Springer Series in Optical Sciences 200

Zbigniew Ficek
Ryszard Tanaś

Quantum-Limit Spectroscopy

Springer

Springer Series in Optical Sciences

Volume 200

Springer Series in Optical Sciences

The Springer Series in Optical Sciences, under the leadership of Editor-in-Chief William T. Rhodes, Florida Atlantic University, USA, provides an expanding selection of research monographs in all major areas of optics: lasers and quantum optics, ultrafast phenomena, optical spectroscopy techniques, optoelectronics, quantum information, information optics, applied laser technology, industrial applications, and other topics of contemporary interest.

With this broad coverage of topics, the series is of use to all research scientists and engineers who need up-to-date reference books.

The editors encourage prospective authors to correspond with them in advance of submitting a manuscript. Submission of manuscripts should be made to the Editor-in-Chief or one of the Editors. See also www.springer.com/series/624

More information about this series at http://www.springer.com/series/624

Zbigniew Ficek · Ryszard Tanaś

Quantum-Limit Spectroscopy

Springer

Zbigniew Ficek
King Abdulaziz City for Science
and Technology (KACST)
National Centre for Applied Physics
Riyadh
Saudi Arabia

Ryszard Tanaś
Nonlinear Optics Division
Faculty of Physics
Adam Mickiewicz University
Poznań
Poland

ISSN 0342-4111 ISSN 1556-1534 (electronic)
Springer Series in Optical Sciences
ISBN 978-1-4939-3738-7 ISBN 978-1-4939-3740-0 (eBook)
DOI 10.1007/978-1-4939-3740-0

Library of Congress Control Number: 2016948595

Printed on acid-free paper

This Springer imprint is published by Springer Nature
The registered company is Springer Science+Business Media LLC
The registered company address is: 233 Spring Street, New York, NY 10013, U.S.A.

To Lila

Preface

At present, we are witnessing the dawn of an era of quantum technology. More and more money is invested in projects that make use of quantum phenomena to achieve new goals of practical applicability. Some people even talk about a *second quantum revolution* that applies the quantum rules to develop new technologies. The increasing ability to manipulate quantum effects is leading to new devices that are superior to traditional devices. It is very important to describe properly the quantum phenomena underlying the new technologies.

Quantum mechanics gives us new opportunities, but it also imposes some restrictions of a fundamental nature. For example, repeated measurement of one of the observable quantities leads to an average value around which there are quantum fluctuations or noise. The quantum noise is a fundamental property of all systems and persists even if all classical sources of error have been eliminated from the measurement process. Quantum fluctuations are present in all systems, including radiation fields in the vacuum state, and it has long been thought that they presented an insuperable barrier to accuracy. They limit the sensitivity achieved by detectors for spectral resolution and the signal-to-noise ratio and hence limit the accuracy to which measurements can be performed. All detection systems are subject to this limit, and it was long believed that this limit could not be suppressed. In the 1980s theoretical studies followed by experimental measurements showed that the quantum limit can be beaten using quantum technologies that employ quantum effects such as quantum interference, squeezing, and entanglement. The search for light fields and physical systems with reduced or even completely suppressed fluctuations has become a new subject in physics to study. The possibility to overcome the quantum limit with new sources of light allows one to perform experiments with greater precision than is possible with laser light. It also allows the transmission of information more accurately than with conventional light. This realm of physics is now known as precision quantum technology. However, some of these quantum technologies are still futuristic; for example, methods of creating and manipulating entanglement are still in their infancy.

The general field of quantum-limit spectroscopy is of importance in connection with the physical theories of noise-free measurements. The field of study of spectroscopic effects at the quantum noise limit is either explicit or implicit in almost all areas of physics and also in many areas of science such as chemistry and biology, and we explore the novel effects and recent developments in spectroscopy of atoms and quantum dots. Quantum effects in atomic radiation, which are distinct from semiclassical theories, arise when it is essential to quantize the electromagnetic field, and it is well known that they were central to the early discussions of the manifestation of the vacuum fluctuations characteristic of quantum fields. In the field of quantum optics the interest in quantum spectroscopic effects has been inspired in part by the work on the fluorescence and absorption spectra by Mollow and Eberly, photon antibunching and squeezing by Kimble, Mandel, Walls, Carmichael, and other workers in the seventies. In recent years quantum spectroscopy has become of interest not only for the basic understanding of complicated quantum structure of atomic systems, but also because it lies at the heart of such important applications as high-resolution spectroscopy, noise-free measurements, and atomic clocks. The latest applications are to quantum computation and to spectroscopy with Bose–Einstein condensates. It has also been demonstrated that quantum and precision spectroscopy methods provide an effective way of controlling quantum fluctuations and decoherence. Other rapidly developing modern topics, such as entanglement, enhanced spectral resolution, and controlled information transfers are, of course, intimately associated with quantum effects in the atom–field interaction. According to quantum mechanics, a coupled system of an atom and the radiation field is not merely an atom exchanging energy with the field: The atom and the radiation field become entangled. They form a composite entity, with superposition states that are entangled states.

Although this book is focused on a small collection of current research areas in atomic spectroscopy, it should nevertheless be evident how strongly atomic spectroscopy relates to basic quantum physics and quantum limits in particular. Quantum-limit spectroscopy lies at the frontier of current experimental and theoretical techniques, and is one of the areas of atomic spectroscopy where the quantization of the sources (atoms) and the field is essential to predict and interpret the existing experimental results. It was recognized as representing a radical departure from the traditional classical spectroscopy where the existing treatments turn out to be less than completely satisfactory. Currently, there is an increasing interest in quantum and precision spectroscopy both theoretically and experimentally, due to a significant progress in trapping and cooling of single atoms and ions. This progress allows us to explore in the most intimate detail the ways in which light interacts with atoms and to measure spectral properties and quantum effects with a large precision. Moreover, it allows us to perform subtle tests of quantum mechanics on the single atom and single photon scale which were hardly even imaginable as “thought experiments” a few years ago.

Some description of the mathematical tools for the study of quantum spectroscopy is required, and therefore we begin in Chap. 1 with an overview of the fundamental concepts relating to quantum fluctuations of the electromagnetic field and the spectroscopic methods of detecting them by means of photoelectron counting. Furthermore, the intensity spectrum, optical power spectrum, and quantum noise spectrum will be defined. The theories of the emission power spectrum, the absorption spectrum, and the phase-dependent spectrum and their relationship to radiating sources are developed in Chap. 2. This chapter also includes a discussion of the homodyne and balanced homodyne techniques for detection of the phase-dependent spectra and quantum fluctuations. In Chap. 3, we begin the analysis of quantum-limit spectroscopy with a consideration of the most fundamental models in atomic spectroscopy. We consider the optical spectra of a coherently driven two-level atom and discuss their properties with a particular attention on signatures of quantum fluctuations and their control. The effect of a tailored vacuum and coherent pumping on the spectral line narrowing is discussed in detail. The chapter concludes with a description of experimental studies of the spectral line narrowing. Chapter 4 is devoted to collective effects in atomic spectroscopy. The role of the collective behavior of the radiating atoms in the cancellation of spontaneous emission is discussed. This chapter also discusses techniques of a selective excitation of the collective states and experimental studies on the preparation of two atoms in a desired collective (entangled) state and the measurement of the subradiance from artificial atoms. The subject of spectroscopy with time-dependent fields is considered in Chap. 5. The theoretical techniques for calculating the fluorescence spectrum are explained in details and illustrated on examples of the excitation with bichromatic and amplitude-modulated fields. Experimental studies on the cancellation of spectral lines are also discussed. The theory of quantum spectroscopy with squeezed light is developed in Chap. 6. The main part of this chapter is devoted to applications of squeezed light in atomic spectroscopy with a particular attention on a class of applications which lead to features unique to quantum nature of squeezed light. Chapter 7 presents experimental studies on atomic spectroscopy with squeezed light. A full description of experiments which aimed to observe alterations in the radiative properties of atoms interacting with squeezed light is presented. A brief discussion of an experiment on ultrahigh frequency measurements, and frequency metrology, is also included. The subject of engineering collective and squeezed field interactions is considered in Chap. 8. The procedures of the adiabatic approximations are used to demonstrate that collective effects between distant atoms and a squeezed field type damping of an atom can be achieved. The chapter also includes experimental studies demonstrating collective behaves of distant atoms. Techniques of beating quantum limits in optical spectroscopy, called quantum strategies, are discussed in Chap. 9. The detailed discussion of different concepts of the fundamental limits in physics accompanies the presentation of experimental studies that demonstrated beating

of the quantum limits and the improvement of the spectral resolution. The final chapter, Chap. 10, deals with various forms of squeezing of the fluctuations of the spin operators. The concepts of dipole, planar, and spin squeezing are introduced, and we demonstrate how to distinguish between these three forms of squeezing. The significance of spin squeezing in detection of entanglement is discussed.

Riyadh, Saudi Arabia — Zbigniew Ficek
Poznań, Poland — Ryszard Tanaś

Contents

About the Authors

Zbigniew Ficek is a professor at the King Abdulaziz City for Science and Technology, Riyadh, Saudi Arabia. He graduated from the Adam Mickiewicz University, Poznań, Poland and worked for many years at the University of Queensland, Australia, where he was ARC QEII Fellow, Senior Research Fellow and then Professorial Research Fellow. He also worked at the Queens University of Belfast as UK EPSRC Professorial Research Fellow. His research speciality is quantum optics and quantum information. He is particularly well known for his contributions to the field of multi-atom effects, spectroscopy with squeezed light, quantum interference and multi-chromatic spectroscopy. He is the co-editor of a book on Quantum Squeezing, the author and co-author of over 160 scientific papers, a research book on Quantum Interference, and two textbooks on Quantum Physics for Beginners and Quantum Optics for Beginners.

Ryszard Tanaś is a professor in the Faculty of Physics at Adam Mickiewicz University, Poznań, Poland. Since 1993 he has served as Head of Nonlinear Optics Division. His research focuses on theoretical quantum optics and quantum information. He is the recipient of the Wojciech Rubinowicz Award of the Polish Physical Society.

Chapter 1
Quantum Fluctuations and Their Measurements

The electromagnetic (radiation) fields are determined by two vector fields, the electric field and magnetic induction, which are subject to fluctuations. Even in a highly stabilized laser, the phase and amplitude of the resulting coherent electromagnetic field exhibit temporal fluctuations. There are several reasons why the radiation field fluctuates. Much of these irregularities arise from random and uncontrolled changes that occur in any radiation source and lead to random changes in the radiation frequency and amplitude. Even if all these sources of fluctuations are eliminated, radiation fields are still subject to fluctuations arising from the laws of quantum physics and are never entirely absent. These fluctuations are called quantum fluctuations and impose the (quantum) limit on the precision of any measurements in physics.

The fluctuations and correlations, which may exist between the fluctuations at two or more space-time points, are manifested in the spectral and statistical properties of the radiation field. In practice, these properties are measured with the help of photoelectric detectors. These devices, however, do not measure the field as the electric field of an electromagnetic wave oscillating at optical frequency varies too fast in time to be measured by the fastest optical detectors available. Instead, physical quantities, such as average radiation intensity, emission and absorption spectra, and field-quadrature noise spectra are measured in typical photodetection experiments. These quantities vary on a much shorter time scale, and can be directly determined from the spectral and statistical properties of photoelectrons. Moreover, the analysis of photoelectric fluctuations has become an important technique for the determination of entirely nonclassical effects, such as sub-Poissionian photon statistics, photon antibunching, and squeezing.

The main purpose of this introductory chapter is to introduce the reader to the fundamental concepts of optical spectra and their measurements by means of photoelectron counting. The radiation intensity, emission and absorption spectra, and field-quadrature noise spectra will be defined in terms of the amplitudes of the detected electromagnetic (EM) field. These quantities are measurable by direct or indirect phase sensitive photocounting techniques and provide

Z. Ficek and R. Tanaś, *Quantum-Limit Spectroscopy*, Springer Series in Optical Sciences 200, DOI 10.1007/978-1-4939-3740-0_1

a method of determining statistical properties of radiation fields. They will also allow us to treat a number of interesting and challenging new problems in atomic spectroscopy and quantum physics.

Another purpose of this introductory chapter is to lay the necessary groundwork in the use of the optical spectra to determine the quantum fluctuations of the radiation field and the methods to modify these fluctuations using external fields or manipulating the density of modes of the field. We have known for quite some time that the radiation spectrum can be altered in a fundamental way by altering the environment surrounding an atomic system or by driving the atomic system with an external near resonant fields.

We start with a brief overview of the quantum theory of radiation. We then introduce the basic concepts of the photodetection theory and define the power spectrum of stationary and nonstationary fields, and spectrum of photocurrent fluctuations, which will be needed in the succeeding chapters of the book. This is followed by a discussion of phase-dependent spectra and their measurements using homodyne detection schemes. A common way to observe field fluctuations is with spectral analyzers, which measures the Fourier transform of the photocurrent during some long-time period. Therefore, the latter part of the chapter introduces the principles of spectral analyzers. The final section deals with the laser modulation techniques for spectroscopic studies.

1.1 Radiation Fields

We begin our study of quantum limit spectroscopy by introducing the fundamental concepts of the quantum theory of radiation which we then apply to the study of statistical and spectral properties of electromagnetic fields radiated by atomic and molecular systems. We proceed to describe the quantum field fluctuations and derive from the quantum theory of photodetection the basic measurable quantities, such as excitation spectrum, emission (fluorescence) spectrum, probe-field absorption spectrum, and quadrature-field fluctuations spectrum. These quantities are directly measurable by means of photoelectron counting, and provide a method of determining the statistical properties of the electromagnetic field. They also carry information about the internal structure of a radiating system [1, 2].

In the quantum theory of radiation, a multimode field is represented by the vector electric field $\hat{\boldsymbol{E}}(\boldsymbol{r}, t)$, which is an operator variable defined at each space point $\boldsymbol{r}$ and any time t. It is convenient to make a Fourier mode decomposition and express the multimode electric field in terms of plane transverse waves whose the amplitudes are quantized and determined by the creation $\hat{a}^{\dagger}_{\boldsymbol{k}s}$ and annihilation $\hat{a}_{\boldsymbol{k}s}$ operators associated with a mode of the electric field of the wave vector $\boldsymbol{k}$ and the orthogonal polarizations s as

$$\hat{\boldsymbol{E}}(\boldsymbol{r},t)=\mathrm{i}\sum_{\boldsymbol{k}s}\sqrt{\frac{\hbar\omega_{\boldsymbol{k}}}{2\varepsilon_0\mathcal{V}}}\left[\boldsymbol{e}_{\boldsymbol{k}s}\hat{a}_{\boldsymbol{k}s}\mathrm{e}^{\mathrm{i}(\boldsymbol{k}\cdot\boldsymbol{r}-\omega_{\boldsymbol{k}}t)}-\boldsymbol{e}^{*}_{\boldsymbol{k}s}\hat{a}^{\dagger}_{\boldsymbol{k}s}\mathrm{e}^{-\mathrm{i}(\boldsymbol{k}\cdot\boldsymbol{r}-\omega_{\boldsymbol{k}}t)}\right], \tag{1.1}$$

where $\mathcal{V}$ is the volume occupied by the field, ε_0 is the permittivity of free space, $\omega_{\boldsymbol{k}}$ is the angular frequency of the $\boldsymbol{k}$th mode connected with the wavevector $\boldsymbol{k}$ by $\omega_{\boldsymbol{k}}=ck$, $\boldsymbol{e}_{\boldsymbol{k}s}$ $(s=1,2)$ are the unit polarization vectors which obey the conditions of a transverse field

$$\boldsymbol{k}\cdot\boldsymbol{e}_{\boldsymbol{k}s}=0,\qquad \boldsymbol{e}^{*}_{\boldsymbol{k}s}\cdot\boldsymbol{e}_{\boldsymbol{k}s'}=\delta_{s,s'},\qquad \boldsymbol{e}_{\boldsymbol{k}1}\times\boldsymbol{e}_{\boldsymbol{k}2}=\boldsymbol{k}/k\,, \tag{1.2}$$

and the asterisk denotes the complex conjugate.

The electric field has been normalized such that the amplitudes represented by the annihilation and creation operators $\hat{a}_{\boldsymbol{k}s}$ and $\hat{a}^{\dagger}_{\boldsymbol{k}s}$ for the $\boldsymbol{k}s$ mode are dimensionless, and obey the usual Bose commutation rules

$$\left[\hat{a}_{\boldsymbol{k}s},\hat{a}_{\boldsymbol{k}'s'}\right]=\left[\hat{a}^{\dagger}_{\boldsymbol{k}s},\hat{a}^{\dagger}_{\boldsymbol{k}'s'}\right]=0,\quad \left[\hat{a}_{\boldsymbol{k}s},\hat{a}^{\dagger}_{\boldsymbol{k}'s'}\right]=\delta_{\boldsymbol{k},\boldsymbol{k}'}\delta_{ss'}\,, \tag{1.3}$$

where $\delta_{i,i'}$ $(i=\boldsymbol{k},s)$ is the Kronecker delta function.

The polarization vector $\boldsymbol{e}_{\boldsymbol{k}s}$ is considered a complex quantity specifically to admit the possibility of different polarizations of the field including circular or elliptical polarizations. In addition, the conditions (1.2) show that the polarization vectors $\boldsymbol{e}_{\boldsymbol{k}1}$, $\boldsymbol{e}_{\boldsymbol{k}2}$ and the unit propagation vector $\boldsymbol{k}/k$ form an orthonormal system

$$\sum_{s=1}^{2}\left(\boldsymbol{e}^{*}_{\boldsymbol{k}s}\right)_i\left(\boldsymbol{e}_{\boldsymbol{k}s}\right)_j+\frac{k_ik_j}{k^2}=\delta_{ij},\qquad i,j=x,y,z\,, \tag{1.4}$$

where $(\boldsymbol{e}_{\boldsymbol{k}s})_i$ is the ith component of the unit polarization vector.

The electric field (1.1) is a physical quantity which is accessible to measurement. It is represented by a Hermitian operator defined in the space of states which describe the field, and can itself be measured for any quantum electromagnetic field state. The results of a succession of measurements will be associated with the expectation value $\langle\hat{\boldsymbol{E}}(\boldsymbol{r},t)\rangle$, representing the most likely value of the field at any space-time point $(\boldsymbol{r},t)$. In the plane wave representation, the electric field is in fact expressed as the sum of two non-Hermitian operators of complex amplitudes, which is often written as

$$\hat{\boldsymbol{E}}(\boldsymbol{r},t)=\hat{\boldsymbol{E}}^{(+)}(\boldsymbol{r},t)+\hat{\boldsymbol{E}}^{(-)}(\boldsymbol{r},t)\,, \tag{1.5}$$

where

$$\hat{\boldsymbol{E}}^{(+)}(\boldsymbol{r},t)=\mathrm{i}\sum_{\boldsymbol{k}s}\sqrt{\frac{\hbar\omega_{\boldsymbol{k}}}{2\varepsilon_0\mathcal{V}}}\boldsymbol{e}_{\boldsymbol{k}s}\hat{a}_{\boldsymbol{k}s}\mathrm{e}^{\mathrm{i}(\boldsymbol{k}\cdot\boldsymbol{r}-\omega_{\boldsymbol{k}}t)} \tag{1.6}$$

represents the positive frequency component of the electric field operator. By definition, the positive frequency component is that proportional to the annihilation operator. The remaining component, which is a Hermitian conjugate of $\hat{\boldsymbol{E}}^{(+)}(\boldsymbol{r}, t)$ and denoted by $\hat{\boldsymbol{E}}^{(-)}(\boldsymbol{r}, t)$, is called the negative frequency component of the field and is proportional to the creation operator.

The decomposition of the electric field operator into two non-Hermitian operators emphasizes the fact that each physical field may be regarded as the sum of two operators which are conjugates of each other and each of them is a combination of the annihilation or creation operators only. As we shall see in Sect. 1.3, the decomposition has a basic significance in photodetection theory, providing insight into the detection process, where atoms being in their ground states and considered as detectors are sensitive to the positive frequency part of the field operator. Moreover, we shall see that the properties of the electromagnetic field may be determined by the expectation values of products of the electric field operators $\hat{\boldsymbol{E}}^{(+)}(\boldsymbol{r}, t)$ and $\hat{\boldsymbol{E}}^{(-)}(\boldsymbol{r}, t)$ at different space-time points.

In the study of the spectral and statistical properties of the radiation field, it will be important to know the commutation relations for the vector components of the positive and negative frequency parts of the electric field at different space-time points. The commutation relations will help us to write expectation values of products of the electric field operators in terms of the normally ordered correlation fusnctions. Since the operators $\hat{a}_{\boldsymbol{k}s}$ and $\hat{a}_{\boldsymbol{k}s}^{\dagger}$ do not commute, it follows that the electric field operators will not commute either. We evaluate the commutation relation between components of the $\hat{\boldsymbol{E}}(\boldsymbol{r}, t)$ vector, and after straightforward calculation using (1.6) together with the commutation relations (1.3), we find

$$\left[\hat{E}_i^{(+)}(\boldsymbol{r}, t), \hat{E}_j^{(-)}(\boldsymbol{r}', t')\right] = \sum_{\boldsymbol{k}s} \left(\frac{\hbar\omega_{\boldsymbol{k}}}{2\varepsilon_0 \mathcal{V}}\right) (\boldsymbol{e}_{\boldsymbol{k}s})_i \left(\boldsymbol{e}_{\boldsymbol{k}s}^*\right)_j \times \exp\left\{\mathrm{i}\left[\boldsymbol{k}\cdot\left(\boldsymbol{r}-\boldsymbol{r}'\right) - \omega_{\boldsymbol{k}}\left(t-t'\right)\right]\right\}, \tag{1.7}$$

where $\hat{E}_i^{(\pm)}(\boldsymbol{r}, t)$ represents the ith vector component of the field.

In order to evaluate the sum over the field modes $\boldsymbol{k}s$, we go over to the large volume limit $\mathcal{V} \to \infty$, at which $\boldsymbol{k}$ varies continuously. This allows us to convert the sum over the wave vector $\boldsymbol{k}$ into an integral

$$\sum_{\boldsymbol{k}s} \longrightarrow \frac{\mathcal{V}}{(2\pi)^3} \sum_{s=1}^{2} \int \mathrm{d}^3\boldsymbol{k}\,. \tag{1.8}$$

Utilizing the above result, and the orthonormality property (1.4), the commutator (1.7) becomes

$$\left[\hat{E}_i^{(+)}(\boldsymbol{r},t),\hat{E}_j^{(-)}(\boldsymbol{r}',t')\right]=\frac{1}{(2\pi)^3}\frac{\hbar}{2\varepsilon_0}\int \mathrm{d}^3\boldsymbol{k}\,\omega_{\boldsymbol{k}}\left(\delta_{ij}-\frac{k_ik_j}{k^2}\right)\times\exp\left\{\mathrm{i}\left[\boldsymbol{k}\cdot\left(\boldsymbol{r}-\boldsymbol{r}'\right)-ck\left(t-t'\right)\right]\right\},\tag{1.9}$$

where the integral is over the magnitudes and directions of $\boldsymbol{k}$ spread over the three-dimensional space of the electromagnetic modes.

In practical situations, bandwidths of optical fields of interest are small compared with some central frequency ω_0. In this case, only a narrow band of frequencies and wave vectors contribute to the integral over $\boldsymbol{k}$. This means that the frequency $\omega_{\boldsymbol{k}}$ can be well approximated by a constant frequency ω_0, the frequency of the central component of the field. Thus, providing that bandwidth of the field is much smaller than the interval over which the integral extends, we can approximate $\omega_{\boldsymbol{k}}$ by ω_0, and then the commutator reduces to

$$\left[\hat{E}_i^{(+)}(\boldsymbol{r},t),\hat{E}_j^{(-)}(\boldsymbol{r}',t')\right]=\frac{1}{(2\pi)^3}\frac{\hbar\omega_0}{2\varepsilon_0}\int \mathrm{d}^3\boldsymbol{k}\left(\delta_{ij}-\frac{k_ik_j}{k^2}\right)\times\exp\left\{\mathrm{i}\left[\boldsymbol{k}\cdot\left(\boldsymbol{r}-\boldsymbol{r}'\right)-ck\left(t-t'\right)\right]\right\}.\tag{1.10}$$

It follows from (1.10) that for equal times, $t=t'$, the integral becomes one of the representations of the three-dimensional *transverse* Dirac delta function $\boldsymbol{\delta}_{ij}^{\mathrm{T}}\left(\boldsymbol{r}-\boldsymbol{r}'\right)$, and we may write

$$\left[\hat{E}_i^{(+)}(\boldsymbol{r},t),\hat{E}_j^{(-)}(\boldsymbol{r}',t)\right]=\frac{\hbar\omega_0}{2\varepsilon_0}\boldsymbol{\delta}_{ij}^{\mathrm{T}}\left(\boldsymbol{r}-\boldsymbol{r}'\right).\tag{1.11}$$

In many problems, we shall be interested in electromagnetic fields propagating in the form of a highly directional beam of a small cross-section area A, where only those modes whose wave vectors lie within a small solid angle over which the field is propagated are important. This simplification is a form of the one-dimensional approximation that variations of the electromagnetic field in the transverse directions are much slower than variations in the longnitudal direction. If the field propagates in one direction, say along the z axis, and has one polarization component only, we evaluate the sum in (1.7) by replacing it with an integral in which we identify the volume $\mathcal{V}$ with AL, where L is some long length parallel to the beam. We allow the length to become infinite, and obtain

$$\left[\hat{E}_i^{(+)}(z,t),\hat{E}_j^{(-)}(z',t')\right]=\frac{\hbar}{2\varepsilon_0 A}\frac{1}{2\pi}\int \mathrm{d}k\,\omega_k\left(\boldsymbol{e}_k\right)_i\left(\boldsymbol{e}_k^*\right)_j\times\exp\left\{\mathrm{i}k\left[\left(z-z'\right)-c\left(t-t'\right)\right]\right\},\tag{1.12}$$

where k now denotes the one-dimensional propagation vector, and we have dropped the sum over the polarization index, assuming that the polarization of the field remains unchanged during propagation of the one-dimensional field. Since $\left(\boldsymbol{e}_k^*\right)_i\left(\boldsymbol{e}_k\right)_j=\delta_{ij}$ and assuming that the beam contains only modes of a wave-number near some central

wave-number k_0, we may replace ω_k by ω_0, and then the commutator (1.12) can be approximated by

$$\left[\hat{E}_i^{(+)}(z,t),\hat{E}_j^{(-)}\left(z',t'\right)\right]=\frac{\hbar\omega_0\delta_{ij}}{2\varepsilon_0 A}\,\delta\left(\left(z-z'\right)-c\left(t-t'\right)\right), \tag{1.13}$$

where $\delta(r)$ is the one-dimensional Dirac delta function.

This is the standard commutation relation for the positive and negative frequency components of the one-dimensional electric field. We shall apply the commutator (1.13) to a broad class of problems involving electromagnetic fields propagating in one direction, for example, focused beams of the output field of optical devices, such as lasers and parametric amplifiers or outputs from an optical cavity, where a strong spatial selection of radiation modes can be achieved. It is worth to note that the commutator (1.13) is a singular function which is zero when $\left(z-z'\right)\neq c\left(t-t'\right)$. Moreover, the components of the electric field commute at any two different points in space ($z\neq z'$) at the same time, and at the same point ($z=z'$) at different times.

It is of some interest to determine the commutation relation for the Fourier components of the one-dimensional electric field. If we make a Fourier decomposition of $\hat{E}_i^{(\pm)}(z,t)$:

$$\hat{E}_i^{(\pm)}(z,\omega)=\int_{-\infty}^{\infty}\mathrm{d}t\,\hat{E}_i^{(\pm)}(z,t)\,\mathrm{e}^{\pm\mathrm{i}\omega t}, \tag{1.14}$$

we obtain

$$\begin{aligned}\left[\hat{E}_i^{(+)}(z,\omega),\hat{E}_j^{(-)}\left(z',\omega'\right)\right]=&\int\int_{-\infty}^{\infty}\mathrm{d}t\,\mathrm{d}t'\mathrm{e}^{\mathrm{i}(\omega t-\omega' t')}\\&\times\left[\hat{E}_i^{(+)}(z,t),\hat{E}_j^{(-)}\left(z',t'\right)\right].\end{aligned} \tag{1.15}$$

With the help of the commutator (1.13) this reduces to

$$\left[\hat{E}_i^{(+)}(z,\omega),\hat{E}_j^{(-)}\left(z',\omega'\right)\right]=\frac{\pi\,\hbar\omega_0\delta_{ij}}{Ac\varepsilon_0}\,\delta\left(z-z'\right)\delta\left(\omega-\omega'\right). \tag{1.16}$$

This commutation relation is found useful in the calculations of correlation functions between the Fourier components of the $\hat{E}$ field, in particular, the output field of a cavity.

1.2 The Field with Multiatom Sources

The electromagnetic fields are not always free fields, but are generated by sources, such as multilevel atoms. In an atom, for example, it is the oscillating dipole moment which usually provides such a source [3]. We now develop a theoretical description

of the radiation field in terms of the source variables. We shall relate properties of the radiation field to the atomic quantities such as coherences and populations of the source atoms. The atomic coherences and populations could be in a steady state as in resonance scattering experiments with a constant exciting field or they could be changing as in experiments where coherences are initially produced by a pulsed light fields.

Consider a combined system composed of the quantum electromagnetic field and a sample of multilevel atoms. The system may be described by the multipolar Hamiltonian and the interaction between the field and atoms given to a good approximation by the electric dipole term [4, 5]. The total electric field operator $\hat{\boldsymbol{E}}(\boldsymbol{r}, t)$ can then be expressed without further approximation as the sum of two terms

$$\hat{\boldsymbol{E}}(\boldsymbol{r}, t) = \hat{\boldsymbol{E}}_F(\boldsymbol{r}, t) + \hat{\boldsymbol{E}}_S(\boldsymbol{r}, t) \ , \tag{1.17}$$

where

$$\hat{\boldsymbol{E}}_F(\boldsymbol{r}, t) = \mathrm{i} \sum_{\boldsymbol{k}s} \sqrt{\frac{\hbar\omega_{\boldsymbol{k}}}{2\varepsilon_0 \mathcal{V}}} \boldsymbol{e}_{\boldsymbol{k}s} \hat{a}_{\boldsymbol{k}s} \mathrm{e}^{\mathrm{i}(\boldsymbol{k}\cdot\boldsymbol{r} - \omega_{\boldsymbol{k}} t)} + \mathrm{H.c.} \tag{1.18}$$

is the *free-field* term which characterizes the vacuum or background field, i.e., the field in the absence of the source atoms, "H.c." stands for the Hermitian conjugate of the first term, and

$$\hat{\boldsymbol{E}}_S(\boldsymbol{r}, t) = \nabla \times \left[\nabla \times \frac{1}{4\pi\varepsilon_0} \sum_{n=1}^{N} \frac{\hat{\boldsymbol{\mu}}_n (t - |\boldsymbol{r} - \boldsymbol{R}_n|/c)}{|\boldsymbol{r} - \boldsymbol{R}_n|} \right. \\ \left. \times \theta (t - |\boldsymbol{r} - \boldsymbol{R}_n|/c) \right] \tag{1.19}$$

is the *source-field* term which characterizes the field radiated by the atoms. For the free field, $\hat{a}_{\boldsymbol{k}s}$ is the annihilation operator of the three-dimensional field which is independent of the presence of sources. For the source field, $\hat{\boldsymbol{\mu}}_n$ is the dipole moment operator associated with the nth atom located at $\boldsymbol{R}_n$, the sum is taken over all the atoms n that contribute to the field at time t, and N is the total number of atoms in the sample. The atomic dipole operator $\hat{\boldsymbol{\mu}}_n$ is given in the form of the usual Heaviside function θ, zero for negative argument and unity for positive argument. The source field is given in retarded form, where the field at an arbitrary point $(\boldsymbol{r}, t)$ is caused by the action of the dipole operator at the retarded time $t - |\boldsymbol{r} - \boldsymbol{R}_n|/c$. The free field has the same time dependence that would apply if there were no atoms present.

In the usual case when the field is observed at a large distance from the source atoms, in the radiation or far-field zone, we can approximate $\hat{\boldsymbol{E}}_S(\boldsymbol{r}, t)$ by an asymptotic form valid for $t > |\boldsymbol{r} - \boldsymbol{R}_n|/c$ and $\boldsymbol{r}$ large, and obtain

$$\hat{\boldsymbol{E}}_S(\boldsymbol{r},t) = \frac{1}{4\pi\varepsilon_0 c^2}\sum_{n=1}^{N}(\boldsymbol{r}-\boldsymbol{R}_n) \times\left[\frac{(\boldsymbol{r}-\boldsymbol{R}_n)\times\ddot{\hat{\boldsymbol{\mu}}}_n(t-|\mathbf{r}-\mathbf{R}_n|/c)}{|\mathbf{r}-\mathbf{R}_n|^3}\right], \tag{1.20}$$

where the double dot over $\hat{\boldsymbol{\mu}}$ indicates the second derivative over time. Equation (1.20) shows the inverse distance dependence of the field at large $|\boldsymbol{r}-\boldsymbol{R}_n|$ and the dependence on the dipole acceleration.

The dipole moment operator for the nth atom can be written as the sum of an upward (raising) component $\hat{\boldsymbol{\mu}}_n^+$ and a downward (lowering) component $\hat{\boldsymbol{\mu}}_n^-$:

$$\hat{\boldsymbol{\mu}}_n = \hat{\boldsymbol{\mu}}_n^+ + \hat{\boldsymbol{\mu}}_n^-, \tag{1.21}$$

and the components can be expanded in terms of the projection operators as

$$\hat{\boldsymbol{\mu}}_n^+ = \left(\hat{\boldsymbol{\mu}}_n^-\right)^\dagger = \sum_{i>j}\boldsymbol{\mu}_{ij}^n\hat{\Lambda}_{ij}^n, \tag{1.22}$$

where the subscripts i,j enumerate the atomic levels, $\boldsymbol{\mu}_{ij}^n = \langle i_n|\hat{\boldsymbol{\mu}}_n|j_n\rangle$ is the matrix element of the atomic dipole operator and the projection operator $\hat{\Lambda}_{ij}^n = |i_n\rangle\langle j_n|$ represents transitions between the atomic energy levels $|i_n\rangle$ and $|j_m\rangle$, whose energies are $\hbar\omega_i$ and $\hbar\omega_j$, such that $\omega_i > \omega_j$ and $i > j$.

With the representation (1.21), the source-field term can be decomposed into a sum of two components, similar to the positive and negative frequency components, as

$$\hat{\boldsymbol{E}}_S(\boldsymbol{r},t) = \hat{\boldsymbol{E}}_S^{(+)}(\boldsymbol{r},t) + \hat{\boldsymbol{E}}_S^{(-)}(\boldsymbol{r},t), \tag{1.23}$$

where

$$\hat{\boldsymbol{E}}_S^{(\pm)}(\boldsymbol{r},t) = \frac{1}{4\pi\varepsilon_0 c^2}\sum_{n=1}^{N}(\boldsymbol{r}-\boldsymbol{R}_n) \times\left[\frac{(\boldsymbol{r}-\boldsymbol{R}_n)\times\ddot{\hat{\boldsymbol{\mu}}}_n^{\mp}(t-|\boldsymbol{r}-\boldsymbol{R}_n|/c)}{|\boldsymbol{r}-\boldsymbol{R}_n|^3}\right). \tag{1.24}$$

Since the dominant contribution to the radiated electric field in a Fourier decomposition would come from certain optical frequencies close to the atomic transition frequencies, it is customary to treat the atomic dipole moment by making the harmonic approximation. In this approximation, it is assumed that the atomic dipole operators evolve with a characteristic harmonic variable, the frequency of an irradiating field or the atomic transition frequency. If the frequency of the radiating atoms is $\omega_{ij} = \omega_i - \omega_j$, the dipole moment oscillates at approximately this same frequency,

and consequently, we may write

$$\hat{\boldsymbol{\mu}}_n(t) = \tilde{\hat{\boldsymbol{\mu}}}_n^{+} \mathrm{e}^{\mathrm{i}\omega_{ij}t} + \tilde{\hat{\boldsymbol{\mu}}}_n^{-} \mathrm{e}^{-\mathrm{i}\omega_{ij}t} , \tag{1.25}$$

where $\tilde{\hat{\boldsymbol{\mu}}}_n^{\pm}$ are the slowly varying parts of the atomic dipole moment. Because $\tilde{\hat{\boldsymbol{\mu}}}_n^{\pm}$ is slowly varying, we have, to a good approximation

$$\ddot{\tilde{\hat{\boldsymbol{\mu}}}}_n^{\pm}(t) = -\omega_{ij}^2 \tilde{\hat{\boldsymbol{\mu}}}_n^{\pm}(t) . \tag{1.26}$$

Hence, the positive frequency component of the source field can be written as

$$\hat{\boldsymbol{E}}_S^{(+)}(\boldsymbol{r}, t) = \sum_{n=1}^{N} \sum_{i>j} \boldsymbol{\Psi}_{ij}^{*}(\boldsymbol{r} - \boldsymbol{R}_n) \hat{\Lambda}_{ji}^{n} \left(t - \frac{|\boldsymbol{r} - \boldsymbol{R}_n|}{c} \right) , \tag{1.27}$$

where

$$\boldsymbol{\Psi}_{ij}(\boldsymbol{r} - \boldsymbol{R}_n) = \frac{\omega_{ij}^2}{4\pi\varepsilon_0 c^2} \left\{ \frac{\boldsymbol{\mu}_{ij}^{n}}{|\boldsymbol{r} - \boldsymbol{R}_n|} - \frac{\left[\boldsymbol{\mu}_{ij}^{n} \cdot (\boldsymbol{r} - \boldsymbol{R}_n) \right] (\boldsymbol{r} - \boldsymbol{R}_n)}{|\boldsymbol{r} - \boldsymbol{R}_n|^3} \right\} \tag{1.28}$$

is the dipole field produced by the nth atom at distance $|\boldsymbol{r} - \boldsymbol{R}_n|$.

Similarly, the negative frequency component of the source field can be written as

$$\hat{\boldsymbol{E}}_S^{(-)}(\boldsymbol{r}, t) = \sum_{n=1}^{N} \sum_{i>j} \boldsymbol{\Psi}_{ij}(\boldsymbol{r} - \boldsymbol{R}_n) \hat{\Lambda}_{ij}^{n} \left(t - \frac{|\boldsymbol{r} - \boldsymbol{R}_n|}{c} \right) . \tag{1.29}$$

The $|\boldsymbol{r} - \boldsymbol{R}_n|$ dependence of $\hat{\Lambda}_{ij}^{n}(t - |\boldsymbol{r} - \boldsymbol{R}_n|/c)$ can be removed with the help of the harmonic approximation, and we can write

$$\hat{\Lambda}_{ij}^{n} \left(t - \frac{|\boldsymbol{r} - \boldsymbol{R}_n|}{c} \right) = \hat{\Lambda}_{ij}^{n}(t) \, \mathrm{e}^{-\mathrm{i}k_0(r - \bar{\boldsymbol{r}} \cdot \boldsymbol{R}_n)} . \tag{1.30}$$

Then the negative frequency component of the electric field becomes

$$\hat{\boldsymbol{E}}^{(-)}(\boldsymbol{r}, t) = \hat{\boldsymbol{E}}_F^{(-)}(\boldsymbol{r}, t) + \sum_{n=1}^{N} \sum_{i>j} \boldsymbol{\Psi}_{ij}(\boldsymbol{r} - \boldsymbol{R}_n) \hat{\Lambda}_{ij}^{n}(t) \, \mathrm{e}^{-\mathrm{i}k_0(r - \bar{\boldsymbol{r}} \cdot \boldsymbol{R}_n)} , \tag{1.31}$$

and the positive frequency component of the electric field is obtained by taking a Hermitian conjugate of (1.31).

Equation (1.31) gives the electric field operator in the radiation zone of the atomic system expressed in terms of the source operators. Therefore, this relation provides the basis for the formal analysis of the properties of the radiation field in terms of the

source variables. It will be used later in the treatment of the spectral and statistical properties of the fields produced by radiating atoms. Further, by applying this relation to the measurable quantities, such as the correlation functions of the electric field operators, we will be able to express the field correlation functions in terms of the correlation functions of the atomic dipole operators. In fact, the correlation functions of the field operators will be the sum of equivalent correlation functions for the free field and for the source field together with interference terms between the source field and the free field. However, for most of the correlation functions, in particular for the normally ordered correlation functions, the free field correlation functions and the interference terms can be zero. Thus, we will be able to relate statistical properties of the radiation field to the statistical properties of its source, the radiating atoms. As we shall see, the source of radiation field fluctuations are fluctuations of the atomic dipoles.

1.3 Photodetection Theory

As we have already mentioned, the electromagnetic field is a physical quantity which can be measured. However, for many purposes the analysis of properties of the electromagnetic field are not based on the field itself but rather on the appropriate correlation functions which are associated with the characteristics of the field and which are measured in experiments. In practice, the correlation functions are measured with the help of photoelectric detectors, and the properties of radiation fields are manifested through the corresponding properties of the photoelectric current. For the purpose of understanding the measurement process, we now introduce the basic concepts of classical and quantum photodetection theory, through which statistical and spectral properties of radiation fields may be studied [6, 7].

The fundamental process in any measurement is the photodetection, and most detection processes (including the visual and photographic processes) are based on the photoelectric effect. In the process, the incident field interacting with a photocathode produces photoelectrons by photoionization. The photoelectrons then are accelerated by a potential applied between the photocathode and anode to form a photocurrent, whose statistical properties are measured. The important point is that in photodetectors the subsequent processes of ionization are independent of each other which leads to statistical properties of the photoelectrons that reflect the statistical properties the incident field. Typical quantities which are measured are the average number of photoelectrons and the variance of the number of photoelectrons, which provide an information about the intensity and fluctuations of the incident field.

The basic quantity for the photodetection theory is the photon counting distribution $P_m(t, T)$ of detecting m photoelectrons emitted by the photocathode illuminated by a light beam in the time interval t to $t+T$. If the intensity of the incident light does

not fluctuate significantly in time,[1] the distribution is the product over all possible probabilities of photoemission in some intervals of time multiplied by the probabilities of no emission in the remaining intervals, which in the limit of large number of intervals gives the distribution

$$P_m(t,T) = \frac{1}{m!}\left[\lambda T \bar{I}(\boldsymbol{r},t,T)\right]^m \exp\left[-\lambda T \bar{I}(\boldsymbol{r},t,T)\right], \tag{1.32}$$

where λ is a constant proportional to the efficiency of the detector

$$\bar{I}(\boldsymbol{r},t,T) = \frac{1}{T}\int_t^{t+T} \mathrm{d}t' I(\boldsymbol{r},t') \tag{1.33}$$

is the average intensity of the light over the detection time T, and

$$I(\boldsymbol{r},t) = 2\varepsilon_0 c\lambda \boldsymbol{E}^*(\boldsymbol{r},t)\cdot\boldsymbol{E}(\boldsymbol{r},t) \tag{1.34}$$

represents the instantaneous intensity of the incident field evaluated at the position of the detector. Here, $\boldsymbol{E}(\boldsymbol{r},t)$ is the positive frequency part of the electric field, the so-called analytic signal. This does not represent the real electric field, it contains all terms which vary as $\exp(-\mathrm{i}\omega t)$, for $\omega > 0$. In reality, the instantaneous intensity of the real field is a rapidly oscillating function of time, with period of order of 10^{-15} s. This is several order of magnitude shorter than the resolution time of the fastest optical detectors available, so that the actual intensity registered by the detector corresponds to an average over many periods of oscillation, and this is represented by (1.34). As we shall see later, the use of the analytic signal instead of the real field has the advantage that it is closely connected with the quantum description of the photodetection theory.

The photon counting distribution (1.32) is a Poisson distribution of the number of photoemissions m, which reflects the fact that the photoelectrons are removed by the incident light independent of each other. This is the randomness introduced solely by the detection process. Although the result (1.32) is based on a classical physics approach, it is often convenient to express the intensity $I(\boldsymbol{r},t)$ in units of photons per second.[2] This has been done by introducing the factor

$$\lambda = \frac{A}{\hbar\omega_0} \tag{1.35}$$

in (1.34), where A is the cross-section area of the light beam as seen by the detector. We assume perfect detectors with efficiency equal to 1.

[1] In the language of the stochastic processes, we assume that the intensity of the incident light is not a stochastic variable, and one considers only a single realization of a possible ensemble of optical fields with intensity $I(\boldsymbol{r},t)$.

[2] The intensity I can be defined in different ways: it can be just $I(\boldsymbol{r},t) = \boldsymbol{E}^*(\boldsymbol{r},t)\cdot\boldsymbol{E}(\boldsymbol{r},t)$ in [V^2/m^2], or multiplied by $2\varepsilon_0 c$ in [W/m^2], or multiplied by $2\varepsilon_0 c\lambda$ in [photons/second].

In what follows, we shall focus only on the temporal behavior of the EM field at an arbitrary position $\boldsymbol{r}$, which we leave implicit. Hence, for convenience, we suppress the position variable $\boldsymbol{r}$, and use the notation for the electric field amplitude $\boldsymbol{E}(t) \equiv \boldsymbol{E}(\boldsymbol{r}, t)$, and for the intensity $I(t) \equiv I(\boldsymbol{r}, t)$.

The probability distribution (1.32), which is valid for a non-fluctuating field may, in fact, be applied to a fluctuating field providing that the detection time T is short compared with the coherence time of the detected field. It is expected that the field intensity remains constant over such a short time. When T is not necessary short compared with the coherence time of the field and, in addition, the intensity of the incident light fluctuates in time, i.e., is a member of a stochastic ensemble, the distribution of the photoelectrons will change. In this case, the distribution (1.32) must be averaged over all possible realizations of $I(t)$, and then, we obtain

$$P_m(t, T) = \frac{1}{m!} \int_0^\infty \mathrm{d}\bar{I} P(\bar{I}) \left(\lambda T \bar{I}\right)^m \exp\left(-\lambda T \bar{I}\right) , \tag{1.36}$$

where $\bar{I} \equiv \bar{I}(t, T)$, and $P(\bar{I})$ is the probability distribution of the average intensity $\bar{I}$. For a stationary field, the average intensity depends only on the detection time T, and then the probability distribution is independent of the origin of time t, and may be written as $P_m(T)$.

Equation (1.36) is the general expression for the probability distribution of detecting m photoelectrons produced by any kind of a fluctuating field. It is no longer a Poisson distribution, it is in the form of an average over Poisson distributions weighted with the distribution $P(\bar{I})$. Although explicit expressions for $P(\bar{I})$ are generally not available, we can readily use the distribution (1.36) to calculate statistical moments of the photoelectron counts. For example, the average number of photoelectron counts measured by a photodetector between the times t and $t + T$ is given by

$$\langle m(t, T)\rangle = \lambda T \langle \bar{I}(t, T)\rangle = \lambda T \int_0^\infty \mathrm{d}\bar{I} \bar{I}(t, T) P(\bar{I}) , \tag{1.37}$$

where the angular brackets denote an average over the intensity fluctuations. The result (1.37) refers to the average number of photoelectrons, but for an ideal photodetector it may be taken as a measure of the average number of photons in the incident field.

If, as is usually the case in typical experiments, the detection time T is much shorter than the coherence time of the light, so that $I(t)$ does not vary appreciably over the detection time, the average number of photoelectrons (1.37) reduces to

$$\langle m(t, T)\rangle = \lambda T \langle I(t)\rangle . \tag{1.38}$$

This formula shows that the intensity of the radiation field is measured by detectors counting the average number of photoelectrons produced by the incident field. This result was of course to be expected from the fact that in the photodetection the subsequent processes of ionization are independent of each other.

One of the most important characterizations of the statistical and spectral properties of the EM field is the variance of the field amplitude which may be investigated by measuring the variance of the number of photoelectric counts. The variance provides us an information about the fluctuations of the field amplitude. These fluctuations impose a limit on the spectral resolution and the accuracy of a measurement of the field and are therefore of fundamental importance. Since

$$\langle m^2(t,T)\rangle = \sum_m m^2 P_m(t,T) = \langle m(t,T)\rangle + (\lambda T)^2 \langle \bar{I}^2(t,T)\rangle \,, \tag{1.39}$$

we find for the variance of the number of photoelectric counts

$$\begin{aligned} \langle [\Delta m(t,T)]^2\rangle &= \langle m^2(t,T)\rangle - \langle m(t,T)\rangle^2 \\ &= \langle m(t,T)\rangle + (\lambda T)^2 \langle \Delta \bar{I}^2(t,T)\rangle \,, \end{aligned} \tag{1.40}$$

where $\langle \Delta \bar{I}^2(t,T)\rangle = \langle \bar{I}^2(t,T)\rangle - \langle \bar{I}(t,T)\rangle^2$ is the variance of the average intensity of the incident field.

The variance (1.40) has a simple physical interpretation. The first term on the right-hand side is the *shot noise* associated with the random generation of discrete photoelectrons in the detector. The second term is the noise in excess of the standard and is called *wave noise*. It is associated with the intensity fluctuations in the incident field. Only for a well-stabilized field whose the intensity does not fluctuate, such as an ideal laser field, the wave noise term is zero, and then the variance of the number of photoelectric counts is equal to the shot noise level. The shot-noise level was believed to be the lowest bound for noise in photodetection. In many applications it limits accuracy of the measurement. Although the variance (1.40) has a simple physical interpretation, it must be used with caution, since the validity of (1.40) is restricted to certain class of radiation fields which are regarded as classical. Later, we will study special class of radiation fields, called nonclassical fields, which can exhibit fluctuations reduced below the shot noise level or even completely suppressed. The availability of such fields opens the possibility of unprecedented precision measurements beyond the shot-noise limit.

If the detection time is much shorter than the coherence time of the field, the variance reduces to

$$\langle [\Delta m(t,T)]^2\rangle = \langle m(t,T)\rangle + (\lambda T)^2 \langle \Delta I^2(t)\rangle T^2 \,. \tag{1.41}$$

The above formula shows that the fluctuations of the photoelectric counts are always expressible as the sum of fluctuations of classical particles obeying the Poisson distribution, for which $\langle [\Delta m(t,T)]^2\rangle = \langle m(t,T)\rangle$, and the fluctuations of the field intensity $\langle \Delta I^2(t)\rangle$. As a consequence, the variance of the number of photoelectric counts produced by a fluctuating field is super-Poissonian. This implies that the photoelectrons are not produced randomly, but have certain characteristic bunching properties. Later, we will see a case of nonclassical light where $\langle : \Delta I^2(t) : \rangle < 0$ may

occur, and consequently a sub-Poissonian statistics of the photoelectric counts may be observed.

The photodetection theory described so far has been based on the classical description of the radiation field. The theory can be easily extended to the quantum description of the field. This can be done by replacing the negative and positive frequency parts of the field, $\boldsymbol{E}^{*}(t)$ and $\boldsymbol{E}(t)$, by Hilbert space operators $\hat{\boldsymbol{E}}^{(-)}(t)$ and $\hat{\boldsymbol{E}}^{(+)}(t)$, respectively. If the electromagnetic field is quantized instead of being classical, then the instantaneous field intensity becomes an operator proportional to the normally ordered field operators

$$\hat{I}(t) = 2\varepsilon_0 c\lambda \hat{\boldsymbol{E}}^{(-)}(t) \cdot \hat{\boldsymbol{E}}^{(+)}(t) \,, \tag{1.42}$$

and the ensemble average $\langle \hat{I}(t) \rangle$ has to be interpreted as a quantum expectation value over an arbitrary state of the field. With these changes, the formula (1.38) for the average number of photoelectrons remains equally valid for a quantum field and a classical one.

Similarly, the variance of the number of photoelectrons produced by a quantum field is written in terms of the time and normally ordered correlation function of the intensity fluctuations as

$$\langle [\Delta m(t,T)]^2 \rangle = \langle m(t,T) \rangle + (\lambda T)^2 \langle : \Delta \hat{\bar{I}}^2(t,T) : \rangle \,, \tag{1.43}$$

where the wave noise is given by

$$\langle : \Delta \hat{\bar{I}}^2(t,T) : \rangle = \int_t^{t+T} \int_t^{t+T} \mathrm{d}t' \mathrm{d}t'' \langle : \Delta \hat{I}(t') \Delta \hat{I}(t'') : \rangle \,, \tag{1.44}$$

and the pair of colons stands for normal ordering of the operators. This means that all annihilation operators are placed to the right of all creation operators in the expectation value. The quantity $\Delta \hat{I}(t) = \hat{I}(t) - \langle \hat{I}(t) \rangle$ is the deviation of the field intensity from the mean value.

It is convenient to introduce the normally ordered first- and second-order correlation functions of the electric field operators

$$G^{(1)}(t) = \langle \hat{\boldsymbol{E}}^{(-)}(t) \cdot \hat{\boldsymbol{E}}^{(+)}(t) \rangle \,, \tag{1.45}$$

$$G^{(2)}(t,t') = \langle \hat{\boldsymbol{E}}^{(-)}(t) \hat{\boldsymbol{E}}^{(-)}(t') : \hat{\boldsymbol{E}}^{(+)}(t') \hat{\boldsymbol{E}}^{(+)}(t) \rangle \,, \tag{1.46}$$

where ":" stands for double scalar product. Then, we can write the variance (1.43) as

$$\langle [\Delta m(t,T)]^2 \rangle = \langle m(t,T) \rangle + (2\varepsilon_0 c\lambda) \int_t^{t+T} \int_t^{t+T} \mathrm{d}t' \mathrm{d}t'' \times \left[G^{(2)}(t',t'') - G^{(1)}(t') G^{(1)}(t'') \right] . \tag{1.47}$$

This shows that the fluctuations of photoelectric counts can be described as having their origin in the second-order correlations of the field intensity. Thus, the problem of determining the fluctuations of photoelectron counts can be studied by determining correlation effects in the radiation field. This is what normally happens in experiments involving the detection of the electromagnetic field with a photodetector and subsequent correlation of the output of the photodetector correspond to the measurement of the correlation functions. Such measurements are referred to as photon correlation or intensity correlation measurements [8].

From the study of the number and variance of photoelectric counts it may appear that with the simple replacement of the classical field amplitudes by field operators there is no much difference between the classical and quantum theory of photodetection. However, there are some peculiar features of the field operators which make their properties different from the corresponding classical amplitudes. The variance (1.47) depends strongly on the correlations between the photoelectric counts, and the term within the square brackets on the right-hand side of (1.47) is not necessarily positive. For example, in a chaotic state of the field, such as for a thermal (blackbody) radiation field

$$G^{(2)}(t', t'') > G^{(1)}(t')G^{(1)}(t'') , \tag{1.48}$$

and the wave noise term is positive leading to the variance of the number of photoelectrons larger than the shot-noise level. The inequality implies that the photoelectric counts do not appear random, but are correlated in the sense that if there is a photoelectron count at time t', there is a larger than average chance that another is produced nearby at a delayed time t''. In other words, we have certain characteristic bunching properties of the photoelectron counts, and this is why this phenomenon is called *photon bunching*. This leads to a photoelectron counting sequence that is more irregular than a Poisson process.

On the other hand, in the vacuum or a coherent state of the field

$$G^{(2)}(t', t'') = G^{(1)}(t')G^{(1)}(t'') , \tag{1.49}$$

i.e., the second-order correlation function factorizes and then the variance of the number of photoelectrons (1.47) is equal to the shot-noise level. The factorization of the correlation function reflects the counting distribution that is given by Poisson statistics. This also shows that even if the amplitude of the field fluctuates, not at all the photoelectron number will still fluctuate.

The properties (1.48) and (1.49) of the second-order correlation function are characteristic of classical fields and can be equally obtained without quantum description of the field amplitudes. However, there are certain states of the field, so-called quantum states with no classical analogues, for which

$$G^{(2)}(t', t'') < G^{(1)}(t')G^{(1)}(t'') . \tag{1.50}$$

The inequality implies that the wave noise of a quantum field is negative. This leads to the variance of the number of photoelectrons smaller than the shot-noise level. We say that in this case the photoelectric counts are anticorrelated in the sense that the appearance of a count at any particular time in the photoelectron count sequence makes it less, rather than more likely, that another will appear nearby. The phenomenon is called *photon antibunching* to contrast it with the photon bunching seen with a thermal field [9–11]. The counting statistics then become sub-Poissonian, and this is often regarded as a characteristic feature of a quantum state of the field.

The above analysis of the photocounting statistics show that the second-order correlation function provides a measure of correlations of the photoelectric counts. Only for those states of the field for which $G^{(2)}(t', t'')$ factorizes, the photoelectric counts become independent.

We can analyze the degree of second-order correlation by introducing the normalized second-order correlation function

$$g_{12}(t, t') = \frac{G^{(2)}(t, t')}{G^{(1)}(t)G^{(1)}(t')} . \tag{1.51}$$

This is the quantity commonly measured in photon correlation experiments and serves to distinguish between fields with different photon number distributions. If $g_{12}(t, t) > g_{12}(t, t')$ for $t' > t$, the photoelectric counts are said to display bunching, and $g_{12}(t, t) = g_{12}(t, t')$ means that the photoelectric counts are completely uncorrelated. If, on other hand, $g_{12}(t, t) < g_{12}(t, t')$, the photoelectric counts display antibunching. Because $g_{12}(t, t) < g_{12}(t, t')$ violates classical probability, antibunching is a quantum phenomenon without classical analogues in the sense that the corresponding (quantum) state of the field cannot be given a diagonal coherent state representation of the density operator ϱ of the field [12, 13]

$$\varrho = \int \mathrm{d}^2\alpha P(\alpha) \, |\alpha\rangle \, \langle\alpha| \, , \tag{1.52}$$

with $P(\alpha)$ in the form of a probability density.

In the following chapters, we will consider different types of the radiation field and determine correlation effects that can lead to a reduction of the quantum fluctuations in the field. Particular attention will be paid to quantum fields with no classical analogs which, as we shall demonstrate, are of particular interest in quantum atomic and molecular spectroscopy. We will show that there exist unusual quantum states for which $G^{(2)}(t, t)$ is proportional to the first power rather than to the second power of the light intensity, which makes $g_{12}(t, t)$ proportional to the reciprocal intensity.

1.4 Definition of the Power Spectrum

Consider now the other quantity of interest when examining radiation fields, the power spectrum or spectral density or spectral distribution, which provides information about the frequency composition of the investigated field. It is typical for a broadband radiation that the intensity of the field is different at different frequencies. Evidently, such a frequency variation of the field intensity would not be revealed by a measurement of the total number of photons in the field, but only after the detected photocurrent is first passed through a spectral analyzer, which provides a measure of the spectral density of the number of photons at various frequencies. The variations are attributed to the field fluctuations at different frequencies of the investigated field. Experiments which measure frequency distributions of the field intensity involve a spectrum analyzer, usually a frequency tunable linear filter located in front of the detector. The spectrum is measured by detecting the transmitted field intensity as a function of the frequency of the spectral analyzer. In this chapter, we will introduce only the general definitions of optical spectra of stationary and nonstationary radiation fields, deferring a more detailed discussion of their calculations to the next chapter, when we consider the spectra of radiation fields emitted by atomic systems.

1.4.1 Power Spectrum of a Stationary Field

In the terminology of the theory of stationary stochastic processes, the so-called Wiener−Khintchine theorem [7], the power spectrum of a stationary field detected at some point $\boldsymbol{r}$ is defined as the Fourier transform with respect to the time difference τ of the two-time normally ordered correlation function of the electric field amplitudes evaluated in the long-time limit

$$S(\omega) = \lim_{t\to\infty} \int_{-\infty}^{\infty} \mathrm{d}\tau \langle \hat{\boldsymbol{E}}^{(-)}(t) \cdot \hat{\boldsymbol{E}}^{(+)}(t+\tau) \rangle \mathrm{e}^{\mathrm{i}\omega\tau}, \tag{1.53}$$

where ω is a spectral frequency, and the electric field operators are evaluated at the position of the detector. The detector has been assumed to have infinite bandwidth and the detection time has been chosen large enough in order to allow for a good resolution of frequency components of the detected field.

It should be pointed out here that the Wiener–Khintchine power spectrum does not arise from an analysis of an experimental situation, and has no obvious relation to the spectrum associated with real experimental observations. Moreover, we note that the power spectrum is *not* the Fourier transform of the field amplitude $\hat{\boldsymbol{E}}(t)$ itself, as is often incorrectly assumed. In fact, in the case of a stationary field, the field amplitude is, in general, not square integrable, so that the Fourier transform of $\hat{\boldsymbol{E}}(t)$ may not even exist.

For a stationary field, the correlation function of the field amplitudes depends only on the time difference τ, not on the time origin t, and therefore we often write the power spectrum as

$$S(\omega) = \int_{-\infty}^{\infty} d\tau \langle \hat{\boldsymbol{E}}^{(-)}(0) \cdot \hat{\boldsymbol{E}}^{(+)}(\tau) \rangle e^{i\omega\tau} . \tag{1.54}$$

where $\hat{\boldsymbol{E}}^{(\pm)}(\tau) \equiv \hat{\boldsymbol{E}}^{(\pm)}(\boldsymbol{r}, \tau)$ and the field amplitude $\hat{\boldsymbol{E}}^{(-)}(0)$ refers to the initial value of the field as the stationary field has no origin in time.

The calculations of the spectrum have to be done for both positive and negative τ. However, we can split the integral appearing in (1.54) into two integrals and, after some rearrangement of the argument τ, we may write the spectrum as

$$\begin{aligned} S(\omega) = &\int_{0}^{\infty} d\tau \langle \hat{\boldsymbol{E}}^{(-)}(0) \cdot \hat{\boldsymbol{E}}^{(+)}(-\tau) \rangle e^{-i\omega\tau} \\ &+ \int_{0}^{\infty} d\tau \langle \hat{\boldsymbol{E}}^{(-)}(0) \cdot \hat{\boldsymbol{E}}^{(+)}(\tau) \rangle e^{i\omega\tau} . \end{aligned} \tag{1.55}$$

Since

$$\langle \hat{\boldsymbol{E}}^{(-)}(0) \cdot \hat{\boldsymbol{E}}^{(+)}(-\tau) \rangle = \langle \hat{\boldsymbol{E}}^{(-)}(-\tau) \cdot \hat{\boldsymbol{E}}^{(+)}(0) \rangle^{*} , \tag{1.56}$$

and making a transformation of the origin of time, we get

$$\langle \hat{\boldsymbol{E}}^{(-)}(0) \cdot \hat{\boldsymbol{E}}^{(+)}(-\tau) \rangle = \langle \hat{\boldsymbol{E}}^{(-)}(0) \cdot \hat{\boldsymbol{E}}^{(+)}(\tau) \rangle^{*} . \tag{1.57}$$

The correlation function is therefore known for both positive and negative values of τ, once it is known for $\tau \geq 0$ and for all values of t. Thus, we can confine the calculations of the power spectrum to only nonnegative values of τ and write the spectrum as the real part of the Fourier transform with respect to $\tau \geq 0$ of the two-time correlation function

$$S(\omega) = \lim_{t \to \infty} \int_{0}^{\infty} d\tau \, \langle \hat{\boldsymbol{E}}^{(-)}(t) \cdot \hat{\boldsymbol{E}}^{(+)}(t + \tau) \rangle e^{i\omega\tau} + \text{c.c.} , \tag{1.58}$$

where 'cc' stands for the complex conjugate of the first term.

We next introduce the oscillatory factors in (1.58) to make the field amplitudes relatively slowly varying functions of time, and write the spectrum as

$$S(\omega) = 2\text{Re} \int_{0}^{\infty} d\tau \lim_{t \to \infty} \langle \hat{\tilde{\boldsymbol{E}}}^{(-)}(t) \cdot \hat{\tilde{\boldsymbol{E}}}^{(+)}(t + \tau) \rangle e^{i(\omega - \omega_0)\tau} , \tag{1.59}$$

in which 'Re' denotes the real part of the integral, ω_0 is some central frequency of the field, and

$$\hat{\tilde{\boldsymbol{E}}}^{(\pm)}(t) = \hat{\boldsymbol{E}}^{(\pm)}(t)\, \mathrm{e}^{\pm \mathrm{i}\omega_0 t} \tag{1.60}$$

are the slowly varying amplitudes which change slowly compared with variations arising from the periodic terms $\exp(\pm \mathrm{i}\omega_0 t)$.

Equation (1.59) is the final expression for the power spectrum which may be applied to the general case of an arbitrary stationary field irrespective of any particular state the field and for any type of the source of the field. The spectrum is evaluated as the Fourier transform of the correlation function of the slowly varying field amplitudes. As we shall see later, the power spectrum provides insights not only into the fluctuations of the radiation field, but also into radiation sources which contribute to the fluctuations. According to (1.31), the power spectrum may be written directly in terms of the correlation function of certain time-independent source variables that produce the radiation field being analyzed. Hence, the spectral properties of the radiated field can be understood from the properties of certain spectral functions of the source variables.

1.4.2 Power Spectrum of a Nonstationary Field

The definition of the power spectrum, introduced above, is based solely on theoretical considerations of the theory of stationary stochastic processes and does not include the method of the detection of the field. Therefore, a question arises whether $S(\omega)$ is physically meaningful quantity in the sense of corresponding to what is actually measured [14]. One can argue that the power spectrum (1.59) is associated with real experimental observations that it corresponds to what is measured by a detector of infinite bandwidth and for a long measurement time. These two properties of the detector ensure the observation of all spectral features of the measured field.

In a laboratory, the power spectra of the electromagnetic field are usually measured via some combination of a spectrometer with a photodetector located in the far-field zone of a radiating system. The spectrometer can be located between the radiator and the detector, as illustrated in Fig. 1.1a, or the radiator can be located inside the spectrometer, as in Fig. 1.1b. The spectrometer serves as a linear, but not necessarily time stationary, frequency filter of the field which is detected. The spectrum is then obtained as an appropriately normalized record of the detected light signal as a function of the transmission frequency of the spectrometer. However, spectrometers have finite rather than infinite bandwidths, the detection of a field usually takes finite time, and the detected fields are not always stationary during the detection process. A radiation field emitted by a system driven by a pulse shape field, for example, exists only for a certain amount of time, and such field is evidently time dependent. A time variation in the amplitude of a continuous wave (cw) driving field also leads to time variations of the emitted field. Therefore, in these cases the detected fields are not strictly stationary and the correlation functions of the field amplitudes are

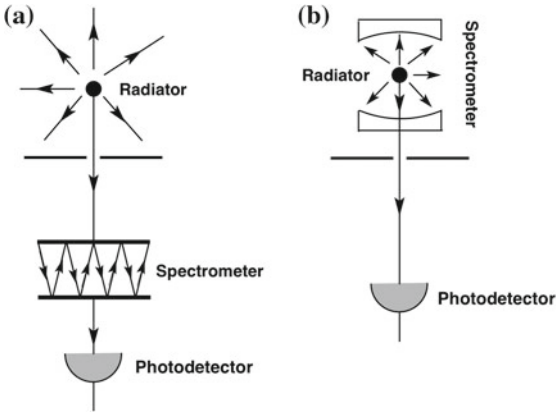

Fig. 1.1 Illustration of apparatus for measuring the power spectrum, consisting of a radiator located **a** outside or **b** inside of a spectrometer, after which is a photodetector

then explicit functions of time, indicating that the formalism used in the derivation of the stationary power spectrum has to be modified.

It is possible, in principle, to proceed with the general definition (1.59) of the power spectrum, allowing the spectrum to be time dependent through a finite Fourier integral [15]. Thus, we might define

$$S(t,\omega) = C\int_0^t \mathrm{d}\tau\langle\hat{\boldsymbol{E}}^{(-)}(t)\cdot\hat{\boldsymbol{E}}^{(+)}(t+\tau)\rangle \mathrm{e}^{\mathrm{i}\omega\tau} + \text{c.c.}\,, \tag{1.61}$$

where C is some constant and t is actual observation time. We might interpret this spectrum as the rate of production of photons of frequency ω at time t. However, despite this interpretation, $S(t,\omega)$ is not a physically meaningful quantity in the sense of being accessible to direct measurement. This spectrum is not consistent with the frequency-time uncertainty relation. In order to resolve spectral features narrower than a given resolution $\delta\omega$ of a spectrometer, a detector must sample over a time interval at least of the order of $1/\delta\omega$. In other words, during the time that $S(t,\omega)$ is changing with respect to its first argument t, the time scale for the variation is of the same order as or less than the reciprocal bandwidth of the spectrometer. A spectrum which changes in times short compared with its reciprocal bandwidth is not really physically meaningful [14, 15].

It was shown by Eberly and Wódkiewicz [16] that this problem may be avoided by introducing a response or filter or transmission function of a spectrometer, and the account for bandwidth effects of the interferometer can then be readily included into the definition of the power spectrum. Suppose that $W(t)$ is the response function of the spectrometer. Then, the effective electric field registered by the detector is a filtered version of the incident field

$$\hat{\boldsymbol{E}}^{(+)}_{\text{eff}}(t) = \int_0^t W(t-t')\hat{\boldsymbol{E}}^{(+)}\left(t'\right)\mathrm{d}t'\,, \tag{1.62}$$

where $\hat{\boldsymbol{E}}^{(+)}_{\text{eff}}(t)$ is the positive frequency part of the electric field transmitted by the spectrometer and $\hat{\boldsymbol{E}}^{(+)}(t)$ is the positive frequency part of the electric field entering the spectrometer directly from a source. The input and output fields of the spectrometer are linearly related and causality is guaranteed by the time order ($t \geq t'$) explicitly incorporated into the integral in (1.62).

Using this model, Eberly and Wódkiewicz introduced the definition of a time-dependent spectrum, dubbed the "physical spectrum" of the detected field, giving the spectrum in terms of a double integral of the normally ordered two-time correlation function of the electric field at the detector

$$\begin{aligned} S(t,\omega) &= \int_0^t \mathrm{d}t_1 \int_0^t \mathrm{d}t_2 \langle \hat{\boldsymbol{E}}^{(-)}_{\text{eff}}(t_1) \cdot \hat{\boldsymbol{E}}^{(+)}_{\text{eff}}(t_2) \rangle \\ &= \int_0^t \mathrm{d}t_1 \int_0^t \mathrm{d}t_2 W^*(t-t_1) W(t-t_2) \\ &\quad \times \langle \hat{\boldsymbol{E}}^{(-)}(t_1) \cdot \hat{\boldsymbol{E}}^{(+)}(t_2) \rangle \,. \end{aligned} \tag{1.63}$$

The spectrum is observed at time t, thereby becoming time dependent without contradicting the frequency-time uncertainty relation. Equation (1.63) relates the spectrum to the time-dependent correlation function of the field operators at the detector which, on the other hand, can be evaluated in terms of the response function $W(t)$ and the time-dependent correlation function of the incident field operators.

The response function $W(t)$ is characteristic for the measurement device which is used to measure the frequency spectrum. We can also interpret the function $W(t)$ as representing the bandwidth limitation inherent in any measurement process. The function $W(t)$ can have different forms, and the relation (1.62) shows that the best filter function would be that represented by a delta function, i.e., $W(t-t') = \delta(t-t')$. In this case, the response of the spectrometer would be immediate and then the detector would register the entire field being analyzed. However, filter functions of real spectrometers are not in form of the delta function. For example, the response function of a Fabry−Perot interferometer is the Airy function whose form is determined by the physical parameters of the interferometer [17]. This function describes the filtering action of the Fabry−Perot interferometer, and in the case of a one-sided plane-mirror interferometer, possesses one perfectly reflecting mirror and one partially transmitting lossless mirror, is given by

$$A(\theta_k, L) = \frac{\left(1-R^2\right)}{(1-R)^2 + 4R\sin^2(kL\cos\theta_k)}\,, \tag{1.64}$$

where $k = \omega/c$, R denotes the (real) reflectivity of the partially transmitting mirror, L is the separation between the mirrors, and θ_k is the angle between the direction of the kth mode and the cavity axis.

A number of interesting conclusions follow from this function. We first observe that the Airy function is sensitive to the separation of the mirrors. Thus, by slightly

changing L, one would change the transmission frequency of the spectrometer, scanning over whole range of frequencies of a measured field. Next, we observe that the Airy function displays a series of sharp peaks representing the cavity modes which propagate in directions θ_k such that $\sin(kL\cos\theta_k) = 0$. The linewidth of the peaks depends on R and becomes very narrow when R is close to one. If $L = \lambda/2$, where λ is the resonance wavelength, the Airy function will exhibit a sharp peak centered at $\cos\theta_k = 1$. This means that the transmission modes of the interferometer are contained only in a small solid angle around the cavity axis. In this idealized case, we can model $W(t)$ as a simple Lorentzian that peaks at the interferometer resonance (transmission) frequency and possesses finite bandwidth, so that we can write

$$W(t - t_0) = \theta(t - t_0)\sqrt{2\Gamma}\exp\left[-(\Gamma + \mathrm{i}\omega)(t - t_0)\right], \tag{1.65}$$

where Γ is the half-width at half-maximum of the transmission peak of the interferometer, ω is its peak transmission frequency, and $\theta(t - t_0)$ is the unit step function which vanishes for $t < t_0$ and is unity for $t \geq t_0$, i.e., the spectrometer is turned on at $t = t_0$. The Lorentzian form of the response function effectively means that only the field detected over a time interval of order of Γ^{-1} prior to the time t will contribute significantly to the spectrum at the time t.

Finally, we combine the result for the response function given by (1.65) with the definition (1.63) of the time-dependent spectrum and obtain the following result for the physical spectrum

$$\begin{aligned} S(t,\omega) = 2\Gamma \int_0^t \mathrm{d}t_1 \int_0^t \mathrm{d}t_2 \mathrm{e}^{-(\Gamma - \mathrm{i}\omega)(t-t_1)}\mathrm{e}^{-(\Gamma+\mathrm{i}\omega)(t-t_2)} \\ \times \langle \hat{\boldsymbol{E}}^{(-)}(t_1)\cdot\hat{\boldsymbol{E}}^{(+)}(t_2)\rangle . \end{aligned} \tag{1.66}$$

The expression for the spectrum is obviously not the Fourier transform of the incident field correlation function. This spectrum is a function of time and has been defined not only as a function of the field parameters, but also as a function of two variables of the measuring apparatus, the frequency and bandwidth of the spectrometer. Consequently, the physical spectrum correctly incorporates the role of the spectrometer in the detection of the field, the possible effects of a finite observation time, and arbitrary initial conditions for the detected field. As previously mentioned, this spectrum has been called the physical spectrum, and we now see the justification as it does represent the outcome of a realizable physical experiment. This definition is also consistent with the quantum theory of measurement, which assumes that there is no unique boundary between the physical system under the observation and the measuring apparatus.

At this time we might very well ask whether the physical spectrum, which takes into account bandwidth of the spectrometer, is the most useful way of detecting available information about the investigated field. One could answer "no", for this fact that the physical spectrum takes into account a property of both the measured field and bandwidth of the spectrometer which in turn affects widths of the observed

spectral lines. The spectral widths provide important information about fluctuations of the detected field. Therefore, alternative definitions of a spectral distribution of the radiation field have been proposed which depend solely on the field properties. The spectrum so defined is more convenient for extracting information about the fluctuations of the radiation field intensity which, on the other hand, yield information about internal properties of radiating systems.

The spectral distribution of a nonstationary field may be defined in terms of an average intensity at various frequencies of the field measured in an element of solid angle $\mathrm{d}\Omega_{\boldsymbol{r}}$ over a finite time interval T as

$$S(\boldsymbol{r}, T, \omega)\mathrm{d}\Omega_{\boldsymbol{r}} = \langle \hat{\boldsymbol{E}}^{(-)}(\omega, T) \cdot \hat{\boldsymbol{E}}^{(+)}(\omega, T)\rangle \mathrm{d}\Omega_{\boldsymbol{r}}\,, \tag{1.67}$$

where $\hat{\boldsymbol{E}}^{(\pm)}(\omega, T)$ are the finite-time (truncated) Fourier transforms of the electric field amplitudes defined by

$$\hat{\boldsymbol{E}}^{(\pm)}(\omega, T) = \int_0^T \mathrm{d}t \hat{\boldsymbol{E}}^{(\pm)}(t)\, \mathrm{e}^{\pm \mathrm{i}\omega t}\,, \tag{1.68}$$

and ω is a positive (real) frequency. The Fourier transforms are interpreted as the ω components of the positive and negative frequency parts of the field at the detector. The time interval T should be taken long enough to allow for a good resolution of the spectral frequency components.

Substituting (1.68) into (1.67), we find that the spectral distribution per unit solid angle can be expressed in terms of a double finite-time Fourier integral

$$S(\boldsymbol{r}, T, \omega) = \int_0^T \mathrm{d}t' \int_0^T \mathrm{d}t'' \langle \hat{\boldsymbol{E}}^{(-)}\left(t'\right) \cdot \hat{\boldsymbol{E}}^{(+)}\left(t''\right)\rangle \mathrm{e}^{\mathrm{i}\omega(t'-t'')}\,, \tag{1.69}$$

which is basically the square of the finite-time Fourier transform of $\hat{\boldsymbol{E}}^{(\pm)}(t)$.

The spectrum (1.69) has the necessary property of being positive, but this expression diverges in the stationary limit and becomes infinite when the length T of the time interval goes to infinity. However, one can easily show that in the limit of long detection times ($T \to \infty$), the spectrum grows linearly with T. Therefore, to avoid the divergence, we can define the spectral distribution normalized over the length T as

$$\begin{aligned} S(\boldsymbol{r}, \omega) = \lim_{T\to\infty} \frac{1}{T} \int_0^T \mathrm{d}t' \int_0^T \mathrm{d}t'' \langle \hat{\boldsymbol{E}}^{(-)}\left(t'\right) \cdot \hat{\boldsymbol{E}}^{(+)}\left(t''\right)\rangle \\ \times \exp\left[\mathrm{i}\omega(t'-t'')\right]\,. \end{aligned} \tag{1.70}$$

This formula for the spectral distribution excludes most of the effects of the measuring apparatus, but it includes a variable which is available to experiments: a finite detection time interval T. Thus, the spectrum incorporates the possible effects of the finite time detection. Although the spectrum (1.70) does not completely incorporate

the measuring apparatus, it reveals many similarities with the physical spectrum of Eberly and Wódkiewicz. In reality, it can be treated as a special case of the physical spectrum in the limit of a very narrow bandwidth spectrometer, i.e., $\Gamma \to 0$. In concluding this section, we must point out that the definition (1.70) enjoys considerable popularity in the study of the spectral distribution of time-dependent radiation fields as it satisfies the requirement of being dependent on the field properties only. Further, in the limit of $T \to \infty$, it reduces to the usual Wiener−Khintchine definition of the stationary power spectrum introduced in Sect. 1.4.1.

1.5 Spectrum of the Intensity Fluctuations

In the preceding section, we have introduced concepts of the power spectrum of the radiation field defined in terms of the Fourier transform of the first-order correlation function of the complex electric field amplitudes. We can carry these concepts to examine spectral properties of the intensity fluctuations of the field, which involve the second-order correlation function of the electric field amplitudes. This is motivated by the fact that in a broadband radiation not only the intensity but also the intensity fluctuations can be different at different frequencies and, in addition, the fluctuations may carry information about noise correlations in the field. Evidently, such frequency-dependent fluctuations and correlations would not be revealed by a direct detection of the photon number fluctuations, as discussed in Sect. 1.3, but only after the detected field is first passed through a frequency filter, which provides a measure of the spectral density of the photon number fluctuations at various frequencies ω. Although the spectrum of the intensity fluctuations can be defined for stationary as well as for time-dependent fields, we shall be concerned in this section with stationary fields only. The discussion of the spectrum will be kept very general in order to make it applicable to any physical system. It will enable us to understand more clearly the basis for and the limitations of the noise contributions to the measured spectra. This study will also lead us to the backgrounds of another phenomenon, the so-called spectrum of squeezing, which will be discussed in more details in Sect. 2.3.

Consider a radiation field with temporal fluctuations that are stationary in time. The spectrum of the stationary intensity fluctuations or the noise spectrum, can be theoretically analyzed by calculating the Fourier transform with respect to the time difference τ of the time ordered correlation function of the stationary intensity fluctuations

$$F(\omega) = \lim_{t\to\infty} \int_{-\infty}^{+\infty} d\tau \langle \mathcal{T} \Delta\hat{I}(t)\, \Delta\hat{I}(t+\tau)\rangle e^{i\omega\tau}, \tag{1.71}$$

where brackets indicate a quantum expectation value, $\Delta\hat{I}(t) = \hat{I}(t) - \langle\hat{I}(t)\rangle$ is the deviation of the radiation intensity operator from the mean value, and the symbol $\mathcal{T}$ indicates time ordering of the field operators.

Before we explain the role of the time ordering in the correlation function appearing in (1.71), let us first examine the symmetric properties of the correlation function which we could use to simplify the calculations of the spectrum. The correlation function appearing in (1.71) has to be calculated for both negative and positive values of τ. However, we can confine the calculations of the correlation function to only nonnegative values of τ by using a procedure similar to that employed previously for the calculations of the correlation function involved in the power spectrum.

As before, in the calculations of the power spectrum, we split the integral over τ into two parts, and obtain

$$F(\omega) = \int_{-\infty}^{0} \mathrm{d}\tau F(\tau)\mathrm{e}^{\mathrm{i}\omega\tau} + \int_{0}^{+\infty} \mathrm{d}\tau F(\tau)\mathrm{e}^{\mathrm{i}\omega\tau}\,, \tag{1.72}$$

where we have introduced the following notation for the time-dependent correlation function

$$F(\tau) = \lim_{t\to\infty} \langle \mathcal{T}\Delta\hat{I}(t)\,\Delta\hat{I}(t+\tau)\rangle\,. \tag{1.73}$$

The first part corresponds to negative values of τ, whereas the second part corresponds to positive values of τ. If in the first integral of (1.72) we replace the variable τ by $-\tau$, the spectrum becomes

$$F(\omega) = \int_{0}^{+\infty} \mathrm{d}\tau F(-\tau)\mathrm{e}^{-\mathrm{i}\omega\tau} + \int_{0}^{+\infty} \mathrm{d}\tau F(\tau)\mathrm{e}^{\mathrm{i}\omega\tau}\,. \tag{1.74}$$

Fortunately, because the correlation function of the stationary intensity fluctuations is independent of t, the correlation function is symmetric with respect to positive and negative τ, so that

$$\begin{aligned} F(-\tau) &= \lim_{t\to\infty} \langle \mathcal{T}\Delta\hat{I}(t)\,\Delta\hat{I}(t-\tau)\rangle = \lim_{t\to\infty} \langle \mathcal{T}\Delta\hat{I}(t-\tau)\,\Delta\hat{I}(t)\rangle \\ &= \lim_{t\to\infty} \langle \mathcal{T}\Delta\hat{I}(t)\,\Delta\hat{I}(t+\tau)\rangle = F(\tau)\,. \end{aligned} \tag{1.75}$$

Hence, in the long-time limit the correlation function is symmetric with respect of τ, and therefore, it is sufficient to evaluate only the correlation function for nonnegative values of τ.

Employing the symmetry property (1.75) to the first term in (1.74), we can express the spectrum of the stationary intensity fluctuations in terms of only the positive time component ($\tau \geq 0$), and obtain

$$F(\omega) = 2\int_{0}^{\infty} \mathrm{d}\tau F(\tau)\cos(\omega\tau)\,. \tag{1.76}$$

The spectrum is the cosine transform of the time ordered correlation function of the stationary intensity fluctuations. Because of the symmetry property (1.75), it follows immediately from (1.76) that the spectrum $F(\omega)$ is always real, positive, and is strictly symmetric about $\omega = 0$, i.e. $F(\omega) = F(-\omega)$. This indicates that the spectrum may be used to determine correlations between photons of frequencies symmetrically located about $\omega = 0$. This property reflects the process of simultaneous creation of pairs of photons at different frequencies, and provides information about two-photon correlations in the field.

Note that the spectrum (1.76) involves the time ordered correlation function in which the operator product is not in the normal order. Consequently, one might argue that the correlation function $F(\tau)$ does not correspond to any measurable correlation function in a photoelectric detection, in which the normally ordered correlation functions of the complex field amplitudes are obtained in a measurement. We can readily relate the correlation function (1.73) to the measurable quantity: the two-time correlation function with the operators written in normal order and in time order. To establish this relation, we start by writing the correlation function $F(\tau)$ in terms of the positive and negative frequency components of the field operators

$$\begin{aligned} F(\tau) &= \lim_{t\to\infty} \langle \mathcal{T}\, \Delta\hat{I}\,(t)\, \Delta\hat{I}\,(t+\tau)\rangle \\ &= (2\varepsilon_0 c\lambda)^2 \lim_{t\to\infty} \Big[\langle \mathcal{T}\hat{\boldsymbol{E}}^{(-)}(t)\,\hat{\boldsymbol{E}}^{(+)}(t) : \hat{\boldsymbol{E}}^{(-)}(t+\tau)\,\hat{\boldsymbol{E}}^{(+)}(t+\tau)\rangle \\ &\quad - \langle \hat{\boldsymbol{E}}^{(-)}(t)\cdot\hat{\boldsymbol{E}}^{(+)}(t)\rangle \langle \hat{\boldsymbol{E}}^{(-)}(t+\tau)\cdot\hat{\boldsymbol{E}}^{(+)}(t+\tau)\rangle \Big] . \end{aligned} \tag{1.77}$$

If we make use of the commutation relation (1.13) to put the operator product $\hat{\boldsymbol{E}}^{(+)}(t)\,\hat{\boldsymbol{E}}^{(-)}(t+\tau)$ in normal order, together with the time ordering which orders the operators among themselves without disturbing the normal order, such that

$$\begin{aligned} \mathcal{T}\hat{\boldsymbol{E}}^{(-)}(t_1)\,\hat{\boldsymbol{E}}^{(-)}(t_2) &= \hat{\boldsymbol{E}}^{(-)}(t_2)\,\hat{\boldsymbol{E}}^{(-)}(t_1) , \qquad t_1 < t_2 , \\ \mathcal{T}\hat{\boldsymbol{E}}^{(+)}(t_1)\,\hat{\boldsymbol{E}}^{(+)}(t_2) &= \hat{\boldsymbol{E}}^{(+)}(t_2)\,\hat{\boldsymbol{E}}^{(+)}(t_1) , \qquad t_1 < t_2 , \end{aligned} \tag{1.78}$$

we obtain the function $F(\tau)$ in terms of the normally ordered second-order correlation function as

$$\begin{aligned} F(\tau) &= (2\varepsilon_0 c\lambda)^2 \lim_{t\to\infty} \langle \hat{\boldsymbol{E}}^{(-)}(t)\,\hat{\boldsymbol{E}}^{(-)}(t+\tau) : \hat{\boldsymbol{E}}^{(+)}(t+\tau)\,\hat{\boldsymbol{E}}^{(+)}(t)\rangle \\ &\quad + \lim_{t\to\infty} \Big[\langle \hat{I}(t)\rangle \delta(\tau) - \langle \hat{I}(t)\rangle \langle \hat{I}(t+\tau)\rangle \Big] . \end{aligned} \tag{1.79}$$

This equation can be written compactly in the form

$$F(\tau) = \lim_{t\to\infty} \Big[\langle \hat{I}(t)\rangle \delta(\tau) + \langle \mathcal{T} : \Delta\hat{I}\,(t)\, \Delta\hat{I}\,(t+\tau) :\rangle \Big] , \tag{1.80}$$

where the pair of colons denotes normal ordering of the operators. The first term in (1.80) represents the random contribution to the correlation function due to uncorrelated events, whereas the second is attributable to correlated fluctuations. Thus, our problem of computing the correlation function $F(\tau)$ reduces to that of computing the normally ordered correlation function, which is a directly measurable quantity. An important feature of this correlation function is the reflection of correlated fluctuations in the measured field.

With the help of (1.80), we can thus express the noise spectrum in terms of the normally ordered correlation function of the intensity fluctuations

$$F(\omega) = \lim_{t\to\infty} \langle \hat{I}(t) \rangle + 2 \lim_{t\to\infty} \int_0^\infty \mathrm{d}\tau \langle \mathcal{T} : \Delta\hat{I}(t)\, \Delta\hat{I}(t+\tau) : \rangle \cos(\omega\tau) \,. \tag{1.81}$$

This equation gives an alternative way of calculating the noise spectrum. It is composed of two terms and involves the measurable correlation function of the intensity fluctuations. The first term on the right-hand side of (1.81) is the shot-noise spectral density, equal to the average intensity of the field incident on the detector. It is white noise, that is, constant over all frequencies. Of much greater interest is the second term. It is the spectral density of the intensity fluctuations and provides a measure of the contribution of the field fluctuations to the noise spectrum relative to the shot-noise fluctuations. This term is always real, but is not necessarily positive. For an ideal coherent field, the second term is zero and only the frequency independent shot noise is present in the noise spectrum. For a classical field, this term is positive at all frequencies, which may be regarded as a reflection of the fact that a classical field of constant intensity yields a constant frequency-independent noise density, and any modulation of the classical intensity can only increase the noise density. Later, we will see a case of a nonclassical (squeezed) field for which this term can be negative at some frequencies, so that the noise density is suppressed below the shot-noise level at those frequencies. This indicates that a nonclassical field fluctuates less than the coherent field, and this feature can be clearly reflected in the noise spectrum.

1.5.1 Contribution of the Background Field

The definitions of the field intensity and the spectral distributions, introduced in Sect. 1.4, are quite general in terms of the electric field at a photodetector, holding equally well the contribution of all signal (source) fields as well as the background field. What then is the distinction between the contribution of the background field and the signal fields, and how we can eliminate the effect of the background field on a measurement of the signal fields.

In the typical optical experiments, we can distinguish three different fields contributing to the total electric field at the detector

$$\hat{\boldsymbol{E}}^{(\pm)}(t) = \hat{\boldsymbol{E}}_e^{(\pm)}(t) + \hat{\boldsymbol{E}}_v^{(\pm)}(t) + \hat{\boldsymbol{E}}_s^{(\pm)}(t) \,. \tag{1.82}$$

The first term in (1.82) is the electric field operator associated with an applied or driving field, which is used to excite a radiating system. This field is often approximated as a classical field, and is the net driving field transmitted through the system. It is a good approximation to the field characterizing a laser beam, and therefore corresponds closely to experimental situations in which source systems are excited by a laser beam. The second term, is the electric field operator associated with a background field contribution, which is responsible for the shot noise at the detector. The final term, is the electric field operator of the signal field produced by the source.

We shall illustrate the role of the different fields in a measurement of correlation functions by analyzing the one-time correlation function of the total electric field registered by a detector. A calculation of the correlation function is accomplished by substituting (1.82) for the total electric field operators in the expression (1.42) and taking an expectation value. Then, the correlation function of the total field splits into correlation functions

$$\begin{aligned}
&\langle \hat{\boldsymbol{E}}^{(-)}(t) \cdot \hat{\boldsymbol{E}}^{(+)}(t) \rangle = \langle \hat{\boldsymbol{E}}_e^{(-)}(t) \cdot \hat{\boldsymbol{E}}_e^{(+)}(t) \rangle + \langle \hat{\boldsymbol{E}}_e^{(-)}(t) \cdot \hat{\boldsymbol{E}}_v^{(+)}(t) \rangle \\
&+ \langle \hat{\boldsymbol{E}}_e^{(-)}(t) \cdot \hat{\boldsymbol{E}}_s^{(+)}(t) \rangle + \langle \hat{\boldsymbol{E}}_v^{(-)}(t) \cdot \hat{\boldsymbol{E}}_e^{(+)}(t) \rangle + \langle \hat{\boldsymbol{E}}_s^{(-)}(t) \cdot \hat{\boldsymbol{E}}_e^{(+)}(t) \rangle \\
&+ \langle \hat{\boldsymbol{E}}_v^{(-)}(t) \cdot \hat{\boldsymbol{E}}_s^{(+)}(t) \rangle + \langle \hat{\boldsymbol{E}}_s^{(-)}(t) \cdot \hat{\boldsymbol{E}}_v^{(+)}(t) \rangle + \langle \hat{\boldsymbol{E}}_v^{(-)}(t) \cdot \hat{\boldsymbol{E}}_v^{(+)}(t) \rangle \\
&+ \langle \hat{\boldsymbol{E}}_s^{(-)}(t) \cdot \hat{\boldsymbol{E}}_s^{(+)}(t) \rangle \,,
\end{aligned} \tag{1.83}$$

where all the products of the field operators are in normal order. It is clear from this equation that the correlation function of the field registered by the detector depends on the correlation functions for both the signal and the background fields and for the driving field together with possible interference terms involving those three fields. The following question then arises: under what conditions can the first-order correlation function for the total field be equated to the normally ordered correlation function for the signal field alone?

In practice it is frequently the case that radiating systems are excited by external fields, which can be in an arbitrary single or multimode state $|\{\alpha\}\rangle$. Since $|\{\alpha\}\rangle$ is the right-hand eigenstate of the positive-frequency field operator and $\langle\{\alpha\}|$ is the left-hand eigenstate of the negative frequency field operator of the driving field, we write

$$\hat{\boldsymbol{E}}_e^{(+)}(t)\,|\{\alpha\}\rangle = \boldsymbol{\mathcal{E}}_e(t)\,|\{\alpha\}\rangle \,, \quad \langle\{\alpha\}|\,\hat{\boldsymbol{E}}_e^{(-)}(t) = \boldsymbol{\mathcal{E}}_e^*(t)\,\langle\{\alpha\}| \,, \tag{1.84}$$

where $\mathcal{E}_e(t)$ is a complex amplitude of the driving field. Then, the driving field operators in (1.83) can be replaced by their right- and left-hand eigenvalues when the correlation functions are evaluated.

However, if we choose the position $\boldsymbol{r}$ of a detector such that it lies well outside the path of the driving beam, we obtain

$$\hat{\boldsymbol{E}}_e^{(+)}(t) \equiv \hat{\boldsymbol{E}}_e^{(+)}(\boldsymbol{r}, t)\,|\{d\}\rangle = 0\,, \tag{1.85}$$

where $|\{d\}\rangle$ is a multimode state of the detection which does not include the state of the driving field $|\{\alpha\}\rangle$. As a result, the amplitudes of the driving fields are zero at the detector and ultimately this enables us to eliminate from (1.83) the correlation function for the driving field and interference terms involving the driving field operators.

In an analogous fashion, we can demonstrate that the choice of the normal ordering allows us to eliminate the contribution of the background field operators to the expression for the correlation function of the total electric field. However, a further condition is required that the background field is in a vacuum state. Hence, if the background field modes are in the vacuum states, for which

$$\hat{\boldsymbol{E}}_v^{(+)}(t)\,|\{0\}\rangle = 0, \qquad \langle\{0\}|\,\hat{\boldsymbol{E}}_v^{(-)}(t) = 0\,, \tag{1.86}$$

then evidently the amplitudes of the vacuum field are zero at the detector and we can eliminate from (1.83) the correlation functions involving the vacuum field operators. It follows that all correlation functions that involve the operators of the driving and the vacuum fields vanish in (1.83) except the correlation function for the signal field.

Consequently, we can conclude that the problem of calculating the normally ordered correlation function of the total electric field at a suitably located detector simplifies to the calculation of the normally ordered correlation function of the signal field, so that

$$\langle \hat{\boldsymbol{E}}^{(-)}(t) \cdot \hat{\boldsymbol{E}}^{(+)}(t) \rangle = \langle \hat{\boldsymbol{E}}_s^{(-)}(t) \cdot \hat{\boldsymbol{E}}_s^{(+)}(t) \rangle\,. \tag{1.87}$$

Although we have illustrated the role of the different fields on the simplest example of the one-time correlation function, we must emphasize that similar results hold for normally ordered multi-time correlation functions, as found in spectral measurements. It does not matter what time ordering is chosen in the normally ordered multi-time correlation functions since all the $\hat{\boldsymbol{E}}^{(-)}(t_1)$ commute with each other independent of the time argument, and all the $\hat{\boldsymbol{E}}^{(+)}(t_2)$ commute with each other. Therefore, we may state that a measured power spectrum is not affected by the vacuum background modes and it follows directly from the Fourier transform of the normally ordered two-time correlation function of the signal field.

The considerations presented in this section show the significance of the normal ordering in the correlation functions which are determined in photodetection measurements. The important property of the normal ordering is that the vacuum field expectation values of the products of the field operators are zero. Thus, the vacuum field gives no contribution to the quantities characterized by those correlation functions. A different situation occurs for other orderings, for example, antinormally ordered products of the field operators. These are not physically measured by normal photodetectors, but are connected with counting devices called quan-

tum counters [18]. These devices, although not generally encountered in laboratory, could detect the field by means of stimulated emission rather than by absorption. An obvious concern, is how to relate these functions to measured functions in normal photodetection. Fortunately, with the help of the commutation relation (1.13), we may always express any correlation function in terms of the normally ordered correlation functions obtained from a photodetection measurement. A good example of this general rule is the correlation function of the intensity fluctuations, discussed in the preceding section, which we split with the help of the commutator (1.13) into two parts of which one was the normally ordered correlation function and the other part was the vacuum field contribution. Strictly speaking, the commutator (1.13) gives the vacuum field contribution which distinguishes any correlation function from the normally ordered correlation function.

1.6 Radiation Intensity

We turn now to the consideration of the average value of the radiation intensity of the electromagnetic field measured by a photoelectric detector located in the radiation zone of an atomic source driven by an external field, as illustrated in Fig. 1.2. The source atoms are contained in a volume with linear dimensions which may be large or small compared with the average wavelength of the emitted radiation field. In Sect. 1.2, we demonstrated how the positive-and negative frequency components of electric field operator are related to the atomic operators, and it would be useful to learn about various contributions of the atomic variables to properties of the emitted field. Therefore, we begin with determining the relation between the radiation intensity and the atomic quantities. Next, on the basis that the source field can be separated from the background field and that the later field does not contribute to any measurable quantity, we find that the intensity can be expressed entirely in terms of the measurable atomic quantities, such as coherences and populations of the source atoms. In the course of the calculations, we shall observe that these quantities carry information about quantum fluctuations of the atomic dipole moments, which affect

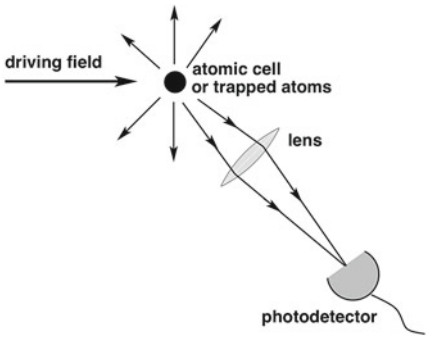

Fig. 1.2 Illustration of a detection scheme to measure the radiation intensity of the electromagnetic field emitted from a group of atoms driven by an external field

the dynamics of the atomic system and are clearly reflected in properties of the emitted field.

The radiation intensity[3] measured by a photoelectric detector located at a point $\boldsymbol{r}$ can be obtained by calculating the average value of the instantaneous intensity of the EM field emitted into an element of solid angle $d\Omega_r = A/r^2$ around the direction $\boldsymbol{r}$ at time t. According to (1.42), the average intensity is proportional to the normally ordered one-time correlation function of the positive and negative frequency components of the electric field at the detector

$$\langle \hat{I}(\boldsymbol{r}, t)\rangle \mathrm{d}\Omega_{\boldsymbol{r}} = \frac{2\varepsilon_0 c r^2}{\hbar\omega_0} \langle \hat{\boldsymbol{E}}^{(-)}(\boldsymbol{r}, t) \cdot \hat{\boldsymbol{E}}^{(+)}(\boldsymbol{r}, t)\rangle \mathrm{d}\Omega_{\boldsymbol{r}}\,, \tag{1.88}$$

where the brackets indicate a quantum expectation value taken over an initial state of the entire system $|\{\alpha\}\rangle = |\{0\}\rangle \otimes |a\rangle$, which is a product of the field vacuum state and an arbitrary state of the source.

Equation (1.88) is perfectly general and gives the average intensity of the electromagnetic field detected at any space-time point $(\boldsymbol{r}, t)$, including the near-zone of the source. Integrating (1.88) over all directions, specified by the solid angles $\mathrm{d}\Omega_{\boldsymbol{r}}$, we obtain the total radiation intensity per unit time

$$\langle \hat{I}(t)\rangle = \int \mathrm{d}\Omega_{\boldsymbol{r}} \langle \hat{I}(\boldsymbol{r}, t)\rangle\,. \tag{1.89}$$

The main interest here is to find the average intensity of the field emitted by an atomic system in the direction $\boldsymbol{r}$ and detected in the radiation (far-field) zone of the source atoms. In this far-field approximation, and with the help of (1.31), the average intensity per unit solid angle can be expressed in terms of expectation values of appropriate atomic operators as

$$\begin{aligned}\langle \hat{I}(\boldsymbol{r}, t)\rangle = \frac{2\varepsilon_0 c r^2}{\hbar\omega_0} \sum_{n,m=1}^{N} \sum_{i>j} \sum_{k>l} \boldsymbol{\Psi}^*_{ij}(\boldsymbol{r} - \boldsymbol{R}_n) \cdot \boldsymbol{\Psi}_{lk}(\boldsymbol{r} - \boldsymbol{R}_m) \\ \times \langle \hat{\Lambda}^n_{ij}(t)\, \hat{\Lambda}^m_{lk}(t)\rangle \mathrm{e}^{\mathrm{i}k_0 \bar{\boldsymbol{r}}\cdot(\boldsymbol{R}_n - \boldsymbol{R}_m)}\,,\end{aligned} \tag{1.90}$$

provided the detection point $\boldsymbol{r}$ is chosen such that it lies outside the driving field, and the background field is in a vacuum state

$$\hat{\boldsymbol{E}}^{(+)}_v(\boldsymbol{r}, t)\,|\{\alpha\}\rangle = 0\,. \tag{1.91}$$

The radiation intensity therefore follows directly from the atomic first-order correlation functions modulated by oscillatory factors induced by relative phases of the fields produced by spatially distributed source atoms. These are the source atoms

[3] The radiation intensity often appears in the literature under different names as the intensity spectrum or excitation spectrum or atomic lineshape.

correlation functions we will be mostly interested in. Later on we shall show that the atomic correlation functions contain all the information about the radiation properties of atomic systems.

Inspection of (1.90) shows that the atomic correlation function contains both the single-atom and multiatom (collective) contributions. We may rewrite (1.90) in a form appropriate to study separately the single-atom and multiatom contributions to the radiation intensity. In order to do this, we split the expression (1.90) into two parts of which one is the contribution involving terms with $n = m$ and the other is the contribution involving terms with $n \neq m$. This splitting leads to the radiation intensity of the form

$$\langle \hat{I}(\boldsymbol{r}, t)\rangle = \sum_{i>j}\sum_{k>l}\left\{\sum_{n=1}^{N}\Phi_{ijlk}^{nn}\langle \hat{\Lambda}_{ij}^{n}(t)\,\hat{\Lambda}_{lk}^{n}(t)\rangle + \sum_{n=1}^{N}\sum_{m\neq n=1}^{N}\Phi_{ijlk}^{nm}\langle \hat{\Lambda}_{ij}^{n}(t)\,\hat{\Lambda}_{lk}^{m}(t)\rangle \mathrm{e}^{\mathrm{i}k_0\hat{\boldsymbol{r}}\cdot\boldsymbol{R}_{nm}}\right\}, \tag{1.92}$$

where $\boldsymbol{R}_{nm} = \boldsymbol{R}_n - \boldsymbol{R}_m$ is the vector distance between two atoms located at $\boldsymbol{R}_n, \boldsymbol{R}_m$, and $\Phi_{ijlk}^{nm} = (2\varepsilon_0 c r^2/\hbar\omega_0)\boldsymbol{\Psi}_{ij}^{*}(\boldsymbol{r} - \boldsymbol{R}_n)\cdot\boldsymbol{\Psi}_{lk}(\boldsymbol{r} - \boldsymbol{R}_m)$ is an effective initial radiation rate into the solid angle $\mathrm{d}\Omega_{\boldsymbol{r}}$ from the atomic dipole moments.

The two contributions to the radiation intensity have distinct physical origin, and in order to appreciate the role played by the atomic correlation functions, we consider some of their general properties. Thus, let us examine the first term on the right-hand side of (1.92). This term contains only a single summation over the atoms and involves correlation functions of the operators belonging to the same atom. Therefore, it represents the contribution to the intensity arising from independently radiating atoms. Since $\langle j_n|l_n\rangle = \delta_{jl}$, it follows that of all the correlation functions contributing to this term only those with $j = l$ are different from zero, so that we arrive at

$$\sum_{i>j}\sum_{k>l}\Phi_{ijlk}^{nn}\langle \hat{\Lambda}_{ij}^{n}(t)\,\hat{\Lambda}_{lk}^{n}(t)\rangle = \sum_{i,k>j}\Phi_{ijjk}^{nn}\langle \hat{\Lambda}_{ij}^{n}(t)\,\hat{\Lambda}_{jk}^{n}(t)\rangle\,. \tag{1.93}$$

We can further split the summation over the atomic energy states into the sum of two terms of which one involves correlation functions with $i = k$ and the other involves correlation functions with $i \neq k$. Hence, it follows that

$$\sum_{i,k>j}\Phi_{ijjk}^{nn}\langle \hat{\Lambda}_{ij}^{n}(t)\,\hat{\Lambda}_{jk}^{n}(t)\rangle = \sum_{i>j}\Phi_{ijji}^{nn}\langle \hat{\Lambda}_{ii}^{n}(t)\rangle + \sum_{i\neq k>j}\Phi_{ijjk}^{nn}\langle \hat{\Lambda}_{ij}^{n}(t)\,\hat{\Lambda}_{jk}^{n}(t)\rangle\,. \tag{1.94}$$

In this expression, the first term describes the contribution to the radiation intensity of the individual atomic dipole transitions. The contribution is proportional to the

populations $\langle \hat{\Lambda}^n_{ii}(t)\rangle = \varrho^n_{ii}$ of the atomic excited states $|i_n\rangle$ weighted with the factor Φ^{nn}_{ijji}, which is the initial radiation rate into $d\Omega_{\boldsymbol{r}}$ for the atomic dipole $\boldsymbol{\mu}_{ij}$. Thus, one of the contributions to the radiation intensity comes from an emission decay of the populations of the excited atomic levels. The second term is quite different. It represents the cross correlations (coherences) between different atomic transitions involving the common lower state $|j_n\rangle$. This term reflects the fact that, as the system decays from the state $|i_n\rangle$, it drives the $|k_n\rangle$ state, and vice versa. This process involves various correlation functions $\langle \hat{\Lambda}^n_{ij}(t)\hat{\Lambda}^n_{jk}(t)\rangle$ which, as we shall see later, are not always real and need not be nonnegative. These correlation functions may create coherent superpositions of the atomic states with reduced and even suppressed decay rates [19]. However, the contribution of the cross correlations to the radiation intensity depends on the mutual orientation of the atomic dipole moments involved and is absent when the dipole moments are orthogonal. In addition, the coherence between two arbitrary excited states $|i_n\rangle$ and $|k_n\rangle$ can contribute to the radiation intensity even if the direct dipole moment between these states is zero.

In order to show this more qualitatively, we require explicit forms of the factors Φ^{nn}_{ijji} and Φ^{nn}_{ijjk} multiplying the correlation functions. From (1.92) we find that the factors are of the form

$$\Phi^{nn}_{ijji} = \frac{3}{8\pi}\gamma_{ij}\left(1-\cos^2\psi_i\right), \tag{1.95}$$

and

$$\Phi^{nn}_{ijjk} = \frac{3}{8\pi}\sqrt{\gamma_{ij}\gamma_{kj}}\left(\cos\theta_{ik}-\cos\psi_i\cos\psi_k\right), \tag{1.96}$$

where θ_{ik} is the angle between the atomic transition dipole moments $\boldsymbol{\mu}_{ij}$ and $\boldsymbol{\mu}_{kj}$, ψ_p $(p = i,k)$ is the angle between the observation direction $\boldsymbol{r}$ and the dipole moment $\boldsymbol{\mu}_{pj}$, and

$$\gamma_{ij} = \frac{1}{4\pi\varepsilon_0}\frac{4\mu^2_{ij}\omega^3_0}{3\hbar c^3} \tag{1.97}$$

is the spontaneous emission rate, equal to the Einstein A coefficient, of the $|i_n\rangle \to |j_n\rangle$ transition. In the derivation of (1.95) and (1.96), we have assumed that the spread of the atomic frequencies satisfies $(\omega_{ij}-\omega_{kj}) \ll \omega_0$, where ω_0 is the average frequency of the atomic transitions, and the observation distance $\boldsymbol{r}$ is much larger than the dimensions of the atomic sample, so that $(\boldsymbol{r}-\boldsymbol{R}_n) \approx \boldsymbol{r}$ and $\omega_{ij}, \omega_{kj} \approx \omega_0$ for all atoms in the sample.

The factor Φ^{nn}_{ijji} is recognized as a radiation pattern of a linear dipole moment. It shows that the maximum of the radiation emitted by a dipole moment is at right angles to the direction of the dipole moment and no radiation along its axis. The factor Φ^{nn}_{ijjk} involves dipole moments of two different atomic transitions and represents an effective initial radiation rate into the solid angle $d\Omega_{\boldsymbol{r}}$ from the interfering atomic

dipole moments $\boldsymbol{\mu}_{ij}$ and $\boldsymbol{\mu}_{kj}$. As we see from (1.96), the rate is sensitive to the mutual polarization of the transition dipole moments, and therefore gives a measure of the coupling between different atomic transitions. If the dipole moments are parallel to each other, the coupling is maximal, while $\Phi^{nm}_{ijil} = 0$ if the dipole moments are orthogonal to each other and the observation point is in the direction orthogonal to the polarization of one of the two dipole moments.

We now turn to the multiatom term in (1.92). This term is more complicated because of the crossnen-correlation functions of operators belonging to different atoms in the double summation. Such operator products represent fields emitted by different atoms and imply interference by the atoms in each others emission process. This is manifested by the presence of the phase factor $\exp(\mathrm{i}k_0\bar{\boldsymbol{r}}\cdot\boldsymbol{R}_{nm})$, which depends on the geometry of the system and represents an effective phase difference between the fields produced by different atoms in the sample. A consequence of this factor is an interference of the fields, which can result in a spatial modulation of the radiation intensity with the position of a photodetector. Since the first part in (1.92) is independent of the interferometric phase factor, it produces a spherically symmetric intensity pattern with the angular distribution the same in all directions. We can conclude from this analysis that the multiatom part of the radiation intensity describes the deviation of the radiation emitted by interacting atoms from that emitted by independent atoms. Clearly, angular variation in the intensity pattern is an evidence of the collective behavior of the atoms and provides an opportunity to determine correlations between the source atoms [20, 21].

There is another interesting phenomenon known as *superradiance* [22–24], which also arise from the correlations between radiating atoms. This phenomenon results from the influence on each atomic dipole of the electromagnetic field produced by the other atomic dipoles which, in certain circumstances, cause each atom to release its energy of excitation more rapidly than it would on its own. The shortening of the atomic lifetime may lead to an enhancement of the emitted radiation with the intensity proportional to the square of the number of atoms. If N identical atoms contribute to the emitted field, we can make the reasonable assumption that the correlation functions appearing in (1.92) are approximately the same for every atom in the sample, and that neither term varies much with positions of the atoms. In addition, we can assume that the interatomic separations are approximately the same for every pair of the atoms in the sample. With these approximations the correlation functions and the exponential phase factors are independent of the indices n and m, and then the radiation intensity (1.92) reduces to

$$\langle \hat{I}(\boldsymbol{r},t)\rangle = \sum_{i>j}\sum_{k>l}\Big\{N\Phi_{ijjk}\langle \hat{\Lambda}_{ij}(t)\,\hat{\Lambda}_{jk}(t)\rangle + N(N-1)\Phi_{ijlk}\langle \hat{\Lambda}^{a}_{ij}(t)\,\hat{\Lambda}^{b}_{lk}(t)\rangle \mathrm{Re}\left(\mathrm{e}^{\mathrm{i}k_0\bar{\boldsymbol{r}}\cdot\boldsymbol{R}_{ab}}\right)\Big\}\,, \tag{1.98}$$

where indices a and b ($b \neq a$) have been introduced to the multiatom correlation functions to indicate that the atomic operators belong to different atoms, and $\boldsymbol{R}_{ab}$ is the interatomic separation, the same for each pair of atoms in the sample. The term

proportional to the number of atoms represents the contribution of N independently radiating atoms, and it is the presence of the N^2-dependent term which accounts for the phenomenon of superradiance.

In the above treatment of the radiation intensity, we have tacitly assumed constant interatomic separations which is equivalent to study of the multiatom effects for an idealized atomic beam consisting with a random distribution of atoms moving with constant velocity. In a real atomic beam, whose atoms move with nonuniform velocities, the interatomic separations are irregular or random. Then, the exponential phase factor $\exp(\mathrm{i}k_0\bar{\boldsymbol{r}}\cdot\boldsymbol{R}_{ab})$, which varies with relative positions of the atoms, rapidly oscillates with changing $\boldsymbol{R}_{ab}$ and averages to zero. Physically, this means that the radiation intensity exhibits no superradiance as the fields produced by different atoms make a negligible contribution by virtue of the rapidly oscillating phase. In this case, the only nonvanishing contribution to the radiation intensity comes from the individually radiating atoms. This brings out the importance of the phase relation in the collective radiation and superradiance [22–24].

In the special case of a small atomic sample that the atoms are confined into a region of space whose linear dimensions are much smaller than the average radiation wavelength, i.e. $k_0 r_{ab} \ll 1$, the phase factors are of order unity for all pairs of atoms in the sample. More generally, $\exp(\mathrm{i}k_0\bar{\boldsymbol{r}}\cdot\boldsymbol{R}_{ab}) \approx 1$ means that all the atoms in the sample lie within the same coherence area and radiate fields of the same phase. Now when the exponential phase factor is reduced to unity, the N^2-dependent term makes a significant contribution to the radiation intensity and for $N \gg 1$ dominates over the linear term. In other words, the emission is superradiant that the system is emitting at a rate approximately N^2 times the single-atom rate. We therefore say that superradiance is a direct manifestation that atoms radiate collectively.

Finally, to complete this section, we point out that the radiation intensity of the field may also be applied as a measure of fluctuations of the field amplitudes. To illustrate this, we introduce a dimensionless ratio

$$q = \frac{\langle \Delta\hat{\boldsymbol{E}}^{(-)}(\boldsymbol{r},t)\cdot\Delta\hat{\boldsymbol{E}}^{(+)}(\boldsymbol{r},t)\rangle}{\langle\hat{\boldsymbol{E}}^{(-)}(\boldsymbol{r},t)\rangle\cdot\langle\hat{\boldsymbol{E}}^{(+)}(\boldsymbol{r},t)\rangle} = g^{(1)}(\boldsymbol{r},t) - 1\,, \tag{1.99}$$

where, as usual

$$\Delta\hat{\boldsymbol{E}}^{(\pm)}(\boldsymbol{r},t) = \hat{\boldsymbol{E}}^{(\pm)}(\boldsymbol{r},t) - \langle\hat{\boldsymbol{E}}^{(\pm)}(\boldsymbol{r},t)\rangle, \tag{1.100}$$

are the fluctuation operators of the field amplitudes and

$$g^{(1)}(\boldsymbol{r},t) = \frac{\langle\hat{\boldsymbol{E}}^{(-)}(\boldsymbol{r},t)\cdot\hat{\boldsymbol{E}}^{(+)}(\boldsymbol{r},t)\rangle}{\langle\hat{\boldsymbol{E}}^{(-)}(\boldsymbol{r},t)\rangle\cdot\langle\hat{\boldsymbol{E}}^{(+)}(\boldsymbol{r},t)\rangle} = \frac{\langle\hat{I}(\boldsymbol{r},t)\rangle}{|\langle\hat{\boldsymbol{E}}^{(-)}(\boldsymbol{r},t)\rangle|^2} \tag{1.101}$$

is the normalized first-order equal-time correlation function of the field amplitudes. The fluctuation operators describe fluctuations of the field amplitudes around their

mean values. Of course, the expectation value of fluctuation operators is zero, but the correlation functions can be different from zero. For instance, one can see from (1.99) and (1.101) that the correlation function of the fluctuation operators is proportional to the first-order equal-time correlation function of the field amplitudes which, on the other hand, is equal to the radiation intensity of the field. Thus, measurements of the radiation intensity would provide information about the first-order correlation as well as the fluctuations of the field amplitudes.

The parameter q represents the basic quantity for investigations of the correlation and fluctuation properties of the field amplitudes and is simply related to directly measurable quantities. It gives a measure of fluctuations of the field amplitudes relative to the fluctuations of the uncorrelated (coherent) amplitudes. The parameter q is known as the *degree of self-coherence* and is one of the important quantities in the elementary theory of optical coherence. It follows from (1.99) that $q = 0$ characterizes a coherent field, whereas a positive value of q ($q > 0$) characterizes an incoherent field. More precisely, $q = 0$ implies first-order coherence, i.e., the correlation function $g^{(1)}(\boldsymbol{r}, t)$ is equal to unity. Thus, a field is said to be coherent in the first order, if the correlation function can be factorized as a product of the mean values of the field amplitudes. As we shall see in the next chapter, the fluorescence field emitted from an atom is usually not coherent in this sense, even if the atom is driven by a coherent field. We should mention that $q = 0$ does not imply non-fluctuating field amplitudes. It means that the fluctuations of the field amplitudes are statistically independent. Although the parameter q refers to the fluctuations of the field amplitudes in general way, to some extent it allows information about quantum fluctuations of the field to be calculated. We thus focus our attention upon cases where quantum fluctuations are important and therefore, the parameter will be of interest to us in searching for optical effects induced by quantum fluctuations.

References

1. W. Heitler: *The Quantum Theory of Radiation*, (Clarendon, Oxford, 1954)
2. W. Louisell: *Quantum Statistical Properties of Radiation*, (Wiley, New York, 1973)
3. L. Allen, J. H. Eberly: *Optical Resonance and Two-Level Atoms*, (Wiley, New York, 1975)
4. E.A. Power, S. Zienau: Philos. Trans. R. Soc. London Ser. A **251**, 427 (1959)
5. W.P. Healy: J. Phys. A **10**, 279 (1977)
6. L. Mandel, E. Wolf: Rev Mod. Phys. **37**, 231 (1965)
7. M. Born, E. Wolf: *Principles of Optics*, (Pergamon, London, 1975)
8. R. Hanbury-Brown, R.Q. Twiss: Nature **177**, 27 (1956)
9. H.J Kimble, L. Mandel: Phys. Rev. A **13**, 2123 (1976)
10. H.J. Carmichael, D.F. Walls: J. Phys. B **9**, 1199 (1976)
11. H.J Kimble, M. Dagenais, L. Mandel: Phys. Rev. Lett. **39**, 691 (1977)
12. R.J. Glauber: Phys. Rev. **131**, 2766 (1963)
13. E.C.G. Sudarshan: Phys. Rev. Lett. **10**, 277 (1963)
14. J.D. Cresser: Phys. Rep. **94**, 47 (1983)
15. B. Renaud, R.M. Whitley, C.R. Stroud, Jr.: J. Phys. B: At. Mol. Phys. **10**, 19 (1977)
16. J.H. Eberly, K. Wódkiewicz: J. Opt. Soc. Am. **67**, 1252 (1977)

17. F. DeMartini, M. Marrocco, P. Mataloni, L. Crescentini, R. Loudon: Phys. Rev. A **43**, 2480 (1991)
18. L. Mandel: Phys. Rev. **152**, 438 (1966)
19. Z. Ficek, S. Swain: *Quantum Interference and Coherence: Theory and Experiments*, (Springer, Berlin Heidelberg New York 2005)
20. M.J. Stephen: J. Chem. Phys. **40**, 669 (1964)
21. R.H. Lehmberg: Phys. Rev. A **2**, 883, 889 (1970)
22. R.H. Dicke: Phys. Rev. **93**, 99 (1954)
23. N.E. Rehler, J.H. Eberly: Phys. Rev. A **3**, 1735 (1971)
24. G.S. Agarwal: In *Quantum Statistical Theories of Spontaneous Emission and their Relation to other Approaches*, ed by G. Höhler, Springer Tracts in Modern Physics, vol 70 (Springer, Berlin Heidelberg New York, 1974)

Chapter 2
Spectra of Radiating Systems

We have already noted that a possible way of measuring fluctuations of the field amplitudes is to detect the intensity of the radiation field emitted by an ensemble of atoms. More useful is the power spectrum, which is attributed to fluctuations of the field amplitudes and gives variations in the field intensity as a function of frequency. As demonstrated in the previous chapter, the calculation of the power spectrum requires the knowledge of the normally-ordered two-time correlation function of the electric field amplitudes evaluated at the position of a detector. In this chapter, we shall take a closer look at the relation of the spectrum to the correlation functions of the source variables and undertake a more detailed discussion of the calculation of the spectrum of radiation field emitted from the atoms. We shall be dealing entirely with power spectra of stationary and quasistationary fields, i.e. fields whose properties are independent of the origin of time. Under this condition, all the two-time correlation functions will involve components that depend on the time arguments only through their difference. Also, we shall follow the definition (1.70) of the power spectrum, which employs a simplified physical model of the detection process. In this model, the radiation field is measured with an ideal Fabry−Perot interferometer of bandwidth $\Gamma \to 0$, and its spectral range much larger than the width of the frequency spectrum of the measured field. The results presented here, however, can be easily extended to include finite bandwidth effects of the interferometer.

2.1 Emission Power Spectrum

Let us begin by considering the normal and time-ordered second-order correlation function of the electric field amplitudes evaluated at the position of a photodetector. As a consequence of the arrangements (1.85) and (1.86), we observe that the correlation function of the field amplitudes at a suitably located detector can be completely determined by the normally ordered correlation function of the source field amplitudes. Under these conditions and for the case of atomic source of the radiation field, we can apply the result (1.31) and write the correlation function of the source field

Z. Ficek and R. Tanaś, *Quantum-Limit Spectroscopy*, Springer Series in Optical Sciences 200, DOI 10.1007/978-1-4939-3740-0_2

amplitudes as a multiple sum of terms involving correlation functions of the atomic dipole operators. The normal and time-ordered correlation function of the electric field amplitudes at the photodetector can then be written in the form as follows:

$$\langle \hat{\boldsymbol{E}}^{(-)}(t) \cdot \hat{\boldsymbol{E}}^{(+)}\left(t'\right)\rangle = \langle \hat{\boldsymbol{E}}_s^{(-)}(t) \cdot \hat{\boldsymbol{E}}_s^{(+)}\left(t'\right)\rangle$$
$$= \sum_{n,m=1}^{N} \sum_{i,k>j,l} \boldsymbol{\Psi}_{ij}^{*}(\boldsymbol{r}-\boldsymbol{R}_n) \cdot \boldsymbol{\Psi}_{lk}(\boldsymbol{r}-\boldsymbol{R}_m) \langle \hat{\Lambda}_{ij}^{n}(t)\, \hat{\Lambda}_{lk}^{m}\left(t'\right)\rangle \mathrm{e}^{\mathrm{i}k_0 \bar{\boldsymbol{r}} \cdot \boldsymbol{R}_{nm}} . \quad (2.1)$$

By taking the double truncated Fourier transform of the two-time correlation function (2.1) and the limit of long detection time, we obtain an expression for the stationary power spectrum of the field radiated per unit solid angle and measured at a point $\boldsymbol{r}$ in the radiation zone

$$S(\boldsymbol{r},\omega) = \lim_{T\to\infty} \frac{1}{T} \sum_{n,m=1}^{N} \sum_{i,k>j,l} \Phi_{ijlk}^{nm} \mathrm{e}^{\mathrm{i}k_0 \bar{\boldsymbol{r}} \cdot \boldsymbol{R}_{nm}}$$
$$\times \int_0^T \mathrm{d}t \int_0^T \mathrm{d}t' \langle \hat{\Lambda}_{ij}^{n}(t)\, \hat{\Lambda}_{lk}^{m}\left(t'\right)\rangle \mathrm{e}^{\mathrm{i}\omega(t-t')} , \quad (2.2)$$

where Φ_{ijlk}^{nm} are the effective initial radiation rates defined in (1.96). This general expression shows that the spectrum of the radiation field emitted by an arbitrary atomic system can be described as having its origin in the correlation functions of the atomic dipole operators. Thus, our concern with the calculation of the spectrum is then with the evaluation of the two-time atomic correlation function. This two-time correlation function is obtained by superposing contributions from different atoms and different atomic transitions together with possible interference terms involving dipole transitions in different atoms and/or different transitions in the same atom.

Usually the source field is composed of a coherent component, corresponding to a field elastically scattered by the source atoms, and an incoherent (noise) component, corresponding to a field produced by fluctuations of the atomic dipoles. In practice this will almost certainly be the case if the source atoms are driven by a coherent field. Therefore, it is often necessary to distinguish between these two contributions to the source field. It is accomplished by expressing the atomic dipole operators $\hat{\Lambda}_{ij}^{n}(t)$ as the sum of its expectation value $\langle \hat{\Lambda}_{ij}^{n}(t)\rangle$ and its fluctuations $\delta\hat{\Lambda}_{ij}^{n}(t)$, so that

$$\hat{\Lambda}_{ij}^{n}(t) = \langle \hat{\Lambda}_{ij}^{n}(t)\rangle + \delta\hat{\Lambda}_{ij}^{n}(t) , \quad (2.3)$$

with $\langle \delta\hat{\Lambda}_{ij}^{n}(t)\rangle = 0$. Accordingly, we can write the atomic correlation function, appearing in (2.2), as a sum of two qualitatively different parts

$$\langle \hat{\Lambda}_{ij}^{n}(t)\, \hat{\Lambda}_{lk}^{m}\left(t'\right)\rangle = \langle \hat{\Lambda}_{ij}^{n}(t)\rangle \langle \hat{\Lambda}_{lk}^{m}\left(t'\right)\rangle + \langle \delta\hat{\Lambda}_{ij}^{n}(t)\, \delta\hat{\Lambda}_{lk}^{m}\left(t'\right)\rangle . \quad (2.4)$$

The first term on the right-hand side of (2.4) is given by the product of the expectation values of the atomic dipole operators and we therefore refer to it as the coherent part of the oscillating atomic dipole moments. The second term is associated with the fluctuations of the atomic dipole moments produced by the coupling of the atoms to the vacuum field. Thus, the effects of the vacuum fluctuations can be reflected through spectral properties of the radiated field, and can be clearly distinguished from coherent effects.

With the result (2.4), we may then clearly resolve the spectrum into two parts. On substituting (2.4) into (2.2), we find that the contribution of the mean dipole operators gives the coherent part of the spectrum

$$S_{\rm coh}(\boldsymbol{r},\omega) = \lim_{T\to\infty}\frac{1}{T}\sum_{n,m=1}^{N}\sum_{i,k>j,l}\Phi_{ijlk}^{nm}\mathrm{e}^{\mathrm{i}k_0\bar{\boldsymbol{r}}\cdot\boldsymbol{R}_{nm}} \times\int_0^T \mathrm{d}t\int_0^T \mathrm{d}t'\langle\hat{\Lambda}_{ij}^{n}(t)\rangle\langle\hat{\Lambda}_{lk}^{m}(t')\rangle\mathrm{e}^{\mathrm{i}\omega(t-t')}\,, \tag{2.5}$$

and the contribution of the quantum fluctuations or quantum noise of the atomic dipoles gives the incoherent part of the spectrum

$$S_{\rm in}(\boldsymbol{r},\omega) = \lim_{T\to\infty}\frac{1}{T}\sum_{n,m=1}^{N}\sum_{i,k>j,l}\Phi_{ijlk}^{nm}\mathrm{e}^{\mathrm{i}k_0\bar{\boldsymbol{r}}\cdot\boldsymbol{R}_{nm}} \times\int_0^T \mathrm{d}t\int_0^T \mathrm{d}t'\langle\delta\hat{\Lambda}_{ij}^{n}(t)\,\delta\hat{\Lambda}_{lk}^{m}(t')\rangle\mathrm{e}^{\mathrm{i}\omega(t-t')}\,. \tag{2.6}$$

From (2.5) and (2.6) it is apparent that the calculation of the coherent part of the spectrum only involves expectation values of the atomic transition operators, whereas the calculation of the incoherent part of the spectrum requires the knowledge of the two-time correlation function of the fluctuation operators. In an alternative way, one can calculate the incoherent part by subtracting the coherent part from the power spectrum $S(\boldsymbol{r},\omega)$. To go further with the evaluation of the correlation functions and thereby the power spectrum, requires the knowledge of an explicit model of the source atoms.

There are a number of theoretical approaches that can be used to calculate the two-time correlation function of the atomic operators. A common method, which we shall be using in the succeeding chapters of the book, involves an application of the master equation describing the evolution of an atomic system and the quantum regression theorem [1]. We shall present some details of this method in Chap. 3, where we calculate and analyse power spectra for the specific source consisting of a single atom.

For the sake of completeness, let us briefly consider the relation between the stationary power spectrum, which is the frequency composition of the emitted field, and the intensity of the entire field emitted by the atoms into an element of solid

angle $\mathrm{d}\Omega_{\boldsymbol{r}}$ around the direction $\boldsymbol{r}$. By integrating (2.5) and (2.6) over the spectral frequency ω we obtain, respectively, the coherent and incoherent contributions to the radiation intensity of the emitted field. Since ω only appears in the exponential, the integration in the limit of the detection time $T \to \infty$ gives the delta function $\delta(t - t')$ and thus the two-time correlation functions reduce to single-time expectation values. The pertinent formula for the stationary value of the coherent part of the radiation intensity, per unit solid angle, is

$$\langle \hat{I}(\boldsymbol{r})\rangle_{\mathrm{coh}} = \int_{-\infty}^{+\infty} \mathrm{d}\omega\; S_{\mathrm{coh}}(\boldsymbol{r},\omega) = \sum_{n,m=1}^{N} \sum_{i,k>j,l} \Phi_{ijlk}^{nm} \mathrm{e}^{\mathrm{i}k_0 \bar{\boldsymbol{r}}\cdot\boldsymbol{R}_{nm}} \times \lim_{T\to\infty} \frac{1}{T} \int_0^T \mathrm{d}t \langle \hat{\Lambda}_{ij}^{n}(t)\rangle \langle \hat{\Lambda}_{lk}^{m}(t)\rangle \,, \tag{2.7}$$

and for the incoherent part is given by

$$\langle \hat{I}(\boldsymbol{r})\rangle_{\mathrm{in}} = \int_{-\infty}^{+\infty} \mathrm{d}\omega\; S_{\mathrm{in}}(\boldsymbol{r},\omega) = \sum_{n,m=1}^{N} \sum_{i,k>j,l} \Phi_{ijlk}^{nm} \mathrm{e}^{\mathrm{i}k_0 \bar{\boldsymbol{r}}\cdot\boldsymbol{R}_{nm}} \times \lim_{T\to\infty} \frac{1}{T} \int_0^T \mathrm{d}t \langle \delta\hat{\Lambda}_{ij}^{n}(t)\, \delta\hat{\Lambda}_{lk}^{m}(t)\rangle \,. \tag{2.8}$$

These equations express the stationary intensity of the emitted field in terms of expectation values and one-time correlation functions of the various transition operators. For the incoherent part populations of the atomic states are involved, since expanding the summation over the atomic energy states yields

$$\sum_{i,k>j} \langle \hat{\Lambda}_{ij}^{n}(t)\, \hat{\Lambda}_{jk}^{n}(t)\rangle = \sum_{i>j} \langle \hat{\Lambda}_{ii}^{n}(t)\rangle + \sum_{i\neq k>j} \langle \hat{\Lambda}_{ij}^{n}(t)\, \hat{\Lambda}_{jk}^{n}(t)\rangle \,, \tag{2.9}$$

where $\langle \hat{\Lambda}_{ii}^{n}(t)\rangle = \varrho_{ii}^{n}$ are populations of the atomic excited states $|i_n\rangle$. Accordingly, the single-atom ($n = m$) contributions to the intensity come from populations of the atomic states and coherences between different atomic transitions. Multiatom contributions with $n \neq m$ cannot be expressed in terms of populations of the single-atom states. They can rather be expressed in term of populations of entangled states of the multiatom system.

2.1.1 Coherent (Elastic) Part of the Spectrum

In the preceding section, we have shown that it is possible to separate the power spectrum into the coherent and incoherent components. It is accomplished by first splitting the two-time correlation function of the atomic operators into coherent

and noise parts. The spectrum is then derived as a sum of the double truncated Fourier transforms of the two parts of the correlation function. We now focus on the coherent part of the spectrum and, for later convenience, we shall introduce a certain simplification which is applicable to an arbitrary atomic system. We shall then find that the stationary coherent spectrum is composed of an infinitely narrow line, represented by a Dirac δ function, or a series of infinitely narrow lines.

Let us consider the relation (2.5) to examine the coherent spectrum when the source field is stationary in time. If the source atoms are driven by an external field, the induced atomic dipole moments continuously oscillate in time at the frequency of the driving field. As far as atoms are concerned, radiative processes such as spontaneous radiative decay, are very slow requiring on the average many millions of cycles of dipole oscillations before they are completed. Therefore, we can extract from the atomic transition operators the rapidly oscillating terms, and write their expectation values as

$$\begin{aligned} \langle \hat{A}_{ij}^{n}(t)\rangle_s &= \langle \hat{A}_{ij}^{n}(t)\rangle \mathrm{e}^{-\mathrm{i}\omega_L t}\,, \\ \langle \hat{A}_{ji}^{n}(t)\rangle_s &= \langle \hat{A}_{ji}^{n}(t)\rangle \mathrm{e}^{\mathrm{i}\omega_L t}\,, \qquad i>j\,, \end{aligned} \tag{2.10}$$

where ω_L is the frequency of the driving field, which does not necessarily coincide with the atomic transition frequencies ω_{ij}, and $\langle \hat{A}_{ij}^{n}(t)\rangle_s$ are expectation values of slowly varying transition operators, which change slowly compared with variations arising from the periodic term $\exp(\mathrm{i}\omega_L t)$.

Written in terms of the slowly varying expectation values, the coherent part of the spectrum (2.5) becomes

$$\begin{aligned} S_{\mathrm{coh}}(\boldsymbol{r},\omega) = \lim_{T\to\infty}\frac{1}{T}\sum_{n,m=1}^{N}\sum_{i,k>j,l}\Phi_{ijlk}^{nm}\mathrm{e}^{\mathrm{i}k_0\bar{\boldsymbol{r}}\cdot\boldsymbol{R}_{nm}} \\ \times\int_0^T \mathrm{d}t\int_0^T \mathrm{d}t'\langle \hat{A}_{ij}^{n}(t)\rangle_s\langle \hat{A}_{lk}^{m}(t')\rangle_s \mathrm{e}^{\mathrm{i}(\omega-\omega_L)(t-t')}. \end{aligned} \tag{2.11}$$

Equation (2.10) shows directly that the atomic dipole moments continue to oscillate in time at the driving frequency and, even after a long time, the expectation values cannot be strictly stationary. However, we may assume that a stationary state is reached after a long time, in the sense that $\langle \hat{A}_{ij}^{n}(t)\rangle_s$ are independent of t, and each of the expectation values in (2.11) becomes independent of time also. If it applies, the expectation values of the slowly varying operators can be replaced by their stationary, time-independent values.

It is then possible to perform the integration explicitly by extracting the time-independent expectation values from the integrals. Provided $T\to\infty$, the double integral can be well approximated by a Dirac δ function, and then the coherent spectrum (2.11) simplifies to

$$S_{\mathrm{coh}}(\boldsymbol{r},\omega)=\sum_{n,m=1}^{N}\sum_{i,k>j,l}\Phi_{ijlk}^{nm}(\boldsymbol{r})\langle\hat{\Lambda}_{ij}^{n}\rangle_{s}\langle\hat{\Lambda}_{lk}^{m}\rangle_{s}\,\pi\,\delta\left(\omega-\omega_{L}\right)\,, \tag{2.12}$$

where $\Phi_{ijlk}^{nm}(\boldsymbol{r})=\Phi_{ijlk}^{nm}\exp(\mathrm{i}k_0\bar{\boldsymbol{r}}\cdot\boldsymbol{R}_{nm})$ and $\langle\hat{\Lambda}_{ij}^{n}\rangle_s$ are stationary coherences, i.e., the time-independent parts of the average atomic transition operators.

The expression (2.12) shows that the coherent spectrum of a stationary field emitted by an atomic source consists of a delta function contribution giving an infinitely narrow line at the frequency of the driving field.[1] It obviously corresponds to a field that is elastically scattered by the atomic system. The intensity of the line depends on magnitudes of the stationary atomic coherences. We should mention that in experimental practice, the exact delta line would not be observed. It would rather show up as a peak of a finite width imposed by the finite spectral resolution of the detecting apparatus.

The procedure of calculating the coherent spectrum is more complicated if the system is not strictly stationary, but rather is in a quasistationary state, even in the long-time limit. The qualifying term *quasistationary* means that the atomic quantities are explicit function of time. In this case, the above formalism has to be modified. Usually, the time dependence arises from nonzero detunings of the driving field frequency from the atomic transition frequencies. It may also arise from a time modulation of the driving field frequency or amplitude. In general, the time dependence may be quite complicated and involve many oscillatory contributions. However, in many practical cases, it occurs that the system oscillates harmonically with a frequency determined by a single parameter δ. The problem is then solved by applying the Floquet method that enables to obtain a formal analytic expression for the stationary part of the time-dependent expectation value $\langle\hat{\Lambda}_{ij}^{n}(t)\rangle_s$. It is done by expanding the time-dependent expectation values into a sum of contributions oscillating at the frequency δ and its harmonics, by means of a Fourier series

$$\langle\hat{\Lambda}_{ij}^{n}(t)\rangle_{s}=\sum_{p=-\infty}^{\infty}\langle\hat{\Lambda}_{ij}^{n}\rangle_{s}^{(p)}\mathrm{e}^{\mathrm{i}p\delta t}\,, \tag{2.13}$$

where p is an integer which determines the order of the harmonics, $\langle\hat{\Lambda}_{ij}^{n}\rangle_s^{(p)}$ are the expansion coefficients that vary slowly with time, and δ is an oscillation (modulation) parameter. As we have already mentioned, the parameter δ can be associated with a detuning of the driving field from atomic resonances or with a time modulation of the driving field frequency and/or amplitude. In the case of a continuous pulse-train driving field, the parameter δ is given by the pulse repetition frequency.

Now that we have determined the method of the explicit treatment of the time-dependent correlation functions, we expand each of the expectation values appearing in (2.11) into a series of slowly varying amplitudes that oscillate at the frequency δ and its harmonics, and arrive at the expression

[1] The delta function occurs only for an infinite observation time. In practice, for a finite observation time T, the width of the contribution is of order T^{-1}.

$$S_{\rm coh}(\boldsymbol{r},\omega) = \lim_{T\to\infty}\frac{1}{T}\sum_{n,m=1}^{N}\sum_{i,k>j,l}\Phi_{ijlk}^{nm}(\boldsymbol{r})\sum_{p,r=-\infty}^{\infty}\int_0^T {\rm d}t\int_0^T {\rm d}t' \times \langle\hat{\Lambda}_{ij}^{n}\rangle_s^{(p)}\langle\hat{\Lambda}_{lk}^{m}\rangle_s^{(r)}{\rm e}^{{\rm i}(p+r)\delta t}{\rm e}^{{\rm i}(\omega-\omega_L-r\delta)(t-t')}. \tag{2.14}$$

The spectrum generally consists of terms which depend on time t and the time difference $t-t'$. For a fixed $t-t'$ and for $p\neq -r$, we see that the time dependent factor $\exp[{\rm i}(p+r)\delta t]$ continuously oscillate in time and becomes negligible after a sufficiently long time t. Thus, in the long-time limit, the terms with $p\neq -r$ make a negligible contribution to the spectrum. There are however "diagonal" terms involving harmonics with $p=-r$. These terms are independent of t, and therefore make a significant contribution to the spectrum even in the long-time limit. This shows that the system eventually settles in a stationary state. Hence, for a sufficiently long detection time T the resultant "stationary" coherent spectrum is given by

$$S_{\rm coh}(\boldsymbol{r},\omega) = \sum_{n,m=1}^{N}\sum_{i,k>j,l}\Phi_{ijlk}^{nm}(\boldsymbol{r}) \times \sum_{r=-\infty}^{\infty}\langle\hat{\Lambda}_{ij}^{n}\rangle_s^{(-r)}\langle\hat{\Lambda}_{lk}^{m}\rangle_s^{(r)}\,\pi\,\delta(\omega-\omega_L-r\delta)\ . \tag{2.15}$$

From this we see that the spectral distribution of the coherently scattered field differs from that of the driving field. It exhibits a series of infinitely sharp peaks located at frequencies $r\delta$ separated by a constant spacing δ. This implies that the coherent scattering on a quasistationary system is not in general elastic. We may conclude that a periodic time modulation of the expectation values introduces new infinitely sharp components at multiples of the modulation frequency δ. The new components reflect the presence of parametric resonances, which are due to the oscillations introduced into the atomic dipole moments at harmonic frequencies $\omega_L+r\delta$. The intensity of a given coherent peak depends on the properties of the stationary Fourier amplitudes of the atomic coherences, whose explicit forms are normally determined from the master equation of a specific atomic system.

As we have already stated, the coherent spectrum is composed of infinitely sharp peaks. Nevertheless, the coherent part of the radiation intensity, obtained after integration of (2.15) over all spectral frequencies, is finite and proportional to the stationary harmonics of the average atomic coherences.

In summary of this section, the expressions (2.12) and (2.15) are our formal results for the coherent part of the power spectrum of a radiation field emitted by stationary and quasistationary systems. The results are instructive because they show how the expectation values of the atomic transition operators and their stationary components enter the spectrum in a simple explicit way. They have simple mathematical structures and allow for a particularly transparent physical interpretation of the coherent spectrum. We emphasize the complete generality of these equations that they are applicable to arbitrary atomic systems and hold for any initial state of the system.

2.1.2 Incoherent (Noise) Part of the Spectrum

Thus far our discussion has been limited to the coherent part of the power spectrum. However, more important is the incoherent part. It arises from quantum fluctuations both of the field and of the atomic source and therefore its measurement may be thought as a method of their detection. Earlier in this chapter, we have defined the incoherent part of the spectrum as a double Fourier transform of the two-time correlation function of the fluctuation operators. Before proceeding further with an examination of the incoherent spectrum for specific atomic systems, we stop for a moment to introduce certain general simplifications to the procedure of calculating the spectrum, which are common for all atomic systems. To be specific, we shall introduce the simplifications to the general form (2.6) of the incoherent part of the power spectrum without a consideration of detailed atomic dynamics.

When dealing with the coherent spectrum it was convenient to introduce slowly oscillating operators that are free from the rapid oscillations at optical frequencies characterizing the atomic operators. In analogy, the common rapid oscillations at the optical frequency ω_L can be removed from the fluctuation operators by transforming to slowly varying operators

$$\delta S_{ij}^{n}(t) = \delta \hat{\Lambda}_{ij}^{n}(t)\, \mathrm{e}^{-\mathrm{i}\omega_L t}\,, \quad \delta S_{ji}^{n}(t) = \delta \hat{\Lambda}_{ji}^{n}(t)\, \mathrm{e}^{\mathrm{i}\omega_L t}\,, \quad i > j\,, \tag{2.16}$$

where, as before, ω_L is the frequency of the driving field. In terms of these new operators, the incoherent part of the power spectrum becomes

$$S_{\mathrm{in}}(\boldsymbol{r},\omega) = \lim_{T\to\infty} \frac{1}{T} \sum_{n,m=1}^{N} \sum_{i,k>j,l} \Phi_{ijlk}^{nm} \mathrm{e}^{\mathrm{i}k_0 \hat{\boldsymbol{r}}\cdot\boldsymbol{R}_{nm}} \times \int_0^T \mathrm{d}t \int_0^T \mathrm{d}t' \langle \delta S_{ij}^{n}(t)\, \delta S_{lk}^{m}(t') \rangle \mathrm{e}^{\mathrm{i}(\omega-\omega_L)(t-t')}\,. \tag{2.17}$$

Although the above expression is rather simple in form, the integrals cannot be evaluated before a detailed solution for the two-time correlation function of the slowly varying operators has been obtained. However, there are two situations in which this formula can further be simplified without a consideration of the solution for the correlation function. The first is the case of steady or stationary systems for which the correlation function depends on the time arguments only through their difference $t'-t$. From this property and employing the basic expression (2.17), giving the incoherent spectrum for a long detection time, it follows that by taking $T \to \infty$ and by changing the variables of integration, the t integral in (2.17) can be carried out explicitly and then the expression for the incoherent spectrum simplifies to

$$S_{\text{in}}(\boldsymbol{r},\omega) = 2\text{Re}\sum_{n,m=1}^{N}\sum_{i,k>j,l}\Phi_{ijlk}^{nm}(\boldsymbol{r}) \times \int_0^\infty \text{d}\tau\langle\delta S_{ij}^n(0)\,\delta S_{lk}^m(\tau)\rangle \text{e}^{\text{i}(\omega-\omega_L)\tau}\,, \tag{2.18}$$

where $\tau = t - t'$ is the delay time, and we have shifted the time origin to $t = 0$ as in the long-time limit the correlation function is independent of the time origin.

Integrating (2.18) over all directions, specified by the solid angles $\text{d}\Omega_{\boldsymbol{r}}$, we obtain the incoherent spectrum of the total radiation field per unit time

$$S_{\text{in}}(\omega) = \int \text{d}\Omega_{\boldsymbol{r}}\, S_{\text{in}}(\boldsymbol{r},\omega) = 2\text{Re}\sum_{n,m=1}^{N}\sum_{i,k>j,l}\sqrt{\gamma_{ij}\gamma_{kl}}\cos\theta_{ik} \times \int_0^\infty \text{d}\tau\,\langle\delta S_{ij}^n(0)\,\delta S_{lk}^m(\tau)\rangle \text{e}^{\text{i}(\omega-\omega_L)\tau}\,. \tag{2.19}$$

The expression (2.19) is one of the fundamental equations in atomic spectroscopy. It is used to determine spectral features of the radiation field emitted by an arbitrary stationary system. This general property makes this expression extremely flexible in that it may be applied in various situations ranging from a single two-level atom to multiatom and multi-level systems in arbitrary spatial distributions and in arbitrary configurations of the energy levels. As we shall explore in this book, the expression (2.19) may also be used to obtain an information about certain quantum features of the field.

This is as far as we can get with the calculation of the stationary spectrum without an explicit calculation of the atomic correlation function. To go further requires a master equation treatment of the stationary atomic correlation function and the quantum regression theorem. Briefly, for a given system, an explicit form of the correlation function can be established from the master equation by deriving a set of coupled differential equations for the density matrix elements and solving it under the stationary condition. Having computed the correlation function, the integration can be performed from which the spectrum of the emitted field may be readily determined for a specific direction of observation $\boldsymbol{r}$. It is worth noting that depending on whether the correlation function is real or complex, the spectrum can be symmetric or asymmetric about its line center, $\omega = \omega_L$. If the correlation function is real, the incoherent spectrum will be symmetric about its line centre, and will be asymmetric if it is not. These points will be further elaborated in the course of specific examples discussed in the next chapter.

Now let us examine the incoherent spectrum for the second situation in which the system is in a quasistationary state. In this case, the two-time correlation function depends explicitly on time t, and we shall not find it possible to proceed with the calculation of the spectrum in quite such a straightforward manner as before for the stationary case. Actually, we have already considered this kind of problem when we have calculated the coherent spectrum of a quasistationary field oscillating slowly

with some frequency δ characterizing the radiating system. We have seen that the temporal oscillations of the one-time atomic variables significantly altered the nature of the coherent field. In this case, it was appropriate to treat the spectrum by employing a Fourier decomposition of the atomic variables in terms of the frequency δ and its harmonics. For the incoherent spectrum we might expect that a similar procedure could be used. This is true; however, we shall see shortly that the calculation of the incoherent spectrum is more complicated than the evolution of the simple expectation values of the atomic operators. It involves two-time correlation functions and, in general, may require a double Fourier decomposition.

Suppose we consider a two-time correlation function $Y(t, t')$, which has a periodic dependence on both t and t', with a period of oscillation δ. Now because the correlation function depends on two different times, we may introduce a double Fourier decomposition taken with respect to the same variable δ. Consequently, the two-time correlation function may be written as

$$\begin{aligned} Y\left(t, t'\right) &= \sum_{p=-\infty}^{\infty} \sum_{r=-\infty}^{\infty} Y^{(p,r)}\left(t, t'\right) \mathrm{e}^{\mathrm{i}p\delta t} \mathrm{e}^{\mathrm{i}r\delta t'} \\ &= \sum_{p=-\infty}^{\infty} \sum_{r=-\infty}^{\infty} Y^{(p,r)}\left(t, t+\tau\right) \mathrm{e}^{\mathrm{i}(p+r)\delta t} \mathrm{e}^{\mathrm{i}r\delta\tau}\,, \end{aligned} \tag{2.20}$$

where $Y^{(p,r)}\left(t, t'\right)$ are two-dimensional slowly varying Fourier amplitudes and, as before, $\tau = t' - t$ is the delay time.

We call the above expansion the double Fourier expansion simply because it is the product of two individual Fourier series, one in time t and the other in time t', or in the delay time τ. From (2.20), we see that the correlation function is periodic in both t and τ, and responds at the fundamental frequency δ and its harmonics. In the long-time limit of $t \to \infty$, the amplitudes $Y^{(p,r)}(t, \tau)$ do not vary with time, that is $\mathrm{d}Y^{(p,r)}(t, \tau)/\mathrm{d}t \approx 0$, and then the Fourier amplitudes become independent of the first argument yielding $Y^{(p,r)}(t, \tau) = Y^{(p,r)}(0, \tau)$. In addition, the t dependent exponential factors cause all terms with $r \neq -p$ to vanish as $t \to \infty$, except the terms with $r = -p$ for which the factors reduce to unity. Hence, in the limit of long times t, the double Fourier expansion reduces to

$$Y(\tau) = \lim_{t\to\infty} Y(t, t+\tau) = \sum_{p=-\infty}^{\infty} Y^{(p,-p)}(0, \tau)\, \mathrm{e}^{-\mathrm{i}p\delta\tau}\,. \tag{2.21}$$

First note that in the stationary limit, in which the two-time correlation function depends only on the time difference τ, the double Fourier expansion reduces to a simpler "diagonal" form. This expansion also tells us that in the stationary limit a system described by the correlation function $Y(t, t+\tau)$ will respond at the fundamental frequency δ at its harmonics. The response at the harmonics is what makes

the quasistationary system different from a stationary system, which responses only at the fundamental frequency δ.

To see how the periodic oscillations of the correlation function affect the incoherent spectrum, we apply the double Fourier decomposition to the two-time correlation function appearing in (2.17), and arrive at the expression

$$S_{\text{in}}(\boldsymbol{r},\omega) = 2\text{Re}\sum_{n,m=1}^{N}\sum_{i,k>j,l}\Phi_{ijlk}^{nm}\mathrm{e}^{\mathrm{i}k_0\bar{\boldsymbol{r}}\cdot\boldsymbol{R}_{nm}}\sum_{p=-\infty}^{\infty}\int_0^{\infty}\mathrm{d}\tau \times\langle\delta S_{ij}^{n}(0)\,\delta S_{lk}^{m}(\tau)\rangle^{(p,-p)}\mathrm{e}^{\mathrm{i}(\omega-\omega_L-p\delta)\tau}\,. \tag{2.22}$$

Equation (2.22) gives the stationary part of the incoherent spectrum in terms of a two-dimensional array of functions. The most interesting feature of the spectrum is the appearance of resonances at harmonics of δ. This feature is not encountered for spectra of the radiation field emitted by a stationary system. Of course, the explicit form of the spectrum and its resonant structure depends crucially on the two-dimensional amplitudes. Once the amplitudes are known, the spectrum can be evaluated to any desired accuracy simply by performing the integration over τ. However, without further calculations two distinctly different types of spectra could be observed depending on whether the diagonal amplitudes are real or not. If the amplitudes are real, the spectrum will be symmetric about its line center, $\omega = \omega_L$. On the other hand, if the diagonal amplitudes are complex, the spectrum will be asymmetric and the imaginary parts of the amplitudes may lead to additional spectral lines or shifts of the harmonic resonances. Consequently, the spectrum can have quite different characteristics, which depend on the specific atomic system.

The method of the double Fourier decomposition, straightforward as it is, becomes cumbersome even in relatively simple problems because of the necessity of dealing with a two-dimensional array of functions. However, there is an equivalent alternative method of treating time dependence of two-time correlation functions, which in many cases is much easier to apply to the calculation of a stationary spectrum. This alternative method consists essentially in evaluating a stationary correlation function in terms of a single Fourier decomposition. For example, if the correlation function $Y(t, t+\tau)$, or its time evolution, depends only on the second argument $(t+\tau)$, we may expand $Y(t, t+\tau)$ into a Fourier series with respect to the time $t+\tau$ as

$$Y(t, t+\tau) = \sum_{p=-\infty}^{\infty} Y^{(p)}(\tau)\,\mathrm{e}^{\mathrm{i}p\delta(t+\tau)}\,. \tag{2.23}$$

Although this expansion differs from (2.20), we emphasize that (2.23) by itself is a perfectly valid mathematical expansion: unknown function Y can always be expressed in terms of a family of unknown functions $Y^{(p)}$. The procedure recognizes that we are actually interested only in the later (delay) time of the two-time correlation. The major advantage of using the decomposition (2.23) over (2.20) is that the real part of the Fourier transform of the stationary harmonic amplitude $Y^{(0)}$ gives

the stationary spectrum of the field emitted by the system described by the correlation function Y. This statement is readily verified by applying the above analysis to the correlation function appearing in (2.17). When the one-time expansion (2.23) is used in (2.17), and the integrals are expressed in terms of time t and time difference $\tau = t' - t$, we readily arrive at the following incoherent spectrum

$$S_{\rm in}(\boldsymbol{r},\omega) = \lim_{T\to\infty}\frac{1}{T}\sum_{n,m=1}^{N}\sum_{i,k>j,l}\Phi_{ijlk}^{nm}\mathrm{e}^{\mathrm{i}k_0\bar{\boldsymbol{r}}\cdot\boldsymbol{R}_{nm}}\sum_{p=-\infty}^{\infty}\int_0^T \mathrm{d}t\int_0^t \mathrm{d}\tau \times \langle \delta S_{ij}^n(t)\,\delta S_{lk}^m(t+\tau)\rangle^{(p)}\mathrm{e}^{\mathrm{i}p\delta(t+\tau)}\mathrm{e}^{\mathrm{i}(\omega-\omega_L)\tau}\,. \tag{2.24}$$

The incoherent spectrum we have found is determined by the Fourier amplitudes which are accompanied by t-dependent exponential factors oscillating at harmonics of δ. Because of these factors, when the integration over the long detection time is performed, the terms with $p \neq 0$ make a negligible contribution to the spectrum except of the term with $p = 0$, which remains constant as $t \to \infty$. Accordingly, we find directly from (2.24) that the long-time spectrum is determined essentially by the temporally stationary harmonic and reaches a stationary value given by

$$S_{\rm in}(\boldsymbol{r},\omega) = 2\mathrm{Re}\sum_{n,m=1}^{N}\sum_{i,k>j,l}\Phi_{ijlk}^{nm}\mathrm{e}^{\mathrm{i}k_0\bar{\boldsymbol{r}}\cdot\boldsymbol{R}_{nm}} \times \int_0^\infty \mathrm{d}\tau\,\langle \delta S_{ij}^n(0)\,\delta S_{lk}^m(\tau)\rangle^{(0)}\mathrm{e}^{\mathrm{i}(\omega-\omega_L)\tau}\,. \tag{2.25}$$

This simplified expression determines the stationary component of the incoherent spectrum of a quasistationary field emitted by an atomic system. It holds for an arbitrary quasistationary state of the system, and is applicable when the time dependence of the atomic correlation function can be expressed in terms of a single frequency parameter δ characterizing the system. Integrating (2.25) over all directions, we obtain the incoherent spectrum of the total radiation field per unit time

$$S_{\rm in}(\omega) = \int \mathrm{d}\Omega_{\boldsymbol{r}}\,S_{\rm in}(\boldsymbol{r},\omega) = 2\mathrm{Re}\sum_{n,m=1}^{N}\sum_{i,k>j,l}\sqrt{\gamma_{ij}\gamma_{kl}}\cos\theta_{ik} \times \int_0^\infty \mathrm{d}\tau\,\langle \delta S_{ij}^n(0)\,\delta S_{lk}^m(\tau)\rangle^{(0)}\mathrm{e}^{\mathrm{i}(\omega-\omega_L)\tau}\,. \tag{2.26}$$

The expression (2.26) will be extensively used in our study of spectral and quantum properties of the field emitted by quasistationary atomic systems. Although the parameter δ does not appear explicitly in the above expression for the stationary spectrum, it certainly will appear in explicit solutions for the time dependent harmonic of the atomic correlation function. As we shall see, the evaluation of the stationary harmonic requires the knowledge of the initial (stationary) values of the correlations, which are given in terms of single-time expectation values of the atomic operators.

They are obtained through another single Fourier decomposition, and then the resultant incoherent spectrum is to be thought of as a superposition of different harmonics of the single-time expectation values. The procedure just described and its applications for evaluation of incoherent spectra of radiation field emitted by specific atomic systems will be discussed in details in the next chapter.

To summarize, we have seen how one may simplify the calculations of incoherent spectra of the radiation field emitted by stationary and quasistationary systems without an explicit calculation of the two-time atomic correlation function. Problems involving stationary fields can be solved by straightforward application of the Fourier transform of the two-time correlation function of slowly varying parts of the atomic operators. In the case of quasistationary fields, the two-time correlation function is properly analyzed by a Fourier expansion, and there are two equivalent approaches available, which allow to study the spectrum analytically. For one, we employ a double Fourier decomposition taken with respect to the same variable characterizing the time dependence of a given system. In the second approach, the spectrum is obtained by employing a more direct approach, utilizing a single Fourier decomposition, which greatly simplifies the calculations. Once the time-dependence of the correlation function is known, it is only a matter of performing the integration over τ to derive the spectrum. It is worth noting, finally, that in general, when the problem involves quasistationary fields whose the time dependence is represented by several different parameters, it is not feasible to attempt a decomposition of the correlation function into a multi-dimensional Fourier series. The analytic description of such a problem is extremely difficult, it may result in multi-dimensional arrays of Fourier amplitudes. In this case, the time evolution is best analysed by numerical methods.

2.2 Absorption Spectrum of a Probe Field

In atomic and molecular spectroscopy one is frequently confronted with a situation in which, in addition to the power (emission) spectrum, changes in the absorption spectrum of a probe beam irradiating an atomic system are observed. The study of the absorption spectrum offers an opportunity for further tests of the role of quantum fluctuations in atomic spectroscopy.

The absorption spectrum is defined as the rate of energy absorption from the probe beam as a function of its frequency. As we shall see, it may be expressed quite generally in terms of a certain atomic correlation function, which is evaluated in the absence of the probe beam. This results from the weak field approximation, in which the probe intensity is assumed to be sufficiently weak that it does not appreciably perturb the atomic system. In addition to weak probe absorption spectra, one can also calculate absorption spectra for a strong probe beam. These spectra are termed "strong probe spectra" and may be significantly different from the spectra obtained with weak probe. However, one may be confused by the use of a strong probe to monitor an atomic system. This requires a word of explanation. If an intense field is used to probe an atomic system, one can argue that what we would normally call

'strong probe' is in fact a contradiction in terms. To put it another way, a strong probe can be viewed as a driving field for the atomic system. In this case, the system should be probed by another weak field. Then, we expect to see qualitatively different properties of the absorption spectrum from those observed in the absence of the strong probe field.

Let us proceed to a more detailed discussion of the procedure of evaluating the absorption spectrum. We stress that there are various ways to evaluate the spectrum. They arise from different experimental arrangements to observe absorptive properties of an atomic system. The method of calculation, we explore in this section, is based on the approach proposed by Mollow [2, 3] although our treatment is more general in some respects. It is appropriate for experiments where the intensity of the radiation field emitted from an atomic system is measured separately in the presence and in the absence of the probe beam. The difference between the two intensities measured as a function of the probe frequency represents the net of absorption at this frequency.

Following closely the approach of Mollow, we may describe the absorption spectrum of a probe beam by first determining the change it produces in the evolution of a probed system. Suppose that an atomic system, described by the total dipole operator $\hat{\boldsymbol{\mu}}$, is monitored by a weak single-mode classical field of a tunable frequency ω_p. If coupling of the atomic system to all other modes of the electromagnetic field is neglected, the interaction between the probe beam and the atomic system, in the electric dipole and rotating-wave approximations, is given by the Hamiltonian

$$\hat{H}(t) = \sum_n -\hat{\boldsymbol{\mu}}^n \cdot \boldsymbol{E}_p(\boldsymbol{R}_n, t) = -\mathrm{i}\hbar \sum_n \sum_{i>j} g_{ij}^n(\boldsymbol{R}_n, t)\hat{\Lambda}_{ij}^n(t) + \mathrm{H.c.}\,, \quad (2.27)$$

where we have used the projection operator representation for the total dipole operator and the mode representation for the probe beam. In (2.27), the atoms are treated as quantum systems represented by the transition operators $\hat{\Lambda}_{ij}^n(t)$, whereas the probe beam is treated as a single-mode classical field of the amplitude

$$\begin{aligned}\boldsymbol{\mathcal{E}}_p(\boldsymbol{r}, t) &= \sqrt{\frac{\hbar\omega_p}{2\varepsilon_0 \mathcal{V}}}\alpha_p \bar{\boldsymbol{e}}_p \mathrm{e}^{\mathrm{i}(\boldsymbol{k}_p\cdot\boldsymbol{r}-\omega_p t)} \\ &= \mathcal{E}_p \bar{\boldsymbol{e}}_p \mathrm{e}^{\mathrm{i}(\boldsymbol{k}_p\cdot\boldsymbol{r}-\omega_p t)}\,, \end{aligned} \quad (2.28)$$

and the coupling constant between the atoms and the field is given in terms of the matrix elements of the atomic transition dipole moments

$$g_{ij}^n(\boldsymbol{R}_n, t) = \hat{\boldsymbol{\mu}}_{ij}^n \cdot \boldsymbol{\mathcal{E}}_p(\boldsymbol{R}_n, t)/\hbar\,. \quad (2.29)$$

Here, α_p is the complex mode amplitude, $\bar{\boldsymbol{e}}_p$ is the unit polarization vector of the probe field mode, and $\hat{\boldsymbol{\mu}}_{ij}^n$ is an atomic transition dipole moment interacting with the probe field. Finally, $\boldsymbol{k}_p$ represents the propagation vector of the field. We point out here, that the probe field is assumed to be tuned near atomic resonances, in the sense that the detunings of the probe field are small compared to optical frequencies,

($|\omega_{ij} - \omega_p| \ll \omega_p$). Moreover, the choice of the classical description for the probe field has an advantage that it corresponds closely to a typical experimental situation in which atoms are probed by a coherent laser field.

With the coupling Hamiltonian (2.27), we are able to study the influence of a probe beam on the dynamics of the atomic system. It is conveniently studied in terms of the density operator describing the system, which obeys the Liouville−von Neumann equation

$$\mathrm{i}\hbar\frac{\partial\varrho(t)}{\partial t} = \left[\hat{H}(t),\, \varrho(t)\right] . \tag{2.30}$$

Formally integrating (2.30) with respect to a measurable time interval, we find that to the lowest order in the probe beam amplitude the interaction (2.27) changes the density operator of the system by

$$\Delta\varrho(t) = \frac{1}{\mathrm{i}\hbar}\int_{-\infty}^{t} \mathrm{d}t' \left[\hat{H}(t'),\, \varrho(t)\right] , \tag{2.31}$$

where we have applied the Markov approximation in which we have replaced $\varrho(t')$ by $\varrho(t)$ under the integral. This is a reasonable approximation for our purposes here, since we look at the response of the system to a weak probe field. For this case, the probe absorption spectrum is determined by the rate at which the system changes linearly under the influence of the probe field [4]. It involves a trace of the time derivative of the interaction Hamiltonian over the internal states of the probed system

$$\begin{aligned} A\left(\omega_p, t\right) &= \mathrm{Tr}\left[\frac{\partial\hat{H}(t)}{\partial t}\Delta\varrho(t)\right] \\ &= \frac{1}{\mathrm{i}\hbar}\int_{-\infty}^{t} \mathrm{d}t' \mathrm{Tr}\left\{\left[\frac{\partial\hat{H}(t)}{\partial t}, \hat{H}(t')\right]\varrho(t)\right\} . \end{aligned} \tag{2.32}$$

When the Hamiltonian (2.27) and its partial time derivative are used in (2.32), it is straightforward to show that in the long time limit the absorption spectrum of the weak field is given by the Fourier transform of the two-time commutator of the atomic dipole operators

$$\begin{aligned} A\left(\omega_p\right) = \lim_{t\to\infty} A\left(\omega_p, t\right) = \sum_{n,m=1}^{N}\sum_{i>j}\sum_{k>l}(\hat{\boldsymbol{\mu}}_{ij}^{n}\cdot\tilde{\boldsymbol{\mathcal{E}}}_p)(\hat{\boldsymbol{\mu}}_{kl}^{m}\cdot\tilde{\boldsymbol{\mathcal{E}}}_p)^* \\ \times\int_{-\infty}^{\infty}\mathrm{d}\tau\langle[\hat{\Lambda}_{ji}^{n},\, \hat{\Lambda}_{kl}^{m}(\tau)]\rangle \mathrm{e}^{\mathrm{i}\boldsymbol{k}_p\cdot\boldsymbol{R}_{nm}}\mathrm{e}^{\mathrm{i}\omega_p\tau} , \end{aligned} \tag{2.33}$$

where, as usual, $\boldsymbol{R}_{nm} = \boldsymbol{R}_n - \boldsymbol{R}_m$ is the vector distance between two atoms in the sample, and $\tilde{\boldsymbol{\mathcal{E}}}_p = (2\omega_p\mathcal{E}_p/\hbar)\tilde{\boldsymbol{e}}_p$. In the derivation of (2.33), we have retained

only the slowly varying terms oscillating with the time difference $\tau = t - t'$ at the probe frequency ω_p. This simplification is obviously a form of the rotating-wave approximation, and for our purposes of a long-time absorption spectrum this is an excellent approximation.

The derivation of the absorption spectrum (2.33) has been kept very general in order to make it applicable to any system probed by a weak field. It is given in terms of a certain two-time atomic correlation function, which is quite different in form than the one which determines the power spectrum for the same system. The correlation function reflects absorptive as well as emissive processes which may take place when the system is probed by a weak field. Mathematically, the absorption spectrum is found by first calculating the expectation value of the commutator, and then taking the Fourier transform of the commutator with respect to τ. It is usually done using the master equation of the atomic system together with the quantum regression theorem. Note that the commutator is evaluated in the absence of the probe field, but the other fields such as the vacuum field and driving fields interacting with the atomic system are always present. The probe and driving fields can be tuned to the same atomic transitions, or alternatively, the probe can be tuned to an auxiliary level. In the first case a Mollow type, whereas in the second case an Autler–Townes type spectrum is monitored.

We recall that the expectation value of the commutator, appearing in (2.33), has an important interpretation in terms of directly measurable quantities. By definition, the commutator may be decomposed into two terms, and consequently we can write

$$\langle [\hat{\Lambda}^n_{ji}, \hat{\Lambda}^m_{kl}(\tau)] \rangle = \langle \hat{\Lambda}^n_{ji} \hat{\Lambda}^m_{kl}(\tau) \rangle - \langle \hat{\Lambda}^m_{kl}(\tau) \hat{\Lambda}^n_{ji} \rangle = A_1 - A_2 \,. \tag{2.34}$$

The physical interpretation of the two terms on the right-hand side of (2.34) is as follows: The first term represents processes corresponding to absorption of the probe field by the atomic system. The second term is attributed to emissive processes corresponding to the stimulated emission into the probe field. The difference of these two terms yields the net absorption of the probe field, which is not necessarily positive. Indeed, when we combine the two terms, the resulting expectation value of the commutator may be positive, equal to zero, or negative. Physically, in the case of $A_1 > A_2$, the total number of absorption processes outweighs the total number of stimulated emission processes resulting in a positive absorption spectrum. Consequently, the probe field is absorbed by the system. In the case of $A_1 = A_2$, the number of absorption is equal to the number of stimulated emission processes resulting in zero net absorption of the probe field. For such a case one speaks of transparency of the system to the probe field. Finally, in the case of $A_1 < A_2$, the stimulated emission outweighs the absorption. Consequently, the absorption becomes negative, i.e. instead of being absorbed the probe field is amplified.

Amplification of a probe field usually requires an inversion of the atomic population on the probed atomic transition, but an amplification without population inversion is also possible. The later, however, requires more than two energy levels to be involved, or equivalently, at least two transition channels simultaneously monitored by the probe field. In this case, an amplification can be achieved through coherences

between the atomic levels which is traditionally understood as quantum interference between various transition channels in the probed system. If only two energy levels are involved, or equivalently the probe field is coupled to a single transition channel, such interference is impossible.

The role of population inversion and interference in the absorption process is seen more explicitly in the integrated absorption spectrum. When we integrate the absorption spectrum over all frequencies, we obtain the total absorption rate

$$\bar{A} = \int_{-\infty}^{\infty} \mathrm{d}\omega_p A\left(\omega_p\right) = 2\pi \sum_{n,m=1}^{N} \sum_{i>j} \sum_{k>l} (\hat{\boldsymbol{\mu}}_{ij}^{n} \cdot \tilde{\boldsymbol{\mathcal{E}}}_p)(\hat{\boldsymbol{\mu}}_{kl}^{m} \cdot \tilde{\boldsymbol{\mathcal{E}}}_p)^* \times (\langle \hat{\Lambda}_{ji}^{n} \hat{\Lambda}_{kl}^{m} \rangle - \langle \hat{\Lambda}_{kl}^{m} \hat{\Lambda}_{ji}^{n} \rangle) \mathrm{e}^{\mathrm{i}\boldsymbol{k}_p \cdot \boldsymbol{R}_{nm}} . \tag{2.35}$$

If we separate the atomic correlation functions into single-atom and multiatom contributions, and further distinguish between populations and coherences in the single-atom terms, we arrive at the expression

$$\begin{aligned} \bar{A}/2\pi = \sum_{n=1}^{N} \Bigg\{ & \sum_{i>j} |\hat{\boldsymbol{\mu}}_{ij}^{n} \cdot \tilde{\boldsymbol{\mathcal{E}}}_p|^2 (\langle \hat{\Lambda}_{jj}^{n} \rangle - \langle \hat{\Lambda}_{ii}^{n} \rangle) \\ & + \sum_{i>j} \sum_{j \neq l} (\hat{\boldsymbol{\mu}}_{ij}^{n} \cdot \tilde{\boldsymbol{\mathcal{E}}}_p)(\hat{\boldsymbol{\mu}}_{jl}^{n} \cdot \tilde{\boldsymbol{\mathcal{E}}}_p)^* (\langle \hat{\Lambda}_{ji}^{n} \hat{\Lambda}_{il}^{n} \rangle - \langle \hat{\Lambda}_{lj}^{n} \hat{\Lambda}_{ji}^{n} \rangle) \Bigg\} \\ & + \sum_{n \neq m=1}^{N} \sum_{i>j} \sum_{k>l} (\hat{\boldsymbol{\mu}}_{ij}^{n} \cdot \tilde{\boldsymbol{\mathcal{E}}}_p)(\hat{\boldsymbol{\mu}}_{kl}^{m} \cdot \tilde{\boldsymbol{\mathcal{E}}}_p)^* \\ & \times (\langle \hat{\Lambda}_{ji}^{n} \hat{\Lambda}_{kl}^{m} \rangle - \langle \hat{\Lambda}_{kl}^{m} \hat{\Lambda}_{ji}^{n} \rangle) \mathrm{e}^{\mathrm{i}\boldsymbol{k}_p \cdot \boldsymbol{R}_{nm}} . \end{aligned} \tag{2.36}$$

From the above expression, we see that the total absorption rate depends crucially on the population distribution and the coherences between the atomic levels. The first term is the contribution resulting from the difference between populations of the lower and upper levels in a given transition. The second term, proportional to the coherences between various atomic transitions, corresponds to absorption induced by quantum interference between the transitions. The final term is the multiatom contribution to the absorption. This arises from the collective interaction between the atoms.

It is apparent from (2.36) that an inequality of the populations gives rise to a net, positive or negative, absorption of the probe field. The negative absorption is understood physically as an amplification of the probe field. Thus, a population inversion ($\langle \hat{\Lambda}_{ii}^{n} \rangle > \langle \hat{\Lambda}_{jj}^{n} \rangle$) leads to the probe amplification on the $|i_n\rangle \longleftrightarrow |j_n\rangle$ transition. This is an example of amplification with population inversion. The contribution of the second term in (2.36), proportional to the difference between atomic coherences, may lead to a negative absorption rate even if the first term is positive (no population inversion). Since there is no population inversion between the upper and lower energy

levels, one obtains amplification without population inversion. We should note that the amplification with population inversion can be obtained on a single two-level transition with a negative population difference. However, the amplification without population inversion is unique to multi-level transitions and is observed when more than two energy levels are involved and nonzero coherences exist between the atomic levels. One can see from (2.36) that in order to have a significant amplification without population inversion, it is necessary for the populations to be nearly equal and the difference of the multi-level coherences to be large and negative.

Referring to the role of quantum fluctuations in the process of probe absorption, we stress that in the case of amplification with population inversion, it is spontaneous emission which imposes a serious restriction in creating an inversion between atomic levels. For example, in a single two-level system with ground state $|j_n\rangle$ and excited state $|i_n\rangle$, the stationary absorptive and emissive processes are governed by the balance condition

$$P_j \gamma_{ji} = P_i \gamma_{ij} \,, \tag{2.37}$$

where $P_j = \langle \hat{\Lambda}^n_{jj} \rangle$ and $P_i = \langle \hat{\Lambda}^n_{ii} \rangle$ are the steady-state populations of the ground and excited states, respectively. The parameter γ_{ji} is the absorptive and γ_{ij} is the emissive rate between the two energy states. It follows from (2.37) that inversion ($P_i > P_j$) can be produced only if $\gamma_{ji} > \gamma_{ij}$. This condition may not be achieved in two-level systems since the stimulated absorptive and emissive rates are the same and spontaneous emission contributes only to the emissive rate, giving $\gamma_{ij} > \gamma_{ji}$. population inversions involving the ground level can, however, be produced in multilevel systems where population can be transferred into level $|i_n\rangle$ through other channels (levels). If we introduce a third level $|k_n\rangle$ which has its absorptive rate γ_{jk} from the ground level and the spontaneous rate γ_{ki} to the excited level much larger than the emissive rate γ_{ij}, a pumping field applied to the $|j_n\rangle - |k_n\rangle$ transition will create a steady-state inversion on the $|i_n\rangle - |j_n\rangle$ transition. Using rate equations for the atomic populations, the ratio P_i/P_j of the steady-state populations of the excited and ground states can be expressed as

$$\frac{P_i}{P_j} = \frac{\gamma_{ki}\,\gamma_{jk}}{\gamma_{ij}\left(\gamma_{ki} + \gamma_{kj}\right)} \,. \tag{2.38}$$

It is seen that the ratio (2.38) depends crucially on the spontaneous emission rate γ_{ij} which depopulates the upper state $|i_n\rangle$. Maximum inversion, with $P_i = 1$ and $P_j = 0$, is obtained for $\gamma_{ij} = 0$, when the population is said to be 'shelved' (trapped) in the state $|i_n\rangle$ from which it cannot decay to the lower state. Thus, in the case of maximum inversion one could expect maximum amplification of a probe field on the $|i_n\rangle - |j_n\rangle$ transition. However, there is another factor which can affect the magnitude of amplification of the probe field. Namely, the dipole moment of the transition, which determines the coupling strength of the probe field to the atom, must be nonzero. According to the balance condition (2.37), an increase of the population inversion can

be achieved by decreasing the emissive rate and the population can be completely inverted only if $\gamma_{ij} = 0$, that is, only if the state $|i_n\rangle$ is a trapping state. Since $\gamma_{ij} \sim |\boldsymbol{\mu}_{ij}|^2$, the trapping results in the cancellation of the dipole moment of the probed transition, and then the inverted transition becomes transparent for the probe field. Therefore, in order to obtain a significant amplification one should produce a large population inversion and simultaneously maintain a strong coupling of the probe field to the inverted transition.

Equation (2.33) applies to the situation of a stationary system in which the commutator depends only on the time difference, and not on t. For a quasistationary system, when commutator depends on t, the treatment may follow the methods we used previously in Sect. 2.1.2 to evaluate the power spectrum. Briefly, if the commutator depends on t, we may first make a harmonic decomposition of the expectation value of the two-time commutator. Next, we substitute the decomposition into the time-dependent spectrum (2.32), and describe the correlation function in terms of the Fourier harmonics of the dipole correlation functions. Calculation of the absorption spectrum then follows exactly the approach that was illustrated in Sect. 2.1.2.

In the foregoing treatment of the absorption spectrum, we have confined our attention to the Mollow's approach in which a probed system is treated as a multi-level quantum system. There is, however, an alternative method of calculating the absorption spectrum in which the atomic system is treated as a homogeneous medium characterized by a (complex) susceptibility χ. The absorption spectrum is then calculated by taking an imaginary part of χ. This method is useful to study spatial propagation effects rather than temporal spectroscopic effects. A complete discussion of the method is out of the scope of this book, and we refer the interested reader to the text by Meystre and Sargent [5] for the complete account of the method.

2.3 Phase-Dependent Spectra and Their Measurements

We have seen that the emission spectrum measures the relative number of photons emitted by a system into vacuum field modes as a function of the spectral frequency of these modes. The absorption spectrum on the other hand measures the relative number of photons absorbed by a system from a probe field as a function of the probe field frequency. It should be noted that the definitions of the emission and absorption spectra involve number of photons which can be measured by direct photocounting techniques.

Additional characterization of the EM field can be found by measuring the amplitude of the field. However, the electric field amplitude is not easy to measure by a direct detection since it is a complex quantity that oscillates at an optical frequency, too fast to be detected by any macroscopic device. It is usually a slowly varying (real) quadrature amplitude of the field and the spectrum of the field-quadrature fluctuations which are measured. The physical quantities that display the field-quadrature fluctuations are Hermitian quadrature components of the electric field operator, which

are specified by a phase θ, an angular frequency ω_c and a wave-vector $\boldsymbol{k}$. They are defined in terms of the positive and negative frequency components of the EM field as

$$\begin{aligned}\hat{E}_\theta(\boldsymbol{r},t) &= \hat{E}^{(+)}(\boldsymbol{r},t)\,\mathrm{e}^{\mathrm{i}\xi} + \hat{E}^{(-)}(\boldsymbol{r},t)\,\mathrm{e}^{-\mathrm{i}\xi}\,,\\ \hat{E}_{\theta+\pi/2}(\boldsymbol{r},t) &= \mathrm{i}\left(\hat{E}^{(+)}(\boldsymbol{r},t)\,\mathrm{e}^{\mathrm{i}\xi} - \hat{E}^{(-)}(\boldsymbol{r},t)\,\mathrm{e}^{-\mathrm{i}\xi}\right)\,,\end{aligned} \tag{2.39}$$

where we have introduced the oscillatory factor

$$\xi = \omega_c t - \boldsymbol{k}\cdot\boldsymbol{r} + \theta \tag{2.40}$$

to make the quadrature components relatively slowly varying functions of time. The phase angle θ may be chosen arbitrary and the quadrature component $\hat{E}_\theta(\boldsymbol{r},t)$ is in phase with θ, whereas $\hat{E}_{\theta+\pi/2}(\boldsymbol{r},t)$ is $\pi/2$ out of phase. Thus, the component $\hat{E}_{\theta+\pi/2}(\boldsymbol{r},t)$ can be obtained from $\hat{E}_\theta(\boldsymbol{r},t)$ by incrementing the phase θ by $\pi/2$. Furthermore, according to (2.39) and (1.5), the electric field operator can be written in terms of the quadrature components as

$$\begin{aligned}\hat{E}(\boldsymbol{r},t) = {}& \hat{E}_\theta(\boldsymbol{r},t)\cos(\omega t - \boldsymbol{k}\cdot\boldsymbol{r} + \theta)\\ &+ \hat{E}_{\theta+\pi/2}(\boldsymbol{r},t)\sin(\omega t - \boldsymbol{k}\cdot\boldsymbol{r} + \theta)\,.\end{aligned} \tag{2.41}$$

This expression shows that the electric field can always be written as a sum of two slowly varying quadrature components oscillating $\pi/2$ out of phase.

The quadrature components do not commute. If, for simplicity, we assume that the detector measures a single polarization component of the field, we find from (2.39) and (1.7) that the quadrature components satisfy the commutation relation

$$\left[\hat{E}_\theta(\boldsymbol{r},t)\,,\,\hat{E}_{\theta+\pi/2}(\boldsymbol{r},t)\right] = 2\mathrm{i}C\,, \tag{2.42}$$

which is a particularly simple relation showing that the quadrature components behave as canonically conjugate variables, and

$$C = \sum_{\boldsymbol{k}} \frac{\hbar\omega_{\boldsymbol{k}}}{2\varepsilon_0 \mathcal{V}} \tag{2.43}$$

is a real positive number called the quantum (shot-noise) level or the standard quantum limit of the electric field fluctuations. In what follows, we will not consider the spatial effects, so we will suppress the position variable $\boldsymbol{r}$.

In terms of the detection theory, the commutation relation (2.42) implies that a simultaneous precise measurement of the two quadrature components is not possible, and from the standard quantum theory, a Heisenberg uncertainty principle applies to the quantum fluctuations in the quadrature components

$$\langle[\Delta\hat{E}_\theta(t)]^2\rangle\langle[\Delta\hat{E}_{\theta+\pi/2}(t)]^2\rangle \geq C^2 , \tag{2.44}$$

where $\Delta\hat{E}_\theta(t) = \hat{E}_\theta(t) - \langle\hat{E}_\theta(t)\rangle$ is the fluctuation operator and the expectation value is taken over an arbitrary state of the field. The relation (2.44) means that the reduction in the fluctuations of one of the quadrature components occurs at the expense of increased fluctuations in the other component.

The variances $\langle[\Delta\hat{E}_\theta(t)]^2\rangle$ and $\langle[\Delta\hat{E}_{\theta+\pi/2}(t)]^2\rangle$ depend on the state of the field, and therefore could serve as distinguishing criteria for different states of the field. To see this, consider possible values of the variances for three different states of the field.

If, for instance, the field is in a chaotic (thermal) state, the fluctuations in both components are large such that

$$\langle[\Delta\hat{E}_\theta(t)]^2\rangle \geq C \qquad \text{and} \qquad \langle[\Delta\hat{E}_{\theta+\pi/2}(t)]^2\rangle \geq C . \tag{2.45}$$

Thus, variances of both quadrature components of a thermal field exceed the standard quantum limit of the electric field fluctuations.

In the case of the vacuum or a coherent state, the fluctuations are independent of θ, as there is no phase reference in the vacuum, and then the variances are equal to the standard quantum limit

$$\langle[\Delta\hat{E}_\theta(t)]^2\rangle = \langle[\Delta\hat{E}_{\theta+\pi/2}(t)]^2\rangle = C . \tag{2.46}$$

This relation expresses the fact that the fluctuations are equally distributed in the two quadrature components. Moreover, the product of the two variances equals the minimum possible value indicating that the vacuum (coherent) state is a minimum uncertainty state.

We may proceed further and introduce the idea of special states of the field for which fluctuations in one of the quadrature components may be reduced below the standard quantum limit of the field fluctuations [6–8]. These special states are called *squeezed states* of the field, and are determined by the requirement that either

$$\langle[\Delta\hat{E}_\theta(t)]^2\rangle < C \qquad \text{or} \qquad \langle[\Delta\hat{E}_{\theta+\pi/2}(t)]^2\rangle < C . \tag{2.47}$$

With the help of the commutator (1.7), the variances of the quadrature components can be written as

$$\begin{aligned}\langle[\Delta\hat{E}_\theta(t)]^2\rangle &= C + \langle: [\Delta\hat{E}_\theta(t)]^2 :\rangle ,\\ \langle[\Delta\hat{E}_{\theta+\pi/2}(t)]^2\rangle &= C + \langle: [\Delta\hat{E}_{\theta+\pi/2}(t)]^2 :\rangle ,\end{aligned} \tag{2.48}$$

where the colons denote normal ordering of the operators. In the vacuum or a coherent state of the field $\langle: [\Delta\hat{E}_\theta(t)]^2 :\rangle = \langle: [\Delta\hat{E}_{\theta+\pi/2}(t)]^2 :\rangle = 0$, independent of θ. Hence, we have an equivalent condition for squeezing

$$\langle : [\Delta \hat{E}_\theta (t)]^2 : \rangle < 0 \qquad \text{or} \qquad \langle : [\Delta \hat{E}_{\theta+\pi/2} (t)]^2 : \rangle < 0 \, . \tag{2.49}$$

It is apparent that a squeezed field has a negative normally ordered variance in one of its quadratures. We shall call this as squeezing in the full sense, because it involves reduction of the fluctuations of the total field.

Note that it is fully consistent with quantum mechanics to shift fluctuations from one of the quadratures to its conjugate. Needless to say, both quadrature variances cannot fall below the quantum limit and beating the the standard quantum limit in this way in $\langle [\Delta \hat{E}_\theta (t)]^2 \rangle$ is achieved at the expense of a corresponding increase in the fluctuations of the other quadrature $\langle [\Delta \hat{E}_{\theta+\pi/2} (t)]^2 \rangle$, for which in view of the inequality (2.44) we must have

$$\langle [\Delta \hat{E}_{\theta+\pi/2} (t)]^2 \rangle > C \, . \tag{2.50}$$

The distribution of the fluctuations among the quadrature components must be such that the product of the variances equals to or is larger than C. Thus, in a squeezed state, the increase of the variance $\langle [\Delta \hat{E}_{\theta+\pi/2} (t)]^2 \rangle$ may exceed the reduction of the variance $\langle [\Delta \hat{E}_\theta (t)]^2 \rangle$. In some cases, however, the field may be in a squeezed state for which the product of the variances is equal to C. Such a state is called the minimum uncertainty squeezed state. Obviously, minimum uncertainty squeezed states are only a subset of a much broader class of squeezed states.

In practice, the usual way to determine fluctuations of the quadrature components of an electric field is to test the criteria (2.45)−(2.49), to which we shall refer as measures of the total field fluctuations. We stress that these measures do not provide the complete information about fluctuations of the field which is measured. For example, for multi-mode fields it is possible for some selected frequencies to exhibit reduced fluctuations or larger fluctuations than that in the total field, which is the integral of the spectral distribution over all frequencies. For this form of fluctuations we shall refer to as spectral component fluctuations and will discuss them in the next section by introducing the concept of phase-dependent noise spectra.

2.4 Homodyne Detection of Quantum Fluctuations

The quadrature components depend on phase. This of course immediately brings up the question how to measure the phase-dependent quadrature components. As we have seen, direct photon counting techniques are not sensitive to the phase of a detected EM field, but only to the field intensity. Therefore, these techniques as a way of detecting phase sensitive quadrature components are impractical. Hence, some alternative techniques are necessary for the measurement of the quadrature components [9, 10]. Typical experimental schemes where phase-dependent fields and their fluctuations are effectively measured are homodyne and heterodyne detection techniques. Homodyning or heterodyning reduces the measurement of a rapidly

oscillating field to the measurement of slowly varying intensities. In the case of optical fields, homodyning or heterodyning is accomplished by adding a strong coherent field to the signal field that is to be measured, and the fluctuations of the superposed field either in photoelectric counting or in photocurrent spectral measurements are detected. The strong coherent field, commonly called the local oscillator, is strictly monochromatic and ideally has a stable amplitude and phase. When the local oscillator frequency is equal to the central frequency of the signal field, we refer to the technique as homodyne detection, and when is different, we refer to as heterodyne detection. The local oscillator provides a controllable fixed phase relative to the signal field that allows to distinguish between the quadrature components of the signal field. The linear superposition of the two fields is achieved using a lossless beam-splitter with the transmissivity very nearly equal unity, so that the signal field is transmitted with a minimal attenuation. As a result, the superposed field emerging from the beam splitter is almost the original signal field together with the much attenuated local oscillator field. What is measured by a detector is the photon count or the photocurrent spectrum of the superposed field as a function of the relative phase difference between the signal field amplitude and the local oscillator amplitude, from which the quadrature components or fluctuations in the quadrature components can be deducted.

A typical homodyne detection scheme is shown in Fig. 2.1. A signal field of an amplitude $\hat{E}_s$ is mixed (beat) at a beam splitter BS with the strong coherent light of a local oscillator field E_{LO} usually derived from an intense, narrow-band laser. In practical realizations of this detection scheme it is necessary to lock the phases of the local oscillator to that of the signal field, and the local oscillator frequency must be equal to the signal field frequency to an accuracy defined by the detection bandwidth. The superposed field E_H (homodyne field) is detected by a detector D placed in one of the outputs of the beam splitter. The resulting photocurrent $i(t)$ is temporary integrated and analyzed by a photoelectron counter C. In this scheme, the

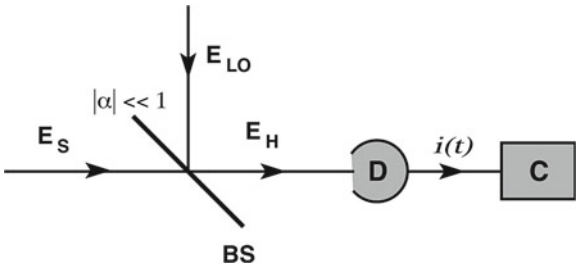

Fig. 2.1 Schematic of a homodyne experiment for detecting phase-dependent quadrature components of the EM field. A signal field E_s is superposed with the local oscillator E_{LO} at a beam splitter BS. The transmissivity of the beam splitter is close to unity, while its reflectivity is very small, $|\alpha| \ll 1$. The superposed field E_H is registered by a detector D and analyzed by a photoelectron counter C. A spectrum analyzer is used instead of the photoelectron counter to detect phase-dependent power spectra of the fluctuations in the selected quadrature of the signal field

beam splitter transmissivity $|\beta|$ is nearly unity while its reflectivity $|\alpha|$ is very small, so that the signal field is transmitted essentially unattenuated. The amplitude of the local oscillator field is kept strong enough that even after a significant attenuation by the beam splitter it still dominates the signal field at the detector.

Let us illustrate the theoretical description of the phase dependence in a homodyne detection scheme, in which a signal field $\hat{E}_s$ is mixed by a beam splitter with a coherent light of a strong local oscillator of the same polarization and angular frequency ω_c, whose phase θ_c can be varied. We will treat the strong local oscillator field classically, even after the much attenuation at the beam splitter, while the signal field amplitude $\hat{E}_s$ will be treated fully quantum-mechanically as an operator. There is only one output field from the beam splitter, the combined (homodyne) field, whose single polarization negative and positive frequency components are given by

$$\begin{aligned} \hat{E}_H^{(-)}(t) &= \alpha E_{LO}^{(-)}(t) + \beta \hat{E}_s^{(-)}(t) \ , \\ \hat{E}_H^{(+)}(t) &= \alpha^* E_{LO}^{(+)}(t) + \beta^* \hat{E}_s^{(+)}(t) \ , \end{aligned} \tag{2.51}$$

where α and β is a complex reflectivity and transmissivity of the beamsplitter satisfying the relations

$$|\alpha|^2 + |\beta|^2 = 1 \ , \qquad \text{and} \qquad \beta\alpha^* + \alpha\beta^* = 0 \ . \tag{2.52}$$

The combined field falls on a photodetector which measures the intensity of the homodyne field, determined by the operator

$$\hat{I}_H(t) = \hat{\boldsymbol{E}}_H^{(-)}(t) \cdot \hat{\boldsymbol{E}}_H^{(+)}(t) \ . \tag{2.53}$$

If we make use of (2.51) for $\hat{E}_H^{(\pm)}(t)$, which assumes that the photodetector measures a single polarization component, we find that the intensity of the homodyne field becomes

$$\begin{aligned} \hat{I}_H(t) = \Big[&|\beta|^2 \, |\hat{E}_s(t)|^2 + |\alpha|^2 \, |\mathcal{E}|^2 \\ &+ |\alpha\beta| \, |\mathcal{E}| \left(\hat{E}_\theta(t) \cos\Phi + \hat{E}_{\theta+\pi/2}(t) \sin\Phi \right) \Big] \ , \end{aligned} \tag{2.54}$$

where $\Phi = \phi + \theta_c - \theta$ is the relative phase difference between the quadrature component and the local oscillator phase θ_c. We have explicitly introduced a constant phase shift ϕ associated with a possible phase change at the beam splitter, $\phi = \arg(\alpha) - \arg(\beta)$, and the phase of the local field has been introduced by writing the positive and negative frequency parts as

$$E_{LO}^{(\pm)}(t) = |\mathcal{E}| \mathrm{e}^{\mp \mathrm{i}(\omega_c t + \theta_c)} \ , \tag{2.55}$$

to show that the intensity of the homodyne field can be made to change with the phase of the local oscillator. The quadrature $\hat{E}_\theta(t)$ is in phase with the local oscillator,

while the amplitude $\hat{E}_{\theta+\pi/2}(t)$ is 90° out of phase, and can be obtained from $\hat{E}_\theta(t)$ by incrementing the phase θ_c by $\pi/2$. An examination of (2.54) shows that the dominant signal field contribution to the intensity of the homodyne field arises from the interference term $|\mathcal{E}|\,\hat{E}_\theta(t)$. This is precisely this interference term that contains quadratures of the signal field and their dependence upon the phase of the local oscillator. Thus, the phase Φ is an important parameter which reflects the phase-dependent signature of the fluctuations of the signal field and determines the measured quadrature component.

Since $|\alpha||\mathcal{E}| \gg |\beta||\langle\hat{E}_s\rangle|$, the first term in (2.54) can be discarded and assuming that the correlation functions involving the local oscillator and the signal field may be factored, we find for the average number of photoelectrons produced by the homodyne field

$$\langle m(t,T)\rangle = 2\varepsilon_0 c\lambda T\langle\hat{I}_H(t)\rangle = \mathcal{U}_T\left[|\alpha|^2|\mathcal{E}|^2 + |\alpha\beta|\,|\mathcal{E}|\left(\langle\hat{E}_\theta(t)\rangle\cos\Phi + \langle\hat{E}_{\theta+\pi/2}(t)\rangle\sin\Phi\right)\right], \quad (2.56)$$

where $\mathcal{U}_T = 2\varepsilon_0 c\lambda T$ is the accumulation of the parameters characteristic of the detection process. Equation (2.56) shows that the measured average number of photoelectrons is a weighted combination of the two quadrature components of the signal field. As the phase Φ is varied, the measured quadrature component changes from the in-phase ($\Phi = 0$) to the out-of-phase ($\Phi = \pi/2$) component. We should notice that the detection of a quadrature component is accompanied by a large coherent component to the measured intensity. This is associated with the local oscillator field reflected by the beam splitter and incident on the detector. It cannot be completely eliminated because the reflectivity of the beam splitter can never be zero.

We have just seen how the average intensity of the measured homodyne field provides a measurement of a quadrature component of the signal field. We now turn to the issue of fluctuations of the signal field and will illustrate the concept of measuring the fluctuations of the field amplitude in the homodyne detection scheme. In general, fluctuations of the field amplitude can be found by measuring the variance of the number of photoelectric counts detected in some time interval T. According to (1.40), the variance of the photoelectric counts carries information about the fluctuations of the detected field intensity. If the photoelectric counting experiment is performed on the homodyne field, then the variance of photoelectric counts in a short detection time T is given by

$$\langle[\Delta m(t,T)]^2\rangle = \mathcal{U}_T\langle\hat{I}_H(t)\rangle + \mathcal{U}_T^2\left[\langle\hat{E}_H^{(-)}(t)\,\hat{E}_H^{(-)}(t)\,\hat{E}_H^{(+)}(t)\,\hat{E}_H^{(+)}(t)\rangle - \langle\hat{E}_H^{(-)}(t)\,\hat{E}_H^{(+)}(t)\rangle^2\right]. \quad (2.57)$$

This relation shows explicitly that in general the contribution of the radiation field fluctuations to the photocurrent fluctuations is provided by the fourth-order correlation function of the homodyne field amplitudes.

We may readily relate the variance of photoelectric counts to the normally ordered variance of the quadrature components $\hat{E}_\theta(t)$ and $\hat{E}_{\theta+\pi/2}(t)$ of the signal field. It is done by substituting (2.54) for $\hat{I}_H(t)$ and (2.51) for $\hat{E}_H^{(\pm)}(t)$ and neglecting all terms of order $|\mathcal{E}|$ and less, as small compared with those of the highest order $|\mathcal{E}|^2$, so that we obtain

$$\begin{aligned}\langle[\Delta m(t,T)]^2\rangle &= \mathcal{U}_T|\alpha|^2|\mathcal{E}|^2 \\ &\quad+\frac{1}{2}\mathcal{U}_T^2|\alpha|^2|\beta|^2|\mathcal{E}|^2\Big\{\langle:[\Delta\hat{E}_\theta(t)]^2:\rangle(1+\cos 2\Phi) \\ &\quad+\langle:[\Delta\hat{E}_{\theta+\pi/2}(t)]^2:\rangle(1-\cos 2\Phi) \\ &\quad+2\langle:\Delta\hat{E}_\theta(t)\,\Delta\hat{E}_{\theta+\pi/2}(t):\rangle\sin 2\Phi\Big\}\,, \end{aligned} \tag{2.58}$$

where $\langle:[\Delta\hat{E}_\theta(t)]^2:\rangle$ and $\langle:[\Delta\hat{E}_{\theta+\pi/2}(t)]^2:\rangle$ are the normally ordered variances of the in-phase and out-of-phase quadrature components of the signal field. We see from (2.58) that fluctuations of the quadrature components are manifested as the phase-dependent noise on the homodyne field. For a strong local oscillator, small fluctuations in the signal field are converted into large homodyne field fluctuations.

The two terms appearing on the right-hand side of (2.58) have the following physical interpretation. The first term is the noise term of the local oscillator, equal to the standard quantum limit. This is an unavoidable background noise level in the detection. The second term is the change of the noise due to the interference of the local oscillator with the signal field. This contribution equals the sum of the normally ordered variances for the in-phase and the out-of-phase components together with an interference term involving fluctuation operators of both components. The interference term vanishes for $\Phi = 0$ or $\Phi = \pi/2$, when either the in-phase or out-of-phase component contribution is maximal.

The expression (2.58) applies to the general case of an EM field irrespective of any particular state of the field and for all types of sources of the field. The variance of photoelectric counts can be greater or less than the standard quantum limit and can be optimized with respect to the choice of the phase Φ and the state of the field. When the signal field is in the vacuum state or a coherent state, the normally ordered variance $\langle:[\Delta\hat{E}_\theta(t)]^2:\rangle = 0$ independent of the phase θ, and then the variance of photoelectric counts is equal to the shot-noise level. When $\langle:[\Delta\hat{E}_\theta(t)]^2:\rangle < 0$ for some value of the phase θ, the variance is less than the shot-noise level. A negative value of $\langle:[\Delta\hat{E}_\theta(t)]^2:\rangle$ is nonclassical in the sense that the corresponding (quantum) state of the field cannot be given a diagonal coherent state representation of the density operator ϱ of the field. In this case, we say that then the fluctuations of the signal field are squeezed. In other words, turning on the squeezed light lowers the fluctuations of the photoelectric counts. This is of course a reflection of the fact that the field fluctuates less in a squeezed state than in the vacuum state. As we shall see later, information could be carried quite accurately with this field, and this is one of the reasons for our interest in squeezed fields.

Since the variance $\langle[\Delta m(t,T)]^2\rangle$ depends crucially on the normally ordered variances of the signal field, it follows that the optimum reduction of the variance of photoelectric counts requires us to find the situation where either $\langle:[\Delta\hat{E}_\theta(t)]^2:\rangle$ or $\langle:[\Delta\hat{E}_{\theta+\pi/2}(t)]^2:\rangle$ is as negative as possible. In this case the variance $\langle[\Delta m(t,T)]^2\rangle$ will be reduced below the standard quantum limit by the largest possible amount.

It is interesting to note that the variance in homodyne detection with a strong local oscillator is determined by second-order correlation functions of the signal field operators. In contrast, the variance in direct detection, given by (1.47), is determined by fourth-order correlation functions of the signal operators. In addition, the variance of photoelectric counts depends on the odd correlation functions $\langle\hat{E}^{(-)}(t)\,\hat{E}^{(-)}(t)\rangle$ and $\langle\hat{E}^{(+)}(t)\,\hat{E}^{(+)}(t)\rangle$ of the complex field amplitudes of the signal field. These functions, called the *anomalous correlation functions*, are explicit functions of time t, and carry information about two-photon correlations and phase properties of the field [11–15]. Consequently, the anomalous correlation functions are zero for one photon fields such as a coherent or thermal field. We shall have much more to say about these correlation functions, but for the present it is sufficient to note that the anomalous correlation functions are responsible for reduction of the field fluctuations below the quantum limit.

We have already seen that a measurement of the normally ordered variance of the quadrature component involves the homodyning of the total field under study with the local oscillator field. A similar analysis may be carried out for the spectrum of the photon number fluctuations of the homodyne field, which requires the total field to be first frequency filtered and then homodyned with a local oscillator field. As was demonstrated earlier in this chapter, the spectrum can be analyzed by calculating the Fourier transform of the two-time correlation function of photocurrent fluctuations. Let us consider the normally ordered part of the correlation function (1.80) under the time-stationary condition. This is consistent with detection experiments which usually run under stationary conditions, with a steady flow of energy from source to photodetector. The normally ordered two-time correlation function of the homodyne field fluctuations can be written as

$$\begin{aligned} F_{\theta_c}(\tau) &= \lim_{t\to\infty}\langle\mathcal{T}:\Delta\hat{I}_H(t)\,\Delta\hat{I}_H(t+\tau):\rangle \\ &= \lim_{t\to\infty}\Big[\langle\mathcal{T}\hat{E}_H^{(-)}(t)\,\hat{E}_H^{(-)}(t+\tau):\hat{E}_H^{(+)}(t)\,\hat{E}_H^{(+)}(t+\tau)\rangle \\ &\quad -\langle\hat{E}_H^{(-)}(t)\cdot\hat{E}_H^{(+)}(t)\rangle\langle\hat{E}_H^{(-)}(t+\tau)\cdot\hat{E}_H^{(+)}(t+\tau)\rangle\Big], \end{aligned} \tag{2.59}$$

where we have put the field operators in the normal order and introduced the the subscript θ_c to indicate the dependence of the homodyne field fluctuations on the phase of the local oscillator.

Applying the time ordering, and after substituting for the homodyne field amplitudes from (2.51), the correlation function (2.59) takes the form

$$
\begin{aligned}
F_{\theta_c}(\tau) &= |\alpha|^2|\beta|^2|\mathcal{E}|^2 F_s(\tau) \\
&= |\alpha|^2|\beta|^2|\mathcal{E}|^2 \lim_{t\to\infty}\Big\{\Big[\langle \Delta\hat{E}_s^{(-)}(t)\,\Delta\hat{E}_s^{(+)}(t+\tau)\rangle e^{i\omega_c\tau} \\
&\quad + \langle \Delta\hat{E}_s^{(-)}(t)\,\Delta\hat{E}_s^{(-)}(t+\tau)\rangle e^{-i\Phi(t,\tau,\theta_c)}\Big] + \text{c.c.}\Big\}\,, \qquad (2.60)
\end{aligned}
$$

where $\Phi(t,\tau,\theta_c) = 2\omega_c t + \omega_c\tau + 2\phi + 2\theta_c$ and we have designated by $F_s(\tau)$ the correlation functions involving the signal field operators only. As before, an approximation has been made that the amplitude $|\mathcal{E}|$ is large. Consequently, the terms of order $|\mathcal{E}|$ and less have been neglected as small compared with those of order $|\mathcal{E}|^2$.

Evaluation of the correlation function (2.60) is usually carried out in terms of the second-order correlation functions of the quadrature components of the signal field. It is done by substituting from (2.39) for the field amplitudes, and after straightforward calculations we arrive at

$$
\begin{aligned}
F_s(\tau) = \frac{1}{2}\lim_{t\to\infty}\Big\{&\langle \mathcal{T} : \Delta\hat{E}_\theta(t)\,\Delta\hat{E}_\theta(t+\tau) :\rangle\,(1+\cos 2\Phi) \\
&+ \langle \mathcal{T} : \Delta\hat{E}_{\theta+\pi/2}(t)\,\Delta\hat{E}_{\theta+\pi/2}(t+\tau) :\rangle\,(1-\cos 2\Phi) \\
&+ \Big[\langle \mathcal{T} : \Delta\hat{E}_\theta(t)\,\Delta\hat{E}_{\theta+\pi/2}(t+\tau) :\rangle \\
&\quad + \langle \mathcal{T} : \Delta\hat{E}_{\theta+\pi/2}(t)\,\Delta\hat{E}_\theta(t+\tau) :\rangle\Big]\sin 2\Phi\Big\}\,, \qquad (2.61)
\end{aligned}
$$

where $\Phi = \phi + \theta_c - \theta$. Note the involvement of the normally ordered and time-ordered correlation functions of the in-phase and the out-of-phase quadrature components together with an interference term.

Once $F_s(\tau)$ has been found, it is only a matter of substitution to derive the stationary spectrum of photocurrent fluctuations. Thus, by substituting (2.61) into (1.81), and replacing $\langle \hat{I}(t)\rangle$ by the dominant term $|\mathcal{E}|^2$, we arrive at the following stationary spectrum of photocurrent fluctuations

$$
F(\omega) = |\alpha|^2|\mathcal{E}|^2\left[1 + |\beta|^2 S(\omega,\Phi)\right]\,, \qquad (2.62)
$$

where we have introduced the so-called squeezing spectrum associated with the signal field fluctuations

$$
S(\omega,\Phi) = 2\int_0^\infty d\tau\, F_s(\tau)\cos(\omega\tau)\,. \qquad (2.63)
$$

Equation (2.62) gives the general expression for the stationary spectrum of photocurrent fluctuations. It relates the measured photocurrent spectral distribution to the squeezing spectrum given in terms of the normally ordered and time-ordered correlation functions for the signal field alone. Thus, the spectrum provides a measure of the contributions of the signal field fluctuations to the photocurrent spectral distribution relative to the vacuum noise level. Just as in the variance of photoelectric counts,

we may identify the first term on the right-hand side of (2.62) with the shot-noise fluctuations of the current. It is white noise, i.e. constant for all frequencies. The second term, proportional to the spectrum of squeezing, depends on frequency and is attributable to the fluctuations of the signal field. Note that the spectrum of squeezing is given by the phase-dependent spectra of quadrature field fluctuations. As the local oscillator phase is varied, the spectrum of squeezing changes from being determined by the quadrature component $\hat{E}_\theta(t)$ to $\hat{E}_{\theta+\pi/2}(t)$ or by any linear combination of the two quadratures. In particular, when the phase is adjusted to satisfy $\Phi = 0$, the squeezing spectrum is determined solely by the in-phase quadrature component

$$S(\omega, 0) = 2\int_0^\infty d\tau \langle : \Delta\hat{E}_\theta(0)\, \Delta\hat{E}_\theta(\tau) : \rangle \cos(\omega\tau) \ , \tag{2.64}$$

and for the choice of $\Phi = \pi/2$, the spectrum simplifies to that determined by the out-of-phase quadrature component

$$S(\omega, \pi/2) = 2\int_0^\infty d\tau \langle : \Delta\hat{E}_{\theta+\pi/2}(0)\, \Delta\hat{E}_{\theta+\pi/2}(\tau) : \rangle \cos(\omega\tau) \ . \tag{2.65}$$

When $S(\omega, \Phi) = 0$, the photocurrent noise is simply the shot noise or vacuum noise seen when the measured signal field is in the vacuum state or in a coherent state. When the signal field is in a squeezed state, the spectrum $S(\omega, \Phi)$ can become negative at some frequencies, resulting in the suppression of the photocurrent noise below the vacuum noise level. The squeezing spectrum has a lower bound of -1 and no upper bound, but the criterion for squeezing as a reduction of the fluctuations below the vacuum level is that the squeezing spectrum must be negative, $S(\omega, \Phi) < 0$. The squeezing will be said to be optimum or perfect at frequency ω when $F(\omega)$ attains its minimum value, $F(\omega) = 0$, with the transmissivity of the beam splitter close to unity, $|\beta|^2 \approx 1$. In this case the squeezing spectrum attains the lower bound $S(\omega, \Phi) = -1$.

A few words should be added at this point about different forms of squeezing. To be specific, for broadband multi-mode fields it is possible that the squeezing spectrum and the normally ordered variance of the total signal field can give different information about squeezing of the field. Namely, if we examine the photocurrent fluctuations $F(\omega)$ for a specific example, we may find that $F(\omega)$ can be smaller than the vacuum noise level for certain ranges of frequencies even though the normally ordered variance of the total signal field is positive. In this case, the field is not squeezed in the full sense. We shall refer to this particular situation as spectral component squeezing. For the case where $F(\omega)$ is smaller than the vacuum noise level for all frequencies, we shall refer to this as homogeneous squeezing. Also, the fluctuations may not be squeezed at some selected frequencies even if $\langle : [\Delta\hat{E}_\theta(t)]^2 : \rangle < 0$, or may exhibit more squeezing than the total field. Nevertheless, in all cases the negative sign of $S(\omega, \Phi)$ indicates the existence of some form of squeezing in the detected field. We shall see that the distinction between squeezing in full sense and squeezing in spectral components is an important one as these two measures give different information about the phase-dependent noise in

the field. These different forms of squeezing will be further elaborated in the course of specific examples studied in Chaps. 6 and 8.

In summary of this section, we have seen that the photoelectron counting technique in homodyne detection differs in two respects from those of direct photon counting techniques. First, intensity fluctuations in the homodyne detection scheme directly measure the fluctuations in a quadrature component of the signal field. Second, the signal field and its variance depend upon the local oscillator phase, which is an external controllable parameter.

2.5 Balanced Homodyne Detection of Quantum Fluctuations

Experimental measurements of quadrature components and their fluctuations based on the scheme shown in Fig. 2.1 are limited by the contribution of the local oscillator noise. This is because in practice the amplitude of the local oscillator is not truly constant as assumed in an ideal theoretical treatment given in the preceding section. The fluctuations of the local field amplitude lead to the so-called excess noise contribution, which in the ordinary homodyne detection scheme cannot be completely suppressed because the reflectivity of the beam splitter can never be zero. For this reason another scheme, called balanced homodyne detection, has been proposed to measure the phase-dependent quadrature components and their variances [9, 10]. The scheme is illustrated in Fig. 2.2. In contrast to the ordinary homodyne detection scheme, a lossless symmetric 50:50 beam splitter is employed, for which $|\alpha| = |\beta| = 1/\sqrt{2}$, and the superimposed fields are detected with a pair of identical photodetectors D_1 and D_2 located at the two output ports of the beam splitter. Photocurrents from the two detectors are then subtracted electronically and

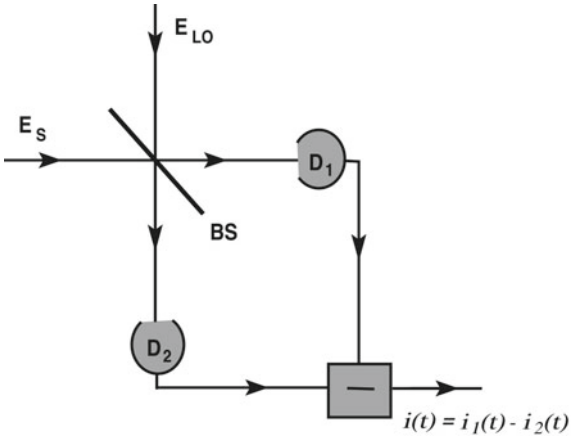

Fig. 2.2 Schematic diagram of a balanced homodyne experiment for detecting noise limited phase-dependent quadrature components of the EM field and its fluctuations

the difference current $i(t) = i_1(t) - i_2(t)$ and its fluctuations are analyzed. In this way, when the photocurrents are subtracted, the difference current provides measurement of the quadrature components and fluctuations of the signal field alone. The advantage of balanced homodyne detection is that the local oscillator noise can be eliminated completely, leaving only the noise of the signal field. This is explained quantitively below.

To examine the balanced homodyne detection scheme more closely, let us assume that in addition to a large coherent component $\mathcal{E}$, the local oscillator amplitude has a certain amount of noise, such that

$$\begin{aligned} E_{LO}^{(+)}(t) &= (\mathcal{E} + \delta\mathcal{E}(t))\, \mathrm{e}^{-\mathrm{i}\omega_c t} \,, \\ E_{LO}^{(-)}(t) &= \left(\mathcal{E}^* + \delta\mathcal{E}^*(t)\right) \mathrm{e}^{\mathrm{i}\omega_c t} \,, \end{aligned} \tag{2.66}$$

where $(\mathcal{E} + \delta\mathcal{E}(t)) = |\mathcal{E} + \delta\mathcal{E}(t)| \exp(-\mathrm{i}\theta_c)$ is the complex amplitude of the fluctuating local oscillator field with a slowly varying noise $\delta\mathcal{E}(t)$ and a constant phase θ_c not affected by the fluctuations.

The local oscillator noise is specified by a Gaussian statistics with zero mean value $\langle \delta\mathcal{E}(t) \rangle = \langle \delta\mathcal{E}^*(t) \rangle = 0$, and the nonzero second-order correlation

$$\langle \delta\mathcal{E}^*(t) \delta\mathcal{E}(t') \rangle = \mathcal{D}\, \delta\left(t - t'\right) \,, \tag{2.67}$$

where $\mathcal{D}$ represents the noise level of the local oscillator. Without loss in generality, we shall assume that the noise level in the local oscillator is negligible compared with the constant amplitude $|\mathcal{E}|^2$, i.e. $\mathcal{D} \ll |\mathcal{E}|^2$.

In the balanced homodyne detection scheme two photodetectors located at the outputs of the lossless beam splitter measure amplitudes of two homodyne fields

$$\begin{aligned} \hat{E}_1^{(\pm)}(t) &= \frac{1}{\sqrt{2}} \left[\pm \mathrm{i} E_{LO}^{(\pm)}(t) + \hat{E}_s^{(\pm)}(t) \right] \,, \\ \hat{E}_2^{(\pm)}(t) &= \frac{1}{\sqrt{2}} \left[E_{LO}^{(\pm)}(t) \pm \mathrm{i} \hat{E}_s^{(\pm)}(t) \right] \,, \end{aligned} \tag{2.68}$$

where the subscripts 1 and 2 refer to the two outputs of the beam splitter, and the positive and negative parts of the classical local field amplitudes are given by (2.66). Here, the factors "$\pm$i" come from a $\phi = \pi/2$ phase shift between the reflected and transmitted fields at the beam splitter, and we have assumed that the beam splitter has equal amplitude reflectivity and transmissivity coefficients, $|\alpha| = |\beta| = 1/\sqrt{2}$. Because of the lossless mixing of the two fields, the output fields are linear, equally weighted, superpositions of the signal field and the local oscillator amplitudes. The two output fields are separately detected and what is measured is the difference signal between the two outputs from which the quadrature amplitudes and their fluctuations can be deducted.

Let us calculate first the average difference number of photoelectrons produced by the homodyne fields in photodetectors during a short detection time T. We begin with (2.54) and (2.68) to evaluate the intensity of the homodyne fields needed to calculate the number of photoelectrons in each photodetector. As before, in the ordinary homodyne detection we assume that $|\mathcal{E}|$ is much greater than $|\langle\hat{E}_s(t)\rangle|$, so we may ignore the contribution of the term $|\langle\hat{E}_s(t)\rangle|^2$. However, the amplitude $|\mathcal{E}|$ need not be nearly so large as in the ordinary homodyne detection, as $|\alpha|$ is not very small. Thus, if we retain only the leading terms in $|\mathcal{E}|$, we find that the numbers of photoelectrons produced by the two homodyne fields (assuming linearly polarized fields) are

$$\begin{aligned} m_1(t,T) &= \mathcal{U}_T\,\hat{\boldsymbol{E}}_1^{(-)}(t)\cdot\hat{\boldsymbol{E}}_1^{(+)}(t) = \frac{1}{2}\mathcal{U}_T\left[|\mathcal{E}+\delta\mathcal{E}(t)|^2\right. \\ &\quad \left. + |\mathcal{E}+\delta\mathcal{E}(t)|\left(\hat{E}_\theta(t)\cos\Phi + \hat{E}_{\theta+\pi/2}(t)\sin\Phi\right)\right], \\ m_2(t,T) &= \mathcal{U}_T\,\hat{\boldsymbol{E}}_2^{(-)}(t)\cdot\hat{\boldsymbol{E}}_2^{(+)}(t) = \frac{1}{2}\mathcal{U}_T\left[|\mathcal{E}+\delta\mathcal{E}(t)|^2\right. \\ &\quad \left. - |\mathcal{E}+\delta\mathcal{E}(t)|\left(\hat{E}_\theta(t)\cos\Phi + \hat{E}_{\theta+\pi/2}(t)\sin\Phi\right)\right]. \end{aligned} \tag{2.69}$$

We see from these expressions that the quadrature components of the signal field are detected against a large background due to the large amplitude and noise of the local oscillator incident on the detectors. This term is certainly of great practical importance since it dominates the interference term, and may be a serious source of limitations in measurement of the quadrature components. Note, however, that this term contributes with the same sign to both numbers of photoelectrons, but the interference term between the local oscillator and the signal field contributes with opposite signs. This suggests that the output photocurrent might be made insensitive to the local oscillator noise if one takes a difference between the two numbers of photoelectrons. Hence, by subtracting the two expressions for the numbers of photoelectrons and taking the expectation value over the initial state of the field, we obtain

$$\begin{aligned} \langle m_-(t,T)\rangle &= \langle m_1(t,T) - m_2(t,T)\rangle \\ &= \mathcal{U}_T\,|\mathcal{E}|\left(\langle\hat{E}_\theta(t)\rangle\cos\Phi + \langle\hat{E}_{\theta+\pi/2}(t)\rangle\sin\Phi\right). \end{aligned} \tag{2.70}$$

This formula shows that for large enough local oscillator amplitude, the expectation value of the difference number of photoelectrons is free from the contribution of the local oscillator noise, it retains only the interference terms between the amplitude of the local oscillator field and the quadrature components of the signal field. Thus, the cancellation of the local oscillator noise in the difference signal can indeed be achieved and the difficulty with measurement of the quadrature components of the signal field can be avoided. This is a distinct advantage when one wants to measure quadrature components of a weak field.

Consider now the fluctuations in the difference between numbers of photoelectrons in the two output fields. In practice, the fluctuations can be measured by analyzing either the squeezing spectrum or the normally ordered variance of the quadrature

components of the signal field, depending on the experimental scheme adopted. Theoretically, the variance of the difference number of photoelectrons produced by the two homodyne fields may be evaluated using (2.69), from which the fluctuations in the quadrature components of the signal field may be calculated. Assuming the linearly polarized fields, the variance of the difference number of photoelectrons is given by the interference term between the local oscillator intensity $|\mathcal{E}|^2$ and the fluctuations in the quadrature components of the signal field. With the help of the commutation relation (1.13), the variance can be written in terms of normally ordered variances of the signal field quadratures as

$$\langle \left[\Delta m_-(t,T)\right]^2 \rangle = \mathcal{U}_T^2 \, |\mathcal{E}|^2 \, [1 + F_\theta(t)] \ , \tag{2.71}$$

where

$$F_\theta(t) = \Big\{ \langle : [\Delta \hat{E}_\theta \, (t)]^2 : \rangle \cos^2 \Phi + \langle : [\Delta \hat{E}_{\theta+\pi/2} \, (t)]^2 : \rangle \sin^2 \Phi + \langle : \Delta \hat{E}_\theta \, (t) \, \Delta \hat{E}_{\theta+\pi/2} \, (t) : \rangle \sin 2\Phi \Big\} \ . \tag{2.72}$$

Again, we have dropped the term $|\langle \hat{E}_s(t) \rangle|^2$ under the usual assumption that $|\mathcal{E}|$ is very large. We see clearly from (2.71) that even though the local oscillator noise, the variance of the difference number of photoelectrons is free from the local oscillator noise and is a weighted combination of the variance of the fluctuations in the two quadratures of the signal field. Thus, the variance of the difference number of photoelectrons immediately provides information about the noise level in the quadrature components of the signal field.

Of much greater interest is the normally ordered two-time correlation function of the difference current fluctuations. This is because the noise level is often measured as a function of frequency which, according to (1.71), is provided by the spectrum of photocurrent fluctuations. Using (1.81) and by substituting (2.68) for the field amplitudes, we easily find the spectrum of the difference photocurrent fluctuations, which written in terms of the squeezing spectrum of the signal field fluctuations takes the form

$$F_-(\omega) = |\mathcal{E}|^2 \, [1 + S \, (\omega, \Phi)] \ , \tag{2.73}$$

where, once again we have retained only dominant terms in $|\mathcal{E}|$ under the assumption of a strong local oscillator field. Note in particular that the spectrum (2.73) is very similar in form to the expression (2.62) for the ordinary homodyne detection. However, there is an essential difference between these two expressions that the spectrum in the balanced homodyne detection is insensitive to the local oscillator noise, whereas it is altered by the noise in the ordinary homodyne detection.

We may summarize this section as follows. The most notable feature of the balanced homodyne detection scheme is that all contributions due to the large amplitude of the local oscillator and its fluctuations cancel, except for the one arising from the

interference between the local oscillator intensity and variances of the quadrature components of the signal field. For this reason, the balanced homodyne detection scheme provides a better method for measuring quadrature components of the electric field and their fluctuations then the ordinary homodyne detection scheme. It is particularly useful and in fact the most frequently used detection scheme for squeezed light. For details of the experimental observation of squeezed light, we refer the interested reader to some of the excellent review papers [16, 17].

References

1. M. Lax: Phys. Rev. **172**, 350 (1968)
2. B.R. Mollow: Phys. Rev. A **5**, 1522 (1972)
3. B.R. Mollow: Phys. Rev. A **5**, 2217 (1972)
4. R. Kubo: J. Phys. Soc. Jap. **12**, 570 (1957)
5. P. Meystre, M. Sargent III: *Elements of Quantum Optics*, (Springer-Verlag, Berlin, 1991)
6. D.F. Walls: Nature **306**, 141 (1983)
7. L. Mandel: Phys. Script. **12**, 42 (1986)
8. R. Loudon, P.L. Knight: J. Mod. Opt. **34**, 709 (1987)
9. H.P. Yuen, J.H. Shapiro: IEEE Trans. Inf. Theory **IT-26**, 78 (1980)
10. H.P. Yuen, V.W.S. Chan; Opt. Lett. **8**, 177 (1983)
11. A.P. Kazantsev, V.S. Smirnov, V.P. Sokolov: Optics Commun. **35**, 209 (1980)
12. G.S. Agarwal: Phys. Rev. A **33**, 2472 (1986)
13. A. Heidmann, S. Reynaud: J. Mod. Opt. **34**, 923 (1987)
14. Z.Y. Ou, C.K. Hong, L. Mandel: J. Opt. Soc. Am. B **4**, 1574 (1987)
15. Z. Ficek, R. Tanaś: Z. Phys. D **9**, 27 (1988)
16. R.E. Slusher, B. Yurke: Sci. Am. **258**, 50 (1988)
17. H.J. Kimble: Phys. Rep. **219**, 227 (1992)

Chapter 3
Spectroscopy with Single Atoms in Atomic Beams

In the preceding chapter, the optical spectra of a signal field and methods of their measurement were defined and discussed. The signal fields are not free fields, but are generated by sources such as atoms or molecules. We now turn more specifically to the subject of spectroscopy with signal fields produced by single multilevel atoms radiating due to the interaction with the ordinary vacuum and irradiated by quasi-resonant fields. The study of spectral properties of the radiation field scattered by atoms or molecules is fundamental to a number of research disciplines in optics and laser physics and provides a convenient ground for rigorous examination of the characteristics of atoms and basic aspects of their interaction with the radiation field. We shall not, however, follow the usual treatment of atomic spectra, which utilizes optical spectra as the basis for the information about splitting of the atomic energy levels, transition frequencies between the levels, and their populations. Here, we shall focus on a different aspect of atomic spectroscopy, which utilizes optical spectra to tackle the problem of quantum fluctuations, their control and effect on the radiative properties of atoms. We consider fluorescence spectra of atoms in atomic beams of low-atomic-number densities and will show that it is possible to exercise extraordinary control of the linewidths of the spectral features and their intensities by imposing strong driving fields on the atoms. The choice of a low density atomic beam takes advantage of the fact that the spacing between the atoms in the low density atomic beam is very much greater than the size of the atoms, so that interaction between the atoms can be neglected. This means that the effect of the driving fields on any atom is substantially the same as if it were the only a single atom present.

We begin by considering the fluorescence spectra of two-level atoms driven by a monochromatic laser field. This is a classic problem in quantum atomic spectroscopy and has been well studied theoretically and experimentally. We explore few aspects of this model in order to provide some insight into the essential properties of the interaction between atoms and radiation fields. What is to be discussed is the kind of information that can be obtained about the atom and the emitted field from measurements of the intensity and the spectrum of the emitted fluorescence field. We will

Z. Ficek and R. Tanaś, *Quantum-Limit Spectroscopy*, Springer Series in Optical Sciences 200, DOI 10.1007/978-1-4939-3740-0_3

show that the spectral features of the fluorescence field provide fundamental insight into the contributions of quantum fluctuations of atomic dipole moments. The fluctuations play important roles in diverse physical phenomena. They limit the spectral resolution and signal-to-noise ratio that are important in spectroscopic experiments, and hence limit the sensitivity of any spectroscopic measurement. After discussing the spectral properties of the radiation field emitted by this fundamental system, a study is made of optical spectra of radiation field emitted by a more complicated system of atoms driven by a multichromatic field. We shall demonstrate that far more detailed information about quantum fluctuations and their control is in fact obtainable by suitable driving of the system.

The latter part of the chapter introduces the concept of a stabilization and control of quantum fluctuations in two- and three-level atoms by locating the atoms in a tailored vacuum field, such as a cavity, or by a suitable driving with laser fields in free space. The stabilization is manifested in a narrowing of resonance fluorescence linewidths to subnatural values. To understand this effect, we apply the dressed-atom model of the system which provides a straightforward interpretation of the linewidth narrowing. This is followed by a discussion of an experiment that demonstrated the existence of line narrowing in coherently driven three-level atoms.

3.1 Spectroscopy with a Monochromatic Excitation

Let us begin the study of the single atom spectroscopy by considering the most fundamental problem, that of a two-level system driven by a monochromatic single-mode continuous wave (cw) laser field [1]. In this section we treat the cw laser field classically and assume that the field is represented as a plane wave with a constant and time-independent amplitude

$$\boldsymbol{E}_L(\boldsymbol{r},t) = \boldsymbol{\mathcal{E}}_L \mathrm{e}^{-\mathrm{i}(\omega_L t - \boldsymbol{k}\cdot\boldsymbol{r}+\psi_L)} + \text{c.c.}\,, \tag{3.1}$$

where ω_L is the frequency, ψ_L is the phase, and $\boldsymbol{\mathcal{E}}_L$ is the amplitude of the field. The amplitude $\boldsymbol{\mathcal{E}}_L$ is independent of time and carries information about polarization of the field, $\boldsymbol{\mathcal{E}}_L = \mathcal{E}_L \bar{\boldsymbol{e}}_L$, where $\bar{\boldsymbol{e}}_L$ is the unit polarization vector of the field. The polarization vector $\bar{\boldsymbol{e}}_L$ is considered as a complex quantity specifically to admit the possibility of different polarizations of the field including circular or elliptical polarizations. For a linearly polarized field, the unit polarization vector $\bar{\boldsymbol{e}}_L$ is a real number, whereas for a circularly or elliptically polarized field, $\bar{\boldsymbol{e}}_L$ is a complex number.

The two-level system is a fictionus atom composed of only two energy levels, that it is represented by a ground state $|g\rangle$, an excited state $|e\rangle$, the atomic transition frequency ω_a, and the transition dipole moment $\boldsymbol{\mu}_a$. In addition to the laser field, the atom interacts with a multimode vacuum field (reservoir) represented by the annihilation and creation operators $\hat{a}_k$ and $\hat{a}_k^\dagger$, satisfying the Bose commutation relation,

$[\hat{a}_k, \hat{a}_{k'}^\dagger] = \delta_{kk'}$. The total Hamiltonian of the system can be written as

$$\hat{H} = \hat{H}_0 + \hat{H}_L + \hat{H}_I \,, \tag{3.2}$$

where

$$\hat{H}_0 = \hbar\omega_a S_z + \hbar \sum_k \omega_k \hat{a}_k^\dagger \hat{a}_k \tag{3.3}$$

is the free Hamiltonian of the atom and the vacuum field,

$$\hat{H}_L = -\frac{1}{2}\mathrm{i}\hbar \left(\Omega S^+ \mathrm{e}^{-\mathrm{i}(\omega_L t - \boldsymbol{k}\cdot\boldsymbol{r} + \psi_L)} - \mathrm{H.c.}\right) \tag{3.4}$$

is the interaction between the atom and the laser field, and

$$\hat{H}_I = -\mathrm{i}\hbar \sum_k \left(g_k \hat{a}_k S^+ - \mathrm{H.c.}\right) \tag{3.5}$$

is the interaction between the atom and the vacuum field, given in the dipole and the rotating-wave approximations. Here, ω_k is the frequency of the kth mode of the field and g_k is the coupling strength of the atom with the k mode of the vacuum field. The choice of a monochromatic driving field reduces the complexity of the atom-field interaction to that determined by a time-independent Rabi frequency Ω, defined as

$$\Omega = 2\boldsymbol{\mu}_{eg} \cdot \boldsymbol{\mathcal{E}}_L / \hbar \,, \tag{3.6}$$

where $\boldsymbol{\mu}_{eg} = \langle e | \boldsymbol{\mu}_a | g \rangle$ is the matrix element of the transition dipole moment between the atomic energy levels.

The dynamics of the atom in the vacuum field are best described in terms of a reduced density operator ϱ, which is obtained by tracing the total density operator of the system ϱ_T over the vacuum field variables. The reduced density operator, written in an interaction picture based on the free Hamiltonian $\hat{H}_0$, satisfies the Liouville equation

$$\mathrm{i}\hbar\dot{\tilde{\varrho}}\,(t) = \mathrm{Tr}_F \left\{\left[\tilde{H}_L\,(t)\,,\, \tilde{\varrho}_T\,(t)\right]\right\} + \mathrm{Tr}_F \left\{\left[\tilde{H}_I\,(t)\,,\, \tilde{\varrho}_T\,(t)\right]\right\} \,, \tag{3.7}$$

where the dot refers to differentiation with respect to time, and

$$\begin{aligned}
\tilde{\varrho} &= \exp\left(\mathrm{i}\hat{H}_0 t/\hbar\right) \varrho \exp\left(-\mathrm{i}\hat{H}_0 t/\hbar\right) \,, \\
\tilde{H}_L &= \exp\left(\mathrm{i}\hat{H}_0 t/\hbar\right) \hat{H}_L \exp\left(-\mathrm{i}\hat{H}_0 t/\hbar\right) \,, \\
\tilde{H}_I &= \exp\left(\mathrm{i}\hat{H}_0 t/\hbar\right) \hat{H}_I \exp\left(-\mathrm{i}\hat{H}_0 t/\hbar\right) \,.
\end{aligned} \tag{3.8}$$

With the condition that the atom and the vacuum field are uncorrelated at the initial time $t = 0$, i.e., $\varrho_T(0) = \varrho(0) \otimes \varrho_F(0)$, where $\varrho_F(0)$ is the density operator of the field, we can solve (3.7) via iteration, which to the second-order in the coupling (Born approximation) leads to

$$\dot{\tilde{\varrho}}(t) = -\frac{\mathrm{i}}{\hbar}\left[\tilde{H}_L(t), \tilde{\varrho}(t)\right] - \frac{1}{\hbar^2}\int_0^t \mathrm{d}t' \mathrm{Tr}_F\left\{\left[\hat{H}_I(t), \left[\hat{H}_I(t'), \tilde{\varrho}(t') \otimes \tilde{\varrho}_F(0)\right]\right]\right\} . \tag{3.9}$$

The evaluation of the trace of the double commutator requires the knowledge of the second-order correlation functions of the vacuum field operators. We choose the ordinary (zero temperature) vacuum characterized by the following correlation functions

$$\begin{aligned} \mathrm{Tr}_F\left\{\hat{a}_k \hat{a}_{k'}^\dagger\right\} &= \delta_{k,k'} , \\ \mathrm{Tr}_F\left\{\hat{a}_k^\dagger \hat{a}_{k'}\right\} &= \mathrm{Tr}_F\left\{\hat{a}_k^\dagger \hat{a}_{k'}^\dagger\right\} = \mathrm{Tr}_F\left\{\hat{a}_k \hat{a}_{k'}\right\} = 0 . \end{aligned} \tag{3.10}$$

The derivation of the master equation simplifies by assuming that the variations of the reduced density operator are slow compared to the atomic frequency ω_a, and by thus making an approximation, $\tilde{\varrho}(t') = \tilde{\varrho}(t)$, which is analogous to the Weisskopf−Wigner approximation of radiation damping theory. Under this approximation, it is the matter of straightforward calculations to arrive at the following master equation for the density operator in the rotated frame

$$\frac{\partial \varrho}{\partial t} = -\mathrm{i}\Delta\left[S_z, \varrho\right] - \frac{1}{2}\Omega\left[S^+ - S^-, \varrho\right] - \frac{1}{2}\gamma\left(\varrho S^+ S^- + S^+ S^- \varrho - 2S^- \varrho S^+\right) , \tag{3.11}$$

where γ is the atomic spontaneous emission rate and $\Delta = \omega_a - \omega_L$ is the detuning of the laser field frequency from the atomic transition frequency. In the derivation of (3.11) we have omitted small imaginary coefficients which represent the Lamb shift of the atomic levels [2]. In addition, we have assumed that the atom is located at the origin and put $\psi_L = 0$. The atomic spontaneous emission rate, a damping rate in short, is given by

$$\gamma = 2\pi \sum_{\boldsymbol{k}s} |g_{\boldsymbol{k}s}|^2 \delta(\omega_a - \omega_k) , \tag{3.12}$$

The summation for k may also be written as

$$\gamma = 2\pi \sum_s \int \mathrm{d}\omega_k \mathrm{d}\Omega_r \, |g_{\omega_k}|^2 D(\omega_k) \, \delta(\omega_k - \omega_a) , \tag{3.13}$$

where g_{ω_k} is the coupling strength at the frequency ω_k and $D(\omega_k)$ is the spectral density of the field modes available for the spontaneously emitted photon

$$D(\omega_k) = \frac{\mathcal{V}\omega_k^2}{\pi^2 c^3}\,, \tag{3.14}$$

with $\mathcal{V}$ as the quantization volume and c as the speed of light in vacuum. In the course of the evaluation, the summation over k wave numbers was changed to integration over frequencies ω_k, and $D(\omega_k)$ can be approximated by $D(\omega_a)$ since the density of the modes is a slowly varying (smooth) function of frequency in the vicinity of the atomic resonance. The dependence of γ on $D(\omega_a)$ means that one can modify the damping rate by modifying the density of the field modes. Note that the spontaneous emission rate results from the presence of quantum fluctuations in the vacuum field. Therefore, a modification of the density of the modes may result in a modification of the quantum fluctuations of the field. Hence, a reduction of the damping rate could be regarded as a stabilization of the quantum fluctuations. In free space, the spectrum of the modes is infinitely broad (flat spectrum). However, inside a cavity or a band gap material or a wave guide, where only a finite number of modes can exist, the density of the modes to which an atom could be coupled is significantly altered which then results in a significantly modified damping rate of an atom located inside the cavity.

Under the influence of the applied field, tuned near resonance with the atomic transition, the atom becomes excited and radiates the fluorescence field which is detected at a distant point $\boldsymbol{r}$. We will consider properties of various quantities, the intensity, fluctuations, and the optical spectra of the fluorescence field. As was demonstrated in Chap. 1, these quantities can be expressed in terms of the correlation functions of the atomic dipole operators which, on other hand, can be evaluated with the help of the master equation (3.11).

3.1.1 Optical Bloch Equations

Having available the master equation for the density operator of a two-level atom, we now turn to the derivation of the equations of motion, the optical Bloch equations for the mean values of the atomic variables $\langle S^+\rangle \equiv \mathrm{Tr}\{S^+\varrho\}$, $\langle S^-\rangle \equiv \mathrm{Tr}\{S^-\varrho\}$ and $\langle S_z\rangle \equiv \mathrm{Tr}\{S_z\varrho\}$. Using the master equation (3.11) we obtain

$$\begin{aligned}
\dot{\langle S^+\rangle} &= -\left(\frac{1}{2}\gamma - \mathrm{i}\Delta\right)\langle S^+\rangle + \Omega\langle S_z\rangle\,,\\
\dot{\langle S^-\rangle} &= -\left(\frac{1}{2}\gamma + \mathrm{i}\Delta\right)\langle S^-\rangle + \Omega\langle S_z\rangle\,,\\
\dot{\langle S_z\rangle} &= -\frac{1}{2}\gamma - \gamma\langle S_z\rangle - \frac{1}{2}\Omega\left(\langle S^+\rangle + \langle S^-\rangle\right)\,.
\end{aligned} \tag{3.15}$$

Alternatively, we may write the optical Bloch equations in terms of the components of the average total atomic spin $\boldsymbol{S} = (\langle S_x\rangle, \langle S_y\rangle, \langle S_z\rangle)$, where

$$S_x = \frac{1}{2}\left(S^- + S^+\right) \ , \quad S_y = \frac{\mathrm{i}}{2}\left(S^- - S^+\right) \ . \tag{3.16}$$

The resulting optical Bloch equations are

$$\begin{aligned}
\langle \dot{S_x}\rangle &= -\frac{1}{2}\gamma\langle S_x\rangle - \Delta\langle S_y\rangle + \Omega\langle S_z\rangle \,, \\
\langle \dot{S_y}\rangle &= -\frac{1}{2}\gamma\langle S_y\rangle + \Delta\langle S_x\rangle \,, \\
\langle \dot{S_z}\rangle &= -\frac{1}{2}\gamma - \gamma\langle S_z\rangle - \Omega\langle S_x\rangle \,.
\end{aligned} \tag{3.17}$$

Note that if the laser frequency is on resonance with the atomic transition frequency, $\Delta = 0$, then the equation of motion for the y component of the spin is decoupled from the other equations. The sets of coupled equations of motion (3.15) and (3.17) can be easy solved. For the purpose of future applications, we confine ourselves to the steady-state solutions. In the steady state, the average values of the spin components are

$$\begin{aligned}
\langle S_x\rangle &= \frac{-\frac{1}{4}\gamma\Omega}{\frac{1}{4}\gamma^2 + \frac{1}{2}\Omega^2 + \Delta^2} \,, \\
\langle S_y\rangle &= \frac{-\frac{1}{2}\Delta\Omega}{\frac{1}{4}\gamma^2 + \frac{1}{2}\Omega^2 + \Delta^2} \,, \\
\langle S_z\rangle &= -\frac{1}{2}\,\frac{\frac{1}{4}\gamma^2 + \Delta^2}{\frac{1}{4}\gamma^2 + \frac{1}{2}\Omega^2 + \Delta^2} \,.
\end{aligned} \tag{3.18}$$

These expressions show that the driven atom decays to nonzero steady state. The quantity $\langle S_z\rangle$ determines the average population inversion in the atom. In the absence of the excitation ($\Omega = 0$), $\langle S_z\rangle = -\frac{1}{2}$ that the atom is in its ground state. On the other hand, if the excitation field is strong, $\langle S_z\rangle \to 0$ indicating that in this limit the atomic levels are equally populated. We say that the atomic transition is saturated. The value $\langle S_z\rangle = 0$ is the maximal value of the average atomic inversion which could ever be achieved in a two-level atom damped in free space to the ordinary vacuum. More interesting is the quantity $\langle S_z\rangle + \frac{1}{2}$, which is equal to the population of the upper atomic state. Specifically

$$\begin{aligned}\langle S_z\rangle + \frac{1}{2} &= \mathrm{Tr}\left\{\left(S_z + \frac{1}{2}\right)\varrho\right\} \\ &= \mathrm{Tr}\left\{\left[\frac{1}{2}\left(|e\rangle\langle e| - |g\rangle\langle g|\right) + \frac{1}{2}\left(|e\rangle\langle e| + |g\rangle\langle g|\right)\right]\varrho\right\} \\ &= \mathrm{Tr}\left\{|e\rangle\langle e|\,\varrho\right\} = \varrho_{ee}\ , \end{aligned} \tag{3.19}$$

where we have used the closure theorem, $|e\rangle\langle e| + |g\rangle\langle g| = 1$. The steady-state values of the components $\langle S_x\rangle$ and $\langle S_y\rangle$ determine the steady-state magnitude and polarization of the induced dipole moment in the atom, $\langle S^-\rangle = \langle S_x\rangle - \mathrm{i}\langle S_y\rangle$. It is easily verified from (3.18) that for small Ω the amplitude of the atomic dipole moment increases with Ω, but decreases inversely with Ω for large Ω. The amplitude of the atomic dipole is maximal when $\Omega^2 = \frac{1}{2}\gamma^2 + 2\Delta^2$.

3.1.2 Excitation Spectrum

To understand how various properties of the radiation field emitted by atoms can be determined from the properties of the atomic dipole correlation functions, we look first at the simple case of a two-level atom driven by a monochromatic laser field. In this section, we consider the intensity of the radiation field and express it in terms of atomic variables. As we shall see, the radiation intensity carries information about the excitation spectrum of an atomic transition, the frequency of the transition, and its linewidth. In experiments, the excitation spectrum is measured as the rate of fluorescence from the excited atoms in a function of detuning of an excitation field. An alternative method is to measure the rate of absorption of the excitation field, but in the steady state the rate of absorption is equal to the rate of fluorescence.

To calculate the excitation spectrum of a two-level atom driven by a coherent laser field, we use the expression (1.92) of the ordinary formula for radiation intensity. In the case of a single ($N = 1$) two-level atom, $\hat{A}_{21}^{n=1} \equiv S^+$, $\hat{A}_{12}^{n=1} \equiv S^-$, and then the expression (1.92) reduces to

$$\langle \hat{I}(\boldsymbol{r}, t)\rangle = \Phi_{2112}^{11}\langle S^+(t)\, S^-(t)\rangle\ , \tag{3.20}$$

where

$$\Phi_{2112}^{11} = \frac{3}{8\pi}\gamma_{21}\left(1 - \cos^2\psi_i\right)\ , \tag{3.21}$$

with $\gamma_{21} \equiv \gamma$. The radiation intensity therefore follows directly from the first-order correlation function of the atomic dipole operators. Integrating (3.20) over all directions $\boldsymbol{r}$, we obtain the total radiation intensity

$$\langle \hat{I}(t)\rangle = \int \mathrm{d}\Omega_{\boldsymbol{r}}\langle \hat{I}(\boldsymbol{r}, t)\rangle = \gamma\langle S^+(t)\, S^-(t)\rangle\ . \tag{3.22}$$

Since $\langle S^+(t)\, S^-(t)\rangle = \langle S_z(t)\rangle + \frac{1}{2} = \varrho_{ee}(t)$, we see that the average radiation intensity equals the population of the atomic excited level times the rate γ the population decays from the level $|e\rangle$.

As time $t \to \infty$, the t-dependent correlation function in (3.22) becomes t-independent, and we find with help of (3.18) that the stationary intensity is

$$\langle \hat{I} \rangle_s = \lim_{t\to\infty} \langle \hat{I}(t)\rangle = \gamma \frac{\frac{1}{4}\Omega^2}{\frac{1}{4}\gamma^2 + \frac{1}{2}\Omega^2 + \Delta^2} \,. \tag{3.23}$$

This expression determines the stationary radiation intensity in terms of the Rabi frequency of the excitation field and of the detuning Δ. As we have already mentioned, the expression is known as the *excitation spectrum*. As a function of the laser field frequency, the spectrum is a Lorentzian centered at the atomic transition frequency and the linewidth $\frac{1}{2}\gamma$ broadened by the Rabi frequency Ω. For a weak excitation with $\Omega \ll \gamma$, the bandwidth of the excitation spectrum is then given by the damping rate of the atomic transition, thus providing an information about the linewidth of the atomic transition.

Finally, we would like to point out that the finite bandwidth of the excitation spectrum indicates that the radiation field emitted by the atom is not coherent. It is especially well seen when one considers the degree of self coherence of the radiation field, given in (1.99). For the driven two-level atom, and in the long-time limit the degree takes the form

$$q = \lim_{t\to\infty} \frac{\langle \hat{I}(\boldsymbol{r}, t)\rangle}{\mathcal{U}_T |\langle \hat{\boldsymbol{E}}^{(-)}(\boldsymbol{r}, t)\rangle|^2} - 1 = \frac{\frac{1}{2}\Omega^2}{\frac{1}{4}\gamma^2 + \frac{1}{2}\Omega^2 + \Delta^2} \,. \tag{3.24}$$

We see that despite the coherent nature of the driving field, the fluorescence field is not coherent in the steady state, since the degree of self coherence is different from zero. As the Rabi frequency of the driving field increases, the fluctuations of the fluorescence field increases, which must be attributed to quantum effects in the interaction between the atom and the field.

3.1.3 Stationary Fluorescence Spectrum

In this section, we apply the optical Bloch equations (3.17) to evaluate the emission power spectrum of the fluorescence field radiated by the coherently driven two-level atom. Although we begin with a general formulation of two-time correlation functions, we will be mostly concerned with a stationary field and evaluate the incoherent (noise) part of the spectrum.

We use the expression (2.19) for the incoherent part of the stationary spectrum, which in the case of a single two-level atom reduces to

$$S_{\text{in}}(\omega) = 2\text{Re}\left\{\gamma \int_0^\infty \mathrm{d}\tau \, \langle \delta S^+(0)\, \delta S^-(\tau)\rangle \mathrm{e}^{\mathrm{i}(\omega-\omega_L)\tau}\right\} . \tag{3.25}$$

The spectrum is determined by the correlation function of the fluctuation parts of the atomic dipole operators. This correlation function can be obtained from the optical Bloch equations with the help of the quantum regression theorem.

$$\begin{aligned}
\frac{\mathrm{d}}{\mathrm{d}\tau} Y_1(\tau) &= -\left(\frac{1}{2}\gamma - \mathrm{i}\Delta\right) Y_1(\tau) + \Omega Y_3(\tau) , \\
\frac{\mathrm{d}}{\mathrm{d}\tau} Y_2(\tau) &= -\left(\frac{1}{2}\gamma + \mathrm{i}\Delta\right) Y_2(\tau) + \Omega Y_3(\tau) , \\
\frac{\mathrm{d}}{\mathrm{d}\tau} Y_3(\tau) &= -\gamma Y_3(\tau) - \frac{1}{2}\Omega \left[Y_1(\tau) + Y_2(\tau)\right] ,
\end{aligned} \tag{3.26}$$

where

$$\begin{aligned}
Y_1(\tau) &= \langle \delta S^+(0) \delta S^+(\tau)\rangle , \quad Y_2(\tau) = \langle \delta S^+(0) \delta S^-(\tau)\rangle , \\
Y_3(\tau) &= \langle \delta S^+(0) \delta S_z(\tau)\rangle
\end{aligned} \tag{3.27}$$

are the correlation functions for the fluctuation operators.

It is convenient at this point to introduce the Laplace transform of the correlations functions

$$Y_j(z) \equiv \int_0^\infty \mathrm{d}\tau \, \mathrm{e}^{-z\tau} Y_j(\tau) . \tag{3.28}$$

Expressed as equations for the Laplace transforms of $Y_j(\tau)$, (3.26) becomes a set of three coupled linear equations

$$\begin{aligned}
\left(z + \frac{1}{2}\gamma - \mathrm{i}\Delta\right) Y_1(z) - \Omega Y_3(z) &= Y_1(0) , \\
\left(z + \frac{1}{2}\gamma + \mathrm{i}\Delta\right) Y_2(z) - \Omega Y_3(z) &= Y_2(0) , \\
(z+\gamma)\, Y_3(z) + \frac{1}{2}\Omega \left[Y_1(z) + Y_2(z)\right] &= Y_3(0) .
\end{aligned} \tag{3.29}$$

Solving for $Y_2(z)$, which is needed to determine the fluorescence spectrum, and taking the steady-state values of $Y_j(0)$, we obtain an analytic expression

$$Y_2(z) = \frac{2\Omega^4}{(\gamma^2 + 2\Omega^2 + 4\Delta^2)^2} \frac{(z+\gamma)^2 + \frac{1}{2}\Omega^2}{(z+\gamma)\left[(z+\frac{1}{2}\gamma)^2 + \Delta^2\right] + (z+\frac{1}{2}\gamma)\Omega^2} . \tag{3.30}$$

Having available the solution for the Laplace transform $Y_2(z)$ it is just a matter of a substitution $z = -\mathrm{i}(\omega - \omega_L)$ in (3.30) to obtain the stationary fluorescence spectrum

$$S_{\rm in}(\omega) = 2{\rm Re}\left\{\gamma\, Y_2(z)|_{z=-{\rm i}(\omega-\omega_L)}\right\}\,. \tag{3.31}$$

Note that the Laplace transform (3.30) is a real function. This implies that the corresponding fluorescence spectrum will be symmetric about $\omega - \omega_L = 0$. The above expression may be simplified substantially for a choice $\Delta = 0$, the laser frequency on resonance with the atomic transition. We can find roots of the cubic polynomial in the denominator of (3.30), which in the case of $\Delta = 0$ have a simple form

$$z_1 = -\frac{1}{2}\gamma\,, \quad z_{2,3} = -\frac{3}{4}\gamma \pm \sqrt{\frac{1}{16}\gamma^2 - \Omega^2}\,. \tag{3.32}$$

Evidently, there is a threshold for Ω at which the roots change character. Below threshold, all roots are real. Therefore, the spectrum will compose of a single spectral line. Above threshold, the roots z_2 and z_3 become complex, and complex conjugate to each other. In this case, the spectrum will be composed of three spectral lines with the central line of the width $\gamma/2$ located at $\omega = \omega_L$, and two sidebands (the Rabi sidebands) of widths $3\gamma/4$ located at $\omega = \omega_L \pm \sqrt{\Omega^2 - \frac{1}{16}\gamma^2}$.

Figure 3.1 shows the incoherent part of the spectrum plotted as a function of frequency and the Rabi frequency. For small Ω the spectrum is composed of a single line and the effect of increasing Rabi frequency is to split the spectrum into a triplet with the side peaks shifted by the Rabi frequency Ω from the central peak. The spectrum is often called the Mollow triplet or Mollow spectrum, after Mollow [3] who first investigated the spectrum of a two-level atom driven by a strong coherent field.

The Mollow spectrum evaluated for the driven two-level atom in free space will serve as a reference for our studies of radiative features indicative of modifications

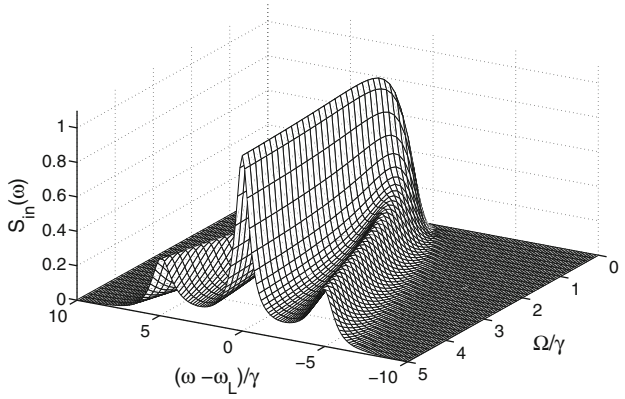

Fig. 3.1 Incoherent part of the stationary fluorescence spectrum plotted as a function of frequency $(\omega - \omega_L)/\gamma$ and the Rabi frequency Ω/γ

of the spontaneous decay. In particular, we will look at features of an atom leading to spectral linewidths narrower than those of the Mollow spectrum. We will refer to the narrowed spectral lines as subnatural linewidths.

From the behavior of the fluorescence field intensity and the fluorescence spectrum of the driven two-level atom we may conclude that the rate $\frac{1}{2}\gamma$ produces the minimum bandwidth of the radiation field emitted by an atom residing in free space, the frequency-independent reservoir. We will refer to the bandwidth $\frac{1}{2}\gamma$ as the *natural linewidth*. The nonzero bandwidth results from the presence of quantum fluctuations in the vacuum field which cause fluctuations of the radiating atomic dipole. The minimum width appears as a barrier for the resolution of spectral lines.

3.2 Spectral Linewidth Narrowing in a Tailored Reservoir

In order to appreciate the role played by the density of the modes in determining the magnitude of the spontaneous emission rate of an atom, we analyze the fluorescence spectrum of a two-level atom driven by a strong laser field and damped by the coupling to a reservoir with a modal density which is substantially frequency dependent in the spectral region of the atomic transition. In particular, the atom resides in an environment in which the density of modes varies appreciably on a frequency scale set by the Rabi frequency of the driving field [4, 5]. In our treatment, we use the dressed-atom model approach for the calculations of the fluorescence spectrum of the strongly driven two-level atom [6, 7]. In these calculations, we first couple the bare atom to the laser field ("dress" the atom in photons of the laser field), and next allow the dressed-atom system to fluoresce into the vacuum field. The dressed-atom system is characterized by three well-separated transition frequencies. If the spectral density of the vacuum field varies sufficiently rapidly with frequency, it should be possible to control separately the three decay rates between the dressed states. We will show that the central component of the Mollow triplet can be narrowed below the free space limit of $\frac{1}{2}\gamma$ if the decay rates of the transitions at the Rabi sidebands are strongly inhibited.

3.2.1 Dressed States of a Driven Atom

In the dressed-atom model approach we treat the driving laser field quantum mechanically [7]. The Hamiltonian of the system composed of a two-level atom and a single-mode laser field, in the electric dipole and rotating-wave approximations can be written as

$$\hat{H} = \hat{H}_0 + \hat{H}_I \,, \tag{3.33}$$

where

$$\hat{H}_0 = \hbar\omega_a S_z + \hbar\omega_L \left(\hat{a}_L^\dagger \hat{a}_L + \frac{1}{2}\right) \tag{3.34}$$

is the unperturbed (noninteracting) Hamiltonian of the atom plus the driving laser field, and

$$\hat{H}_I = -\mathrm{i}\hbar g \left(S^+ \hat{a}_L - S^- \hat{a}_L^\dagger\right) \tag{3.35}$$

is the interaction Hamiltonian of the atom and the driving field. Here, $\hat{a}_L$ and $\hat{a}_L^\dagger$ are the annihilation and creation operators for the driving field of frequency ω_L, and g is the coupling constants between the atom and the laser field mode.

The noninteracting atom+laser field Hamiltonian $\hat{H}_0$ has eigenstates, ("undressed" states), $|g, n\rangle = |g\rangle \otimes |n\rangle$ and $|e, n-1\rangle = |e\rangle \otimes |n-1\rangle$, where $|i\rangle$ is an atomic state ($i = g, e$), $|n\rangle$ is the state of the laser mode, and n is the number of photons in the laser mode. The undressed states form a ladder of doublets with the intra-doublet spacing $\Delta = \omega_a - \omega_L$, the detuning of the laser field frequency from the atomic transition frequency. We diagonalize the total Hamiltonian (3.33) in the basis formed by these undressed states. The diagonalization results in superposition states, the dressed states of the system

$$\begin{aligned} \left|\tilde{1}, n\right\rangle &= \cos\phi\,|g, n\rangle + \sin\phi\,|e, n-1\rangle \ , \\ \left|\tilde{2}, n\right\rangle &= \sin\phi\,|g, n\rangle - \cos\phi\,|e, n-1\rangle \ , \end{aligned} \tag{3.36}$$

with energies

$$E_{\tilde{1},n} = \hbar\left(n\omega_L - \frac{1}{2}\Omega\right) \ , \quad E_{\tilde{2},n} = \hbar\left(n\omega_L + \frac{1}{2}\Omega\right) \ , \tag{3.37}$$

where

$$\cos^2\phi = \frac{1}{2} + \frac{\Delta}{2\Omega} \ , \tag{3.38}$$

in which $\Omega = \sqrt{\Omega_0^2 + \Delta^2}$ is the Rabi frequency in the detuned field, and $\Omega_0 = 2g\sqrt{\langle n\rangle}$ is the on resonance Rabi frequency. In the derivation of the dressed states, we have assumed that the laser field is strong, $\langle n\rangle \gg 1$, and have approximated $g\sqrt{n+1} \approx g\sqrt{n} \approx g\sqrt{\langle n\rangle} = \Omega_0/2$.

3.2.2 Transition Rates

The dressed states, shown in Fig. 3.2, form an infinite ladder of doublets with inter-doublet spacing ω_L and intra-doublet spacing Ω. It is clear that in the dressed-atom basis the system, the two-level atom driven by a laser field, is no longer a two-level system. It is a multilevel system with three different transition frequencies, ω_L and $\omega_L \pm \Omega$. If the atom has no permanent dipole moments, transitions between dressed states occur with dipole moments

$$\begin{aligned}
\boldsymbol{\mu}_{\tilde{1}\tilde{1}} &= \left\langle n, \tilde{1} \right| \boldsymbol{\mu} \left| \tilde{1}, n-k \right\rangle = \boldsymbol{\mu}_{eg} \sin\phi\cos\phi \left(\delta_{n,n-1-k} + \delta_{n-1,n-k}\right) , \\
\boldsymbol{\mu}_{\tilde{2}\tilde{2}} &= \left\langle n, \tilde{2} \right| \boldsymbol{\mu} \left| \tilde{2}, n-k \right\rangle = -\boldsymbol{\mu}_{eg} \sin\phi\cos\phi \left(\delta_{n,n-1-k} + \delta_{n-1,n-k}\right) , \\
\boldsymbol{\mu}_{\tilde{1}\tilde{2}} &= \left\langle n, \tilde{1} \right| \boldsymbol{\mu} \left| \tilde{2}, n-k \right\rangle = -\boldsymbol{\mu}_{eg} \sin^2\phi \left(\delta_{n,n-1-k} + \delta_{n-1,n-k}\right) , \\
\boldsymbol{\mu}_{\tilde{2}\tilde{1}} &= \left\langle n, \tilde{2} \right| \boldsymbol{\mu} \left| \tilde{1}, n-k \right\rangle = \boldsymbol{\mu}_{eg} \cos^2\phi \left(\delta_{n,n-1-k} + \delta_{n-1,n-k}\right) ,
\end{aligned} \tag{3.39}$$

where $\boldsymbol{\mu}_{eg}$ is the transition dipole moment of the atom. The presence of the Kronecker delta functions, which are different from zero only for $k = \pm 1$, indicates that transitions with nonzero dipole moments occur only between dressed states of neighboring manifolds.

When we include the interaction of the dressed system with the vacuum field, spontaneous emission will occur from states of $|\tilde{i}, n\rangle$ to states $|\tilde{i}, n-1\rangle$, where $i = 1, 2$. According to (3.13), spontaneous emission damping rate from a state $|i\rangle$ to a state $|j\rangle$ is proportional to the absolute square of the transition dipole moment between these states. Therefore, the spontaneous emission damping rates between dressed states of two neighboring manifolds are of the form

$$\begin{aligned}
\gamma_{11} &= \gamma\tilde{D}(\omega_L)\sin^2\phi\cos^2\phi , \quad \gamma_{12} = \gamma\tilde{D}(\omega_L - \Omega)\sin^4\phi , \\
\gamma_{21} &= \gamma\tilde{D}(\omega_L + \Omega)\cos^4\phi , \quad \gamma_{22} = \gamma\tilde{D}(\omega_L)\sin^2\phi\cos^2\phi ,
\end{aligned} \tag{3.40}$$

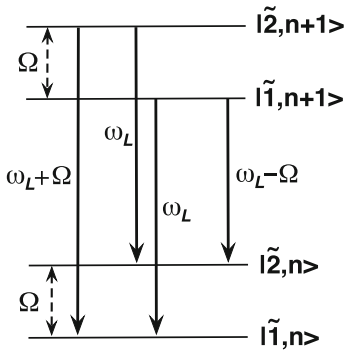

Fig. 3.2 Dressed states of a strongly driven two-level atom. The arrows indicate the allowed spontaneous transitions at frequencies ω_L and $\omega_L \pm \Omega$

where γ is the free space damping rate and $\tilde{D}(\omega_i) = D(\omega_i)/D(\omega_a)$ is the density of the field modes at a frequency ω_i relative to the density of the field modes at the atomic transition frequency ω_a in free space. Note that in free space $D(\omega_a)$ is a constant equal to $\mathcal{V}\omega_a^2/(\pi^2 c^3)$.

In distinction to free space in which the damping rates are constants, the rates (3.40) depend on the density of the vacuum field modes at the dressed-atom transition frequencies. In free space $\tilde{D}(\omega_L) = \tilde{D}(\omega_L \pm \Omega) = 1$. However, in a frequency-dependent reservoir of a finite bandwidth, say λ, the damping rates can be significantly altered if $\Omega \gg \lambda$. For example, if the distribution of the field modes is a simple Lorentzian that peaks at the laser frequency ω_L and the bandwidth $\lambda \ll \Omega$, then $\tilde{D}(\omega_L \pm \Omega) \approx 0$. In such a case, $\gamma_{12} = \gamma_{21} \approx 0$. Thus, the spontaneous emission from the dressed states can be significantly modified by a suitable choice of the Rabi frequency of the laser field. This kind of modification of spontaneous emission rates is called a dynamical modification of spontaneous emission rates, since it is imposed on the atom by a strong driving field.

3.2.3 Populations and Coherences

We now proceed to evaluate populations of the dressed states and coherences between them. We follow the master equation approach of Cohen-Tannoudji and Reynaud [6] with the usual simplifying approximations and assumptions:

- n is sufficiently large that the Rabi frequency determining the splitting of the doublets is taken to be constant.
- The Rabi frequency, and consequently the splitting of the doublets is taken to be large compared to the spontaneous emission rate γ.
- The coupling between the populations and coherences introduces correction terms of order γ/Ω. Because of assumption $\Omega \gg \gamma$, such terms are negligible, and therefore the coupling between the populations and coherences is ignored.

With these approximations, the reduced populations

$$P_{ii} = \sum_n \left\langle n, \tilde{i} \right| \varrho \left| \tilde{i}, n \right\rangle , \tag{3.41}$$

which are the diagonal elements of the density matrix of the system, satisfy the following set of coupled equations of motion

$$\dot{P}_{ii}(t) = -\gamma_i P_{ii}(t) + \sum_j \gamma_{ij} P_{jj}(t) , \tag{3.42}$$

where

$$\gamma_i = \sum_j \gamma_{ij} \tag{3.43}$$

is the total spontaneous emission decay rate from the dressed state $|\tilde{i}, n\rangle$ into the manifold below. In (3.42) the first term on the right-hand side is due to transitions out of $|\tilde{i}, n\rangle$ into the manifold below, and the second term to transitions into $|\tilde{i}, n\rangle$ from the states $|\tilde{j}, n+1\rangle$ of the manifold above.

The coherences between the dressed states are determined by the off-diagonal density matrix elements

$$\varrho_{ij,n} = \left\langle n, \tilde{i} \right| \varrho \left| \tilde{j}, n-1 \right\rangle . \tag{3.44}$$

If there is only one transition which has frequency ω_{ij} and the frequencies of the other transitions are significantly different from ω_{ij}, the reduced coherence $\varrho_{ij} = \sum_n \varrho_{ij,n}$ obeys the equation

$$\dot{\varrho}_{ij}(t) = -\left[\mathrm{i}\omega_{ij} + \frac{1}{2}\left(\gamma_i + \gamma_j\right) + \gamma_{ii} \right] \varrho_{ij}(t) . \tag{3.45}$$

If two or more transitions degenerate that they have the same transition frequency, the evolution of their corresponding reduced coherences satisfies a set of coupled equations

$$\dot{\varrho}_{ii}(t) = -\left(\mathrm{i}\omega_{ii} + \gamma_i\right) \varrho_{ii}(t) + \sum_j \gamma_{ji} \varrho_{jj}(t) . \tag{3.46}$$

Thus, the populations of the dressed states (3.36) satisfy the following set of coupled equations of motion

$$\begin{aligned} \dot{P}_{11}(t) &= -\gamma_{12} P_{11}(t) + \gamma_{21} P_{22}(t) , \\ \dot{P}_{22}(t) &= -\gamma_{21} P_{22}(t) + \gamma_{12} P_{11}(t) , \end{aligned} \tag{3.47}$$

with the condition $P_{11} + P_{22} = 1$.

Consider now the equations of motion for the coherences. It is easy to see that between two neighboring manifolds of the dressed states (3.36) there is only one transition of frequency $\omega_L + \Omega$, $|\tilde{2}, n\rangle \to |\tilde{1}, n-1\rangle$, and only one transition of frequency $\omega_L - \Omega$, $|\tilde{1}, n\rangle \to |\tilde{2}, n-1\rangle$, but there are two transitions of frequency ω_L, $|\tilde{1}, n\rangle \to |\tilde{1}, n-1\rangle$ and $|\tilde{2}, n\rangle \to |\tilde{2}, n-1\rangle$. Hence, for the corresponding coherences, we get the following equations of motion for the nondegenerate transitions

$$\begin{aligned} \dot{\varrho}_{21}(t) &= -\left[\mathrm{i}(\omega_L + \Omega) + \frac{1}{2}\left(\gamma_{11} + 3\gamma_{22} + \gamma_{12} + \gamma_{21}\right) \right] \varrho_{21}(t) , \\ \dot{\varrho}_{12}(t) &= -\left[\mathrm{i}(\omega_L - \Omega) + \frac{1}{2}\left(3\gamma_{11} + \gamma_{22} + \gamma_{12} + \gamma_{21}\right) \right] \varrho_{12}(t) , \end{aligned} \tag{3.48}$$

and a set of two coupled equations of motion for the degenerate transitions

$$\begin{aligned}\dot{\varrho}_{11}(t) &= -(\mathrm{i}\omega_L + \gamma_{12})\,\varrho_{11}(t) + \gamma_{21}\varrho_{22}(t)\,,\\ \dot{\varrho}_{22}(t) &= -(\mathrm{i}\omega_L + \gamma_{21})\,\varrho_{22}(t) + \gamma_{12}\varrho_{11}(t)\,.\end{aligned} \tag{3.49}$$

Setting the derivatives in (3.47) to zero, we obtain the steady-state populations of the dressed states

$$P_{11}(\infty) = \frac{\gamma_{21}}{\gamma_{12}+\gamma_{21}}\,, \quad P_{22}(\infty) = \frac{\gamma_{12}}{\gamma_{12}+\gamma_{21}}\,. \tag{3.50}$$

Note that the populations satisfy the detailed-balance condition

$$\gamma_{12}P_{11}(\infty) = \gamma_{21}P_{22}(\infty)\,. \tag{3.51}$$

The solution of (3.48) is easily found to be

$$\begin{aligned}\varrho_{21}(t) &= \varrho_{21}(0)\exp\{-[\mathrm{i}(\omega_L+\Omega)+\gamma_s]\,t\}\,,\\ \varrho_{12}(t) &= \varrho_{12}(0)\exp\{-[\mathrm{i}(\omega_L-\Omega)+\gamma_s]\,t\}\,,\end{aligned} \tag{3.52}$$

where

$$\gamma_s = \frac{1}{2}\,(4\gamma_{11}+\gamma_{12}+\gamma_{21})\,, \tag{3.53}$$

and we have used the fact that $\gamma_{22} = \gamma_{11}$. Note that the coherences decay with the same rate γ_s.

To solve the set of coupled equations (3.49), we introduce the Laplace transform of the coherences

$$\varrho_{ii}(z) \equiv \int_0^\infty \mathrm{d}t\,\mathrm{e}^{-zt}\varrho_{ii}(t)\,. \tag{3.54}$$

Then in terms of the Laplace transforms, (3.49) becomes

$$\begin{pmatrix} z+\gamma_{12}+\mathrm{i}\omega_L & -\gamma_{21} \\ -\gamma_{12} & z+\gamma_{21}+\mathrm{i}\omega_L \end{pmatrix}\begin{pmatrix}\varrho_{11}(z)\\ \varrho_{22}(z)\end{pmatrix} = \begin{pmatrix}\varrho_{11}(0)\\ \varrho_{22}(0)\end{pmatrix}\,. \tag{3.55}$$

The solutions for the Laplace transforms are easily obtained and can be written as

$$\begin{aligned}\varrho_{11}(z) &= \frac{(z+\mathrm{i}\omega_L+\gamma_{21})\varrho_{11}(0)+\gamma_{21}\varrho_{22}(0)}{(z+\mathrm{i}\omega_L)(z+\mathrm{i}\omega_L+\gamma_{12}+\gamma_{21})}\,,\\ \varrho_{22}(z) &= \frac{(z+\mathrm{i}\omega_L+\gamma_{12})\varrho_{22}(0)+\gamma_{12}\varrho_{11}(0)}{(z+\mathrm{i}\omega_L)(z+\mathrm{i}\omega_L+\gamma_{12}+\gamma_{21})}\,.\end{aligned} \tag{3.56}$$

By inverting the Laplace transforms $\varrho_{11}(z)$ and $\varrho_{22}(z)$, we transform the solutions back to the time domain and find

$$\begin{aligned}\varrho_{11}(t) &= \frac{\gamma_{21}\left[\varrho_{11}(0)+\varrho_{22}(0)\right]}{\gamma_{12}+\gamma_{21}}\mathrm{e}^{-\mathrm{i}\omega_L t}+\frac{\gamma_{12}\varrho_{11}(0)-\gamma_{21}\varrho_{22}(0)}{\gamma_{12}+\gamma_{21}}\mathrm{e}^{-(\gamma_c+\mathrm{i}\omega_L)t}\,,\\ \varrho_{22}(t) &= \frac{\gamma_{12}\left[\varrho_{11}(0)+\varrho_{22}(0)\right]}{\gamma_{12}+\gamma_{21}}\mathrm{e}^{-\mathrm{i}\omega_L t}\\ &\quad+\frac{\gamma_{21}\varrho_{22}(0)-\gamma_{12}\varrho_{11}(0)}{\gamma_{12}+\gamma_{21}}\mathrm{e}^{-(\gamma_c+\mathrm{i}\omega_L)t}\,,\end{aligned} \tag{3.57}$$

where $\gamma_c = \gamma_{12} + \gamma_{21}$ is the decay rate of the coherences.

3.2.4 Incoherent Fluorescence Spectrum

To evaluate the fluorescence spectrum of the field emitted by the dressed-atom system we use the expression (2.19) which describes the incoherent part of the spectrum of the total field radiated by a multilevel system. Adopted to our single-atom ($N = 1$) dressed-atom system, the spectrum can be written as

$$\begin{aligned}S_{\mathrm{in}}(\omega) &= 2\mathrm{Re}\sum_{i,k>j,l}\sqrt{\gamma_{ij}\gamma_{kl}}\cos\theta_{ik}\\ &\quad\times\int_0^\infty \mathrm{d}\tau\,\langle\delta S_{ij}(0)\,\delta S_{lk}(\tau)\rangle\mathrm{e}^{\mathrm{i}(\omega-\omega_L)\tau}\,,\end{aligned} \tag{3.58}$$

where $S_{ij} = |\tilde{i}, n\rangle\langle n-1, \tilde{j}|$ and $S_{lk} = |\tilde{l}, n\rangle\langle n-1, \tilde{k}|$ are projection operators between the dressed states. The terms ($i = k$, $j = l$) are the contributions to the spectrum from the dressed-atom transitions, whereas terms $i \neq k$, $j \neq l$ are cross (interference) terms between the transitions.

Since we assume $\Omega \gg \gamma$, the transition frequencies differ significantly from each other, so we can neglect the contributions of the interference term. Hence, the expression (3.58) reduces to

$$S_{\mathrm{in}}(\omega) = 2\mathrm{Re}\sum_{i,j}\gamma_{ij}\int_0^\infty \mathrm{d}\tau\,\langle\delta S_{ij}(0)\,\delta S_{ji}(\tau)\rangle\mathrm{e}^{\mathrm{i}(\omega-\omega_L)\tau}\,. \tag{3.59}$$

According to the quantum regression theorem, the two-time correlation function $\langle\delta S_{ij}(0)\,\delta S_{ji}(\tau)\rangle$ satisfies the same equation of motion as the one-time average $\langle\delta S_{ji}(\tau)\rangle = \tilde{\varrho}_{ij}(\tau)$ with the initial condition

$$\langle\delta S_{ij}(0)\,\delta S_{ji}(0)\rangle = P_{ii}\,, \tag{3.60}$$

where P_{ii} is the steady-state population of the state $|\tilde{i}, n\rangle$.

The one-time average $\langle \delta S_{ji}(\tau) \rangle$ satisfies the same equation of motion as $\tilde{\varrho}_{ji}(\tau) = \varrho_{ji}(\tau) \exp(i\omega_L t)$, the slowly varying part of the coherence $\varrho_{ji}(\tau)$. When the spectral lines do not overlap, the Fourier transform of the two-time correlation function is simply a sum of Lorentzians

$$F(\omega - \omega_{ij}) = \gamma_{ii} P_{ii} \frac{\gamma_s}{(\omega - \omega_{ij})^2 + \gamma_s^2}, \quad i \neq j,$$
$$F(\omega - \omega_L) = (\gamma_{12} P_{11} + \gamma_{21} P_{22}) \frac{\gamma_c}{(\omega - \omega_L)^2 + \gamma_c^2}, \tag{3.61}$$

which yields the incoherent fluorescence spectrum

$$S_{\text{in}}(\omega) = P_{11} P_{22} \frac{4(\gamma_{11} + \gamma_{22})\gamma_c}{(\omega - \omega_L)^2 + \gamma_c^2} + P_{11} \frac{2\gamma_{12}\gamma_s}{(\omega - \omega_L + \Omega)^2 + \gamma_s^2} + P_{22} \frac{2\gamma_{21}\gamma_s}{(\omega - \omega_L - \Omega)^2 + \gamma_s^2}. \tag{3.62}$$

The first term in (3.62) represents the central component of the spectrum, the next two are the Rabi sidebands. The widths of the spectral lines, what interests us the most here, are

$$\gamma_c = \gamma \left[\tilde{D}(\omega_L - \Omega) \sin^4 \phi + \tilde{D}(\omega_L + \Omega) \cos^4 \phi \right],$$
$$\gamma_s = \frac{1}{2}\gamma \Big[4\tilde{D}(\omega_L) \sin^2\phi \cos^2\phi + \tilde{D}(\omega_L - \Omega) \sin^4\phi + \tilde{D}(\omega_L + \Omega) \cos^4\phi \Big]. \tag{3.63}$$

Let us discuss in more details the variation of the spectral widths with the density of the vacuum field modes. For clarity, assume that $\Delta = 0$ ($\phi = \pi/4$). In this case the expressions for the widths simplify to

$$\gamma_c = \frac{1}{4}\gamma \left[\tilde{D}(\omega_L - \Omega) + \tilde{D}(\omega_L + \Omega) \right],$$
$$\gamma_s = \frac{1}{2}\gamma \left\{ \tilde{D}(\omega_L) + \frac{1}{4} \left[\tilde{D}(\omega_L - \Omega) + \tilde{D}(\omega_L + \Omega) \right] \right\}. \tag{3.64}$$

The linewidths are sensitively dependent on the density of the field modes at different components of the spectrum. The linewidth of the central component at frequency ω_L depends on the density of the modes at the Rabi sideband frequencies. In other words, the decay at frequency ω_L is induced by the vacuum fluctuations at the Rabi sidebands. Hence, the linewidth of the central component can be narrower that the natural linewidth $\gamma/2$ and can even be reduced to zero when $\tilde{D}(\omega_L \pm \Omega) = 0$. Quantum fluctuations at frequency ω_L do not induce the spontaneous decay at that frequency. They may still induce the decay at the Rabi sideband frequencies.

In summary of this section, the linewidth of the central component of the Mollow triplet can be narrower than the natural linewidth if the atom decays to a frequency-dependent reservoir of a finite bandwidth. The decay can even be inhibited if the vacuum field does not support quantum fluctuations at frequencies of the Rabi sidebands of the spectrum.

3.3 Atomic Population Inversion in a Tailored Vacuum

The decay of an atom in a tailored (frequency dependent) reservoir of a finite bandwidth may result not only in the narrowing of the spectral lines, but also can lead to a steady-state population inversion between bare atomic states. In this section, we investigate the influence of the tailored vacuum on the steady-state population inversion between the bare atomic states of a two-level atom driven by a coherent laser field. As we have seen, the population inversion between the bare atom excited state $|e\rangle$ and ground state $|g\rangle$ is determined by the quantity $\langle S_z\rangle$ defined as a difference between the populations of the excited and ground states

$$\langle S_z\rangle = \frac{1}{2}\left(\varrho_{ee} - \varrho_{gg}\right) . \tag{3.65}$$

In Sect. 3.1.1 we have shown that $\langle S_z\rangle \leq 0$, indicating that the population of the atom cannot be inverted when the vacuum field is that of free space.

3.3.1 Enhancement and Suppression of the Atomic Excitation

Consider now a two-level atom placed in an empty cavity and driven by an off-resonant laser field, $\Delta \neq 0$. According to (3.40), if the density of the cavity modes varies rapidly with frequency such that the cavity bandwidth λ is smaller than the Rabi frequency Ω then it should be possible to control separately the three decay rates (3.40) and hence modify the steady-state population distribution. It is not difficult to show, using the solution (3.50) for the steady-state population of the dressed states, that in the case $\Omega \gg \gamma$, the population of the excited state is

$$\begin{aligned}\varrho_{ee} &= \frac{\gamma_{12}\cos^2\phi + \gamma_{21}\sin^2\phi}{\gamma_{12}+\gamma_{21}} \\ &= \frac{\tilde{D}(\omega_L-\Omega)\sin^4\phi\cos^2\phi + \tilde{D}(\omega_L+\Omega)\cos^4\phi\sin^2\phi}{\tilde{D}(\omega_L-\Omega)\sin^4\phi + \tilde{D}(\omega_L+\Omega)\cos^4\phi} .\end{aligned} \tag{3.66}$$

We see that the population depends only on the transition rates at the Rabi sideband frequencies. In free space $\tilde{D}(\omega_L \pm \Omega) = 1$, and then

$$\varrho_{ee} = \frac{\sin^2\phi\cos^2\phi}{\sin^4\phi + \cos^4\phi} = \frac{1}{2}\left[1 - \frac{\cos^2(2\phi)}{\sin^4\phi + \cos^4\phi}\right]. \tag{3.67}$$

Clearly, ϱ_{ee} cannot be larger than $1/2$, that population inversion between bare atomic states is not possible to achieve in free space.

The situation differs when the atom is placed inside the cavity. If the Rabi frequency of the driving field is much larger than the cavity bandwidth, $\Omega \gg \lambda$, then the cavity field can be tuned to only one of the three transition frequencies of the dressed-atom system. Consequently, either γ_{12} or γ_{21} will be equal to zero. Suppose that the cavity field is tuned to the higher frequency Rabi sideband. In this case $\tilde{D}(\omega_L - \Omega) = 0$ and then the expression (3.66) reduces to

$$\varrho_{ee} = \sin^2\phi\,. \tag{3.68}$$

For $\Delta < 0$, $\sin^2\phi > \frac{1}{2}$, which implies that $\varrho_{ee} > \frac{1}{2}$. Thus, it is possible for the cavity to create a steady-state atomic population inversion. The population inversion may even reach total inversion, which can happen for $|\Delta| \gg \gamma$, at which $\sin^2\phi \approx 1$. On the other hand, for $\Delta > 0$, $\sin^2\phi < \frac{1}{2}$, which implies a reduction of the population of the atomic excited state. It is interesting that the population ϱ_{ee} varies with the density of the modes only when $\Delta \neq 0$. For $\Delta = 0$, the population ϱ_{ee} is independent of $\tilde{D}(\omega)$.

3.3.2 *Enhancement and Suppression of the Atomic Excitation: Experiment*

The variation of the excited state population with the density of the modes was demonstrated experimentally by the Mossberg's group at Oregon [8]. Their apparatus shown schematically in Fig. 3.3 involved an optical cavity formed by two spherical

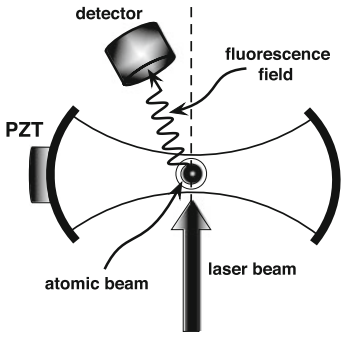

Fig. 3.3 The main features of the apparatus used by Zhu et al. [8] for observing the fluorescence from a driven two-level atom alternated by the finite bandwidth vacuum mode structure of a cavity

mirrors separated by 1 cm and mounted in an Invar holder which was equipped with piezoelectric transducer (PZT) for cavity tuning. A beam of barium atoms was made to pass the center of the cavity in the direction normal to the cavity axis. The output of a cw ring dye laser, propagating normal to both the cavity axis and the barium beam, was used to excite the ${}^1S_0 - {}^1P_1$ transition in atoms. The atomic fluorescence into side modes was detected along a direction 10° away from antiparallel with the laser beam and normal to the atomic beam.

Figure 3.4 shows the experimental results for the fluorescence intensity, and hence the population of the atomic excited state, obtained for varying the cavity frequency. The trace (a) shows the variation of the fluorescence intensity for a large negative detuning, $\Delta < 0$, whereas the trace (c) shows the corresponding results for $\Delta > 0$. The intensity of the fluorescence field varies with the cavity detuning with maximum (minimum) at the cavity frequency tuned to the Rabi sidebands of the fluorescence field. For $\Delta > 0$, the fluorescence is enhanced when the cavity frequency is tuned to the lower frequency Rabi sideband ($\gamma_{12} \neq 0$), and reduced when the cavity frequency is tuned to the higher frequency Rabi sideband, ($\gamma_{21} \neq 0$). The observed variation of the fluorescence intensity with the laser frequency agrees perfectly with the theoretical result given in (3.66). Trace (b) shows the variation of the fluorescence intensity for $\Delta = 0$. Clearly, the intensity remains almost constant independent of the cavity frequency. This is consistent with the theoretical result (3.66) which shows that for $\Delta = 0$, the population ϱ_{ee} is constant ($=\frac{1}{2}$) and independent of any frequency.

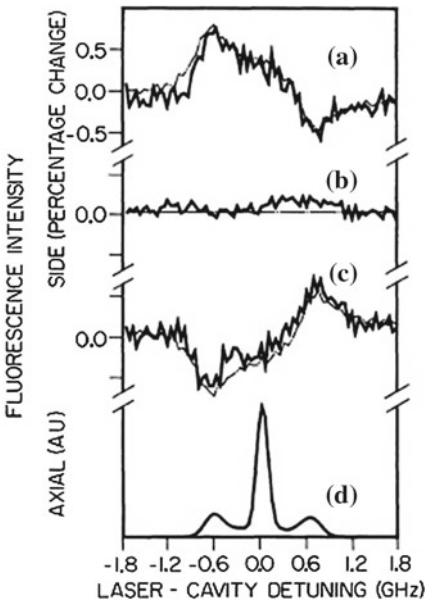

Fig. 3.4 Observation by Zhu et al. [8] of the variation of the fluorescence intensity with the cavity frequency for different detunings Δ of the laser field from the atomic resonance: trace **a** $\Delta < 0$, trace **b** $\Delta = 0$, and trace **c** $\Delta > 0$. Trace **d** shows the observed Mollow triplet. The experiment aimed to demonstrate that the cavity field appears as a finite bandwidth reservoir to the driven atoms. Reprinted with permission from Y. Zhu, A. Lezama, T.W. Mossberg, M. Lewenstein: Phys. Rev. Lett. **61**, 1946 (1988). Copyright (1988) by the American Physical Society

3.4 Spectral Linewidth Narrowing in Free Space

Before we move to discuss further examples of the dynamical suppression of spectral linewidths, we show that a narrowing below the natural linewidth appears in the spectrum of the fluorescence field of a weakly driven two-level atom in free space.

It is easily verified that in the absence of the driving field ($\Omega = 0$), an initially excited atom ($\varrho_{ee}(0) = 1$) decays to the ground state producing the radiation whose the spectral distribution is a Lorentzian centered on the atomic transition frequency ω_a and bandwidth equal to the natural linewidth $\gamma/2$:

$$S_{\rm in}(\omega) = \frac{\gamma^2}{\frac{1}{4}\gamma^2 + (\omega - \omega_a)^2} \,. \tag{3.69}$$

In Sect. 3.1.3, we derived the Laplace transform of the correlation function needed to determine the fluorescence spectrum, expression (3.30), which is valid for an arbitrary strength of the excitation field, given by the Rabi frequency Ω. For $\Delta = 0$ and in the limit of a weak driving field ($\Omega \ll \gamma$) the function $Y_2(z)$ can be written as

$$Y_2(z) = \frac{2\Omega^4}{(\gamma^2 + 2\Omega^2)^2} \frac{(z+\gamma)^2 + \frac{1}{2}\Omega^2}{(z+\frac{1}{2}\gamma)(z+\frac{1}{2}\gamma + \frac{2\Omega^2}{\gamma})(z+\gamma - \frac{2\Omega^2}{\gamma})} \,. \tag{3.70}$$

When we invert (3.70) to the time domain, we find that up to the second-order in Ω/γ:

$$Y_2(\tau) = \frac{1}{2}\left(\frac{\Omega}{\gamma}\right)^2 \left\{ e^{-[\frac{1}{2}\gamma - i(\omega-\omega_a)]\tau} - e^{-\left[\left(\frac{1}{2}\gamma + \frac{2\Omega^2}{\gamma}\right) - i(\omega-\omega_a)\right]\tau} \right\} \,. \tag{3.71}$$

By substituting (3.71) into (3.25), we obtain the stationary incoherent spectrum

$$S_{\rm in}(\omega) = \frac{\Omega^2}{\gamma}\left[\frac{\frac{1}{2}\gamma}{\frac{1}{4}\gamma^2 + (\omega-\omega_a)^2} - \frac{\frac{1}{2}\gamma\left(1 + \frac{4\Omega^2}{\gamma^2}\right)}{\frac{1}{4}\gamma^2\left(1 + \frac{4\Omega^2}{\gamma^2}\right)^2 + (\omega-\omega_a)^2} \right] \,. \tag{3.72}$$

The spectrum is composed of two Lorentzians centered at frequency ω_a with one of the Lorentzians contributing with negative weight. It was first noted by Mollow [3]. The subtraction of the Lorentzians results in a square of a Lorentzian

$$S_{\rm in}(\omega) = \frac{1}{2}\left(\frac{\Omega}{\gamma}\right)^2 \frac{\gamma^2\Omega^2}{\left[\frac{1}{4}\gamma^2 + (\omega-\omega_a)^2\right]^2} \,. \tag{3.73}$$

The square of the Lorentzian results in the spectrum falling off as $(\omega - \omega_0)^{-4}$ in the wings instead of a $(\omega - \omega_0)^{-2}$ falling which would result if all spectral components were positive. What this means is that the spectral line becomes narrower than that of

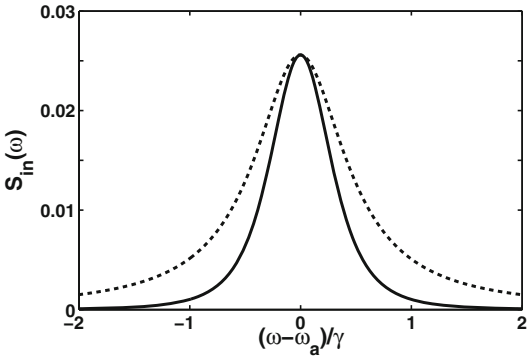

Fig. 3.5 Incoherent part of the fluorescence spectrum for a weak driving field ($\Omega = 0.2\gamma$) (*solid line*). The *dashed line* is the Lorentzian $2\Omega^4/\gamma^2[\frac{1}{4}\gamma^2 + (\omega - \omega_a)^2]$

the natural linewidth $\gamma/2$. This is illustrated in Fig. 3.5, where we plot the spectrum (3.73) together with a Lorentzian of the bandwidth $\gamma/2$. We see a narrowing of the spectral line below the linewidth $\gamma/2$.

The interpretation of the spectral line narrowing can be provided by relating the incoherent spectrum to the quadrature fluctuations (squeezing) spectra. It was shown by Rice and Carmichael [9] that the negative weight of the spectral component can be attributed to squeezing of the fluctuations of the induced atomic dipole moment. They have also demonstrated that the two Lorentzians correspond to the quadrature noise spectrum, squeezing spectrum of the fluorescence field. In other words, the induced squeezed fluctuations of its own atomic dipole moment allow the partial inhibition of spontaneous emission from the atom even in free space, the ordinary vacuum field. We defer the detailed analysis of the source of the narrowing of the spectral line to Chap. 8, after first introducing the concept of squeezing and the squeezing spectrum in Chap. 6.

3.5 Spectral Linewidth Narrowing in Free Space via Coherent Pumping

In Sect. 3.2 we have seen how the concept of a frequency-dependent reservoir led to the prediction of a dynamical reduction of spontaneous emission which resulted in a line narrowing in the fluorescence spectrum and even fluorescence quenching at frequency of the central component of the Mollow triplet. In this section, we will investigate the line narrowing in a three-level atom driven by two coherent laser fields such that each laser is coupled only to one of the two possible transitions. We are particularly interested in the manner in which a weak laser field coupled to one of the two atomic transitions affects the fluorescence field emitted from the other transition driven by a strong laser field. Using the master equation technique, we calculate the steady-state fluorescence spectrum of the field emitted on the transition driven by the strong laser field.

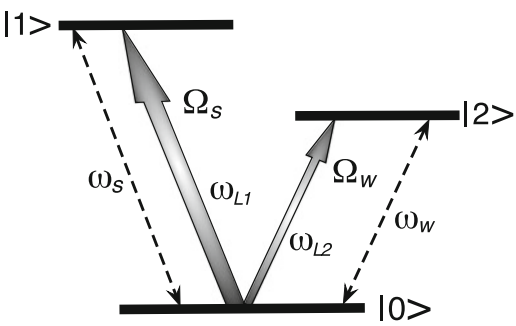

Fig. 3.6 Energy level diagram of a three-level Vee-type system driven by two lasers of frequencies ω_{L1} and ω_{L2} which are exactly equal to the atomic transition frequencies ω_w and ω_s, respectively

Our physical interpretation of the spectral features is based on the quantum dressed-atom model of the system. The dressed states of the system are identified, and the spectral features are explained in terms of the transitions among these dressed states.

The possibility of modifying linewidths of the spectral lines of the fluorescence field emitted by a three-level Vee-type atom using intense laser fields was first noted by Narducci et al. [10]. The details of the energy-level structure of the system and the configuration of the driving fields are shown in Fig. 3.6. The atom in the Vee configuration is driven by two single-mode coherent laser fields and simultaneously interacts with the quantized multimode radiation field whose the modes are in the vacuum state. The first laser of the Rabi frequency Ω_s is coupled to the atomic transition $|1\rangle \leftrightarrow |0\rangle$ and has an angular frequency ω_{L1} which is exactly equal to the atomic transition frequency ω_s, i.e., the one-photon detuning $\Delta_s = \omega_s - \omega_{L1}$ is zero. The second laser of the Rabi frequency Ω_w is coupled to the atomic transition $|2\rangle \leftrightarrow |0\rangle$ and has an angular frequency ω_{L2} which is exactly equal to the atomic transition frequency ω_w, i.e., the one-photon detuning $\Delta_w = \omega_w - \omega_{L2}$ is zero. On the other hand, the frequency ω_s is significantly different from ω_w, so that each laser is coupled only to one of the two possible transitions in the three-level atom.

3.5.1 *Fluorescence Spectrum*

We want to find the incoherent part of the steady-state spectrum of the fluorescence field emitted on the $|1\rangle \rightarrow |0\rangle$ transition that is not superimposed on the fluorescence field emitted on the $|2\rangle \rightarrow |0\rangle$ transition. This is done by finding the Fourier transform of the two-time correlation function of the atomic dipole operators

$$S_{\rm in}(\omega) = 2{\rm Re}\sum_{i,j=1}^{2}\int_0^\infty {\rm d}\tau \lim_{t\to\infty}\Big[\langle S_i^+(t)S_j^-(t+\tau)\rangle - \langle S_i^+(t)\rangle\langle S_j^-(t+\tau)\rangle\Big]{\rm e}^{{\rm i}\omega\tau}\,. \tag{3.74}$$

For well-separated atomic transition frequencies, that the frequency difference between the two atomic transitions is much larger than the Rabi frequencies of the laser fields and the spontaneous emission rates of the transitions, i.e., $\Delta = \omega_s - \omega_w \gg \Omega_s, \Omega_w, \gamma_s, \gamma_w$, the spectrum (3.74) can be written as a sum of two independent terms corresponding to the frequency separated fluorescence fields

$$S_{\rm in}(\omega) = 2{\rm Re}\int_0^\infty {\rm d}\tau \lim_{t\to\infty}\left\{\left[\langle\tilde{S}_1^+(t)\tilde{S}_1^-(t+\tau)\rangle - \langle\tilde{S}_1^+(t)\rangle\langle\tilde{S}_1^-(t+\tau)\rangle\right]{\rm e}^{{\rm i}(\omega-\omega_s)\tau}\right.$$
$$\left. + \left[\langle\tilde{S}_2^+(t)\tilde{S}_2^-(t+\tau)\rangle - \langle\tilde{S}_2^+(t)\rangle\langle\tilde{S}_2^-(t+\tau)\rangle\right]{\rm e}^{{\rm i}(\omega-\omega_w)\tau}\right\} , \tag{3.75}$$

where

$$\tilde{S}_1^\pm(t) = S_1^\pm(t)\exp(\mp{\rm i}\omega_s\tau) ,$$
$$\tilde{S}_2^\pm(t) = S_2^\pm(t)\exp(\mp{\rm i}\omega_w\tau) , \tag{3.76}$$

are the slowly varying parts of the atomic operators.

The first term on the right-hand side of (3.75) will differ significantly from zero only for those frequencies ω which are near the laser frequency ω_s. Similarly, the second term differs significantly from zero only for those frequencies ω which are near the laser frequency ω_w. Therefore, the incoherent part of the spectrum of the fluorescence field emitted with frequencies ω near the frequency ω_s of the $|1\rangle \to |0\rangle$ transition driven by the resonant laser field of frequency ω_s is given by

$$S_{\rm in}(\omega-\omega_s) = 2{\rm Re}\int_0^\infty {\rm d}\tau\, G(\tau){\rm e}^{{\rm i}(\omega-\omega_s)\tau} , \tag{3.77}$$

where

$$G(\tau) = \lim_{t\to\infty}\left[\langle\tilde{S}_1^+(t)\tilde{S}_1^-(t+\tau)\rangle - \langle\tilde{S}_1^+(t)\rangle\langle\tilde{S}_1^-(t+\tau)\rangle\right] . \tag{3.78}$$

Thus, in order to calculate the incoherent spectrum of the fluorescence field emitted on the $|1\rangle \to |0\rangle$ transition, we have to determine the time evolution of the atomic correlation function $G(\tau)$. This is done in the usual way by applying the quantum regression theorem, which says that for $\tau > 0$ the two-time correlation function $\langle\tilde{S}_1^+(t)\tilde{S}_1^-(t+\tau)\rangle$ satisfies the same equations of motion as the one-time average $\langle\tilde{S}_1^-(\tau)\rangle$. On the other hand, the average $\langle\tilde{S}_1^-(\tau)\rangle$ satisfies the same equation of motion as the density matrix element

$$\tilde{\varrho}_{10}(\tau) = \varrho_{10}\exp({\rm i}\omega_s\tau) . \tag{3.79}$$

The time evolution of the density matrix element is found from the master equation for the reduced density operator of the system, which in the Schrödinger picture is given by

$$\frac{\mathrm{d}\varrho}{\mathrm{d}t} = -\frac{\mathrm{i}}{\hbar}\left[\hat{H}_0, \varrho\right] - \frac{1}{2}\gamma_1\left(S_1^+ S_1^- \varrho + \varrho S_1^+ S_1^- - 2S_1^- \varrho S_1^+\right) - \frac{1}{2}\gamma_2\left(S_2^+ S_2^- \varrho + \varrho S_2^+ S_2^- - 2S_2^- \varrho S_2^+\right) , \tag{3.80}$$

where γ_1 and γ_2 are the spontaneous decay rates of the $|1\rangle \rightarrow |0\rangle$ and $|2\rangle \rightarrow |0\rangle$ transitions, respectively, and $\hat{H}_0$ is the Hamiltonian composed of two terms

$$\hat{H}_0 = \hat{H}_A + \hat{H}_{\mathrm{int}} , \tag{3.81}$$

where

$$\hat{H}_A = \hbar\left[\omega_s |1\rangle\langle 1| + \omega_w |2\rangle\langle 2|\right] \tag{3.82}$$

is the Hamiltonian of the atom, and

$$\hat{H}_{\mathrm{int}} = \frac{1}{2}\mathrm{i}\hbar\Omega_s\left[S_1^+(t)\exp\left(-\mathrm{i}\omega_s t\right) - S_1^-(t)\exp\left(\mathrm{i}\omega_s t\right)\right] + \frac{1}{2}\mathrm{i}\hbar\Omega_w\left[S_2^+(t)\exp\left(-\mathrm{i}\omega_w t\right) - S_2^-(t)\exp\left(\mathrm{i}\omega_w t\right)\right] \tag{3.83}$$

is the interaction between the atom and the driving laser fields. The parameters Ω_s and Ω_w that appear in (3.83) are the Rabi frequencies of the laser fields coupled to the strong and weak transitions, respectively.

Suppose that each of the atomic transitions is driven by a resonant laser field. In this case, the master equation (3.80) leads to the following set of coupled equations of motion for the density matrix elements

$$\begin{aligned}
\dot{\varrho}_{11} &= -\gamma_s \varrho_{11} + \frac{1}{2}\Omega_s\left(\tilde{\varrho}_{10} + \tilde{\varrho}_{01}\right) , \\
\dot{\varrho}_{22} &= -\gamma_w \varrho_{22} + \frac{1}{2}\Omega_w\left(\tilde{\varrho}_{02} + \tilde{\varrho}_{20}\right) , \\
\dot{\tilde{\varrho}}_{01} &= \frac{1}{2}\Omega_s - \frac{1}{2}\gamma_s\tilde{\varrho}_{01} - \frac{1}{2}\Omega_s\left(2\varrho_{11} + \varrho_{22}\right) - \frac{1}{2}\Omega_w\varrho_{21} , \\
\dot{\tilde{\varrho}}_{10} &= \frac{1}{2}\Omega_s - \frac{1}{2}\gamma_s\tilde{\varrho}_{10} - \frac{1}{2}\Omega_s\left(2\varrho_{11} + \varrho_{22}\right) - \frac{1}{2}\Omega_w\varrho_{12} , \\
\dot{\tilde{\varrho}}_{02} &= \frac{1}{2}\Omega_w - \frac{1}{2}\gamma_w\tilde{\varrho}_{02} - \frac{1}{2}\Omega_s\varrho_{12} - \frac{1}{2}\Omega_w\left(2\varrho_{22} + \varrho_{11}\right) , \\
\dot{\tilde{\varrho}}_{20} &= \frac{1}{2}\Omega_w - \frac{1}{2}\gamma_w\tilde{\varrho}_{20} - \frac{1}{2}\Omega_s\varrho_{21} - \frac{1}{2}\Omega_w\left(2\varrho_{22} + \varrho_{11}\right) , \\
\dot{\varrho}_{21} &= -\frac{1}{2}\left(\gamma_s + \gamma_w\right)\varrho_{21} + \frac{1}{2}\Omega_w\tilde{\varrho}_{01} + \frac{1}{2}\Omega_s\tilde{\varrho}_{20} , \\
\dot{\varrho}_{12} &= -\frac{1}{2}\left(\gamma_s + \gamma_w\right)\varrho_{12} + \frac{1}{2}\Omega_w\tilde{\varrho}_{10} + \frac{1}{2}\Omega_s\tilde{\varrho}_{02} ,
\end{aligned} \tag{3.84}$$

where

$$\tilde{\varrho}_{20}(t) = \varrho_{20}(t)\exp(\mathrm{i}\omega_w t)\ , \qquad \tilde{\varrho}_{10}(t) = \varrho_{10}(t)\exp(\mathrm{i}\omega_s t)\ , \tag{3.85}$$

are the slowly varying parts of the off-diagonal density matrix elements. In the derivation of (3.84), we have assumed that the frequencies ω_{L1} and ω_{L2} of the driving fields are on resonance with the $|0\rangle \rightarrow |1\rangle$ and $|0\rangle \rightarrow |2\rangle$ transitions, respectively.

The size of the density matrix of the system makes it difficult to solve the set of coupled equations (3.84) analytically. Therefore we will use numerical methods. For purposes of numerical computation it is convenient to rewrite the set of the equations of motion in a matrix form

$$\dot{\boldsymbol{X}}(t) = \mathbf{Q}\boldsymbol{X}(t) + \boldsymbol{I}\ , \tag{3.86}$$

where $\mathbf{Q}$ is a 8×8 matrix of the coefficients of the differential equations for the density matrix elements, $\boldsymbol{X}(t)$ is a 8×1 column vector composed of the eight density matrix elements

$$\boldsymbol{X}(t) = \mathrm{col}\,(\varrho_{11}, \varrho_{22}, \tilde{\varrho}_{01}, \tilde{\varrho}_{10}, \tilde{\varrho}_{02}, \tilde{\varrho}_{20}, \varrho_{21}, \varrho_{12})\ , \tag{3.87}$$

and $\boldsymbol{I}$ is a 8×1 column vector with the components

$$\boldsymbol{I} = \mathrm{col}\,(0, 0, \Omega_s/2, \Omega_s/2, \Omega_w/2, \Omega_w/2, 0, 0)\ . \tag{3.88}$$

We first find the steady-state solution of (3.86), which is obtained by taking the limit of $t \rightarrow \infty$, or more directly by setting the left-hand side of (3.86) equal to zero. Thus

$$\boldsymbol{X}(\infty) = -\mathbf{Q}^{-1}\boldsymbol{I}. \tag{3.89}$$

Next, we consider two-time correlation function $G(\tau)$ involved in the calculation of the spectrum (3.77). Since the function $G(\tau)$ involves fluctuations operators, one can easily find by applying the quantum regression theorem to (3.86) that the two-time correlations functions of the fluctuation operators satisfy an equation of motion

$$\frac{\mathrm{d}}{\mathrm{d}\tau}\delta\boldsymbol{Y}(\tau) = \mathbf{Q}\delta\boldsymbol{Y}(\tau), \tag{3.90}$$

where the components of the vector $\delta\boldsymbol{Y}(t, \tau)$ are

$$\begin{aligned}\delta\boldsymbol{Y}(\tau) = \mathrm{col}\,\big\{&\langle\delta S_1^+\delta[S_1^+(\tau)S_1^-(\tau)]\rangle, \langle\delta S_1^+\delta[S_2^+(\tau)S_2^-(\tau)]\rangle,\\ &\langle\delta S_1^+\delta S_1^+(\tau)\rangle, \langle\delta S_1^+\delta S_1^-(\tau)\rangle, \langle\delta S_1^+\delta S_2^+(\tau)\rangle, \langle\delta S_1^+\delta S_2^-(\tau)\rangle,\\ &\langle\delta S_1^+\delta[S_1^+(\tau)S_2^-(\tau)]\rangle, \langle\delta S_1^+\delta[S_2^+(\tau)S_1^-(\tau)]\rangle\big\}\ .\end{aligned} \tag{3.91}$$

Applying the Laplace transform to (3.90), we find

$$\Delta \boldsymbol{Y}(z) = (z\mathbf{I} - \mathbf{Q})^{-1}\, \Delta \boldsymbol{Y}(0), \tag{3.92}$$

where the "initial" vector $\Delta \boldsymbol{Y}(0)$ is composed of the steady-state values of the density matrix elements

$$\begin{aligned}\Delta \boldsymbol{Y}(0) = \mathrm{col}\,\{&-\tilde{\varrho}^s_{01}\varrho^s_{11}, -\tilde{\varrho}^s_{01}\varrho^s_{22}, \varrho^s_{11} - \tilde{\varrho}^s_{01}\tilde{\varrho}^s_{10}, -(\tilde{\varrho}^s_{01})^2, \varrho^s_{21} - \tilde{\varrho}^s_{01}\tilde{\varrho}^s_{20},\\ &-\tilde{\varrho}^s_{01}\tilde{\varrho}^s_{02}, -\tilde{\varrho}^s_{01}\tilde{\varrho}^s_{12}, -\tilde{\varrho}^s_{01}\tilde{\varrho}^s_{21}\},\end{aligned} \tag{3.93}$$

and the superscript "s" stands for the steady-state values of the density matrix elements.

Having available the solution (3.92) for the Laplace transform of the correlation functions of the fluctuation operators, we then easily find the incoherent part of the spectrum as

$$S_{\mathrm{in}}(\omega - \omega_s) = 2\mathrm{Re}\left\{\delta Y_4(z)|_{z=-\mathrm{i}(\omega-\omega_s)/\gamma_w}\right\}, \tag{3.94}$$

where $\delta Y_4(z)$ is a component of the vector $\Delta \boldsymbol{Y}(z)$.

The incoherent part of the spectrum of the fluorescence field emitted on the $|1\rangle \to |0\rangle$ transition is plotted in Fig. 3.7 for $\gamma_s = 3\gamma_w$, $\Omega_s = 7\gamma_w$ and different Ω_w. In the absence of the driving field on the $|2\rangle \to |0\rangle$ transition ($\Omega_w = 0$), the spectrum is the Mollow triplet. It is easy to understand, in the absence of the driving field on the weak transition, the atom behaves as a two-level system with the upper state $|1\rangle$ and the ground state $|0\rangle$. As we discussed in Sect. 3.1.3, the linewidth of the central

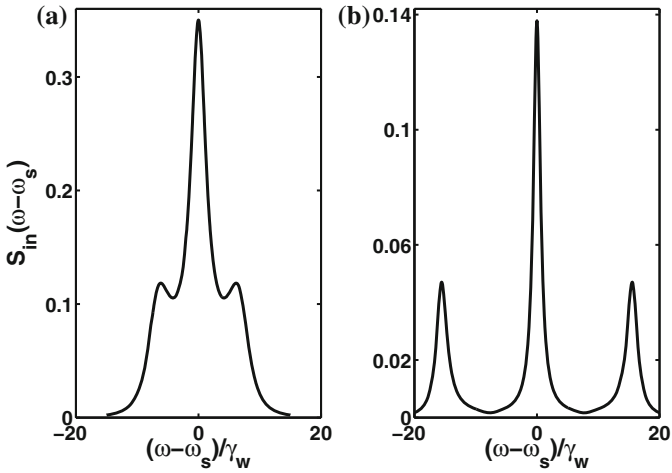

Fig. 3.7 Incoherent part of the power spectrum of the fluorescence field emitted on the $|1\rangle \to |0\rangle$ transition for $\gamma_s = 3\gamma_w$, $\Omega_s = 7\gamma_w$ and two values of Ω_w: **(a)** $\Omega_w = 0$ and **(b)** $\Omega_w = 14\gamma_w$

component of the spectrum is equal to the natural linewidth of the transition involved, in the present case $\gamma_s/2$. However, when the other transition is simultaneously driven, the linewidth narrows and the narrowing increases with an increasing Ω_w until it becomes equal to $\gamma_w/2$, the natural linewidth of the other transition.

It is clearly seen from the figure that the effect of applying a strong driving field on the weak transition, in particular of the Rabi frequency Ω_w much larger than Ω_s, is to narrow the linewidth of the central component of the spectrum. The linewidth is reduced from $\gamma_s/2$, the natural linewidth of the $|1\rangle \rightarrow |0\rangle$ transition, to approximately $\gamma_w/2$, the natural linewidth of the $|2\rangle \rightarrow |0\rangle$ transition.

3.5.2 *Dressed-Atom Model Explanation of the Linewidth Narrowing*

It is difficult to understand the physical origin of the line narrowing from the calculations described above. A physical interpretation of the line narrowing can be achieved from a dressed-atom description of the atom-field system. In such a description, we treat the laser fields quantum mechanically, and first derive the eigenstates (dressed states) of the combined system: atom plus the laser fields. We then use these states to calculate transition rates and the incoherent part of the fluorescence spectrum.

Let us present the main features of the dressed-atom model for the three-level Vee-type atom interacting with two single-mode laser fields. In a fully quantum-mechanical description of the atom and the driving fields, the Hamiltonian of the system (in the rotating-wave approximation) may be written as

$$\hat{H} = \hat{H}_0 + \hat{W} \,, \tag{3.95}$$

where

$$\hat{H}_0 = \hbar\omega_s \,|1\rangle\langle 1| + \hbar\omega_w \,|2\rangle\langle 2| + \hbar\omega_{L1}\hat{a}_1^\dagger\hat{a}_1 + \hbar\omega_{L2}\hat{a}_2^\dagger\hat{a}_2 \,, \tag{3.96}$$

is the unperturbed (noninteracting) Hamiltonian of the atom plus the driving laser fields, and

$$\hat{W} = -\mathrm{i}\hbar g_s\left(S_1^+\hat{a}_1 - S_1^-\hat{a}_1^\dagger\right) - \mathrm{i}\hbar g_w\left(S_2^+\hat{a}_2 - S_2^-\hat{a}_2^\dagger\right) \,, \tag{3.97}$$

is the interaction Hamiltonian of the atom and the driving fields. Here, $\hat{a}_1(\hat{a}_2)$ and $\hat{a}_1^\dagger(\hat{a}_2^\dagger)$ are the annihilation and creation operators for the driving laser field of frequency $\omega_{L1}(\omega_{L2})$, and g_s and g_w are the coupling strengths of the laser fields to the atomic transition.

In the semiclassical description of the system, presented above, we have treated the driving fields classically, and the basic states states for the system were simply the atomic states $|0\rangle$, $|1\rangle$, and $|2\rangle$. For the quantum treatment, the basic states are product

states $|i\rangle \otimes |n_1\rangle \otimes |n_2\rangle$ involving products of atomic $|i\rangle$ $(i = 0, 1, 2)$ and driving field states $|n_1\rangle$ and $|n_2\rangle$, where n_1 is the number of photons in mode 1 and n_2 is the number of photons in mode 2. For convenience, we write $n = n_1 + n_2$ as the total number of photons in the laser fields and $m = n_1 - n_2$ as the photon-number difference. In order to relate the quantum model to the semiclassical model, we assume that the driving fields are single-mode laser fields in the coherent states $|\alpha_1\rangle$ and $|\alpha_2\rangle$ with the mean photon numbers $\langle n_1\rangle = |\alpha_1|^2 \gg 1$ and $\langle n_2\rangle = |\alpha_2|^2 \gg 1$, respectively. Moreover, we assume that the driving lasers are on resonance with the transitions to which are coupled, i.e., $\omega_{L1} = \omega_s$ and $\omega_{L2} = \omega_w$.

The eigenstates (undressed states) of the noninteracting Hamiltonian form manifolds composed of threefold-degenerate states $|0, n_1, n_2\rangle$, $|1, n_1 - 1, n_2\rangle$, and $|2, n_1, n_2 - 1\rangle$ of energy

$$E_{nm} = \hbar\,(n_1\omega_s + n_2\omega_w) = \hbar\left(n\omega_0 + \frac{1}{2}m\Delta\right)\,, \tag{3.98}$$

where $\omega_0 = (\omega_s + \omega_w)/2$ and $\Delta = \omega_s - \omega_w$.

When we include the interaction $\hat{W}$ between the atom and the driving fields, the degeneracy is lifted, resulting in triplets $|i, n, m\rangle$ (dressed states) that satisfy the eigenvalue equation

$$(\hat{H}_0 + \hat{W})\,|i, n, m\rangle = E_{inm}\,|i, n, m\rangle \qquad i = 0, 1, 2\,, \tag{3.99}$$

in which

$$\begin{aligned}
|0, n, m\rangle &= \frac{1}{\Omega}\left(-\Omega_2\,|1, n_1 - 1, n_2\rangle + \Omega_1\,|2, n_1, n_2 - 1\rangle\right)\,,\\
|1, n, m\rangle &= \frac{1}{\sqrt{2}\Omega}\left(\Omega_1\,|1, n_1 - 1, n_2\rangle\right.\\
&\quad \left. + \mathrm{i}\Omega\,|0, n_1, n_2\rangle + \Omega_2\,|2, n_1, n_2 - 1\rangle\right)\,,\\
|2, n, m\rangle &= \frac{1}{\sqrt{2}\Omega}\left(\Omega_1\,|1, n_1 - 1, n_2\rangle\right.\\
&\quad \left. - \mathrm{i}\Omega\,|0, n_1, n_2\rangle + \Omega_2\,|2, n_1, n_2 - 1\rangle\right)\,,
\end{aligned} \tag{3.100}$$

are the dressed states of the system corresponding to energies

$$\begin{aligned}
E_{0nm} &= E_{nm}\,,\\
E_{1nm} &= E_{nm} - \frac{1}{2}\hbar\Omega\,,\\
E_{2nm} &= E_{nm} + \frac{1}{2}\hbar\Omega\,,
\end{aligned} \tag{3.101}$$

where $\Omega = \left(\Omega_s^2 + \Omega_w^2\right)^{1/2}$ with $\Omega_s = 2g_s\langle n_1\rangle^{1/2}$ and $\Omega_w = 2g_w\langle n_2\rangle^{1/2}$.

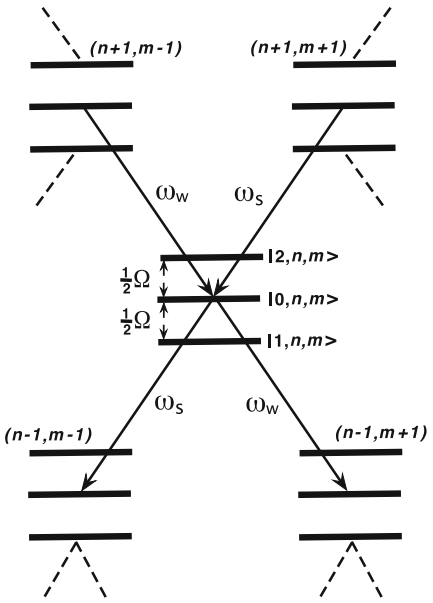

Fig. 3.8 Dressed states of a driven three-level atom in the Vee configuration. The manifold (n, m) is separated from the manifolds $(n \pm 1, m \pm 1)$ by the frequency ω_s, and from the manifolds $(n \pm 1, m \mp 1)$ by the frequency ω_w

The dressed states, shown in Fig. 3.8, group into manifolds, each containing three states. Neighboring manifolds are separated by ω_s and ω_w, while the states inside each manifold are separated by $\frac{1}{2}\Omega$. Considering only the energy diagram, it is apparent that the possibility of transitions exists at five different frequencies about each of the atomic transition frequencies, either ω_s or ω_w. For example, about ω_s, transitions are possible at frequencies

$$\begin{aligned} \omega_{00} = \omega_{11} = \omega_{22} &= \omega_s \,, \\ \omega_{01} = \omega_{20} &= \omega_s - \frac{1}{2}\Omega \,, \\ \omega_{10} = \omega_{02} &= \omega_s + \frac{1}{2}\Omega \,, \\ \omega_{12} &= \omega_s + \Omega \,, \\ \omega_{21} &= \omega_s - \Omega \,. \end{aligned} \tag{3.102}$$

Interaction between the atom and the vacuum modes of the electromagnetic field leads to a spontaneous emission cascade by the dressed atom down its energy manifold ladder. The probability of a transition between any two dressed states is proportional to the absolute square of the dipole transition moment connecting these two states, and is given by the Fermi golden rule

$$\begin{aligned} \gamma_{ij} = {} & \gamma_s \left| \langle i, n, m | \, S_1^+ \, | j, n-1, m-1 \rangle \right|^2 \\ & + \gamma_w \left| \langle i, n, m | \, S_2^+ \, | j, n-1, m+1 \rangle \right|^2 \,, \end{aligned} \tag{3.103}$$

where we have assumed that the atomic transition dipole moments $\boldsymbol{\mu}_{10}$ and $\boldsymbol{\mu}_{20}$ of the Vee-type atom are perpendicular to each other.

Using (3.100), we find that the dipole matrix elements, involved in the expression (3.103), connecting dressed states of the manifold $|i, n, m\rangle$ with states of the manifold $|j, n-1, m-1\rangle$, and also connecting $|i, n, m\rangle$ with $|j, n-1, m+1\rangle$. Then, we find using (3.103) that the transitions between dressed states of the neighboring manifolds occur with rates

$$\begin{aligned} \gamma_{00} = \gamma_{10} = \gamma_{20} &= 0 \,, \\ \gamma_{01} = \gamma_{02} &= \frac{\Omega_w^2}{2\Omega^2}\gamma_s + \frac{\Omega_s^2}{2\Omega^2}\gamma_w \,, \\ \gamma_{12} = \gamma_{21} = \gamma_{11} = \gamma_{22} &= \frac{\Omega_s^2}{4\Omega^2}\gamma_s + \frac{\Omega_w^2}{4\Omega^2}\gamma_w \,. \end{aligned} \tag{3.104}$$

One can see that all transition rates into the state $|0, n, m\rangle$ are zero. This indicates that there is no spontaneous emission into this state. Since there are nonzero transition rates out of the state $|0, n, m\rangle$ the population in this state will decrease in time and in the steady state the population will be depopulated. This feature effectively reduces the dressed-atom system to that of a two-level atom. This explains why the fluorescence spectrum of the radiation emitted from the system, like that shown in Fig. 3.7 is always a triplet despite the fact that there are five different frequencies possible between the dressed states (3.100).

To obtain information on the spectral linewidths, one must consider the off-diagonal elements (coherences) of the density operator of the system. However, the dressed-atom system of the driven three-level atom effectively behaves as that for a strongly driven two-level atom. Therefore, we can use the results of Sect. 3.1.3, from which we have that the linewidth of the central component of the spectrum is

$$\gamma_c = \gamma_{12} + \gamma_{21} = \frac{\Omega_s^2}{2\Omega^2}\gamma_s + \frac{\Omega_w^2}{2\Omega^2}\gamma_w \,. \tag{3.105}$$

Clearly, the linewidth of the central spectral component on the $|1\rangle \rightarrow |0\rangle$ transition is a function of the Rabi frequencies of the driving fields and the natural linewidths of *both* atomic transitions. When $\Omega_w = 0$, the linewidth of the central component is determined solely by the natural linewidth γ_s of the driven transition. However, if $\Omega_w \neq 0$, the linewidth is determined by both γ_s and γ_w, and approaches γ_w when $\Omega_w \gg \Omega_s$.

Figure 3.9 shows how the linewidth of the central component of the spectrum $S_{in}(\omega - \omega_s)$ changes as the Rabi frequency of the laser driving the weak transition is varied from 0 to $50\gamma_s$. The linewidth decreases rapidly as Ω_w increases so that the central component exhibits dramatic narrowing and approaches asymptotically the width $\gamma_w/2$ when $\Omega_w \gg \Omega_s$, that is the damping rate of the other transition. Thus, contrary to what might have been expected, the linewidth of the spectral lines of the fluorescence emitted on the $|1\rangle \rightarrow |0\rangle$ transition is determined by the spontaneous emission rate of the $|2\rangle \rightarrow |0\rangle$ transition. Therefore, we may conclude that the

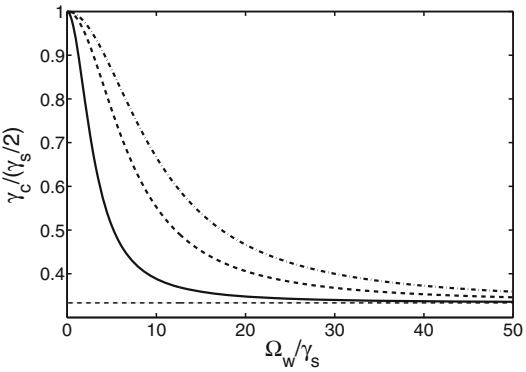

Fig. 3.9 Variation of the linewidth of the central component of the fluorescence spectrum $S_{in}(\omega - \omega_s)$ with the Rabi frequency Ω_w of the weak transition for $\gamma_w = \frac{1}{3}\gamma_s$ and several values of Ω_s: $\Omega_s = 3\gamma_s$ (*solid line*), $\Omega_s = 7\gamma_s$ (*dashed line*), and $\Omega_s = 10\gamma_s$ (*dashed-dotted line*). The *horizontal dashed line* represents the natural linewidth $(\gamma_w/2)$ of the weak transition

coupling between the atomic transitions through a common level suppresses the quantum fluctuations of the strong transition at the expense of increasing the fluctuations of the weak transition.

3.6 Experimental Studies of the Spectral Line Narrowing

Evidence of line narrowing in the fluorescence spectrum of a driven three-level Vee-type atom has been observed in experiments by the Mossberg's group at the University of Oregon [11]. The experiments involved measuring the resonance fluorescence spectrum emitted by a collimated beam of barium (Ba) atoms using a Fabry−Perot interferometer which enabled the frequency selection of the fluorescence signal at frequency of the $|1\rangle \rightarrow |0\rangle$ transition. The relevant energy levels of the Ba atom, the decay paths, and the coupling configuration of the driving fields are shown in Fig. 3.10.

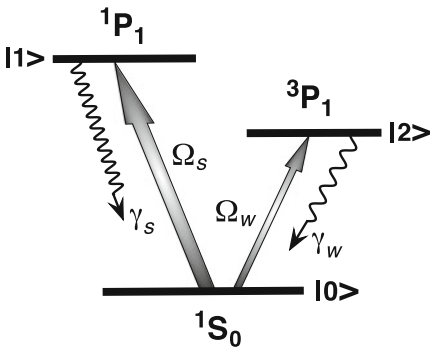

Fig. 3.10 A partial energy-level diagram of a Ba atom relevant for observation of line narrowing in the fluorescence spectrum. The atomic transitions are driven by two resonant laser fields of the Rabi frequencies Ω_s and Ω_w. The damping rates of the atomic $^1P_1 \rightarrow {}^1S_0$ and $^3P_1 \rightarrow {}^1S_0$ transitions are γ_s and γ_w, respectively

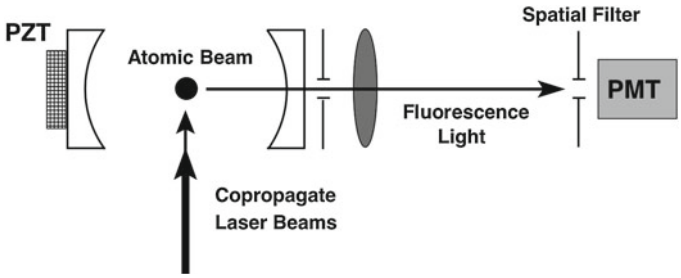

Fig. 3.11 Outline of the apparatus used by Gauthier et al. [11] for observing the line narrowing in the fluorescence spectrum of driven barium atoms

The atomic level $^1P_1$ has a short spontaneous lifetime of 8.37 ± 0.08 ns, whereas the level $^3P_1$ has a long spontaneous lifetime of 3.35 ± 0.5 μs. Therefore, the transitions $^1P_1 \leftrightarrow {}^1S_0$ and $^3P_1 \leftrightarrow {}^1S_0$ were called "strong" and "weak" transitions, respectively. The atomic transitions were driven by two monochromatic and well stabilized continuous wave (cw) laser beams tuned to the $^1P_1 \rightarrow {}^1S_0$ and $^3P_1 \rightarrow {}^1S_0$ transitions such that each laser was coupled only to one of the two atomic transitions. The laser beam applied to the strong transition had maximum power of 20 mW, whereas the weak transition was driven by a strong laser beam of the power of 200 mW. Strong here implies that the Rabi frequency of the laser field is substantially greater than the $^1P_1 \rightarrow {}^1S_0$ transition natural width of 19 MHz.

The apparatus used in the experiment involved a confocal Fabry−Perot cavity that increased the fluorescence signal without modification of the total spontaneous emission rate of the atom. Figure 3.11 shows a schematic view of the experimental setup.

The laser beams were collimated, superimposed, and made incident on the barium atoms as they were passing through the center of the cavity. The laser beams, the atomic beam, and the cavity axis were all aligned to be mutually orthogonal thereby providing for nearly Doppler-free atom-field interaction. One of the cavity mirrors was mounted on a piezoelectric crystal, piezoelectric transducer (PZT), which allowed the cavity frequency to be varied by varying the cavity spacing. The fluorescence spectrum was obtained by recording the fluorescence intensity transmitted through one of the cavity mirrors as a function of cavity length and therefore cavity transmission frequency. Imaging and spatial-filtering techniques were employed to select only that fluorescence light which was emitted nearly orthogonal to the atomic beam and which originated from a source volume approximately 850 μm in diameter. In order to detect only the fluorescence field emitted on the strong atomic transition, a spectral filtering was introduced and the resulting atomic fluorescence field was imaged on a cooled photon counting photomultiplier tube (PMT), as shown in the figure.

Figure 3.12 shows the results of the measured strong-transition fluorescence spectra obtained for the strong-transition Rabi frequency $\Omega_s = 35$ MHz without (Fig. 3.12a) and with (Fig. 3.12b) simultaneous excitation of the weak transition. On

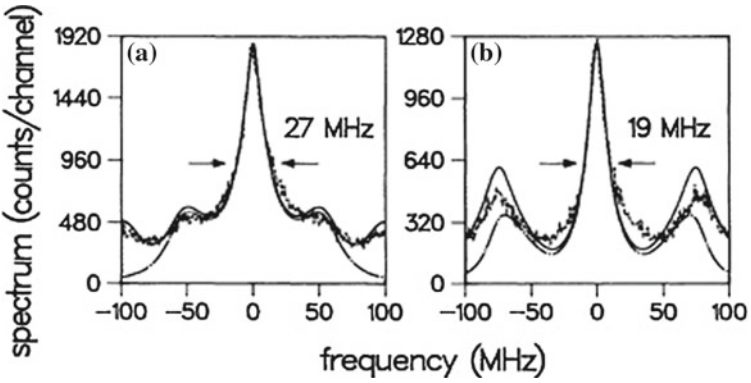

Fig. 3.12 Fluorescence spectra observed by Gauthier et al. [11], demonstrating the line narrowing in the fluorescence spectrum of a three-level Vee-type atom driven by coherent laser fields. Reprinted with permission from D.J. Gauthier, Y. Zhu, T.W. Mossberg: Phys. Rev. Lett. **66**, 2460 (1991). Copyright (1991) by the American Physical Society

each graph, the dotted lines represent the theoretically predicted spectra calculated from the model outlined in the previous section. Note the dramatic narrowing of the central component of the spectrum in the presence of the laser field on the weak transition, from 27 MHz to 19 MHz. The measured fluorescence spectra are found to be in good agreement with the theoretical predictions. Thus, it was confirmed that a coherent mixing of the atomic states can lead to a stabilization of quantum fluctuations in a driven atomic system.

The interpretation of the experimental results is that in the absence of the driving field on the weak transition, the linewidth of the central component of the fluorescence spectrum is given by the natural linewidth of the transition. But in the presence of the driving field on the weak transition, the fluorescence spectrum is dramatically different that the linewidth of the central component of the spectrum observed on the strong transition is significantly narrower than the natural linewidth of the transition. The 25 MHz width found in the former case is slightly larger than the 19 MHz natural width of the strong transition and results from the effects of the finite cavity resolution, the Doppler broadening, approximately 3 MHz, the angular spread of the atomic beam, and not fully resolved Mollow sidebands.

The experiments clearly demonstrated that it is possible to manipulate atomic systems to obtain dramatically reduced and controlled spontaneous emission rates. In other words, the observed subnatural linewidth of the spectral line is the signature of the fluctuations stabilization in a driven atom by a coherent mixing of the atomic energy levels.

References

1. P.L. Knight, P.W. Milonni: Phys. Rep. **66**, 21 (1980)
2. W.E. Lamb, Jr.: Phys. Rev. **134**, A1429 (1964)

3. B.R. Mollow: Phys. Rev. **188**, 1969 (1969)
4. M. Lewenstein, T.W. Mossberg, R.J. Glauber: Phys. Rev. Lett. **59**, 775 (1987)
5. M. Lewenstein, T.W. Mossberg: Phys. Rev. A **37**, 2048 (1988)
6. C. Cohen-Tannoudji and S. Reynaud: J. Phys. B **10**, 345 (1977)
7. C. Cohen-Tannoudji, J. Dupont-Roc, G. Grynberg: *Atom-Photon Interactions* (Wiley, New York, 1992)
8. Y. Zhu, A. Lezama, T.W. Mossberg, M. Lewenstein: Phys. Rev. Lett. **61**, 1946 (1988)
9. P.R. Rice, H.J. Carmichael: J. Opt. Soc. Am. B **5**, 1661 (1988)
10. L.M. Narducci, M.O. Scully, G.-L. Oppo, P.Ru, J.R. Tredicce: Phys. Rev. A **42**, 1630 (1990)
11. D.J. Gauthier, Y. Zhu, T.W. Mossberg: Phys. Rev. Lett. **66**, 2460 (1991)

Chapter 4
Collective Multiatom Spectroscopy

The radiative properties of atomic systems are, in general, much more complicated than those discussed in the previous chapter, in which we considered optical spectra of single multilevel atoms separated by large distances. The complication arises from the fact that in practice atomic separations are small, even in low density atomic beams, and can be of the order of a resonant wavelength. In this case, the atoms do not radiate independently so the interatomic interactions cannot be neglected. Therefore, in this chapter we shall consider a class of phenomena which arises from the collective interaction between atoms. Our main effort will be devoted to the study of the radiative properties of a small number of interacting atoms, since the solution of these problems for a large number of atoms can be accomplished only with the aid of some approximations, for example suitable decoupling procedures. Although the several atom systems are admittedly an elementary model, it offers some advantages over the multiatom problem. Because of its simplicity, one may obtain detailed and almost exact dynamical solutions with variety of initial conditions. Many of these results are analogous to phenomena that one would expect in multiatom systems. In the simplest case, we consider a pair of two-level atoms separated by an arbitrary distance, and therefore capable of developing a quantum formalism to study radiative effects sensitive to the atomic separation. Moreover, this will enable us to differentiate the single-atom effects from those arising from interactions between the atoms. We then proceed to a consideration of the radiative properties of a general two-atom system of arbitrary size relative to the radiation wavelength. We will consider radiation intensity and show that the inclusion of the interatomic interactions can lead to subnatural linewidths in the radiation intensity.

A major portion of this chapter is devoted to the angular distribution of the radiation field emitted by interacting atoms. We will show that the spontaneous emission by the atoms can be strongly directional with some directions in which the radiation can be completely suppressed. This prediction is intriguing because it gives a new class of systems in which directions of emission can be manipulated and the effects directly observed. The mutual influence of radiating systems may result in a cancelation of the radiation in some directions. In order to understand the situation better we take a simple system composed of two two-level atoms located close to

Z. Ficek and R. Tanaś, *Quantum-Limit Spectroscopy*, Springer Series in Optical Sciences 200, DOI 10.1007/978-1-4939-3740-0_4

each other and collectively interacting with the electromagnetic field. We focus on the directional properties of the radiation field emitted by the system.

We conclude the chapter with a qualitative discussion of different techniques of the selective excitation of the collective states of strongly interacting atoms. We also describe a method of the preparation of collective states between distant atoms coupled to a common field mode. Finally, we discuss a series of experiments demonstrating the preparation of two trapped ions deterministically in both the symmetric and antisymmetric states, the subradiant decay of the excitation of a large cloud of trapped atoms, the subradiance of two distant artificial atoms, and collective suppression of linewidths of multiple artificial atoms.

4.1 Collective Atomic States

For most of the topics in this chapter it will be possible to obtain a transparent interpretation in terms of superradiant and subradiant states of a collective multiatom system. The concept of the superradiant and subradiant states was introduced by Dicke in 1954, who discussed the quantum theory of spontaneous emission from an assembly of N atoms, and showed that the influence on each atomic dipole of the electromagnetic field produced by the other atomic dipoles could, in certain circumstances, cause each atom to radiate more or less rapidly than it would on its own [1]. An understanding of these multiatom phenomena is of great use since it represents modifications of the interaction of the atoms with the radiation field [2].

The simplest model by which one can illustrate the concept of superradiant and subradiant states consists of two identical atoms separated by a fixed distance R_{12} and coupled to a quantized electromagnetic field [3]. We take the atoms to be two-level systems composed of energy levels $|g_i\rangle$ and $|e_i\rangle$ with energies $-\hbar\omega_a/2$ and $\hbar\omega_a/2$, respectively, and connected by an electric transition dipole moment $\boldsymbol{\mu}_i$. When the atoms are both coupled to a radiation field photons emitted spontaneously by each atom can be absorbed by the other atom thus inducing an oscillation of its dipole moment. The oscillations induced in each atom are partly coherent with their own oscillations and thus lead to a coherent coupling between the atoms, called the dipole-dipole interaction [2, 3]. The Hamiltonian of the dipole-dipole interacting atoms is

$$\hat{H}_0 = \hat{H}_a + \hat{H}_{dd} \,, \tag{4.1}$$

where $\hat{H}_a$ is the unperturbed Hamiltonian of the atoms

$$\hat{H}_a = \hbar \sum_{i=1}^{2} \omega_a S_i^z \tag{4.2}$$

and $\hat{H}_{dd}$ is the dipole-dipole interaction among the atoms

$$\hat{H}_{dd} = \hbar\Omega_{12}\left(S_1^+ S_2^- + S_2^+ S_1^-\right) . \tag{4.3}$$

Here, $S_i^+ = |e_i\rangle\langle g_i|$ and $S_i^- = |g_i\rangle\langle e_i|$ are the dipole raising and lowering operators of atom i, and $S_i^z = \left(|e_i\rangle\langle e_i| - |g_i\rangle\langle g_i|\right)/2$ describes its energy. The parameter Ω_{ij} stands for the dipole-dipole interaction strength between the atoms. The strength depends on the distance between the atoms and the orientation of the atomic dipole moments in respect to the interatomic axis, and is given by the expression [3]

$$\begin{aligned}\Omega_{12} = \frac{3}{4}\gamma\Bigg\{ &-\left[1-\left(\bar{\boldsymbol{\mu}}\cdot\bar{\boldsymbol{R}}_{ij}\right)^2\right]\frac{\cos\left(k_0 R_{ij}\right)}{k_0 R_{ij}} \\ &+\left[1-3\left(\bar{\boldsymbol{\mu}}\cdot\bar{\boldsymbol{R}}_{ij}\right)^2\right]\left[\frac{\sin\left(k_0 R_{ij}\right)}{\left(k_0 R_{ij}\right)^2}+\frac{\cos\left(k_0 R_{ij}\right)}{\left(k_0 R_{ij}\right)^3}\right]\Bigg\} ,\end{aligned} \tag{4.4}$$

where $\bar{\boldsymbol{\mu}} \equiv \bar{\boldsymbol{\mu}}_1 = \bar{\boldsymbol{\mu}}_2$, $\bar{\boldsymbol{R}}_{ij}$ are unit vectors along the atomic transition dipole moments and the vector $\boldsymbol{R}_{ij} = \boldsymbol{R}_j - \boldsymbol{R}_i$, respectively, and γ is the single-atom damping rate.

As is well known, the Hamiltonian of the dipole-dipole interacting atoms when diagonalized results in collective states of the interacting atoms

$$\begin{aligned}|g\rangle &= |g_1\rangle\otimes|g_2\rangle , \qquad |e\rangle = |e_1\rangle\otimes|e_2\rangle , \\ |s\rangle &= \frac{1}{\sqrt{2}}\left(|e_1\rangle\otimes|g_2\rangle + |g_1\rangle\otimes|e_2\rangle\right) , \\ |a\rangle &= \frac{1}{\sqrt{2}}\left(|e_1\rangle\otimes|g_2\rangle - |g_1\rangle\otimes|e_2\rangle\right) ,\end{aligned} \tag{4.5}$$

with energies

$$E_g = -\hbar\omega_a , \qquad E_e = \hbar\omega_a , \qquad E_s = \hbar\Omega_{12} , \qquad E_a = -\hbar\Omega_{12} . \tag{4.6}$$

The states $|s\rangle$ and $|a\rangle$, which are linear equally weighted symmetric and antisymmetric superpositions of the product states, are the superradiant and subradiant states of the two-atom system, for the reason which will be clarified below when we calculate transition rates between the collective states. The states $|s\rangle$ and $|a\rangle$ are often called in the literature as the Bell triplet and singlet states, respectively. We see that in terms of the collective states the system behaves as a single four-level system, with the ground state $|g\rangle$, the upper state $|e\rangle$, and two intermediate states: the symmetric state $|s\rangle$ and the antisymmetric state $|a\rangle$. The energies of the intermediate states depend on the dipole-dipole interaction and these states suffer a large shift when the interatomic separation is small.

The interaction of the atoms, or equivalently, the collective atomic system with the vacuum modes of the electromagnetic field leads to spontaneous transitions between the collective states. From the Fermi golden rule, it is known that the probability of a transition between two energy states is determined by the damping rate of the transition and is proportional to the absolute square of the dipole transition moment

connecting these states. The lowering dipole moment operator for emission of a photon of wave vector $\boldsymbol{k}$ by the collective system is

$$\begin{aligned}\boldsymbol{D}^{(-)} = {} & \boldsymbol{d}_{se}\,|s\rangle\langle e| + \boldsymbol{d}_{ae}\,|a\rangle\langle e| + \boldsymbol{d}_{ge}\,|g\rangle\langle e| \\ & + \boldsymbol{d}_{gs}\,|g\rangle\langle s| + \boldsymbol{d}_{ga}\,|g\rangle\langle a| + \boldsymbol{d}_{as}\,|a\rangle\langle s| \ , \end{aligned} \tag{4.7}$$

where

$$\boldsymbol{d}_{ij} = \langle i|\,\boldsymbol{\mu}_1 e^{i\boldsymbol{k}\cdot\boldsymbol{R}_1} + \boldsymbol{\mu}_2 e^{i\boldsymbol{k}\cdot\boldsymbol{R}_2}\,|j\rangle \tag{4.8}$$

is the matrix element of the dipole transition moment between $|i\rangle$ and $|j\rangle$ states. If the atoms have no permanent dipole moments, we find using (4.5) that the matrix elements of the dipole transition moments between the collective states are

$$\begin{aligned}\boldsymbol{D}^{(-)}_{eg} &= \boldsymbol{D}^{(-)}_{sa} = 0\,, \\ \boldsymbol{D}^{(-)}_{es} &= \boldsymbol{D}^{(-)}_{sg} = \frac{1}{\sqrt{2}}\left(\tilde{\boldsymbol{\mu}}_1 e^{i\boldsymbol{k}\cdot\boldsymbol{R}_1} + \tilde{\boldsymbol{\mu}}_2 e^{i\boldsymbol{k}\cdot\boldsymbol{R}_2}\right)\,, \\ \boldsymbol{D}^{(-)}_{ea} &= -\boldsymbol{D}^{(-)}_{ag} = \frac{1}{\sqrt{2}}\left(\tilde{\boldsymbol{\mu}}_1 e^{i\boldsymbol{k}\cdot\boldsymbol{R}_1} - \tilde{\boldsymbol{\mu}}_2 e^{i\boldsymbol{k}\cdot\boldsymbol{R}_2}\right)\,, \end{aligned} \tag{4.9}$$

where $\tilde{\boldsymbol{\mu}}_1 = \langle g_1|\,\mu_1\,|e_1\rangle$ and $\tilde{\boldsymbol{\mu}}_2 = \langle g_2|\,\mu_2\,|e_2\rangle$ are matrix elements of the transition dipole moments of the atoms.

The transition rates between the collective states, equal to the damping rates of the transitions, are obtained by integrating $|\boldsymbol{D}^{(-)}_{ij}|^2$ over all possible wave vectors $\boldsymbol{k}$ and polarizations $\boldsymbol{e}_k$ of the emitted photon. It is straightforward to show that the damping rates of the transitions between the collective states are

$$\begin{aligned}\gamma_{eg} &= \gamma_{sa} = 0\,, \\ \gamma_{es} &= \gamma_{sg} = \gamma + \gamma_{12}\,, \\ \gamma_{ea} &= \gamma_{ag} = \gamma - \gamma_{12}\,, \end{aligned} \tag{4.10}$$

where γ_{12} depends on the distance between the atoms and the polarization of the transition dipole moments with respect to the interatomic axis

$$\begin{aligned}\gamma_{12} = \gamma_{21} = \frac{3}{2}\gamma \Bigg\{ & \left[1 - \left(\bar{\boldsymbol{\mu}}\cdot\bar{\boldsymbol{R}}_{12}\right)^2\right]\frac{\sin\left(k_0 R_{12}\right)}{k_0 R_{12}} \\ & + \left[1 - 3\left(\bar{\boldsymbol{\mu}}\cdot\bar{\boldsymbol{R}}_{12}\right)^2\right]\left[\frac{\cos\left(k_0 R_{12}\right)}{\left(k_0 R_{12}\right)^2} - \frac{\sin\left(k_0 R_{12}\right)}{\left(k_0 R_{12}\right)^3}\right]\Bigg\}\ . \end{aligned} \tag{4.11}$$

The parameter γ_{12} is the collective damping rate of atom 1 caused by the radiation field of atom 2 and vice versa. It reflects the dependence of the coupling between the atoms and the vacuum field upon spatial distribution and polarization of the radiation field.

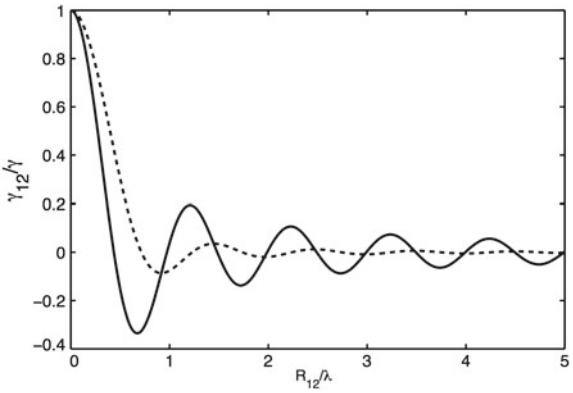

Fig. 4.1 The collective damping rate γ_{12}/γ as a function of the interatomic separation R_{12}/λ for two polarizations of the atomic dipole moments in respect to the interatomic axis; $\bar{\boldsymbol{\mu}} \parallel \bar{\boldsymbol{R}}_{12}$ (*solid line*) and $\bar{\boldsymbol{\mu}} \perp \bar{\boldsymbol{R}}_{12}$ (*dashed line*)

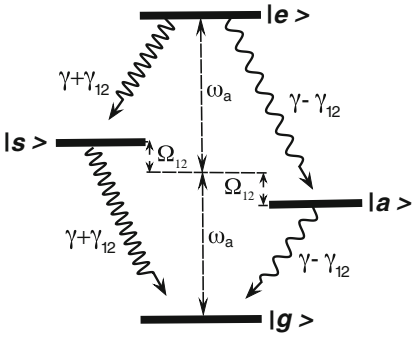

Fig. 4.2 Energy states and spontaneous transitions in the collective states representation of two interacting atoms. The energies of the intermediate states $|s\rangle$ and $|a\rangle$ are shifted from the single-atom energy by Ω_{12} and the damping rates between the collective states are modified by the collective damping rate γ_{12}

In Fig. 4.1 the collective damping rate is illustrated for different polarizations of the atomic dipole moments in respect to the interatomic axis. For large distances between the atoms, the collective damping rate is very small and vanishes when $R_{12} \to \infty$. At the other extreme of interatomic distances much smaller than the radiation wavelength, the damping rate varies rapidly with R_{12} and attains its maximal value $\gamma_{12} = \gamma$ for $R_{12} \ll \lambda$. This limit corresponds to the small-sample model of the system. For moderate R_{12}, the collective damping rate is small, alternatively positive and negative.

The effects of the dipole-dipole interaction and the mutual influence of the atoms on their radiative properties include the shift of the collective levels from the single-atom energy and a change in the lifetime (damping rates) of each collective levels from the single-atom radiative lifetime. The effective two-atom system is shown in Fig. 4.2.

Clearly, we can distinguish two dissipation channels $|e\rangle \to |s\rangle \to |g\rangle$ and $|e\rangle \to |a\rangle \to |g\rangle$, each with two cascade nondegenerate transitions. The superradiant transitions decay with an enhanced rate $(\gamma + \gamma_{12})$, whereas the subradiant transitions decay with a reduced rate $(\gamma - \gamma_{12})$. To say this in another way: The radiative decay of superradiant transitions is much shorter, whereas the decay of subradiant transi-

tions is much longer than the radiative decay of a single atom. For small $k_0 R_{ij}$, the $|s\rangle$ state is superradiant, with the decay rate double that of the single atom γ; the $|a\rangle$ state is subradiant, with the decay rate of order $(k_0 R_{ij})^2\,\gamma$. For large distances between the atoms, the effects of the atomic interactions become negligible, and the states decay with rates identical to those of a single atom. For $\gamma_{12} = \gamma$, which appears when the interatomic separation is much smaller than the resonant wavelength, the superradiant transitions do not decay, and consequently decouple from the vacuum field. Hence, for $\gamma_{12} = \gamma$ the system reduces to a three-level cascade system, referred to as the small-sample model or two-atom Dicke model.

4.1.1 Master Equation for the Density Operator

We now proceed to consider the radiative properties of the collective system. In order to do this, we shall make use of the master equation for the reduced density operator of the two-atom system, which can be derived from the general integro-differential equation (3.9). The corresponding interaction Hamiltonian between the two-atom system and the ordinary vacuum (reservoir) field, written in the interaction picture is given by

$$\tilde{H}_I = -\mathrm{i}\hbar \sum_{i=1}^{2} \sum_{\boldsymbol{k}} \left(g_k^{(i)} \hat{a}_k S_i^+ \mathrm{e}^{\mathrm{i}\boldsymbol{k}\cdot\boldsymbol{R}_i} - \mathrm{H.c.} \right) , \tag{4.12}$$

where $\hat{a}_k$ is the annihilation operator of mode k and $g_k^{(i)}$ is the coupling strength of the ith atom to the kth mode of the vacuum field. Using (4.12) for the evaluation of the commutators in (3.9), and applying the usual Born−Markov approximation, it is straightforward to write down the master equation

$$\begin{aligned}
\frac{\partial \varrho}{\partial t} = &-\mathrm{i} \sum_{i=1}^{2} \omega_0 \left[S_i^z, \varrho \right] - \mathrm{i} \sum_{i \neq j=1}^{2} \Omega_{ij} \left[S_i^+ S_j^-, \varrho \right] \\
&+ \frac{1}{2} \mathrm{i} \sum_{i=1}^{2} \left[\Omega\left(\boldsymbol{R}_i\right) S_i^+ \mathrm{e}^{-\,\mathrm{i}(\omega_L t + \phi_L)} + \Omega^*\left(\boldsymbol{R}_i\right) S_i^- \mathrm{e}^{+\,\mathrm{i}(\omega_L t + \phi_L)}, \varrho \right] \\
&- \frac{1}{2} \sum_{i=1}^{2} \gamma \left(\varrho S_i^+ S_i^- + S_i^+ S_i^- \varrho - 2 S_i^- \varrho S_i^+ \right) \\
&- \frac{1}{2} \sum_{i \neq j=1}^{2} \gamma_{ij} \left(\varrho S_i^+ S_j^- + S_i^+ S_j^- \varrho - 2 S_j^- \varrho S_i^+ \right) .
\end{aligned} \tag{4.13}$$

The first term on the right-hand side represents the evolution of ϱ due to the unperturbed atomic Hamiltonian. The second term contains the contribution of the dipole-dipole interaction between the atoms. The third term contains the interaction of the atoms with an external coherent field, which is treated classically in our calculations and is characterized by its frequency ω_L and the phase ϕ_L. The strength of the interaction between the atoms and the laser field is determined by the Rabi frequency $\Omega(\boldsymbol{R}_i)$. The final two terms in (4.13) represent the interaction of the atoms with the vacuum field. It gives rise to dissipation of the atomic energy through the process of spontaneous emission.

We have already demonstrated that it is convenient to study the properties of the two-atom system in the basis of the collective states. If we relate the atomic bare operators $S_i^{\pm}$ to operators $A_{ij} = |i\rangle\langle j|$ in the collective state basis, $i, j = e, a, s, g$, through the following identities

$$\begin{aligned} S_1^+ &= \left(A_{es} - A_{ea} + A_{sg} + A_{ag}\right)/\sqrt{2}\,, \\ S_2^+ &= \left(A_{es} + A_{ea} + A_{sg} - A_{ag}\right)/\sqrt{2}\,, \end{aligned} \tag{4.14}$$

we then may transform the master equation (4.13) into the following form

$$\frac{\partial \varrho}{\partial t} = -\frac{\mathrm{i}}{\hbar}\left[\hat{H}_0 + \hat{H}_L, \varrho\right] + \left(\frac{\partial}{\partial t}\varrho\right)_S + \left(\frac{\partial}{\partial t}\varrho\right)_A , \tag{4.15}$$

where

$$\hat{H}_0 = \hbar\Delta_L\left(A_{ss} + A_{aa} + 2A_{ee}\right) + \hbar\Omega_{12}\left(A_{ss} - A_{aa}\right)\,, \tag{4.16}$$

and

$$\begin{aligned} \hat{H}_L = \frac{\hbar}{2}\Big\{&\tilde{\Omega}_1\left(A_{es} + A_{sg} + A_{ag} - A_{ea}\right) \\ &+ \tilde{\Omega}_2\left(A_{es} + A_{sg} - A_{ag} + A_{ea}\right) + \text{H.c.}\Big\}\,. \end{aligned} \tag{4.17}$$

Here, $\tilde{\Omega}_1 = \Omega(\boldsymbol{R}_1)/\sqrt{2}$, $\tilde{\Omega}_2 = \Omega(\boldsymbol{R}_2)/\sqrt{2}$, and $\Delta_L = \omega_a - \omega_L$ is the detuning of the laser field frequency from the atomic transition frequency.

The dissipative part of the master equation (4.13) consists of two terms corresponding to the two decay (fluorescent emission) channels; the symmetric channel $|e\rangle \to |s\rangle \to |g\rangle$ in which the transitions decay with an enhanced rate $\gamma_s = \gamma + \gamma_{12}$:

$$\begin{aligned} \left(\frac{\partial}{\partial t}\varrho\right)_S = -\frac{1}{2}\gamma_s\Big\{&\left(A_{ee} + A_{ss}\right)\varrho + \varrho\left(A_{ee} + A_{ss}\right) + A_{se}\varrho A_{sg} + A_{gs}\varrho A_{es} \\ &-2\left(A_{se}\varrho A_{es} + A_{gs}\varrho A_{sg}\right)\Big\}\,, \end{aligned} \tag{4.18}$$

and the antisymmetric channel $|e\rangle \rightarrow |a\rangle \rightarrow |g\rangle$ in which the transitions decay with a reduced rate $\gamma_a = \gamma - \gamma_{12}$

$$\left(\frac{\partial}{\partial t}\varrho\right)_A = -\frac{1}{2}\gamma_a \left\{(A_{ee} + A_{aa})\,\varrho + \varrho\,(A_{ee} + A_{aa}) + A_{ae}\varrho A_{ag} + A_{ga}\varrho A_{ea} - 2\left(A_{ae}\varrho A_{ea} + A_{ga}\varrho A_{ag}\right)\right\}. \tag{4.19}$$

The Rabi frequencies appearing in (4.17) depend on the positions of the atoms. Since

$$\Omega_i \equiv \Omega\left(\boldsymbol{R}_i\right) = 2\boldsymbol{\mu}_i \cdot \boldsymbol{\mathcal{E}}_L^{(+)} \mathrm{e}^{\mathrm{i}\boldsymbol{k}_L \cdot \boldsymbol{R}_i}/\hbar\,, \tag{4.20}$$

we see that the atoms can experience different amplitudes and phases of the laser field, even if their transition dipole moments are identical. For example, if the dipole moments of the atoms are parallel, the Rabi frequencies Ω_1 and Ω_2 of the atoms separated by a distance R_{12} are related to each other by

$$\Omega_2 = \Omega_1 \frac{|\boldsymbol{\mu}_2|}{|\boldsymbol{\mu}_1|} \exp\left(\mathrm{i}\boldsymbol{k}_L \cdot \boldsymbol{R}_{12}\right)\,. \tag{4.21}$$

Thus, for two identical atoms the Rabi frequencies differ by the phase factor $\exp(\mathrm{i}\boldsymbol{k}_L \cdot \boldsymbol{R}_{12})$ arising from different position coordinates of the atoms. However, the phase factor depends on the orientation of the interatomic axis in respect to the direction of propagation of the driving field, and can be equal to one, even for large interatomic separations R_{12}. This happens when the direction of propagation of the laser field is perpendicular to the interatomic axis, $\boldsymbol{k}_L \perp \boldsymbol{R}_{12}$. For directions different from perpendicular, $\boldsymbol{k}_L \cdot \boldsymbol{R}_{12} \neq 0$, and then the atoms are in nonequivalent positions in the driving field, with different Rabi frequencies ($\Omega_2 \neq \Omega_1$). For a very special geometrical configuration of the system that the atoms are confined to a volume with linear dimensions that are much smaller compared to the laser wavelength, the phase factor reduces to one independent of the atomic positions, and then the Rabi frequencies are the same for both atoms.

If we write the Rabi frequencies as $\Omega_1 = |\Omega_1| \exp(\mathrm{i}\phi_1)$ and $\Omega_2 = |\Omega_2| \exp(\mathrm{i}\phi_2)$, then the interaction Hamiltonian (4.17) can be written as

$$\hat{H}_L = \mathrm{i}\hbar\left[\Omega_\alpha\left(A_{es} + A_{sg}\right) + \Omega_\beta\left(A_{ea} + A_{ag}\right) - \mathrm{H.c.}\right]\,, \tag{4.22}$$

where

$$\begin{aligned}\Omega_\alpha &= \tilde{\Omega}_d \sin\phi_d - \mathrm{i}\tilde{\Omega}_0 \cos\phi_d\,,\\ \Omega_\beta &= \tilde{\Omega}_0 \sin\phi_d - \mathrm{i}\tilde{\Omega}_d \cos\phi_d\,,\end{aligned} \tag{4.23}$$

in which

$$\tilde{\Omega}_0 = \frac{1}{2}\left(|\tilde{\Omega}_1| + |\tilde{\Omega}_2|\right), \quad \tilde{\Omega}_d = \frac{1}{2}\left(|\tilde{\Omega}_1| - |\tilde{\Omega}_2|\right), \tag{4.24}$$

and $\phi_d = (\phi_1 - \phi_2)/2$ is the phase difference between the Rabi frequencies of the atoms. Equation (4.22) demonstrates that the transitions of the symmetric channel are driven at the Rabi frequency Ω_α, while the transitions of the antisymmetric channel are driven at the Rabi frequency Ω_β. Thus, by a suitable choice of the Rabi frequencies and their phases, one can selectively drive either the symmetric or antisymmetric channels.

4.1.2 Equations of Motion for the Density Matrix Elements

In the basis of the collective states the master equation leads to a set of 15 coupled differential equations for the density matrix elements. Among them we can distinguish eight equations for the density matrix elements determining transitions between the symmetric states

$$\begin{aligned}
\dot{\varrho}_{ss} &= -\gamma_s(\varrho_{ss} - \varrho_{ee}) + \left[\Omega_\alpha(\varrho_{gs} - \varrho_{se}) + \text{c.c.}\right], \\
\dot{\varrho}_{ee} &= -2\gamma\,\varrho_{ee} + \left(\Omega_\alpha\varrho_{se} - \Omega_\beta\varrho_{ae} + \text{c.c.}\right), \\
\dot{\varrho}_{sg} &= -\left[\frac{1}{2}\gamma_s + \mathrm{i}(\Delta + \Omega_{12})\right]\varrho_{sg} - \frac{1}{2}\gamma_s\varrho_{es} + \Omega_\alpha(\varrho_{gg} - \varrho_{ss}) - \Omega_\alpha^*\varrho_{eg} - \Omega_\beta\varrho_{sa}, \\
\dot{\varrho}_{se} &= -\left[\frac{1}{2}(2\gamma_s + \gamma_a) - \mathrm{i}(\Delta - \Omega_{12})\right]\varrho_{se} + \Omega_\alpha^*(\varrho_{ss} - \varrho_{ee}) + \Omega_\alpha\varrho_{ge} - \Omega_\beta^*\varrho_{sa}, \\
\dot{\varrho}_{eg} &= -(\gamma + 2\mathrm{i}\Delta)\varrho_{eg} + \Omega_\alpha(\varrho_{sg} - \varrho_{es}) - \Omega_\beta(\varrho_{ag} + \varrho_{ea}), \\
\dot{\varrho}_{gs} &= -\left[\frac{1}{2}\gamma_s - \mathrm{i}(\Delta + \Omega_{12})\right]\varrho_{gs} - \frac{1}{2}\gamma_s\varrho_{se} + \Omega_\alpha^*(\varrho_{gg} - \varrho_{ss}) - \Omega_\alpha\varrho_{ge} - \Omega_\beta^*\varrho_{as}, \\
\dot{\varrho}_{es} &= -\left[\frac{1}{2}(2\gamma_s + \gamma_a) + \mathrm{i}(\Delta - \Omega_{12})\right]\varrho_{es} + \Omega_\alpha(\varrho_{ss} - \varrho_{ee}) + \Omega_\alpha^*\varrho_{eg} - \Omega_\beta\varrho_{as}, \\
\dot{\varrho}_{ge} &= -(\gamma - 2\mathrm{i}\Delta)\varrho_{ge} + \Omega_\alpha^*(\varrho_{gs} - \varrho_{se}) - \Omega_\beta^*(\varrho_{ga} + \varrho_{ae}),
\end{aligned} \tag{4.25}$$

and seven equations determining transitions between antisymmetric states

$$\begin{aligned}
\dot{\varrho}_{aa} &= -\gamma_a(\varrho_{aa} - \varrho_{ee}) + \left[\Omega_\beta(\varrho_{ga} + \varrho_{ae}) + \text{c.c.}\right], \\
\dot{\varrho}_{ae} &= -\left[\frac{1}{2}(\gamma_s + 2\gamma_a) - \mathrm{i}(\Delta + \Omega_{12})\right]\varrho_{ae} - \Omega_\beta^*(\varrho_{aa} - \varrho_{ee}) + \Omega_\beta\varrho_{ge} + \Omega_\alpha^*\varrho_{as}, \\
\dot{\varrho}_{ag} &= -\left[\frac{1}{2}\gamma_a + \mathrm{i}(\Delta - \Omega_{12})\right]\varrho_{ag} - \frac{1}{2}\gamma_a\varrho_{ea} + \Omega_\beta(\varrho_{gg} - \varrho_{aa}) + \Omega_\beta^*\varrho_{eg} - \Omega_\alpha\varrho_{as}, \\
\dot{\varrho}_{as} &= -(\gamma - 2\mathrm{i}\Omega_{12})\varrho_{as} - \Omega_\alpha\varrho_{ae} + \Omega_\alpha^*\varrho_{ag} + \Omega_\beta\varrho_{gs} + \Omega_\beta^*\varrho_{es},
\end{aligned}$$

$$\dot{\varrho}_{ea} = -\left[\frac{1}{2}(\gamma_s + 2\gamma_a) + \mathrm{i}(\Delta + \Omega_{12})\right]\varrho_{ea} - \Omega_\beta(\varrho_{aa} - \varrho_{ee}) + \Omega_\beta^*\varrho_{eg} + \Omega_\alpha\varrho_{sa}\,,$$

$$\dot{\varrho}_{ga} = -\left[\frac{1}{2}\gamma_a - \mathrm{i}(\Delta - \Omega_{12})\right]\varrho_{ga} - \frac{1}{2}\gamma_a\varrho_{ae} + \Omega_\beta^*(\varrho_{gg} - \varrho_{aa}) + \Omega_\beta\varrho_{ge} - \Omega_\alpha^*\varrho_{sa}\,,$$

$$\dot{\varrho}_{sa} = -(\gamma + 2\mathrm{i}\Omega_{12})\varrho_{sa} - \Omega_\alpha^*\varrho_{ea} + \Omega_\alpha\varrho_{ga} + \Omega_\beta^*\varrho_{sg} + \Omega_\beta\varrho_{se}\,. \tag{4.26}$$

The remaining equation of motion for ϱ_{gg} is found from the closure relation $\varrho_{gg} = 1 - \varrho_{ss} - \varrho_{ee} - \varrho_{aa}$. We see from the equations that the transitions between the symmetric states are driven at the Rabi frequency Ω_α and are coupled to the antisymmetric states with a strength proportional to Ω_β. On the other hand, transitions between the antisymmetric modes are driven at the Rabi frequency Ω_β and are also coupled by Ω_β to the transitions between the symmetric states. Thus, in the case of $\Omega_\beta = 0$, the dynamics of the symmetric and antisymmetric states are independent of each other.

4.2 Stationary Intensity

We now proceed to study the radiative properties of the collective two-atom system. In particular, we will search for signatures of the collective effects which lead to modifications of the radiative properties of the atoms. We shall calculate the intensity spectrum of the radiation emitted from a two-atom system continuously driven by a coherent laser field. The calculations will be performed for arbitrary atomic separations relative to the radiation wavelength, and will fully incorporate the effects of the dipole-dipole interaction. In the calculation of the intensity spectrum we shall concentrate on two distinct cases of the direction of propagation of the laser field in respect to the interatomic axis. In the first case, we assume that the laser field propagates in the direction perpendicular to the interatomic axis ($\boldsymbol{k}_L \perp \boldsymbol{R}_{ij}$). This case has the mathematical advantage that at most only nine coupled differential equations for the density matrix elements of the system have to be solved instead of 15, as in the general case of $\Omega_1 \neq \Omega_2$. Physically, in this situation the antisymmetric state does not participate in the interaction with the driving field. Correspondingly, we shall refer to this case as the symmetric excitation, because only transitions between states of the same symmetry with respect to the exchange of the atoms are excited. In the second case, the laser field is assumed to propagate in the direction parallel to the interatomic axis. In this case, the atoms are not in equivalent positions in the driving field, so that the atoms experience different amplitudes and phases of the driving field. Physically, in this situation the antisymmetric state fully participates in the interaction with the driving field.

4.2.1 General Features of the Radiation Intensity

We start off by discussing some general features of the intensity of the radiation field emitted from a two-atom system. Following the general expression (1.92), the resultant average intensity of the field emitted from two two-level atoms and measured in the direction $\boldsymbol{r}$ at time t is given by

$$\langle \hat{I}(\boldsymbol{r},t)\rangle = \Phi(\bar{\boldsymbol{r}})\left\{\sum_{n=1}^{2}\langle S_n^+(t)S_n^-(t)\rangle + \sum_{m\neq n=1}^{2}\langle S_n^+(t)S_m^-(t)\,(t)\rangle \mathrm{e}^{\mathrm{i}k_0\bar{\boldsymbol{r}}\cdot\boldsymbol{R}_{nm}}\right\}, \tag{4.27}$$

where $S_n^+(t)\equiv\hat{A}_{21}^n(t)$, $S_n^-(t)\equiv\hat{A}_{12}^n(t)$, and

$$\Phi(\bar{\boldsymbol{r}})\equiv\Phi_{1221}^{nn}=\frac{3}{8\pi}\gamma\left(1-\cos^2\psi\right), \tag{4.28}$$

In writing (4.27), we have assumed that the atomic dipole moments are parallel to each other and oriented in a direction forming the angle ψ with the direction of observation $\bar{\boldsymbol{r}}$.

The intensity (4.27) can be written in terms of four contributions involving the correlation functions and geometrical factors

$$\begin{aligned} I(\boldsymbol{r},t) = \Phi(\bar{\boldsymbol{r}})\big\{&\langle S_1^+(t)S_1^-(t)\rangle + \langle S_2^+(t)S_2^-(t)\rangle \\ &+\big[\langle S_1^+(t)S_2^-(t)\rangle + \langle S_2^+(t)S_1^-(t)\rangle\big]\cos(kR_{12}\cos\theta) \\ &+\mathrm{i}\big[\langle S_1^+(t)S_2^-(t)\rangle - \langle S_2^+(t)S_1^-(t)\rangle\big]\sin(kR_{12}\cos\theta)\big\}, \end{aligned} \tag{4.29}$$

where θ is the angle between $\boldsymbol{R}_{12}$ and the direction of observation $\bar{\boldsymbol{r}}$. The radiation intensity therefore exhibits a variation with θ that we refer to as the radiation pattern. Certain general features of the radiation intensity follow from (4.29):

1. The first term expresses the intensity of the emitted radiation created by spontaneous emission from atom 1. The second term expresses the intensity of the radiation spontaneously emitted by atom 2. These two terms are always positive and independent of θ. The contribution of these two terms obviously leads to a spherical shape of the radiation pattern.
2. The third and fourth terms result from the interference between the radiation fields emitted by different atoms. If nonzero, these terms can lead to a nonspherical shape of the radiation pattern and the emitted radiation can exhibit a strong enhancement or reduction in a direction θ at which $\cos(kR_{12}\cos\theta)=\pm1$ and/or $\sin(kR_{12}\cos\theta)=\pm1$.

It is convenient, in particular for physical interpretation, to write the intensity in terms of the density matrix elements of the density operator of the two-atom system represented in the basis of the superposition (collective) states. It is easily shown that in terms of the density matrix elements the correlation functions appearing in (4.29) can be expressed as

$$\begin{aligned}
&\langle S_1^+(t)S_1^-(t)\rangle + \langle S_2^+(t)S_2^-(t)\rangle = \varrho_{ss}(t) + \varrho_{aa}(t) + 2\varrho_{ee}(t)\,,\\
&\langle S_1^+(t)S_2^-(t)\rangle + \langle S_2^+(t)S_1^-(t)\rangle = \varrho_{ss}(t) - \varrho_{aa}(t)\,,\\
&\mathrm{i}\left[\langle S_1^+(t)S_2^-(t)\rangle - \langle S_2^+(t)S_1^-(t)\rangle\right] = 2\mathrm{Im}[\varrho_{as}(t)]\,.
\end{aligned} \tag{4.30}$$

We see from (4.30) that the interference term proportional to $\cos(kR_{12}\cos\theta)$ will contribute to the intensity only when $\varrho_{ss}(t) \neq \varrho_{aa}(t)$, i.e., when the symmetric and antisymmetric states are unequally populated. On the other hand, the interference term proportional to $\sin(kR_{12}\cos\theta)$ will contribute to the intensity only when $\mathrm{Im}[\varrho_{as}(t)] \neq 0$.

In terms of the density matrix elements of the collective atomic system the intensity of the radiation field observed at a point $\boldsymbol{r}$ can be written as

$$\begin{aligned}
\langle I(\boldsymbol{r},t)\rangle = \Phi(\bar{\boldsymbol{r}})\,\{&2\varrho_{ee}(t) + \varrho_{ss}(t)\,[1+\cos(kR_{12}\cos\theta)]\\
&+ \varrho_{aa}(t)\,[1-\cos(kR_{12}\cos\theta)]\\
&+ \mathrm{i}\,(\varrho_{sa}(t) - \varrho_{as}(t))\sin(kR_{12}\cos\theta)\}\,.
\end{aligned} \tag{4.31}$$

In examining (4.31), we note the dependence of the intensity spectrum on the direction relative to the interatomic axis. This indicates that the emission process from two atoms is strongly directional. The first term on the right-hand side of (4.31) is due to the radiation field emitted on transitions from the upper state $|e\rangle$ to the states $|s\rangle$ and $|a\rangle$. This contribution is spherically symmetric, i.e., is independent of the direction of observation. The second term represents the radiation field emitted on the $|s\rangle \to |g\rangle$ transition. The third term arises from the $|a\rangle \to |g\rangle$ transition. These two terms describe two different channels of transitions for which the angular distribution varies as $[1 \pm \cos(kR_{12}\cos\theta)]$. The last term in (4.31) originates from interference between these two radiation channels. Clearly, the emission process from the symmetric and antisymmetric states depends in a simple way on the geometry of the system and on populations of the states.

As we have already mentioned, the radiation field emitted on the symmetric transitions exhibits completely different directional properties then that emitted on the antisymmetric transitions. For example, the emission from the antisymmetric state is zero in the direction perpendicular to the interatomic axis, as for $\theta = \pi/2$ the factor $[1-\cos(kR_{12}\cos\theta)]$ vanishes independent of the interatomic separation R_{12}. Maximum radiation takes place at $\theta = 0$, but varies with R_{12}. The maximum value appears for $R_{12} = n\lambda/2$, corresponding to the integer multiple of the half-wavelength of the radiation field. By contrast, the emission from the symmetric state is most intense in the $\theta = \pi/2$ direction. The intensity is also different from zero in the $\theta = 0$

direction, but reduces to zero for $R_{12} = n\lambda/2$, i.e., for interatomic distances at which the radiation from the antisymmetric state is maximal.[1] Thus, we see that the radiation pattern of the emitted field is not spherically symmetric unless $\varrho_{ss}(t) = \varrho_{aa}(t)$ and then the angular distribution is spherically symmetric independent of the interatomic separation. Therefore, an asymmetry in the angular distribution of the fluorescence field would be a compelling evidence that the collective states $|s\rangle$ and $|a\rangle$ are not equally populated. If the fluorescence is detected in the direction perpendicular to the interatomic axis the observed intensity (if any) would correspond to the fluorescence field emitted from the symmetric state $|s\rangle$ and/or the upper state $|e\rangle$. On the other hand, if there is no fluorescence detected in the direction perpendicular to the atomic axis, the population is entirely in a superposition of the antisymmetric state $|a\rangle$ and the ground state $|g\rangle$.

4.2.2 Radiation Intensity for Symmetric Driving

We now proceed to investigate the radiative properties of two interacting atoms by examining the angular distribution of the average radiation intensity for the case in which the driving laser field propagates transverse to the interatomic axis [4–8]. This limiting case corresponds to a situation where both atoms experience the same amplitude and phase of the driving field. Accordingly, $\tilde{\Omega}_1 = \tilde{\Omega}_2$ and $\phi_1 = \phi_2$, so that the Rabi frequencies (4.23) become $\Omega_\alpha = -\mathrm{i}\Omega_0$ and $\Omega_\beta = 0$. This implies that the laser field drives only the symmetric transitions between the collective states of the system. Hence, we need only to solve the set of equations of motion (4.25) to get nonzero steady-state density matrix elements. Solving (4.25) with $\Omega_\alpha = -\mathrm{i}\Omega_0$ and $\Omega_\beta = 0$ is straightforward and results in the following steady-state values of the diagonal density matrix elements (populations)

$$\varrho^s_{ee} = \varrho^s_{aa} = \frac{\tilde{\Omega}_0^4}{D}\,, \quad \varrho^s_{ss} = \frac{\left(\tilde{\Omega}_0^2 + \gamma^2 + 4\Delta_L^2\right)\tilde{\Omega}_0^2}{D}\,, \tag{4.32}$$

and the off-diagonal elements (coherences)

$$\varrho^s_{sg} = \mathrm{i}\frac{\left\{\gamma\left(\tilde{\Omega}_0 + 2\mathrm{i}\Delta_L\right)\tilde{\Omega}_0 + \left(\gamma^2 + 4\Delta_L^2\right)\left[\tfrac{1}{2}(\gamma + \gamma_{12}) + \mathrm{i}(\Delta_L - \Omega_{12})\right]\right\}\tilde{\Omega}_0}{D}\,,$$

$$\varrho^s_{es} = \mathrm{i}\frac{(\gamma + 2\mathrm{i}\Delta_L)\,\tilde{\Omega}_0^3}{D}\,,$$

$$\varrho^s_{ge} = -\frac{(\gamma + 2\mathrm{i}\Delta_L)\left[\tfrac{1}{2}\,(\gamma + \gamma_{12}) + \mathrm{i}\,(\Delta_L - \Omega_{12})\right]\tilde{\Omega}_0^2}{D}\,,$$

[1] It should be kept in mind that there is no radiation in the direction parallel to the transition dipole moments of the atoms because $\Phi(\bar{\boldsymbol{r}}) = 0$ for $\boldsymbol{r} \parallel \boldsymbol{\mu}$.

$$\varrho_{gs}^{s} = \left(\varrho_{sg}^{s}\right)^{*} , \quad \varrho_{se}^{s} = \left(\varrho_{es}^{s}\right)^{*} , \quad \varrho_{eg}^{s} = \left(\varrho_{ge}^{s}\right)^{*} , \tag{4.33}$$

where the superscript "s" stands for steady-state values, and

$$D = 4\tilde{\Omega}_0^4 + \left(\gamma^2 + 4\Delta_L^2\right)\left[2\tilde{\Omega}_0^2 + \frac{1}{4}\left(\gamma + \gamma_{12}\right)^2 + \left(\Delta_L - \Omega_{12}\right)^2\right]. \tag{4.34}$$

With the stationary solutions (4.33), the intensity of the radiation field, which depends on the direction of observation, takes the form

$$\langle \hat{I}\left(\boldsymbol{r}\right)\rangle = \lim_{t\to\infty}\langle \hat{I}\left(\boldsymbol{r}, t\right)\rangle = \Phi(\bar{\boldsymbol{r}})\left\{\frac{3\tilde{\Omega}_0^4}{4D}\left[1 - \frac{1}{3}\cos\left(kR_{12}\cos\theta\right)\right]\right.$$
$$\left. + \frac{\tilde{\Omega}_0^4 + 2\tilde{\Omega}_0^2\left(\gamma^2 + 4\Delta_L^2\right)}{4D}\left[1 + \cos\left(kR_{12}\cos\theta\right)\right]\right\} . \tag{4.35}$$

It is seen that the radiation intensity depends strongly on the Rabi frequency of the driving field. We may distinguish two distinct regimes of values of the Rabi frequency with markedly different intensity behaviors; the weak, $\Omega \ll \gamma, \Delta_L$, and strong Rabi frequency regime, $\Omega \gg \gamma, \Delta_L$. In the strong Rabi frequency regime, at which the magnitudes of the first and the second term on the right-hand side of (4.35) are comparable, the intensity is smallest in directions determined by

$$\cos\theta = \frac{n}{2(R_{12}/\lambda)} , \quad (n = \pm 1, \pm 3, \pm 5, \ldots) , \tag{4.36}$$

but it can never vanish. Note from (4.35) that the directivity can be improved by detuning of the laser field from the atomic resonance.

In the limit of a weak driving field, $\Omega \ll \gamma, \Delta_L$, the first term on the right-hand side of (4.35) is negligible in comparison to the second term. We therefore ignore its contribution to the intensity distribution and arrive at the result

$$\langle I\left(\boldsymbol{r}\right)\rangle = \Phi(\bar{\boldsymbol{r}})\frac{\Omega^2\left(\gamma^2 + 4\Delta_L^2\right)}{2D}\left[1 + \cos\left(kR_{12}\cos\theta\right)\right] . \tag{4.37}$$

Unlike the intensity for a strong driving, which can never vanish, the intensity (4.37) can vanish for directions determined by (4.36). For example, when the atoms are separated by the distance $R_{12} = \lambda/2$, the intensity (4.37) vanishes in directions $\theta = 0$ and π, i.e., in directions along the interatomic axis. The number of directions for which the intensity (4.37) vanished increases with an increasing distance between the atoms. When $R_{12} = \lambda$, the intensity vanishes in directions $\theta = \pi/3, 2\pi/3, 4\pi/3$ and $5\pi/3$.

It is important to note that the distance $R_{12} = \lambda/2$ is the minimum distance between the atoms at which the intensity (4.37) could vanish. Since $|\cos\theta| \leq 1$, after simple calculations one can show that (4.36) leads to the following restriction

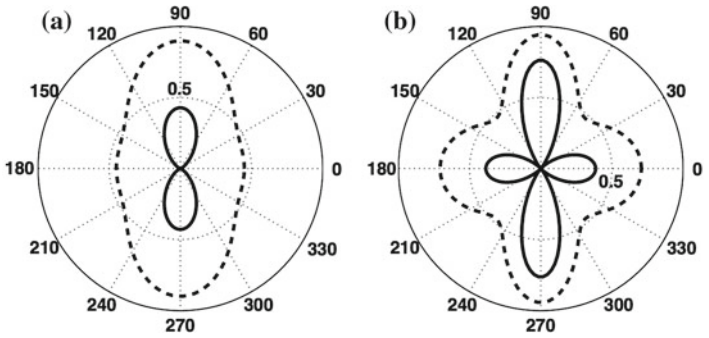

Fig. 4.3 Angular distribution of the stationary radiation intensity for $\boldsymbol{\mu} \perp \boldsymbol{R}_{12}$ and different separations between the atoms and different Rabi frequencies of the laser field. In frame **a**, $R_{12} = \lambda/2$ and $\Omega = 0.1\gamma$ (*solid line*), $\Omega = \gamma$ (*dashed line*). In frame **b**, $R_{12} = 3\lambda/4$ and $\Omega = 0.1\gamma$ (*solid line*), $\Omega = \gamma$ (*dashed line*)

on R_{12}:

$$R_{12} = \frac{1}{2}\left|\frac{n}{\cos\theta}\right|\lambda\,. \tag{4.38}$$

Obviously, the lower limit on R_{12} is for $n = 1$ and $\cos\theta = 1$ at which the radiation intensity is suppressed in the direction perpendicular to the interatomic axis.

Since the radiation intensity (4.35) is independent of the azimuthal angle ϕ, we can display it graphically in a polar form for a variety of different sizes of the system, i.e., different distances between the atoms. The angular distribution of the average radiation intensity (4.35) is illustrated graphically in Fig. 4.3 for two different Rabi frequencies and separations between the atoms. It is seen that the radiation pattern is not spherically symmetric. The asymmetry depends strongly on the Rabi frequency and the distance between the atoms. For a weak driving field and the atomic separation $R_{12} = \lambda/2$, the asymmetry is very pronounced and the intensity is identically equal to zero in the direction of the interatomic axis. When the atoms are separated by $R_{12} = 3\lambda/4$, there are four directions in which the intensity vanishes. The asymmetry of the radiation pattern decreases with increasing Ω and for a strong driving there are no directions in which the intensity vanishes. We may summarize that in the case of a weak driving of the atoms there are directions in which the radiation can be dynamically suppressed.

4.2.3 Radiation Intensity for Nonsymmetric Driving

We now turn to investigate the possibility of a directional suppression of the radiation intensity in the case of a nonsymmetric driving corresponding to $\Omega_\alpha \neq 0$ and $\Omega_\beta \neq 0$. According to (4.23), the laser field can now excite both, the symmetric and antisymmetric transitions in the system. For clarity, two kinds of a nonsymmet-

ric driving are discussed, corresponding to the choices of either different phases or different amplitudes of the driving field at the positions of the atoms [9–11].

Since in the case of $\Omega_\beta \neq 0$, the sets of the differential equations (4.25) and (4.26) cannot be solved separately, we will use numerical methods to find the stationary values of the density matrix elements. For purposes of numerical computation, it is more convenient to write (4.25) and (4.26) in a matrix form

$$\dot{\boldsymbol{X}}(t) = M\boldsymbol{X}(t) + \boldsymbol{I} \ , \tag{4.39}$$

where M is a 15×15 matrix of the coefficients of the differential equations (4.25) and (4.26), $\boldsymbol{X}(t)$ is a 15×1 column vector of the fifteen density matrix elements, and $\boldsymbol{I}$ is a 15×1 column vector of the inhomogeneous terms. The stationary values for the density matrix elements are found by setting the left-hand side of (4.39) equal to zero, so that

$$\boldsymbol{X}(\infty) = M^{-1}\boldsymbol{I} \ , \tag{4.40}$$

or, explicitly, in component form

$$X_i(\infty) = -\sum_{j=1}^{15} (M^{-1})_{ij} I_j \ . \tag{4.41}$$

Angular distributions of the average radiation intensity are illustrated in Figs. 4.4 and 4.5. Two different physical situations are considered for the Rabi frequency of the driving field at the positions of the atoms: phase difference only ($\phi_d \neq 0$, $\Omega_d = 0$) in Figs. 4.4a and 4.5a, and magnitude difference only ($\Omega_d \neq 0$, $\phi_d = 0$) in Figs. 4.4b and 4.5b.

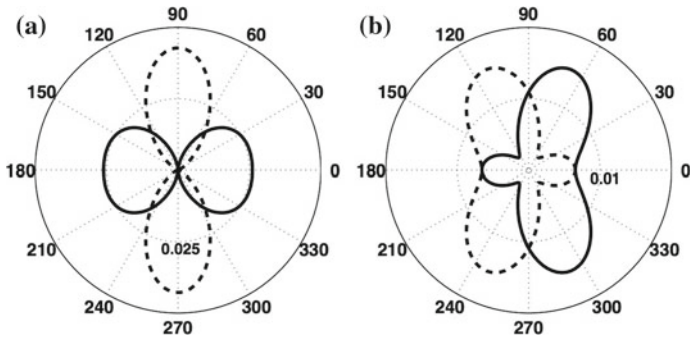

Fig. 4.4 Angular distribution of the stationary radiation intensity for $\bar{\boldsymbol{\mu}} \perp \boldsymbol{R}_{12}$, $R_{12} = \lambda/2$ and different phases and Rabi frequencies of the laser field at the positions of the atoms. In frame **a**, $\Omega_1 = \Omega_2 = 0.1\gamma$ and $\phi_d = \pi/2$ (*solid line*), $\phi_d = 0$ (*dashed line*). In frame **b**, $\phi_d = 0$ and $\Omega_1 = 0.1\gamma$, $\Omega_2 = 0$ (*solid line*), $\Omega_1 = 0$, $\Omega_2 = 0.1\gamma$ (*dashed line*)

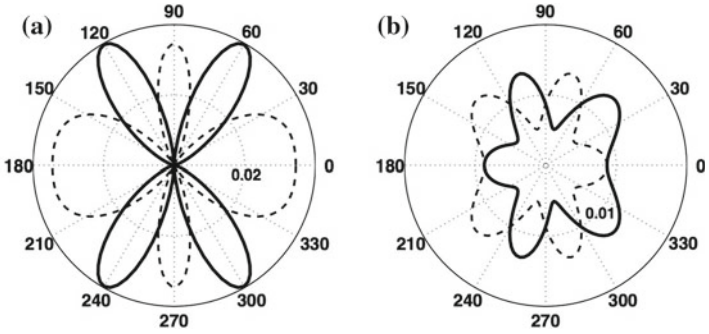

Fig. 4.5 Angular distribution of the stationary radiation intensity for $\bar{\boldsymbol{\mu}} \perp \boldsymbol{R}_{12}$, $R_{12} = \lambda$ and different phases and Rabi frequencies of the laser field at the positions of the atoms. In frame **a**, $\Omega_1 = \Omega_2 = 0.1\,\gamma$ and $\phi_d = \pi/2$ (*solid line*), $\phi_d = 0$ (*dashed line*). In frame **b**, $\phi_d = 0$ and $\Omega_1 = 0.1\gamma$, $\Omega_2 = 0$ (*solid line*), $\Omega_1 = 0$, $\Omega_2 = 0.1\gamma$ (*dashed line*)

In Fig. 4.4a we compare the angular distribution for the phase difference $\phi_d = 0$ with that for $\phi_d = \pi/2$ when the atoms are separated by a distance $R_{12} = \lambda/2$. The phase difference $\phi_d = \pi/2$ corresponds to the dipole moments of the atoms driven with opposite phases, $\phi_1 = \pi$, $\phi_2 = 0$. As discussed in the previous section, the case of $\phi_d = 0$ corresponds to the situation where the laser field drives only the symmetric modes of the system, while in the case of $\phi_d = \pi/2$ the laser effectively drives only the antisymmetric modes. We see that for $\phi_d = 0$ the emission is inhibited in the direction along the interatomic axis. The phase difference $\phi_d = \pi/2$ has the effect of forcing the atoms to radiate along the interatomic axis, with zeros in the emission occurring in the perpendicular directions, $\theta = \pi/2$ and $\theta = 3\pi/2$.

In frame (b) of Fig. 4.4 we compare angular distributions for the same phases ($\phi_d = 0$) but different magnitudes of the Rabi frequencies at the positions of the atoms. We have chosen the magnitudes $\Omega_1 \neq 0, \Omega_2 = 0$ and $\Omega_1 = 0, \Omega_2 \neq 0$ to suit the situation where the symmetric and antisymmetric modes are driven by the same Rabi frequency, $\Omega_\alpha = \Omega_\beta$. A comparison of Fig. 4.4a, b immediately shows the difference that different phases and different magnitudes have on the radiation intensity. The most obvious difference between the results is the absence of directions in which the radiation intensity is completely canceled. Different magnitudes of the Rabi frequency lead to a destructive interference in some directions but the interference is not maximal. However, we see that the radiation is mainly on one side of the system. Thus, the un-driven atom steers the system to radiate toward one side of the pattern. The direction of the emission reverses when Ω_d reverses its sign. The one-sided emission behavior seen in Fig. 4.4b can be understood by referring to the effect of the angular factor $\sin(kR_{12}\cos\theta)$ appearing in the expression for the radiation pattern. The contribution of this factor is determined by $\mathrm{Im}[\varrho_{as}(t)]$. It is easily shown that $\mathrm{Im}[\varrho_{as}(t)] \neq 0$ for $\Omega_d \neq 0$ such that $\mathrm{Im}[\varrho_{as}(t)]|_{\Omega_d>0} = -\mathrm{Im}[\varrho_{as}(t)]|_{\Omega_d<0}$.

The number of directions in which the emission can be inhibited increases with an increasing separation between the atoms. This is illustrated in Fig. 4.5a, which

shows the radiation pattern for the atomic separation $R_{12} = \lambda$ and two values of ϕ_d. The increase of the separation shows up clearly in the presence of four directions in which the emission is inhibited. It is interesting that a change of ϕ_d from 0 to $\pi/2$ rotates the directions of the inhibited emission by $\pi/4$.

When the atoms experience different magnitudes of the Rabi frequency the asymmetry of the radiation pattern is less pronounced, as illustrated in Fig. 4.5b, that the larger dimensions of the atomic system the smaller confining of the radiation in particular directions.

In summary of this section, the results presented in Figs. 4.4 and 4.5 show clearly that a phase difference between the Rabi frequencies at the positions of the atoms is a crucial factor for achievement of the complete inhibition of the emission in some directions. It is simple to interpret this behavior by referring to the expression for the radiation intensity, (4.31). The intensity contains two interference terms, one proportional to $\cos(kR_{12}\cos\theta)$ and the other proportional to $\sin(kR_{12}\cos\theta)$. Radiation at an angle θ from atom 2 has a distance $R_{12}\cos\theta$ farther to travel to the observation point than that from atom 1. Its electric field is therefore retarded by an extra amount $kR_{12}\cos\theta$. The fields of the atoms interfere destructively in the direction $\theta = \pi/2$ if the phases ϕ_2 at which the atom 2 and the phase ϕ_1 at which atom 1 is driven, are opposite, $\phi_1 - \phi_2 = \pi$. In the direction $\theta = 0$, the interference of the fields emitted depends on the distance between the atoms. For $R_{12} = \lambda/2$ the oscillation phases of the atoms are opposite. Therefore, for $\phi_d = 0$ there is a destructive interference of the fields emitted in the direction of the interatomic axis. An additional phase difference $\phi_d = \pi/2$ makes the atoms to oscillate in phase, so then there is a constructive interference of the fields along the interatomic axis. However, then there is a destructive interference in the directions perpendicular to the interatomic axis. Since cosine is a symmetric function, there are always two directions at which the interference is constructive or destructive. The situation changes when $\phi_d = 0$ and the magnitudes of the Rabi frequencies are different. In this case, the interference term $\cos(kR_{12}\cos\theta) = 1$ whereas $\sin(kR_{12}\cos\theta)$ can be negative. Hence, the symmetry of the emission direction can be broken simply because $\cos\theta > 0$ gives $\sin(kR_{12}\cos\theta)$ positive whereas $\cos\theta < 0$ gives $\sin(kR_{12}\cos\theta)$ negative. As a result, the radiation intensity can have different magnitudes in the $\cos\theta > 0$ and $\cos\theta < 0$ parts of the pattern. In physical terms one-sided emission reflects constructive and destructive interference effects on the two sides of the pattern.

4.3 Selective Excitation of the Collective States

In this section, we will look at different methods of preparing two identical two-level atoms in a selected excited collective state. As we have seen in the preceding section, the preparation of the system in either symmetric or antisymmetric state can lead to the complete inhibition of the emission in some directions. The directions in which the symmetric and antisymmetric states do not radiate are quite different and vary with the distance between the atoms.

The preparation of two atoms in a desired state can be done by using short laser pulses. Alternatively, one can use a cw laser field which after a long interaction time could drive the system to a selected stationary state. In the first method, the conditions for a selective excitation of the collective atomic states are analyzed from the interaction Hamiltonian of the laser field with the two-atom system. If we make the unitary transformation

$$\tilde{H}_L = \mathrm{e}^{\mathrm{i}\hat{H}_a t/\hbar}\hat{H}_L \mathrm{e}^{-\mathrm{i}\hat{H}_a t/\hbar}\,, \tag{4.42}$$

where $\hat{H}_a$ is given in (4.2), we find that the interaction Hamiltonian (4.17) takes the form

$$\begin{aligned}\tilde{H}_L = -\frac{\hbar}{2}\Big\{&\left(\tilde{\Omega}_1+\tilde{\Omega}_2\right)\left(A_{es}\mathrm{e}^{\mathrm{i}(\Delta_L+\Omega_{12})t}+A_{sg}\mathrm{e}^{\mathrm{i}(\Delta_L-\Omega_{12})t}\right)\\ &+\left(\tilde{\Omega}_2-\tilde{\Omega}_1\right)\left(A_{ag}\mathrm{e}^{\mathrm{i}(\Delta_L+\Omega_{12})t}+A_{ea}\mathrm{e}^{\mathrm{i}(\Delta_L-\Omega_{12})t}\right)+\mathrm{H.c.}\Big\}\,.\end{aligned} \tag{4.43}$$

The Hamiltonian (4.43) represents the interaction of the laser field with the collective two-atom system, and in the transformed form contains terms oscillating at frequencies $\Delta_L \pm \Omega_{12}$, which correspond to the two separate groups of transitions between the collective atomic states occurring at frequencies $\omega_L = \omega_0 + \Omega_{12}$ and $\omega_L = \omega_0 - \Omega_{12}$. It is now apparent that the $\Delta_L + \Omega_{12}$ frequencies are separated from $\Delta_L - \Omega_{12}$ frequencies by $2\Omega_{12}$, and hence the two sets of the transitions evolve separately when $\Omega_{12} \gg \gamma$. Thus, depending on the frequency, the laser can be selectively tuned to either of the two sets of the transitions. When $\omega_L = \omega_0 + \Omega_{12}$, which corresponds to $\Delta_L - \Omega_{12} = 0$, the laser is tuned to exact resonance with the $|e\rangle - |a\rangle$ and $|g\rangle - |s\rangle$ transitions, and then the terms, appearing in the Hamiltonian (4.43), and corresponding to these transitions have no explicit time dependence. In contrast, the $|g\rangle - |a\rangle$ and $|e\rangle - |s\rangle$ transitions are off-resonant and the terms corresponding to these transitions have an explicit time dependence $\exp(\pm 2\mathrm{i}\Omega_{12}t)$. If $\Omega_{12} \gg \gamma$, the off-resonant terms rapidly oscillate with the frequency $2\Omega_{12}$, and then we can make a secular approximation in which we neglect all those rapidly oscillating terms. After the secular approximation, the interaction Hamiltonian (4.43) takes the simplified form

$$\tilde{H}_L = -\frac{\hbar}{2}\left[\left(\tilde{\Omega}_1+\tilde{\Omega}_2\right)A_{sg}+\left(\tilde{\Omega}_2-\tilde{\Omega}_1\right)A_{ea}+\mathrm{H.c.}\right]\,. \tag{4.44}$$

It is seen that the laser field couples to the transitions with significantly different Rabi frequencies. The coupling strength of the laser to the $|g\rangle - |s\rangle$ transition is proportional to the sum of the Rabi frequencies $\tilde{\Omega}_1 + \tilde{\Omega}_2$, whereas the coupling strength of the laser to the $|a\rangle - |e\rangle$ transition is proportional to the difference of the Rabi frequencies $\tilde{\Omega}_1 - \tilde{\Omega}_2$. According to (4.21), the Rabi frequencies $\tilde{\Omega}_1$ and $\tilde{\Omega}_2$ even if of equal amplitudes can differ in phase. Thus, in order to selectively couple the laser field to the symmetric $|g\rangle - |s\rangle$ transition, the driving laser field should

be in phase with both atoms, i.e., $\tilde{\Omega}_1 = \tilde{\Omega}_2$. This can be achieved by choosing the direction of propagation of the laser perpendicular to the interatomic axis.

Of course, the Rabi frequency cannot be too strong in order to avoid the coupling of the laser to the $|s\rangle - |e\rangle$ transition, which could lead to a slight pumping of the population to the state $|e\rangle$. On the other hand, the Rabi frequency cannot be too small as for a small $\tilde{\Omega}$ the duration of the pulse, required for the complete transfer of the population into the state $|s\rangle$, becomes longer and then spontaneous emission can occur during the excitation process. Therefore, the transfer of the population to the state $|s\rangle$ cannot be made arbitrarily fast and, in addition, requires a careful estimation of the optimal Rabi frequency, which could be difficult to achieve in a real experimental situation.

If we choose the laser frequency such that $\Delta_L + \Omega_{12} = 0$, the laser field is then resonant to only two of the transitions: $|a\rangle - |g\rangle$ and $|e\rangle - |s\rangle$. Thus, after the secular approximation the Hamiltonian (4.43) reduces to

$$\tilde{H}_L = -\frac{\hbar}{2}\left[\left(\tilde{\Omega}_2 - \tilde{\Omega}_1\right) A_{ag} + \left(\tilde{\Omega}_1 + \tilde{\Omega}_2\right) A_{es} + \text{H.c.}\right] . \tag{4.45}$$

Clearly, for $\tilde{\Omega}_1 = -\tilde{\Omega}_2$ the laser couples only to the $|a\rangle - |g\rangle$ transition. Thus, in order to selectively excite the antisymmetric $|g\rangle - |a\rangle$ transition, the atoms should experience the same magnitudes but opposite phases of the laser field. How to realize this situation in practice? This can be achieved by choosing the propagation vector $\boldsymbol{k}_L$ of the laser along the interatomic axis, and adjusting the atomic separations such that

$$\phi_2 - \phi_1 = (2n+1)\,\pi\,, \qquad n = 0, 1, 2, \ldots\,. \tag{4.46}$$

One can also produce atoms in a single collective state by turning on the atoms a standing laser field instead of the running-wave field. In this method, the laser amplitudes differ by the sign, i.e., $\boldsymbol{\mathcal{E}}_{L_1} = -\boldsymbol{\mathcal{E}}_{L_2} = \boldsymbol{\mathcal{E}}_0$, and the phases also differ by the sign, $\boldsymbol{k}_{L_1} \cdot \boldsymbol{R}_1 = -\boldsymbol{k}_{L_2} \cdot \boldsymbol{R}_2$, so the Rabi frequencies experienced by the atoms are

$$\begin{aligned} \Omega_1 &= \frac{2\mathrm{i}}{\hbar}\boldsymbol{\mu}_1 \cdot \boldsymbol{\mathcal{E}}_0 \sin\left(\frac{1}{2}\boldsymbol{k}_L \cdot \boldsymbol{R}_{12}\right) , \\ \Omega_2 &= -\frac{2\mathrm{i}}{\hbar}\boldsymbol{\mu}_2 \cdot \boldsymbol{\mathcal{E}}_0 \sin\left(\frac{1}{2}\boldsymbol{k}_L \cdot \boldsymbol{R}_{12}\right) , \end{aligned} \tag{4.47}$$

where $\boldsymbol{k}_L = \boldsymbol{k}_{L_1} = \boldsymbol{k}_{L_2}$ and we have chosen the reference frame such that $\boldsymbol{R}_1 = \boldsymbol{R}_{12}/2$ and $\boldsymbol{R}_2 = -\boldsymbol{R}_{12}/2$. It follows from (4.47) that the Rabi frequencies oscillate with opposite phases independent of the separation between the atoms.

There are other techniques which could be used to produce atoms in a single collective state. For example, when the driving field is propagated such that the symmetric and antisymmetric transitions experience the same Rabi frequency, i.e., $\Omega_\alpha = \Omega_\beta$, selective population of the collective states can be achieved by varying the detuning of the laser field from the atomic resonance. Figure 4.6 shows the stationary

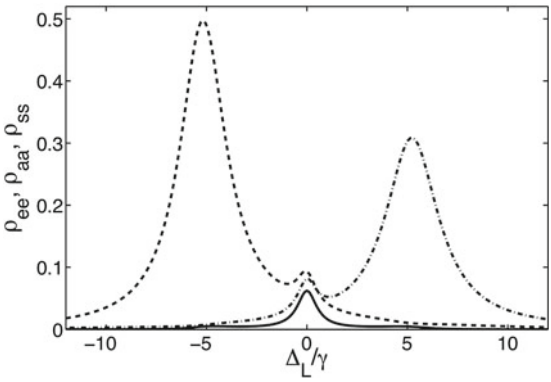

Fig. 4.6 Stationary populations of the collective atomic states of two identical atoms plotted as a function of Δ_L for the laser field driving the atoms with Rabi frequencies $\Omega_1 = 2.5\gamma$, $\Omega_2 = 0$, $\phi_1 = \phi_2 = 0$, the atomic separation $R_{12} = 0.08\lambda$ and $\bar{\boldsymbol{\mu}} \perp \boldsymbol{R}_{12}$: ϱ_{ee} (*solid line*), ϱ_{aa} (*dashed line*), and ϱ_{ss} (*dashed-dotted line*)

populations of the collective excited states as a function of the laser detuning Δ_L. The populations are obtained from the numerical solution (4.41) of the coupled sets of equations of motion for the density matrix elements (4.25) and (4.26). We see from the figure that the collective state $|e\rangle$ is populated at $\Delta_L = 0$, the symmetric state is significantly populated at $\Delta_L = \Omega_{12}$, whereas the antisymmetric state is significantly populated at $\Delta_L = -\Omega_{12}$. At these detunings the laser field frequency is resonant with the frequency of the corresponding transition between the collective states.

4.3.1 Experimental Preparation of Two Atoms in a Collective State

The examples discussed above on the preparation of two atoms in a single collective state relay on the requirement of a strong dipole-dipole interaction between the atoms which allows to address individually each of the transitions between the collective states. This, however, requires the atoms to be located at very small distances which, on the other hand, put a significant limit on experimental realizations of the selective excitation of the collective states.

It is possible, however, to create superposition states of distant atoms coupled to a common EM mode [12, 13]. For example, Cirac and Zoller [14] proposed a scheme for the creation of superposition (entangled) states of atomic ions confined in a linear trap and coupled to a common quantized motional mode. In their scheme the ions are assumed to be trapped at large distances so there is no direct interaction between them and each ion is driven by a standing-wave laser beam. Other proposals, which we will discuss in details in Chap. 8, involve coupling of distant atoms to a cavity mode.

Following the Cirac-Zoller proposal, Turchette et al. [15] have realized experimentally a non-maximally superposed single excitation collective state between two

trapped ions coupled to a quantized mode of the ions' motional mode cooled to the ground state.

Theoretical Background

Let us first briefly outline the theory behind the experiment in order to provide some insight into the essential requirements for the creation of a single excitation collective state. The calculation follows very closely the experimental situation.

Consider two two-level systems (ions) interacting with a single-mode EM field. The interaction Hamiltonian of the ions with the field, under the rotating-wave approximation, can be written as

$$\hat{H}_I = -\mathrm{i}\hbar g_1 \left(S_1^+ \hat{a} - \hat{a}^\dagger S_1^-\right) - \mathrm{i}\hbar g_2 \left(S_2^+ \hat{a}\, \mathrm{e}^{-\mathrm{i}kR_{12}} - \hat{a}^\dagger S_2^- \mathrm{e}^{\mathrm{i}kR_{12}}\right) , \tag{4.48}$$

where S_i^+ and S_i^- are the spin-up and spin-down operators of ion i, $\hat{a}$ and $\hat{a}^\dagger$ are the annihilation and creation operators of the field mode, g_1 and g_2 are the coupling strengths of the ions to the field mode, and we have introduced the phase factor $\exp(\pm \mathrm{i}kR_{12})$ in the coupling coefficients reflecting a phase difference in the oscillation of the dipole moments of the ions separated by a finite distance R_{12}.

The calculation of the dynamics of the ions is based on the solution of the Schrödinger equation for the state vector of the system

$$\mathrm{i}\hbar \frac{\partial}{\partial t} |\tilde{\Psi}(t)\rangle = \hat{H}_I |\tilde{\Psi}(t)\rangle , \tag{4.49}$$

where $|\tilde{\Psi}\rangle$ is the state vector of the system in the interaction picture.

Assume that only a single excitation is present in the system. Then the state vector can be expanded in terms of three terms

$$|\tilde{\Psi}(t)\rangle = C_F(t)\, |g_1, g_2, 1\rangle + C_1(t)\, |e_1, g_2, 0\rangle + C_2(t)\, |g_1, e_2, 0\rangle \ , \tag{4.50}$$

where $C_F(t)$ is a slowly varying part of the probability amplitude that both ions are in their ground states and a single excitation is present in the field mode, $C_1(t)$ is a slowly varying part of the probability amplitude that ion 1 is in excited state, ion 2 is in ground state and no excitation is present in the field mode, and $C_2(t)$ is a slowly varying part of the probability amplitude that ion 1 is in ground state, ion 2 is in excited state and no excitation is present in the field mode.

By substituting the wave function (4.50) into (4.49), we obtain the following system of coupled differential equations for the probability amplitudes

$$\dot{C}_F = \frac{1}{2}\Omega_1 C_1 + \frac{1}{2}\Omega_2 \mathrm{e}^{\mathrm{i}\phi} C_2 \ , \ \dot{C}_1 = -\frac{1}{2}\Omega_1 C_F \ , \ \dot{C}_2 = -\frac{1}{2}\Omega_2 \mathrm{e}^{-\mathrm{i}\phi} C_F \ , \tag{4.51}$$

where $\Omega_i = 2g_i/\hbar$ is the single-photon Rabi frequency of ion i, and $\phi = kR_{12}$. Solving (4.51) with the initial condition $|\Psi(0)\rangle = |g_1\rangle\, |e_2\rangle\, |0\rangle$, we find

$$|\tilde{\Psi}(t)\rangle = \frac{\Omega_2 e^{i\phi}}{\Omega} \sin\left(\frac{1}{2}\Omega t\right) |g\rangle\,|1\rangle + \left\{\left[\frac{\Omega_2^2}{\Omega^2}\left(\cos\frac{1}{2}\Omega t - 1\right) + 1\right] |g_1\rangle\,|e_2\rangle + e^{i\phi}\left[\frac{\Omega_1\Omega_2}{\Omega^2}\left(\cos\frac{1}{2}\Omega t - 1\right)\right] |e_1\rangle\,|g_2\rangle\right\} |0\rangle \ , \tag{4.52}$$

where $\Omega = \sqrt{\Omega_1^2 + \Omega_2^2}$. For the duration of the driving laser fields $\Omega t = 2\pi$, the superposition state (4.52) reduces to a non-maximally superposed collective state

$$|\tilde{\Psi}(t = 2\pi/\Omega)\rangle = |\Psi_c(\phi)\rangle\,|0\rangle \ , \tag{4.53}$$

where

$$|\Psi_c(\phi)\rangle = \frac{\Omega_1^2 - \Omega_2^2}{\Omega^2} |g_1\rangle\,|e_2\rangle - e^{i\phi}\frac{2\Omega_1\Omega_2}{\Omega^2} |e_1\rangle\,|g_2\rangle \tag{4.54}$$

is a non-maximally superposed ions' collective state. We see that the crucial for the preparation of the collective state is to drive the atoms with unequal Rabi frequencies.

We can evaluate the fidelity (overlapping) of the state (4.54) with either the symmetric state $|s\rangle$ or the antisymmetric state $|a\rangle$ and find

$$|\langle s\,|\Psi_c(\phi)\rangle|^2 = |\langle a\,|\Psi_c(\phi)\rangle|^2 = \frac{1}{2}\left(\frac{\Omega_1^2 + 2\Omega_1\Omega_2 - \Omega_2^2}{\Omega^2}\right)^2 . \tag{4.55}$$

It is straightforward to show that the fidelity (4.55) is maximal for $\Omega_1 = 2\Omega_2$ at which

$$|\langle s\,|\Psi_c(\phi)\rangle|^2 = |\langle a\,|\Psi_c(\phi)\rangle|^2 = 0.98 \ , \tag{4.56}$$

and the state (4.54) reduced to

$$|\Psi_c(\phi)\rangle = \frac{3}{5} |g_1, e_2\rangle - e^{i\phi}\frac{4}{5} |e_1, g_2\rangle \ . \tag{4.57}$$

One can see that for $\phi = 0$ or π, the state $|\Psi_c(\phi)\rangle$ is a good approximation of the antisymmetric state $|a\rangle$ or the symmetric state $|s\rangle$.

Experiment

We now turn to describe in details the experiment by Turchette et al. [15] demonstrating the creation of the collective state (4.54) between two berylium $^9Be^+$ ions trapped in an elliptical rf (Paul) trap. Figure 4.7a is a schematic view of the apparatus used in the experiment and Fig. 4.7b shows the relevant energy levels of the berylium ion. The preparation of a collective state between the ions was done in several steps. In the first step, the beams D1, D2, and D3 were turned on for about 10 μs to Doppler cool the ions to the Lamb-Dicke regime, corresponding to the ions' confinement much smaller than the laser wavelength. The cold ions held in the trap

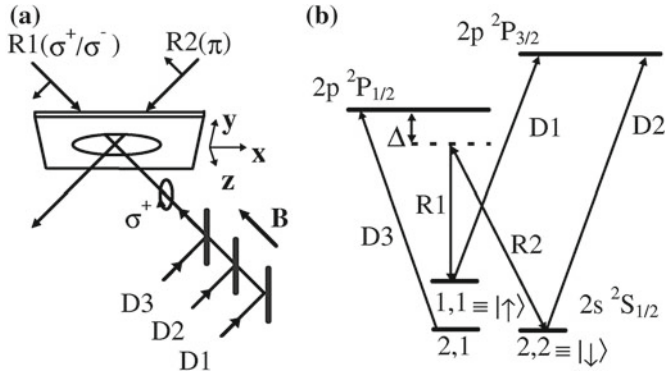

Fig. 4.7 **a** Main features of the apparatus used by Turchette et al. [15]. **b** berylium $^9Be^+$ energy levels and laser driven transitions relevant in the experiment. Laser beams D1 and D2 provide Doppler pre-cooling in all three dimensions, and laser D3 prevents optical pumping to the $|F = 2, m_F = 1\rangle$, (2, 1) state. Reprinted with permission from Q.A. Turchette, C.S. Wood, B.E. King, C.J. Myatt, D. Leibfried, W.M. Itano, C. Monroe, D.J. Wineland: Phys. Rev. Lett. **81**, 3631 (1998). Copyright (1998) by the American Physical Society

were undergoing small oscillations about their equilibrium positions. For the ions lying along the $\boldsymbol{x}$ axis there were two modes associated with the motion of the ions along this axis: the center-of-mass mode of frequency ω_x and the stretch mode of frequency $\sqrt{3}\omega_x$ associated with the motion of the ions in opposite directions.

In the second step, the beam D2 was turned off leaving beams D1 and D3 on for 5 μs to optically pump both ions to the $^2S_{1/2}$ $(F = 2, m_F = 2)$ hyperfine state, abbreviated in Fig. 4.7b as the $2, 2 \equiv |\downarrow\rangle$ state. Next, the beams D1 and D3 were turned off and two laser beams R1 and R2 (R1⊥R2) were then applied to drive stimulated Raman transitions between the $^2S_{1/2}$ $(F = 1, m_F = 1)$ hyperfine state, abbreviated in Fig. 4.7b as the $1, 1 \equiv |\uparrow\rangle$ state, and the $|\downarrow\rangle$ state through the virtual $2p\,^2P_{1/2}$ state. The beams R1 and R2 were detuned by Δ from the $2p\,^2P_{1/2}$ state and their frequency difference ω_d was tuned to the transition frequency ω_0 between the hyperfine states $|\uparrow\rangle$ and $|\downarrow\rangle$ with a small detuning $\delta_{\rm pr}$, $\omega_d = \omega_0 + \delta_{\rm pr}$. By varying $\delta_{\rm pr}$, two types of transitions were driven: the carrier transition ($\delta_{\rm pr} = 0$) causing the population to oscillate between the $|\uparrow\rangle$ and $|\downarrow\rangle$ states without changing the vibrational level n of the quantized motion along the $\boldsymbol{x}$ axis, and the red motional sideband transition ($\delta_{\rm pr} = -\omega_x$) causing the population to oscillate between the states $|\downarrow, n\rangle$ and $|\uparrow, n-1\rangle$.

In the third step, the Raman beams were tuned to the carrier frequency and the D2 beam was turned on to measure the ions' fluorescence to determine the Rabi frequencies Ω_1 and Ω_2. The Rabi frequencies of the ions were varied by applying a static electric field to push the ions in the same direction along $\boldsymbol{x}$ axis, moving ion 2 away from and ion 1 toward the resonant field null position. In this case, the ion 2, moved away from the null position, experienced a smaller Rabi frequency whereas the ion 1, moved toward the null position, experienced a larger Rabi frequency. The D2-driven fluorescence signal (intensity) at time t is proportional to

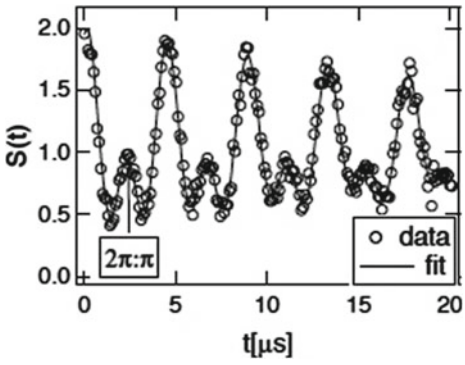

Fig. 4.8 The time evolution of the fluorescence signal $S(t)$ for $\Omega_1 = 2\Omega_2$. The initial state of the ions was $|\downarrow\downarrow\rangle \otimes |0\rangle$. Reprinted with permission from Q.A. Turchette, C.S. Wood, B.E. King, C.J. Myatt, D. Leibfried, W.M. Itano, C. Monroe, D.J. Wineland: Phys. Rev. Lett. **81**, 3631 (1998). Copyright (1998) by the American Physical Society

$$\begin{aligned} S(t) \equiv I(t) &\sim \langle S_1^+(t) S_1^-(t)\rangle + \langle S_2^+(t) S_2^-(t)\rangle \\ &= 2P_{\downarrow\downarrow}(t) + P_{\downarrow\uparrow}(t) + P_{\uparrow\downarrow}(t)\,, \end{aligned} \tag{4.58}$$

where $P_{lk}(t) = \langle |l,k\rangle \langle k,l| \rangle$ is the population of the product state $|l,k\rangle = |l\rangle \otimes |k\rangle$ of the ions' hyperfine states, $l, k \in \{\uparrow, \downarrow\}$. Figure 4.8 shows the Rabi oscillations of the fluorescence signal of the ions driven on the $\boldsymbol{x}$ carrier with the Rabi frequencies $\Omega_1 = 2\Omega_2$ and prepared initially in the state $|\downarrow\downarrow\rangle \otimes |n = 0\rangle$. The local maximum, indicated in the figure by the $2\pi : \pi$ point, corresponds to the time at which the ion 1 has undergone a 2π pulse while ion 2 has undergone a π pulse resulting in the $|\downarrow\uparrow\rangle \otimes |0\rangle$ state of the ions.

Once the ions were prepared in the $|\downarrow\uparrow, 0\rangle$ state, the Raman beams were tuned to the red motional sideband transition and driven for time t to create the state (4.52). Simultaneously, the beam D2 was turned on for a time $\tau_d = 500\,\mu$s and the number of photons m detected in time τ_d. From the measured photon-number distributions of the four product states it was determined that the detected number of photons $m \leq 3$ means that the ions were in the $|\uparrow\uparrow\rangle$ state, when $3 < m < 17$ was detected the state of the ions was either $|\uparrow\downarrow\rangle$ or $|\downarrow\uparrow\rangle$, and a detection of $m \geq 17$ means that the state was $|\downarrow\downarrow\rangle$.

Different states were generated deterministically and described by the density operator $\varrho_{(s,a)}$ in which the populations measured were $P_{\downarrow\uparrow} \approx P_{\uparrow\downarrow} \approx 0.4$, $P_{\downarrow\downarrow} \approx 0.15$ and $P_{\uparrow\uparrow} \approx 0.05$. A spin J transformation was made to determine which of the states was generated, the antisymmetric or symmetric or a mixed state. Since the antisymmetric state has the total spin $J = 0$, any J-preserving transformation, such as an equal rotation of both spins, must leave this pure state unchanged, whereas such a rotation on a mixed state will exhibit a time evolution.

Figure 4.9 shows the time evolution of experimentally generated states which approximate the antisymmetric state, Fig. 4.9a, and the symmetric state, Fig. 4.9b. When the ions are prepared in the antisymmetric state the population remains constant during the evolution. By contrast, when the ions are prepared in the symmetric state,

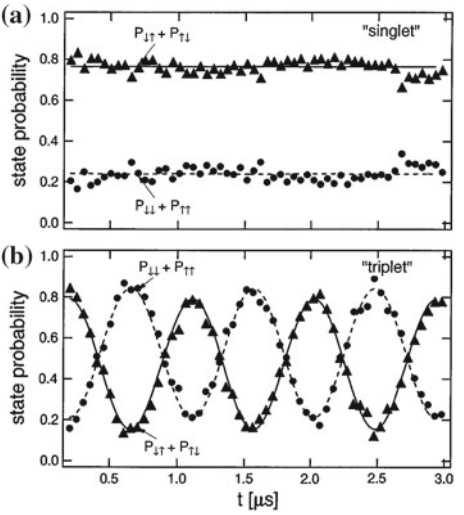

Fig. 4.9 Time evolution of the populations $P_{\downarrow\uparrow} + P_{\uparrow\downarrow}$ and $P_{\downarrow\downarrow} + P_{\uparrow\uparrow}$ for the initial collective states: **a** $|\Psi_c(0)\rangle$ and **b** $|\Psi_c(\pi)\rangle$. Reprinted with permission from Q.A. Turchette, C.S. Wood, B.E. King, C.J. Myatt, D. Leibfried, W.M. Itano, C. Monroe, D.J. Wineland: Phys. Rev. Lett. **81**, 3631 (1998). Copyright (1998) by the American Physical Society

the population exhibits periodic evolution in time. The experimental data show that the density operator of the generated states $\varrho_{(s,a)}$ can be well approximated by the decompositions

$$\varrho_a = C\,|a\rangle\,\langle a| + (1-C)\varrho_m\,, \quad \varrho_s = C\,|s\rangle\,\langle s| + (1-C)\varrho_m\,, \tag{4.59}$$

where ϱ_m is a part of the density operator which has no coherences connecting $|\downarrow\uparrow\rangle$ with $|\uparrow\downarrow, 0\rangle$ and $|\downarrow\downarrow, 0\rangle$ with $|\uparrow\uparrow, 0\rangle$. The parameter C is the contrast factor of the curves in Fig. 4.9, $C = 0.6$, which leads to the fidelity

$$\langle s|\,\varrho_s\,|s\rangle = \langle a|\,\varrho_a\,|a\rangle = \frac{1}{2}\left(P_{\downarrow\uparrow} + P_{\uparrow\downarrow} + C\right) \approx 0.7\,. \tag{4.60}$$

The fidelity (4.60) is close to (4.56), the fidelity of the collective states predicted theoretically for the same parameters. The discrepancy was interpreted as arising from some experimental imperfections such as the Raman laser intensity noise which caused a damping of the sinusoidal Rabi oscillations between the $|\uparrow\rangle$ and $|\downarrow\rangle$ states of the ions.

4.4 Experimental Evidence of Suppressed Spontaneous Emission from a Large Cloud of Atoms

The above discussed experiment demonstrating subradiance, the reduced spontaneous emission rate of atoms, was done on a small system involving only two atoms. The subradiance of a large number of atoms was first observed at University of Nice

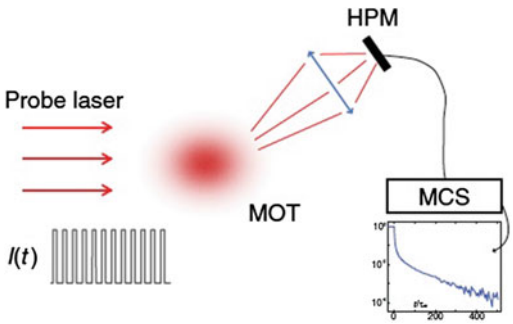

Fig. 4.10 Schematic diagram of the experiment of Guerin et al. [16] to observe superradiance of a large cloud of atoms. Reprinted with permission from W. Guerin, M.O. Arújo, R. Kaiser: Phys. Rev. Lett. **116**, 083601 (2016). Copyright (2016) by the American Physical Society

Sophia-Antipolis by Guerin et al. [16]. They loaded a large cloud of cold ^{87}Rb atoms ($N \approx 10^9$) into a magneto-optical trap (MOT) for 50 ms, at which time they could control the size of the cloud, density, and temperature. Then the MOT was switched off for 3 ms to optically pump all atoms into the upper hyperfine ground state $F = 2$. Next, the atoms were excited with a probe laser, a series of 12 weak laser pulses of duration 30 μs and separated by 1 ms. The pulses were obtained by using two acousto-optical modulators and their angular frequency was detuned by δ from the atomic transition $F = 2 \rightarrow F' = 3$. The fluorescence was collected at angle $\theta = 35°$ from the direction of the probe laser by a hybrid photomultiplier (HPM) and recorded on a multichannel scaler (MCS). Figure 4.10 is a schematic view of the experimental setup.

The pulses were switched off rapidly with the fall time about 15 ns, and the excitation was repeated 500,000 times. Between subsequent pulses of each series, the size of the cloud increases because of thermal expansion and the number of atoms decreased due to of-resonant pumping into the $F = 1$ hyperfine state. The corresponding change of the optical depth b_0 allowed to measure the decay of the fluorescence as a function of b_0.

Experimental results for the decay time of the fluorescence after switching off the probe laser are shown in Fig. 4.11. The graphs show the fluorescence signal normalized to the steady-state level and are displayed in the logarithmic scale. Frame (a) shows the decay time of the fluorescence detected for a fixed detuning δ and several different values of the depth b_0. Initially, the signal decays fast, but a slow decay is observed for latter times when the signal drops below 10^{-4}. The slow decay and its appearance at the latter times was attributed to subradiance. The slope of the fast decaying signals varies with b_0 but the amplitude of the slow decay remains almost the same. Frame (b) displays the decay time of the fluorescence detected for a fixed b_0 and several different values of the detuning δ. In this case, the slope of the decaying fluorescence is independent of δ but the amplitudes of the slow decay vary with δ. Note that the lifetime of the detected signal was about 300 times longer than the atomic lifetime τ_{at}. This can be regarded as another evidence that the atoms were prepared in a subradiant state.

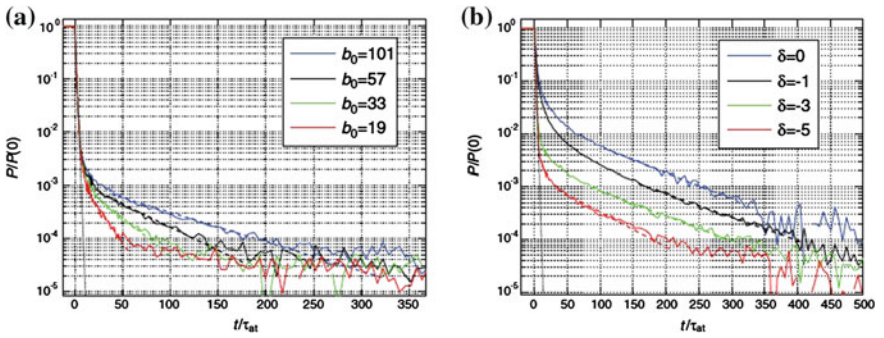

Fig. 4.11 The observed time evolution of the normalized fluorescence signal after switching off the probe laser. **a** The time evolution of the fluorescence signal for $\delta = -6\gamma$, where γ is the damping rate of the transition, and several different values of the optical depth b_0. **b** The fluorescence signal for $b_0 = 108$ and several different values of δ. Reprinted with permission from W. Guerin, M.O. Arújo, R. Kaiser: Phys. Rev. Lett. **116**, 083601 (2016). Copyright (2016) by the American Physical Society

4.5 Atom Physics Meets Solid State Physics: Spectroscopy with Artificial Atoms

So far we have discussed experiments to reduce spontaneous decay using trapped atoms an ions. However, the interest in suppression of spontaneous emission extends well beyond the atom physics, especially to the solid state physics. Recent advances in semiconductor physics had led to the realization of semiconducting quantum circuits, which are becoming the most experimentally advanced solid state quantum two-level systems (qubits) [17–20]. Unlike atoms or ions on which the systems of quantum spectroscopy are based, superconducting quantum circuits are based on the electrical (LC) oscillator and are macroscopic systems with a large number of circuits assembled in the shape of plates or metallic wires. The operation of semiconducting quantum circuits is based on two phenomena: superconductivity, which is the frictionless flow of electrical fluid through the metal at low temperature, and the Josephson effect, which endows the circuit with nonlinearity without introducing dissipation or dephasing. The Josephson junction can be placed in parallel with the inductor, or can even replace the inductor completely, the case called superconducting charge qubit. A superconducting charge qubit which has reduced sensitivity to charge noise is called transmon qubit [21]. A possibility of tunneling of charges through the Josephson junction transforms the circuit into a true artificial atom, for which the transition from the ground state $|g\rangle$ to the excited state $|e\rangle$ can be selectively excited and used as a qubit. The artificial atoms are fabricated with thin film technology and operate at temperatures below 100 mK. Measurements are performed with integrated on-chip instruments. Coupling between artificial atoms can be made strong. In principle the systems composed of artificial atoms are scalable to large numbers [22].

4.5.1 Measurement of Subradiance of Two Distant Artificial Atoms

Evidence of superradiance and subradiance in a system composed of two distant artificial atoms was observed by Wallraff's group at ETH Zurich [23]. In their experiments, two artificial atoms (superconducting transmon qubits) were capacitively coupled to a single high-Q superconducting coplanar waveguide transmission line, as illustrated in Fig. 4.12. The separation between the atoms was fixed at $d = 18.6$ mm which corresponded to one-photon wavelength λ. The effective separation between the atoms given in terms λ was varied by changing the transition frequencies of the atoms. The atomic transition frequencies 6.4 and 4.8 GHz corresponded to effective separations λ and $3\lambda/4$, respectively. The natural linewidth of the atoms at frequency 6.4 GHz was determined to be $\gamma/2\pi = 26 \pm 1$ MHz. The atoms were driven by a coherent field and the field transmitted through or reflected from the sample was amplified and then down converted using an analog microwave frequency mixer. The power spectrum $S(\omega)$ was obtained by measuring the down-converted field amplitudes of the reflected field as a function of time at a sampling rate of 1 GHz. Then each time trace was Fourier transformed and multiplied with its complex conjugate using fast digital electronics to obtain the power spectrum.

Figure 4.13 shows experimental results for the power spectrum of the field measured in reflection for the atomic separation $d = \lambda$ and several different values of the Rabi frequency of the driving field. There are two distinct features of the observed spectrum manifesting the collective behavior of the atoms, namely, the width of the central component of the observed Mollow triplet, shown in frame A of Fig. 4.13 is approximately $\gamma_c \sim 26$ MHz, which is twice as large as the width of the central component of the single atom Mollow triplet, $\gamma/2 \sim 13$ MHz. The width of the very narrow line seen in frame B of Fig. 4.13 is approximately $\gamma_c \sim 0.4$ MHz, which shows that the width is reduced by a factor of about 100 compared to the single atom width.

Referring to the energy level structure of the two-atom system and the transition rates between the collective states, shown in Fig. 4.2, we see that the broadening of the central component to 2γ is a manifestation of the superradiant behavior of

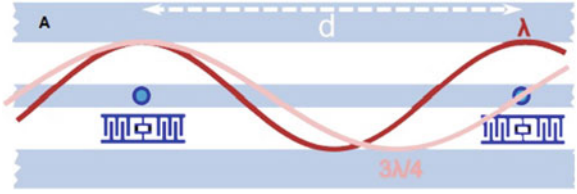

Fig. 4.12 Schematic diagram of the van Loo et al. [23] experiment. Two semiconducting transmon qubits are couple to a 1D coplanar waveguide transmission line at a fixed separation d. From A.F. van Loo, A. Fedorov, K. Lalumiere, B.C. Sanders, A. Blais, A. Wallraff: Science **342**, 1494 (2013). Reprinted with permission from AAAS

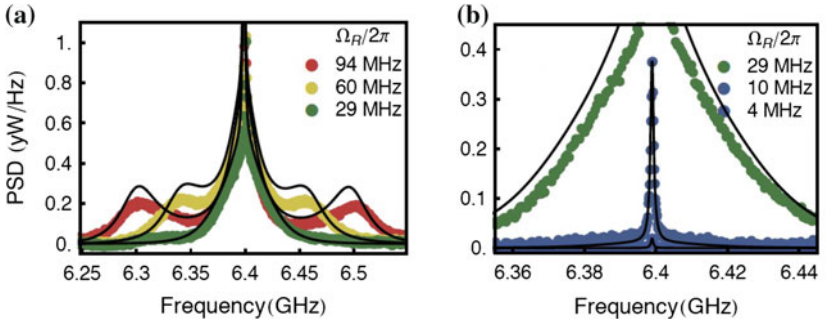

Fig. 4.13 Measured power spectrum $S(\omega)$ of the scattered field for the atoms in resonance at separation $d = \lambda$ and for different Rabi frequencies Ω_R of the driving field. The spectra for large powers of the driving field are displayed in frame **a**, while the spectra corresponding to weak powers are displayed in frame **b**. The *solid lines* are theoretical spectra. From A.F. van Loo, A. Fedorov, K. Lalumiere, B.C. Sanders, A. Blais, A. Wallraff: Science **342**, 1494 (2013). Reprinted with permission from AAAS

the system resulting from $|s\rangle \rightarrow |g\rangle$ transitions occurring with the enhanced rate $\gamma + \gamma_{12} \approx 2\gamma$. On the other hand, the very narrow spectral line seen in frame B of Fig. 4.13 is a manifestation of the subradiant behavior of the system resulting from $|a\rangle \rightarrow |g\rangle$ transitions occurring with the suppressed rate $\gamma - \gamma_{12} \approx 0$.

In summary, the experimental results clearly demonstrate a strong collective behavior of distant artificial atoms coupled to a waveguide transmission line. The presence of the subnatural linewidths is a clear manifestation of the stabilization of the quantum fluctuations by strongly interacting atoms. The experiment was also performed for the atomic separation $d = 3\lambda/4$ with the results showing a splitting of the spectral line due to the dipole-dipole interaction between the atoms.

4.5.2 *Measurement of Suppressed Linewidths of Multiple Artificial Atoms*

The Wallraff's group carried out a closely related experiment to that discussed in the preceding section [24]. The aim of the experiment was to demonstrate collective suppression of linewidths of multiple artificial atoms (qubits) coupled to a microwave cavity field and damped by a dephasing process arising from the interaction of the atoms with a reservoir characterized by a $1/\omega$ noise spectrum.

Theoretical Background

Let us first demonstrate in some details how the spontaneous decay rates could depend on the inverse of the number of atoms when the atoms are coupled to a single-mode cavity and undergo a dephasing due to a reservoir with a $1/\omega$ spectrum. We start from the total Hamiltonian of the system, which can be written in the form

$$H = H_0 + H_1 + H_2 \,, \tag{4.61}$$

where H_0 is the Hamiltonian of the reservoir

$$H_0 = \hbar \sum_k \omega_k \hat{b}_k^\dagger \hat{b}_k \,, \tag{4.62}$$

H_1 is the Hamiltonian of the atoms plus the interaction with the cavity field

$$H_1 = \hbar \sum_{i=1}^{N} \omega_0 S_i^z + \hbar \sum_{i=1}^{N} g \left(S_i^+ \hat{a} + \text{H.c.} \right) , \tag{4.63}$$

and H_2 is the Hamiltonian of the collective coupling of the atoms to the reservoir

$$H_2 = \hbar \sum_k g_k \left(\hat{b}_k + \hat{b}_k^\dagger \right) S_z \,. \tag{4.64}$$

Here $\hat{a}$ is the annihilation operator of the cavity mode, $\hat{b}_k^\dagger$ and $\hat{b}_k$ are the creation and annihilation operators of mode k of frequency ω_k of the reservoir, $S_i^+ (S_i^-)$ is the raising (lowering) operator and S_i^z is the population difference operator of the ith atom, $S_z = \sum_{i=1}^{N} S_i^z$ is the collective operator of the atomic inversion, g is the coupling strength of the atoms to the cavity field, assumed the same for all atoms, and g_k is the coupling strength of the mode k of the reservoir to the atoms.

In order to analyze the effect of the dephasing reservoir on the atoms, we define a unitary operator [25–28]

$$U = \mathrm{i}\hbar \sum_k \frac{g_k}{\omega_k} \left(b_k^\dagger - b_k \right) S_z \,, \tag{4.65}$$

and make the unitary transformation of the Hamiltonian (4.61). Hence, we obtain

$$H_T = \mathrm{e}^{-\mathrm{i}U/\hbar} H \mathrm{e}^{\mathrm{i}U/\hbar} = H_R + H_I \,, \tag{4.66}$$

where

$$H_R = \mathrm{e}^{-\mathrm{i}U/\hbar} (H_0 + H_2) \mathrm{e}^{\mathrm{i}U/\hbar} = \sum_k \hbar \omega_k \hat{b}_k^\dagger \hat{b}_k - \hbar \sum_k \frac{g_k^2}{4\omega_k} \,, \tag{4.67}$$

and

$$H_I = \hbar \sum_{i=1}^{N} g \left(S_i^+ \hat{a} + \text{H.c.} \right) + \left[\hbar \sum_{i=1}^{N} \sum_k \frac{g_k g}{\omega_k} \left(\hat{b}_k^\dagger - \hat{b}_k \right) S_i^+ + \text{H.c.} \right] + \ldots \,. \tag{4.68}$$

The first term in (4.67) represents the energy of the reservoir, while the second term is the Lamb shift of the energy levels of the atoms due to the interaction with the reservoir. The shift is usually considered to be absorbed into the atomic transition frequency and is not included explicitly in the dynamics of the system. The first term on the right-hand side of (4.68) contains the interaction of the atoms with the cavity field. The second term represents the interaction of the atoms with the reservoir. It is in a form of the electric dipole interaction in which the reservoir couples to the dipole transition of the atoms. In the derivation of (4.68), we have performed a Taylor expansion and have kept only the terms up to first-order in g_k. With the higher-order terms ignored, we simply limit the interaction of the atoms with the reservoir to one-photon processes only.

We may transform the Hamiltonian (4.66) into the interaction picture with the unitary operator $W(t) = \exp(\mathrm{i}H_R t/\hbar)$, and find

$$\begin{aligned}\tilde{H}_T &= \mathrm{e}^{-\mathrm{i}H_R t/\hbar} H_T \mathrm{e}^{\mathrm{i}H_R t/\hbar} \\ &= \sum_{i=1}^{N} \sum_{k} J(\omega_k) \left\{ \left[\hat{b}_k^{\dagger} \mathrm{e}^{\mathrm{i}(\omega_k + \Omega_N)t} - \hat{b}_k \mathrm{e}^{-\mathrm{i}(\omega_k - \Omega_N)t} \right] S_i^{+} + \mathrm{H.c.} \right\}, \end{aligned} \tag{4.69}$$

where $J(\omega_k) = g g_k/\omega_k$ is the effective coupling strength of the atoms to the reservoir, and $\Omega_N = g\sqrt{N}$ is the N-atom Rabi frequency of the interaction of the atoms with the cavity field. It is clear from the form of $J(\omega_k)$ that the reservoir has a spectrum corresponding to $1/\omega$ noise. Note from (4.69) that the interaction contains terms which oscillate at two frequencies $\omega_k - \Omega_N$ and $\omega_k + \Omega_N$. These two frequencies arising from the splitting of the dressed states of the atoms plus the cavity field system. When there are N atoms in the cavity, the atomic ground state is

$$|g_N\rangle = |g_1\rangle \otimes |g_2\rangle \ldots |g_{N-1}\rangle \otimes |g_N\rangle \ , \tag{4.70}$$

and the first atomic excited state is

$$|e_1\rangle = \frac{1}{\sqrt{N}} \sum_{i=1}^{N} S_i^{+} |g_N\rangle \ . \tag{4.71}$$

Then, the single excitation dressed states of the atoms plus the cavity field system are

$$|\pm, 0\rangle = \frac{1}{\sqrt{2}} \left[|g_N, 1\rangle \pm |e_1, 0\rangle \right] \ , \tag{4.72}$$

and since the transition dipole moment between $|g_N\rangle$ and $|e_1\rangle$ is $\mu\sqrt{N}$, the first doublet splitting of the atom-cavity system is $\Omega_N = g\sqrt{N}$. Transitions between the single excitation dressed states and the ground state generate the "vacuum" Rabi peaks at frequencies $\omega_+ = \omega_0 + g\sqrt{N}$ and $\omega_- = \omega_0 - g\sqrt{N}$.

In what follows we consider the situation where $\omega_k \approx \Omega_N$ that the reservoir is centered about one of the two dressed state transitions. This prompts us to make the rotating-wave approximation in which we ignore rapidly oscillating terms at frequency $2\omega_k$, and obtain

$$\tilde{H}_T = -\sum_{i=1}^{N}\sum_{k} J(\omega_k)\left[\hat{b}_k S_i^+ \mathrm{e}^{-\mathrm{i}(\omega_k-\Omega_N)t} + \mathrm{H.c.}\right] . \tag{4.73}$$

Having derived the effective interaction Hamiltonian of the atom-cavity system with the reservoir, we now turn to the derivation of the master equation for the reduced density operator of the atoms

$$\varrho(t) = \mathrm{Tr}_F\{\varrho_T(t)\} , \tag{4.74}$$

where $\varrho_T(t)$ is the density operator of the total system, the atom-cavity system plus the reservoir field. We choose an initial state with no correlations between the atoms and the reservoir modes, $\varrho_T(0) = \varrho_F(0)\otimes\varrho(0)$, and specify the reservoir as a vacuum thermal bath with the following correlations

$$\langle b_k\rangle = \langle b_k^\dagger\rangle = 0 , \quad \langle b_k^\dagger b_{k'}\rangle = \bar{n}\,\delta(k-k') , \quad \langle b_k b_{k'}^\dagger\rangle = (\bar{n}+1)\,\delta(k-k') , \tag{4.75}$$

where $\bar{n}$ is the average number of thermal photons.

After tracing over the phonon bath operators, and using the standard Born-Markov approximations, we arrive at the master equation

$$\begin{aligned}\frac{\partial}{\partial t}\varrho &= (\bar{n}+1)\gamma_a(2S^-\rho S^+ - S^+S^-\rho - \rho S^+S^-) \\ &\quad + \bar{n}\gamma_a(2S^+\rho S^- - S^-S^+\rho - \rho S^-S^+) ,\end{aligned} \tag{4.76}$$

where $S^\pm = \sum_{i=1}^{N} S_i^\pm$ are the collective atomic operators, and

$$\gamma_a = 2\pi|J(\omega_+)|^2 = 2\pi g^2\left(\frac{g_{\omega_+}}{\Omega_N}\right)^2 \tag{4.77}$$

is the damping rate of the atoms. Clearly, the damping rate is inversely proportional to N that γ_a decreases with an increasing N. Hence, the damping rate can be suppressed by increasing the number of atoms because the collective Rabi frequency is enhanced by $\sqrt{N}$ over the single-atom value.

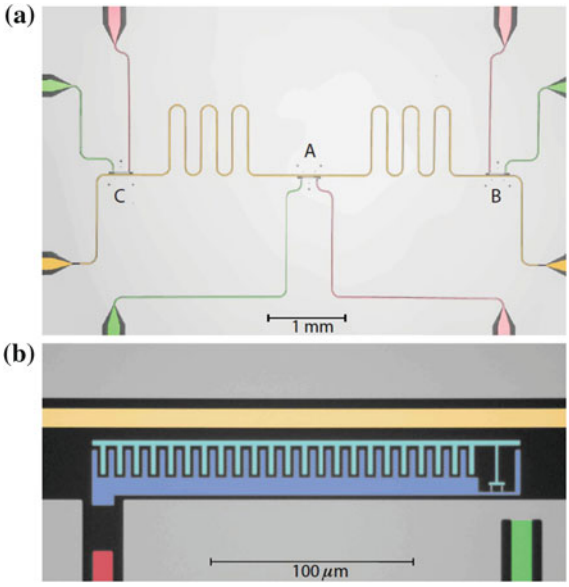

Fig. 4.14 Schematic diagram of the experiment of Nissen et al. [24]. **a** The experimental setup consisting of three qubits, A, B and C, coupled to a waveguide resonator, indicated in yellow color. **b** An enlarged view of the transmon qubit C. Reprinted with permission from F. Nissen, J.M. Fink, J.A. Mlynek, A. Wallraff, J. Keeling: Phys. Rev. Lett. **110**, 203602 (2013). Copyright (2013) by the American Physical Society

Experiment

In the experiment of Nissen et al. [24], transmon-type superconducting qubits, A, B and C, were capacitively coupled to a single electric field mode of a coplanar microwave resonator, as shown in Fig. 4.14.

The qubits were located at antinodes of the first harmonic mode of the resonator of frequency $\omega_r/2\pi = 7.023$ GHz. The transition frequencies of the qubits, $\omega_j/2\pi = 9.58, 8.65, 8.23$ GHz were designed such that all three frequencies can be tuned into resonance with the cavity frequency. The coupled atom-cavity system was then driven by a weak field and the coherently scattered transmission amplitude for one, two and three atoms was measured.

Figure 4.15 shows the measured linewidths of one, two, and three qubits, together with the theoretical linewidths. We see that the linewidth decreases with an increasing number of atoms when the atoms are collectively coupled to the reservoir. Inversely, the linewidth increases with an increasing number of atoms when the atoms are individually coupled to the reservoir. The insert of the figure shows the experimental spectrum of the coherently scattered transmission amplitude. The experiment demonstrated that the decay rates of atoms damped by a dephasing process decrease with an increasing number of atoms. As it is evident from Fig. 4.15, the linewidth becomes smaller when the number of atoms is increased.

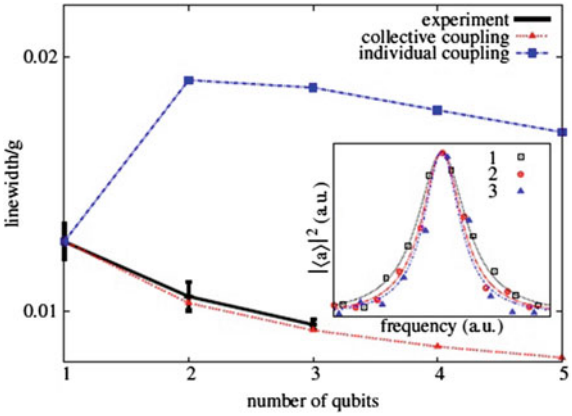

Fig. 4.15 Experimentally measured linewidths (*black solid line*) of an N-qubit-cavity system. Superimposed on the experimental *curves* are *red* and *blue dashed lines* indicating the theoretical linewidths. The *upper blue-dashed line* represents the theoretical linewidths calculated for the case when atoms individually couple to the reservoir, while the lower red line is for the collective coupling. The inset shows the experimental spectrum of the coherently scattered transmission amplitude for one, two and three qubits, normalized such that peaks are centered at the same frequency. The *lines* are the corresponding Lorentzian fits to the experimental data. Only one of the two Rabi peaks of the dressed atom-cavity system is shown. The narrowing of the spectral line with increasing N is evident. Reprinted with permission from F. Nissen, J.M. Fink, J.A. Mlynek, A. Wallraff, J. Keeling: Phys. Rev. Lett. **110**, 203602 (2013). Copyright (2013) by the American Physical Society

References

1. R.H. Dicke: Phys. Rev. **93**, 99 (1954)
2. Z. Ficek, R. Tanaś: Phys. Rep. **372**, 369 (2002)
3. R.H. Lehmberg: Phys. Rev. A **2**, 883, 889 (1970)
4. Z. Ficek, R. Tanaś, S. Kielich: Optics Commun. **36**, 121 (1981)
5. T. Richter: Optica Acta **29**, 265 (1982)
6. Z. Ficek, R. Tanaś, S. Kielich: Optica Acta **30**, 713 (1983)
7. H.S. Freedhoff: Phys. Rev. A **26**, 684 (1982)
8. Z. Ficek, R. Tanaś, S. Kielich: Phys. Rev. A **29**, 2004 (1984)
9. T. Richter: Optica Acta **30**, 1769 (1983)
10. Z. Ficek, B.C. Sanders: Phys. Rev. A **41**, 359 (1990)
11. T.G. Rudolph, Z. Ficek, B.J. Dalton: Phys. Rev. A **52**, 636 (1995)
12. S. Filipp, A.F. van Loo, M. Baur, L. Steffen, A. Wallraff: Phys. Rev. A **84**, 061805 (2011)
13. B. Casabone, K. Friebe, B. Brandstatter, K. Schuppert, R. Blatt, T. E. Northup: Phys. Rev. Lett. **114**, 023602 (2015)
14. J.I. Cirac, P. Zoller: Phys. Rev. Lett. **74**, 4091 (1995)
15. Q.A. Turchette, C.S. Wood, B.E. King, C.J. Myatt, D. Leibfried, W.M. Itano, C. Monroe, D.J. Wineland: Phys. Rev. Lett. **81**, 3631 (1998)
16. W. Guerin, M.O. Araújo, R. Kaiser: Phys. Rev. Lett. **116**, 083601 (2016)
17. A. Wallraff, D.I. Schuster, A. Blais, L. Frunzio, R.- S. Huang, J. Majer, S. Kumar, S.M. Girvin, R.J. Schoelkopf: Nature **431**, 162 (2004)
18. A. Blais, J. Gambetta, A. Wallraff, D.I. Schuster, S.M. Grivin, M.H. Devoret, R.J. Schoelkopf: Phys. Rev. A **75**, 032329 (2007)

19. D.I. Schuster, A.A. Houck, J.A. Schreier, A. Wallraff, J.M. Gambetta, A. Blais, L. Frunzio, J. Majer, B. Johnson, M.H. Devoret, S.M. Girvin, R.J. Schoelkopf: Nature (London) **445**, 515 (2007)
20. G. de Lange, B. van Heck, A. Bruno, D.J. van Woerkom, A. Geresdi, S.R. Plissard, E.P.A.M. Bakkers, A.R. Akhmerov, L. DiCarlo: Phys. Rev. Lett. **115**, 127002 (2015)
21. J. Koch, T.M. Yu, J. Gambetta, A.A. Houck, D.I. Schuster, J. Majer, A. Blais, M.H. Devoret, S.M. Girvin, R. J. Schoelkopf: Phys. Rev. A **76**, 042319 (2007)
22. J.A. Mlynek, A.A. Abdumalikov, Jr., F.M. Fink, L. Steffen, M. Baur, C. Lang, A.F. van Loo, A. Wallraff: Phys. Rev. A **86**, 053838 (2012)
23. A.F. van Loo, A. Fedorov, K. Lalumiere, B.C. Sanders, A. Blais, A. Wallraff: Science **342**, 1494 (2013)
24. F. Nissen, J.M. Fink, J.A. Mlynek, A. Wallraff, J. Keeling: Phys. Rev. Lett. **110**, 203602 (2013)
25. R. Alicki, M. Horodecki, P. Horodecki, R. Horodecki, L. Jacak, P. Machnikowski: Phys. Rev. A **70**, 010501(R) (2004)
26. D.P.S. McCutcheon, A. Nazir: New J. Phys. **12**, 113042 (2010)
27. C. Roy, S. Hughes: Phys. Rev. Lett. **106**, 247403 (2011)
28. H. Huang, G.-X. Li, W.-J. Gu, Z. Ficek: Phys. Rev. A **90**, 023815 (2014)

Chapter 5
Time-Dependent Fluorescence Spectroscopy

In Chap. 3 we treated the external laser field driving an atom as a single mode continuous wave monochromatic field, which is characterized by a constant and time-independent amplitude. We illustrated solutions for the dynamics of the driven atom and the steady-state spectral distributions of the emitted radiation field in the presence of a such monochromatic field. As we have seen, in the case of a two-level atom the excitation field has played no significant role in the modification and control of the atomic spontaneous decay rate. In this chapter, we focus on a two-level atom and the response of the atom to a continuous wave multi-chromatic driving field. This is especially interesting, and as we shall see, the amplitude of a multi-chromatic field varies in time and then the fluorescence spectra display additional information about the quantum fluctuations and their control not observed in the fluorescence spectra with a monochromatic excitation. Just as in the case of the monochromatic driving field, we assume that the driven atom is also coupled to a reservoir, whose the modes are in the ordinary vacuum state.

Although we begin with a general formulation of different forms of the multi-chromatic field, we shall be mostly concerned with driving fields composed of two and three frequency components. These studies represent a striking departure from traditional studies of resonance fluorescence and bring into sharp focus some of the most basic features of quantum spectroscopy. The most significant for our studies is the control of spontaneous emission in atomic systems. We will describe how the control of spontaneous emission may be useful in more general problems of coherent control of a quantum system. The goal in coherent control is to guide the evolution of a system along a particular path to a desired final state. In our system, the evolution can be controlled by the amplitude and frequency of the modulating fields, and the system can radiate only at desired frequencies.

We analyze the fluorescence spectrum for features indicative of dynamical modifications of spontaneous emission. We are particularly interested in the possibility of spectral line narrowing by the presence of the additional frequency component of the driving field. As we shall see, this system may demonstrate a dynamical stabi-

Z. Ficek and R. Tanaś, *Quantum-Limit Spectroscopy*, Springer Series in Optical Sciences 200, DOI 10.1007/978-1-4939-3740-0_5

lization of quantum fluctuations which are manifested by the vanishing of spectral components on some transitions between dressed states of the system. This suggest that one can, in principle, suppress spontaneous emission from a two-level system.

5.1 Modulation Spectroscopy

Suppose, we are dealing with a polychromatic laser field consisting of a superposition of $k = 2p + 1$ independent mutually coherent modes having the same direction of propagation and the same state of polarization. In this case, the total electric field of a continuous wave driving field is given by

$$\begin{aligned} \boldsymbol{E}_L(t) &= \sum_{k=-p}^{p} \boldsymbol{\mathcal{E}}_k \mathrm{e}^{-\mathrm{i}(\omega_k t+\psi_k)} + \text{c.c.} \\ &= \mathrm{e}^{-\mathrm{i}(\omega_L t+\psi_0)} \sum_{k=-p}^{p} \boldsymbol{\mathcal{E}}_k \mathrm{e}^{-\mathrm{i}(\delta_k t+\phi_k)} + \text{c.c.}\,, \end{aligned} \tag{5.1}$$

where $\boldsymbol{\mathcal{E}}_k$ is the amplitude of the k-th component of the field, $\delta_k = \omega_k - \omega_L$ is the detuning (beating frequency) between frequency ω_k of a sideband component ($k \neq 0$) and frequency $\omega_{k=0} \equiv \omega_L$ of the central (carrier) component of the field, ψ_k is the initial phase of the kth component and $\phi_k = \psi_k - \psi_0$ is the relative phase difference between the carrier component and the sideband components of the field at $t = 0$.

It follows from (5.1) that the interaction Hamiltonian of the external laser field with an atom, under the rotating-wave approximation, will involve a time-dependent Rabi frequency

$$\hat{H}_L = -\frac{1}{2}\mathrm{i}\hbar\left[\Omega(t) S^{+} \mathrm{e}^{-\mathrm{i}(\omega_L t+\psi_0)} - \text{H.c.}\right], \tag{5.2}$$

where

$$\Omega(t) = 2\boldsymbol{\mu} \cdot \tilde{\boldsymbol{\mathcal{E}}}(t)/\hbar \tag{5.3}$$

is the time-dependent Rabi frequency in which $\boldsymbol{\mu}$ is the dipole matrix element of an atomic transition, and

$$\tilde{\boldsymbol{\mathcal{E}}}(t) = \frac{1}{2} \sum_{k=-p}^{p} \boldsymbol{\mathcal{E}}_k \mathrm{e}^{-\mathrm{i}(\delta_k t+\phi_k)} \tag{5.4}$$

is the slowly varying part of the electric field amplitude, since under the RWA the beat frequency is assumed small compared with the carrier frequency ω_L.

When we make use of the Hamiltonian (5.2) in the master equation (3.11), we readily find that the optical Bloch equations for the expectation values of the atomic dipole moment and population inversion operators, written in a reference frame rotating at the frequency ω_L, are of the form

$$\begin{aligned}
\frac{\mathrm{d}}{\mathrm{d}t}\langle\tilde{S}^{+}(t)\rangle &= -\left(\frac{1}{2}\gamma - \mathrm{i}\Delta\right)\langle\tilde{S}^{+}(t)\rangle + \Omega(t)\langle S_z(t)\rangle\,, \\
\frac{\mathrm{d}}{\mathrm{d}t}\langle\tilde{S}^{-}(t)\rangle &= -\left(\frac{1}{2}\gamma + \mathrm{i}\Delta\right)\langle\tilde{S}^{-}(t)\rangle + \Omega^{*}(t)\langle S^{z}(t)\rangle\,, \\
\frac{\mathrm{d}}{\mathrm{d}t}\langle S_z(t)\rangle &= -\frac{1}{2}\gamma - \gamma\langle S_z(t)\rangle - \frac{1}{2}\Omega(t)\langle\tilde{S}^{-}(t)\rangle - \frac{1}{2}\Omega^{*}(t)\langle\tilde{S}^{+}(t)\rangle\,, \qquad (5.5)
\end{aligned}$$

where the asterisk denotes a complex conjugate, γ is the spontaneous emission rate, $\Delta = \omega_a - \omega_L$, and

$$\langle\tilde{S}^{\pm}(t)\rangle = \langle S^{\pm}(t)\rangle \mathrm{e}^{\mp\mathrm{i}(\omega_L t+\psi_0)} \qquad (5.6)$$

are the slowly varying parts of the expectation values of the atomic dipole operators.

The optical Bloch equations (5.5) supplemented with appropriate initial conditions determine fully the evolution of single-time expectation values of the atomic variables and thereby of the radiated field. On the other hand, spectral properties of the radiated field are determined by the two-time correlation functions of the atomic variables. We know from the quantum regression theorem [1] that for $t' > t$ the two-time average $\langle\tilde{S}^{+}(t)\tilde{S}^{-}(t')\rangle$ satisfies the same equation of motion as the one-time average $\langle\tilde{S}^{-}(t')\rangle$ with the initial condition $\langle\tilde{S}^{+}(t)\tilde{S}^{-}(t)\rangle$.

If we define the two-time correlation functions of the fluctuation parts of the atomic dipole operators

$$\begin{aligned}
Y_1(t,t') &= \langle\delta\tilde{S}^{+}(t)\,\delta\tilde{S}^{+}(t')\rangle\,, \quad Y_2(t,t') = \langle\delta\tilde{S}^{+}(t)\,\delta\tilde{S}^{-}(t')\rangle\,, \\
Y_3(t,t') &= \langle\delta\tilde{S}^{+}(t)\,\delta\tilde{S}_z(t')\rangle\,, \qquad (5.7)
\end{aligned}$$

we then readily find from the optical Bloch equations (5.5) and the quantum regression theorem that $Y_i(t,t')$ obey the following equations

$$\begin{aligned}
\frac{\mathrm{d}}{\mathrm{d}t'}Y_1(t,t') &= -\left(\frac{1}{2}\gamma - \mathrm{i}\Delta\right)Y_1(t,t') + \Omega(t')Y_3(t,t')\,, \\
\frac{\mathrm{d}}{\mathrm{d}t'}Y_2(t,t') &= -\left(\frac{1}{2}\gamma + \mathrm{i}\Delta\right)Y_2(t,t') + \Omega^{*}(t')Y_3(t,t')\,, \\
\frac{\mathrm{d}}{\mathrm{d}t'}Y_3(t,t') &= -\gamma\,Y_3(t,t') - \frac{1}{2}\Omega(t')Y_1(t,t') - \frac{1}{2}\Omega^{*}(t')Y_2(t,t')\,, \qquad (5.8)
\end{aligned}$$

which we shall refer to as the two-time optical Bloch equations.

Mathematically, the equations (5.5) and (5.8) are coupled linear differential equations with time-dependent coefficients which are quasi-periodic in time with periodicity δ_k. In general, the time dependence of $\Omega(t)$ as given in (5.3) involves k different parameters δ_k. The analytic treatment of any problem involving such a complicated Rabi frequency is extremely difficult [2, 3]. However, in certain special cases, where the frequencies of the field components are equidistant such that $\delta_k = k\delta$, one can determine the time dependence of $\Omega(t)$ in terms of multiples of a single parameter δ as

$$\Omega(t) = \sum_{k=-p}^{p} \Omega_k e^{-i(k\delta t+\phi_k)} , \tag{5.9}$$

where $\Omega_k = 2\boldsymbol{\mu} \cdot \boldsymbol{\mathcal{E}}_k/\hbar$ is the Rabi frequency associated with the k-th component of the field. Furthermore, if the field components are symmetrically distributed about the central (carrier) mode, so that $\phi_{-k} = \phi_k$ and $\Omega_{-k} = \Omega_k$, the Rabi frequency (5.9) simplifies to

$$\Omega(t) = \Omega_0 + 2\sum_{k=1}^{p} \Omega_k e^{-i\phi_k} \cos(k\delta t) . \tag{5.10}$$

This shows that the symmetrically detuned sideband fields act as a modulator of the Rabi frequency Ω_0 of the central component.

Note that the Rabi frequency (5.10) depends on the phase difference ϕ_k between the central and the sideband components of the field. Hence, depending on the phase ϕ_k the sideband fields can modulate the amplitude or the phase of Ω_0. For example, when $\phi_k = 0$ or π, the sidebands modulate the amplitude of Ω_0 and then

$$\Omega(t) = \Omega_0 \left[1 \pm \sum_{k=1}^{p} a_k \cos(k\delta t) \right] , \tag{5.11}$$

where $a_k = 2\Omega_k/\Omega_0$ is the modulation amplitude and the sign "+" corresponds to $\phi_k = 0$, while "−" corresponds to $\phi_k = \pi$. When $\phi_k = \pi/2$ or $3\pi/2$, the sideband fields modulate the phase of Ω_0, so that

$$\Omega(t) = \Omega_0 \left[1 \mp i \sum_{k=1}^{p} a_k \cos(k\delta t) \right] . \tag{5.12}$$

In the following sections, we will illustrate mathematical methods, which to some extend can be considered as analytical methods of solving the optical Bloch equations for excitations with time-dependent Rabi frequency. For this purpose some explicit time-dependent forms of the multimode driving field will be used. In particular, we will consider three different types of the multimode driving field. A bichromatic driving field, which we solve using the Floquet method [4]. Driving the

atom with two independent laser fields of equal frequencies, which we solve with a dressed-atom model, and an amplitude modulated field with a single pair of modulating fields, which we will solve analytically using the Fourier decomposition of the modulation terms.

5.2 Bichromatic Excitation

As a first example of a multi-field excitation of a two-level atom let us consider a bichromatic field, illustrated in Fig. 5.1, composed of one component resonant with the atomic transition frequency and the other component detuned from the atomic frequency by δ.

The explicit time dependence of the Rabi frequency of the bichromatic field can be found from (5.9). Suppose that the resonant component of the field is the carrier component. In this case, $\Delta = 0$ and the resonant component corresponds to $p = 0$. The detuned component corresponds to $p = -1$. Thus, we have

$$\Omega(t) = \Omega_0 + \Omega_1 e^{i(\delta t - \phi_1)} . \tag{5.13}$$

Insertion of this form of the Rabi frequency into the optical Bloch equations (5.5) yields

$$\begin{aligned}
\frac{d}{dt}\langle \tilde{S}^+(t)\rangle &= -\frac{1}{2}\gamma\langle \tilde{S}^+(t)\rangle + \Omega_0\left(1+\alpha e^{i\delta t}\right)\langle S_z(t)\rangle , \\
\frac{d}{dt}\langle \tilde{S}^-(t)\rangle &= -\frac{1}{2}\gamma\langle \tilde{S}^-(t)\rangle + \Omega_0\left(1+\alpha^* e^{-i\delta t}\right)\langle S^z(t)\rangle , \\
\frac{d}{dt}\langle S_z(t)\rangle &= -\frac{1}{2}\gamma - \gamma\langle S_z(t)\rangle - \frac{1}{2}\Omega_0\left(1+\alpha e^{i\delta t}\right)\langle \tilde{S}^-(t)\rangle \\
&\quad - \frac{1}{2}\Omega_0\left(1+\alpha^* e^{-i\delta t}\right)\langle \tilde{S}^+(t)\rangle ,
\end{aligned} \tag{5.14}$$

where $\alpha = \Omega_1 e^{-i\phi_1}/\Omega_0$ is the ratio between the Rabi frequencies of the detuned (Ω) and the resonant (Ω_0) components.

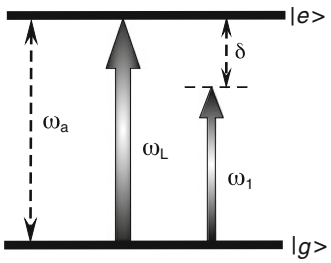

Fig. 5.1 Two-level atom with transition frequency ω_a driven by a bichromatic field composed of a resonant frequency component ω_L and a nonresonant component ω_1 detuned from the atomic resonance by $\delta \ll \omega_a$

The optical Bloch equations (5.14) are coupled linear differential equations with time-dependent coefficients, which are periodic in time with periodicity δ, and we merely have to solve these three simultaneous equations in order to find the expectation values of the atomic variables. An inspection of (5.14) shows that there is no rotating frame which could transform (5.14) into a system of coupled differential equations with time independent coefficients [5]. Therefore, in order to solve the system of equations (5.14), we use the Floquet method approach supplemented with a continued fraction or a matrix inversion method [6–12].

5.2.1 Floquet Method Approach

In the Floquet method we express the dynamical variables, $\langle \tilde{S}^{-}(t) \rangle$, $\langle \tilde{S}^{+}(t) \rangle$, and $\langle S_z(t) \rangle$, as Fourier series in terms of amplitudes which oscillate at the frequency δ and its harmonics. In other words, the time evolution of the atomic variables can be written as

$$X_i(t) = \sum_{\ell=-\infty}^{+\infty} X_i^{(\ell)}(t)\, \mathrm{e}^{\mathrm{i}\ell\delta t}\,, \qquad i = 1, 2, 3\,, \tag{5.15}$$

where $X_i^{(\ell)}(t)$ is the Fourier amplitude of the ℓth harmonic of the ith component of the vector

$$\boldsymbol{X}(t) = \begin{pmatrix} X_1(t) \\ X_2(t) \\ X_3(t) \end{pmatrix} = \begin{pmatrix} \langle \tilde{S}^{-}(t) \rangle \\ \langle \tilde{S}^{+}(t) \rangle \\ \langle S_z(t) \rangle \end{pmatrix}\,, \tag{5.16}$$

The Fourier expansion (5.15) shows that the atomic variables will respond at harmonics of δ and the knowledge of the Fourier amplitudes $X_i^{(\ell)}(t)$ gives all the information about the time evolution of the atomic variable $X_i(t)$.

If we substitute (5.15) into (5.14) and compare coefficients of the same powers of $\ell\delta$, we find that the optical Bloch equations for the amplitudes $\boldsymbol{X}^{(\ell)}(t)$ take the form

$$\begin{aligned} \frac{\mathrm{d}}{\mathrm{d}t}\boldsymbol{X}^{(\ell)}(t) = &-\frac{1}{2}\gamma\delta_{\ell,0}\boldsymbol{U}_0 \\ &- A_0\boldsymbol{X}^{(\ell-1)}(t) - B_\ell\boldsymbol{X}^{(\ell)}(t) - C_0\boldsymbol{X}^{(\ell+1)}(t)\,, \end{aligned} \tag{5.17}$$

in which $\delta_{\ell,0}$ is the Kronecker delta function, and the terms are products of matrices and vectors with

$$\boldsymbol{X}^{(\ell)}(t) = \begin{pmatrix} X_1^{(\ell)}(t) \\ X_2^{(\ell)}(t) \\ X_3^{(\ell)}(t) \end{pmatrix}, \qquad \boldsymbol{U}_0 = \begin{pmatrix} 0 \\ 0 \\ 1 \end{pmatrix}, \tag{5.18}$$

and A_0, B_ℓ, and C_0 are 3×3 matrices

$$A_0 = \begin{pmatrix} 0 & 0 & -\Omega_0 \\ 0 & 0 & -\Omega_1 \\ \Omega_1 & \Omega_0 & 0 \end{pmatrix}, \qquad B_\ell = \begin{pmatrix} \frac{1}{2}\gamma + \mathrm{i}\ell\delta & 0 & 0 \\ 0 & \frac{1}{2}\gamma + \mathrm{i}\ell\delta & 0 \\ 0 & 0 & \gamma + \mathrm{i}\ell\delta \end{pmatrix},$$

$$C_0 = \begin{pmatrix} 0 & 0 & -\Omega_1 \\ 0 & 0 & -\Omega_0 \\ \Omega_0 & \Omega_1 & 0 \end{pmatrix}, \tag{5.19}$$

obtained from the coefficients appearing in the optical Bloch equations.

We see that the equations of motion (5.17) are in form of a vector recurrence relation. In terms of the components of the vector $\boldsymbol{X}(t)$, the relation (5.17) represents a system of an infinite number of linear coupled differential equations with constant, time-independent coefficients. Thus, the time-dependence appearing in the Bloch equations (5.14) has been removed by splitting the time evolution of the atomic variables into an infinite number of harmonics oscillating at frequencies $n\omega_a \pm m\omega_2$, where n and m are integers. The atomic variables are then obtained by solving the recurrence relation for $\boldsymbol{X}^{(\ell)}(t)$ with appropriate initial conditions.

Among many numerical methods there are two common methods of solving the recurrence relation (5.17):

1. Continued fraction method, in which one finds $\boldsymbol{X}^{(\ell)}(t)$ in terms of continued fraction using a truncated basis of Fourier amplitudes.
2. Matrix inversion method, in which one can write the relation (5.17) in a form of a matrix differential equation of a truncated dimension n, and solve it for $\boldsymbol{X}^{(\ell)}(t)$ by the matrix inversion.

Both techniques lead, of course, to identical solutions and are based on powerful methods of solving an infinite hierarchy of simultaneous differential equations with time-independent coefficients. In what follows, we present a relatively accurate formulation of these methods and illustrate an application to the calculation of the fluorescence spectrum of a two-level atom driven by a bichromatic field.

5.2.2 *Continued Fraction Method*

To illustrate the solution of the recurrence relation (5.17) in terms of continued fraction, it is convenient to apply the Laplace transform, which converts the recurrence relation (5.17) into a three-term relation

$$A_0 \boldsymbol{X}^{(\ell-1)}(z) + B_\ell(z)\boldsymbol{X}^{(\ell)}(z) + C_0 \boldsymbol{X}^{(\ell+1)}(z) = \boldsymbol{X}^{(\ell)}(0) \ , \tag{5.20}$$

in which $\boldsymbol{X}^{(\ell)}(z)$ is a column vector

$$\boldsymbol{X}^{(\ell)}(z) = \begin{pmatrix} X_1^{(\ell)}(z) \\ X_2^{(\ell)}(z) \\ X_3^{(\ell)}(z) \end{pmatrix} \ , \tag{5.21}$$

$\boldsymbol{X}^{(\ell)}(0)$ is a column vector of the initial values of the transformed atomic variables

$$\boldsymbol{X}^{(\ell)}(0) = \begin{pmatrix} X_1^{(\ell)}(0) \\ X_2^{(\ell)}(0) \\ X_3^{(\ell)}(0) - \frac{\gamma}{2z}\delta_{\ell,0} \end{pmatrix} \ , \tag{5.22}$$

and $B_\ell(z)$ is a diagonal matrix

$$B_\ell(z) = \begin{pmatrix} z + \frac{1}{2}\gamma + \mathrm{i}\ell\delta & 0 & 0 \\ 0 & z + \frac{1}{2}\gamma + \mathrm{i}\ell\delta & 0 \\ 0 & 0 & z + \gamma + \mathrm{i}\ell\delta \end{pmatrix} \ . \tag{5.23}$$

In the derivation of (5.20), we have used the following definition for the Laplace transform

$$\mathcal{L}\left[X_i^{(\ell)}(t)\right] \equiv X_i^{(\ell)}(z) \equiv \int_0^\infty \mathrm{d}t\, X_i^{(\ell)}(t)\, \mathrm{e}^{-zt} \ , \qquad i = 1, 2, 3 \ , \tag{5.24}$$

together with the relation

$$\mathcal{L}\left[\frac{\mathrm{d}}{\mathrm{d}t} X_i^{(\ell)}(t)\right] = z X_i^{(\ell)}(z) - X_i^{(\ell)}(0) \ , \tag{5.25}$$

where z is the Laplace transform parameter and $X_i^{(\ell)}(0)$ is the value of $X_i^{(\ell)}(t)$ at $t = 0$.

We now proceed to solve the recurrence relation (5.20) to determine all the Fourier amplitudes $X_i^{(\ell)}(z)$. By multiplying both sides of (5.20) by the inverse matrix $B_\ell^{-1}(z)$ from the left-hand side, the relation translates into

$$D_\ell \boldsymbol{X}^{(\ell-1)} + \boldsymbol{X}^{(\ell)} + G_\ell \boldsymbol{X}^{(\ell+1)} = \boldsymbol{d}_\ell \ , \tag{5.26}$$

where $\boldsymbol{X}^{(\ell)} \equiv \boldsymbol{X}^{(\ell)}(z)$, and

$$D_\ell = B_\ell^{-1}(z) A_0 \ , \quad G_\ell = B_\ell^{-1}(z) C_0 \ , \quad \boldsymbol{d}_\ell = B_\ell^{-1}(z) \boldsymbol{X}^{(\ell)}(0) \ . \tag{5.27}$$

In order to obtain a solution to (5.26), we have to truncate the Fourier series at a very large index $\ell = n \gg 1$, i.e., we set $\boldsymbol{X}^{(\ell)} = 0$ for $\ell \geq n$. The procedure then consists of the iterative elimination of $\boldsymbol{X}^{(\ell)}$, $\boldsymbol{X}^{(\ell-1)}$ and so on till we reach the amplitude $\boldsymbol{X}^{(0)}$. The number n must be chosen to be so large that the components of $\boldsymbol{X}^{(\ell)}$ not change, for given precision, as n is increased or reduced by one.

Since we have to find the amplitudes $\boldsymbol{X}^{(\ell)}$ for both positive and negative ℓ, it is helpful to consider separately the recurrence relation for $\ell > 0$ and $\ell < 0$. For $\ell > 0$, the system terminating at $\ell = n$ indicates that the recurrence relation (5.26) for $\ell = n$ can be written as

$$D_n \boldsymbol{X}^{(n-1)} + \boldsymbol{X}^{(n)} = \boldsymbol{d}_n \ , \tag{5.28}$$

and after solving for $\boldsymbol{X}^{(n)}$, we obtain

$$\boldsymbol{X}^{(n)} = \boldsymbol{d}_n - D_n \boldsymbol{X}^{(n-1)} \ . \tag{5.29}$$

Similarly, for $\ell = n - 1$, the relation (5.26) becomes

$$D_{n-1} \boldsymbol{X}^{(n-2)} + \boldsymbol{X}^{(n-1)} + G_{n-1} \boldsymbol{X}^{(n)} = \boldsymbol{d}_{n-1} \ . \tag{5.30}$$

Solving for $\boldsymbol{X}^{(n-1)}$ and substituting for $\boldsymbol{X}^{(n)}$ from (5.29), we get

$$\begin{aligned} \boldsymbol{X}^{(n-1)} = {} & (I - G_{n-1} D_n)^{-1} (\boldsymbol{d}_{n-1} - D_{n-1} \boldsymbol{d}_n) \\ & - (I - G_{n-1} D_n)^{-1} D_{n-1} \boldsymbol{X}^{(n-2)} \ , \end{aligned} \tag{5.31}$$

where I stands for 3×3 identity matrix.

We continue this iterative method in a similar fashion, defining the larger index Fourier amplitudes in terms of the lower index Fourier amplitudes, until we reach the amplitude for $n = 1$. This relation has the following form

$$\begin{aligned} \boldsymbol{X}^{(1)} = {} & \Big(I - G_1 \Big\{ I - G_2 \big[\ldots G_{n-2} (I - G_{n-1} D_n)^{-1} D_{n-1} \ldots \big]^{-1} D_3 \Big\}^{-1} \\ & \times D_2 \Big)^{-1} D_1 \boldsymbol{X}^{(0)} \\ & + \Big(I - G_1 \Big\{ I - G_2 \big[\ldots G_{n-2} (I - G_{n-1} D_n)^{-1} D_{n-1} \ldots \big]^{-1} D_3 \Big\}^{-1} \\ & \times D_2 \Big)^{-1} \big(d_1 - G_1 \big\{ I - G_2 \big[\ldots G_{n-2} (I - G_{n-1} D_n)^{-1} \\ & \times (d_{n-1} - G_{n-1} d_n) \big] \big\} (I - G_2 D_3)^{-1} (d_2 - G_2 d_3) \big) \ . \end{aligned} \tag{5.32}$$

We can write this relation in a simpler form as

$$\boldsymbol{X}^{(1)} = d^{+} + M^{+} \boldsymbol{X}^{(0)} \ , \tag{5.33}$$

where d^{+} and M^{+} are the continued fraction matrices.

Repeating the same procedure for $\ell < 0$ and starting with $\ell = -n$, until we reach the amplitude for $n = -1$, we get

$$\begin{aligned} \boldsymbol{X}^{(-1)} = & \Big(I - G_{-1}\Big\{I - G_{-2}\big[\ldots G_{-n+2}\left(I - G_{-n+1}D_n\right)^{-1} D_{-n+1}\ldots\big]^{-1} \\ & \times D_{-3}\Big\}^{-1} D_{-2}\Big)^{-1} D_{-1}\boldsymbol{X}^{(0)} \\ & + \Big(I - G_{-1}\Big\{I - G_{-2}\big[\ldots G_{-n+2}\left(I - G_{-n+1}D_n\right)^{-1} D_{-n+1}\ldots\big]^{-1} \\ & \times D_{-3}\Big\}^{-1} D_{-2}\Big)^{-1} \left(d_{-1} - G_{-1}\{I - G_{-2}[\ldots \right. \\ & \left. G_{-n+2}\left(I - G_{-n+1}D_n\right)^{-1}\left(d_{-n+1} - G_{-n+1}d_n\right)\big]\Big\} \\ & \times \left(I - G_{-2}D_{-3}\right)^{-1}\left(d_{-2} - G_{-2}d_{-3}\right)\Big) \ . \end{aligned} \tag{5.34}$$

Again we can write this relation in a simplified form as

$$\boldsymbol{X}^{(-1)} = d^{-} + M^{-}\boldsymbol{X}^{(0)} \ . \tag{5.35}$$

The final step is to find $\boldsymbol{X}^{(0)}$. For $n = 0$, the recurrence relation (5.26) yields

$$D_0\boldsymbol{X}^{(-1)} + \boldsymbol{X}^{(0)} + G_0\boldsymbol{X}^{(1)} = \boldsymbol{d}_0 \ . \tag{5.36}$$

Having obtained $\boldsymbol{X}^{(1)}$ and $\boldsymbol{X}^{(-1)}$, we can solve (5.36) and determine $\boldsymbol{X}^{(0)}$. The result is

$$\boldsymbol{X}^{(0)} = \left(D_0M^{-} + G_0M^{+} + I\right)^{-1}\left(d_0 - D_0d^{-} - G_0d^{+}\right) \ . \tag{5.37}$$

This equation forms the basis for the formal analysis of the dynamics of a two-level atom driven by the bichromatic field with one component on resonance and the other detuned from the atomic transition frequency. It is readily evaluated numerically by computer, giving us complete dynamical solutions for any of the harmonic amplitudes. These solutions are a function of four parameters, the spontaneous emission rate γ, the detuning δ, and the Rabi frequencies Ω_0 and Ω_1.

5.2.3 *Matrix Inversion Method*

An alternative but more elegant approach to solve the recurrence relation (5.17) is the matrix inversion method [13, 14]. This method arises from a treatment based on the diagonalization of tridiagonal matrices, in which the solutions for the harmonic amplitudes are determined in terms of eigenvalues and eigenvectors of an infinite-dimensional matrix of time-independent coefficients. In this way, we construct a matrix differential equation by arranging the amplitudes $X^{(\ell)}(t)$ in the order

$$\boldsymbol{\Upsilon}(t) = \begin{pmatrix} \vdots \\ X^{(1)}(t) \\ X^{(0)}(t) \\ X^{(-1)}(t) \\ \vdots \end{pmatrix} . \tag{5.38}$$

Then, the recurrence relation (5.17) can be simply written as the matrix differential equation

$$\frac{\mathrm{d}}{\mathrm{d}t}\boldsymbol{\Upsilon}(t) = \boldsymbol{K}\boldsymbol{\Upsilon}(t) + \boldsymbol{P} , \tag{5.39}$$

where $\boldsymbol{K}$ is an infinite-dimensional tridiagonal matrix composed of the 3×3 matrices A_0, B_ℓ and C_0, and $\boldsymbol{P}$ is an infinite-dimensional vector with the nonzero component $-\frac{1}{2}\gamma\delta_{\ell,0}\boldsymbol{X}^{(\ell)}(0)$.

The matrix equation (5.39) is a simple differential equation with time independent coefficients, and is solved by direct integration. For an arbitrary initial time t_0, the integration of (5.39) leads to the following formal solution for $\boldsymbol{\Upsilon}(t)$:

$$\boldsymbol{\Upsilon}(t) = \mathrm{e}^{\boldsymbol{K}t}\boldsymbol{\Upsilon}(t_0) - \left(1 - \mathrm{e}^{\boldsymbol{K}t}\right)\boldsymbol{K}^{-1}\boldsymbol{P} , \tag{5.40}$$

where $\boldsymbol{\Upsilon}(t_0)$ is an initial value of $\boldsymbol{\Upsilon}(t)$ proper for a given type of evolution.

In order to proceed further, we have to truncate the dimension of the vector $\boldsymbol{\Upsilon}(t)$. The validity of the truncation is ensured by requiring that the solution (5.40) not change as the dimension of $\boldsymbol{\Upsilon}(t)$ increases or decreases by one. Because the determinant of the finite-dimensional (truncated) matrix $\boldsymbol{K}$ is different from zero, there exists a complex invertible matrix $\boldsymbol{T}$ which diagonalizes $\boldsymbol{K}$, and $\lambda = \boldsymbol{T}^{-1}\boldsymbol{K}\boldsymbol{T}$ is the diagonal matrix of complex eigenvalues. By introducing $\boldsymbol{L} = \boldsymbol{T}^{-1}\boldsymbol{\Upsilon}$ and $\boldsymbol{R} = \boldsymbol{T}^{-1}\boldsymbol{P}$, we can rewrite (5.40) as

$$\boldsymbol{L}(t) = \boldsymbol{L}(t_0)\,\mathrm{e}^{\lambda t} - \left(1 - \mathrm{e}^{\lambda t}\right)\lambda^{-1}\boldsymbol{R} , \tag{5.41}$$

or, in component form

$$L_i(t) = L_i(t_0)\,\mathrm{e}^{\lambda_i t} - \sum_{j=1}^{n}\left(\lambda^{-1}\right)_{ij}\left(1 - \mathrm{e}^{\lambda_j t}\right)R_j , \tag{5.42}$$

where n is the dimension of the truncated matrix. Equation (5.42) makes possible the easy evaluation of the amplitudes $X^{(\ell)}(t)$. It is done by determining the eigenvalues λ_i and the corresponding eigenvectors $L_i(t)$ using, for example, a numerical method of diagonalization of the matrix $\boldsymbol{K}$.

5.2.4 Fluorescence Spectrum

In Sect. 3.1.3, we illustrated how to calculate the fluorescence spectrum of a two-level atom driven by a monochromatic laser field. This was accomplished by first determining the master equation of the system from which we found equations of motion for the expectation values of the atomic operators. The equations of motion are then solved analytically or numerically by direct integration and the required two-time correlation function of the atomic operators is found by applying the quantum regression theorem.

In this section, we implement the Floquet method by calculating the fluorescence spectrum of a two-level atom driven by the bichromatic field composed of a resonant and a detuned frequency components [13]. Since, the bichromatic field is an example of a quasistationary field, the spectrum can be calculated from the general expression (2.26), which in the case of a single two-level atom takes the form

$$\begin{aligned} S_{\text{in}}(\omega) &= 2\gamma \text{Re} \int_0^\infty \mathrm{d}\tau \, \langle \delta S^+(0) \, \delta S^-(\tau) \rangle^{(0)} \mathrm{e}^{\mathrm{i}(\omega-\omega_L)\tau} \\ &= 2\gamma \text{Re} \int_0^\infty \mathrm{d}\tau \, Y_2^{(0)}(0,\tau) \mathrm{e}^{\mathrm{i}(\omega-\omega_L)\tau} \, , \end{aligned} \tag{5.43}$$

where $Y_2^{(0)}(0,\tau) = \langle \delta S^+(0) \, \delta S^-(\tau) \rangle^{(0)}$ is the zeroth-order harmonic of the two-time correlation function of the atomic fluctuation operators.

Thus, we need to obtain the zeroth-order harmonic $Y_2^{(0)}(0,\tau)$, which could be calculated through (5.8). Owing to the time dependence of the coefficients of the differential equations (5.19), we apply the Floquet method in which we make a harmonic decomposition

$$Y_i\left(t,t'\right) = \sum_{\ell=-\infty}^{+\infty} Y_i^{(\ell)}\left(t,t'\right) \mathrm{e}^{\mathrm{i}\ell\delta t'} \, , \qquad i = 1,2,3 \, . \tag{5.44}$$

Upon substitution of (5.44) into (5.8), we find that harmonics of $Y_i(t,t')$ satisfy the following set of coupled differential equations

$$\begin{aligned} \frac{\mathrm{d}}{\mathrm{d}t'} Y_1^{(l)} &= -\left(\frac{1}{2}\gamma + \mathrm{i}l\delta\right) Y_1^{(l)} + \Omega_0 Y_3^{(l)} + \tilde{\Omega}_1 Y_3^{(l-1)} \, , \\ \frac{\mathrm{d}}{\mathrm{d}t'} Y_2^{(l)} &= -\left(\frac{1}{2}\gamma + \mathrm{i}l\delta\right) Y_2^{(l)} + \Omega_0 Y_3^{(l)} + \tilde{\Omega}_1^* Y_3^{(l+1)} \, , \\ \frac{\mathrm{d}}{\mathrm{d}t'} Y_3^{(l)} &= -\left(\gamma + \mathrm{i}l\delta\right) Y_3^{(l)} - \frac{1}{2}\Omega_0 \left(Y_1^{(l)} + Y_2^{(l)}\right) \\ &\quad - \frac{1}{2}\tilde{\Omega}_1^* Y_1^{(l+1)} - \frac{1}{2}\tilde{\Omega}_1 Y_2^{(l-1)} \, , \end{aligned} \tag{5.45}$$

where $\tilde{\Omega}_n = \Omega_n e^{-i\phi_n}$. The way we shall compute $Y_1^{(l)}(0,\tau)$ is that we take the Laplace transform of (5.45) and first compute $Y_3^{(l)}$. Thus, taking the Laplace transform of (5.45) and then eliminating $Y_1^{(l)}(z)$ and $Y_2^{(l)}(z)$ we arrive to the following inhomogeneous three-term recurrence relation for $Y_3^{(l)}(z)$:

$$\begin{aligned}\left[(z+\gamma+il\delta) + \frac{\Omega_0^2}{P_l(z)} + \frac{|\tilde{\Omega}_1|^2}{2P_{l+1}(z)} + \frac{|\tilde{\Omega}_1|^2}{2P_{l-1}(z)}\right] Y_3^{(l)}(z) \\ + \frac{1}{2}\Omega_0\tilde{\Omega}_1\left[\frac{1}{P_l(z)} + \frac{1}{P_{l-1}(z)}\right] Y_3^{(l-1)}(z) \\ + \frac{1}{2}\Omega_0\tilde{\Omega}_1^*\left[\frac{1}{P_l(z)} + \frac{1}{P_{l+1}(z)}\right] Y_3^{(l+1)}(z) = g_l(z)\ , \quad (5.46)\end{aligned}$$

where $P_l(z) = z + \frac{1}{2}\gamma + il\delta$, z is a complex (Laplace transform) parameter, and

$$g_l(z) = Y_3^{(l)}(0) - \frac{\Omega_0[Y_1^{(l)}(0)+Y_2^{(l)}(0)]}{2P_l(z)} - \frac{\tilde{\Omega}_1^* Y_1^{(l+1)}(0)}{2P_{l+1}(z)} - \frac{\tilde{\Omega}_1 Y_2^{(l-1)}(0)}{2P_{l-1}(z)} \quad (5.47)$$

is an inhomogeneous term given by the initial values of the atomic correlation functions

$$\begin{aligned}Y_1^{(l)}(0) \equiv Y_1^{(l)}(t,t) &= \frac{1}{2}\delta_{l,0} + X_3^{(l)}(t) - \sum_{r=-\infty}^{\infty} X_1^{(l-r)}(t)X_2^{(r)}(t)\ , \\ Y_2^{(l)}(0) \equiv Y_2^{(l)}(t,t) &= -\sum_{r=-\infty}^{\infty} X_2^{(l-r)}(t)X_2^{(r)}(t)\ , \\ Y_3^{(l)}(0) \equiv Y_3^{(l)}(t,t) &= -\sum_{r=-\infty}^{\infty}\left(\frac{1}{2}\delta_{r,0} + X_3^{(r)}(t)\right) X_2^{(l-r)}(t)\ . \quad (5.48)\end{aligned}$$

In the above equation, $X_i^{(l)}$ are stationary harmonic amplitudes of the components of the Bloch vector given in terms of the expectation values of the atomic variables

$$\begin{aligned}X_1(t) = \langle\tilde{S}^-(t)\rangle &= \sum_{l=-\infty}^{\infty} X_1^{(l)}(t')\, e^{il\delta t}\ , \\ X_2(t) = \langle\tilde{S}^+(t)\rangle &= \sum_{l=-\infty}^{\infty} X_2^{(l)}(t)\, e^{il\delta t}\ , \\ X_3(t) = \langle S_z(t)\rangle &= \sum_{l=-\infty}^{\infty} X_3^{(l)}(t)\, e^{il\delta t}\ . \quad (5.49)\end{aligned}$$

The stationary values of the harmonics $X_k^{(l)}$ are obtained by taking the $z \to 0$ limit in either the continued fraction solution for $\boldsymbol{X}^{(n)}$, expressions (5.28)−(5.37), or in the matrix inversion solution, expression (5.42).

To illustrate the structure of the spectrum, we first find $Y_3^{(l)}(z)$ by solving the recurrence relation (5.46), using either the continued fraction or matrix inversion method. This $Y_3^{(l)}(z)$ can then be used to calculate $Y_1^{(l)}(z)$, the Laplace transform of the equation of motion for the $Y_1^{(l)}$ component

$$\left(z + \frac{1}{2}\gamma + il\delta\right) Y_2^{(l)}(z) = Y_2^{(l)}(0) + \Omega_0 Y_3^{(l)}(z) + \tilde{\Omega}_1^* Y_3^{(l+1)}(z) \,, \tag{5.50}$$

and the result for $Y_2^{(0)}(z)$ used to evaluate the fluorescence spectrum from the relation

$$S_{\text{in}}(\omega) = 2\gamma \text{Re}\left\{ Y_2^{(0)}(z)\Big|_{z=-\text{i}\nu} \right\} \,, \tag{5.51}$$

where $\nu = (\omega - \omega_L)/\gamma$.

Figure 5.2 shows the fluorescence spectrum for $\Omega_0 = 50\gamma$, $\Omega_1 = 5\gamma$ and several different values of $\Delta_1 = \delta - \Omega_0$, a detuning of the weaker laser component from the Rabi frequency of the strong component. When the frequency of the weaker component is far away from the Rabi frequency of the strong component, the spectrum is a triplet, the familiar Mollow triplet of a monochromatically driven atom. In this

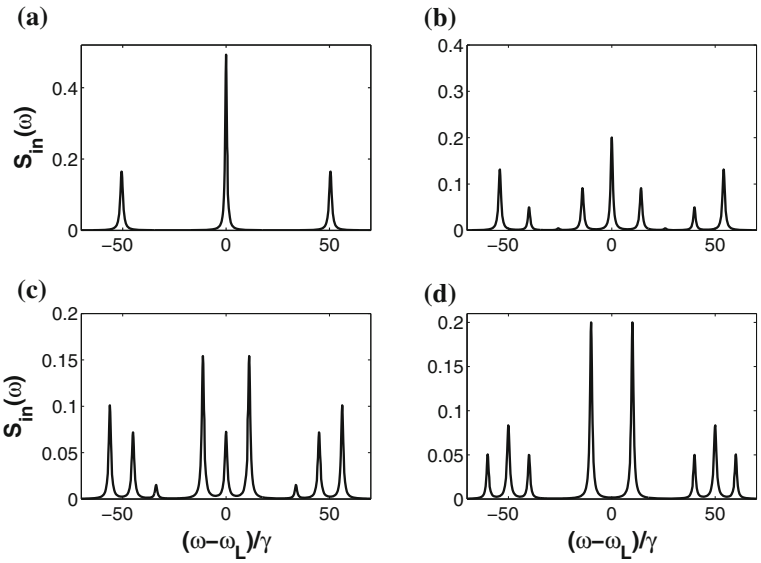

Fig. 5.2 The fluorescence spectrum of the doubly driven atom for $\omega_L = \omega_a, \omega_1 = \omega_L - \Omega_0 - \Delta_1$, $\Omega_0 = 50\gamma$, $\Omega_1 = 5\gamma$, and for several different detunings $\Delta_1 = \delta - \Omega_0$: **a** $\Delta_1 = 100\gamma$, **b** $\Delta_1 = 10\gamma$, **c** $\Delta_1 = 5\gamma$, and **d** $\Delta_1 = 0$

case, the atom is effectively driven only by the strong resonant component. As the detuning Δ_1 decreases, the central component of the Mollow triplet and the Rabi sidebands split into triplets. However, as the detuning Δ_1 decreases further toward zero the central component of the spectrum rapidly declines and completely disappears when $\Delta_1 = 0$. In this case, the weaker component of the driving field is tuned to exact resonance with the lower Rabi sideband of the Mollow triplet. Under this circumstance, there is no fluorescence at the atomic transition frequency ω_a that the spontaneous emission is completely cancelled at the atomic transition frequency.

5.2.5 *Dressed-Atom Model Analysis of the Dynamical Suppression of the Spectral Component*

We have seen that the effect of bichromatic excitation on the radiative properties of a two-level atom is to modify the spectral properties. The most interesting feature of the spectral properties is the apparent suppression of the central component of the spectrum when the weaker component is detuned from the atomic resonance by an amount equal to the Rabi frequency of the strong component. The Floquet method supplement with either the continuous fraction method or matrix inversion method led us to plotting the fluorescence spectrum in a very direct manner. However, the Floquet method approach is too restricted in a physical interpretation of the solutions and do not lead to a physical understanding of the characteristics of the fluorescence spectrum, in particular the origin of the suppression of the central component of the spectrum.

A physical understanding of the suppression of the central component of the spectrum can be obtained by the dressed-atom approach, which provides a convenient ground for rigorous examination of the spectral features and facilitates the explicit study of the positions of the spectral lines, their bandwidths and intensities [15].

Let us illustrate the dressed-atom approach to the case of a bichromatic driving field, corresponding to the situation presented in Fig. 5.1. As we have seen in Sect. 3.2.1, the idea of the "dressing" technique is to neglect, in a first step, the effect of spontaneous emission and find the eigenstates of the combined system: the atom plus the driving field. Since the bichromatic field is composed of two frequency components, we effectively have two "dressing" fields. Therefore, we will first dress the atom with the strong resonant component, and then, we will apply the second component to the dressed states of the strong component. This procedure is often called in the literature as dressing dressed states technique [13, 14]. Hence, we first dress the atom with the strong resonant component of the bichromatic field, which results in what we refer to the "singly" dressed states

$$\left|\tilde{i}, n\right\rangle = \frac{1}{\sqrt{2}}\left(|1, n\rangle - (-1)^i |2, n-1\rangle\right) , \quad i = 1, 2, \tag{5.52}$$

which are linear combinations of the product states $|1, n\rangle \equiv |1\rangle \otimes |n\rangle$ and $|2, n-1\rangle \equiv |2\rangle \otimes |n-1\rangle$, where n is the number of photon in the mode of the resonant component, and $|1\rangle$, $|2\rangle$ are the bare states of the atom. As illustrated in Sect. 3.2.1, the singly dressed states constitute a ladder of an infinite number of doublets. The centers of adjacent dressed-state doublets are separated by the atomic frequency ω_a, and the splitting between two states $|n, \tilde{1}\rangle$ and $|n, \tilde{2}\rangle$ within each doublet is equal to the Rabi frequency of the strong component.

In the next step of the procedure, we add the weaker component at frequency $\omega_1 = \omega_a - \Omega_0$ to the singly dressed atom, which results in new "undressed" states

$$\begin{aligned} \left|\tilde{1}, n, m\right\rangle &= \left|\tilde{1}, n\right\rangle \otimes |m\rangle \ , \\ \left|\tilde{2}, n, m\right\rangle &= \left|\tilde{2}, n\right\rangle \otimes |m\rangle \ , \end{aligned} \tag{5.53}$$

with energies

$$E_{\overline{n},\pm} = \overline{n}\omega_0 - m\left(\Omega_0 + \Delta_1\right) \pm \frac{1}{2}\Omega_0 \ , \tag{5.54}$$

where $\Delta_1 = \delta - \Omega_0$ is the detuning of the weaker component from the Rabi sideband frequency $\omega_a - \Omega_0$, $\overline{n} = n + m$ is the total number of photons in the field modes, and m is the number of photons in the weaker field mode. In state $|n, +, m\rangle$, for example, the singly dressed atom is in state $|n, +\rangle$ and there are m photons in the weaker field. The combined undressed states (5.53) group into manifolds each containing an infinite number of doublets. For $\Delta_1 = 0$, the states in a given doublet are degenerate, but are nondegenerate for $\Delta_1 \neq 0$. We treat the states (5.53) as basis states and calculate how they are affected by the interaction between the singly dressed atom and the weaker field. The interaction Hamiltonian is given in the rotating-wave approximation by

$$\hat{H}_1 = \mathrm{i}\hbar g_1 \left(\hat{a}_1^\dagger S^- - S^+ \hat{a}_1\right) \ , \tag{5.55}$$

where g_1 is the coupling constant and $\hat{a}_1^\dagger \left(\hat{a}_1\right)$ is the creation (annihilation) operator of the detuned field mode.

Applying the interaction (5.55) to the states (5.53), we find the "doubly dressed states" of the system

$$\begin{aligned} |\overline{n}, +, p\rangle &= \sin\varphi\, |n + 1 - p, +, m - 1 + p\rangle \\ &\quad + \cos\varphi\, |n - p, -, m + p\rangle \ , \\ |\overline{n}, -, p\rangle &= \cos\varphi\, |n + 1 - p, +, m - 1 + p\rangle \\ &\quad - \sin\varphi\, |n - p, -, m + p\rangle \ , \end{aligned} \tag{5.56}$$

and their energies

$$E_{\bar{n},p,\pm} = \bar{n}\omega_0 + \left(m + p + \frac{1}{2}\right)\Omega_0 - (m+p)\,\Delta_1 \pm \frac{1}{2}G\,, \tag{5.57}$$

where

$$\cos^2\varphi = \frac{1}{2} + \frac{\Delta_1}{2G}\,, \tag{5.58}$$

with $G = \sqrt{\Omega_1^2 + \Delta_1^2}$.

The doubly dressed states (5.56) group into manifolds each containing an infinite number of doublets, labeled by p. Neighboring doublets are separated by Ω_0, while the intra-doublet separation is G.

With the dressed states of the doubly driven system available, it is straightforward to show that the dipole transition moments between dressed states $|\bar{n}, \pm, p\rangle$ and $|\bar{n}-1, \pm, q\rangle$ of two neighboring manifolds are

$$\begin{aligned}
\langle p, +, \bar{n}|\, S^+ |\bar{n}-1, -, q\rangle &= -\frac{1}{2}\sin 2\varphi\,\delta_{p,q} + \frac{1}{2}\cos^2\varphi\,\delta_{p,q+1} + \frac{1}{2}\sin^2\varphi\,\delta_{p,q-1}\,,\\
\langle p, -, \bar{n}|\, S^+ |\bar{n}-1, +, q\rangle &= -\frac{1}{2}\sin 2\varphi\,\delta_{p,q} - \frac{1}{2}\sin^2\varphi\,\delta_{p,q+1} - \frac{1}{2}\cos^2\varphi\,\delta_{p,q-1}\,,\\
\langle p, -, \bar{n}|\, S^+ |\bar{n}-1, -, q\rangle &= -\frac{1}{2}\cos 2\varphi\,\delta_{p,q} - \frac{1}{4}\sin 2\varphi\left(\delta_{p,q+1} - \delta_{p,q-1}\right)\,,\\
\langle p, +, \bar{n}|\, S^+ |\bar{n}-1, +, q\rangle &= \frac{1}{2}\cos 2\varphi\,\delta_{p,q} + \frac{1}{4}\sin 2\varphi\left(\delta_{p,q+1} - \delta_{p,q-1}\right)\,.
\end{aligned} \tag{5.59}$$

The presence of the Kronecker delta functions in (5.59) indicates that from a given doublet $|\bar{n}, \pm, p\rangle$ spontaneous emission can occur to doublets $|\bar{n}-1, \pm, q\rangle$ with $q = p, p \pm 1$ only. Rates at which the spontaneous transitions occur are determined by

$$\gamma_{pi,qj} = \gamma\left|\langle \bar{n}, i, p|\, S^+ \,|\bar{n}-1, j, q\rangle\right|^2\,, \tag{5.60}$$

where $i, j = \pm$. By examining (5.59) one can find that, in general, the transitions occur with nine different frequencies. This explains why the fluorescence spectrum, shown in Fig. 5.2, exhibits at most nine lines.

What interests us most is the reason for the disappearance of the central component of the spectrum when $\Delta_1 = 0$. It is easily verified that the transitions from $|\bar{n}, +, p\rangle$ to $|\bar{n}-1, +, p\rangle$ and from $|\bar{n}, -, p\rangle$ to $|\bar{n}-1, -, p\rangle$, which occur at the frequency ω_a and thus give rise to the central component of the spectrum occur with rates

$$\gamma_{p\pm,p\pm} = \frac{1}{4}\gamma\cos^2 2\varphi\,. \tag{5.61}$$

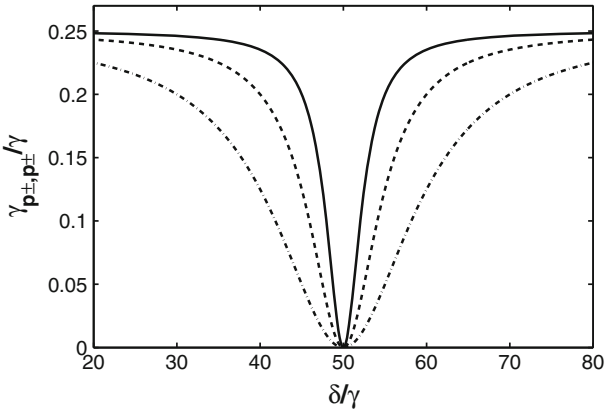

Fig. 5.3 Spontaneous emission rates $\gamma_{p\pm,p\pm}$ as a function of δ for $\Omega_0 = 50\,\gamma$ and different Ω_1: $\Omega_1 = 5\gamma$ (*solid line*), $\Omega_1 = 10\gamma$ (*dashed line*), $\Omega_1 = 20\gamma$ (*dashed-dotted line*)

It is apparent from (5.61), that the spontaneous emission rates vanish for $\varphi = \pi/4$, which corresponds to $\Delta_1 = 0$. Consequently, there is no spectral component at ω_a when $\Delta_1 = 0$.

Figure 5.3 illustrates the variation of $\gamma_{p\pm,p\pm}$ with the detuning $\delta = \Omega_0 + \Delta_1$. It is apparent that the spontaneous emission rate of the transitions at the atomic frequency ω_a depends strongly on the detuning δ. For δ significantly different from Ω_0, the transition rates are almost the same as for the monochromatic driving field. The transition rates decrease as δ approaches Ω_0, and vanish when δ is exactly equal to the Rabi frequency of the resonant component. Consequently, there are no fluctuations of the vacuum field at the atomic frequency.

5.3 Excitation with an Amplitude−Modulated Field

In this section, we will describe another theoretical method used to calculate the response of an atom to a multi-chromatic field. The method was initiated by Blind et al. [16] and involves semiclassical dressed states of the system, which are eigenstates of an atom and a classically treated driving field. Under the assumption that at least one component of the driving field is strong, the evolution of the system is obtained by solving the optical Bloch equations through the direct integration. The method, although approximate, allows to analyze analytically the evolution of the system and the fluorescence spectrum. We illustrate the method on example of a two-level atom driven by an amplitude modulated field.

In Sect. 5.1 the optical Bloch equations for the one- and two-time correlation functions of the atomic dipole operators were derived, valid for an arbitrary time dependence of the Rabi frequency of the driving field. We model the driving field

as being of an amplitude modulated field with the Rabi frequency given by (5.11). The Hamiltonian describing the interaction of the amplitude modulated field with a two-level atom, in a frame rotating with frequency ω_L, depends explicitly on time and can be written as

$$\hat{H}_L(t) = \hat{H}_0 + \hat{H}_m(t) \,, \tag{5.62}$$

where

$$\hat{H}_0 = \hbar\Delta S_z - \frac{1}{2}\mathrm{i}\hbar\Omega_0 \left(S^+ - S^-\right) \tag{5.63}$$

is the Hamiltonian of the atom plus the interaction between the atom and the central component of the driving field, and

$$\hat{H}_m(t) = -\mathrm{i}\Omega_1 \cos\delta t \left(S^+ - S^-\right) \tag{5.64}$$

is the interaction of the atom with the time-dependent amplitude modulating fields.

In what follows we consider the situation where the Rabi frequency Ω_0 is much larger than the spontaneous emission rate γ, the modulation frequency δ, and the Rabi frequency Ω_1 of the modulating fields, the so-called weak modulation, i.e., $\Omega_0 \gg \gamma, \delta, \Omega_1$. In this case, we can diagonalize the Hamiltonian (5.63) to find the so-called semiclassical dressed states. Assuming that the frequency of the central component is on resonance with the atomic transition frequency, $\Delta = 0$, the semiclassical dressed states are

$$\left|\tilde{1}\right\rangle = \frac{1}{\sqrt{2}}\left(|g\rangle + \mathrm{i}\,|e\rangle\right) \,, \quad \left|\tilde{2}\right\rangle = \frac{1}{\sqrt{2}}\left(|g\rangle - \mathrm{i}\,|e\rangle\right) \,, \tag{5.65}$$

where $|g\rangle$ and $|e\rangle$ are the atomic ground and upper bare states, respectively.

We now introduce the dressed-state raising, lowering, and population difference operators, $R_{21} = |\tilde{2}\rangle\langle\tilde{1}|$, $R_{12} = |\tilde{1}\rangle\langle\tilde{2}|$, and $R_3 = (|\tilde{2}\rangle\langle\tilde{2}| - |\tilde{1}\rangle\langle\tilde{1}|)/2$. Using (5.65), we easily find that the dressed-atom operators are related to the atomic dipole and inversion operators by the relations

$$\begin{aligned} R_{21} &= S_z - \frac{\mathrm{i}}{2}\left(S^+ + S^-\right) \,, \quad R_{12} = S_z + \frac{\mathrm{i}}{2}\left(S^+ + S^-\right) \,, \\ R_3 &= \frac{\mathrm{i}}{2}\left(S^+ - S^-\right) \,. \end{aligned} \tag{5.66}$$

It follows from (5.5) and (5.66) that the optical Bloch equations written in terms of the dressed-atom operators become

$$\frac{\mathrm{d}}{\mathrm{d}t}\langle R_{12}(t)\rangle = -\frac{1}{2}\gamma - \frac{3}{4}\gamma\,\langle R_{12}(t)\rangle - \frac{1}{4}\gamma\,\langle R_{21}(t)\rangle + \mathrm{i}\Omega\,(t)\,\langle R_{12}(t)\rangle\,,$$
$$\frac{\mathrm{d}}{\mathrm{d}t}\langle R_{21}(t)\rangle = -\frac{1}{2}\gamma - \frac{3}{4}\gamma\,\langle R_{21}(t)\rangle - \frac{1}{4}\gamma\,\langle R_{12}(t)\rangle - \mathrm{i}\Omega\,(t)\,\langle R_{21}(t)\rangle\,,$$
$$\frac{\mathrm{d}}{\mathrm{d}t}\langle R_3(t)\rangle = -\frac{1}{2}\gamma\,\langle R_3(t)\rangle\,, \tag{5.67}$$

We see that the equation of motion for $\langle R_3(t)\rangle$ is independent of the driving field and is decoupled from the remaining equation. On the other hand, the equations of motion for $\langle R_{12}(t)\rangle$ and $\langle R_{21}(t)\rangle$ are coupled to one another through the damping term $\gamma/4$. It is clear that in the limit of negligibly small damping, the equations decouple from each other. In this limit, we can directly integrate (5.67) and readily find that $\langle R_{12}(t)\rangle$ and $\langle R_{21}(t)\rangle$ oscillate at frequencies $+\Omega(t)$ and $-\Omega(t)$, respectively. Since $\Omega_0 \gg \gamma, \Omega_1$, we may introduce slowly varying dynamical variables, $\langle \tilde{R}_{12}(t)\rangle = \langle R_{12}(t)\rangle \exp(-\mathrm{i}\Omega_0 t)$ and $\langle \tilde{R}_{21}(t)\rangle = \langle R_{21}(t)\rangle \exp(\mathrm{i}\Omega_0 t)$ which are free from the rapid oscillations at Ω_0. In terms of these new variables (5.67) becomes

$$\frac{\mathrm{d}}{\mathrm{d}t}\langle \tilde{R}_{12}(t)\rangle = -\frac{1}{2}\gamma \mathrm{e}^{-\mathrm{i}\Omega_0 t} - \left(\frac{3}{4}\gamma - 2\mathrm{i}\Omega_1 \cos\delta t\right)\langle \tilde{R}_{12}(t)\rangle - \frac{1}{4}\gamma\,\langle \tilde{R}_{21}(t)\rangle \mathrm{e}^{-2\mathrm{i}\Omega_0 t}\,,$$
$$\frac{\mathrm{d}}{\mathrm{d}t}\langle \tilde{R}_{21}(t)\rangle = -\frac{1}{2}\gamma \mathrm{e}^{\mathrm{i}\Omega_0 t} - \left(\frac{3}{4}\gamma + 2\mathrm{i}\Omega_1 \cos\delta t\right)\langle \tilde{R}_{21}(t)\rangle - \frac{1}{4}\gamma\,\langle \tilde{R}_{12}(t)\rangle \mathrm{e}^{2\mathrm{i}\Omega_0 t}\,,$$
$$\frac{\mathrm{d}}{\mathrm{d}t}\langle R_3(t)\rangle = -\frac{1}{2}\gamma\,\langle R_3(t)\rangle\,. \tag{5.68}$$

In these equations we recognize certain terms oscillating at twice the Rabi frequency Ω_0. When the equations are integrated over any time interval, these oscillatory terms make a negligible contribution. Thus, the secular approximation can be applied, which involves dropping these rapidly oscillating terms. Hence, after discarding the rapidly oscillating terms we obtain a set of decoupled differential equations

$$\frac{\mathrm{d}}{\mathrm{d}t}\langle \tilde{R}_{12}(t)\rangle = -\frac{1}{2}\gamma \mathrm{e}^{-\mathrm{i}\Omega_0 t} - \left(\frac{3}{4}\gamma - 2\mathrm{i}\Omega_1 \cos\delta t\right)\langle \tilde{R}_{12}(t)\rangle\,,$$
$$\frac{\mathrm{d}}{\mathrm{d}t}\langle \tilde{R}_{21}(t)\rangle = -\frac{1}{2}\gamma \mathrm{e}^{\mathrm{i}\Omega_0 t} - \left(\frac{3}{4}\gamma + 2\mathrm{i}\Omega_1 \cos\delta t\right)\langle \tilde{R}_{21}(t)\rangle\,,$$
$$\frac{\mathrm{d}}{\mathrm{d}t}\langle R_3(t)\rangle = -\frac{1}{2}\gamma\,\langle R_3(t)\rangle\,. \tag{5.69}$$

These approximate differential equations can be solved by the direct integration.

Let us illustrate the method of integrating the differential equations on the equation for $\langle \tilde{R}_{12}(t)\rangle$. The method of integrating the equation for $\langle \tilde{R}_{21}(t)\rangle$ follows by a similar analysis. If we integrate the equation using the integrating factor method, we first ignore the inhomogeneous term $-\frac{1}{2}\gamma \mathrm{e}^{-\mathrm{i}\Omega_0 t}$, and by integration of the homogeneous term over a finite time interval from 0 to t, we obtain

$$\langle \tilde{R}_{12}(t)\rangle = C\mathrm{e}^{-\left(\frac{3}{4}\gamma t - \mathrm{i}\beta\sin\delta t\right)}\,, \tag{5.70}$$

where $\beta = 2\Omega_1/\delta$ and C is a constant. We now determine the constant C by letting C to be a time-dependent variable, $C \to C(t)$. Hence, substituting (5.70) back to the equation of motion for $\langle \tilde{R}_{12}(t)\rangle$, we obtain a differential equation for $C(t)$:

$$\frac{\mathrm{d}}{\mathrm{d}t}C(t) = -\frac{1}{2}\gamma\mathrm{e}^{(\frac{3}{4}\gamma - \mathrm{i}\Omega_0)t - \mathrm{i}\beta\sin\delta t}\,. \tag{5.71}$$

We can decompose the modulation term $(\sin\delta t)$ into Fourier components [17]

$$\mathrm{e}^{\pm\mathrm{i}\beta\sin(\delta t)} = \sum_n J_n(\pm\beta)\,\mathrm{e}^{\mathrm{i}n\delta t}\,, \tag{5.72}$$

where $J_n(\beta)$ is the nth order Bessel function. When the relation (5.72) is used in (5.71) we have, after integration

$$C(t) = -\frac{1}{2}\gamma\sum_n \frac{J_n(-\beta)}{\left[\frac{3}{4}\gamma - \mathrm{i}(\Omega_0 - n\delta)\right]}\mathrm{e}^{\frac{3}{4}\gamma t - \mathrm{i}(\Omega_0 - n\delta)t} + C(0)\,. \tag{5.73}$$

Once $C(t)$ has been found, it is only a matter of substitution to derive $\langle R_{12}(t)\rangle$ from (5.70). Thus, we obtain the complete time dependence of $\langle R_{12}(t)\rangle$ in the framework of the secular approximation, valid at any time t and for any initial state

$$\begin{aligned}\langle R_{12}(t)\rangle = &-\frac{1}{2}\gamma\sum_{n,m}\frac{J_n(-\beta)J_m(\beta)}{\left[\frac{3}{4}\gamma - \mathrm{i}(\Omega_0 - n\delta)\right]}\mathrm{e}^{\mathrm{i}(n+m)\delta t}\\ &+\left\{R_{12}(0) + \frac{1}{2}\gamma\sum_n\frac{J_n(-\beta)}{\left[\frac{3}{4}\gamma - \mathrm{i}(\Omega_0 - n\delta)\right]}\right\}\\ &\times\sum_m J_m(\beta)\mathrm{e}^{-\frac{3}{4}\gamma t + \mathrm{i}(\Omega_0 + m\delta)t}\,.\end{aligned} \tag{5.74}$$

The solution of equation for $\langle R_{21}(t)\rangle$ is similarly found to be

$$\begin{aligned}\langle R_{21}(t)\rangle = &-\frac{1}{2}\gamma\sum_{n,m}\frac{J_n(-\beta)J_m(\beta)}{\left[\frac{3}{4}\gamma + \mathrm{i}(\Omega_0 + n\delta)\right]}\mathrm{e}^{\mathrm{i}(n+m)\delta t}\\ &+\left\{R_{21}(0) + \frac{1}{2}\gamma\sum_n\frac{J_n(-\beta)}{\left[\frac{3}{4}\gamma + \mathrm{i}(\Omega_0 + n\delta)\right]}\right\}\\ &\times\sum_m J_m(\beta)\mathrm{e}^{-\frac{3}{4}\gamma t - \mathrm{i}(\Omega_0 - m\delta)t}\,,\end{aligned} \tag{5.75}$$

and the solution of equation for $\langle R_3(t)\rangle$ is obtained by a simple integration

$$\langle R_3(t)\rangle = \langle R_3(0)\rangle \mathrm{e}^{-\frac{1}{2}\gamma t} \,. \tag{5.76}$$

Note that both terms in (5.74) and (5.75) depend on time, but only the second terms fall off exponentially with t. This means that for $t \to \infty$ the state of the system is not strictly stationary that, in general, $\langle R_{12}(t)\rangle$ and $\langle R_{21}(t)\rangle$ do not become t independent. However, there are terms, those with $m = -n$, which are independent of t. Consequently, in the long-time limit $t \to \infty$, we have

$$\begin{aligned}
\langle R_3^s\rangle &\equiv \langle R_3(t\to\infty)\rangle = 0 \,, \\
\langle R_{12}^s\rangle &\equiv \langle R_{12}(t\to\infty)\rangle = -\frac{1}{2}\gamma \sum_n \frac{J_n^2(\beta)}{\left[\frac{3}{4}\gamma - \mathrm{i}(\Omega_0 - n\delta)\right]} \,, \\
\langle R_{21}^s\rangle &\equiv \langle R_{21}(t\to\infty)\rangle = -\frac{1}{2}\gamma \sum_n \frac{J_n^2(\beta)}{\left[\frac{3}{4}\gamma + \mathrm{i}(\Omega_0 + n\delta)\right]} \,.
\end{aligned} \tag{5.77}$$

Note that in the long-time limit, the populations of the two dressed states are exactly equal, $\langle R_3^s\rangle = 0$, but the coherences between the dressed states are different from zero.

We now turn to the solution of the Bloch equations for the two-time correlation functions which are required to evaluate the fluorescence spectrum. The correlation functions can be determined from the two-time optical Bloch equations (5.8). Instead of the three components $Y_1(t,t')$, $Y_2(t,t')$ and $Y_3(t,t')$, we introduce the following linear combinations

$$\begin{aligned}
V\left(t,t'\right) &= \frac{1}{2}\left[Y_1\left(t,t'\right) - Y_2\left(t,t'\right)\right] \,, \\
U\left(t,t'\right) &= Y_3\left(t,t'\right) + \frac{\mathrm{i}}{2}\left[Y_1\left(t,t'\right) + Y_2\left(t,t'\right)\right] \,, \\
W\left(t,t'\right) &= Y_3\left(t,t'\right) - \frac{\mathrm{i}}{2}\left[Y_1\left(t,t'\right) + Y_2\left(t,t'\right)\right] \,,
\end{aligned} \tag{5.78}$$

where $Y_k\left(t,t'\right)$ are defined in (5.7). In terms of the new variables, and assuming $\Delta = 0$ and $\phi_1 = 0$, the two-time optical Bloch equations (5.8) take the form

$$\begin{aligned}
\frac{\mathrm{d}}{\mathrm{d}t'} V\left(t,t'\right) &= -\frac{1}{2}\gamma V\left(t,t'\right) \,, \\
\frac{\mathrm{d}}{\mathrm{d}t'} U\left(t,t'\right) &= -\frac{3}{4}\gamma U\left(t,t'\right) - \frac{1}{4}\gamma W\left(t,t'\right) + \mathrm{i}\Omega\left(t'\right) U\left(t,t'\right) \,, \\
\frac{\mathrm{d}}{\mathrm{d}t'} W\left(t,t'\right) &= -\frac{3}{4}\gamma W\left(t,t'\right) - \frac{1}{4}\gamma U\left(t,t'\right) - \mathrm{i}\Omega\left(t'\right) W\left(t,t'\right) \,.
\end{aligned} \tag{5.79}$$

It follows from (5.79) that $V\left(t,t'\right)$ is independent of the driving field and is decoupled from the remaining variables. Its solution has the simple exponential form

$$V\left(t,t'\right)=V\left(t,t\right)\exp\left[-\frac{1}{2}\gamma\left(t'-t\right)\right]\,,\quad t'>t\,, \tag{5.80}$$

where $V\left(t,t\right)$ is the initial value of $V\left(t,t'\right)$.

The remaining variables $U\left(t,t'\right)$ and $W\left(t,t'\right)$, which depend on the driving field, are coupled to each other through the damping term $\gamma/4$. Proceeding in the same manner as in solving (5.71), we assume that $\Omega_0 \gg \gamma, \Omega_1$ and after introducing new variables

$$\tilde{U}\left(t,t'\right)=U\left(t,t'\right)\mathrm{e}^{-\mathrm{i}\Omega_0(t'-t)}\,,\quad \tilde{W}\left(t,t'\right)=W\left(t,t'\right)\mathrm{e}^{\mathrm{i}\Omega_0(t'-t)}\,, \tag{5.81}$$

we find that in terms of these new variables (5.79) becomes

$$\begin{aligned}\frac{\mathrm{d}}{\mathrm{d}t'}\tilde{U}\left(t,t'\right)&=-\left(\frac{3}{4}\gamma-2\mathrm{i}\Omega_1\cos\delta t'\right)\tilde{U}\left(t,t'\right)-\frac{1}{4}\gamma\tilde{W}\left(t,t'\right)\mathrm{e}^{-2\mathrm{i}\Omega_0 t'}\,,\\ \frac{\mathrm{d}}{\mathrm{d}t'}\tilde{W}\left(t,t'\right)&=-\left(\frac{3}{4}\gamma+2\mathrm{i}\Omega_1\cos\delta t'\right)\tilde{W}\left(t,t'\right)-\frac{1}{4}\gamma\tilde{U}\left(t,t'\right)\mathrm{e}^{2\mathrm{i}\Omega_0 t'}\,.\end{aligned} \tag{5.82}$$

We see that certain terms are slowly varying while others oscillate rapidly at twice the Rabi frequency Ω_0. After dropping these rapidly oscillating terms we obtain approximate equations of motion for $\tilde{U}\left(t,t'\right)$ and $\tilde{W}\left(t,t'\right)$, which are decoupled from one another. These approximate equations of motion can now be solved by a direct integration and the results are

$$\begin{aligned}U\left(t,t'\right)&=U\left(t,t\right)\mathrm{e}^{-\left(\frac{3}{4}\gamma-\mathrm{i}\Omega_0\right)\left(t'-t\right)+\mathrm{i}\beta\left(\sin\delta t'-\sin\delta t\right)}\,,\\ W\left(t,t'\right)&=W\left(t,t\right)\mathrm{e}^{-\left(\frac{3}{4}\gamma+\mathrm{i}\Omega_0\right)\left(t'-t\right)-\mathrm{i}\beta\left(\sin\delta t'-\sin\delta t\right)}\,.\end{aligned} \tag{5.83}$$

When the Fourier decomposition (5.72) is used in (5.83), we obtain

$$\begin{aligned}U\left(t,t'\right)&=U(t,t)\sum_{n,m}J_n(\beta)J_m(-\beta)\mathrm{e}^{-\left[\frac{3}{4}\gamma-\mathrm{i}(\Omega_0+n\delta)\right]\left(t'-t\right)}\mathrm{e}^{\mathrm{i}(n+m)\delta t}\,,\\ W\left(t,t'\right)&=W(t,t)\sum_{n,m}J_n(-\beta)J_m(\beta)\mathrm{e}^{-\left[\frac{3}{4}\gamma+\mathrm{i}(\Omega_0+n\delta)\right]\left(t'-t\right)}\mathrm{e}^{\mathrm{i}(n+m)\delta t}\,.\end{aligned} \tag{5.84}$$

If in (5.84) we make the change of variable $t'-t=\tau$ and take the long-time limit $t\to\infty$, we find that only terms with $m=-n$ become independent of t. We then obtain

$$\begin{aligned}U_s(\tau)&\equiv\lim_{t\to\infty}U(t,t+\tau)=\lim_{t\to\infty}U(t,t)\sum_n J_n^2\left(\beta\right)\mathrm{e}^{-\left[\frac{3}{4}\gamma-\mathrm{i}(\Omega_0+n\delta)\right]\tau}\,,\\ W_s(\tau)&\equiv\lim_{t\to\infty}W(t,t+\tau)=\lim_{t\to\infty}W(t,t)\sum_n J_n^2\left(\beta\right)\mathrm{e}^{-\left[\frac{3}{4}\gamma+\mathrm{i}(\Omega_0+n\delta)\right]\tau}\,.\end{aligned} \tag{5.85}$$

The long-time values of $V(t,t)$, $U(t,t)$, and $W(t,t)$ can be expressed in terms of the expectation values of the dressed-atom operators as

$$\begin{aligned} V_s &\equiv \lim_{t\to\infty} V(t,t) = -\frac{1}{4}\left(\langle R_{12}^s\rangle + \langle R_{21}^s\rangle + 1\right) , \\ U_s &\equiv \lim_{t\to\infty} U(t,t) = \frac{\mathrm{i}}{4}\left[1 + 2\langle R_2^s\rangle\left(\langle R_{12}^s\rangle - \langle R_{21}^s\rangle + 1\right)\right] , \\ W_s &\equiv \lim_{t\to\infty} W(t,t) = -\frac{\mathrm{i}}{4}\left[1 + 2\langle R_{21}^s\rangle\left(\langle R_{21}^s\rangle - \langle R_{12}^s\rangle + 1\right)\right] . \end{aligned} \tag{5.86}$$

Note from (5.74) that $\langle R_{12}^s\rangle$ and $\langle R_{21}^3\rangle$ decrease to zero as the Rabi frequency Ω_0 increases, i.e., as $\Omega_0 \to \infty$. Provided the limit $\Omega_0 \gg \gamma, \Omega_1$, the long-time solutions (5.86) can be approximated, without introducing any significant errors, by $V_s = -1/4$, $U_s = \mathrm{i}/4$ and $W_s = -\mathrm{i}/4$.

Having the two-time correlation functions available, we can evaluate the incoherent part of the spectrum. According to the definition (2.17), the incoherent part of the spectrum is determined by the two-time correlation function $\langle \delta S^+(t)\delta S^-(t')\rangle \equiv Y_2\left(t,t'\right)$. Using (5.78), we readily find that $Y_2\left(t,t'\right)$ can be expressed by the linear combinations $V(t,t')$, $U(t,t')$ and $W(t,t')$ as

$$Y_2\left(t,t'\right) = -V\left(t,t'\right) + \frac{\mathrm{i}}{2}\left[W\left(t,t'\right) - U\left(t,t'\right)\right] . \tag{5.87}$$

Since in the long-time limit $V(t,t')$, $U(t,t')$ and $W(t,t')$ are independent of t, we may use the expression (2.19) for the spectrum, which in the case of a single two-level atom reads

$$\begin{aligned} S_{\mathrm{in}}(\omega) &= 2\gamma \mathrm{Re}\int_0^\infty \mathrm{d}\tau\, \langle \delta S^+(0)\, \delta S^-(\tau)\rangle \mathrm{e}^{\mathrm{i}(\omega-\omega_L)\tau} \\ &= 2\gamma \mathrm{Re}\int_0^\infty \mathrm{d}\tau Y_2(0,\tau)\, \mathrm{e}^{\mathrm{i}(\omega-\omega_L)\tau} . \end{aligned} \tag{5.88}$$

When the relation (5.87) is inserted in (5.88) together with (5.80) and (5.85), and we pass to the long-time limit at which $V_s = -1/4$, $U_s = \mathrm{i}/4$ and $W_s = -\mathrm{i}/4$, we readily find the explicit analytical expression of the fluorescence spectrum

$$\begin{aligned} S_{\mathrm{in}}(\omega) = {} & \frac{\frac{1}{4}\gamma^2}{\frac{1}{4}\gamma^2 + (\omega-\omega_L)^2} + \frac{3}{16}\sum_n \frac{J_n^2(\beta)\,\gamma^2}{\frac{9}{16}\gamma^2 + (\omega-\omega_L+\Omega_0+n\delta)^2} \\ & + \frac{3}{16}\sum_n \frac{J_n^2(\beta)\,\gamma^2}{\frac{9}{16}\gamma^2 + (\omega-\omega_L-\Omega_0+n\delta)^2} . \end{aligned} \tag{5.89}$$

Clearly, the spectrum (5.89) consists of three components, the central component, essentially the same as those of the Mollow triplet of a monochromatically driven

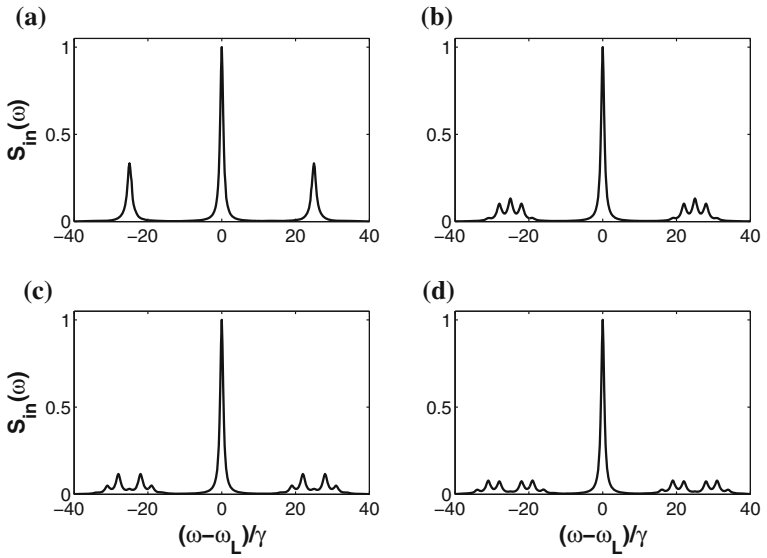

Fig. 5.4 The fluorescence spectrum of a two-level atom driven by an amplitude modulated field for $\omega_L = \omega_a, \delta = 3\gamma, \Omega_0 = 25\,\gamma$, and for several values of Ω_1: **a** $\Omega_1 = 0$, **b** $\Omega_1 = 2\gamma$, **c** $\Omega_1 = 3\gamma$, and **d** $\Omega_1 = 4\gamma$

atom, and two multi-peak structures of discrete lines centered about $\pm\Omega_0$ and separated by $n\delta$.

In Fig. 5.4 we plot the fluorescence spectrum for $\delta = 3\gamma$, $\Omega_0 = 25\gamma$, and several different values of Ω_1. We see that the central component is not sensitive to the presence of the modulating fields. Moreover, positions and widths are insensitive to the Rabi frequencies of the driving fields. The number of sidebands, however, increases with an increasing Rabi frequency of the modulating fields. Thus, the spectral lines do not suffer power broadening and the Stark shift, indicating that spontaneous emission from the system occurs at the well defined frequencies.

As we have already mentioned, the most interesting feature of the spectrum is the insensitivity of the central component to the presence of the modulating fields. Hence, not all spectral lines are sensitive to the modifications of the driving field. Behavior of this kind can be interpreted as being a consequence of the cancelation of dipole moments at frequencies ω_λ close to but different than ω_a. We treat the system in a manner similar to that of Sect. 5.2.5, as a doubly dressed system in which the atom is first dressed by the strong resonant component of the driving field, and the resulting singly dressed atom then dressed again by the weaker detuned (modulating) fields, which can be treated as a single bichromatic field with the components equally detuned from the atomic transition frequency.

The Hamiltonian of the noninteracting singly dressed-atom characterized by the dressed states $|n, \tilde{i}\rangle$, and two single-mode modulating fields is given by

$$\hat{H}_0 = \hat{H}_d + \hbar\,(\omega_a + \delta)\,\hat{a}_+^\dagger \hat{a}_+ + \hbar\,(\omega_a - \delta)\,\hat{a}_-^\dagger \hat{a}_- \,, \tag{5.90}$$

where $\hat{H}_d$ is the Hamiltonian of the singly dressed atom, which satisfies the eigenvalue equation

$$\hat{H}_d \left| n, \tilde{i} \right\rangle = \hbar \left[n\omega_a + (-1)^i \frac{1}{2}\Omega_0 \right] \left| n, \tilde{i} \right\rangle \,, \tag{5.91}$$

and $\hat{a}_\pm^\dagger$ ($\hat{a}_\pm$) are the creation (annihilation) operators of the modulating field modes of frequencies $\omega_a \pm \delta$, respectively.

The Hamiltonian $\hat{H}_0$ has the eigenvalue equation

$$\hat{H}_0 \left| n, \tilde{i}, s \right\rangle = \hbar \left[n\omega_a + (-1)^i \frac{1}{2}\Omega_0 + (2m + s)\,\delta \right] \left| n, \tilde{i}, s \right\rangle \,, \tag{5.92}$$

where $|n, \tilde{i}, s\rangle \equiv |(n-2m)\,, \tilde{i}\rangle \otimes |m\,+\,s\rangle \otimes |m\rangle$ are the undressed states of the non-interacting singly dressed-atom system and the modulating fields, $|m + s\rangle$ is the eigenstate of the sideband mode $\omega_a + \delta$, and $|m\rangle$ is the eigenstate of the mode $\omega_a - \delta$. The states $|n, \tilde{i}, s\rangle$ group into manifolds separated by ω_a. Each manifold is composed of two sets of an infinite number of states with an interset splitting Ω_0 and an intra-set splitting δ.

When we include the interaction

$$\hat{H}_I = -\mathrm{i}\hbar g_1 \left(\hat{a}_+ S^+ - S^- \hat{a}_+^\dagger \right) - \mathrm{i}\hbar g_1 \left(\hat{a}_- S^+ - S^- \hat{a}_-^\dagger \right) \tag{5.93}$$

between the singly dressed atom and the modulating fields, the nondegenerate states $|n, \tilde{i}, s\rangle$ recombine into nondegenerate doubly dressed states $|n, \tilde{i}, p\rangle$, which satisfy the eigenvalue equation

$$\left(\hat{H}_0 + \hat{H}_I \right) \left| n, \tilde{i}, p \right\rangle = E_{n,\tilde{i}}^{(p)} \left| n, \tilde{i}, p \right\rangle \,, \tag{5.94}$$

where

$$\left| n, \tilde{i}, p \right\rangle = \sum_{s=-\infty}^{\infty} J_{s-p} \left(-\frac{2\Omega_1}{\delta} \right) \left| n, \tilde{i}, s \right\rangle \,, \tag{5.95}$$

and

$$E_{n,\tilde{i}}^{(p)} = \hbar \left[n\omega_a + (-1)^i \frac{1}{2}\Omega_0 + \, p\delta \right] \,. \tag{5.96}$$

The doubly dressed states group into an infinite ladder of manifolds separated by ω_a, with each manifold composed of two sub-manifolds separated by Ω_0. Each sub-manifold is composed of an infinite number of states separated by δ.

Let us check what would be a possible structure of the spectrum at the central component, which results from $|n, \tilde{1}, p\rangle \rightarrow |n-1, \tilde{1}, q\rangle$ and from $|n, \tilde{2}, p\rangle \rightarrow |n-1, \tilde{2}, q\rangle$ transitions within neighboring manifolds. The transitions occur with frequencies

$$\omega_{pq} = \frac{1}{\hbar}\left(E^{(p)}_{n,\tilde{i}} - E^{(q)}_{n-1,\tilde{i}}\right) = \omega_a + (p-q)\delta \,. \tag{5.97}$$

This suggests that a multi-peak structure at the central component of the spectrum should be expected. The number of lines in fact depends on the transition dipole moments between the corresponding dressed states. We show this by considering the transition dipole moments corresponding to the frequencies $\omega_a + (p-q)\delta$. Using the dressed states (5.95) and the summation properties of the Bessel functions, we find that the relevant transition dipole moments are

$$\boldsymbol{\mu}_{pq} = \left\langle p, \tilde{i}, n \middle| \boldsymbol{\mu} \middle| n-1, \tilde{i}, q \right\rangle = \frac{1}{2}\boldsymbol{\mu}_a \delta_{pq} \,. \tag{5.98}$$

It is clear from this result that the dipole moments corresponding to transitions with $p \neq q$ are all equal to zero, indicating a suppression of spontaneous emission at those frequencies. Under this circumstance only a single peak at ω_a can be present in the spectrum. This also shows that the central line of the spectrum is not attributable to a multi-peak splitting by the amplitude modulated field.

5.4 Excitation with Two Fields of Equal Frequencies

The phenomena described in the previous section arise from the excitation of a two-level atom by two fields having different frequencies. In this section, we consider driving the atom with two laser beams of equal frequencies [18]. We assume that the two beams are derived from separate sources and have no fixed phase relation. If the two beams have had a fixed relative phase this would be equivalent to driving the atom with a monochromatic field whose electric field is the vector sum of those of the two fields. With the mutual random phases of the beams, the two beams could be regarded as a single beam with a phase that performs a random walk.

We calculate the fluorescence spectrum assuming that the angular frequencies of both fields are equal to the atomic transition frequency ω_a, but again consider that the two fields have significantly different Rabi frequencies, $\Omega_0 \gg \Omega_1$. Since one of the fields is intense, a dressed-atom model provides a good approach for studying the problem. Although the Floquet method, developed in the preceding section, can

be adopted to this situation, but it becomes cumbersome when the frequencies are degenerate.

The starting point of our calculation is the singly dressed system, produced by the the strong laser field interacting with the two-level atom. The dressed states $|n, \tilde{i}\rangle$ $(i = 1, 2)$ are of the same form as those given in (5.52). The presence of the weaker field results in product (undressed) states $|n, \tilde{i}\rangle \otimes |p\rangle$, where $p = 1, 2, \ldots, \infty$ is the number of photons in the weaker field. The Hamiltonian $\hat{H}_0$ of the noninteracting dressed-atom + weaker field satisfies the eigenvalue equation

$$\hat{H}_0 \left| (n-p)\,\tilde{i},\, p \right\rangle = \hbar \left[n\omega_a + (-1)^i \frac{1}{2}\Omega_0 \right] \left| (n-p)\,\tilde{i},\, p \right\rangle , \tag{5.99}$$

where $|\,(n-p)\,\tilde{i},\, p\rangle \equiv |(n-p)\,\tilde{i}\rangle \otimes |p\rangle$. We treat the states $|(n-p)\,\tilde{i},\, p\rangle$ as basis states for the dressing of the singly dressed system with the weaker field.

The undressed states group into manifolds each containing two sets of an infinite number of degenerate states, as illustrated in Fig. 5.5a. We now include the interaction between the singly dressed atom and the weaker field which is described by the interaction Hamiltonian of the same form as (5.55). In the limit of $\Omega_0 \gg \Omega_1$, the interaction $\hat{H}_I$ has matrix elements given by

$$\begin{aligned} H_{pq}^{(i)} &= \left\langle (n-p)\,\tilde{i},\, p \right| \hat{H}_I \left| (n-q)\,\tilde{i},\, q \right\rangle \\ &= (-1)^i \frac{1}{2}\hbar g_1 \left(\sqrt{p+1}\,\delta_{p+1,q} + \sqrt{p}\,\delta_{p-1,q} \right) . \end{aligned} \tag{5.100}$$

The matrix which represents $\hat{H}_I$ in the manifold $|(n-p)\,\tilde{i},\, p\rangle$ is the infinite two-diagonal matrix

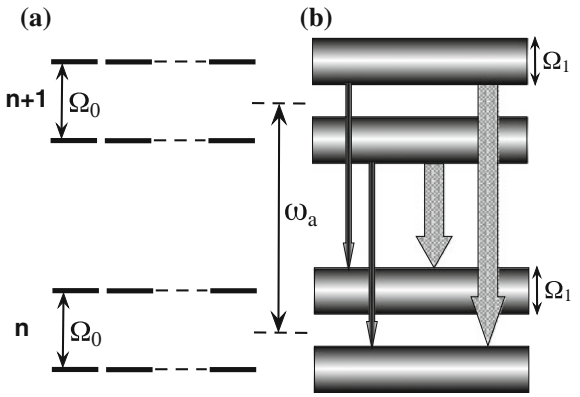

Fig. 5.5 Energy level spectra of the **a** undressed states and **b** doubly dressed states. The arrows represent spontaneous transitions

$$M = \pm\frac{1}{2}\hbar g_1 \begin{pmatrix} 0 & \sqrt{1} & 0 & 0 & \cdots \\ \sqrt{1} & 0 & \sqrt{2} & 0 & \cdots \\ 0 & \sqrt{2} & 0 & \sqrt{3} & \cdots \\ 0 & 0 & \sqrt{3} & 0 & \cdots \\ \vdots & \vdots & \vdots & \vdots & \end{pmatrix} . \tag{5.101}$$

The eigenvalues λ of M are found by setting $\det|M - \lambda I| \equiv 0$, where I is the unit matrix. Note that the matrix M has the same form as that which represents the position operator in the basis of the energy eigenstates of the one-dimensional harmonic oscillator. Therefore, λ is an arbitrary real number.

If we represent the eigenvectors by the column vector $\boldsymbol{a} \equiv (a_0, a_1, a_2, \ldots)$, we then find that the eigenvalue equation $M\boldsymbol{a} = \lambda\boldsymbol{a}$ yields the recursion relation

$$\sqrt{p}a_{p-1} + \sqrt{p+1}a_{p+1} = \pm\lambda a_p , \tag{5.102}$$

If we choose

$$a_p = \frac{1}{\sqrt{2^p\, p!}}U_p , \tag{5.103}$$

where U_p is a function we want to determine, we then find that the recurrence relation (5.102) takes the form

$$2\frac{(\pm\lambda)}{\sqrt{2}}U_p = 2pU_{p-1} + U_{p+1} . \tag{5.104}$$

Comparing (5.104) with the recursion relation for the Hermite polynomials $H_p(x)$ [17],

$$2xH_p(x) = 2pH_{p-1}(x) + H_{p+1}(x) , \tag{5.105}$$

we find that $x = \pm\lambda/\sqrt{2}$ and the eigenvector is defined by

$$a_p = \left(\sqrt{2\pi}\, 2^p\, p!\right)^{-\frac{1}{2}} H_p\,(x)\, \mathrm{e}^{-\frac{1}{2}x^2} . \tag{5.106}$$

Thus, the eigenvectors (doubly dressed states) can thus be written in the form

$$|n\pm, \lambda\rangle = \sum_{p=0}^{\infty} \phi_p \left(\pm\frac{\lambda}{\sqrt{2}}\right) |(n-p)\pm, p\rangle , \tag{5.107}$$

with corresponding energies

$$E_{n\lambda}^{(\pm)} = \hbar\left[n\omega_a \pm \left(\Omega_0 + \frac{1}{2}\lambda g_1\right)\right] , \qquad -\infty < \lambda < \infty , \tag{5.108}$$

where

$$\phi_p(x) = \left(\sqrt{2\pi}\, 2^p p!\right)^{-\frac{1}{2}} H_p(x)\, \mathrm{e}^{-\frac{1}{2}x^2} , \tag{5.109}$$

and $H_p(x)$ is the Hermite polynomial of order p.

The doubly dressed states (5.107) obey the orthonormality and completeness relations

$$\langle \lambda', \pm n | m\pm, \lambda \rangle = \delta_{nm}\delta(\lambda - \lambda') , \tag{5.110}$$

and

$$\sum_{n,\pm} \int \mathrm{d}\lambda\, |n\pm, \lambda\rangle \langle \lambda, \pm n| = 1 . \tag{5.111}$$

The energy levels of the doubly dressed atom group into manifolds each containing doublet of finite size continua, as illustrated in Fig. 5.5b. Neighboring manifolds are separated by frequency ω_a, while the pair of continua making up each doublet is separated by Ω_0. The finite size of the continua results from the fact that the population distribution inside a continuum is determined by $|\phi_p(\lambda/\sqrt{2})|^2$. From the theory of the quantum harmonic oscillator, it is well known that the function $|\phi_p(\lambda/\sqrt{2})|^2$ is nonzero for $|\lambda| < |\lambda_p|$, where $\pm\lambda_p/\sqrt{2}$ are the classical turning points of the oscillator, and goes rapidly to zero for $|\lambda| > |\lambda_p|$.

The structure of the doubly dressed states would seem to suggest that the emitted radiation (fluorescence) should have a spectrum consisting of three continuum structures, one centered at frequency ω_a and the other two centered at the Rabi sidebands, $\omega_a \pm \Omega_0$. This, however, is not the case. In order to see it, let us calculate the dipole transition moments between the doubly dressed states. With the help of the orthonormality and completeness relations (5.110) and (5.111), we find

$$\begin{aligned} \langle \lambda, \pm n| S^+ \left|(n-1)\pm, \lambda'\right\rangle &= \mp\frac{1}{2}\delta(\lambda - \lambda') , \\ \langle \lambda, \mp n| S^+ \left|(n-1)\pm, \lambda'\right\rangle &= \pm\frac{1}{2}\delta(\lambda + \lambda') , \end{aligned} \tag{5.112}$$

where the difference in sign within the arguments of the delta functions originates from the parity of the eigenstates

$$\phi_p(-x) = (-1)^p\, \phi_p(x) . \tag{5.113}$$

Transition rates between the continua of neighboring manifolds are given by the expressions

$$\gamma_{\pm\pm} = \gamma \left|\langle N \pm \lambda| S^+ \left|(N-1) \pm \lambda'\right\rangle\right|^2 = \frac{1}{4}\gamma_\delta\left(\lambda - \lambda'\right) ,$$
$$\gamma_{\pm\mp} = \gamma \left|\langle N \pm \lambda| S^+ \left|(N-1) \mp \lambda'\right\rangle\right|^2 = \frac{1}{4}\gamma_\delta\left(\lambda + \lambda'\right) , \qquad (5.114)$$

and correspond to transition frequencies

$$\omega_{\pm\lambda,\pm\lambda'} = \hbar^{-1}\left(E^{(\pm)}_{n\lambda} - E^{(\pm)}_{(n-1)\lambda'}\right) = \omega_a + \frac{1}{2}(\lambda - \lambda')g_1 ,$$
$$\omega_{\pm\lambda,\mp\lambda'} = \hbar^{-1}\left(E^{(\pm)}_{n\lambda} - E^{(\mp)}_{(n-1)\lambda'}\right) = \omega_a \pm \Omega_0 + \frac{1}{2}(\lambda - \lambda')g_1 . \qquad (5.115)$$

From (5.114) we see that the dipole moments corresponding to transitions at frequencies $\omega_{\pm\lambda,\pm\lambda'}$ with $\lambda \neq \lambda'$ are all equal to zero, indicating a suppression of spontaneous emission at those frequencies. These modifications will exhibit themselves through changes in the resonance fluorescence spectrum. This means that the central line of the spectrum is expected to be a Lorentzian-like structure with the effective width $\gamma/2$ rather than a continuum structure. On the other hand, at the Rabi sidebands only those dipole moments are zero which correspond to transitions with $\lambda \neq -\lambda'$. Clearly, the Rabi sidebands will be in a form of broad continua created by a set of transitions at frequencies $\omega_a \pm \Omega_0 + \lambda g_1$. Thus, quantum fluctuations of the vacuum field are stable at the transitions corresponding to the central component of the spectrum, but are very unstable at frequencies corresponding to the Rabi sidebands.

With the spontaneous emission included, the behavior of the system is governed by the master equation

$$\frac{\partial \varrho}{\partial t} = -\frac{\mathrm{i}}{\hbar}\left[\hat{H}_0 + \hat{H}_I, \varrho\right] - \frac{1}{2}\gamma\left(\varrho S^+ S^- + S^+ S^- \varrho - 2S^- \varrho S^+\right) , \qquad (5.116)$$

where ϱ is the reduced density operator, which in the representation of the doubly dressed states (5.108) can be written as

$$\varrho = \sum_{i,j=1}^{2}\sum_{n,m}\int\int \mathrm{d}\lambda \mathrm{d}\lambda' \varrho_{ij,n,m}(\lambda,\lambda')\left|n,\tilde{i},\lambda\right\rangle\left\langle\lambda',\tilde{j},m\right| , \qquad (5.117)$$

where the diagonal matrix elements $P_{i,n}(\lambda,t) = \langle\lambda,\tilde{i},n|\varrho(t)|n,\tilde{i},\lambda\rangle$ are the populations of the doubly dressed states and the off-diagonal matrix elements $\varrho_{ij,n}(t)$ are the coherences between them.

We use the master equation to calculate the populations of the dressed state continua and coherences between them, needed for the evaluation of the fluorescence spectrum. For the populations of the dressed states, we project the master equation (5.116) onto $|n,\tilde{i},\lambda\rangle$ on the right and $\langle\lambda,\tilde{i},n|$ on the left, and average over n. The resulting equations of motion for the reduced populations, $P_i(\lambda,t) = \sum_n \varrho_{ii,n}(\lambda,\lambda)$ are

$$\dot{P}_1(\lambda,t) = -\frac{1}{4}\gamma P_1(\lambda,t) + \frac{1}{4}\gamma P_2(\lambda,t)\ ,$$
$$\dot{P}_2(\lambda,t) = -\frac{1}{4}\gamma P_2(\lambda,t) + \frac{1}{4}\gamma P_1(\lambda,t)\ . \tag{5.118}$$

It is easy to find that the steady-state populations of the doubly dressed states are

$$P_1(\lambda,t) = P_2(\lambda,t) = \frac{1}{2}\left|\phi_p\left(\frac{\lambda}{\sqrt{2}}\right)\right|^2\ , \tag{5.119}$$

where $\phi_p\left(\lambda/\sqrt{2}\right)$ is given in (5.109). We see that the continua are equally populated. Within each continuum, however, the population distribution depends on λ; it has maxima for $\lambda/\sqrt{2}$ in the vicinity of the classical turning points of the harmonic oscillator eigenfunction $\phi_p\left(\lambda/\sqrt{2}\right)$, i.e., for $\lambda_p \approx \pm 2\sqrt{p+\frac{1}{2}}$, or for energies $\frac{1}{2}\left|\lambda_p\right|\hbar g_1 \approx \hbar g_1\sqrt{p} = \frac{1}{2}\hbar\Omega_1$. For $|\lambda| < \left|\lambda_p\right|$ the population $P(\lambda)$ is nonzero, while for $|\lambda| > \left|\lambda_p\right|$, $P(\lambda)$ goes rapidly to zero.

For the coherences between the dressed states, we project the master equation (5.116) onto $|n-1,\tilde{j},\lambda\rangle$ on the right and $\langle\lambda,\tilde{i},n|$ on the left, and average over n. The resulting equations are

$$\dot{\varrho}_{12}(\lambda,\lambda') = -\left\{\frac{3}{4}\gamma + \mathrm{i}\left[\omega_a + \Omega_0 + \left(\lambda-\lambda'\right)g_1\right]\right\}\varrho_{12}(\lambda,\lambda')\ ,$$
$$\dot{\varrho}_{21}(\lambda,\lambda') = -\left\{\frac{3}{4}\gamma + \mathrm{i}\left[\omega_a - \Omega_0 + (\lambda-\lambda')g_1\right]\right\}\varrho_{21}(\lambda,\lambda')\ , \tag{5.120}$$

and

$$\dot{\varrho}_{11}(\lambda,\lambda') = -\left\{\frac{1}{4}\gamma + \mathrm{i}\left[\omega_a + \left(\lambda-\lambda'\right)g_1\right]\right\}\varrho_{11}(\lambda,\lambda') + \frac{1}{4}\gamma\varrho_{22}(\lambda,\lambda')\ ,$$
$$\dot{\varrho}_{22}(\lambda,\lambda') = -\left\{\frac{1}{4}\gamma + \mathrm{i}\left[\omega_a + (\lambda-\lambda')g_1\right]\right\}\varrho_{22}(\lambda,\lambda') + \frac{1}{4}\gamma\varrho_{11}(\lambda,\lambda')\ . \tag{5.121}$$

The fluorescence spectrum is given by the real part of the Fourier transform of the two-time correlation function of the atomic dipole moments. Following the standard dressed-atom procedure, we find that the incoherent part of the fluorescence spectrum is given by

$$S_{\text{in}}(\omega) = \frac{\frac{1}{4}\gamma^2}{(\omega-\omega_L)^2+\left(\frac{1}{2}\gamma\right)^2} + \int_{-\infty}^{\infty} d\lambda \left|\phi_p\left(\frac{\lambda}{\sqrt{2}}\right)\right|^2 \left[\frac{\frac{3}{16}\gamma^2}{(\omega-\omega_L-\Omega_0-\lambda g_1)^2+\left(\frac{3}{4}\gamma\right)^2} + \frac{\frac{3}{16}\gamma^2}{(\omega-\omega_L+\Omega_0-\lambda g_1)^2+\left(\frac{3}{4}\gamma\right)^2}\right]. \quad (5.122)$$

This result shows that the central component of the spectrum is a Lorentzian of the width $\gamma/2$, which is the same as in the case of the monochromatic excitation. The Rabi sidebands consist of a convolution of Lorentzians, centered at $\omega_L \pm \Omega_0 - \lambda g_1$ and having widths $3\gamma/4$, multiplied by a weight factor $|\phi_p(\lambda/\sqrt{2})|^2$. Because $|\phi_p(\lambda/\sqrt{2})|^2$ has maxima near the classical turning points, the sidebands display continua centered at $\omega_L \pm \Omega_0$ of widths $\sim \Omega_1$. The spectrum given by the expression (5.122) is plotted in Fig. 5.6 for $\Omega = 20\gamma$ and $\Omega_1 = 7\gamma$.

Comparison of Figs. 5.2 and 5.6 immediately shows the difference that unequal and equal angular frequencies of the components of the driving field have on the spectrum. The driving bichromatic field can result in a multiplet structure of the spectrum and suppression of the central component of the spectrum, whereas for the driving field with two equal frequencies, the spectrum exhibits triplet component, characteristic of the monochromatic driving, with the central component unaffected by the presence of the second field. In fact, in both cases the dynamical suppression of spontaneous emission takes place but the effect appears at different frequencies. For the bichromatic field, the suppression can appear at frequency of the stronger com-

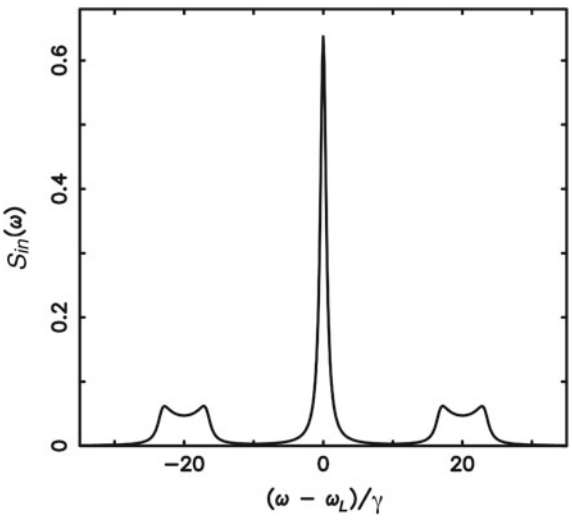

Fig. 5.6 The fluorescence spectrum of a two-level atom driven by two fields of equal frequencies, $\omega_L = \omega_1 = \omega_a$, but different Rabi frequencies, $\Omega = 20\gamma$ and $\Omega_1 = 7\gamma$

ponent of the driving field, whereas for the driving field with two equal frequencies the suppression appears at frequencies different from the driving fields.

5.5 Experimental Verification of the Dynamical Suppression of Spontaneous Emission

It was predicted in Sect. 5.2.5 that a two-level atom driven by a bichromatic field with one strong component on resonance with the atomic transition and the other on resonance with the Rabi sideband does not radiate at the atomic frequency. Consequently, the central component at the atomic frequency is absent leaving the fluorescence spectrum composed of spectral lines at frequencies different from the atomic frequency. Moreover, it was predicted that the central component of the fluorescence spectrum of a two-level atom driven by two equal frequency fields or by an amplitude modulated field is the same as in the case of the monochromatic driving field. This was interpreted also as the result of the cancelation of spontaneous emission at some spectral frequencies close to the atomic frequency [13, 19]. Interesting modifications of the spectrum such as continuous or multi-peak structures have been predicted at spectral frequencies significantly different from the atomic frequency. In this section, we focus on experimental studies which were aimed to verify some of these interesting features of the fluorescence spectrum. We start describing experiments by the Mossberg's group in Oregon involving atomic beams [20]. It is followed by describing very elegant experiments performed by the Pan's group at the Hefei National Laboratory in China which involved deposited quantum dots [21].

5.5.1 Experiments with Doubly Driven Atomic Beams

The modifications of the fluorescence spectrum of barium atoms under a bichromatic field excitation and a variety of conditions were observed in a series of experiments carried out by the Mossberg's group in Oregon [20]. The experiments showed the fluorescence spectra with multi-peak structures, intensity-independent peak separation, intensity-dependent peak quantity, and alternating peak linewidths due to the time variation of the Rabi frequency of the driving field. Here, we focus on the experimental study which was aimed to verify the fluorescence spectrum for the special case of a bichromatic field composed of one (strong) frequency component resonant to the atomic transition and the other (weaker) component detuned from the atomic resonance by $\delta = \Omega_0$. As demonstrated in Sect. 5.2.5, the theory predicts the absence of the central component of the spectrum.

The schematic setup of the experiment is given in Fig. 5.7. The apparatus involved a beam of barium atoms driven by a bichromatic field inside a confocal Fabry–Perot cavity. The atoms traveled in a collimated atomic beam at right angle to the opti-

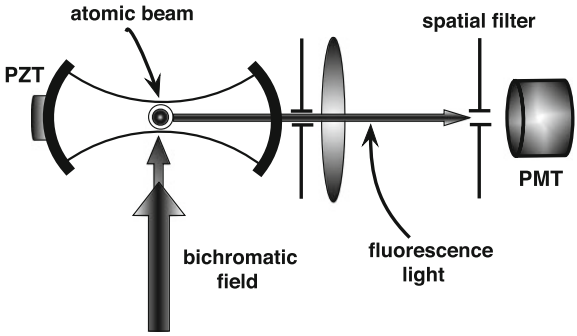

Fig. 5.7 Schematic diagram of the experiment to observe the fluorescence spectrum of a two-level atom driven by a bichromatic field

cal axis of the cavity. The linearly polarized output of a single-mode cw, ring laser was frequency-locked via saturation spectroscopy techniques to frequency ω_a of the $^1S_0 \leftrightarrow {}^1P_1$ transition in the ^{138}Ba barium atoms. Since ^{138}Ba has zero nuclear spin, the $^1S_0 \leftrightarrow {}^1P_1$ transition closely approximates a two-level system. An acusto-optic modulator (AOM) was used to create the second tunable driving field component with frequency $\omega_2 = \omega_a - 2\Delta_{\rm rf}$, where $\Delta_{\rm rf} = 110$ MHz is the AOM drive frequency. The frequency difference between the two field components $\delta = \omega_a - \omega_2 = 220$ MHz was equal to the Rabi frequency Ω_0 of the resonant component. An electro-optic modulator (EOM) was employed to vary the Rabi frequency of the ω_2 driving field component. Since both the resonant and detuned components of the driving bichromatic field originated from the same laser source and traveled along essentially the same optical path, their relative phase was fixed by the relative phase of a rf field used to create the bichromatic field. To ensure uniform laser intensity throughout the atom-field interaction region, the atomic beam was collimated to 0.75 mm in diameter and the bichromatic field was collimated to a full-width-at-half-maximum (FWHM) diameter of 3 mm to create a spatially homogeneous excitation field. Both components of the bichromatic field were linearly polarized in the same direction, and intersected the atomic beam at right angles.

The fluorescence spectra were measured by monitoring the fluorescence intensity emitted out one end of the cavity as a function of cavity length and therefore the cavity transmission frequency. The cavity length was varied by using a piezoelectric crystal (PZT) mounted on one of the cavity mirrors. The resolution of the observed fluorescence spectra was limited by an instrumental resolution $\gamma_c \approx 13$ MHz arising from finite cavity resolution and residual atomic beam Doppler broadening. The experimental spectral resolution γ_c was deducted from the observed width of weak signal elastic scattering. When probed by a weak monochromatic laser field, the atomic beam displayed an absorption linewidth of 21 MHz, with the excess width as compared to $\gamma = 19$ MHz attributed to the angular spread of the atomic beam and excitation laser bandwidth ($\sim$1 MHz).

Figure 5.8 shows a series of fluorescence spectra observed experimentally for $\delta = \Omega_0 = 220$ MHz and several values of Ω_2. Traces (i) show experimental results, while traces (ii) illustrate the theoretical spectra predicted for the same parameters.

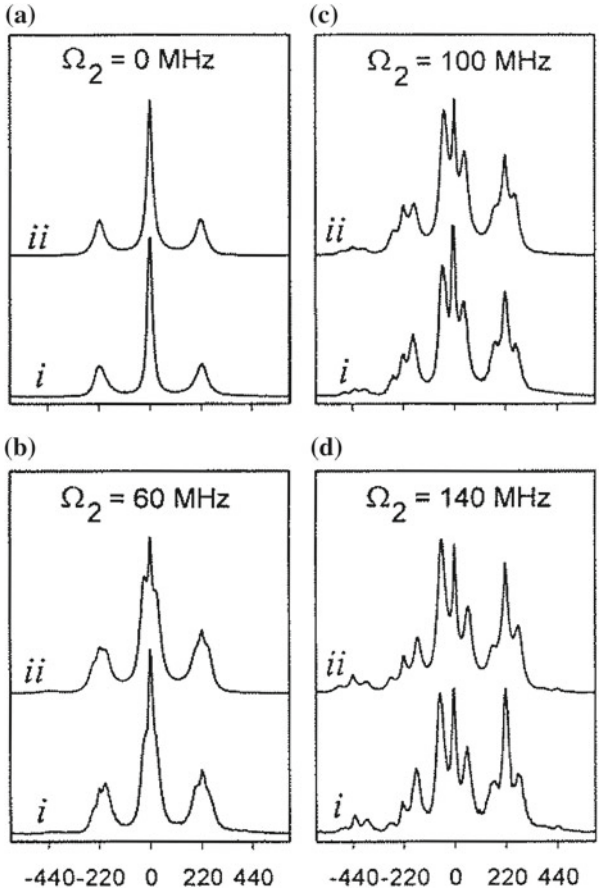

Fig. 5.8 Experimentally observed spectra (*lines i*) together with theoretical spectra (*lines ii*) of doubly driven Ba atoms with a strong resonant field of Rabi frequency $\Omega_0 = 220$ MHz and a weaker field of several Rabi frequencies Ω_2 and detuned from the resonance by $\delta = \Omega_0$

To obtain agreement it was necessary to include as well in the theoretical curves both the finite instrumental resolution $\gamma_c = 13$ MHz and the contribution of the other six stable Ba isotopes (about 22% total abundance) that were nonresonantly driven by the excitation fields. The observed spectrum exhibits triplet features at the central component of the spectrum and at the harmonics of the Rabi frequency Ω_0. As predicted by the theory, the splitting of the spectral lines is equal to $\Omega_2/2$. One can see from Fig. 5.8 that there is a large, but very narrow line at the center of the observed spectrum. The theoretical curves in Fig. 5.8 show that unlike the sideband structures of the fluorescence spectrum whose general characteristics remain largely insensitive to the presence of multiple isotopes, the central sharp line arises from the elastic scattering from the isotopes of the Ba atoms. Unfortunately, the presence of multiple

isotopes greatly distorted the central spectral feature away from that expected for a pure single-isotope two-level atom. Hence, the experiment demonstrated the double dressing of the atom, but did not explicitly explore the vanishing of the central component at ω_a, thereby did not confirm the dynamical suppression of spontaneous emission at the central line of the spectrum.

Bochinski et al. [22] have developed an experimental technique that isolates the signals of a single strongly driven isotope in the presence of multiple spectator isotopes, but this technique has not been yet applied to observe the fluorescence spectrum of a single-isotope species.

5.5.2 *Experiments with a Doubly Driven Quantum Dot*

The suppression of the central component of the spectrum was not possible in the previously described experiment involving an atomic beam of barium atoms due to the presence of isotopes of the barium atoms elastically scattering the strong component of the driving field.

Such suppression has been observed experimentally by the Pan's group at the Hefei National Laboratory in China [21]. Their experiment, shown schematically in Fig. 5.9, considered a quantum dot, a low-Q planar semiconductor micro-cavity, bath cryostat, two laser beams, and a spectral analyzer. A self-assembled layer of InGaAs quantum dots with a density of 20 μm^2 was embedded in a distributed-Bragg-reflector micro-cavity with 24 (lower) and 5 (upper) pairs of $Al_{90\%}Ga_{10\%}As$ and GaAs $\lambda/4$ layers, as shown in Fig. 5.9b. The sample was kept in a cryogen-free bath cryostat with the temperature stabilized within ± 5 mK around 4.2 K. The lifetime of the exciton state of the quantum dot was 390 ps.

The quantum dot was excited by two cw lasers, a strong (driving) laser tuned to the transition frequency of the quantum dot, and a weaker (coupling) tunable laser field.

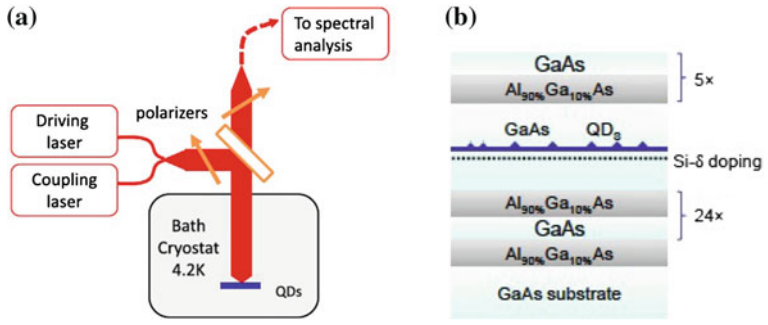

Fig. 5.9 **a** The main features of the apparatus used by He et al. [21]. **b** The structure of a distributed-Bragg-reflector cavity with 24 (*lower*) and 5 (*upper*) pairs of $Al_{90\%}Ga_{10\%}As$ and GaAs $\lambda/4$ layers containing a layer of InGaAs quantum dots. Reprinted with permission from Y. He, Y.M. He, J. Liu, Y.J. Wei, H. Ramirez, M. Atatüre, C. Schneider, M. Kamp, S. Höfling, C.Y. Lu, J.W. Pan: Phys. Rev. Lett. **114**, 097402 (2015). Copyright (2015) by the American Physical Society

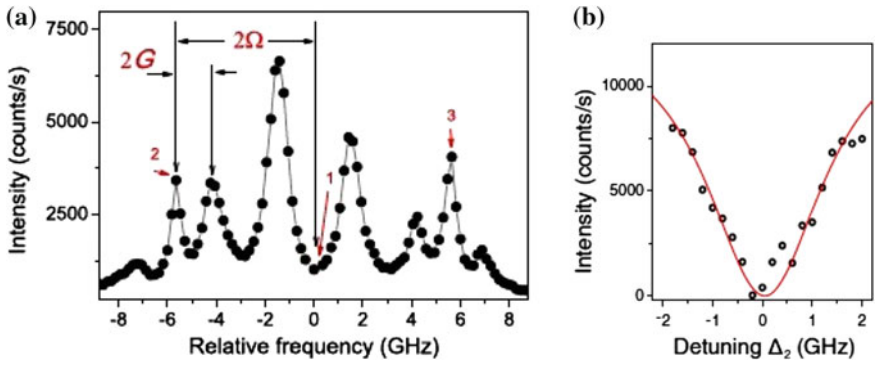

Fig. 5.10 **a** Evidence of the cancelation of the central component of the fluorescence spectrum for the Rabi frequency of the driving laser $2\Omega = 5.8$ GHz and the Rabi frequency of the coupling laser $2G = 0.6\Omega$. The coupling laser was tuned to the Rabi sideband of the driving laser frequency. **b** Variation of the intensity of the central component of the fluorescence spectrum with the detuning Δ_2 of the coupling laser from the Rabi sideband frequency of the strong driving laser. Reprinted with permission from Y. He, Y.M. He, J. Liu, Y.J. Wei, H. Ramirez, M. Atatüre, C. Schneider, M. Kamp, S. Höfling, C.Y. Lu, J.W. Pan: Phys. Rev. Lett. **114**, 097402 (2015). Copyright (2015) by the American Physical Society

The laser frequencies were stabilized to the neutral exciton state X_0 of the quantum dot to an accuracy within ± 5 MHz, which was much narrower than the linewidth of the quantum dot fluorescence. A cross-polarization configuration was used to excite the quantum dot and collect fluorescence photons. In the cross-polarization configuration the polarizers in the input and output ports were placed orthogonal to each other to separate the quantum dot fluorescence from the excitation lasers. A Fabry–Perot interferometer was used as the spectral analyser to resolve the resonance fluorescence spectra with a spectral resolution of $\sim 2\pi \times 67$ MHz. High resolution resonance fluorescence spectra from the neutral exciton state were measured for various strength of the laser fields.

Figure 5.10a shows the experimental results for the fluorescence spectrum when the coupling laser frequency was tuned to the Rabi sideband of the strong driving field.[1] The solid line shows the theoretical spectrum which agrees excellently with the measurements represented by black circles. Note the observation of the complete suppression of the central line of the spectrum. Figure 5.10b shows the variation of the magnitude of the central component with the detuning of the driving laser frequency from the frequency of the Rabi sideband frequency of the coupling laser. This demonstrates the complete cancelation of the central component of of the spectrum when the driving laser is tuned to the Rabi sideband frequency of the coupling laser.

With a very small modification of the experimental setup, just by driving the quantum dot with two independent (phase unlocked) lasers of equal angular frequencies, the experimental team was also able to demonstrate the insensitivity of the central component of the spectrum to the random phase distribution of the unlocked laser

[1] Note a different notation used by He et al. [21] to that in Sect. 5.2 for the Rabi frequencies and detunings.

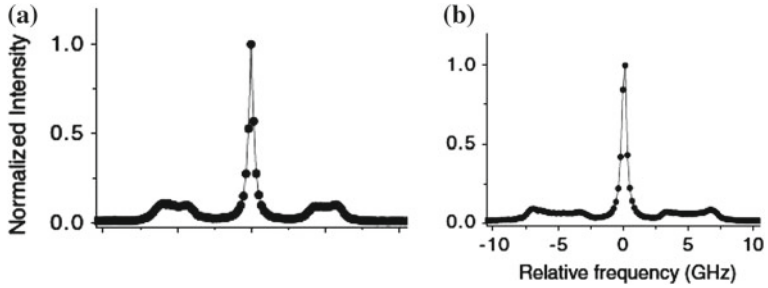

Fig. 5.11 Experimentally measured fluorescence spectra of a two-level quantum dot subjected to driving with two independent lasers of equal angular frequencies, $\omega_{L1} = \omega_{L2} = \omega_a$, and for two different ratios $\alpha = \Omega/G$. In **a** $\alpha = 0.2$ and in **b** $\alpha = 0.4$. Reprinted with permission from Y. He, Y.M. He, J. Liu, Y.J. Wei, H. Ramirez, M. Atatüre, C. Schneider, M. Kamp, S. Höfling, C.Y. Lu, J.W. Pan: Phys. Rev. Lett. **114**, 097402 (2015). Copyright (2015) by the American Physical Society

and the continuous spread of the Mollow sidebands. The experimental results for two different ratios of the Rabi frequencies of the lasers are shown in Fig. 5.11. The experimental results clearly demonstrate that the central component of the spectrum is not affected by the random phase noise of the lasers. The random phase noise produces continua at the frequency of the Rabi sideband of the strong field.

References

1. M. Lax: Phys. Rev. **172**, 350 (1968)
2. T.-S. Ho, S.-I. Chu, J.V. Tietz: Chem. Phys. Lett. **96**, 464 (1983)
3. A. Verdeny, J. Puig, F. Mintert: arXiv:1603.03923 [quant-ph] (2016)
4. G. Floquet: Ann. Ecole Norm. Sup. **12**, 47 (1883)
5. Z. Ficek, H.S. Freedhoff: Progress in Optics **40**, 389 (2000)
6. M.A. Newbold, G.J. Salamo, Phys. Rev. A **22**, 2098 (1980)
7. K. Rzażewski, M. Florjańczyk: J. Phys. B **17**, L509 (1984)
8. N. Nayak, G.S. Agarwal: Phys. Rev. A **31**, 3175 (1985)
9. Y. Zhu, A. Lezama, D.J. Gauthier, T.W. Mossberg: Phys. Rev. A **41**, 6574 (1990)
10. G.S. Agarwal, Y. Zhu, D.J. Gauthier, T.W. Mossberg: J. Opt. Soc. Am. B **8**, 1163 (1991)
11. M. Janowicz: Phys. Rev. A **44**, 3144 (1991)
12. A.D. Greentree, C. Wei, N.B. Manson: Phys. Rev. A **59**, 4083 (1999)
13. Z. Ficek, H.S. Freedhoff: Phys. Rev. A **53**, 4275 (1996)
14. T. Rudolph, H.S. Freedhoff, Z. Ficek: Phys. Rev. A **58**, 1296 (1998)
15. H.S. Freedhoff, Z. Chen: Phys. Rev. A **41**, 6013 (1990)
16. B. Blind, P.R. Fontana, P. Thomann: J. Phys. B **13**, 2717 (1980)
17. M. Abramowitz, I. Stegun: *Handbook of Mathematical Functions* (Dover, New York, 1972), p. 361
18. H.S. Freedhoff, Z. Ficek: Phys. Rev. A **55**, 1234 (1997)
19. Z. Ficek, T. Rudolph: Phys. Rev. A **60**, R4245 (1999)
20. C.C. Yu, J.R. Bochinski, T.M.V. Kordich, T.W. Mossberg, Z. Ficek: Phys. Rev. A **56**, R4381 (1997)
21. Y. He, Y.M. He, J. Liu, Y.J. Wei, H. Ramirez, M. Atature, C. Schneider, M. Kamp, S. Höfling, C.Y. Lu, J.W. Pan: Phys. Rev. Lett. **114**, 097402 (2015)
22. J.R. Bochinski, T. Loftus, T.W. Mossberg: Phys. Rev. A **61**, 041404(R) (2000)

Chapter 6
Quantum Spectroscopy with Squeezed Light

In Chap. 2 we introduced the concept and definition of squeezed states of the EM field and briefly discussed how squeezed states could be detected using the standard heterodyne or homodyne detection schemes. Squeezed states are an example of quantum (nonclassical) states of the EM field with fluctuations in one of the quadrature component of the field reduced below the standard quantum limit. For a squeezed state the Glauber-Sudarshan P representation of the density operator does not exist as a classical probability density, and this is well-known signature of a nonclassical field. Therefore, it is essential to use quantum theory in the description of squeezed states, they cannot be understood by using semiclassical techniques that assume a classical electromagnetic field interacting with quantized atoms or detectors.

We do not intend to discuss examples illustrating of how squeezed states could be generated in an optical system. It is assumed that the reader is acquainted with the elementary facts concerning the generation of squeezed states of the EM field in nonlinear optical systems. An extended literature on various aspects of squeezed states and their generation exists, and is also discussed in several textbooks. Our main efforts of this chapter will be devoted to applications of squeezed light in atomic spectroscopy, in particular, we focus our discussion on a class of applications which lead to features unique to quantum nature of squeezed light. In order to accomplish this aim, we start with a review of the theory of sources of squeezed light suitable for spectroscopic applications. The most successful in the applications have been the degenerate (DPO) and nondegenerate (NDPO) parametric oscillators whose one of the output quadratures exhibits a noise reduction below the standard quantum limit observable over a wide range of frequencies. This property makes these sources the most suitable for excitation of a variety of atomic systems.

We then proceed to a consideration of the influence of a squeezed vacuum field on two fundamental atomic radiative processes, spontaneous emission and dynamics of three-level atoms. These applications have been proposed more than 35 years ago and are still some of the most prominent applications of squeezed light in atomic spectroscopy. Next discussed is a mapping of the quantum correlations from a squeezed

Z. Ficek and R. Tanaś, *Quantum-Limit Spectroscopy*, Springer Series in Optical Sciences 200, DOI 10.1007/978-1-4939-3740-0_6

field to atoms. We will illustrate how the correlations contained in the squeezed vacuum can be mapped on a three-level atom in ladder configuration of its energy states and also on a system of two two-level atoms. We will find that these multilevel systems when illuminated by a squeezed vacuum field decay to a pure rather than the expected mixed state. In particular, the two-atom system decays to a pure entangled state.

6.1 Squeezed Light for Spectroscopic Applications

Squeezed light or a squeezed vacuum field can be obtained in many nonlinear optical processes [1, 2], but the most effective scheme to produce squeezed light turned out to be degenerate (DPO) and nondegenerate (NDPO) parametric oscillators [3–5]. These schemes base on the process of parametric down conversion in which a photon of the pump field of frequency $2\omega_0$ generates through the interaction with a nonlinear medium two lower frequency photons of frequencies ω_1 and ω_2, such that $2\omega_0 = \omega_1 + \omega_2$. In the degenerate process both photons have the same frequency and occupy a single mode of frequency $\omega_0 = \omega_1 = \omega_2$, whereas in the nondegenerate process the output photons have different frequencies $\omega_1 \neq \omega_2$ and occupy two distinct, momentum-conserving and phase-matched modes called signal and idler modes. The photons in the output modes usually have a wide bandwidth and they appear "simultaneously" or nearly simultaneously as a pair of strongly correlated photons. The strong correlations between the photons produce a squeezed state with reduced quantum fluctuations in one of the quadratures of the output field.

The parametric down conversion is a nonlinear process and is characterized by a threshold that the output field exhibits different properties above and below the threshold. Above threshold, the output field is in a squeezed coherent state, often called a displayed squeezed state, while below the threshold the output field is in a squeezed vacuum state.

6.1.1 Squeezed Light from a Degenerate Parametric Oscillator: Experiment

Squeezed states or shortly squeezing in the output of a degenerate parametric oscillator was first observed at Caltech by Wu et al. [5]. In the experiment, shown schematically in Fig. 6.1, a $Ba_2NaNb_5O_{15}$ crystal was placed inside a Nd: YAG ring-laser cavity to produce the second harmonic of the fundamental infrared laser wavelength 1.06 μm. The two orthogonally polarized output fields, the fundamental beam and the generated second-harmonic beam of wavelength 0.53 μm, were separated by the polarizer P. The second-harmonic field pumping the DPO was sufficiently strong to be treated as a classical nondepleted field, and was used to pump the DPO cavity

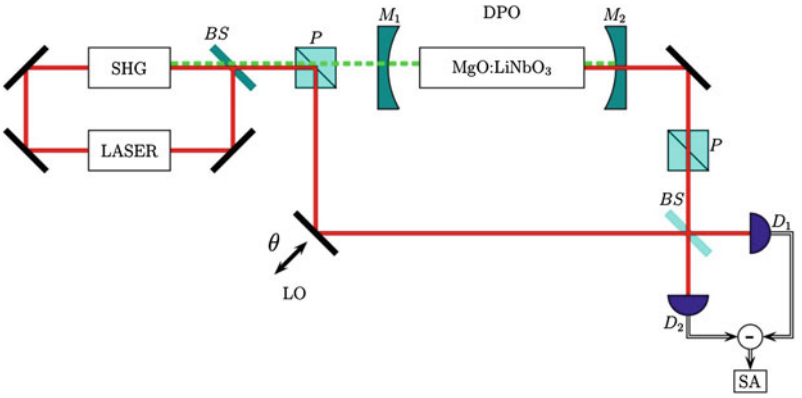

Fig. 6.1 Schematic diagram of the principal elements of the experiment by Wu et al. [5] for generation of squeezed light in DPO operating *below* threshold

consisting of two mirrors M_1 and M_2 and a MgO:LiNbO$_3$ crystal. The DPO, working below the threshold of oscillation, produced a squeezed vacuum state of the output mode at the fundamental beam frequency. The DPO cavity mirrors were prepared in such a way that the mirror M_1 had about 3.5% transmission at 0.53 μm and a very small transmission (0.06%) at 1.06 μm. The mirror M_2 had low transmission for 0.53 μm and 4.3 or 7.3% transmission for 1.06 μm. This means that from the point of view of the generated signal at 1.06 μm, the DPO cavity can be considered as a single-ended cavity. The output from the DPO was superimposed at the beamsplitter of a balanced homodyne detection system with the local oscillator field being a part of the fundamental laser beam. The photocurrents registered by two photodetectors (photodiodes) were subtracted and the noise of the difference current was spectrally analyzed. The rms noise voltage from the balanced homodyne detector was measured as a function of the phase θ of the local oscillator at fixed frequency and bandwidth of the spectral distribution of the photocurrent fluctuations. The phase θ was varied by vibrating the mirror in the path of the local oscillator.

The experimental results are shown in Fig. 6.2. When the output of the DPO was blocked to enter the detection system, the detected noise voltage was insensitive to the phase θ. This is shown by the horizontal dashed line. However, with the DPO output present, a variation of the noise voltage with the phase was observed dropping at some phases down below the level of vacuum fluctuations. This indicates squeezing in the output mode of the DPO, and the 50% reduction of the fluctuations below the vacuum level was observed.

In an improved version of the experiment [6], the experimental team reported an observation of a 63% reduction of the noise voltage below the vacuum level.

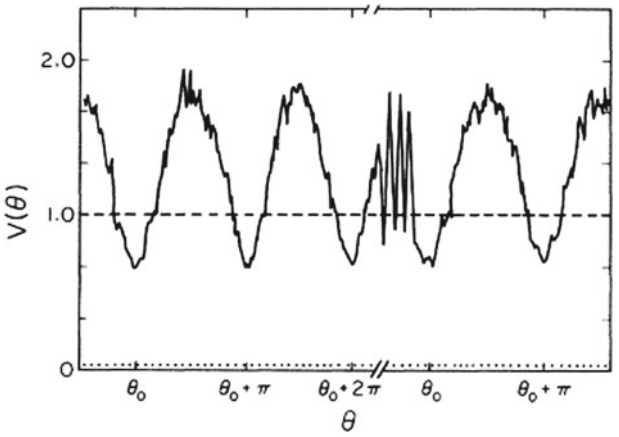

Fig. 6.2 Measured voltage $V(\theta)$ as a function of the local oscillator phase θ. The dashed line represents the level of vacuum fluctuations measured in the absence of the output from the DPO. The dotted line is the amplifier noise level. The solid line represents the measured noise voltage with the DPO output present. Reprinted with permission from L.A. Wu, H.J. Kimble, J.L. Hall, H. Wu: Phys. Rev. Lett. **57**, 2520 (1986). Copyright (1986) by the American Physical Society

6.1.2 The Input–Output Theory

To characterize the nonclassical properties of light produced by the DPO we need a relation between the field outside the DPO cavity that is accessible for measurement, and the field inside the DPO cavity which is produced in a nonlinear process of parametric down conversion. The relation has been found by Collett and Gardiner [7] who developed the input–output formalism applicable to such situations.

To illustrate how the formalism works, in particular, in the situation of the experiment discussed in the preceding section, we consider a single-sided cavity formed by one perfect mirror M_1 and one output mirror M_2 of finite transmissivity, as shown in Fig. 6.3. We assume that the field inside the cavity is represented by a single mode of frequency ω_c, which is coupled through the output mirror to the external field appearing to the cavity as a broadband multimode reservoir.

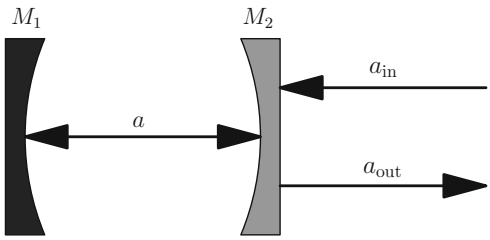

Fig. 6.3 Single-sided cavity configuration for the input–output theory. The mirror M_1 is totally reflecting and the mirror M_2 of finite transmissivity acts as the input as well as the output port of the single cavity mode a, the input field $a_{\rm in}$, and the output field $a_{\rm out}$

To describe the evolution of such a system it is convenient to start with the Hamiltonian, which can be written as

$$\hat{H} = \hat{H}_S + \hat{H}_R + \hat{H}_I \,, \tag{6.1}$$

where

$$\hat{H}_S = \hbar\omega_c \hat{a}^\dagger \hat{a} \tag{6.2}$$

is the Hamiltonian of the cavity mode,

$$\hat{H}_R = \int_0^\infty \mathrm{d}\omega\, \hbar\omega \hat{b}^\dagger(\omega)\hat{b}(\omega) \tag{6.3}$$

is the Hamiltonian of the external multimode (reservoir) field, and

$$\hat{H}_I = \mathrm{i}\hbar \int_0^\infty \mathrm{d}\omega\, K(\omega)[\hat{b}^\dagger(\omega)\hat{a} - \hat{a}^\dagger \hat{b}(\omega)] \tag{6.4}$$

is the interaction between the cavity mode and the reservoir.

In (6.1), $\hat{a}$ and $\hat{a}^\dagger$ are the annihilation and creation operators of the cavity mode, $\hat{b}(\omega)$ and $\hat{b}^\dagger(\omega)$ are the annihilation and creation operators of a mode of frequency ω of the reservoir, and $K(\omega)$ is the coupling constant of the cavity mode to the mode of frequency ω of the reservoir. The interaction Hamiltonian $\hat{H}_I$ retains only the terms which play dominant role in the rotating-wave approximation. Antiresonant terms which would make much smaller contributions have been omitted. The annihilation and creation operators of the cavity field and the reservoir satisfy the Bose commutation relations

$$\left[\hat{a}, \hat{a}^\dagger\right] = 1 \,, \tag{6.5}$$

$$\left[\hat{b}(\omega), \hat{b}^\dagger(\omega')\right] = \delta(\omega - \omega') \,. \tag{6.6}$$

The Heisenberg equations of motion for the annihilation operators are

$$\dot{\hat{a}} = -\mathrm{i}\omega_c \hat{a} - \int_0^\infty \mathrm{d}\,\omega\, K(\omega)\hat{b}(\omega) \,, \tag{6.7}$$

$$\dot{\hat{b}}(\omega) = -\mathrm{i}\omega \hat{b}(\omega) + K(\omega)\hat{a} \,, \tag{6.8}$$

along with the corresponding equations for the adjoint operators. It is clear from (6.7) that the free evolution of the annihilation operator for the cavity mode has the form $\hat{a}(t) = \exp[-\mathrm{i}\omega_c(t - t_0)]\hat{a}(t_0)$. If ω_c corresponds to an optical frequency, then the annihilation operator rapidly oscillates in time. We can factor out the rapid oscillations introducing the slowly varying operator $\hat{a}_s(t)$ by the relation $\hat{a}(t) = \hat{a}_s(t)\exp(-\mathrm{i}\omega_c t)$. Since we assume that the rotating-wave approximation is valid, we expect that the essential contributions to the interaction come from the

reservoir operators oscillating with frequencies ω close to ω_c. Thus, we may write $\hat{b}(\omega) = \hat{b}_s(\omega)\exp(-\mathrm{i}\omega_c t)$, and then (6.7) and (6.8) written in terms of the slowly varying operators take the form

$$\dot{\hat{a}}_s = -\int_0^\infty \mathrm{d}\,\omega\, K(\omega)\hat{b}_s(\omega)\,, \tag{6.9}$$

$$\dot{\hat{b}}_s(\omega) = -\mathrm{i}(\omega-\omega_c)\hat{b}_s(\omega) + K(\omega)\hat{a}_s\,. \tag{6.10}$$

In its time integrated form (6.10) is

$$\hat{b}_s(\omega) = \mathrm{e}^{-\mathrm{i}(\omega-\omega_c)(t-t_0)}\hat{b}_{0s}(\omega) + K(\omega)\int_{t_0}^{t}\mathrm{d}t'\mathrm{e}^{-\mathrm{i}(\omega-\omega_c)(t-t')}\hat{a}_s(t')\,, \tag{6.11}$$

and when this relation is substituted into (6.9), we find

$$\begin{aligned}\dot{\hat{a}}_s = &-\int_0^\infty \mathrm{d}\omega K(\omega)\mathrm{e}^{-\mathrm{i}(\omega-\omega_c)(t-t_0)}\hat{b}_{0s}(\omega)\\ &-\int_0^\infty \mathrm{d}\omega K^2(\omega)\int_{t_0}^{t}\mathrm{d}t'\mathrm{e}^{-\mathrm{i}(\omega-\omega_c)(t-t')}\hat{a}_s(t')\,.\end{aligned} \tag{6.12}$$

If we change the variable $\omega-\omega_c \to \omega$, and extend the integration over the new variable from $-\omega_c$ to $-\infty$, we arrive at

$$\begin{aligned}\dot{\hat{a}}_s = &-\int_{-\infty}^\infty \mathrm{d}\omega K(\omega_c+\omega)\mathrm{e}^{-\mathrm{i}\omega(t-t_0)}\hat{b}_{0s}(\omega_c+\omega)\\ &-\int_{-\infty}^\infty \mathrm{d}\omega K^2(\omega_c+\omega)\int_{t_0}^{t}\mathrm{d}t'\mathrm{e}^{-\mathrm{i}\omega(t-t')}\hat{a}_s(t')\,,\end{aligned} \tag{6.13}$$

which, after going back to the original operators gives

$$\begin{aligned}\dot{\hat{a}} = &-\mathrm{i}\omega_c\hat{a} - \int_{-\infty}^\infty \mathrm{d}\omega\, K(\omega_c+\omega)\mathrm{e}^{-\mathrm{i}(\omega_c+\omega)(t-t_0)}\hat{b}_0(\omega_c+\omega)\\ &-\int_{-\infty}^\infty \mathrm{d}\omega\, K^2(\omega_c+\omega)\int_{t_0}^{t}\mathrm{d}t'\,\mathrm{e}^{-\mathrm{i}(\omega_c+\omega)(t-t')}\hat{a}(t')\,.\end{aligned} \tag{6.14}$$

Expression (6.14) indicates that the integration over ω is centered around the cavity resonance frequency ω_c. However, if we keep in mind this fact, we can make replacement $\omega_c+\omega \to \omega$ obtaining the standard form of the formula [7]

$$\begin{aligned}\dot{\hat{a}} = &-\mathrm{i}\omega_c\hat{a} - \int_{-\infty}^\infty \mathrm{d}\omega\, K(\omega)\mathrm{e}^{-\mathrm{i}\omega(t-t_0)}\hat{b}_0(\omega)\\ &-\int_{-\infty}^\infty \mathrm{d}\omega\, K^2(\omega)\int_{t_0}^{t}\mathrm{d}t'\,\mathrm{e}^{-\mathrm{i}\omega(t-t')}\hat{a}(t')\,.\end{aligned} \tag{6.15}$$

This integro-differential form can be obtained directly from the Hamiltonian (6.1) simply by taking the integrations over ω from $-\infty$ to $+\infty$. One could comment that the integrations over negative frequencies in the Hamiltonian is a nonsense on the physical ground. However, if the main contributions to the process in question come from the frequencies that are high, like optical frequencies, we can safely include negative frequencies in the integral because their contribution is negligible. This is true as far as the rotating-wave approximation is valid. A reward for using this approach is a very simple formalism in which we deal with the standard Fourier transforms.

We now make what is called the first Markov approximation [8], i.e., we assume that the coupling constant is independent of frequency

$$K(\omega) = \sqrt{\frac{\kappa}{2\pi}}\,. \tag{6.16}$$

Then, we use of the properties

$$\int_{-\infty}^{\infty} \mathrm{e}^{-\mathrm{i}\omega(t-t')}\,\mathrm{d}\omega = 2\pi\delta(t-t')\,, \tag{6.17}$$

$$\int_{t_0}^{t} a(t')\delta(t-t')\,\mathrm{d}t' = \frac{1}{2}a(t)\,, \tag{6.18}$$

and get

$$\dot{\hat{a}} = -\mathrm{i}\omega_c\hat{a} - \sqrt{\kappa}\hat{a}_{\mathrm{in}}(t) - \frac{\kappa}{2}\hat{a}\,, \tag{6.19}$$

where

$$\hat{a}_{\mathrm{in}}(t) = \int_{-\infty}^{\infty} \mathrm{d}\omega \mathrm{e}^{-\mathrm{i}\omega(t-t_0)}\hat{b}_0(\omega) \tag{6.20}$$

defines the input field to the cavity. This field satisfy the commutation relation

$$[\hat{a}_{\mathrm{in}}(t), \hat{a}^{\dagger}_{\mathrm{in}}(t')] = \delta(t-t')\,. \tag{6.21}$$

When solving (6.10), we have assumed that $t > t_0$, that is the $\hat{b}_0$ represents the field "in the past". It is possible, however, to find a solution for $t < t_1$, defining the initial conditions "in the future".

$$\hat{b}_s(\omega) = \mathrm{e}^{-\mathrm{i}(\omega-\omega_c)(t-t_1)}\hat{b}_{1s}(\omega) + K(\omega)\int_{t}^{t_1} \mathrm{d}t'\,\mathrm{e}^{-\mathrm{i}(\omega-\omega_c)(t-t')}\hat{a}_s(t')\,, \tag{6.22}$$

which leads to

$$\dot{\hat{a}} = -\mathrm{i}\omega_c \hat{a} - \sqrt{\kappa}\hat{a}_{\mathrm{out}}(t) + \frac{\kappa}{2}\hat{a}\,, \tag{6.23}$$

where

$$\hat{a}_{\mathrm{out}}(t) = \int_{-\infty}^{\infty} \mathrm{d}\omega\, \mathrm{e}^{-\mathrm{i}\omega(t-t_1)}\hat{b}_1(\omega) \tag{6.24}$$

represents the "out" (outgoing) field from the cavity. Subtracting (6.19) from (6.23), we obtain the input–output relation

$$\hat{a}_{\mathrm{out}}(t) - \hat{a}_{\mathrm{in}}(t) = \sqrt{\kappa}\hat{a}(t)\,. \tag{6.25}$$

Relation (6.25) is a sort of a boundary condition which makes explicit connection of the field inside the cavity with the field outside the cavity. The connection involves the cavity damping rate κ, as one could expect.

The formalism outlined above is the well-known input–output formalism developed by Collett and Gardiner [7, 8]. It has been found very useful and applicable in many physical situations. The simplest situation is an empty cavity discussed above, but it can be easily extended to situations where the cavity is filled with the nonlinear medium.

6.1.3 Correlations Functions of the Output DPO Field

Let us consider the experimental situation, discussed above in Sect. 6.1.1 and illustrated in Fig. 6.1, in which the downconversion from frequency $2\omega_c$ to frequency ω_c occurs inside a resonant cavity of length L and cross section A containing a nonlinear medium. The cavity is formed by one near-perfect mirror and one output mirror with a finite transmissivity. We make use of the relation derived by Collett and Gardiner [7] between the Fourier amplitude $\hat{E}^{(\pm)}_{\mathrm{out}}(\omega)$ of the downconverted light emerging from the cavity and the Fourier amplitude $\hat{E}^{(\pm)}_{\mathrm{in}}(\omega)$ of the input pumping beam

$$\hat{E}^{(+)}_{\mathrm{out}}(\omega) = U_1(\omega)\hat{E}^{(+)}_{\mathrm{in}}(\omega) + U_2(\omega)\hat{E}^{(-)}_{\mathrm{in}}(2\omega_c - \omega)\,, \tag{6.26}$$

where

$$\begin{aligned} U_1(\omega) &= -\frac{\kappa^2/4 + \epsilon^2 + (\omega-\omega_c)^2}{\kappa^2/4 - \epsilon^2 - (\omega-\omega_c)^2 - \mathrm{i}\kappa(\omega-\omega_c)}\,, \\ U_2(\omega) &= -\frac{\kappa\epsilon}{\kappa^2/4 - \epsilon^2 - (\omega-\omega_c)^2 - \mathrm{i}\kappa(\omega-\omega_c)}\,, \end{aligned} \tag{6.27}$$

in which κ is the cavity damping rate and ϵ is the amplitude of the pump field.

From the expression (6.26) we can evaluate the spectral correlation functions of the output field amplitudes. If we evaluate the normally ordered correlation function $\langle \Delta \hat{E}^{(-)}_{\text{out}}(\omega) \Delta \hat{E}^{(+)}_{\text{out}}(\omega') \rangle$ according to (6.26), we find the result

$$\begin{aligned}\langle \Delta \hat{E}^{(-)}_{\text{out}}(\omega) \Delta \hat{E}^{(+)}_{\text{out}}(\omega') \rangle &= U_1^*(\omega) U_1(\omega') \langle \Delta \hat{E}^{(-)}_{\text{in}}(\omega) \Delta \hat{E}^{(+)}_{\text{in}}(\omega') \rangle \\ &+ U_1^*(\omega) U_2(\omega) \langle \Delta \hat{E}^{(-)}_{\text{in}}(\omega') \Delta \hat{E}^{(-)}_{\text{in}}(2\omega_c - \omega') \rangle \\ &+ U_2^*(\omega) U_1(\omega') \langle \Delta \hat{E}^{(+)}_{\text{in}}(2\omega_c - \omega) \Delta \hat{E}^{(+)}_{\text{in}}(\omega') \rangle \\ &+ U_2^*(\omega) U_2(\omega') \langle \Delta \hat{E}^{(+)}_{\text{in}}(2\omega_c - \omega) \Delta \hat{E}^{(-)}_{\text{in}}(2\omega_c - \omega') \rangle \, . \end{aligned} \tag{6.28}$$

If the state of the input field is a vacuum or a coherent state $|\alpha\rangle$, it will have zero normally ordered variance, that is

$$\begin{aligned}\langle \Delta \hat{E}^{(-)}_{\text{in}}(\omega) \Delta \hat{E}^{(+)}_{\text{in}}(\omega') \rangle &= \langle \Delta \hat{E}^{(-)}_{\text{in}}(\omega') \Delta \hat{E}^{(-)}_{\text{in}}(2\omega_c - \omega') \rangle \\ &= \langle \Delta \hat{E}^{(+)}_{\text{in}}(2\omega_c - \omega) \Delta \hat{E}^{(+)}_{\text{in}}(\omega') \rangle = 0 \, . \end{aligned} \tag{6.29}$$

Hence, the only nonvanishing contribution to $\langle \Delta \hat{E}^{(-)}_{\text{out}}(\omega) \Delta \hat{E}^{(+)}_{\text{out}}(\omega') \rangle$ comes from the last term in (6.28), which is in antinormal order

$$\begin{aligned}\langle \Delta \hat{E}^{(-)}_{\text{out}}(\omega) \Delta \hat{E}^{(+)}_{\text{out}}(\omega') \rangle &= U_2^*(\omega) U_2(\omega') \\ &\times \langle \Delta \hat{E}^{(+)}_{\text{in}}(2\omega_c - \omega) \Delta \hat{E}^{(-)}_{\text{in}}(2\omega_c - \omega') \rangle \, . \end{aligned} \tag{6.30}$$

The correlation function appearing on the right-hand side of (6.30) can be readily evaluated with the help of the commutation relation (1.16), and we obtain

$$\langle \Delta \hat{E}^{(-)}_{\text{out}}(\omega) \Delta \hat{E}^{(+)}_{\text{out}}(\omega') \rangle = |U_2(\omega)|^2 \frac{\pi \hbar \omega_c}{A c \varepsilon_0} \delta(\omega - \omega') \, . \tag{6.31}$$

This expression can be written as

$$\langle \Delta \hat{E}^{(-)}_{\text{out}}(\omega) \Delta \hat{E}^{(+)}_{\text{out}}(\omega') \rangle = \frac{\pi \hbar \omega_c}{A c \varepsilon_0} N(\omega) \delta(\omega - \omega') \, , \tag{6.32}$$

where $N(\omega) \equiv |U_2(\omega)|^2$ is the intensity spectrum, and using (6.27) we find that

$$N(\omega) = \frac{\epsilon^2 \kappa^2}{\left[\kappa^2/4 - \epsilon^2 - (\omega - \omega_c)^2\right]^2 + \kappa^2 (\omega - \omega_c)^2} \, . \tag{6.33}$$

It is easily shown that the expression (6.33) can be written as a difference of two Lorentzians centered at the output field frequency ω_c:

$$N(\omega) = \Phi_\mu(\omega) - \Phi_\lambda(\omega) \, , \tag{6.34}$$

where

$$\Phi_\mu(\omega) = \frac{\lambda^2-\mu^2}{4}\frac{1}{(\omega-\omega_c)^2+\mu^2}\,,$$
$$\Phi_\lambda(\omega) = \frac{\lambda^2-\mu^2}{4}\frac{1}{(\omega-\omega_c)^2+\lambda^2}\,, \tag{6.35}$$

in which λ and μ are related to the cavity damping rate κ and the amplitude of the pump field ϵ of the parametric oscillator according to

$$\lambda = \frac{\kappa}{2}+\epsilon\,, \qquad \mu = \frac{\kappa}{2}-\epsilon\,. \tag{6.36}$$

We now calculate $\langle \Delta\hat{E}^{(-)}_{\rm out}(\omega)\Delta\hat{E}^{(-)}_{\rm out}(\omega')\rangle$ in a similar manner, and with the help of the commutation relation (1.16), we arrive at the following expression:

$$\langle \Delta\hat{E}^{(-)}_{\rm out}(\omega)\Delta\hat{E}^{(-)}_{\rm out}(\omega')\rangle = U_1^*(\omega)U_2^*(2\omega_c-\omega)\frac{\pi\hbar\omega_c}{Ac\varepsilon_0}\delta(2\omega_c-\omega-\omega')\,. \tag{6.37}$$

Using the expressions (6.27), we find

$$\langle \Delta\hat{E}^{(-)}_{\rm out}(\omega)\Delta\hat{E}^{(-)}_{\rm out}(\omega')\rangle = \frac{\pi\hbar\omega_c}{Ac\varepsilon_0}M(\omega)\delta(2\omega_c-\omega-\omega')\,. \tag{6.38}$$

where $M(\omega)\equiv U_1^*(\omega)U_2^*(2\omega_c-\omega)$ and with the help of (6.27) we find that

$$M(\omega) = \frac{\epsilon\kappa\left[\kappa^2/4+\epsilon^2+(\omega-\omega_c)^2\right]}{\left[\kappa^2/4-\epsilon^2-(\omega-\omega_c)^2\right]^2+\kappa^2(\omega-\omega_c)^2}\,, \tag{6.39}$$

This expression can be written as a sum of the two Lorentzians (6.35), that

$$M(\omega) = \Phi_\mu(\omega)+\Phi_\lambda(\omega)\,. \tag{6.40}$$

When the optical parametric oscillator works in the nondegenerate regime (NDPO), the frequency dependence of the spectral functions $N(\omega)$ and $M(\omega)$ is given by [7]

$$N(\omega) = \frac{1}{2}\left[\Phi_\mu(\omega-\alpha)+\Phi_\mu(\omega+\alpha)-\Phi_\lambda(\omega-\alpha)-\Phi_\lambda(\omega+\alpha)\right]\,,$$
$$M(\omega) = \frac{1}{2}\left[\Phi_\mu(\omega-\alpha)+\Phi_\mu(\omega+\alpha)+\Phi_\lambda(\omega-\alpha)+\Phi_\lambda(\omega+\alpha)\right]\,, \tag{6.41}$$

where $\alpha = (\omega_1-\omega_2)/2$ is the displacement of the frequencies of the output idler and signal modes from the frequency of the pumping mode.

From (6.32) and (6.38), it is clear that $N(\omega)$ is related to the mean number of photons at frequency ω, while $M(\omega)$ describes the correlation between the two photons created in the down conversion process. As we will see, these correlations lead to the unequal partition of the quantum fluctuations between two quadrature components of the output field. The frequency dependence of the two parameters, $N(\omega)$ and $M(\omega)$, is governed by two Lorentzian functions with the widths λ and μ defined by the cavity damping rate and the amplitude of the pump field. Below threshold, $\epsilon < \kappa/2$, both λ and μ are positive, and $\lambda > \mu$. For the case of a weak pumping ($\epsilon \to 0$), both parameters reduce to $\kappa/2$, while in the opposite extreme of very strong pumping approaching the DPO threshold ($\epsilon \to \kappa/2$), $\lambda \to \kappa$ and $\mu \to 0$. Clearly, the bandwidth of the squeezed field is limited to the bandwidth of the DPO cavity. Thus, if the bandwidth of the cavity is large that $N(\omega)$ and $M(\omega)$ are constant over a frequency range much greater than all other frequencies which appear in the problem under consideration, the frequency dependence of $N(\omega)$ and $M(\omega)$ can be omitted and the squeezed vacuum is then considered as a *broadband squeezed vacuum*. In such situations the squeezed vacuum is parametrized by two constants N and M.

In concluding this section, we would like to point out that in the broadband approximation, there is no difference between the fields from DPO and NDPO, both can be described by the parameters N and M that are constants independent of frequency. Therefore, in the broadband approximation, the output fields of both DPO and NDPO can be equally used in modeling the interaction of squeezed light with a quantum system. However, if λ and μ are finite, the two fields differ dramatically: DPO produces the field with one peak centered at the squeezing carrier frequency, while NDPO produces light with two spectral peaks symmetrically shifted by α with respect to the carrier frequency ω_s. This fact can have important consequences when, for example, an atom interacts with the squeezed vacuum. If μ is much greater than the atomic linewidth γ, the broadband approximation can be used, and the squeezed vacuum can be treated as a reservoir to the atom.

6.2 Fluctuations and Correlations of Squeezed Light

The squeezing parameters we have defined in the preceding section cannot be treated separately. The expressions for $N(\omega)$ and $M(\omega)$ show explicitly that the parameters are related to each other. The relation results from the fact that two (in the case of DPO) and four (in the case of NDPO) Lorentzians determine both $N(\omega)$ and $M(\omega)$ parameters. In this section, we will determine how the parameters are associated with the squeezing spectrum and how strong squeezing can be obtained in the DPO. Moreover, we will distinguish between different forms of squeezing. In particular, we will define a classically squeezed field. As we will see, both quantum and classically squeezed fields have an anisotropic distribution of the fluctuations between the quadrature components but only the quantum squeezed field has the fluctuations in one of the quadrature components reduced below the quantum limit. In addition,

we introduce a function that measures the degree of two-photon correlations relative to the number of photons in the field, which also distinguishes between the quantum and classical squeezing.

6.2.1 Nonclassical Fluctuations of Squeezed Light

Having the photon number and two-photon correlation functions specified, we may determine the squeezing spectrum of the output DPO field. According to (2.63) the squeezing spectrum is defined as the Fourier transform of the correlation function of the normally ordered quadrature components

$$\begin{aligned} 2\pi S_\theta(\omega, 0)\delta(\omega+\omega') &= \langle : \Delta\hat{E}_\theta(\omega)\Delta\hat{E}_\theta(\omega') : \rangle \, , \\ 2\pi S_\theta(\omega, \pi/2)\delta(\omega+\omega') &= \langle : \Delta\hat{E}_{\theta+\pi/2}(\omega)\Delta\hat{E}_{\theta+\pi/2}(\omega') : \rangle \, , \end{aligned} \tag{6.42}$$

where

$$\begin{aligned} \langle : \Delta\hat{E}_\theta(\omega)\Delta\hat{E}_\theta(\omega') : \rangle = {} & \langle \Delta\hat{E}^{(+)}_{\text{out}}(\omega)\Delta\hat{E}^{(+)}_{\text{out}}(\omega')\rangle e^{2i\theta} \\ & + \langle \Delta\hat{E}^{(-)}_{\text{out}}(\omega)\Delta\hat{E}^{(+)}_{\text{out}}(\omega')\rangle + \langle \Delta\hat{E}^{(-)}_{\text{out}}(\omega')\Delta\hat{E}^{(+)}_{\text{out}}(\omega)\rangle \\ & + \langle \Delta\hat{E}^{(-)}_{\text{out}}(\omega)\Delta\hat{E}^{(-)}_{\text{out}}(\omega')\rangle e^{-2i\theta} \, . \end{aligned} \tag{6.43}$$

Substituting the expressions (6.32) and (6.38) into (6.43), we arrive at

$$S_\theta(\omega, 0) = 2N(\omega) + 2|M(\omega)|\cos(\phi - 2\theta) \, , \tag{6.44}$$

where ϕ is the phase of the squeezed field. Similarly, for $S_\theta(\omega, \pi/2)$, we find

$$S_\theta(\omega, \pi/2) = 2N(\omega) - 2|M(\omega)|\cos(\phi - 2\theta) \, . \tag{6.45}$$

With the particular choice $\theta = \phi/2$, the squeezing spectra are

$$\begin{aligned} S_\theta(\omega, 0) &= 2N(\omega) + 2|M(\omega)| = 4\Phi_\mu(\omega) \, , \\ S_\theta(\omega, \pi/2) &= 2N(\omega) - 2|M(\omega)| = -4\Phi_\lambda(\omega) \, . \end{aligned} \tag{6.46}$$

We see that each squeezing spectrum is determined by a single Lorentzian line. The spectrum $S_\theta(\omega, 0)$ is determined by $\Phi_\mu(\omega)$ whereas $S_\theta(\omega, \pi/2)$ is determined by $\Phi_\lambda(\omega)$. Note that $S_\theta(\omega, \pi/2)$ is negative for all frequencies, so the output DPO field is squeezed for all frequencies. It is clear by inspection of $\Phi_\lambda(\omega)$ that maximum squeezing is obtained when $\omega = \omega_c$ and the pumping approaching the threshold $\epsilon \to \kappa/2$, in which case $S_\theta(0, \pi/2) = -1$. Thus, perfect squeezing can be observed in principle in the output field of the DPO. Figure 6.4 shows the squeezing spectrum $S_\theta(\omega, \pi/2)$ for several different values of ϵ. It is apparent that squeezing is present for all frequencies and maximum squeezing is achieved at the cavity frequency.

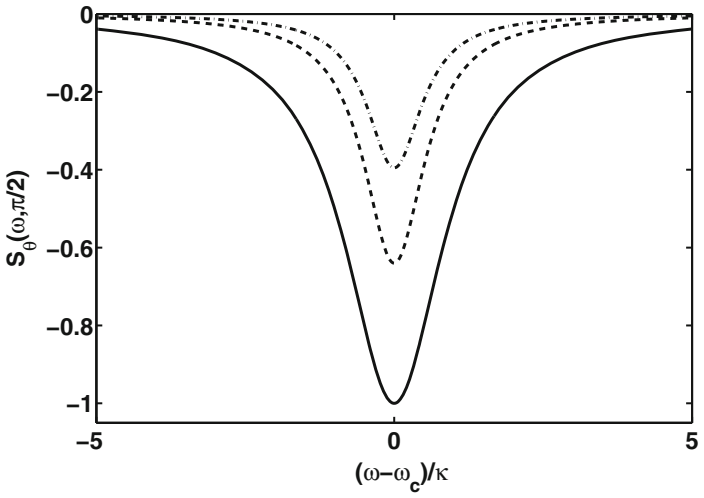

Fig. 6.4 Squeezing spectrum $S_\theta(\omega, \pi/2)$ plotted for several different values of ϵ: $\epsilon = \kappa/2$ (*solid line*), $\epsilon = \kappa/8$ (*dashed line*), and $\epsilon = \kappa/16$ (*dashed-dotted line*)

6.2.2 Quantum and Classical Correlations in Squeezed Light

As we have already mentioned, the parameters $N(\omega)$ and $M(\omega)$ are related to each other that the degree of the two-photon correlations between photons in the output DPO field depends on the number of photons in the output mode. Here, we determine the relation between these parameters on the example of the output field of the DPO, but the approach we take works equally well for the case of nondegenerate modes.

Suppose that the DPO works below the threshold that the output field has zero average electric field amplitude $\langle \hat{E}^{(\pm)}_{\rm out}(\omega)\rangle = 0$. Then the correlation functions (6.32) and (6.38) for the fluctuation operators reduce to

$$\begin{aligned}
\langle \hat{E}^{(-)}_{\rm out}(\omega)\hat{E}^{(+)}_{\rm out}(\omega)\rangle &= \frac{\pi\hbar\omega_c}{Ac\varepsilon_0}N(\omega)\ ,\\
\langle \hat{E}^{(-)}_{\rm out}(2\omega_c-\omega)\hat{E}^{(+)}_{\rm out}(2\omega_c-\omega)\rangle &= \frac{\pi\hbar\omega_c}{Ac\varepsilon_0}N(2\omega_c-\omega)\ ,\\
\langle \hat{E}^{(-)}_{\rm out}(\omega)\hat{E}^{(-)}_{\rm out}(2\omega_c-\omega)\rangle &= \frac{\pi\hbar\omega_c}{Ac\varepsilon_0}M(\omega)\ .
\end{aligned} \tag{6.47}$$

These correlation functions will be used to help evaluate the relation between the squeezing parameters.

Let us take a linear, not necessary Hermitian combination of the output field operators at frequencies ω and $2\omega_c - \omega$:

$$\hat{O}(\omega) = c_\omega \hat{E}^{(+)}_{\rm out}(\omega) + c^*_{-\omega}\hat{E}^{(-)}_{\rm out}(2\omega_c-\omega)\ , \tag{6.48}$$

where c_ω and $c_{-\omega}$ are complex numbers, and evaluate the expectation value $\langle \hat{O}^\dagger(\omega)\hat{O}(\omega)\rangle$. We find

$$\begin{aligned}\langle \hat{O}^\dagger(\omega)\hat{O}(\omega)\rangle &= |c_\omega|^2 \langle \hat{E}^{(-)}_{\rm out}(\omega)\hat{E}^{(+)}_{\rm out}(\omega)\rangle + c_\omega c_{-\omega}\langle \hat{E}^{(+)}_{\rm out}(\omega)\hat{E}^{(+)}_{\rm out}(2\omega_c-\omega)\rangle \\ &+ c^*_\omega c^*_{-\omega}\langle \hat{E}^{(-)}_{\rm out}(\omega)\hat{E}^{(-)}_{\rm out}(2\omega_c-\omega)\rangle \\ &+ |c_{-\omega}|^2 \langle \hat{E}^{(+)}_{\rm out}(2\omega_c-\omega)\hat{E}^{(-)}_{\rm out}(2\omega_c-\omega)\rangle \,. \end{aligned} \tag{6.49}$$

If we use the commutation relation (1.16), we can write

$$\begin{aligned}\langle \hat{E}^{(+)}_{\rm out}(2\omega_c-\omega)\hat{E}^{(-)}_{\rm out}(2\omega_c-\omega)\rangle &= \frac{\pi\hbar\omega_c}{Ac\varepsilon_0} \\ \langle \hat{E}^{(-)}_{\rm out}(2\omega_c-\omega)\hat{E}^{(+)}_{\rm out}(2\omega_c-\omega)\rangle &= \frac{\pi\hbar\omega_c}{Ac\varepsilon_0}\,[1+N(2\omega_c-\omega)] \,. \end{aligned} \tag{6.50}$$

It is convenient to write the expectation value (6.49) in a matrix form. Expressed as a matrix equation, with the help of (6.47) and (6.50), it becomes

$$\langle \hat{O}^\dagger(\omega)\hat{O}(\omega)\rangle = \frac{\pi\hbar\omega_c}{Ac\varepsilon_0}\begin{pmatrix} c^*_\omega & c_{-\omega}\end{pmatrix}\begin{pmatrix} N(\omega) & M(\omega) \\ M^*(\omega) & 1+N(2\omega_c-\omega)\end{pmatrix}\begin{pmatrix} c_\omega \\ c^*_{-\omega}\end{pmatrix} \,. \tag{6.51}$$

Since $\langle \hat{O}^\dagger(\omega)\hat{O}(\omega)\rangle \geq 0$, the determinant of the matrix is positive, so we get an inequality

$$|M(\omega)| \leq \sqrt{N(\omega)[N(2\omega_c-\omega)+1]} \,. \tag{6.52}$$

Clearly, the number of photons $N(\omega)$ imposes an upper limit on $M(\omega)$. Note that $|M(\omega)| > N(\omega)$, which is due to the presence of the term "1" arising from the quantum nature of the field, from the fact that the field operators $\hat{E}^{(-)}_{\rm out}(\omega)$ and $\hat{E}^{(+)}_{\rm out}(\omega)$ do not commute. Only in the limit of $N(\omega)\to\infty$, the parameter $|M(\omega)|$ approaches $N(\omega)$.

If the output of a source of a correlated field is treated as a classical field, then we can replace the field operators $\hat{E}^{(\pm)}_{\rm out}(\omega)$, appearing in (6.49), by classical amplitudes, $\hat{E}^{(-)}_{\rm out}(\omega)\to\mathcal{E}^*_{\rm out}(\omega)$ and $\hat{E}^{(+)}_{\rm out}(\omega)\to\mathcal{E}_{\rm out}(\omega)$. Since for classical amplitudes

$$\langle \mathcal{E}_{\rm out}(2\omega_c-\omega)\mathcal{E}^*_{\rm out}(2\omega_c-\omega)\rangle = \langle \mathcal{E}^*_{\rm out}(2\omega_c-\omega)\mathcal{E}_{\rm out}(2\omega_c-\omega)\rangle \,, \tag{6.53}$$

the expression (6.51) takes a form

$$\langle \mathcal{O}^*(\omega)\mathcal{O}(\omega)\rangle = \frac{\pi\hbar\omega_c}{Ac\varepsilon_0}\begin{pmatrix} c^*_\omega & c_{-\omega}\end{pmatrix}\begin{pmatrix} N(\omega) & M(\omega) \\ M^*(\omega) & N(2\omega_c-\omega)\end{pmatrix}\begin{pmatrix} c_\omega \\ c^*_{-\omega}\end{pmatrix} \,, \tag{6.54}$$

and as the determinant of the matrix in (6.54) must be positive, it follows that

$$|M(\omega)| \leq \sqrt{N(\omega)N(2\omega_c-\omega)} \,. \tag{6.55}$$

When $N(2\omega_c - \omega) = N(\omega)$, the inequality (6.55) reduces to $|M(\omega)| \leq N(\omega)$. We see that the correlations $|M(\omega)|$ between photons can be no larger than $N(\omega)$ that the maximal possible correlation one could achieve in a classical field is $|M(\omega)| = N(\omega)$. In this case, the squeezing spectra are positive, $S_\theta(\omega, 0) = 4N(\omega)$ and $S_\theta(\omega, \pi/2) = 0$. Thus, none of the quadrature components is reduced below the quantum limit. In this sense the classically squeezed field is always clearly distinguishable from the quantum squeezed field. For this reason, the limit $|M(\omega)| = N(\omega)$ is called in the literature as a classical limit for the two-photon correlations.

The quantum nature of the field is manifested by the increase of the two-photon correlations above the classical limit of $|M(\omega)| = N(\omega)$. What is also interesting and perhaps surprising that the largest increase of the correlations above the classical limit occurs for weak squeezed fields, i.e., for small $N(\omega)$, at which the reduction of the fluctuations below the quantum limit is not so significant. To see this more clearly, we define the normalized two-photon correlation function

$$C(\omega) = \frac{|M(\omega)|^2}{N(\omega)N(2\omega_c - \omega)} \,. \tag{6.56}$$

In the case of a classically squeezed field $|M(\omega)| \leq N(\omega)$ and then $C(\omega) \leq 1$. When $M(\omega)$ represents correlations in a quantum squeezed field, the function $C(\omega)$ is greater than one and increases dramatically at low intensity of a maximally squeezed field with $|M(\omega)| = \sqrt{N(\omega)[N(2\omega_c - \omega) + 1]}$, at which

$$C(\omega) = \frac{1 + N(\omega)}{N(\omega)} \,. \tag{6.57}$$

The result is a highly nonclassical correlation which is greatest for $N(\omega) < 1$. As we have already noticed, the nonclassical character of the correlations is manifested by the term "1" in (6.57), which arises from the quantum nature of the field. Therefore, any effect arising from the excess correlations over that for a classical field has a nonclassical character.

In summary of this section, the above discussion was introduced in order to provide some insight into the properties of squeezed fields and to distinguish characteristics which could give rise to nonclassical effects in the interaction of squeezed light with a quantum system. Examples of the effects in the radiative properties of two- and three-level atoms are given in section which follows.

6.3 Application of Squeezed Light in Atomic Spectroscopy

The experimental successes in generating squeezed light make possible to consider a wide variety of important applications. It is, however, outside the scope of the present book to do much more than examine a number of applications in atomic spectroscopy. The topics to be considered in this section are those on signatures of

quantum squeezing excitation. In particular, modifications of the atomic decay in a squeezed vacuum, signatures of quantum squeezing in three-level atoms, creation of pure states and mapping of quantum correlations contained in the squeezed field on atoms. These particular topics have been chosen because of their great influence on the development of atomic spectroscopy with nonclassical light and also because the solutions are quite readily obtained and provide an elegant demonstration of the quantum nature of squeezed states of light.

6.3.1 Radiative Decay in Squeezed Vacuum

The interaction of an atom with the ordinary, zero temperature vacuum field leads to a spontaneous decay of an atomic excitation enforced by the quantum fluctuations of the field. The decay occurs with a rate γ defined by

$$\gamma = \pi |g_\omega|^2 D(\omega) \,, \tag{6.58}$$

where $D(\omega)$ is the spectral density of the field modes at frequency ω and g_ω is the coupling strength between the atom and the field at that frequency. At a nonzero temperature, the rate is enhanced by the increased fluctuations of the thermal field and increases with an increasing temperature, $\gamma_T = N\gamma$, where N is the number of photons in the thermal field.

In the ordinary (zero temperature) or thermal vacuum field the quantum fluctuations have an isotropic distribution that two quadratures of the field amplitudes are equally modified by the quantum fluctuations. A squeezed vacuum field is characterized by an unequal distribution of the quantum fluctuations between the two quadrature components. Then, an interesting question arises if this unequal distribution of the quantum fluctuations (quantum noise) could modify the spontaneous decay of the atom.

This question was first addressed by Gardiner who considered the decay of a two-level atom in a broadband squeezed vacuum field [9]. Let us outline the major steps in the derivation of the master equation, which determines the dynamics of the atom in the squeezed field described in terms of the reduced density operator ϱ. A detailed derivation can be found, for example, in [10].

In practice the interaction of an atom with a squeezed vacuum field can be realized by the pumping of the atomic transition by the output field of a DPO or NDPO operating below threshold. However, it requires the squeezed field to cover a substantial region of the spectrum of the electromagnetic field to which the atom is coupled. The output of a typical DPO or NDPO has a finite bandwidth. Therefore, the bandwidth of the output field although finite should be broad enough compared to the atomic linewidth ($\kappa \gg \gamma/2$) that it could be treated as a broadband squeezed vacuum field.

Consider a two-level atom represented by its ground state $|1\rangle$, an excited state $|2\rangle$, the atomic transition frequency ω_a, and the transition dipole moment $\boldsymbol{\mu}_a$. The squeezed vacuum is treated as a broadband multimode field represented by the anni-

hilation and creation operators $\hat{a}_k$ and $\hat{a}_k^\dagger$, satisfying the Bose commutation relation, $[\hat{a}_k, \hat{a}_{k'}^\dagger] = \delta_{kk'}$. The total Hamiltonian of the system can be written as

$$\hat{H} = \hat{H}_0 + \hat{H}_I \ , \tag{6.59}$$

where

$$\hat{H}_0 = \hbar\omega_a S_z + \hbar \sum_k \omega_k \hat{a}_k^\dagger \hat{a}_k \tag{6.60}$$

is the free Hamiltonian of the atom and the field, and

$$\hat{H}_I = -\mathrm{i}\hbar \sum_k \left(g_k \hat{a}_k S^+ - \mathrm{H.c.}\right) \tag{6.61}$$

is the interaction between the atom and the vacuum field, given in the dipole and the rotating-wave approximations. Here, ω_k is the frequency of the kth mode of the field and g_k is the coupling strength of the atom with the k mode of the vacuum field.

The dynamics of the atom in the vacuum field are best described in terms of a reduced density operator ϱ, which is obtained by tracing the total density operator of the system ϱ_T over the vacuum field variables. The reduced density operator, written in the interaction picture, satisfies the Liouville equation

$$\mathrm{i}\hbar\dot{\tilde{\varrho}}\,(t) = \mathrm{Tr}_F \left\{ \left[\hat{H}_I\,(t)\,, \tilde{\varrho}_T\,(t) \right] \right\} \ , \tag{6.62}$$

where $\tilde{\varrho}$ is the density operator in the interaction picture and $\hat{H}_I(t)$ is given in (6.61). With the condition that the atom and the vacuum field are uncorrelated at the initial time $t = 0$, i.e. $\varrho_T(0) = \varrho(0) \otimes \varrho_F(0)$, where $\varrho_F(0)$ is the density operator of the field, we can solve (6.62) via iteration, which to the second order in the coupling (Born approximation) leads to

$$\dot{\tilde{\varrho}}\,(t) = -\frac{1}{\hbar^2} \int_0^t \mathrm{d}t' \mathrm{Tr}_F \left\{ \left[\hat{H}_I\,(t)\,, \left[\hat{H}_I\,(t')\,, \tilde{\varrho}\,(t') \otimes \tilde{\varrho}_F\,(0) \right] \right] \right\} \ . \tag{6.63}$$

The evaluation of the trace of the double commutator requires the knowledge of the second-order correlation functions of the squeezed vacuum field operators. We choose, of course, the output of the DPO characterized by the correlation functions (6.32) and (6.38), calculated in Sect. 6.1.3. In terms of the annihilation and creation operators, these correlation functions can be written as

$$\begin{aligned} &\mathrm{Tr}_F \left\{ \hat{a}_k \hat{a}_{k'}^\dagger \right\} = (1+N)\delta_{k,k'} \ , \quad \mathrm{Tr}_F \left\{ \hat{a}_k^\dagger \hat{a}_{k'} \right\} = N\delta_{k,k'} \ , \\ &\mathrm{Tr}_F \left\{ \hat{a}_k^\dagger \hat{a}_{k'}^\dagger \right\} = M\delta_{2k_c-k,k'} \ , \quad \mathrm{Tr}_F \left\{ \hat{a}_k \hat{a}_{k'} \right\} = M^*\delta_{2k_c-k,k'} \ . \end{aligned} \tag{6.64}$$

The derivation of the master equation simplifies by assuming that the variations of the reduced density operator are slow compared to the atomic frequency ω_a, and by thus making an approximation, $\tilde{\varrho}(t') = \tilde{\varrho}(t)$, which is analogous to the Weisskopf−Wigner approximation of radiation damping theory. Under this approximation, it is the matter of straightforward calculations to arrive at the following master equation

$$\begin{aligned}\frac{\partial\tilde{\varrho}}{\partial t} &= -\frac{1}{2}\gamma(1+N)\left(\tilde{\varrho}S^+S^- + S^+S^-\tilde{\varrho} - 2S^-\tilde{\varrho}S^+\right)\\ &\quad -\frac{1}{2}\gamma N\left(\tilde{\varrho}S^-S^+ + S^-S^+\tilde{\varrho} - 2S^+\tilde{\varrho}S^-\right)\\ &\quad -\gamma M^*S^+\tilde{\varrho}S^+\mathrm{e}^{-2\mathrm{i}\Delta t} - \gamma MS^-\tilde{\varrho}S^-\mathrm{e}^{2\mathrm{i}\Delta t}\,,\end{aligned} \tag{6.65}$$

where $\Delta = \omega_c - \omega_a$ is the detuning of the squeezed field carrier frequency from the atomic transition frequency. In the derivation of (6.65) we have omitted small imaginary coefficients which represent the Lamb shift of the atomic levels.

We are interested in determining the properties of the fluorescence field emitted by the atom damped to the squeezed vacuum field. In Chap. 1 we showed, expression (1.31), that the negative-frequency component of the electric field (fluorescence) emitted by an atom is proportional to the atomic dipole raising operator. In the case of a single two-level atom ($\hat{\Lambda}_{21} \equiv S^+$), the expression (1.31) takes the form

$$\hat{\mathbf{E}}^{(-)}(\mathbf{r},t) = \hat{\mathbf{E}}_F^{(-)}(\mathbf{r},t) + \boldsymbol{\Psi}(\mathbf{r})S^+(t-r/c)\,. \tag{6.66}$$

The major benefit of this expression is that it allows to consider the properties of the emitted field entirely in terms of the atomic dipole operators. Therefore, we can readily relate the quadrature components of the fluorescence field $\hat{\mathbf{E}}_\theta(\mathbf{r},t)$ and $\hat{\mathbf{E}}_{\theta+\pi/2}(\mathbf{r},t)$ to the quadrature components of the atomic dipole operators, obtaining the result

$$\begin{aligned}\hat{\mathbf{E}}_\theta(\mathbf{r},t) &= \hat{\mathbf{E}}_\theta^F(\mathbf{r},t) + 2\boldsymbol{\Psi}(\mathbf{r})S_\theta(t)\,,\\ \hat{\mathbf{E}}_{\theta+\pi/2}(\mathbf{r},t) &= \hat{\mathbf{E}}_{\theta+\pi/2}^F(\mathbf{r},t) + 2\boldsymbol{\Psi}(\mathbf{r})S_{\theta+\pi/2}(t)\,,\end{aligned} \tag{6.67}$$

where the quadratures of the atomic variables are defined with

$$\begin{aligned}S_\theta(t) &= \frac{1}{2}\left[S^-(t-r/c)\mathrm{e}^{\mathrm{i}\theta} + S^+(t-r/c)\mathrm{e}^{-\mathrm{i}\theta}\right]\,,\\ S_{\theta+\pi/2}(t) &= \frac{\mathrm{i}}{2}\left[S^-(t-r/c)\mathrm{e}^{\mathrm{i}\theta} - S^+(t-r/c)\mathrm{e}^{-\mathrm{i}\theta}\right]\,.\end{aligned} \tag{6.68}$$

Note that for $\theta = 0$, the quadratures S_θ and $S_{\theta+\pi/2}$ coincide, respectively, with the S_x and S_y polarization component of the atomic dipole moment.

We consider first the evolution of the expectation values of the dipole quadrature components. The corresponding equations of motion are obtained from the master

equation (6.65). When the squeezed vacuum field frequency is on resonance with the atomic transition frequency ($\Delta = 0$), the equations of motion for the expectation values of the dipole quadrature components are

$$\begin{aligned} \langle \dot{S}_\theta(t) \rangle &= -\gamma_x \langle S_\theta(t) \rangle + \gamma |M| \sin \Phi \langle S_{\theta+\pi/2}(t) \rangle \ , \\ \langle \dot{S}_{\theta+\pi/2}(t) \rangle &= -\gamma_y \langle S_{\theta+\pi/2}(t) \rangle + \gamma |M| \sin \Phi \langle S_\theta(t) \rangle \ , \end{aligned} \tag{6.69}$$

where $\langle S_i \rangle = \mathrm{Tr}[S_i(t)\varrho]$, $(i = \theta, \theta + \pi/2)$, $\Phi = 2\theta - \phi$, and

$$\begin{aligned} \gamma_x &= \frac{1}{2}\gamma \left[1 + 2N + 2|M| \cos \Phi\right] \ , \\ \gamma_y &= \frac{1}{2}\gamma \left[1 + 2N - 2|M| \cos \Phi\right] \ . \end{aligned} \tag{6.70}$$

Note that if $\Phi = 0$ or π, the equations of motion decouple from each other and then the quadratures S_θ and $S_{\theta+\pi/2}$ simply decay with the rates γ_x and γ_y, respectively. It is easy to see by comparing (6.70) with (6.46) that the damping rates of the atomic quadratures are related to the variances of the quadratures of the incident squeezed vacuum field. For $\Phi = 0$, the quadrature components S_θ and $S_{\theta+\pi/2}$ coincide with the maximally unsqueezed and maximally squeezed quadratures of the vacuum field, respectively.

We see that in the case of damping into the classically squeezed field, either γ_x or γ_y can be maximally reduced to its normal vacuum rate, $\gamma/2$. On the other hand, when the atom is damped into the quantum squeezed field, one of the damping rates can be reduced below its ordinary vacuum rate. For example, for $\Phi = 0$ and $N \gg 1$, the damping rate γ_y can be reduced to $\gamma_y \approx \gamma/(8N)$. Clearly, the reduction of either γ_x or γ_y below γ is a feature that is unique to quantum squeezing in that it only occurs when $M > N$.

It is instructive to calculate the evolution of the atomic population determined by the expectation value of the inversion operator $S_z(t)$. As showed in Sect. 1.6, the quantity $\langle S_z(t) \rangle + \frac{1}{2}$ is a measure of the fluorescence light intensity radiated by the atom. The master equation (6.65) gives the following equation of motion for $\langle S_z(t) \rangle$:

$$\langle \dot{S}_z(t) \rangle = -\frac{1}{2}\gamma - \gamma_z \langle S_z(t) \rangle \ , \tag{6.71}$$

in which

$$\gamma_z = \gamma_x + \gamma_y = \gamma \left(1 + 2N\right) \ . \tag{6.72}$$

We see that the population decays with the rate which is independent of M and therefore is also independent of the phase. This is to be expected, since two strongly correlated photons characteristic of the squeezed field cannot be simultaneously absorbed when interacting with a single photon transition of the two-level atom.

Thus, the fluorescence intensity, which is proportional to the population of the upper state of the atom is not a useful indicator of the quantum nature of the squeezed

field since the population decays with the rate γ_z which is not affected by the correlations M. Therefore, in any attempt to measure signatures of quantum squeezing one should perform an experiment in which the decay rate of the dipole quadrature component is directly measured or to measure quantities which are directly related to the decay rates of quadrature components.

An example of the directly measurable quantities whose properties are related to the decay rates of the dipole quadrature components is the fluorescence or the absorption spectrum of a strongly driven atom. The fluorescence spectrum, defined in (1.6) follows directly from the two-time correlation function of the atomic variables $\langle S^+(t)S^-(t+\tau)\rangle$, which can be evaluated from the optical Bloch equations of the form

$$\begin{aligned}
\langle \dot{S}_x(t)\rangle &= -\gamma_x \langle S_x(t)\rangle \,, \\
\langle \dot{S}_y(t)\rangle &= -\gamma_y \langle S_y(t)\rangle + \Omega \langle S_z\rangle \,, \\
\langle \dot{S}_z(t)\rangle &= -\frac{1}{2}\gamma - \gamma_z \langle S_z(t)\rangle - \Omega \langle S_y(t)\rangle \,,
\end{aligned} \tag{6.73}$$

where Ω is the Rabi frequency of the driving laser field. In the derivation of (6.73), we have assumed that both squeezed vacuum field and the laser field are on resonance with atomic transition. Making use of (6.73) and by taking the Fourier transform of $\langle S^+(t)S^-(t+\tau)\rangle$ with respect of τ, we obtain the incoherent part of the fluorescence spectrum. To illustrate the analytic structure of the spectrum, we consider the strong-field limit $\Omega \gg \gamma$ on resonance, when $\Delta = 0$, and find

$$\begin{aligned}
S_{in}(\omega) = \frac{\gamma}{4\pi}\Bigg[& \frac{\gamma_x}{\gamma_x^2 + (\omega-\omega_a)^2} \\
& + \frac{\frac{1}{2}\gamma_s}{\gamma_s^2 + (\omega-\omega_a-\Omega)^2} + \frac{\frac{1}{2}\gamma_s}{\gamma_s^2 + (\omega-\omega_a+\Omega)^2}\Bigg] \,,
\end{aligned} \tag{6.74}$$

where γ_x is the width of the central line, given in (6.70), and $\gamma_s = \gamma(3 + 6N - 2|M|\cos\Phi)/4$ is the width of the Rabi sidebands.

We see that the bandwidth of the central component of the spectrum is determined by the damping rate of the in-phase quadrature component S_x of the atomic dipole. Therefore, the central component of the spectrum can be significantly narrowed with a choice of phase $\Phi = \pi/2$. However, the bandwidth of the Rabi sidebands is determined by a mixture of the damping rates and could only be broadened relative to their linewidth in the ordinary vacuum. Since the linewidth of the central component of the spectrum is given by γ_x, it can be used as a measure of the damping rate of the in-phase quadrature component S_x. A measurement of the linewidth of the spectral line narrower than that for the ordinary vacuum would appear to be a direct measurement of the reduction of the decay rate γ_x below the vacuum rate. The first successful observation of the phase dependent fluorescence spectrum of a two-level atom in a squeezed vacuum field was made by Siddiqi and coworkers at University of California. Details of the experiment will be discussed in Sect. 7.3.

In closing this section, we briefly comment on the relation (6.66) which connects the frequency components of the electric field with the atomic dipole operators [11–16]. As we have seen, the relation leads to a direct connection between the quadrature components of the field and the the corresponding quadrature component of the atomic spin. However, this is not always the case that there are quantities for which the relation (6.66) gives a direct correspondence between the field and atomic spin quantities. For example, using (6.66) the normally ordered variance of the field quadrature can be written as

$$\langle : [\Delta \hat{E}_\theta(\mathbf{r}, t)]^2 : \rangle = \langle : [\Delta \hat{E}^F_\theta(\mathbf{r}, t)]^2 : \rangle + 4\mathbf{\Psi}^2(\mathbf{r}) \langle : [\Delta S_\theta(t)]^2 : \rangle \, . \tag{6.75}$$

Provided that the free field is in vacuum, $\langle : [\Delta \hat{E}^F_\theta(\mathbf{r}, t)]^2 : \rangle = 0$, and then

$$\langle : [\Delta \hat{E}_\theta(\mathbf{r}, t)]^2 : \rangle = 4\mathbf{\Psi}^2(\mathbf{r}) \langle : [\Delta S_\theta(t)]^2 : \rangle \, . \tag{6.76}$$

It follows that the criterion for squeezing in the field variables is equivalent to the condition that the normally ordered variance of the corresponding atomic quadrature component is negative. However, not alway $\langle : [\Delta S_\theta(t)]^2 : \rangle$ is negative when the fluctuations in the quadrature component $S_\theta(t)$ are squeezed.

The spin quadrature components (6.68) satisfy a commutation relation

$$[S_\theta(t), S_{\theta+\pi/2}(t)] = \mathrm{i} S_z(t) \, . \tag{6.77}$$

Therefore, referring to the definition of squeezing (2.47), the fluctuations of the in-phase quadrature (S_θ) are squeezed if

$$\langle [\Delta S_\theta(t)]^2 \rangle < \frac{1}{2} |\langle S_z(t) \rangle| \, . \tag{6.78}$$

Since

$$\langle [\Delta S_\theta(t)]^2 \rangle = \langle : [\Delta S_\theta(t)]^2 : \rangle - \frac{1}{2} \langle S_z(t) \rangle \, , \tag{6.79}$$

we see that in terms of the normally ordered variance the condition for squeezing is

$$\langle : [\Delta S_\theta(t)]^2 : \rangle - \frac{1}{2} \langle S_z(t) \rangle - \frac{1}{2} |\langle S_z(t) \rangle| < 0 \, . \tag{6.80}$$

The expectation value $\langle S_z(t) \rangle$ is a real number which may in general be positive or negative. If $\langle S_z(t) \rangle$ is negative, $\langle S_z(t) \rangle = -|\langle S_z(t) \rangle|$, and then the criterion for squeezed fluctuations in $S_\theta(t)$ is that the normally ordered variance should be negative, $\langle : [\Delta S_\theta(t)]^2 : \rangle < 0$. Thus, the negativity of $\langle : [\Delta S_\theta(t)]^2 : \rangle$ as the condition for squeezing requires negativity of the expectation value $\langle S_z(t) \rangle$. For a positive $\langle S_z(t) \rangle$ the normally ordered variance $\langle : [\Delta S_\theta(t)]^2 : \rangle$ can be positive even though the corresponding quadrature component of the atomic spin is squeezed. Therefore, the atom

can radiate unsqueezed light even though the atomic dipole fluctuations are squeezed. This situation is encountered in the theory of transient resonance fluorescence from a two-level atom driven by a monochromatic field.

We may summarize that $\langle : [\Delta S_\theta(t)]^2 : \rangle < 0$ as the condition for squeezing is equivalent to the dual requirements that the expectation value $\langle S_z(t) \rangle$ is negative and that the in-phase quadrature component of the atomic spin should be squeezed. We will return to this problem in Chap. 10 which is devoted to squeezing in spin variables.

6.3.2 *Signatures of Squeezing Excitation in a Three-Level Atom*

In the preceding section the effect of the output DPO squeezed vacuum field on the dynamics of a two-level atom were discussed. We have seen that the population of the atomic states of a two-level atom is not affected by the two-photon correlations M characteristic of the squeezed field. Since the squeezed field is characterized of the presence of strongly correlated pairs of photons, it suggests that systems in which two-photon transitions are possible could be more suitable for spectroscopy with squeezed light than a single two-level atom. Such a situation may be realized in a three-level atom in the ladder configuration, in which two-photon transitions could be possible between its upper and ground levels via a nonresonant intermediate level [17–22]. Figure 6.5 illustrates the level structure of the three-level atom consisting of upper level $|3\rangle$, intermediate level $|2\rangle$, and ground level $|1\rangle$ separated by frequencies ω_2 and ω_1, respectively. The energy levels are connected by transition dipole moments, $\boldsymbol{\mu}_1 = \langle 2| \boldsymbol{\mu} |1\rangle$ and $\boldsymbol{\mu}_2 = \langle 3| \boldsymbol{\mu} |2\rangle$. We assume that the transition dipole moment $\boldsymbol{\mu}_3 = \langle 3| \boldsymbol{\mu} |1\rangle = 0$ that the transition $|3\rangle \rightarrow |1\rangle$ is forbidden in the electric-dipole approximation.

The atomic transitions decay to a multimode squeezed vacuum field which can be the output field of the NDPO cavity. For clarity we restrict our considerations to perfect coupling of the squeezed vacuum field to the atom and work in the broadband limit of the squeezed field that the field provides a broad reservoir to the atom. We remain within the broadband field by regarding the squeezing parameters N and M as constant independent of frequency. We will demonstrate the occurrence of signatures of the quantum nature of the squeezed field in the populations of the atomic levels.

In the dipole and rotating-wave approximations, the atom-field interaction Hamiltonian is given by

$$\hat{H}_I = -\mathrm{i}\hbar \sum_{i=1}^{2} \sum_{k} \left(g_k^{(i)} \hat{a}_k S_i^+ - \mathrm{H.c.} \right) , \tag{6.81}$$

where $S_1^+ = |2\rangle\langle 1|$ ($S_1^- = |1\rangle\langle 2|$) and $S_2^+ = |3\rangle\langle 2|$ ($S_2^- = |2\rangle\langle 3|$) are the atomic raising (lowering) operators of the transitions $|2\rangle \rightarrow |1\rangle$ and $|3\rangle \rightarrow |2\rangle$, respectively.

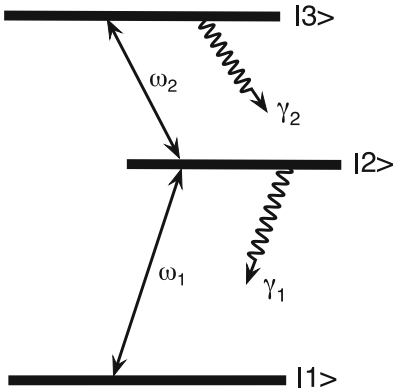

Fig. 6.5 Energy-level structure of a three-level atom in the ladder configuration. The upper level $|3\rangle$ decays to the intermediate level $|2\rangle$ with a rate γ_2, while the level $|2\rangle$ decays to the ground level $|1\rangle$ with a rate γ_1. The transition $|3\rangle \rightarrow |1\rangle$ and the decay of the upper level to the ground level are forbidden in the electric-dipole approximation

The master equation can be derived from (6.63) by substitution of the interaction Hamiltonian (6.81). After straightforward but somewhat tedious manipulation of terms, we arrive at the following master equation

$$\begin{aligned}\frac{d\tilde{\varrho}}{dt} = &-\frac{1}{2}\sum_{i,j=1}^{2}\gamma_{ij}(N+1)\left(S_i^+S_j^-\tilde{\varrho}+\tilde{\varrho}S_i^+S_j^- - 2S_j^-\tilde{\varrho}S_i^+\right)\mathrm{e}^{\mathrm{i}(\omega_i-\omega_j)t}\\ &-\frac{1}{2}\sum_{i,j=1}^{2}\gamma_{ij}N\left(S_i^-S_j^+\tilde{\varrho}+\tilde{\varrho}S_i^-S_j^+ - 2S_j^+\tilde{\varrho}S_i^-\right)\mathrm{e}^{\mathrm{i}(\omega_i-\omega_j)t}\\ &-\frac{1}{2}\sum_{i,j=1}^{2}\gamma_{ij}M\left(S_i^-S_j^-\tilde{\varrho}+\tilde{\varrho}S_i^-S_j^- - 2S_j^-\tilde{\varrho}S_i^-\right)\mathrm{e}^{-\mathrm{i}(2\omega_c-\omega_i-\omega_j)t}\\ &-\frac{1}{2}\sum_{i,j=1}^{2}\gamma_{ij}M^*\left(S_i^+S_j^+\tilde{\varrho}+\tilde{\varrho}S_i^+S_j^+ - 2S_j^+\tilde{\varrho}S_i^+\right)\mathrm{e}^{\mathrm{i}(2\omega_c-\omega_i-\omega_j)t}\,, \qquad (6.82)\end{aligned}$$

where $\tilde{\varrho}$ is the reduced density operator of the atom in the interaction picture, $\gamma_{11}=\gamma_1$ and $\gamma_{22}=\gamma_2$ are the damping rates of the atomic transitions $|2\rangle \rightarrow |1\rangle$ and $|3\rangle \rightarrow |2\rangle$, respectively, and $\gamma_{12}=\gamma_{21}$ are the cross damping rates between the transitions. The cross damping rates represent the effect of the coupling between the atomic transitions induced by spontaneous emission that the decay from the level $|3\rangle$ induces a decay from level $|2\rangle$, and vice versa. The rates are very sensitive to the mutual polarization of the transition dipole moments. For example, if $\boldsymbol{\mu}_1$ is parallel to $\boldsymbol{\mu}_2$, then $\gamma_{12}=\sqrt{\gamma_1\gamma_2}$ and the cross damping is maximal. If $\boldsymbol{\mu}_1$ is perpendicular to $\boldsymbol{\mu}_2$, then $\gamma_{12}=0$ and the levels decay independently. In what follows we will assume that $\gamma_{12}=\sqrt{\gamma_1\gamma_2}$.

Having available the master equation for the density operator of the atom, we turn our attention to the dynamics of the atom. Here, we concentrate on the stationary populations of the atomic levels. Let us start by writing a complete set of the equations of motion for the populations of the atomic levels and the involved coherence between

them. For simplicity, let us assume that the double frequency $2\omega_c$ of the squeezed vacuum field is resonant with the two-photon atomic transition from $|1\rangle$ to $|3\rangle$, i.e., $2\omega_c = \omega_1 + \omega_2$. The equations of motion are of the form

$$\begin{aligned}
\dot{\varrho}_{22} &= N\gamma_1 - [N\gamma_2 + (2N+1)\gamma_1]\,\varrho_{22} + [(N+1)\gamma_2 - N\gamma_1]\,\varrho_{33} + \gamma_{12}|M|\tilde{\varrho}_{13}\,, \\
\dot{\varrho}_{33} &= -(N+1)\,\gamma_2\varrho_{33} + N\gamma_2\varrho_{22} - \frac{1}{2}\gamma_{12}|M|\tilde{\varrho}_{13}\,, \\
\dot{\tilde{\varrho}}_{13} &= -\gamma_{12}|M| - \frac{1}{2}\,[N\gamma_1 + (N+1)\,\gamma_2]\,\tilde{\varrho}_{13} + 3\gamma_{12}|M|\varrho_{22}\,,
\end{aligned} \tag{6.83}$$

where $\tilde{\varrho}_{13} = \varrho_{13}\exp(\mathrm{i}\phi) + \varrho_{31}\exp(-\mathrm{i}\phi)$ is the real part of the two-photon coherence, and ϕ is the phase of the squeezed field.

Equations (6.83) show that the populations of the three-level atom can be sensitive to the two-photon correlations M and the sensitivity is brought by the cross damping rate. Therefore, the effect of the two-photon correlations on the three-level atom is expected to be more drastic than on a two-level atom. To check it, let us consider the steady-state populations of the atomic levels. These are obtained from (6.83) by putting the left-hand side of the equations to zero. It is then straightforward to find that the steady-state solutions for the populations of the atomic levels are

$$\begin{aligned}
\varrho_{22} &= \frac{N\,(N+1) - |M|^2}{3N^2 + 3N + 1 - 3|M|^2}\,, \\
\varrho_{33} &= \frac{N^2 W - |M|^2\,(W - 1 - \alpha)}{W\left(3N^2 + 3N + 1 - 3\,|M|^2\right)}\,,
\end{aligned} \tag{6.84}$$

where $W = \alpha + N\,(1+\alpha)$, and $\alpha = \gamma_2/\gamma_1$.

To examine the occurrence of signatures of the quantum nature of the squeezed field we look at the variation of the populations with the squeezing parameter M. Note that the range of $|M| \leq N$ corresponds to the excitation with a classically squeezed light whereas $|M| > N$ corresponds to the excitation with a quantum squeezed field.

Figure. 6.6 shows the populations ϱ_{22} and ϱ_{33} as a function of the degree of two-photon correlations $|M|$ for several different values of N. We see that for $|M| \leq N$ the populations are almost unchanged from their values in the thermal field. Thus, classical two-photon correlations do not affect the populations of the atomic levels. Once $|M|$ reaches the value corresponding to the boundary for quantum squeezing ($|M| = N$) the populations change drastically with $|M|$. For $|M| > N$, the population ϱ_{22} falls almost instantaneously to zero whereas ϱ_{33} jumps to values much larger than those corresponding to the equilibrium distribution predicted by the Boltzmann distribution, $\varrho_{33} = \frac{1}{3}$. Thus, the effect of going into the regime of quantum correlations is to decrease the population of the intermediate level to zero. This is readily understood if it is recalled that the in the quantum squeezed field photons are strongly correlated in pair. One photon of a correlated pair excites the atom to the intermediate state $|2\rangle$ and its twin immediately takes the population to the upper state $|3\rangle$. In this

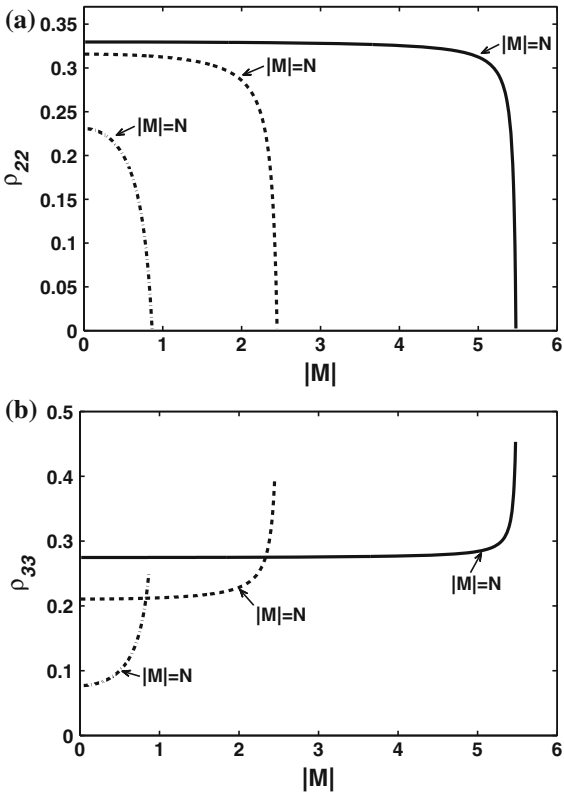

Fig. 6.6 Variation of the steady-state populations of the excited states **a** ϱ_{22} and **b** ϱ_{33} with the squeezing parameter $|M|$ for $\alpha = 1$ and different N: $N = 5$ (*solid line*), $N = 2$ (*dashed line*), and $N = 0.5$ (*dashed-dotted line*)

case, the population is transferred from the ground state $|1\rangle$ to the upper state $|3\rangle$ without population of the state $|2\rangle$.

The reduction of the population of the intermediate level to zero leads to population inversion between the atomic levels. It is easily found from the steady-state solutions (6.84) that for a classical squeezed field with $|M| = N$ the stationary populations of the excited atomic levels are

$$\varrho_{22} = \frac{N}{3N+1}, \tag{6.85}$$

and

$$\varrho_{33} = \frac{N^2\,(1+\alpha)}{W\,(3N+1)}. \tag{6.86}$$

In this case, the ratios of the populations are

$$\frac{\varrho_{33}}{\varrho_{22}} = 1 - \frac{\alpha}{\alpha + N\,(1+\alpha)}\,, \tag{6.87}$$

and

$$\frac{\varrho_{22}}{\varrho_{11}} = 1 - \frac{W + \alpha N}{W\,(N+1) + \alpha N}\,. \tag{6.88}$$

It is straightforward to see that the ratios are smaller than one so that the populations are not inverted, indicating that in the classically squeezed field the populations obey a Boltzmann distribution with $\varrho_{11} > \varrho_{22} > \varrho_{33}$. Moreover, in the limit of low intensities ($N \ll 1$) of the squeezed field the population ϱ_{33} is proportional to N^2, showing that in classical fields the population exhibits a quadratic dependence on the intensity. This dependence reflects a two step excitation $|1\rangle \rightarrow |2\rangle$ and $|2\rangle \rightarrow |3\rangle$, each proportional to N.

The situation is different for a quantum squeezed field with $|M| > N$. If we write

$$|M| = \sqrt{N^2 + \beta N}\,, \tag{6.89}$$

where $0 \leq \beta \leq 1$ measures the excess of the two-photon correlations above the classical limit of $|M| = N$, (6.84) now give us

$$\varrho_{22} = \frac{(1-\beta)\,N}{3\,(1-\beta)\,N + 1}\,, \tag{6.90}$$

and

$$\varrho_{33} = \frac{\beta N + (1-\beta)\,(1+\alpha)\,N^2}{(\alpha + \alpha N + N)\,[3\,(1-\beta)\,N + 1]}\,. \tag{6.91}$$

The ratio between the populations ϱ_{33} and ϱ_{22} is now given by

$$\frac{\varrho_{33}}{\varrho_{22}} = 1 + \frac{(1+\alpha)\beta - \alpha}{(1-\beta)\,[\alpha + (1+\alpha)\,N]}\,. \tag{6.92}$$

It is easy to see that the ratio can be larger than one when $\beta > \alpha/\,(1+\alpha)$. This indicates that in the case of the decay in the quantum squeezed vacuum, the level populations no longer obey the Boltzmann distribution. Furthermore, for $\alpha \ll 1$ and $\beta \approx 1$ the population in the state $|3\rangle$ approaches one ($\varrho_{33} \approx 1$). Thus, a nearly-complete population inversion can be achieved when the atom is damped by the quantum squeezed vacuum. This is another notable feature of quantum nature of the squeezed field.

It should be noted that the population inversions are very sensitive to the degree of two-photon correlations in the squeezed vacuum. From the population inversion condition, $\beta > \alpha/\,(1+\alpha)$, it is clear that for α small enough a significant inversion can be obtained even with an imperfect correlations. This is an important conclusion since the theory of the DPO or NDPO, discussed in Sect. 6.2.1, predicts an imperfectly squeezed output field with $\beta < 1$.

Let us now comment about the population ϱ_{33} in the quantum squeezed vacuum, expression (6.91). It is seen that the population exhibits both linear and quadratic

dependence on N. The quadratic term vanishes for a squeezed vacuum with perfect correlations, ($\beta \approx 1$). For weak fields ($N \ll 1$) the linear term dominates indicating that in a low intensity quantum squeezed field the population ϱ_{33} depends linearly on the intensity. This distinctive feature reflects the direct modifications of the two-photon absorption that in the quantum squeezed field the photon correlations $|M|$ enable the transition $|1\rangle \rightarrow |3\rangle$ to occurs in a "single step" proportional to N.

In addition, we find that the population ϱ_{33}, for $N \ll 1$, can be written as

$$\varrho_{33} \approx \frac{\beta^2}{\alpha} N \ , \tag{6.93}$$

which shows that even for an imperfect squeezed vacuum the population depends linearly on N. A small degree of the correlations diminishes only the value of the population in the state $|3\rangle$. Thus, we have a feature unique to the quantum nature of the squeezed vacuum which is not disturbed by an correlations and can be observed even for a small degree of the correlations β, independent of α.

This feature has led to a successful experiment observation of the linear dependence on intensity of the population ϱ_{33} in a cesium atom illuminated by the output field from the NDPO. Details of the experiment are presented in Sect. 7.4.

6.3.3 Spontaneous Decay to a Correlated Pure State

In the previous section we have determined the stationary distribution of the population in a three-level atom decaying to a squeezed vacuum field. In this section we will examine the stationary state of the atom and demonstrate the occurrence of yet another feature unique to the quantum nature of the squeezed vacuum. The squeezed vacuum appears to the atom as a nonzero temperature reservoir characterized by two-photon correlations. Therefore, it is quite natural to expect that an atom interacting with the squeezed vacuum should decay to a mixed state. However, we will find that the stationary state of the atom illuminated by a quantum squeezed vacuum field is not a mixed state but a pure superposition state [23–26].

Let us start with determining steady-state values of the density matrix elements. From the equations of motion for the populations (6.83) we see that only different from zero could be the diagonal elements (populations) and the real part of the off-diagonal element ϱ_{13}. The remaining off-diagonal elements are not coupled to the populations and as such, even if nonzero initially, will evolve to zero values in the steady-state. Therefore, the steady-state density matrix of the system is of the form

$$\varrho = \begin{pmatrix} \varrho_{11} & 0 & \varrho_{13} \\ 0 & \varrho_{22} & 0 \\ \varrho_{31} & 0 & \varrho_{33} \end{pmatrix} \ , \tag{6.94}$$

where ϱ_{ij} are the nonzero density matrix elements obtained by solving (6.83) for the steady-state, and are given by

$$\begin{aligned}
\varrho_{11} &= \frac{[\gamma_2 + N(\gamma_1+\gamma_2)](1+N)^2 - [(1+N)\gamma_1 + (2+N)\gamma_2]|M|^2}{(3N^2+3N+1-3|M|^2)[\gamma_2+N(\gamma_1+\gamma_2)]}\,,\\
\varrho_{22} &= \frac{N(N+1)-|M|^2}{3N^2+3N+1-3|M|^2}\,,\\
\varrho_{33} &= \frac{N^2[\gamma_2+N(\gamma_1+\gamma_2)] - |M|^2[N(\gamma_1+\gamma_2)-\gamma_1]}{(3N^2+3N+1-3|M|^2)[\gamma_2+N(\gamma_1+\gamma_2)]}\,,\\
\varrho_{13} &= \frac{\sqrt{\gamma_1\gamma_2}|M|e^{-i\phi}}{(3N^2+3N+1-3|M|^2)[\gamma_2+N(\gamma_1+\gamma_2)]}\,.
\end{aligned} \tag{6.95}$$

It is evident from (6.94) that in the squeezed vacuum the stationary density matrix of the system is not diagonal due to the presence of the two-photon coherencies ϱ_{13} and ϱ_{31}. This indicates that the atom decays to states different than the bare atomic states. To find these states, we diagonalize the matrix (6.94) and find the diagonal probabilities

$$P_1 = \frac{1}{2}(\varrho_{11}+\varrho_{33}+D)\;,\;\; P_2 = \frac{1}{2}(\varrho_{11}+\varrho_{33}-D)\;,\;\; P_3 = \varrho_{22}\,, \tag{6.96}$$

and the corresponding states

$$\begin{aligned}
|\Psi_1\rangle &= \cos\vartheta\,|1\rangle + \sin\vartheta\,|3\rangle\;,\\
|\Psi_2\rangle &= \sin\vartheta\,|1\rangle - \cos\vartheta\,|3\rangle\;,\\
|\Psi_3\rangle &= |2\rangle\;,
\end{aligned} \tag{6.97}$$

where

$$\cos^2\vartheta = \frac{1}{2} + \frac{\varrho_{11}-\varrho_{33}}{2D}\,, \tag{6.98}$$

with

$$D = \left[(\varrho_{11}-\varrho_{33})^2 + 4|\varrho_{31}|^2\right]^{\frac{1}{2}}\;. \tag{6.99}$$

It is clearly seen from (6.97) that the squeezed vacuum causes the atom to decay into superposition states which are linear combinations of the atomic ground $|1\rangle$ and the upper $|3\rangle$ states. The intermediate state $|2\rangle$ remains unchanged under the squeezed vacuum excitation.

In general, the stationary state of the atom is a mixed state. Since the populations depend on the two-photon correlations, one can expect that the state of the atom may change with M. In order to check it, we evaluate the quantity

$$\mathrm{Tr}\left(\varrho^2\right) = P_1^2 + P_2^2 + P_3^2 \,, \tag{6.100}$$

which is a measure of the purity of the atomic state. $\mathrm{Tr}(\varrho^2) = 1$ corresponds to a pure state of the atom, while $\mathrm{Tr}(\varrho^2) < 1$ corresponds to a mixed state. $\mathrm{Tr}(\varrho^2) = \frac{1}{3}$ describes a completely mixed state of the atom.

Figure 6.7 shows $\mathrm{Tr}(\varrho^2)$ as a function of $|M|$ for several values of N. We see that the purity is almost constant in the range of the correlations $0 \leq |M| < \sqrt{N(N+1)}$ and then at $|M|$ very close to the maximal value of $\sqrt{N(N+1)}$ the purity suddenly "jumps" to the maximum value of unity. Thus, at $|M| \approx \sqrt{N(N+1)}$ the atom suddenly turns from a mixed state to a pure state. For a strong field with $N \gg 1$ the state of the atom at $|M| < \sqrt{N(N+1)}$ is exactly the same as in the case of a thermal field. A correlated atomic state is produced suddenly at $|M| = \sqrt{N(N+1)}$.

It is easily verified that for maximal correlations $|M|^2 = N(N+1)$, the populations P_2 and P_3 are zero leaving the state $|\Psi_1\rangle$ of only populated state of the atom. Hence, in the quantum squeezed vacuum with maximal correlations the atom decays to a pure state $|\Psi_1\rangle$ which is a linear superposition of only the ground and the upper states. It is easily verified that for $|M|^2 = N(N+1)$ and $\gamma_1 = \gamma_2$, $D = 1$ and $\varrho_{11} - \varrho_{33} = 1/(2N+1)$. In this case the atomic pure state is of the form

$$|\Psi_1\rangle = \frac{1}{\sqrt{2N+1}} \left(\sqrt{N+1}\,|1\rangle + \sqrt{N}\,|3\rangle \right) \,. \tag{6.101}$$

The creation of the two-photon superposition state reflects the fact that two-photon correlations contained in the squeezed vacuum are transferred to the atom. However, the created superposition of the atomic states is not maximal despite the fact that the correlations in the squeezed field are maximal. The superposition becomes maximal

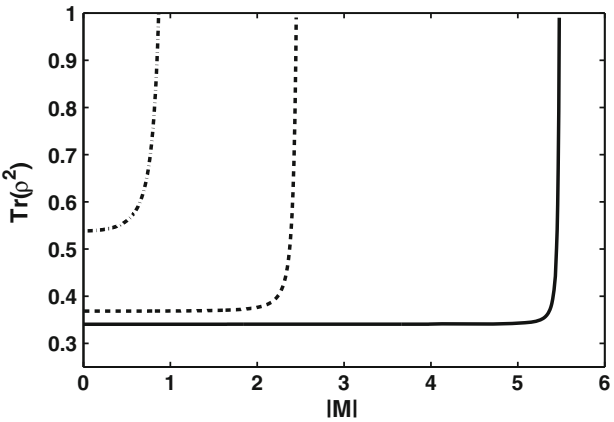

Fig. 6.7 Variation of $\mathrm{Tr}(\varrho^2)$ with the squeezing parameter $|M|$ for $\gamma_2 = \gamma_1$ and different N: $N = 5$ (*solid line*), $N = 2$ (*dashed line*), and $N = 0.5$ (*dashed-dotted line*)

in the limit of $N \to \infty$. According to (6.46), the limit $N \to \infty$ corresponds to perfect squeezing of the squeezed vacuum field, in which case the squeezing spectrum is given by

$$S_\theta(\omega_c, \pi/2) = 2N - 2|M| \to 2N - 2N\left(1 + \frac{1}{2N} - \cdots\right) \approx -1 \,. \quad (6.102)$$

Thus, the maximal superposition of the atomic ground and the upper states is created by perfectly squeezed vacuum field.

6.3.4 Mapping of Squeezed Fluctuations on Atoms

The pure highly correlated stationary state of the atom results from the transfer of the two-photon correlations from the squeezed vacuum to the atoms. A question arises how efficient is the transfer of the correlations? In particular, we look at the mapping of squeezed fluctuations on the atoms and determine the relation between squeezing in the incident squeezed vacuum and that produced by the atomic dipoles [27–30]. In other words, we look at conditions the atomic dipole fluctuations mirror the fluctuations in the squeezed vacuum.

A measurable quantity associated with the correlations produced by the NDPO cavity is the normally ordered variance of the field operators

$$\begin{aligned}\langle : [\Delta \hat{E}^S_\theta(\omega)]^2 : \rangle = {} & 2\langle \Delta \hat{E}^{(-)}_\theta(\omega) \Delta \hat{E}^{(+)}_\theta(\omega) \rangle + \langle \Delta \hat{E}^{(+)}_\theta(\omega) \Delta \hat{E}^{(+)}_\theta(\omega) \rangle e^{2i\theta} \\ & + \langle \Delta \hat{E}^{(-)}_\theta(\omega) \Delta \hat{E}^{(-)}_\theta(\omega) \rangle e^{-2i\theta} \,, \end{aligned} \quad (6.103)$$

where the superscript "S" stands for the squeezed vacuum field.

The correlation functions, which are needed to determine the normally ordered variance, are obtained from previously derived expressions (6.32) and (6.38). We find that

$$\langle : (\Delta \hat{E}^S_\theta)^2 : \rangle = E_0 \, (2N + 2|M| \cos \Phi) \,, \quad (6.104)$$

where E_0 is a constant and $\Phi = 2\theta - \phi$. For $\Phi = \pi$ and $|M| = \sqrt{N(N+1)}$, we see from (6.104) that the normally ordered variance is negative indicating squeezing of the vacuum field.

On the other hand, the normally ordered variance of the stationary fluorescence field emitted from a three-level atom in a ladder configuration is given by

$$\langle : (\Delta \hat{E}^A_\theta)^2 : \rangle = \langle : (\Delta \hat{E}^F_\theta)^2 : \rangle + 4\Psi^2(\mathbf{r}) \langle : (\Delta S_\theta)^2 : \rangle \,, \quad (6.105)$$

where the superscript "A" stands for the field produced by the atom, and

$$S_\theta = \frac{1}{2}\left[(S_1^- + S_2^-)e^{i\theta} + (S_1^+ + S_2^+)e^{-i\theta}\right] \quad (6.106)$$

is the in-phase quadrature component of the total atomic dipole. It involves dipole operators of the two transitions in the atom. In writing (6.105) we have assumed that both atomic transitions contribute equally, i.e., $\mathbf{\Psi}_{32}^2(\mathbf{r}) = \mathbf{\Psi}_{21}^2(\mathbf{r}) \equiv \mathbf{\Psi}^2(\mathbf{r})$.

The variance of the atomic quadrature component, written in terms of the density matrix elements is of the form

$$\langle : (\Delta E_\theta^A)^2 : \rangle = E_0 \left(2\varrho_{22} + 2\varrho_{33} + 2|\varrho_{13}| \cos 2\theta\right) , \tag{6.107}$$

where we have retained only those density matrix elements which are nonzero in the steady-state.

To determine the variance, we make use of the previously found steady-state solutions (6.95) and take $|M| = \sqrt{N(N+1)}$ and $\gamma_1 = \gamma_2$. We then find

$$\langle : (\Delta E_\theta^A)^2 : \rangle = E_0 \frac{(2N + 2|M| \cos \Phi)}{2N + 1} . \tag{6.108}$$

The variances (6.104) and (6.108) differ by a factor $2N + 1$. The normally ordered variances given by (6.104) and (6.108) are plotted in Fig. 6.8 as a function of N. The variances are almost identical when the squeezed vacuum is relatively weak, $N \ll 1$. In this limit, the atomic dipole fluctuations mirror the fluctuations in the squeezed vacuum. In other words, the squeezed fluctuations of the incident field are perfectly mapped onto the atomic system. However, as the intensity of the squeezed vacuum increases, the variances deviate from each other and the squeezing in the fluorescence field disappears when $N \to \infty$ at which the squeezed vacuum is perfectly squeezed. The increasing deviation of the variances with N can be ascribed to quantum fluctuations induced during the interaction of the squeezed vacuum with the atom. The

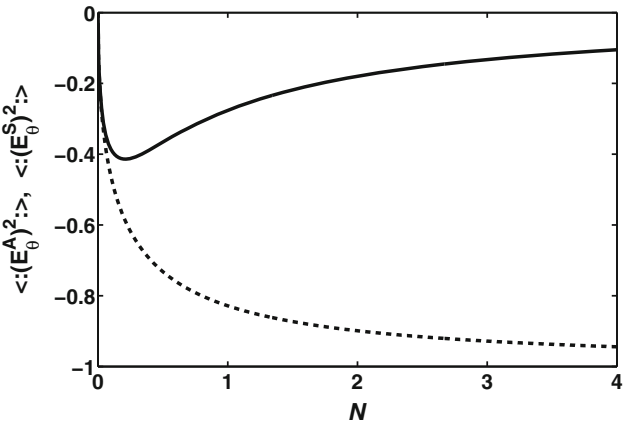

Fig. 6.8 Normally ordered variances of the squeezed vacuum field and the fluorescence field of the atom are plotted as a function of N: $\langle : (\Delta E_\theta^A)^2 : \rangle / E_0$ (*solid line*) and $\langle : (\Delta E_\theta^S)^2 : \rangle / E_0$ (*dashed line*)

stronger the squeezed field is, the greater are the fluctuations of the fluorescence field. We see from the figure that the optimum squeezing in the fluorescence field is produced at low N when the squeezed vacuum is only weakly squeezed.

Perhaps the interesting aspect of squeezing in the three-level atom relates to the superposition state that the maximal superposition of the atomic ground and upper levels does not produce squeezing in the fluorescence field. Dalton et al. [31] showed that the state for maximum noise reduction (optimum squeezing) in a quadrature component of the dipole moment of a three-level ladder system is a superposition state of the form

$$|\psi\rangle = \frac{1}{\sqrt{2}}\sqrt{\left(1+\frac{1}{\sqrt{2}}\right)}\,|1\rangle + \frac{1}{\sqrt{2}}\sqrt{\left(1-\frac{1}{\sqrt{2}}\right)}\,|3\rangle\ . \tag{6.109}$$

The normally ordered variance of the fluorescence field corresponding to the state (6.109) is given by

$$\langle :(\Delta E_\theta^A)^2: \rangle / E_0 = -(\sqrt{2}-1) \approx -0.41\ . \tag{6.110}$$

We may write the state (6.101) in the form

$$|\Psi_1\rangle = \frac{1}{\sqrt{2}}\sqrt{\left(1+\frac{1}{2N+1}\right)}\,|1\rangle + \frac{1}{\sqrt{2}}\sqrt{\left(1-\frac{1}{2N+1}\right)}\,|3\rangle\ , \tag{6.111}$$

and when comparing with (6.109), we find that the state producing optimum squeezing that is, the minimum normally ordered variance of the fluorescence field can be created by a weak squeezed field of the intensity $N = (\sqrt{2}-1)/2 \approx 0.21$.

6.3.5 *Signatures of Squeezing Excitation in the Dicke Model*

A related model to a three-level atom in a ladder configuration is a system composed of two two-level atoms contained in a volume with linear dimensions that are small compared to the radiation wavelength. This model is known in the literature as the Dicke model, and in this section we deal briefly with the dynamics of the model in a squeezed vacuum field. We will demonstrate that somewhat similar effects appear in this model to those observed in the three-level atom. However, there are some important differences which we would like to explore in this section. In particular, no two-photon inversion can be created in the Dicke model but one can create a pure maximally entangled state between the atoms.

The Dicke model is the simplest model of a group of atoms with a collective decay. The model does not include features such as spatial separation of the atoms and dipole–dipole interactions. It assumes that atomic separations are small compared to the radiation wavelength. In this case, the collective damping parameter

γ_{12}, introduced in Chap. 3, can be approximated by γ. As a result, the antisymmetric state, which decays with the rate $\gamma - \gamma_{12}$, becomes optically inactive and decouples from the remaining states of the system. Therefore, the dynamics of the Dicke model can be described in terms of the collective states but confined to the subspace of only three states, the ground $|g_1, g_2\rangle$, symmetric $|s\rangle$ and the upper $|e_1, e_2\rangle$ states. Clearly, the collective states form a three-level ladder system. The upper state $|e\rangle$ and the intermediate state $|s\rangle$ decay with equal rates 2γ. This makes the Dicke model different from the three-level ladder atom in which the excited states can decay with different rates.

The interaction Hamiltonian of the Dicke model with the squeezed vacuum field, in the electric-dipole and rotating-wave approximations, can be written as

$$\hat{H}_I = -\mathrm{i}\hbar \sum_k \left(g_k \hat{a}_k S^+ - g_k^* S^- \hat{a}_k^\dagger \right) , \tag{6.112}$$

where S^+ and S^- are the total (collective) atomic raising and lowering operators

$$S^+ = \sum_{n=1}^{2} S_n^+ , \quad S^- = \sum_{n=1}^{2} S_n^- . \tag{6.113}$$

The master equation can be derived for the density operator of the Dicke system damped to a squeezed vacuum starting from the general equation of motion for the reduced density operator (6.63). When the interaction Hamiltonian (6.112) together with the field correlation functions (6.64) is substituted into (6.63), we arrive to the following master equation

$$\begin{aligned} \frac{d\tilde{\varrho}}{dt} = & -\frac{1}{2}\gamma(N+1)\left(S^+S^-\tilde{\varrho} + \tilde{\varrho}S^+S^- - 2S^-\tilde{\varrho}S^+\right) \\ & -\frac{1}{2}\gamma N\left(S^-S^+\tilde{\varrho} + \tilde{\varrho}S^-S^+ - 2S^+\tilde{\varrho}S^-\right) \\ & -\frac{1}{2}\gamma M\left(S^-S^-\tilde{\varrho} + \tilde{\varrho}S^-S^- - 2S^-\tilde{\varrho}S^-\right)\mathrm{e}^{-2\mathrm{i}(\omega_c-\omega_0)t} \\ & -\frac{1}{2}\gamma M^*\left(S^+S^+\tilde{\varrho} + \tilde{\varrho}S^+S^+ - 2S^+\tilde{\varrho}S^+\right)\mathrm{e}^{2\mathrm{i}(\omega_c-\omega_0)t} . \end{aligned} \tag{6.114}$$

Using the master equation (6.114), with the system confined to space of collective states $\{|g\rangle, |s\rangle, |e\rangle\}$, we can derive equations of motion for the diagonal and off-diagonal density matrix elements. By examining the equations of motion, we find that only four matrix elements, ϱ_{gg}, ϱ_{ss}, ϱ_{ee} and ϱ_u can have nonzero steady-state solutions. None of the other density matrix elements can have nonzero steady-state solutions. The equations of motion for these four density matrix elements are

$$\begin{aligned}
\dot{\varrho}_{gg} &= 2\gamma\,(N+1)\,\varrho_{ss} - 2\gamma N\,\varrho_{gg} + \gamma|M|\varrho_u\,,\\
\dot{\varrho}_{ee} &= -2\gamma\,(N+1)\,\varrho_{ee} + 2\gamma N\,\varrho_{ss} + \gamma|M|\varrho_u\,,\\
\dot{\varrho}_{ss} &= -2\gamma\,(2N+1)\,\varrho_{ss} + 2\gamma(N+1)\varrho_{ee} + 2\gamma N\varrho_{gg} - 2\gamma|M|\varrho_u\,,\\
\dot{\varrho}_u &= 2\gamma|M| - \gamma\,(2N+1)\,\varrho_u - 6\gamma|M|\varrho_{ss}\,,
\end{aligned} \tag{6.115}$$

where $\varrho_u = \varrho_{eg}\exp(-i\phi_s) + \varrho_{ge}\exp(i\phi_s)$ and, for simplicity, we have assumed that the carrier frequency ω_s of the squeezed vacuum field is resonant with the atomic transition frequency ω_0.

The steady-state solution of (6.115) is easy to obtain, and is of the form

$$\begin{aligned}
\varrho_{gg} &= \frac{(2N+1)\,(N+1)^2 - (2N+3)\,|M|^2}{(2N+1)\left(3N^2+3N+1-3|M|^2\right)}\,,\\
\varrho_{ee} &= \frac{N^2\,(2N+1) - (2N-1)\,|M|^2}{(2N+1)\left(3N^2+3N+1-3|M|^2\right)}\,,\\
\varrho_{ss} &= \frac{N\,(N+1) - |M|^2}{3N^2+3N+1-3|M|^2}\,,\\
\varrho_u &= \frac{2|M|}{(2N+1)\left(3N^2+3N+1-3|M|^2\right)}\,.
\end{aligned} \tag{6.116}$$

Comparing the steady-state results of the Dicke model (6.116) to those of a three-level atom (6.95), we find that the only difference is in the dependence on the damping rate. The steady-state of the three-level atom depends on the ratio of the damping rates of the two atomic transitions, the dependence which is absent in the steady-state of the Dicke model. As we have seen, this dependence yields a two-photon population inversion. Obviously, no two-photon population inversion is possible in the Dicke model.

Of course, with the assumption of equal decay rates, the results for the three-level atom and the Dicke model share many common features. For example, when the atoms are damped by a classically squeezed field with the maximal correlations $M = N$, the expressions (6.116) reduce to

$$\begin{aligned}
\varrho_{ss} &= \frac{N}{3N+1}\,, \quad \varrho_{gg} = \frac{8N^2+4N+1}{(2N+1)\,(3N+1)}\,,\\
\varrho_{ee} &= \frac{2N^2}{(2N+1)\,(3N+1)}\,, \quad \varrho_u = \frac{2N}{(2N+1)\,(3N+1)}\,.
\end{aligned} \tag{6.117}$$

We find that, as before for the three-level atom, the populations are not inverted, $\varrho_{gg} > \varrho_{ss} > \varrho_{ee}$. Moreover, in the limit of low intensities ($N \ll 1$), the population ϱ_{ee} is proportional to N^2, showing that in classical fields the population exhibits a quadratic dependence on the intensity.

Also there are many similarities between these two systems in the case of damping by a quantum squeezed field. With the maximal correlations $|M|^2 = N(N+1)$, the expressions (6.116) reduce to

$$\varrho_{ss} = 0\,, \quad \varrho_{gg} = \frac{N+1}{2N+1}\,,$$
$$\varrho_{ee} = \frac{N}{2N+1}\,, \quad \varrho_u = \frac{2\sqrt{N(N+1)}}{2N+1}\,. \tag{6.118}$$

We see that similar to the three-level atom, the intermediate level (symmetric state) is not populated. Consequently, there is a one-photon population inversion. Moreover, in a weak quantum squeezed field the population ϱ_{ee} depends linearly on the intensity.

As we have already mentioned, and it is easy to see from (6.118), that $\varrho_{gg} > \varrho_{ee}$ always. Consequently, there is no possibility for a two-photon population inversion in the Dicke model.

There are interesting properties of the final state of the Dicke model, that it can be a maximally entangled state. Since the only nonzero steady-state density matrix elements are those given in (6.116), the steady-state density matrix is of the form

$$\varrho = \begin{pmatrix} \varrho_{gg} & 0 & \varrho_{ge} \\ 0 & \varrho_{ss} & 0 \\ \varrho_{eg} & 0 & \varrho_{ee} \end{pmatrix}\,. \tag{6.119}$$

The density matrix is not diagonal, and when diagonalized, we find that the final state of the system is, in general, a mixed state determined by a set of three entangled states

$$|\Upsilon_1\rangle = \cos\vartheta\,|g_1, g_2\rangle + \sin\vartheta\,|e_1, e_2\rangle\,,$$
$$|\Upsilon_2\rangle = \sin\vartheta\,|g_1, g_2\rangle - \cos\vartheta\,|e_1, e_2\rangle\,,$$
$$|\Upsilon_3\rangle \equiv |s\rangle = \frac{1}{\sqrt{2}}\left(|e_1, g_2\rangle + |g_1, e_2\rangle\right)\,, \tag{6.120}$$

where

$$\cos^2\vartheta = \frac{1}{2} + \frac{\varrho_{gg} - \varrho_{ee}}{2D}\,, \tag{6.121}$$

with

$$D = \left[\left(\varrho_{gg} - \varrho_{ee}\right)^2 + 4\left|\varrho_{eg}\right|^2\right]^{\frac{1}{2}}\,, \tag{6.122}$$

and the corresponding probabilities are

$$P_1 = \frac{1}{2}\left(\varrho_{gg} + \varrho_{ee} + D\right)\,,\ P_2 = \frac{1}{2}\left(\varrho_{gg} + \varrho_{ee} - D\right)\,,\ P_3 = \varrho_{ss}\,. \tag{6.123}$$

However, the involvement of the entangled states does not necessarily result in an entanglement between the atoms. In order to see this, let us consider the concurrence, a measure of entanglement between two atoms in a mixed state. With the density matrix of the X form, such as the matrix (6.119), the concurrence can be calculated analytically and can be expressed as

$$\mathcal{C} = \max\{0, C_1, C_2\} \ , \tag{6.124}$$

where

$$C_1 = 2\left(\varrho_{ss} - \sqrt{\varrho_{gg}\varrho_{ee}}\right) \ , \tag{6.125}$$

$$C_2 = \varrho_u - \varrho_{ss} \ . \tag{6.126}$$

There are two quantities which determine a nonzero concurrence, C_1 and C_2. These quantities are functions of the populations of the collective states and the coherence between them. Obviously, either $C_1 > 0$ or $C_2 > 0$ is required for the atoms to be entangled. It is easily verified that with the steady-state (6.116), the quantity C_1 is always negative, whereas C_2 can be positive.

The variation of the concurrence with N for the classical ($|M| = N$) and quantum ($|M| = \sqrt{N(N+1)}$) squeezed vacuum field is illustrated in Fig. 6.9. We see that the atoms can be entangled by both classical and quantum squeezed fields. However, the degree of entanglement with the classically squeezed field is very low. The most positive value of C_2 is achieved when $N = 0.15$, in which case $C_2 = 0.05$, so that we can speak of 5% entanglement. Moreover, the entanglement occurs in the limited range of the squeezing intensity, $N < 1/2$. In the quantum squeezed field, the atoms are entangled over the entire range of N. For $N \to \infty$, $\mathcal{C} \to 1$, which indicates that in this limit the atoms are perfectly entangled. This shows that the

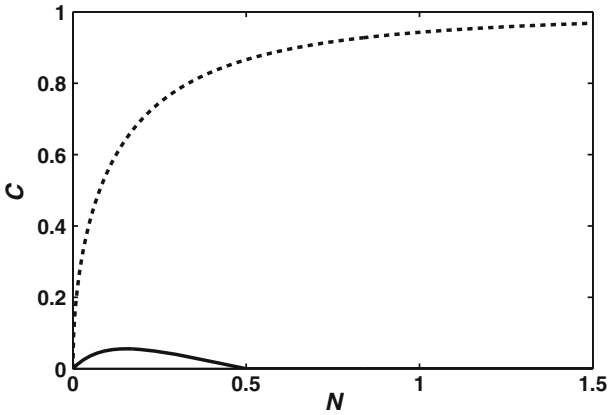

Fig. 6.9 Concurrence $\mathcal{C}$ plotted as a function of N for a classically squeezed field with $|M| = N$ (*solid line*) and a quantum squeezed field with $|M| = \sqrt{N(N+1)}$ (*dashed line*)

entangled properties of the atoms change dramatically for the change from classical to quantum correlations. Note that in the case of the quantum squeezed field with maximal correlations $|M|^2 = N(N+1)$, the state of the system reduces to a pure state

$$|\Upsilon_1\rangle = \frac{1}{\sqrt{2N+1}}\left[\sqrt{N+1}\,|g_1, g_2\rangle + \sqrt{N}\,|e_1, e_2\rangle\right], \tag{6.127}$$

which in the limit of $N \to \infty$ becomes a maximally entangled state. Thus, the perfectly squeezed vacuum field drives the atoms to a pure maximally entangled state.

References

1. R. Loudon, P.L. Knight: J. Mod. Opt. **34**, 709 (1987)
2. A.S. Parkins: in *Modern Nonlinear Optics, Part II*, eds. M. Evans S. Kielich (Wiley, New York, 1993), p. 607
3. R.E. Slusher, L.W. Hollberg, B. Yurke, J.C. Mertz, J.F. Valley: Phys. Rev. Lett. **55**, 2409 (1985)
4. R.M. Shelby, M.D. Levenson, S.H. Perlmutter, R.G. Devoe, D.F. Walls: Phys. Rev. Lett. **57**, 691 (1986)
5. L.A. Wu, H. J. Kimble, J.L. Hall, H. Wu: Phys. Rev. Lett. **57**, 2520 (1986)
6. L.A. Wu, M. Xiao, H.J. Kimble: J. Opt. Soc. Am. B **4**, 1465 (1987)
7. M.J. Collett C.W. Gardiner: Phys. Rev. A **30**, 1386 (1984)
8. C.W. Gardiner: *Quantum Noise* (Springer-Verlag, Berlin, 1991)
9. C.W. Gardiner: Phys. Rev. Lett. **56**, 1917 (1986)
10. B.J. Dalton, Z. Ficek, S. Swain: J. Mod. Opt. **46**, 379 (1999)
11. Z. Ficek, R. Tanaś, S. Kielich: J. Opt. Soc. Am. B **4**, 882 (1984)
12. Z. Ficek, R. Tanaś, S. Kielich: Acta Phys. Pol. **A67**, 583 (1985)
13. S.M. Barnett: Optics Commun. **61**, 432 (1987)
14. K. Wódkiewicz, P.L. Knight, S.J. Buckle, S.M. Barnett: Phys. Rev. A **35**, 2567 (1987)
15. P.K. Aravind: J. Opt. Soc. Am. B **3**, 1712 (1986)
16. S.M. Barnett, P.L. Knight: Phys. Scr. **21**, 5 (1988)
17. J. Janszky, Yushin: Phys. Rev. A **36**, 1288 (1987)
18. J. Gea-Banacloche: Phys. Rev. Lett. **62**, 1603 (1989)
19. J. Javanainen, P. L. Gould: Phys. Rev. A **41**, 5088 (1990).
20. Z. Ficek, P. D. Drummond: Phys. Rev. A **43**, 6247 (1991); **43**, 6258 (1991)
21. V. Buzek, P.L. Knight, I.K. Kudryavtsev: Phys. Rev. A **44**, 1931 (1991)
22. P. Zhou, S. Swain: Phys. Rev. A **55**, 772 (1997)
23. G.M. Palma, P.L. Knight: Phys. Rev. A **39**, 1962 (1989)
24. G.S. Agarwal, R.R. Puri: Phys. Rev. A **41**, 3782 (1990)
25. Z. Ficek, M.R.B. Wahiddin: Optics Commun. **134**, 387 (1997)
26. Z. Ficek, R. Tanaś: Optics Commun. **153**, 245 (1998)
27. A.E. Kozhekin, K. Molmer, E. Polzik: Phys. Rev. A **62**, 033809 (2000)
28. J. Hald, J.L. Sorensen, L. Leich, E.S. Polzik: Opt. Express **2**, 93 (1998)
29. J. Hald, J.L. Sorensen, C. Schori, E.S. Polzik: Phys. Rev. Lett. **83**, 1319 (1999)
30. M. Fleischhauer, S.F. Yelin, M.D. Lukin: Optics Commun. **179**, 395 (2000).
31. B.J. Dalton, Z. Ficek, P.L. Knight: Phys. Rev. A **50**, 2646 (1994)

Chapter 7
Experiments with Squeezed Light Excitation of Atoms

The experimental generation of squeezed light has opened possibilities for many useful applications and the study of novel phenomena in the interaction of atoms with light. The first investigation by Gardiner of the interaction of a squeezed vacuum with a two-level atom showed that the two quadratures of the atomic polarization can decay at vastly different rates [1]. The decay of a particular atomic polarization quadrature may be greatly inhibited, the phenomenon unique to quantum squeezing. The resonance fluorescence spectrum of a two-level atom was studied by Carmichael et al. [2, 3] who showed that the components of the familiar Mollow triplet depend strongly on the relative phase of the driving coherent field and the squeezed vacuum. Depending on the phase, the linewidth of the central component of the spectrum can be reduced below its natural linewidth. These pioneering applications of squeezed light have faced many practical problems and it has taken 27 years for their first experimental verification [4, 5].

In addition to these applications, a number of other investigations of the effect of squeezed light on the atomic radiative processes was also reported. It has been predicted that the squeezed field can result in the extreme sensitivity of the resonance fluorescence spectra, may produce unusual spectral features such as the hole burning and the dispersive profiles [6, 7], transparency of a weak probe field and gain without population inversion [8, 9]. Other aspects of the interaction of atoms with the squeezed field have also been investigated. The problem of the influence of squeezed light on multi-photon processes, dynamics of three-level atoms, laser cooling, and the dynamics of atoms in the cavity environment have been also treated [10]. Thus, a plethora of novel and exciting effects have been predicted since the initial proposals, and it will be exciting to observe which of these phenomena are verified experimentally. In particular, a verification of phenomena in which the quantum nature of the squeezed field plays an essential role would be a powerful demonstration of the ability of squeezed light to modify atomic radiative processes in a fundamental way.

In this chapter, we continue our study of the interaction of atoms with squeezed light, but we now turn our attention to a number of experiments which aimed to

Z. Ficek and R. Tanaś, *Quantum-Limit Spectroscopy*, Springer Series in Optical Sciences 200, DOI 10.1007/978-1-4939-3740-0_7

observe alterations in the radiative properties of atoms interacting with squeezed light. In fact, there are only three experiments in the area of atomic spectroscopy attempting to demonstrate features unique to quantum nature of the squeezed field. The small number of the experimental demonstrations can be attributed to a general lack of squeezed light sources coincident with convenient atomic transitions, to the difficulty of achieving an efficient coupling of squeezed light to the atoms and also to complications in generating broadband squeezed light. The output field of a conventional source of squeezed light is in the form of a "beam", which can overlap with only a small fraction of the 4π dipole radiation pattern of an atom. The atom−squeezed-light coupling is then so weak that any effect of the squeezing reduced fluctuations below the quantum limit is masked by the "normal" vacuum fluctuations in modes not occupied by the squeezed field with which the atom nonetheless interacts. Moreover, most of the squeezed light sources produce a narrow rather than broadband squeezed light. Therefore, the usual broadband treatment of the interaction of atoms with squeezed light is inadequate for the experimental realization. A more complicated theoretical approach must be taken to account for the finite bandwidth of the squeezed light which, on other hand, limits the degree of quantum effects. Despite these difficulties, there have been few but successful experiments demonstrating features in the radiative properties of atoms unique to quantum nature of the squeezed field.

We review experiments in which some of the predictions of atomic spectroscopy with squeezed light have been realized in laboratory. In particular, the verification of the phenomena of inhibited spontaneous decay of a two-level atom, phase dependent fluorescence spectra and the linear dependence of the two-photon absorption rate on the intensity of a squeezed vacuum field are a powerful demonstration of the ability of squeezed light to modify atomic radiative processes in a fundamental way. The chapter concludes with a brief discussion of an experiment on ultra high frequency measurements, frequency metrology, based on the two-photon excitation of three-level atoms with a squeezed vacuum field.

7.1 Experimental Investigations of Atom−Squeezed-Light Interaction in a Cavity

Suppression of the decay rate of an atom interacting with a squeezed vacuum field could be realized experimentally with atoms located or passing through an optical cavity, because inside the cavity atoms effectively couple to a limited number of modes whose propagation vectors lie within a small solid angle about a line perpendicular to the mirror surfaces. In this case, only the cavity modes need to be squeezed to overlap the squeezed field with the dipole radiation pattern of the atoms. This is an approximate one-dimensional situation often called as the one-dimensional atom (1D atom) regime. Hence, with the use of a cavity one can perform experiments with

essentially one-dimensional beams of squeezed light, which offers the possibility of seeing effects of squeezed light in atomic spectroscopy.

Experiments of the type just described were performed by the Kimble's group at Caltech [11]. They have developed a frequency-tunable source of squeezed light exhibiting approximately 75% squeezing, with a cavity bandwidth parameter $\kappa/2 = 5.8$ MHz, i.e., $N = 9/16$, $M = 15/16$, $\mu = 3.87$ MHz, and $\lambda = 7.73$ MHz. The aim of the experiments was to measure by direct spectroscopy the absorption spectrum of a transmitted weak probe beam incident on a high-finesse optical cavity containing two-level atoms and illuminated by a squeezed field produced by a degenerate parametric down conversion [11].

Theoretical Background

Let us first briefly outline the analytic theory of the system investigated in the experiment in order to provide some insight into the essential properties of the atom-cavity system interacting with the squeezed field. As we described in Chap. 6, the starting point for the calculations of the atomic dynamic in squeezed light is the master equation for the density operator describing the properties of the atom-cavity system. In the case of the resonant interaction between a two-level atom of frequency ω_a and a single mode cavity of frequency $\omega_c (= \omega_a)$ driven by squeezed light injected into the cavity through one of its mirrors, the master equation is of the form

$$\begin{aligned}\frac{\partial \varrho}{\partial t} = &-\frac{\mathrm{i}}{\hbar}\left[\hat{H}_0, \varrho\right] - \frac{1}{2}\gamma_a\left(S^+S^-\varrho + \varrho S^+S^- - 2S^-\varrho S^+\right)\\ &-\kappa(N+1)\left(\hat{a}^\dagger\hat{a}\varrho + \varrho\hat{a}^\dagger\hat{a} - 2\hat{a}\varrho\hat{a}^\dagger\right) - \kappa N\left(\hat{a}\hat{a}^\dagger\varrho + \varrho\hat{a}\hat{a}^\dagger - 2\hat{a}^\dagger\varrho\hat{a}\right)\\ &-\kappa M\left(\hat{a}^\dagger\hat{a}^\dagger\varrho + \varrho\hat{a}^\dagger\hat{a}^\dagger - 2\hat{a}^\dagger\varrho\hat{a}^\dagger\right) - \kappa M^*\left(\hat{a}\hat{a}\varrho + \varrho\hat{a}\hat{a} - 2\hat{a}\varrho\hat{a}\right), \qquad (7.1)\end{aligned}$$

where ϱ is the reduced density operator in the interaction picture, S^+ and S^- are the atomic raising and lowering operators, $\hat{a}$ and $\hat{a}^\dagger$ are the annihilation and creation operator for the cavity mode,

$$\hat{H}_0 = -\mathrm{i}\hbar g_0\left(S^+\hat{a} - \hat{a}^\dagger S^-\right) \qquad (7.2)$$

is the interaction Hamiltonian of the atom with the cavity mode in which g_0 is the coupling strength of the atom to the cavity mode. The master equation (7.1) describes the dynamics of a composite atom-cavity-mode system interacting with a broadband squeezed vacuum field, injected into the cavity through one of its mirrors. The system radiates via two distinct channels, the coupling of the atom to modes different than the cavity mode leading to spontaneous emission of the atom with the rate γ_a, and by loss through the cavity mirrors with the rate κ. The decay process of the cavity mode is modified by the injected squeezed vacuum field which appears as a broadband reservoir to the cavity mode. As described earlier in this chapter, the squeezed field is characterized by parameters N and M, which for a broadband field are independent of frequency and obey the following inequality $|M|^2 \leq N(N+1)$.

To ensure the validity of the broadband squeezing assumption, the bandwidth of the injected squeezed field would need be large compared to κ.

Working in the bad cavity regime for which $\kappa \gg g_0, \gamma_a$, the cavity mode dynamics can be adiabatically eliminated leaving the atom undergoing spontaneous emission with the cavity modified decay rate. The adiabatic elimination procedure leads to a set of equations for the atomic variables only, that is, the optical Bloch equations for the mean in-phase S_x and out-phase S_y quadrature components of the atomic polarization and inversion S_z:

$$\begin{aligned}
\langle \dot{S}_x \rangle &= -\gamma_x \langle S_x \rangle \,, \\
\langle \dot{S}_y \rangle &= -\gamma_y \langle S_y \rangle \,, \\
\langle \dot{S}_z \rangle &= -\frac{1}{2}\gamma_a \,(1 + 2C_1) - \gamma_z \langle S_z \rangle \,,
\end{aligned} \tag{7.3}$$

where

$$\begin{aligned}
\gamma_x &= \frac{1}{2}\gamma_a \,[1 + 2C_1 \,(2N - 2\epsilon M + 1)] \,, \\
\gamma_y &= \frac{1}{2}\gamma_a \,[1 + 2C_1 \,(2N + 2\epsilon M + 1)] \,, \\
\gamma_z &= \gamma_x + \gamma_y \,,
\end{aligned} \tag{7.4}$$

with $\epsilon = \pm 1$ corresponding to the x component of the atomic spin in phase ($\epsilon = 1$) or out of phase ($\epsilon = -1$), respectively, with the maximally squeezed quadrature of the squeezed input field, and $C_1 = g_0^2/(2\kappa\gamma_a)$ is the single-atom cooperativity parameter which is the part of the decay governed by the cavity. The parameters γ_x and γ_y are the modified decay rates of the x and the y components of the atomic polarization, respectively, and γ_z is the decay rate of the atomic population inversion. It is clear that the components of the atomic polarization are damped at different rates so that a squeezed field injected into the cavity can strongly influence of the cavity modified radiative dynamics of the atom. However, for the effect of squeezing on the atomic dynamics to be visible, one evidently requires $C_1 \sim 1$, which can be achieved for large values of g_0/γ_a.

After the atom-cavity system has attained steady-state conditions, the cavity mode is illuminated by a probe beam of a tunable frequency ω_p and amplitude $\boldsymbol{E}_p$ propagating in the direction parallel to the cavity axis. The probe is assumed to be sufficiently weak so that it does not appreciably perturb the atom-cavity system. According to the linear response theory, the probe absorption spectrum is defined in terms of the Fourier transform of the mean value of the two-time commutator of the cavity field operators as

$$A_p(\omega_p) = \left(\frac{2\omega_p}{\hbar}\right)\left|\boldsymbol{\mu} \cdot \boldsymbol{E}_p\right|^2 \mathrm{Re} \int_0^\infty \mathrm{d}\tau \, \mathrm{e}^{\mathrm{i}\omega_p \tau} \lim_{t\to\infty} \left\langle \left[a(t+\tau), a^\dagger(t)\right]\right\rangle \,, \tag{7.5}$$

where μ is the transition electric dipole moment of the atom. In the expression for $A_p(\omega_p)$ the commutator is calculated in the absence of the probe beam, but the

squeezed field is always present. Hence, we may concentrate only on the real part of the integral appearing in the absorption spectrum

$$A_p(\nu) = \mathrm{Re}\int_0^\infty \mathrm{d}\tau\, \mathrm{e}^{\mathrm{i}\nu\tau} \lim_{t\to\infty} \left\langle \left[\tilde{a}(t+\tau), \tilde{a}^\dagger(t)\right]\right\rangle = \mathrm{Re}\, \Phi_p(z)|_{z=-\mathrm{i}\nu}\,, \tag{7.6}$$

where $\nu = \omega_p - \omega_c$, $\tilde{a}(t) = a(t)\exp(\mathrm{i}\omega_c t)$ is the slowly varying part of the cavity field operator, $\Phi_p(z)$ is the Laplace transform of the steady-state value of the commutator in (7.5), and z is the complex Laplace transform parameter.

In the bad cavity regime, considered in the experiment, the correlation function of the cavity field operators appearing in (7.6) can be approximated by

$$\lim_{t\to\infty} \left\langle \left[\tilde{a}(t+\tau), \tilde{a}^\dagger(t)\right]\right\rangle \approx \mathrm{e}^{-\frac{1}{2}\kappa\tau} - \frac{2\gamma_a C}{\kappa} \lim_{t\to\infty} \left\langle \left[S^-(t+\tau), S^+(t)\right]\right\rangle\,, \tag{7.7}$$

where $C = \sum_{i=1}^{n_a} g_{0_i}^2/(2\kappa\gamma_a)$ is the multi-atom (collective) cooperativity parameter, and n_a is the number of atoms in the atomic beam. It determines the collective coupling of all the atoms simultaneously interacting with the cavity mode.

In order to obtain the time evolution of the commutator in (7.7), we solve the Bloch equations (7.3) using the Laplace transforms. Applying the quantum regression theorem, we calculate the absorption spectrum. The Laplace transform of the steady-state value of the commutator in (7.7) leads to

$$\Phi_p(z)|_{z=-\mathrm{i}\nu} = \frac{1}{\frac{1}{2}\tilde{\kappa} - \mathrm{i}\tilde{\nu}} - \frac{2C}{\tilde{\kappa}} \frac{(1+2C)}{(1+2N_c)} \frac{\mathrm{i}\tilde{\nu} - \frac{1}{2}(1+2N_c)}{D(\tilde{\nu})}\,, \tag{7.8}$$

with

$$D(\tilde{\nu}) = \left[\tilde{\nu} + \frac{1}{2}\mathrm{i}(1+2N_c)\right]^2 + 4|M_c|^2\,, \tag{7.9}$$

where $N_c = C(2N+1)$, $M_c = 2C|M|$, $\tilde{\kappa} = \kappa/\gamma_a$, and $\tilde{\nu} = \nu/\gamma_a$.

The actual absorption spectrum, given by (7.6) can be easily obtained simply by extracting the real part of the right-hand side of (7.8), and is given by

$$A_p(\nu) = \mathcal{L}_1(\nu) + \mathcal{L}_2(\nu) + \mathcal{L}_3(\nu)\,, \tag{7.10}$$

where

$$\begin{aligned}
\mathcal{L}_1(\nu) &= \frac{1}{\frac{1}{4}\tilde{\kappa}^2 + \tilde{\nu}^2}\,,\\
\mathcal{L}_2(\nu) &= -\frac{C}{\tilde{\kappa}} \frac{(1+2C)}{(1+2N_c)} \frac{\gamma_y}{\tilde{\nu}^2 + \gamma_y^2}\,,\\
\mathcal{L}_3(\nu) &= -\frac{C}{\tilde{\kappa}} \frac{(1+2C)}{(1+2N_c)} \frac{\gamma_x}{\tilde{\nu}^2 + \gamma_x^2}\,.
\end{aligned} \tag{7.11}$$

The absorption spectrum is composed of three Lorentzians, one of a positive weight ($\mathcal{L}_1$) and two of a negative weight ($\mathcal{L}_2$) and ($\mathcal{L}_3$), all centered on $\tilde{\nu} = 0$ but having different linewidths. Thus, the absorption features of the atom-cavity system are locked to the cavity frequency. The first component of the absorption spectrum ($\mathcal{L}_1$) is a broad, positive, Lorentzian peak of the linewidth $\kappa/2$, the second component is a broad negatively weighted Lorentzian peak and therefore will contribute a broad feature forming a flat background of the spectrum, whereas the third also negatively weighted component has a reduced bandwidth and therefore may produce a sharp negative feature which may result in a narrow hole bored in the spectrum. A hole burning indicates a reduction of the absorption of the probe beam or equivalently an enhancement of the transmission of the probe beam passing through the atom-cavity system. Note that the negative weight Lorentzians are present even in the absence of squeezing, $M_c = 0$. The effect of squeezing, which we are interested in here, is to alter the width of the negative weight features from $\frac{1}{2}(1 + 2N_c)\gamma_a$ to $\frac{1}{2}(1 + 2N_c \pm 2M_c)\gamma_a$.

In the limit of strong quantum squeezing, $|M| \approx N + 1/2$, and then the widths of the negative weight Lorentzians reduce to

$$\gamma_y = \frac{1}{2}\left(1 + 4N_c\right)\gamma_a\,, \quad \gamma_x = \frac{1}{2}\gamma_a\,. \tag{7.12}$$

This shows that there is a complete cancellation of the cavity enhanced broadening of the absorption spectrum. As a result, one could observe a narrow dip of the width $\gamma_a/2$ in the absorption spectrum of the probe beam. For a comparison, in the case of a classically squeezed field, $|M| = N$, and then the widths of the negative weight Lorentzians are

$$\gamma_y = \frac{1}{2}\left[1 + 2C\left(1 + 4N\right)\right]\gamma_a\,, \quad \gamma_x = \frac{1}{2}\left(1 + 2C\right)\gamma_a\,. \tag{7.13}$$

Clearly, a feature of the absorption spectrum unique to the quantum nature of squeezing ($|M| > N$) is the reduction of the width γ_x below $\frac{1}{2}(1 + 2C)\gamma_a$.

Figure 7.1 shows the effect of various kinds of the illuminating fields on the absorption spectrum of a probe beam transmitted through the atom-cavity system. The illuminating fields are characterized by the squeezing parameters $|M|$ and N and are distinguished from each other by different values of the parameter $|M|$. A thermal field has $|M| = 0$, and we see from the figure that in this case the absorption spectrum is composed of a broad Lorentzian of the linewidth $\kappa/2$. When the system is illuminated by a classically squeezed field, a broad hole is burned at line center. When the illuminating field is replaced by a quantum squeezed field, the hole becomes deeper and narrower with the linewidth reduced to $\gamma_a/2$.

Experiment

It was the primary aim of the Turchette et al. [11] experiment to observe a narrow peak in the spectrum of the transmitted probe beam of the linewidth reduced below $\frac{1}{2}(1 + 2C)\gamma_a$ since, as we have shown above, could be attributed unequivocally to

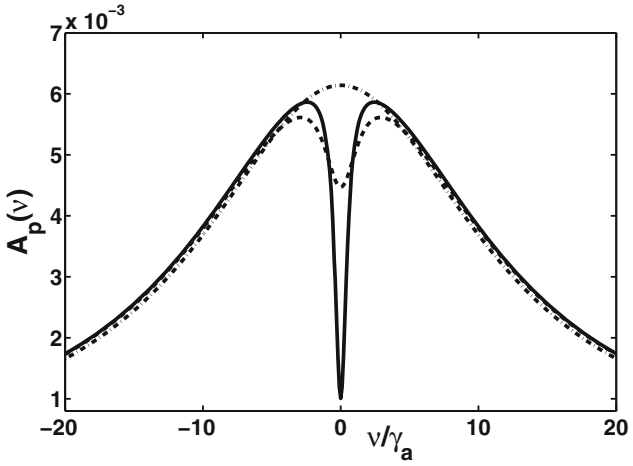

Fig. 7.1 Absorption spectrum $A_p(\nu)$ of a probe beam transmitted through an atom-cavity system plotted as a function of the probe field frequency ν for $\kappa = 25\gamma_a$, $N = 10$, $C = 1$, corresponding to $g_0 = 7\gamma_a$, and various kinds of the illuminating field distinguished by different values of the parameter $|M|$: quantum squeezed field, $|M| = \sqrt{N(N+1)}$ (*solid line*), classically squeezed field, $|M| = N$ (*dashed line*), and thermal field, $|M| = 0$ (*dashed-dotted line*)

the quantum nature of the squeezed field. The width of the transmitted probe beam corresponds to the width of the deep in the absorption spectrum. Schematic diagram of the experiment is shown in Fig. 7.2. Cesium (Cs) atoms were passed through the cavity slow compared with the cavity decay rate to let the atoms to remain inside the cavity for enough time to allow the atom-cavity system to reach a stationary state. Before the beam entered the cavity the number of atoms which could interact with the cavity mode was controlled by the "Cs beam control" adjusting the $F = 4$ ground-state population of the atoms. In addition, the beam was optically pumped (OP) for preparation of two-state atoms. The cavity length was locked such that a TEM_{00} mode was exactly resonant with the atomic transition frequency, $\omega_c = \omega_a$. The squeezed light was injected into the cavity through mirror M_2 and the cavity mode was probed with a weak tunable field injected through mirror M_1. The probe was transmitted out of the cavity through mirror M_2 and then recorded on a balanced heterodyne detector. The detected probe field was analyzed by a spectrum analyzer (SA) set to measure the beat note between the local oscillator (LO) and the probe. From the size of the heterodyne photocurrent beat note, the average intracavity probe field amplitude $|\langle a_p(\nu)\rangle|$ was inferred and values of $|\langle a_p(\nu)\rangle|^2$ recorded for a variety of parameters involved. The results for the spectrum of the transmitted probe field in the presence of squeezed light were compared with those in the presence of thermal light with identical properties, i.e., the same number of photons N, bandwidth and line shape. This was done by exciting the cavity mode with the output field of the degenerate OPO with both modes illuminating the atom (squeezed light) and only with a single mode of the NOPO illuminating the atom (thermal light). This technique was based

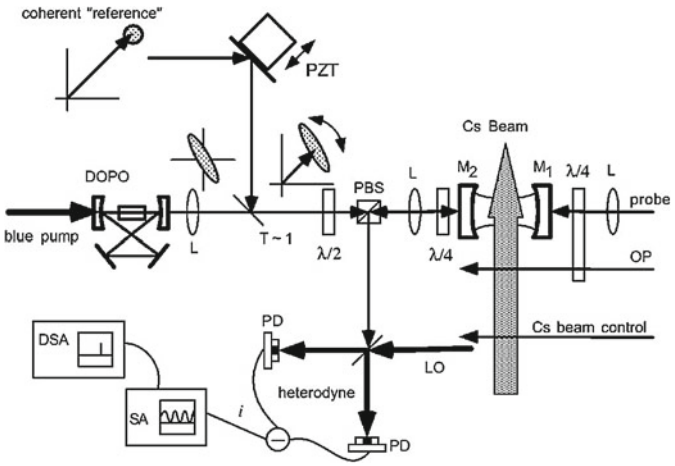

Fig. 7.2 Schematic diagram of the Turchette et al. [11] experiment to demonstrate a strong atom−squeezed-light coupling in a cavity. Reprinted with permission from Q.A. Turchette, N.Ph. Georgiades, C.J. Hood, H.J. Kimble, A.S. Parkins: Phys. Rev. A **58**, 4056 (1998). Copyright (1998) by the American Physical Society

on the fact that the thermal light from a single mode of the NOPO is identical in all respects to the squeezed light from the degenerate OPO. To extract the probe transmission in the presence of atoms inside the cavity the normalized atom-cavity transmission was measured, $T_i = T_{\text{with atoms}}/T_{\text{no atoms}}$ in the presence of squeezed T_s or thermal T_t fields and without the input fields T_v. Then, two quantities Δ_s and Δ_t were compared

$$\Delta_s \equiv T_s - T_v \,, \quad \text{and} \quad \Delta_t \equiv T_t - T_v \,. \tag{7.14}$$

The results of measurements of Δ_s and Δ_t are shown in Fig. 7.3. Analysis of these transmitted probe beam spectra demonstrates that the effect of the input fields, squeezed or thermal, is rather small making incapable of distinguishing the probe spectrum in the presence of a squeezed field from that in the presence of a thermal field, although the shape of these spectra is different, especially in the wings. Consequently, it has not been possible to make any definitive statement that the observed differences are manifestations of the nonclassical interaction between atoms and squeezed light.

It was commented that the lack of convincing results can be attributed to the effects of atomic beam fluctuations, which lead to additional loss mechanisms that reduce the effects of the squeezed field interaction with atoms. This could also be attributed to the fact that the damping rates are very sensitive to the matching of the incident squeezed modes to the vacuum modes coupled to the atom. An imperfect matching is equivalent in replacing the parameters N and M by $\tilde{N} = \eta N$ and $\tilde{M} = \eta M$, respectively, where η describes the matching of the incident squeezed

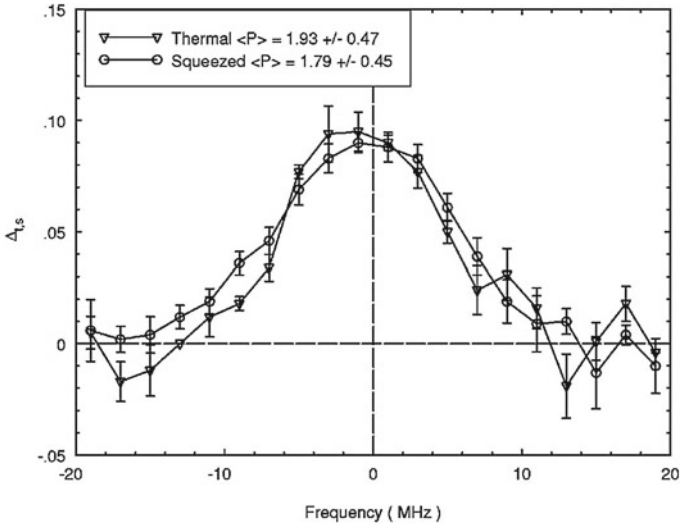

Fig. 7.3 The measured difference spectra with squeezed light Δ_s and thermal light Δ_t, averaged over the power in the squeezed and thermal fields. Reprinted with permission from Q.A. Turchette, N.Ph. Georgiades, C.J. Hood, H.J. Kimble, A.S. Parkins: Phys. Rev. A **58**, 4056 (1998). Copyright (1998) by the American Physical Society

vacuum modes to the vacuum modes coupled to the atom. For perfect matching, $\eta = 1$, whereas for an imperfect matching $\eta < 1$. When the parameters N and M appearing in the expressions (7.4) for the decay rates are replaced by the effective parameters $\tilde{N}$ and $\tilde{M}$, respectively, we find that in the case of a classically squeezed field the damping rate γ_x is not affected by η, $\gamma_x = \frac{1}{2}(1 + 2C)\gamma_a$, whereas for the quantum squeezed field with maximal correlations, $|M| = \sqrt{N(N+1)}$, the decay rate γ_x takes the form

$$\gamma_x = \frac{1}{2}\left[1 + 2C\,(1-\eta)\right]\gamma_a\ . \tag{7.15}$$

We see that even if a perfectly correlated source of squeezed light is employed, the imperfect matching η acts to considerably affect the cancellation of the cavity enhanced part of the damping rate. The rate depends linearly on η which means that, for example, a 20% reduction of the damping rate below the classical limit requires 20% of the modes occupying the 4π solid angle to be squeezed.

Additional experiments were performed by including a resonant coherent displacing (reference) field, which was mixed with the squeezed vacuum output of the OPO on a beam splitter and the resulting field was then injected into the cavity. The phase of the squeezing relative to the phase of the reference field was controlled by the piezoelectric transducer, see Fig. 7.2. The response of the weak probe transmission to the modulation of the relative phase of the fields was measured. Figure 7.4 shows the results for the response of the weak probe transmission to the modulation

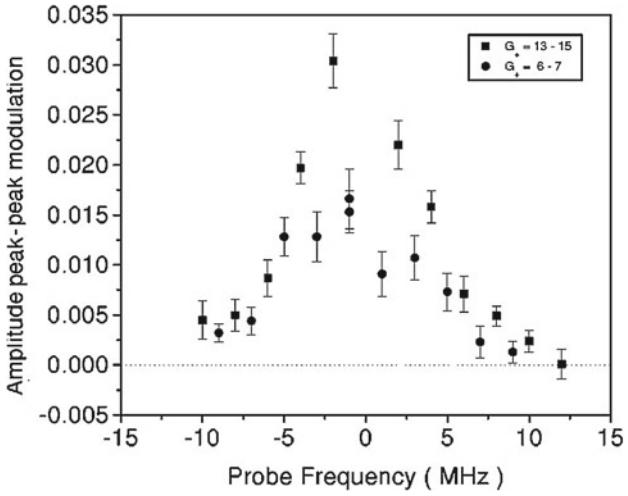

Fig. 7.4 The amplitude fractional modulation as a function of the probe field frequency for the reference field powers $P_{\text{ref}} = 40$ pW ($G_+ = 6 - 7$ data) and $P_{\text{ref}} = 60$ pW ($G_+ = 13 - 15$ data). The frequency of the squeezed field was fixed on resonance. Reprinted with permission from Q.A. Turchette, N.Ph. Georgiades, C.J. Hood, H.J. Kimble, A.S. Parkins: Phys. Rev. A **58**, 4056 (1998). Copyright (1998) by the American Physical Society

of the relative phase of the fields. A change of the relative phase corresponds to a rotation of the squeezing ellipse which leads to a change of the degree of squeezing of the injected field. The results displayed in Fig. 7.4 are for the amplitude peak-peak modulation as a function of the probe detuning for two fixed reference field powers, $P_{\text{ref}} = 40$ and 60 pW, and two degrees of squeezing quantified by the phase sensitive OPO gain, $G_+ = 6.5$ and $G_+ = 14$. The amplitude peak-peak modulation is given by the amplitude fractional modulation defined as

$$\alpha_{pp} = \frac{\left|A_p^+(\nu) - A_p^-(\nu)\right|}{\left|A_p^{\text{no sqz}}(\nu)\right|} , \tag{7.16}$$

where $A_p^{\text{no sqz}}(\nu)$ is the amplitude of the transmitted probe beam in the absence of the squeezed field. The plus and minus refer to orthogonal phases of the squeezing which are correlated with the maxima and minima of the probe modulation. The phase sensitive OPO gain G_+ is defined as

$$G_+ = \frac{1}{(1 + \frac{\varepsilon}{\kappa_s/2})^2} , \tag{7.17}$$

where ε is the strength of the parametric driving rate and κ_s is the full width at half maximum of the OPO cavity. One can see from Fig. 7.4 that the effect of squeezing on the transmitted probe beam is most noticeable on resonance ($\nu = 0$), where a significant variation of the fractional modulation with the degree of squeezing (squeezing phase) was observed. However, from the size of the modulation, it is

not possible to clearly distinguish if this could be regarded as a manifestation of the nonclassical interaction between atoms and squeezed light. Nevertheless, the experiment clearly demonstrated a phase sensitive modulation of the transmitted probe beam resulting from an asymmetric distribution of the fluctuations between the quadratures of the squeezed vacuum field.

7.2 Experimental Realization of the Suppression of the Atomic Decay Rate

As we have seen, there were practical problems in the experimental attempt to realize the canonical prediction of atomic spectroscopy with squeezed light, the reduction of the decay rate of an atom interacting with a squeezed vacuum field below its natural linewidth. This was found as a difficult task and for this reason has been largely lacking from subsequent investigations for more than 25 years.

It was until 2013 when Murch et al. [4] made the first demonstration of the suppression of the spontaneous relaxation time of atomic coherence in a squeezed vacuum field. They studied the effect of a broadband squeezed vacuum field on the relaxation time of the two-level system. In contrast to the indirect spectroscopic measurement of Turchette et al. [11], they measured the quadrature decay constants directly. Their experiment, shown schematically in Fig. 7.5b, consisted of a superconducting transmon circuit which behaves as a controllable atom, and whose ground and excited states form an effective two-level atom or equivalently an effective spin one-half $\boldsymbol{S}$ with eigenstates $|g\rangle \equiv |S_z = -1/2\rangle$ and $|e\rangle \equiv |S_z = +1/2\rangle$. The transition frequency of the effective two-level atom was $\omega_q/2\pi = 5.8989$ GHz and the atomic line was broadened purely radiatively with the longitudinal relaxation time $T_1 = 0.65\,\mu$s arising from the coupling of the system to the 50 Ω environment. The squeezed vac-

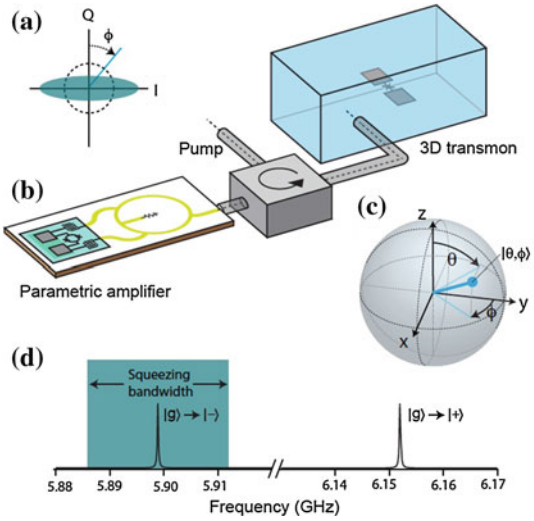

Fig. 7.5 Experimental setup of Murch et al. [4] to observe the suppression of the spontaneous emission rate of atomic coherence in a squeezed vacuum field. Reprinted by permission from Macmillan Publishers Ltd: [Nature] (K.W. Murch, S.J. Weber, K.M. Beck, E. Ginossar, I. Siddiqi: Nature 499, 62 (2013)), copyright (2013)

uum was generated by pumping a lumped-element Josephson parametric amplifier with a field composed of two frequencies ω_1 and ω_2 symmetrically located about a central frequency that was set equal to the two-level system transition frequency ω_q, i.e., $(\omega_1 + \omega_2)/2 = \omega_q$. The bandwidth of the squeezed field, 13 MHz, was 50 times larger than the atomic linewidth, $\gamma_a/2\pi = 240$ kHz. Thus, the squeezing bandwidth was sufficient to fulfill the requirement for the field to be considered as a broadband squeezed vacuum field.

The Ramsey spectroscopy method was used to measure the relaxation times T_x, T_y and T_z of the spin components into the squeezed vacuum. Two phase coherent microwave pulses of frequency $\omega \approx \omega_q$ were applied to prepare the atom in an arbitrary superposition state $|\Psi\rangle = \alpha\,|g\rangle + \beta\,|e\rangle$. The first pulse corresponded to a $\pi/2$ rotation of the initial spin $|0\rangle$ about the $-\hat{x}\cos\phi + \hat{y}\sin\phi$ axis, and the second pulse delayed by Δt corresponded to a $\pi/2$ rotation about the $-\hat{x}\sin\omega_{\rm mod}t - \hat{y}\cos\omega_{\rm mod}t$ axis. Modulation of the rotation angle of the second pulse at frequency $\omega_{\rm mod}$ resulted in oscillatory Ramsey fringes.

To help gain insight into the Ramsey spectroscopy method used in the experiment, we have graphically displayed in Fig. 7.6 the trajectory on the Bloch sphere of the spin vector in the four steps taken to determine the average population inversion $\langle S_z(t)\rangle$ for the case of $\phi = \pi/2$. In the first step, the atom was prepared in the state $|e\rangle \equiv |S_z = +1/2\rangle$, as illustrated in Fig. 7.6a. In the second step, a microwave $\pi/2$ pulse was applied which for $\phi = \pi/2$ performed a 90° rotation of the spin around the $+\hat{y}$ axis, Fig. 7.6b. As a result, the spin was aligned along the $+\hat{x}$ axis. Then in the third step, the spin was allowed to evolve freely in the presence of the squeezed vacuum until a time t at which the second $\pi/2$ pulse was applied. During the free evolution, no rotation or precession of the spin occurred since, according to the optical Bloch equations (7.3), the spin components evolve independently when the squeezed field is resonant with the atomic transition frequency. However, the amplitude of the $\langle S_x(t)\rangle$ component was decreasing during the free evolution with

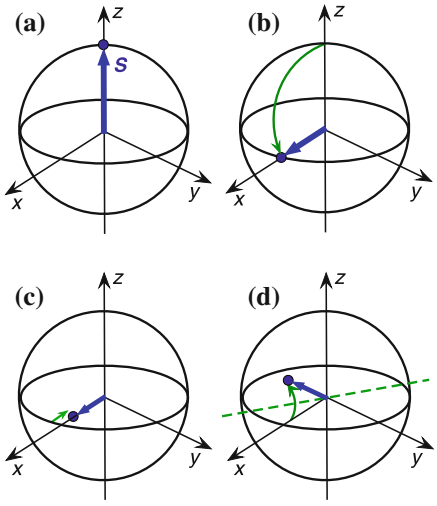

Fig. 7.6 Schematic illustration of the evolution of the spin $\boldsymbol{S}$ in the Ramsey spectroscopy method. **a** Orientation of the spin vector for the atom prepared in its excited state. **b** Rotation of the spin vector by a $\pi/2$ pulse. **c** Spontaneous decay of the spin vector during the free evolution. **d** A $\pi/2$ rotation of the spin vector around a direction determined by the dashed green line

the rate the x component decays. This behavior is illustrated in Fig. 7.6c and can be expressed by

$$\langle S_x(t)\rangle = \mathrm{e}^{-t/T_x}\,, \quad \langle S_y(t)\rangle = 0\,, \quad \langle S_z(t)\rangle = 0\,, \tag{7.18}$$

where $T_x = 1/\gamma_x = 1/(N-|M|+1/2)$. Note, the result (7.18) is the solution of the Bloch equations for the atomic spin, which are the same as those given by (7.3) in an earlier discussion of the radiation damping in a squeezed field. The solution (7.18) is for the initial condition $\langle S_x(0)\rangle = 1$, $\langle S_y(0)\rangle = 0$ and $\langle S_z(0)\rangle = 0$, corresponding to the situation illustrated in Fig. 7.6b. Finally, in the fourth step, illustrated in Fig. 7.6d, a second microwave $\pi/2$ pulse was applied, but this time with a phase such that it performed a 90° rotation around the $-\hat{x}\sin\omega_{\mathrm{mod}}t - \hat{y}\cos\omega_{\mathrm{mod}}t$ axis. After these four steps, the population of the atom was measured to determine the average population inversion $\langle S_z(t)\rangle$. This way, the relaxation time, or equivalently, the decay rate of the quadrature component $\langle S_x\rangle$ was measured. By repeating the procedure for the rotation angles $\phi = \pi$ and no rotation, the relaxation times, respectively, of the $\langle S_y\rangle$ and $\langle S_z\rangle$ components can be determined.

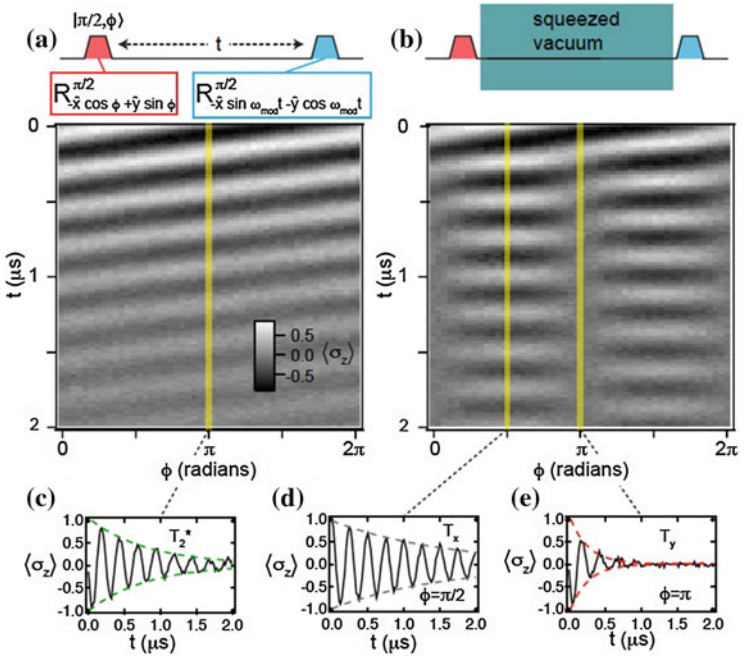

Fig. 7.7 Observation by Murch et al. [4] of the time evolution of the atomic inversion $\langle\sigma_z\rangle = 2\langle S_z\rangle$ after the application of two time delayed $\pi/2$ pulses and its modulation with the phase ϕ of the first $\pi/2$ pulse rotation. Frame **a** shows the evolution in the absence of the squeezed vacuum between the pulses, whereas Frame **b** shows the evolution in the presence of the squeezed vacuum field. Reprinted by permission from Macmillan Publishers Ltd: [Nature] (K.W. Murch, S.J. Weber, K.M. Beck, E. Ginossar, I. Siddiqi: Nature 499, 62 (2013)), copyright (2013)

The experimental results for these three cases are shown in Fig. 7.7. It is seen that in the case of $\phi = \pi/2$, corresponding to the evolution of only the x component of the spin, the population inversion decayed with the rate T_x which was much longer than the longitudinal relaxation time T_2. By contrast, when the first $\pi/2$ pulse aligned the spin vector along the $+\hat{y}$ axis, the population inversion decayed with the rate T_y, which was much shorter than T_2. In other words, the experimental results clearly demonstrate that the S_x component decays in the squeezed vacuum with a time constant T_x^s which is longer than the time constant of the decay in the normal vacuum, $T_x^s > T_x^v = T_2$. As we have mentioned before, the decay of the x quadrature component with the time constant $T_x > T_2$ ($\gamma_x < \gamma_a/2$) is attributed unequivocally to the quantum nature of the squeezed vacuum field.

7.3 Experimental Observation of the Phase Dependent Fluorescence Spectra

Shortly after the successful demonstration of the suppression of the atomic decay rate, Siddiqi and coworkers at the University of California succeeded in the observation of the phase dependent fluorescence spectra in squeezed vacuum [5]. An outline of the experiment, which is closely related to the above-discussed experiment on the suppression of the atomic decay rate, is shown in Fig. 7.8. A squeezed vacuum field of a noise reduction up to 3.1 dB below the standard vacuum level was generated by a Josephson parametric amplifier (JPA) and then directed by a detuning to an aluminum microwave waveguide cavity containing a superconducting transmon circuit. The circuit formed an artificial atom and was coupled to the cavity mode of resonance frequency $\omega_c/2\pi = 7.1051$ GHz with the coupling strength $g/2\pi = 202$ MHz. The strong coupling of the circuit to the cavity mode produced well-separated polariton states. This ensured that the transition between the ground state and lower energy level of the polariton of frequency $\omega_a/2\pi = 7.091$ GHz behaved like a two-level

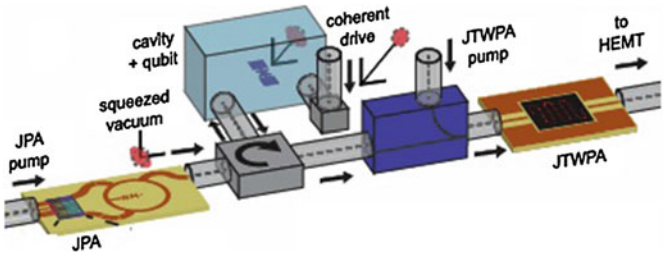

Fig. 7.8 Outline of the principal elements of the apparatus used by Toyli et al. [5] for observing the phase dependent fluorescence spectrum of a driven two-level atom in a squeezed vacuum field. Reprinted with permission from D.M. Toyli, A.W. Eddins, S. Boutin, S. Puri, D. Hover, V. Bolkhovsky, W.D. Oliver, A. Blais, I. Siddiqi: Phys. Rev. X **6**, 031004 (2016). Copyright (2016) by the American Physical Society

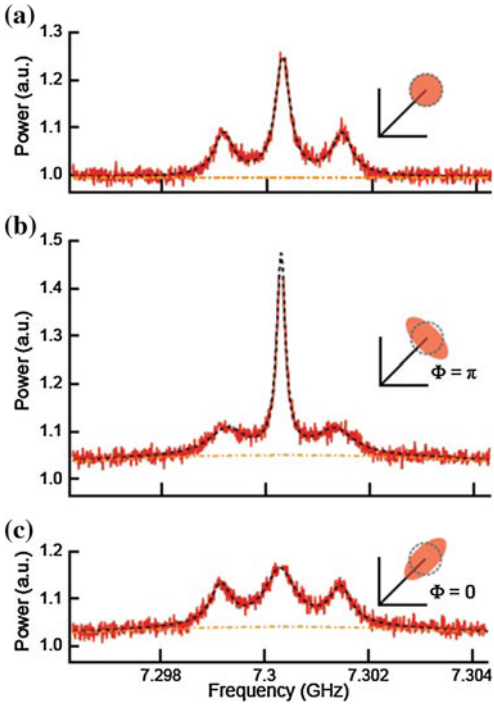

Fig. 7.9 First evidence of the phase dependent spectrum of the fluorescence field emitted by a coherently driven two-level atom in a squeezed vacuum. The *dashed-dotted horizontal line* indicates the linewidth of the ordinary vacuum. The *black dashed line* is the theoretical spectrum arbitrary normalized to the same magnitude of the central peak. Reprinted with permission from D.M. Toyli, A.W. Eddins, S. Boutin, S. Puri, D. Hover, V. Bolkhovsky, W.D. Oliver, A. Blais, I. Siddiqi: Phys. Rev. X **6**, 031004 (2016). Copyright (2016) by the American Physical Society

quantum system. The linewidth of the atomic transition $\gamma = 290$ kHz was much smaller than the bandwidth of the squeezed field, 38 MHz, which ensured a broadband excitation of the atom. The cavity was kept at temperature 30 mK at which the number of thermal photons is small and thus had negligible effect on the cavity environment.

The cavity was accessed by two ports, one strongly and the other weakly coupled to the cavity mode. The squeezed field was directed to the cavity through the strongly coupled port, while the weakly coupled port was used to direct a coherent field to drive the atom. Both JPA pump field and the coherent field driving the atom were generated from the same microwave source, which allows to control the relative phase between the driving and squeezed fields. As we have seen in Chap. 6, the phase difference plays an important role in the form of the fluorescence spectrum. The fluorescence light emitted was collected through the strongly coupled port and then directed through the circulator towards the Josephson traveling wave parametric amplifier (JTWPA) for amplification. After the amplification the fluorescence spectrum was measured with a microwave spectrum analyzer.

Figure 7.9 shows the observed fluorescence spectra, the Mollow triplet in ordinary vacuum, squeezed vacuum with relative phase $\Phi = \pi$ and $\Phi = 0$, respectively. The spectra were normalized such that the background level in the ordinary vacuum was one. The observed spectra clearly demonstrate the dependence of the Mollow triplet on the phase of the squeezed vacuum field, with the linewidth of the central peak

varying between subnatural and supernatural values. It is also noticeable that the Rabi sidebands exhibit broadening compared to their ordinary vacuum width. The subnatural linewidth of the central peak for $\Phi = \pi$ is a clear signature of quantum squeezing.

7.4 Experimental Realization of Nonclassical Excitation of a Three-Level Atom

Although the reduction of the atomic decay rate and the variation of the fluorescence spectrum with the squeezing phase have been confirmed in the above discussed experiments, it was in fact the phenomenon of the linear dependence of the two-photon absorption rate on the intensity of a squeezed vacuum field in a three-level atom which is regarded as the first experimental confirmation of the unique quantum squeezing modification of the radiative atomic processes. The experiment was carried out by the Kimble's group at Caltech in 1995 [12]. Specifically, the rate of a two-photon transition in cesium atoms illuminated by a squeezed vacuum field generated via nondegenerate parametric down conversion was measured and the experimental team observed that in the limit of a weak excitation the rate growth linearly with the field intensity, in contrast with the quadratic growth produced by classical light sources.

Theoretical Background

Before going into the details of the experiment and presenting the results, let us first demonstrate the connection between the population of the upper atomic state $|3\rangle$ and the two-photon transitions in the atom.

Suppose that the atom was initially at $t = 0$ in its ground state $|1\rangle$, while the field was in a squeezed vacuum state $\left|S_\phi\right\rangle$. We then write for the initial state of the combined system

$$|\Psi(0)\rangle = |1\rangle \otimes \left|S_\phi\right\rangle \ . \tag{7.19}$$

We assume that at $t = 0$ the atom and the field were uncorrelated, and choose for the initial state of the field, the multimode squeezed field determined by the correlation functions (6.64).

If the atom interacts with the field through an electric dipole interaction, then after a time t the state in the interaction picture will be of the form

$$|\Psi(t)\rangle = \hat{U}(t)\,|\Psi(0)\rangle \ , \tag{7.20}$$

where $\hat{U}(t)$ is an evolution operator

$$\hat{U}(t) = \exp\left[-\frac{\mathrm{i}}{\hbar}\int_0^t \mathrm{d}t'\,\hat{H}_I(t')\right] , \tag{7.21}$$

with

$$\hat{H}_I = -\mathrm{i}\hbar \sum_{i=1}^{2} \sum_{k} \left(g_k^{(i)} \hat{a}_k S_i^+ - \mathrm{H.c.} \right) , \tag{7.22}$$

where $g_k^{(i)}$ is the coupling strength of the ith atomic transition to mode k of the squeezed field.

The total density operator of the system can be defined from (7.20) as

$$\varrho_T(t) = \hat{U}(t)\varrho_T(0)\hat{U}^\dagger(t) , \tag{7.23}$$

where $\varrho_T(0) = \varrho(0) \otimes \varrho_F(0)$ is the total density operator of the system, which we assume is in factorized form at the initial time $t = 0$, $\varrho(0)$ is the reduced density operator of the atom, and $\varrho_F(0)$ is the density operator of the field. Applying perturbation theory to the operator (7.21) and keeping only the second-order (two-photon) terms, we get

$$\begin{aligned} \tilde{\varrho}_T(t) &\approx \frac{1}{4}\hat{U}^{(2)}(t)\tilde{\varrho}_T(0)\hat{U}^{(2)\dagger}(t) \\ &= \frac{1}{4}\int_0^t \mathrm{d}t_1 \int_0^{t_1} \mathrm{d}t_2 \int_0^{t_2} \mathrm{d}t_3 \int_0^{t_3} \mathrm{d}t_4 \, \hat{H}_I(t_1)\hat{H}_I(t_2)\tilde{\varrho}_T(0)\hat{H}_I(t_3)\hat{H}_I(t_4) , \end{aligned} \tag{7.24}$$

where $\tilde{\varrho}_T$ is the density operator in the interaction picture.

Taking the trace over the field operators and averaging over the upper state $|3\rangle$ of the atom, we obtain the population of the state $|3\rangle$ as

$$\begin{aligned} \varrho_{33}(t) = \langle 3| \, \mathrm{Tr}_F\{\tilde{\varrho}_T(t)\} \, |3\rangle = \gamma_1\gamma_2 \int_0^t \mathrm{d}t_1 \int_0^{t_1} \mathrm{d}t_2 \int_0^{t_2} \mathrm{d}t_3 \int_0^{t_3} \mathrm{d}t_4 \\ \times \, G^{(2)}(t_1, t_2; t_3, t_4) \mathrm{e}^{\mathrm{i}\omega_1(t_2 - t_3)} \mathrm{e}^{\mathrm{i}\omega_2(t_1 - t_4)} , \end{aligned} \tag{7.25}$$

where

$$G^{(2)}(t_1, t_2; t_3, t_4) = \left\langle S_\phi \right| \hat{\mathcal{A}}^\dagger(t_1)\hat{\mathcal{A}}^\dagger(t_2)\hat{\mathcal{A}}(t_3)\hat{\mathcal{A}}(t_4) \left| S_\phi \right\rangle , \tag{7.26}$$

in which

$$\hat{\mathcal{A}}(t) = \frac{1}{2\pi} \int_0^\infty \mathrm{d}\omega_k \, \hat{a}_k \mathrm{e}^{-\mathrm{i}\omega_k t} . \tag{7.27}$$

is the Fourier integral decomposition of the boson field operator, and γ_i $(i = 1, 2)$ is the damping rate of the ith atomic transition. We see that to the second order the contribution of the field to the population ϱ_{33} comes from the second order correlation function $G^{(2)}(t_1, t_2; t_3, t_4)$.

Since the field operators of a vacuum field are Gaussian variables, the fourth order correlation function appearing in (7.25) can be factorized into second-order

correlation functions as

$$
\begin{aligned}
G^{(2)}(t_1,t_2;t_3,t_4) &= \langle S_\phi|\,\hat{\mathcal{A}}^\dagger(t_1)\hat{\mathcal{A}}^\dagger(t_2)\hat{\mathcal{A}}(t_3)\hat{\mathcal{A}}(t_4)\,|S_\phi\rangle \\
&= \langle S_\phi|\,\hat{\mathcal{A}}^\dagger(t_1)\hat{\mathcal{A}}^\dagger(t_2)\,|S_\phi\rangle\langle S_\phi|\,\hat{\mathcal{A}}(t_3)\hat{\mathcal{A}}(t_4)\,|S_\phi\rangle \\
&+ \langle S_\phi|\,\hat{\mathcal{A}}^\dagger(t_1)\hat{\mathcal{A}}(t_3)\,|S_\phi\rangle\langle S_\phi|\,\hat{\mathcal{A}}^\dagger(t_2)\hat{\mathcal{A}}(t_4)\,|S_\phi\rangle \\
&+ \langle S_\phi|\,\hat{\mathcal{A}}^\dagger(t_1)\hat{\mathcal{A}}(t_4)\,|S_\phi\rangle\langle S_\phi|\,\hat{\mathcal{A}}^\dagger(t_2)\hat{\mathcal{A}}(t_3)\,|S_\phi\rangle\ . \qquad (7.28)
\end{aligned}
$$

Using (6.64), we find

$$
\begin{aligned}
G^{(2)}(t_1,t_2;t_3,t_4) &= |M|^2 e^{2i\omega_c(t_1-t_3)}\delta(t_1-t_2)\delta(t_3-t_4) \\
&+ N^2\delta(t_1-t_3)\delta(t_2-t_4) + N^2\delta(t_1-t_4)\delta(t_2-t_3)\ , \qquad (7.29)
\end{aligned}
$$

where we have assumed that the squeezing parameters N and M are independent of frequency. By substituting (7.29) into (7.25), we find for the population

$$
\varrho_{33}(t) = 2\gamma_1\gamma_2\left\{N^2t^2 + \frac{|M|^2}{\Delta^2}\left[1-\cos(\Delta t)\right]\right\}\ , \qquad (7.30)
$$

where $\Delta = 2\omega_c - \omega_1 - \omega_2$ is the detuning of the double frequency of the squeezed field from the atomic two-photon resonance.

Thus, the two-photon excitation of the atom can be studied by analyzing the population of the upper state. For a thermal field, $|M| = 0$, and then the population (7.30) reduces to

$$
\varrho_{33}(t) = 2\gamma_1\gamma_2N^2t^2\ , \qquad (7.31)
$$

which shows that in the thermal field the population exhibits a quadratic dependence on N. For a low intensity ($N \ll 1$) squeezed vacuum with $|M| = \sqrt{N(N+1)}$ and the vanishing detuning $\Delta \to 0$, the expression (7.30) reduces to

$$
\varrho_{33}(t) = \gamma_1\gamma_2Nt^2\ . \qquad (7.32)
$$

In this case, the population $\varrho_{33}(t)$ linearly depends on N. Both results for the behavior of the population, (7.31) and (7.32), agree with the results discussed in Sect. 6.3.2.

Experiment

As has been already pointed out, the dependence of the population ϱ_{33} on the intensity of the squeezed vacuum was investigated experimentally by the Kimble's group at Caltech [12]. The experimental apparatus is shown in Fig. 7.10. In the experiment a cloud of cesium atoms in a magneto-optical trap (MOT) was irradiated by a squeezed vacuum field produced by an optical parametric oscillator (OPO). As we have seen, the output of the OPO consists of two strongly correlated beams of frequencies ω_i and ω_s, symmetrically located about the carrier (pump) frequency $\omega_0 = (\omega_i + \omega_s)/2$.

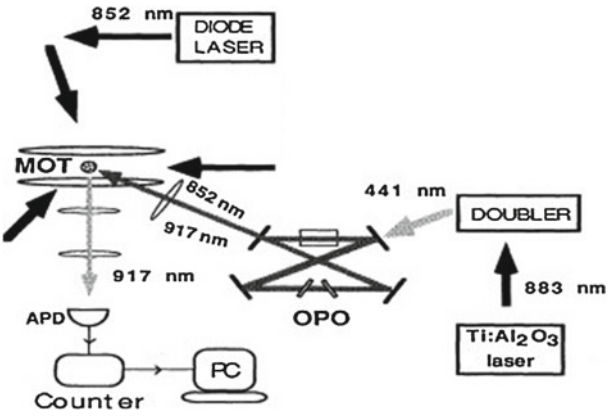

Fig. 7.10 Schematics of the Georgiades et al. [12] experiment on nonclassical spectroscopy to observe a linear dependence of the two-photon transition rate, a feature unique to quantum nature of the squeezed vacuum field. Reprinted with permission from N.Ph. Georgiades, E.S. Polzik, K. Edamatsu, H.J. Kimble, A.S. Parkins: Phys. Rev. Lett. **75**, 3426 (1995). Copyright (1995) by the American Physical Society.

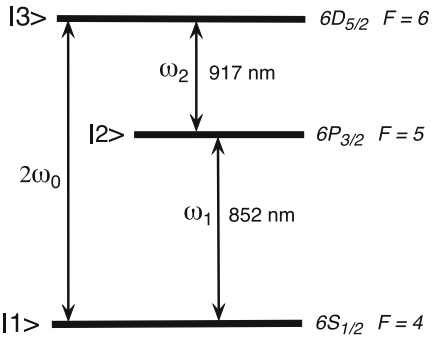

Fig. 7.11 Cesium energy levels and transition frequencies relevant in the experiment of the Kimble's group on the two-photon absorption in a squeezed vacuum field

The atomic cesium with the energy levels structure relevant to the experiment is shown in Fig. 7.11. The cesium atom behaves as a three-level atom in a ladder configuration with transition wavelengths $\lambda_{32} = 917$ nm and $\lambda_{21} = 852$ nm. The correlated squeezed vacuum beams were tuned to these atomic transitions. The cesium's fluorescence at 917 nm (which is proportional to the population ϱ_{33}) was recorded with an avalanche photodiode (APD) and analyzed by computer.

Figure 7.12 shows the experimental results for the variation of the population ϱ_{33} with N in a log-log scale. Superimposed on the experimental results are two dashed lines, one of slope $\delta = 1$ and the other of slope $\delta = 2$. The departure of the experimental results from the slope $\delta = 2$, corresponding to the N^2 variation of the population, gives compelling evidence for quantum nature of the excitation squeezed vacuum field.

In comparing the experimental result shown in Fig. 7.12 with the theoretical result, given in (6.93), one can notice that the experimental result departures from the

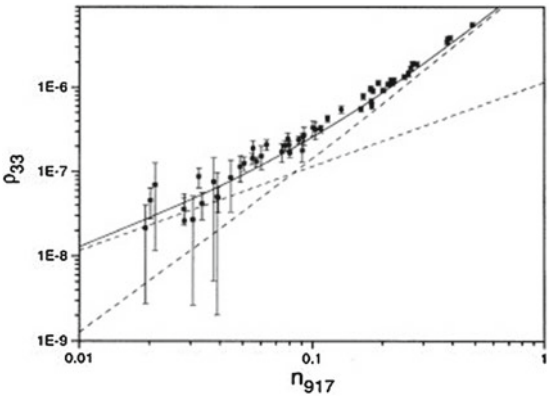

Fig. 7.12 Observation by Georgiades et al. [12] of the variation of the population ϱ_{33} with the intensity of the squeezed vacuum field. The plot shows evidence of the departure of the variation of ϱ_{33} from slope $\delta = 2$ to $\delta < 2$, ($\delta \sim 1.3$). Reprinted with permission from N.Ph. Georgiades, E.S. Polzik, K. Edamatsu, H.J. Kimble, A.S. Parkins: Phys. Rev. Lett. **75**, 3426 (1995). Copyright (1995) by the American Physical Society.

theoretical prediction that the observed variation of the population with N consists of not only a linear part but also a quadratic part. The reason for this discrepancy is in the assumption made in the derivation of the theoretical expression (6.93) of the perfect matching of the squeezed vacuum field to the atom. In other words, it was assumed that the squeezed field couples to the atom through a full 4π solid angle. Such an assumption does not suit the experimental arrangement that in the experiment the squeezed field focused on the atoms covered only a fraction of the 4π solid angle of space of the vacuum modes coupled to the atom.

Taking into account an imperfect coupling of the squeezed field to the atom is equivalent to replace the parameters N and M by $\tilde{N} = \eta N$ and $\tilde{M} = \eta M$, where η is the coupling efficiency of the incident squeezed vacuum modes to the vacuum modes surrounding the atom. For perfect matching, $\eta = 1$, whereas for an imperfect matching $\eta < 1$. We see that the effect of an imperfect matching is to degrade the squeezed field parameters N and M. The criterion $|M| = \sqrt{N(N+1)}$ is modified to

$$|\tilde{M}| = \eta\sqrt{N(N+1)} < \sqrt{N(N+1)}\,. \tag{7.33}$$

Thus, even if the output of the OPO has perfect two-photon correlations, in the interaction region with the atom it behaves like a squeezed field with imperfect two-photon correlations. Note that although M is decreased, its quantum nature persists.

When the parameters N and M appearing in the expression (6.82) are replaced by the effective parameters $\tilde{N}$ and $\tilde{M}$, respectively, we find that in the case of a quantum squeezed field with maximal correlations, $|M| = \sqrt{N(N+1)}$, the upper state population reduces to

$$\varrho_{33} = \frac{\eta^2 N\gamma_1 + (1-\eta)\eta^2 N^2(\gamma_1+\gamma_2)}{[\eta N(\gamma_1+\gamma_2)+\gamma_2]\,[3\eta(1-\eta)N+1]}\,. \tag{7.34}$$

This population consists of both linear and quadratic dependence terms on N, which is in agreement with the experimental result. The linear part is associated with the

factor η, a part of the 4π solid angle of space of the vacuum modes coupled to the atom occupied by the squeezed modes. The quadratic part is associated with $(1-\eta)$, a part of the 4π solid angle of space of the modes not covered by the squeezed vacuum modes.

Finally, we would like to emphasize that the linear dependence of the population on the intensity N is not crucially dependent on the perfect matching of the squeezed modes to the vacuum modes surrounding the atom. For $N \ll 1$, the expression (7.34) simplifies to

$$\varrho_{33} \approx \frac{\eta^2 \gamma_1 N}{\gamma_2} , \tag{7.35}$$

which shows that the linear dependence on the intensity of the population ϱ_{33} is not destroyed by an imperfect matching. This is of great importance in practice, since this makes it necessary only to match a fraction of the vacuum modes to the squeezed modes, and this, in fact, was done in the experiment.

7.5 Ultra-High Frequency Metrology with Squeezed Light

For a range of applications of squeezed light, it is necessary to determine accurately the absolute frequencies of the correlated signal and idler beams generated by parametric down-conversion. Well separated frequencies are usually measured in conventional homodyne photo-detection schemes where each of the frequencies can be separately mixed with a local oscillator field resulting in well resolved interference fringes observed in the intensity of the superposed fields. In the output field of a typical NDPO strong correlations between the signal and idler beams are usually manifested at frequency differences very small compared to the pump frequency, $\Delta\omega \equiv |\omega_s - \omega_i| \ll \omega_c$. It could be extremely difficult in practice to resolve such a small frequency difference in the conventional homodyne detection scheme since the small frequency difference could lead to a modulation of the interference fringes resulting in a degradation of the resolution of the interference fringes.

7.5.1 Two-Photon Interference

A high resolution of two correlated beams could be achieved in a two-photon interference scheme involving the joint two-photon excitation with signal and idler beams mixed with a coherent reference (local oscillator) beam. This situation might be encountered in a cascade three-level atom when the signal and idler beams of the NDPO are mixed with a strong coherent reference beam coupled to a quadrupole moment of the atomic two-photon transition, and one looks for two-photon interference effects. A schematic representation of the two-photon excitation of the three-level atom is shown in Fig. 7.13.

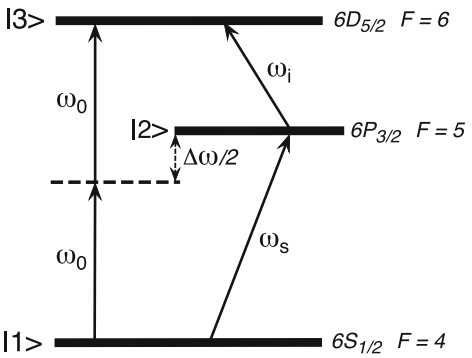

Fig. 7.13 Illustration of excitation paths of the state $|3\rangle$ in a cascade three-level atom. The signal and idler beams of frequencies ω_s and ω_i, respectively, excite the upper level $|3\rangle$ from the ground level $|1\rangle$ through the off-resonant intermediate level $|2\rangle$. The local oscillator of frequency ω_0 excites the level $|3\rangle$ directly from the ground level through the coupling to a quadrupole moment of the $|1\rangle \rightarrow |3\rangle$ transition

The principle of the two-photon interference is based on the excitation of the state $|3\rangle$ via two pathways, i.e., through two dipole stepwise transitions $|1\rangle \rightarrow |2\rangle \rightarrow |3\rangle$ and the direct $|1\rangle \rightarrow |3\rangle$ quadrupole transition. The amplitudes for these two indistinguishable excitation pathways interfere coherently to result in a quantum interference which can manifest itself as a modulation of the two-photon transition rate. We have shown in Sect. 7.4 that there is a direct connection between the two-photon absorption rate and the population of the state $|3\rangle$. Therefore, two-photon interference effects can be observed by monitoring the variation of the excited state population ϱ_{33} with the phase of the local oscillator. The two-photon interference scheme might reasonably be called "two-photon homodyne detection scheme" since it involves beating of a two signal fields with two photons of a strong classical field playing the role of a local oscillator.

Let us discuss the two-photon interference problem involving nonclassical and coherent light beams. A convenient way of describing two-photon processes is through the two-time intensity correlation function of the radiation field in normal order

$$\begin{aligned}&\langle \mathcal{T} : \hat{I}(\boldsymbol{r}, t)\hat{I}(\boldsymbol{r}, t+\tau) :\rangle \\ &= \langle \hat{E}^{(-)}(\boldsymbol{r}, t)\hat{E}^{(-)}(\boldsymbol{r}, t+\tau) : \hat{E}^{(+)}(\boldsymbol{r}, t+\tau)\hat{E}^{(-)}(\boldsymbol{r}, t)\rangle, \end{aligned} \tag{7.36}$$

where $\mathcal{T}$ and : : are time-ordering and normal ordering symbols. In the following we will drop the position label $\boldsymbol{r}$ for brevity, with understanding that $\boldsymbol{r}$ is in the far-field of the radiating atom.

In the two-photon interference scheme considered here, the total electric field is a sum of two fields

$$\hat{E}^{(-)}(t) = \hat{E}^{(-)}_{\rm out}(t) + \mathcal{E}(t)\ , \tag{7.37}$$

where $\mathcal{E}(t)$ is the amplitude of the local oscillator field of frequency ω_0 and phase β, which can be varied in some way,

$$\mathcal{E}(t) = |\mathcal{E}|\mathrm{e}^{\mathrm{i}(\omega_0 t+\beta)}\ , \tag{7.38}$$

and $\hat{E}^{(-)}_{\rm out}(t)$ is the amplitude of the output field of the NDPO cavity. The intensity correlation function of the resultant field is then

$$\begin{aligned}
\langle \mathcal{T}:\hat{I}(t)\hat{I}(t+\tau):\rangle &= \langle[\hat{E}^{(-)}_{\rm out}(t)+\mathcal{E}(t)][\hat{E}^{(-)}_{\rm out}(t+\tau)+\mathcal{E}(t+\tau)]\\
&\times[\hat{E}^{(+)}_{\rm out}(t+\tau)+\mathcal{E}^*(t+\tau)][\hat{E}^{(+)}_{\rm out}(t)+\mathcal{E}^*(t)]\rangle\\
&= |\mathcal{E}|^4 + \sigma_r^2\frac{|\mathcal{E}|^3 A}{r^2}\left\{\left[\langle\hat{E}^{(+)}_{\rm out}(t)\rangle\mathrm{e}^{\mathrm{i}(\omega_0 t+\beta)}+\mathrm{c.c.}\right]\right.\\
&+\left.\left[\langle\hat{E}^{(+)}_{\rm out}(t+\tau)\rangle\mathrm{e}^{\mathrm{i}(\omega_0 t+\omega_0\tau+\beta)}+\mathrm{c.c.}\right]\right\}\\
&+|\mathcal{E}|^2\left\{\langle\hat{E}^{(-)}_{\rm out}(t)\hat{E}^{(+)}_{\rm out}(t)\rangle+\langle\hat{E}^{(-)}_{\rm out}(t+\tau)\hat{E}^{(+)}_{\rm out}(t+\tau)\rangle\right.\\
&+\left[\langle\hat{E}^{(-)}_{\rm out}(t)\hat{E}^{(+)}_{\rm out}(t+\tau)\rangle\mathrm{e}^{\mathrm{i}\omega_0\tau}+\mathrm{c.c.}\right]\\
&+\left.\left[\langle\hat{E}^{(-)}_{\rm out}(t)\hat{E}^{(-)}_{\rm out}(t+\tau)\rangle\mathrm{e}^{-\mathrm{i}[\omega_0(2t+\tau)+2\beta]}+\mathrm{c.c.}\right]\right\}\ ,
\end{aligned} \tag{7.39}$$

where the terms of order $|\mathcal{E}|$ and less have been neglected as small compared with those of order $|\mathcal{E}|^2$.

We now go to the steady state limit ($t\to\infty$) in the sense that the correlation functions appearing in (7.39) become independent of t. Since the output field of the NDPO is in a vacuum state, we put the average amplitudes $\langle\hat{E}^{(+)}_{\rm out}(t)\rangle$ and $\langle\hat{E}^{(+)}_{\rm out}(t+\tau)\rangle$ equal to zero.

Let us introduce the notation

$$\begin{aligned}
D(\tau) &= \lim_{t\to\infty}\langle\mathcal{T}:\hat{I}(t)\hat{I}(t+\tau):\rangle\ ,\\
G^{(1)}_N(\tau) &= \lim_{t\to\infty}\langle\hat{E}^{(-)}_{\rm out}(t)\hat{E}^{(+)}_{\rm out}(t+\tau)\rangle\mathrm{e}^{-\mathrm{i}\omega_0\tau}\ ,\\
G^{(1)}_M(\tau) &= \lim_{t\to\infty}\langle\hat{E}^{(-)}_{\rm out}(t)\hat{E}^{(-)}_{\rm out}(t+\tau)\rangle\mathrm{e}^{\mathrm{i}\omega_0(2t+\tau)}\ .
\end{aligned} \tag{7.40}$$

Hence, we can write (7.39) in the form

$$D(\tau) = |\mathcal{E}|^4+|\mathcal{E}|^2\left\{G^{(1)}_N(0)+G^{(1)}_N(\tau)+G^{(1)}_M(\tau)\mathrm{e}^{-2\mathrm{i}\beta}+\mathrm{c.c}\right\}\ . \tag{7.41}$$

If we take the Fourier transform of $D(\tau)$:

$$D(\omega) = \int_0^\infty \mathrm{d}\tau\, D(\tau)\mathrm{e}^{\mathrm{i}\omega\tau}\,, \tag{7.42}$$

we arrive at

$$\begin{aligned} D(\omega) = 2\pi|\mathcal{E}|^4\delta(\omega) + |\mathcal{E}|^2 \Big\{ &\langle \hat{E}^{(-)}_{\mathrm{out}}(\omega)\hat{E}^{(+)}_{\mathrm{out}}(\omega')\rangle \\ &+ \langle \hat{E}^{(-)}_{\mathrm{out}}(\omega)\hat{E}^{(+)}_{\mathrm{out}}(\omega'+\omega_0)\rangle + \langle \hat{E}^{(-)}_{\mathrm{out}}(\omega)\hat{E}^{(-)}_{\mathrm{out}}(\omega')\rangle \mathrm{e}^{-2\mathrm{i}\beta} \\ &+ \langle \hat{E}^{(+)}_{\mathrm{out}}(\omega)\hat{E}^{(+)}_{\mathrm{out}}(\omega')\rangle \mathrm{e}^{2\mathrm{i}\beta} \Big\}\,. \end{aligned} \tag{7.43}$$

Using the results (6.32) and (6.38) for the correlation functions, we then have

$$D(\omega) = 2\pi I_c^2 \left[1 + \frac{2\tilde{M}}{I_c}\cos\Phi \right] + 4\pi I_c \tilde{N}\,, \tag{7.44}$$

where $\Phi = 2\beta - \phi$, $I_c = |\mathcal{E}|^2$ is the intensity of the local oscillator field, $\tilde{N} = AN$ and $\tilde{M} = AM$ are the effective squeezing parameters reflecting the fact that the squeezed vacuum is acting over the cross-section area A.

The normalized intensity correlation function $g^{(2)}(\omega, \Phi)$ can be obtained by dividing $D(\omega)$ by $2\pi I_c^2$. Hence, we obtain

$$g^{(2)}(\omega, \Phi) = 1 + \frac{2\tilde{N}}{I_c} + \frac{2\tilde{M}}{I_c}\cos\Phi\,. \tag{7.45}$$

Since $\varrho_{33} \propto D(\omega)$, the population ϱ_{33} therefore exhibits a periodic variation with the phase Φ that we refer to as interference. The interference may be regarded as reflecting the presence of two-photon correlations in the squeezed vacuum and, therefore offers an alternative procedure for establishing the existence of the correlations in the squeezed field. The relative modulation amplitude or the visibility of the interference pattern is given by the ratio $2\tilde{M}/I_c$, which is smaller than one. Note that the periodic variation is there even if the field is classically squeezed ($|M| = N$). However, the visibility, although small, it could be used to distinguish between the classical and quantum squeezing. In order to distinguish between the classical and intrinsically quantum correlations associated with the nonclassical nature of the quantum squeezed field, we concentrate on the region of small N where, as we have shown in Sect. 6.2.2, the distinction between classical and quantum correlations is maximal. For small N, we find that the visibility with a quantum squeezed field is proportional to $\sqrt{N}$, while for a classically squeezed field with $|M| = N$ the visibility is proportional to N. The distinction between $\sqrt{N}$ and N is apparently an unambiguous signature of a nonclassical effect.

It is worth mentioning that also the normalized intensity correlation function $g^{(2)}(\omega, \Phi)$ can be used to distinguish between the classical and quantum squeezing.

Note from (7.45) that for a classically squeezed field, $g^{(2)}(\omega, \Phi) \geq 1$ indicating that the emitted photons from the state $|3\rangle$ exhibit photon bunching. In the absence of the squeezed field, $(N = |M| = 0)$, the correlation function $g^{(2)}(\omega, \Phi) = 1$ corresponding to the coherent state of the excitation with the local oscillator alone. However, in the presence of the quantum squeezed field $g^{(2)}(\omega, \Phi)$ can be smaller than one, which occurs for the relative phase $\Phi = \pi$. Therefore, for the quantum squeezed field, the emitted photons exhibit the nonclassical phenomenon of antibunching.

7.5.2 *Observations of the Two-Photon Interference*

The phase sensitive two-photon excitation of the three-level atom with a squeezed vacuum was studied experimentally by the Kimble's group at Caltech [13] using the $6S_{1/2}F = 4 \rightarrow 6P_{3/2}F' = 5 \rightarrow 6D_{5/2}F'' = 6$ transition in atomic cesium. More specifically, the atomic transition was excited by the output of a NDPO whose signal and idler frequencies $\omega_s = \omega_0 + \frac{1}{2}\Delta\omega$ and $\omega_i = \omega_0 - \frac{1}{2}\Delta\omega$ were tuned to the atomic transition frequencies ω_1 and ω_2, respectively. The frequency separation between the signal and idler beams was $\Delta\omega/2\pi \approx 25$ THz. Simultaneously, the atom was illuminated with a coherent laser field of frequency $\omega_0 = \frac{1}{2}(\omega_1 + \omega_2)$ corresponding to half that of the $6S_{1/2}F = 4 \rightarrow 6D_{5/2}F'' = 6$ transition frequency, as shown in the insert of Fig. 7.14. The laser field was interacting with the atomic transition $|1\rangle \rightarrow |3\rangle$ through an electric quadrupole interaction. Thus, the state $|3\rangle$

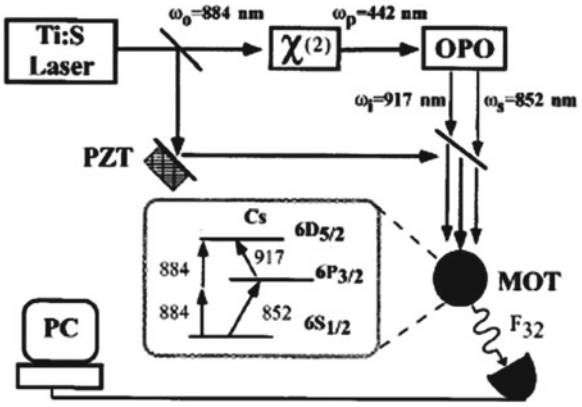

Fig. 7.14 Schematic of the experiment for detecting a phase sensitive two-photon excitation of cesium atoms using the output of a OPO cavity and a reference laser field (local oscillator). The fluorescence field at frequency 917 nm was detected and the power spectrum of the resulting photocurrent was analyzed on PC computer. The insert shows the energy levels of a cesium atom in the excitation paths of the upper level, a direct two-photon excitation path at 884 nm and the two-step excitation path through the intermediate level at 852 nm and 917 nm. Reprinted with permission from N.Ph. Georgiades, E.S. Polzik, H.J. Kimble: Phys. Rev. A **55**, R1605 (1997). Copyright (1997) by the American Physical Society

was excited via two pathways, i.e. the stepwise transitions $|1\rangle \rightarrow |2\rangle \rightarrow |3\rangle$ driven by the squeezed vacuum field and the direct $|1\rangle \rightarrow |3\rangle$ quadrupole transition driven by the laser field. As we have demonstrated above, quantum interference between the amplitudes of these two excitation paths leads to a phase-sensitive dependence of ϱ_{33} on the two-photon correlations M.

The objective of the experiment was to explore explicitly the issue of the phase-sensitivity of the excitation process and to provide a method of probing quantum correlations between two field separated in frequency by tens of THz, i.e. by ultra-high frequencies in a range 10–100 THz. In the experiment, shown in Fig. 7.14, cesium atoms, trapped and cooled in a magneto-optical trap (MOT) were illuminated by the output field of the OPO cavity and a laser beam, local oscillator, extracted from the Ti:S laser beam driving the OPO cavity. The phase of the local oscillator was modulated with a piezoelectric transducer (PZT).

In order to observe the signatures of the two-photon correlations present in the squeezed field, the first measurement of the fluorescence from the level $|3\rangle$ was done in the absence of the squeezed field for the phase Φ varied by modulating the phase β of the local oscillator as $\beta(t) = \beta_0 + \omega_m t$. Experimental data were obtained by measuring the power spectrum of the photocurrent due to the fluorescence from the level $|3\rangle$. The results are shown in Fig. 7.15a. The second observation was of the fluorescence in the presence of the squeezed field. Figure 7.15b shows the photocurrent spectrum which was measured. The measured spectra clearly show that in the absence of the squeezed field no frequency peaks are present at frequencies corresponding to the modulation frequency $f_m = \omega_m/2\pi = 11$ Hz and its harmonic

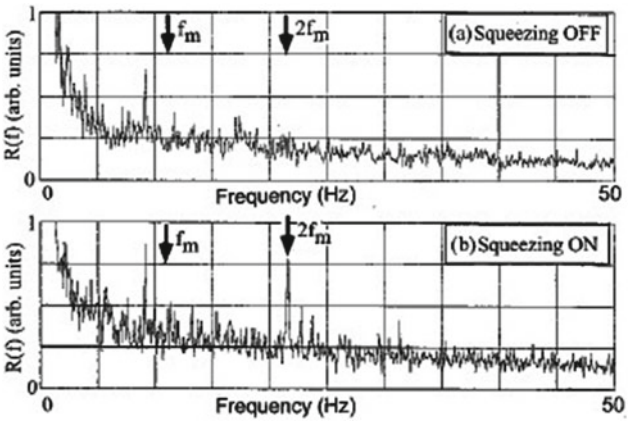

Fig. 7.15 Measured power spectrum of the photocurrent produced by the fluorescence detected at 917 nm. The fluorescence intensity is proportional to the population of the upper atomic level $|3\rangle$. Frame **a** shows the measured power spectrum in the absence of the squeezed field. The atom was excited alone with the local oscillator field. Frame **b** shows the power spectrum in the presence of both, the squeezed field and the local oscillator. The arrows indicate the positions of the interference peaks at the modulation frequency f_m and its harmonic $2f_m$. Reprinted with permission from N.Ph. Georgiades, E.S. Polzik, H.J. Kimble: Phys. Rev. A **55**, R1605 (1997). Copyright (1997) by the American Physical Society.

$2f_m$. When the squeezed field was turned on, a pronounced peak was observed at $2f_m$ signaling the presence of two-photon correlations in the squeezed field. The observed phase-sensitive modulation of the fluorescence field is a clear indication of the presence of the two-photon correlations in the output field of the NDPO.

References

1. C.W. Gardiner: Phys. Rev. Lett. **56**, 1917 (1986)
2. H.J. Carmichael, A.S. Lane, D.F. Walls: J. Mod. Opt. **34**, 821 (1987)
3. H.J. Carmichael, A.S. Lane, D.F. Walls: Phys. Rev. Lett. **58**, 2539 (1987)
4. K.W. Murch, S.J. Weber, K.M. Beck, E. Ginossar, I. Siddiqi: Nature **499**, 62 (2013)
5. D.M. Toyli, A.W. Eddins, S. Boutin, S. Puri, D. Hover, V. Bolkhovsky, W.D. Oliver, A. Blais, I. Siddigi: Phys. Rev. X **6**, 031004 (2016)
6. P. Zhou, S. Swain: Phys. Rev. Lett. **89**, (1999).
7. P. Zhou, S. Swain: Phys. Rev. A **59**, (1999).
8. Z. Ficek, B.J. Dalton: Opt. Commun. **102**, 231 (1993)
9. Z. Ficek, W. S. Smyth, S. Swain: Opt. Commun. **110**, 555 (1994)
10. A.S. Parkins: in *Modern Nonlinear Optics, Part II*, eds. M. Evans S. Kielich (Wiley, New York, 1993), p. 607
11. Q.A. Turchette, N.Ph. Georgiades, C.J. Hood, H.J. Kimble, A.S. Parkins: Phys. Rev. A **58**, 4056 (1998)
12. N.Ph. Georgiades, E.S. Polzik, K. Edamatsu, H.J. Kimble, A.S. Parkins: Phys. Rev. Lett. **75**, 3426 (1995)
13. N.Ph. Georgiades, E.S. Polzik, H.J. Kimble: Phys. Rev. A **55**, R1605 (1997)

Chapter 8
Engineering Collective and Squeezed Field Interactions

In this chapter, we shall consider methods of engineering collective interactions between atoms and a squeezed field-type damping of an atom. The concept of the collective behavior of atoms discussed in Chap. 4 was based on the assumption that distances between the atoms are smaller or comparable to the resonant wavelength. At such small distances, the atoms can behave collectively and we have seen that the collective effects are manifested in the presence of the collective damping, which alters the damping rates of the transitions, and the dipole–dipole interaction which shifts the energies of the atomic single-excitation levels. However, it is not easy in practice to bring trapped atoms into very small distances and keep the interacting atoms at fixed positions. The current experimental schemes can trap atoms at distances much larger than their resonant wavelengths.

We shall show that these difficulties may in principle be avoided by engineering an interaction between distant atoms inside a microcavity. The microcavity can provide several other advantages for the atoms. First, it can provide a shielding mechanism against environment effects on the atoms. Second, by placing atoms inside the cavity, atoms can be easily manipulated to reduce the spontaneous emission such that the system can decohere slower. In the approach, we shall use adiabatic methods to eliminate the cavity mode. Once the cavity mode is eliminated by either a fast damping or a large detuning from the atomic resonance, the atoms behave collectively either by the presence of the collective decay mechanism or the dipole–dipole coupling potential.

The remaining sections of the chapter are devoted to the field of spectral line narrowing by engineering atom-squeezed field type interactions. We have already seen in the preceding two chapters, Chaps. 6 and 7, that the major difficulty with the alteration of radiative properties of atoms is the requirement that the atoms interact exclusively with squeezed modes of the radiation field. External sources of squeezed light produce a beam which can couple to only a small fraction of the modes to which the atoms are coupled. In this chapter, we shall demonstrate two methods of engineering a squeezed field-type damping in an atom coupled to the ordinary vacuum.

Z. Ficek and R. Tanaś, *Quantum-Limit Spectroscopy*, Springer Series in Optical Sciences 200, DOI 10.1007/978-1-4939-3740-0_8

In the first, we shall demonstrate that this type of damping naturally manifested in a weakly driven two-level atom through the presence of spectral components with a negative weight. We shall arrive to this conclusion when explaining the origin of the negative weight of one of the Lorentzian in the fluorescence spectrum calculated in Sect. 3.4. By expressing the incoherent part of the fluorescence spectrum in terms squeezing spectra of the fluctuations of the fluorescence field, we shall show that the negative weight can be related to squeezing produced in the emitted field. However, on two further examples we shall demonstrate that negative-weighted Lorentzians can be present in the spectrum even if there is no squeezing in the field. The second method involves a four-level system driven by laser fields and damped to the ordinary vacuum. We shall show that under the adiabatic approximation of fast damped transitions, this system may effectively behave as a two-level system damped to quantum squeezed reservoir.

8.1 Engineering Long Distance Collective Interactions

It is our purpose in this section to address the question of how to create (engineer) the collective damping mechanism and dipole–dipole interactions between distant atoms. We study the simplest example, two identical two-level atoms separated by a large distance R_{12} (large compare to the resonance wavelength so the direct coupling between the atoms can be ignored), and interacting with a common EM field. There are two cases to be considered: (1) a fast damped cavity, the so-called bad cavity, containing two atoms located at a large distance from each other and resonant with the cavity frequency, and (2) the case of a good cavity but of frequency significantly detuned from the atomic resonance. In both the above cases our main efforts will be devoted to the derivation of the master equation for the reduced density operator of the atoms. The approach we shall take is to eliminate the cavity mode through either the fast damping of the cavity mode or a large detuning of the cavity frequency from the atomic resonance. In so doing, we shall demonstrate that in (1) the collective damping mechanism can be generated, analogous to the collective damping of the Dicke model, whereas in (2) we shall predict existence of a coherent coupling between the atoms, analogous to the dipole–dipole interaction. With the master equations obtained, we then investigate a possibility of the population transfer between the distant atoms interacting with a single-mode cavity field and discuss the experimental studies, performed by the Haroche's group in Paris, which demonstrated the population transfer.

8.1.1 Two Distant Atoms in a Cavity

Consider two identical two-level atoms of transition frequency ω_a located inside a cavity and separated by a large distance ($R_{12} \gg \lambda$) such that the collective parameters

$\gamma_{12} \approx 0$ and $\Omega_{12} \approx 0$. We assume that the atoms are coupled to a single mode of the cavity of frequency ω_c with coupling constants $g(\boldsymbol{R}_1)$ and $g(\boldsymbol{R}_2)$, respectively. We choose the reference frame such that

$$g(\boldsymbol{R}_1) = g_0, \quad \text{and} \quad g(\boldsymbol{R}_2) = g_0 \cos(kR_{12}) \ , \tag{8.1}$$

where $R_{12} = R_2 - R_1$ is the distance between the atoms, and $k = \omega_c/c$. This choice of the reference frame corresponds to a situation where atom 1 is kept exactly at an antinode of the standing wave and the atom 2 is moved through successive nodes and antinodes of the standing wave. This choice, of course, involves no loss of generality. We also assume that the atoms are stationary during the interaction with the cavity mode, i.e., the distance between the atoms is independent of time (the Raman-Nath approximation). This is a good approximation for many experiments on cooling of trapped atoms, where the storage time of the trapped atoms is long, so that they are essentially motionless and lie at known and controllable distances from one another [1].

Suppose that the cavity mode is damped with a rate κ, and the atoms are damped with rates γ_c. Since the cavity subtends a small solid angle of the EM modes to which the atoms are coupled, one would not expect a modification of the spontaneous decay rates of the atoms from those in free space γ, so that $\gamma_c \approx \gamma$. In addition, the cavity mode is driven by a laser field of the angular frequency ω_L and the Rabi frequency Ω.

A quantum state of the combined system; two atoms plus the cavity mode, labeled by the suffices a and c, respectively, is described by the density operator ϱ_{ac}. In the Schrödinger picture, the density operator satisfies the master equation

$$\frac{\partial \varrho_{ac}}{\partial t} = -\frac{\mathrm{i}}{\hbar}\left[\hat{H}, \varrho_{ac}\right] - \frac{1}{2}\gamma \mathcal{L}_a \varrho_{ac} - \frac{1}{2}\kappa \mathcal{L}_c \varrho_{ac} \ , \tag{8.2}$$

where

$$\begin{aligned} \hat{H} = {} & \hbar \sum_{i=1}^{2} \omega_0 S_z^{(i)} + \hbar\omega_c \hat{a}^\dagger \hat{a} + \frac{1}{2}\hbar\Omega\left(\hat{a}\mathrm{e}^{\mathrm{i}\omega_L t} + \hat{a}^\dagger \mathrm{e}^{-\mathrm{i}\omega_L t}\right) \\ & - \frac{1}{2}\hbar \sum_{i=1}^{2} g(\boldsymbol{R}_i)\left(S_i^- \hat{a}^\dagger + \hat{a} S_i^+\right) \end{aligned} \tag{8.3}$$

is the Hamiltonian of the system, and

$$\begin{aligned} \mathcal{L}_a \varrho_{ac} &= \sum_{i=1}^{2}\left(S_i^+ S_i^- \varrho_{ac} + \varrho_{ac} S_i^+ S_i^- - 2S_i^- \varrho_{ac} S_i^+\right) \ , \\ \mathcal{L}_c \varrho_{ac} &= \hat{a}^\dagger \hat{a} \varrho_{ac} + \varrho_{ac} \hat{a}^\dagger \hat{a} - 2\hat{a}\varrho_{ac}\hat{a}^\dagger \ , \end{aligned} \tag{8.4}$$

are operators representing the damping of the atoms by spontaneous emission and of the field by cavity decay, respectively; $\hat{a}$ and $\hat{a}^\dagger$ are the cavity mode annihilation and

creation operators, and S_i^+, S_i^- and $S_z^{(i)}$ are the dipole raising, lowering, and energy difference operators of atom i.

In the following two sections, we derive the master equation for the reduced density operator ϱ_a of the two atoms alone. As we have already mentioned, we consider two cases, (1) the bad cavity limit and (2) a good cavity limit with the cavity mode frequency significantly detuned from the atomic resonance.

8.1.2 Dynamics of the Atoms in Bad Cavity

We consider in this section the bad cavity limit. For simplicity, we assume that the frequencies ω_c, ω_L, and ω_0 are all equal. In a rotating frame defined by the unitary transformation

$$U = \mathrm{e}^{\mathrm{i}\left(\sum_{i=1}^{2}\omega_L S_z^{(i)} + \omega_L \hat{a}^\dagger \hat{a}\right)t} , \tag{8.5}$$

the master equation (8.2) takes the form

$$\begin{aligned}\frac{\partial \tilde{\varrho}_{ac}}{\partial t} = &-\frac{1}{2}\mathrm{i}\Omega\left[\hat{a}+\hat{a}^\dagger, \tilde{\varrho}_{ac}\right] - \frac{1}{2}\mathrm{i}\sum_{i=1}^{2} g(\boldsymbol{R}_i)\left[S_i^-\hat{a}^\dagger + \hat{a}S_i^+, \tilde{\varrho}_{ac}\right] \\ &-\frac{1}{2}\gamma\,\mathcal{L}_a\tilde{\varrho}_{ac} - \frac{1}{2}\kappa\,\mathcal{L}_c\tilde{\varrho}_{ac} ,\end{aligned} \tag{8.6}$$

where $\tilde{\varrho}_{ac} = U\varrho_{ac}U^\dagger$.

We now derive the master equation for the reduced density operator ϱ_a describing the evolution of the atomic state only. In order to do it, we perform the unitary transformation on the density operators ϱ_{ac} as

$$\varrho_T = \hat{D}(-\eta)\tilde{\varrho}_{ac}\hat{D}(\eta) , \tag{8.7}$$

where

$$\hat{D}(\eta) = \mathrm{e}^{\mathrm{i}\eta(\hat{a}+\hat{a}^\dagger)} \tag{8.8}$$

is the displacement operator, and $\eta = \Omega/\kappa$. Under the transformation (8.7), the master equation (8.6) takes the form

$$\begin{aligned}\frac{\partial \varrho_T}{\partial t} = &\frac{1}{2}\mathrm{i}\eta\sum_{i=1}^{2} g(\boldsymbol{R}_i)\left[S_i^+ + S_i^-, \varrho_T\right] - \frac{1}{2}\mathrm{i}\sum_{i=1}^{2} g(\boldsymbol{R}_i)\left[S_i^-\hat{a}^\dagger + \hat{a}S_i^+, \varrho_T\right] \\ &-\frac{1}{2}\gamma\,\mathcal{L}_a\varrho_T - \frac{1}{2}\kappa\,\mathcal{L}_c\varrho_T .\end{aligned} \tag{8.9}$$

We now introduce the photon number representation for the density operator ϱ_T with respect to the cavity mode

$$\varrho_T = \sum_{m,n=0}^{\infty} \varrho_{mn} \left| m \right\rangle \left\langle n \right| \ , \tag{8.10}$$

where ϱ_{mn} are the density matrix elements in the basis of the photon number states of the cavity mode.

Suppose that the cavity mode is strongly damped, that is

$$\kappa \gg g_0, \gamma \ . \tag{8.11}$$

This condition defines the bad cavity limit and implies that photons rapidly escape from the cavity leaving only the low excitation states populated. Therefore, we may neglect populations of the highly excited cavity modes and truncate the mode expansion at $m, n = 1$. Under this approximation, it is straightforward to write down the equations of motion for the density matrix elements. Thus, from the master equation (8.9) we obtain the following set of coupled equations of motion for the density matrix elements

$$\begin{aligned}
\dot{\varrho}_{00} &= \kappa \varrho_{11} - \frac{1}{2} \mathrm{i} \sum_{i=1}^{2} g(\boldsymbol{R}_i) \left(S_i^+ \varrho_{10} - \varrho_{01} S_i^- \right) + \mathcal{L} \varrho_{00} \ , \\
\dot{\varrho}_{10} &= -\frac{1}{2} \kappa \varrho_{10} - \frac{1}{2} \mathrm{i} \sum_{i=1}^{2} g(\boldsymbol{R}_i) \left(S_i^- \varrho_{00} - \varrho_{11} S_i^- \right) + \mathcal{L} \varrho_{10} \ , \\
\dot{\varrho}_{01} &= -\frac{1}{2} \kappa \varrho_{01} + \frac{1}{2} \mathrm{i} \sum_{i=1}^{2} g(\boldsymbol{R}_i) \left(\varrho_{00} S_i^+ - S_i^+ \varrho_{11} \right) + \mathcal{L} \varrho_{01} \ , \\
\dot{\varrho}_{11} &= -\kappa \varrho_{11} - \frac{1}{2} \mathrm{i} \sum_{i=1}^{2} g(\boldsymbol{R}_i) \left(S_i^- \varrho_{01} - \varrho_{10} S_i^+ \right) + \mathcal{L} \varrho_{11} \ ,
\end{aligned} \tag{8.12}$$

where

$$\mathcal{L} \varrho_{nm} = \frac{1}{2} \mathrm{i} \eta \sum_{i=1}^{2} g(\boldsymbol{R}_i) \left[S_i^+ + S_i^- , \varrho_{nm} \right] - \frac{1}{2} \gamma \mathcal{L}_a \varrho_{nm} \ . \tag{8.13}$$

We note that the field matrix elements ϱ_{mn} are still operators with respect to the atoms. Moreover

$$\varrho_{00} + \varrho_{11} = \mathrm{Tr}_F \left(\varrho_T \right) = \varrho_a \tag{8.14}$$

is the reduced density operator of the atoms.

Under the condition (8.11), the most populated state of the cavity field is the ground state $|0\rangle$, and then we can make a fundamental physical assumption: The coherences ϱ_{10} and ϱ_{01} change slowly in time, in the sense that $\dot{\varrho}_{10} \ll \omega_c \varrho_{10}$ and $\dot{\varrho}_{01} \ll \omega_c \varrho_{01}$, so that we can put $\dot{\varrho}_{10} = 0$ and $\dot{\varrho}_{01} = 0$. Under this approximation, the coherences ϱ_{10} and ϱ_{01} become simply

$$\begin{aligned} \varrho_{10} &\approx -\mathrm{i} \sum_{i=1}^{2} \frac{g(\boldsymbol{R}_i)}{\kappa} \left(S_i^- \varrho_{00} - \varrho_{11} S_i^- \right) , \\ \varrho_{01} &\approx \mathrm{i} \sum_{i=1}^{2} \frac{g(\boldsymbol{R}_i)}{\kappa} \left(\varrho_{00} S_i^+ - S_i^+ \varrho_{11} \right) , \end{aligned} \tag{8.15}$$

provided $\kappa \gg \eta g(\boldsymbol{R}_i), \gamma$. The above approximation is known as the adiabatic approximation. Mathematically, it allows to eliminate the coherences ϱ_{10} and ϱ_{01} from the dynamics of the system. By substituting the expressions (8.15) into the equations of motion for ϱ_{00} and ϱ_{11} in (8.12), we get

$$\begin{aligned} \dot{\varrho}_{00} &= \mathcal{L}\varrho_{00} + \kappa \varrho_{11} - \frac{1}{2} \sum_{i,j=1}^{2} \gamma_{ij} \left(S_i^+ S_j^- \varrho_{00} + \varrho_{00} S_i^+ S_j^- - 2 S_i^+ \varrho_{11} S_j^- \right) , \\ \dot{\varrho}_{11} &= \mathcal{L}\varrho_{11} - \kappa \varrho_{11} - \frac{1}{2} \sum_{i,j=1}^{2} \gamma_{ij} \left(S_i^- S_j^+ \varrho_{11} + \varrho_{11} S_i^- S_j^+ - 2 S_i^- \varrho_{00} S_j^+ \right) , \end{aligned} \tag{8.16}$$

where

$$\gamma_{ij} = \frac{g(\boldsymbol{R}_i) g(\boldsymbol{R}_j)}{\kappa} . \tag{8.17}$$

Next, we add together the two equations in (8.16) and then neglect the population of the state $|1\rangle$ as negligibly small. When we do that, we find the master equation for the reduced density operator of the atoms

$$\begin{aligned} \frac{\partial \varrho_a}{\partial t} &= \frac{1}{2} \mathrm{i} \sum_{i=1}^{2} \Omega(\boldsymbol{R}_i) \left[S_i^+ + S_i^-, \varrho_a \right] - \frac{1}{2} \gamma \mathcal{L}_a \varrho_a \\ &\quad - \frac{1}{2} \sum_{i,j=1}^{2} \gamma_{ij} \left(S_i^+ S_j^- \varrho_a + \varrho_a S_i^+ S_j^- - 2 S_j^- \varrho_a S_i^+ \right) , \end{aligned} \tag{8.18}$$

where $\Omega(\boldsymbol{R}_i) = \eta g(\boldsymbol{R}_i)$ is the effective Rabi frequency of the laser field at the position of atom i.

The master equation (8.18) is formally identical to the master equation (4.13) describing the dynamics of two *directly* interacting atoms. The only difference is the absence of the dipole–dipole interaction term. Thus, the adiabatic elimination of the

cavity mode, under the bad cavity limit, mimics the collective damping of the atoms. The first term in (8.18) is due to the interaction of the atoms with the driving field of an effective Rabi frequency $\Omega(\boldsymbol{R}_i)$. The second term is due to the damping of the atoms by spontaneous emission to modes different than the cavity mode. Finally, the last term describes radiation damping in the atomic system due to the coupling of the atoms to the fast damped cavity mode. It is composed of four terms involving γ_{ij}; with γ_{ii} describing damping of atom i, and γ_{ij} $(i \neq j)$ the damping of atom i caused by the radiation of atom j. The parameters γ_{11} and γ_{22} are recognized as the cavity-induced decay rates of the atoms 1 and 2, respectively.

The parameter $\gamma_{12}(=\gamma_{21})$, on the other hand, gives the collective damping mechanism of the system. Hence, effectively we engineer, with the help of the adiabatic approximation, a collective damping mechanism between the atoms. It should be noted that the damping rates γ_{11} and γ_{22} are, in general, not equal. They become equal only if the atoms are in equivalent positions inside the cavity mode, i.e., when $g(\boldsymbol{R}_1) = g(\boldsymbol{R}_2)$. Therefore, we can conclude that a system of two identical atoms coupled to a fast damped cavity mode may effectively behave as a system of two *nonidentical* atoms *collectively* damped by the cavity field.

If we choose the parameters such that the collective damping by the cavity field is much larger than the spontaneous rates of the atoms to the side cavity modes, the second term in (8.18) can be ignored, and then the master equation (8.18) describes the evolution of the density operator of the collective damped two-atom system.

Finally, we may show that the cavity-induced damping term in (8.18) is the same as the damping term of transitions between the symmetric states of a two-atom system. If we introduce symmetric and antisymmetric combinations of the atomic dipole operators

$$\begin{aligned} S_s^{\pm} &= \sqrt{\frac{\gamma_{11}}{\gamma_{11}+\gamma_{22}}}S_1^{\pm} + \sqrt{\frac{\gamma_{22}}{\gamma_{11}+\gamma_{22}}}S_2^{\pm}\,, \\ S_a^{\pm} &= \sqrt{\frac{\gamma_{22}}{\gamma_{11}+\gamma_{22}}}S_1^{\pm} - \sqrt{\frac{\gamma_{11}}{\gamma_{11}+\gamma_{22}}}S_2^{\pm}\,, \end{aligned} \tag{8.19}$$

representing the symmetric and antisymmetric mode of the atomic system, we readily find that in terms of these new operators (8.18) then becomes

$$\begin{aligned} \frac{\partial \varrho_a}{\partial t} &= \frac{1}{2}\mathrm{i}\Omega_s\left[\left(S_s^{+}+S_s^{-}\right),\varrho_a\right] + \frac{1}{2}\mathrm{i}\Omega_a\left[\left(S_a^{+}+S_a^{-}\right),\varrho_a\right] - \frac{1}{2}\gamma\,\mathcal{L}_a\varrho_a \\ &\quad - \frac{1}{2}\gamma_s\left(S_s^{+}S_s^{-}\varrho_a + \varrho_a S_s^{+}S_s^{-} - 2S_s^{-}\varrho_a S_s^{+}\right)\,, \end{aligned} \tag{8.20}$$

where

$$\begin{aligned} \Omega_s &= \sqrt{\frac{\gamma_{11}}{\gamma_{11}+\gamma_{22}}}\Omega(\boldsymbol{R}_1) + \sqrt{\frac{\gamma_{22}}{\gamma_{11}+\gamma_{22}}}\Omega(\boldsymbol{R}_2)\,, \\ \Omega_a &= \sqrt{\frac{\gamma_{22}}{\gamma_{11}+\gamma_{22}}}\Omega(\boldsymbol{R}_1) - \sqrt{\frac{\gamma_{11}}{\gamma_{11}+\gamma_{22}}}\Omega(\boldsymbol{R}_2)\,, \end{aligned} \tag{8.21}$$

and $\gamma_s = \gamma_{11} + \gamma_{22}$. Clearly, the master equation (8.20) involves damping of only the symmetric mode. The antisymmetric mode of the system does not decay. However, the antisymmetric mode is driven by the laser field with an effective Rabi frequency Ω_a. We note that $\Omega_a \neq 0$ only if the atoms are in nonequivalent positions inside the cavity mode, $g(\boldsymbol{R}_1) \neq g(\boldsymbol{R}_2)$. Otherwise, $\Omega_a = 0$.

8.1.3 Dynamics of the Atoms in Off-Resonant Cavity

In the preceding section we have shown how to create the collective decay mechanism in a system of two distant atoms. This has been done by eliminating the cavity field variables under the bad cavity limit. We now consider a good cavity with a small damping rate but we shall assume that the cavity mode frequency is significantly detuned from the atomic resonance [2, 3]. In this case, we can make the adiabatic approximation in respect to the large detuning to eliminate the cavity mode. In the following calculation, we take $\Omega = 0$, i.e., no external driving field.

When the cavity mode frequency is detuned from the atomic resonance, at the detuning $\Delta = \omega_c - \omega_a$, the master equation (8.2), can be written in the form

$$\frac{\partial \tilde{\varrho}_{ac}}{\partial t} = -\mathrm{i}\omega_c \left[\hat{a}^\dagger \hat{a}, \tilde{\varrho}_{ac}\right] - \frac{1}{2}\mathrm{i} \sum_{i=1}^{2} g(\boldsymbol{R}_i) \left[S_i^- \hat{a}^\dagger \mathrm{e}^{-\mathrm{i}\omega_0 t} + \hat{a} S_i^+ \mathrm{e}^{\mathrm{i}\omega_0 t}, \tilde{\varrho}_{ac}\right] - \frac{1}{2}\gamma \mathcal{L}_a \tilde{\varrho}_{ac} - \frac{1}{2}\kappa \mathcal{L}_c \tilde{\varrho}_{ac} , \tag{8.22}$$

where $\tilde{\varrho}_{ac} = U \varrho_{ac} U^\dagger$ is the density operator in the rotating frame determined by the unitary operator

$$U = \mathrm{e}^{\mathrm{i}\omega_0 (S_z^{(1)} + S_z^{(2)})t} . \tag{8.23}$$

In a good cavity, the atoms interchange photons more effectively with the cavity mode than with the side modes, but the cavity mode itself loses photons with the rate κ. Hence, in order to avoid the process of losing photons, we introduce *the limit of large detuning*, that $\Delta \gg g(\boldsymbol{R}_i) \gg \gamma, \kappa$. In this limit there is no energy exchange between the atoms and the cavity mode, the atoms exchange virtual photons. Under this approximation, we find from the master equation (8.22) that the populations of the two lowest energy levels and coherence between them satisfy the following equations of motion

$$\dot{\tilde{\varrho}}_{00} = -\mathrm{i} \sum_{i=1}^{2} g(\boldsymbol{R}_i) \left(S_i^+ \tilde{\varrho}_{10} - \tilde{\varrho}_{01} S_i^-\right) - \frac{1}{2}\gamma \mathcal{L}_a \varrho_{00} ,$$

$$\dot{\tilde{\varrho}}_{01} = \mathrm{i}\Delta \tilde{\varrho}_{01} - \mathrm{i} \sum_{i=1}^{2} g(\boldsymbol{R}_i) \left(S_i^+ \varrho_{11} - \varrho_{00} S_i^+\right) - \frac{1}{2}\gamma \mathcal{L}_a \tilde{\varrho}_{01} ,$$

$$\dot{\tilde{\varrho}}_{10} = -\mathrm{i}\Delta\tilde{\varrho}_{10} + \mathrm{i}\sum_{i=1}^{2} g(\boldsymbol{R}_i)\left(\varrho_{11}S_i^- - S_i^-\varrho_{00}\right) - \frac{1}{2}\gamma\,\mathcal{L}_a\tilde{\varrho}_{10}\,,$$

$$\dot{\varrho}_{11} = -\mathrm{i}\sum_{i=1}^{2} g(\boldsymbol{R}_i)\left(S_i^-\tilde{\varrho}_{01} - \tilde{\varrho}_{10}S_i^+\right) - \frac{1}{2}\gamma\,\mathcal{L}_a\varrho_{11}\,, \tag{8.24}$$

where $\tilde{\varrho}_{10} = \varrho_{10}\mathrm{e}^{\mathrm{i}\omega_a t}$ and $\tilde{\varrho}_{01} = \varrho_{01}\mathrm{e}^{-\mathrm{i}\omega_a t}$ are the slowly varying parts of the coherences.

Now, we explicitly apply the adiabatic approximation that for a large detuning, the coherences $\tilde{\varrho}_{01}$ and $\tilde{\varrho}_{10}$ vary slowly in time, so we can assume that $\dot{\tilde{\varrho}}_{01} \approx 0$ and $\dot{\tilde{\varrho}}_{10} \approx 0$. In this case, we find from (8.24) that in the limit of $\Delta \gg g(\boldsymbol{R}_i) \gg \gamma$, the coherences can be approximated by

$$\tilde{\varrho}_{01} \approx \sum_{i=1}^{2} \frac{g(\boldsymbol{R}_i)}{\Delta}\left(S_i^+\varrho_{11} - \varrho_{00}S_i^+\right),$$

$$\tilde{\varrho}_{10} \approx \sum_{i=1}^{2} \frac{g(\boldsymbol{R}_i)}{\Delta}\left(\varrho_{11}S_i^- - S_i^-\varrho_{00}\right). \tag{8.25}$$

As in the previous section, we substitute (8.25) into the equations of motion for ϱ_{00} and ϱ_{11} in (8.24). In so doing, we get

$$\dot{\varrho}_{00} = \mathrm{i}\sum_{i,j=1}^{2} \frac{g(\boldsymbol{R}_i)g(\boldsymbol{R}_j)}{\Delta}\left[S_i^+S_j^-, \varrho_{00}\right] - \frac{1}{2}\gamma\,\mathcal{L}_a\varrho_{00}, \tag{8.26}$$

$$\dot{\varrho}_{11} = -\mathrm{i}\sum_{i,j=1}^{2} \frac{g(\boldsymbol{R}_i)g(\boldsymbol{R}_j)}{\Delta}\left[S_i^-S_j^+, \varrho_{11}\right] - \frac{1}{2}\gamma\,\mathcal{L}_a\varrho_{11}. \tag{8.27}$$

Next, by adding (8.26) and (8.27) and neglecting the population ϱ_{11}, we arrive at the master equation for the density operator ϱ_a of the atoms

$$\frac{\partial\varrho_a}{\partial t} = \mathrm{i}\sum_{i=1}^{2}\delta_i\left[S_z^{(i)}, \varrho_a\right] + \mathrm{i}\sum_{i\neq j=1}^{2}\Omega_{ij}\left[S_i^+S_j^-, \varrho_a\right] - \frac{1}{2}\gamma\,\mathcal{L}_a\varrho_a\,, \tag{8.28}$$

where

$$\delta_i = \frac{g^2(\boldsymbol{R}_i)}{\Delta}, \quad \text{and} \quad \Omega_{ij} = \Omega_{ji} = \frac{g(\boldsymbol{R}_i)g(\boldsymbol{R}_j)}{\Delta}. \tag{8.29}$$

The first term in the master equation (8.28) gives rise to frequency shifts of the atomic levels. It is an analog of a dynamic Stark shift. The second term depends on the position coordinates of the atoms and represents the shift in energy separation of the levels of atom i due to its interaction with the atom j via virtual photon exchange.

The third term represents the damping of the atoms through the interaction with the environment. From the structure of the second term in (8.29) one can recognize that Ω_{ij} is an analog of the familiar dipole–dipole interaction between the atoms [4, 5]. This shows that the interaction of the atoms with a detuned cavity fields produces a structure in the master equation analogous to the dipole–dipole interaction between the atoms. This happens because the photons emitted spontaneously by each atom induce in the other atom the oscillations which, on other hand, are partially coherent with their own spontaneous oscillations.

The above procedure shows that the adiabatic elimination of the cavity mode creates a shift of the atomic transition frequencies and an effective interaction between two distant atoms. Thus, the dynamics of the system composed of two identical atoms in nonequivalent positions in the cavity mode is equivalent to those of two nonidentical atoms of different transition frequencies. In other words, the procedure is an example of how one can "engineer" the dipole–dipole type interaction between distant atoms.

8.1.4 Application to Population Transfer

As an example of the application of the master equation (8.28) to a situation of the collective behavior of two distant atoms, we consider the evolution of the state vector of the atomic system. For simplicity, we consider the case when the atoms are in equivalent positions inside the cavity mode at which $\delta_1 = \delta_2 \equiv \delta$.

If we choose the direct-product basis

$$\begin{aligned} |1\rangle &= |g_1\rangle \otimes |g_2\rangle\,, \quad |2\rangle = |g_1\rangle \otimes |e_2\rangle\ , \\ |3\rangle &= |e_1\rangle \otimes |g_2\rangle\,, \quad |4\rangle = |e_1\rangle \otimes |e_2\rangle\ , \end{aligned} \tag{8.30}$$

the state vector $|\Psi_a(t)\rangle$ of the two-atom system can then be written as

$$|\Psi_a(t)\rangle = C_1(t)\,|1\rangle + C_2(t)\,|2\rangle + C_3(t)\,|3\rangle + C_4(t)\,|4\rangle\ , \tag{8.31}$$

where $C_i(t)$ is the probability amplitude of the state $|i\rangle$. Note that $|C_i(t)|^2 = \varrho_{ii}(t)$ is the occupation probability (population) of the state $|i\rangle$. Hence, we can determine the time evolution of the state vector simply by finding the time evolution of the populations of the product states. Using the master equation (8.28), we find the following equations of motion for the populations

$$\begin{aligned} \dot{\varrho}_{11} &= \gamma\,(\varrho_{22} + \varrho_{33})\ , \\ \dot{\varrho}_{22} &= -\gamma\varrho_{22} + \gamma\varrho_{44} - \mathrm{i}\Omega_{12}\,(\varrho_{23} - \varrho_{32})\ , \\ \dot{\varrho}_{33} &= -\gamma\varrho_{33} + \gamma\varrho_{44} + \mathrm{i}\Omega_{12}\,(\varrho_{23} - \varrho_{32})\ , \\ \dot{\varrho}_{44} &= -2\gamma\varrho_{44}\,, \end{aligned} \tag{8.32}$$

while the off-diagonal density matrix elements (coherences) obey the equations

$$\begin{aligned}\dot{\varrho}_{23} &= -\gamma\varrho_{23} - \mathrm{i}\Omega_{12}\,(\varrho_{22} - \varrho_{33})\ ,\\ \dot{\varrho}_{32} &= -\gamma\varrho_{32} + \mathrm{i}\Omega_{12}\,(\varrho_{22} - \varrho_{33})\ .\end{aligned} \tag{8.33}$$

If we introduce linear combinations

$$\varrho_{ss} = \varrho_{22}+\varrho_{33}\ ,\ u = \varrho_{23}+\varrho_{32}\ ,\ v = \mathrm{i}(\varrho_{23}-\varrho_{32})\ ,\ w = \varrho_{22} - \varrho_{33}\ , \tag{8.34}$$

we readily find that (8.32) and (8.33) take a simplified form

$$\begin{aligned}\dot{\varrho}_{11} &= \gamma\varrho_{ss},\\ \dot{\varrho}_{ss} &= -\gamma\varrho_{ss} + 2\gamma\varrho_{44}\ ,\\ \dot{\varrho}_{44} &= -2\gamma\varrho_{44}\ ,\end{aligned} \tag{8.35}$$

and

$$\begin{aligned}\dot{u} &= -\gamma\, u\ ,\\ \dot{v} &= -\gamma\, v + 2\Omega_{12} w\ ,\\ \dot{w} &= -\gamma\, w - 2\Omega_{12} v\ .\end{aligned} \tag{8.36}$$

Note that the equations of motion (8.36) are the exact equivalent of the optical Bloch equations of a two-level system driven by a coherent field, where the dipole–dipole interaction Ω_{12} couples to the levels like the Rabi frequency of the coherent field. The upper and lower energy levels $|2\rangle$ and $|3\rangle$ thus show a dynamics that is analogous to that of a driven two-level system.

The general solution of (8.35) and (8.36), valid for arbitrary initial conditions, is given by

$$\begin{aligned}\varrho_{ss}(t) &= \varrho_{ss}(0)\mathrm{e}^{-\gamma t} + 2\varrho_{44}(0)\left(1 - \mathrm{e}^{-\gamma t}\right)\mathrm{e}^{-\gamma t}\ ,\\ u(t) &= u(0)\mathrm{e}^{-\gamma t}\ ,\quad \varrho_{44}(t) = \varrho_{44}(0)\mathrm{e}^{-2\gamma t}\ ,\\ v(t) &= \mathrm{e}^{-\gamma t}\left[v(0)\cos(2\Omega_{12}t) + w(0)\sin(2\Omega_{12}t)\right]\ ,\\ w(t) &= \mathrm{e}^{-\gamma t}\left[v(0)\sin(2\Omega_{12}t) + w(0)\cos(2\Omega_{12}t)\right]\ ,\end{aligned} \tag{8.37}$$

where $w(0)$, $u(0)$ and $v(0)$ stand for the initial values.

If initially only atom 1 was excited, $\varrho_{33}(0) = 1$, and then it is easy to find that the populations of the product states (8.30) are

$$\begin{aligned}\varrho_{11}(t) &= 1 - \mathrm{e}^{-\gamma t}\ ,\quad \varrho_{44}(t) = 0\ ,\\ \varrho_{22}(t) &= \mathrm{e}^{-\gamma t}\sin^2(\Omega_{12}t)\ ,\quad \varrho_{33}(t) = \mathrm{e}^{-\gamma t}\cos^2(\Omega_{12}t)\ .\end{aligned} \tag{8.38}$$

In this case, the state vector of the system at time $t > 0$ is

$$|\Psi_a(t)\rangle = \sqrt{1-e^{-\gamma t}}\,|1\rangle + e^{-\frac{1}{2}\gamma t}\sin(\Omega_{12}t)|2\rangle + e^{-\frac{1}{2}\gamma t}\cos(\Omega_{12}t)|3\rangle \ . \quad (8.39)$$

We see that the amplitudes of $|2\rangle$ and $|3\rangle$ states periodically oscillate at the frequency Ω_{12}. The atoms exchange virtual photons through the highly detuned cavity mode which results in a reversible coherent evolution. The atoms also spontaneously emit photons into the side modes. Consequently, the reversible oscillations are damped with the rate γ leading to an increase of the population of the state $|1\rangle$. At times shorter than the lifetime of the excitation in the system, $t \ll 1/\gamma$, the initial population evolves entirely between the single excitation states $|2\rangle$ and $|3\rangle$. At times $t = n\pi/4\Omega_{12}$, $(n = 1, 3, 5, \ldots)$, when $\sin\Omega_{12}t = \cos\Omega_{12}t = 1/\sqrt{2}$, the system is in the maximally entangled state.

8.1.5 *Experimental Evidence of the Population Transfer*

Evidence for the population transfer between two distant atoms coupled to a nonresonant cavity mode was observed in experiments by the Haroche's group in Paris, Osnaghi et al. [6]. The apparatus used for observing the population transfer is shown in Fig. 8.1. Atoms of rubidium emerging from an oven O were velocity selected before entering into area B by laser optical pumping, and then prepared in the area B by a combination of laser and radio frequency excitation in the circular Rydberg states with principal quantum numbers $n = 51$ or $n = 50$. This preparation procedure assured that an atom in the beam behaved as a two-level system with upper state $|e\rangle$ $(n = 51)$, lower state $|g\rangle$ $(n = 50)$ and transition frequency $\omega_0/2\pi = 51.1$ GHz.

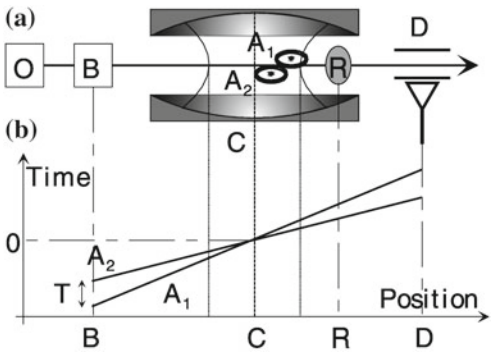

Fig. 8.1 **a** The apparatus used by Osnaghi et al. [6] for the demonstration of the population transfer between atoms while they cross together a nonresonant cavity. **b** Space-time diagram showing different stages of the experiment. Step R, shown in the diagram, was not applied for the detection of the population exchange. Reprinted with permission from S. Osnaghi, P. Bertet, A. Auffeves, P.Maioli, M. Brune, J.M. Raimond, S. Haroche: Phys. Rev. Lett. **87**, 037902 (2001). Copyright (2001) by the American Physical Society

The Rydberg states were chosen because the large transition dipole moment ($\mu_{eg} \sim n^2$) ensured a strong coupling to the cavity mode, while the low (microwave) transition frequency allowed the cavity decay time to be long.

The velocity selection was based on the Doppler effect selection. It was performed by emptying the $F = 3$ hyperfine ground state of rubidium with an optical pumping laser beam propagating orthogonal to the atomic beam. The level was then repopulated with a second pulsed laser beam propagating in a direction at angle 55° with the atomic beam. Atoms with well defined velocities $v_1 = 300$ m/s (A_1) and $v_2 = 243$ m/s (A_2) were prepared with the delay of the preparation $T = 78$ μs, and the mean velocities determined by the frequency of the repumping laser. The well- adjusted delay time T ensured that the atoms A_1 and A_2, moving with different velocities, simultaneously crossed the cavity axis. In other words, the atoms crossed the cavity axis in pairs. The delay in the preparation also allowed to independently excite the atoms A_1 and A_2 into different states. In this way, pairs of atoms with excitations $(|e_1\rangle, |g_2\rangle)$, $(|g_1\rangle, |e_2\rangle)$, $(|g_1\rangle, |g_2\rangle)$, and $(|e_1\rangle, |e_2\rangle)$ were separately prepared.

The selectively prepared atoms then passed through a cavity C formed by two spherical semiconducting niobium mirrors spaced 2.75 cm apart and cooled to 1.3 K. This was able to oscillate in two TEM_{900} modes with linear orthogonal polarizations and transverse Gaussian profiles, with mode waist 6 mm. The frequencies ω_a and ω_b of the cavity modes were nondegenerate due to a small mirror anisotropy and were detuned from the atomic transition frequency ω_0 by variable detunings δ_a and δ_b. The detunings were varied by varying the mirror separation.

Due to large dipole moments, the Rydberg atoms are very sensitive to the van der Waals interaction leading to collisions between the atoms. When colliding, the atoms exchange their energy. It was expected, and demonstrated by Osnaghi et al. [6], that the collision rate can be significantly enhanced when the atoms interact inside a cavity. Large detunings between the cavity frequency and atomic transition frequency result in the complete transfer of the excitation between the atoms that after the collision the cavity mode remains in its vacuum state. The presence of the population exchanging collisions inside the cavity was detected by monitoring the population of the atoms leaving the cavity. The detections was done in the area D, where atoms in the excited state were ionized by an electric field thereby determining the state of the atoms leaving the cavity. With 1000 atomic pairs recorded, the detection probabilities $P(|i_1\rangle, |j_2\rangle)$ to find atom 1 in state i and atom 2 in state j as a function of the detuning δ were reconstructed.

Figure 8.2 shows recordings of the probabilities $P(|i_1\rangle, |j_2\rangle)$ plotted as a function of the detuning parameter $\eta = (\omega_a/\delta_a + \omega_a/\delta_b)$, which is related to the dipole–dipole coupling between the atoms. The experiment showed oscillations of the probabilities $P(|e_1\rangle, |g_2\rangle)$ and $P(|g_1\rangle, |e_2\rangle)$ with the detuning parameter η, and the absence of the oscillations of the probabilities $P(|e_1\rangle, |e_2\rangle)$ and $P(|g_1\rangle, |g_2\rangle)$. Thus, the experiment showed evidence for the population transfer between atoms coupled to a detuned cavity field.

The experimental results are consistent with the theoretical analysis presented in Sect. 8.1.3. Since the measured probabilities $P(|i_1\rangle, |j_2\rangle)$ correspond to the populations of the product states (8.30), i.e., $P(|e_1\rangle, |g_2\rangle) \equiv \varrho_{33}$, $P(|g_1\rangle, |e_2\rangle) \equiv \varrho_{22}$, $P(|e_1\rangle, |e_2\rangle) \equiv \varrho_{44}$, and $P(|g_1\rangle, |g_2\rangle) \equiv \varrho_{11}$, we then see from (8.38) that ϱ_{22}

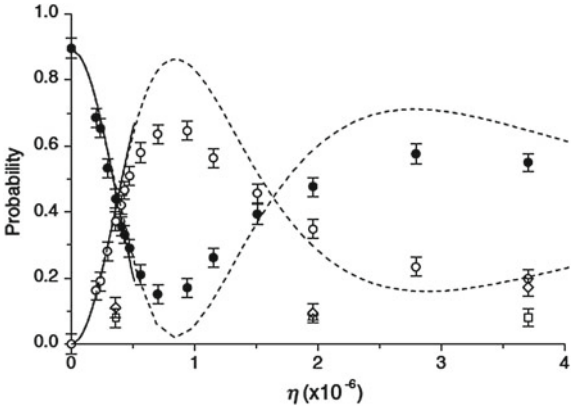

Fig. 8.2 The detection probabilities as a function of the detuning parameter η: $P(|e_1\rangle, |g_2\rangle)$ (*black circles*), $P(|g_1\rangle, |e_2\rangle)$ (*white circles*), $P(|e_1\rangle, |e_2\rangle)$ (*white squares*), and $P(|g_1\rangle, |g_2\rangle)$ (*white diamonds*). *Dashed lines* indicate theoretical results for $P(|e_1\rangle, |g_2\rangle)$ and $P(|g_1\rangle, |e_2\rangle)$. Reprinted with permission from S. Osnaghi, P. Bertet, A. Auffeves, P. Maioli, M. Brune, J.M. Raimond, S. Haroche: Phys. Rev. Lett. **87**, 037902 (2001). Copyright (2001) by the American Physical Society

and ϱ_{33} oscillate with Ω_{12} (note that $\Omega_{12} \sim \eta$), while the populations ϱ_{11} and ϱ_{44} are insensitive to Ω_{12}. These results confirm the agreement between theory and the experiment.

8.2 Engineering Atom-Squeezed Light Interaction

In Sect. 3.4 we found that the fluorescence spectrum of a weakly driven two-level atom can be decomposed into two Lorentzians, one of a positive and the other of a negative weight. A particular consequence of the negative weight of one of the Lorentzians was a narrowing of the spectral line below the natural linewidth. In this section, we shall explain the origin of the negative weight of one of the Lorentzian by considering the incoherent part of the fluorescence spectrum in terms of squeezing spectra of the fluctuations of the fluorescence field. We shall show that the negative weight can be related to squeezing produced in the interaction of the driven atom with the ordinary vacuum field [7].

Let us briefly outline the concept of squeezing spectra for the fluorescence field of a two-level atom. Consider the expression (3.25) for the incoherent part of the stationary fluorescence spectrum of a single two-level atom, which may be written in the form

$$S_{\rm in}(\omega) = \gamma \int_{-\infty}^{\infty} {\rm d}\tau \, \langle \delta S^{+}(0) \, \delta S^{-}(\tau) \rangle {\rm e}^{{\rm i}(\omega-\omega_L)\tau} \, . \tag{8.40}$$

Using the definition of the quadrature components of the dipole operators, we may express $\delta S^{+}(0)$ and $\delta S^{-}(\tau)$ in terms of the fluctuation parts of the quadrature components

$$\begin{aligned}\delta S^{+}(0) &= \left[S_{\theta}(0) + \mathrm{i}S_{\theta+\pi/2}(0)\right]\mathrm{e}^{\mathrm{i}\theta}\,,\\ \delta S^{-}(\tau) &= \left[S_{\theta}(\tau) - \mathrm{i}S_{\theta+\pi/2}(\tau)\right]\mathrm{e}^{-\mathrm{i}\theta}\,.\end{aligned} \tag{8.41}$$

Then, the spectrum can be decomposed into the sum of three phase dependent terms

$$S_{\mathrm{in}}(\omega) = S_{\theta}(\omega) + S_{\theta+\pi/2}(\omega) + S_{\mathrm{asy}}(\omega)\,, \tag{8.42}$$

where

$$\begin{aligned}S_{\theta}(\omega) &= \gamma\int_{-\infty}^{\infty}\mathrm{d}\tau\,\langle :\delta S_{\theta}\,(0)\,\delta S_{\theta}\,(\tau):\rangle\mathrm{e}^{\mathrm{i}(\omega-\omega_L)\tau}\,,\\ S_{\theta+\pi/2}(\omega) &= \gamma\int_{-\infty}^{\infty}\mathrm{d}\tau\,\langle :\delta S_{\theta+\pi/2}\,(0)\,\delta S_{\theta+\pi/2}\,(\tau):\rangle\mathrm{e}^{\mathrm{i}(\omega-\omega_L)\tau}\,,\end{aligned} \tag{8.43}$$

are spectral functions of the normally ordered quadrature phase components of the atomic dipole operators, and $S_{\mathrm{asy}}(\omega)$ is the asymmetric contribution given by

$$\begin{aligned}S_{\mathrm{asy}}(\omega) = \mathrm{i}\gamma\int_{-\infty}^{\infty}\mathrm{d}\tau\,\Big[&\langle :\delta S_{\theta+\pi/2}\,(0)\delta S_{\theta}(\tau):\rangle\\ &-\langle :\delta S_{\theta}(0)\delta S_{\theta+\pi/2}\,(\tau):\rangle\Big]\mathrm{e}^{\mathrm{i}(\omega-\omega_L)\tau}\,.\end{aligned} \tag{8.44}$$

The spectral functions that we have introduced may all are related to the correlation functions $Y_i(\tau)$, determined by the Bloch equations (3.26). In order to show this, we first note symmetry properties of the correlation functions

$$\begin{aligned}\langle\delta S^{+}\,(0)\,\delta S^{-}\,(-\tau)\rangle &= \langle\delta S^{+}\,(0)\,\delta S^{-}\,(\tau)\rangle^{*}\,,\\ \langle\delta S^{\pm}\,(0)\,\delta S^{\pm}\,(-\tau)\rangle &= \langle\delta S^{\mp}\,(0)\,\delta S^{\mp}\,(\tau)\rangle^{*}\,,\end{aligned} \tag{8.45}$$

which help us to write (8.43) and (8.44) in the form

$$\begin{aligned}S_{\theta}(\omega) &= \gamma\,\mathrm{Re}\int_{0}^{\infty}\mathrm{d}\tau\,\cos[(\omega-\omega_L)\,\tau]\,[Y_2(\tau)+Y_1(\tau)]\,,\\ S_{\theta+\pi/2}(\omega) &= \gamma\,\mathrm{Re}\int_{0}^{\infty}\mathrm{d}\tau\,\cos[(\omega-\omega_L)\,\tau]\,[Y_2(\tau)-Y_1(\tau)]\,,\end{aligned} \tag{8.46}$$

and

$$S_{\mathrm{asy}}(\omega) = -2\gamma\int_{0}^{\infty}\mathrm{d}\tau\,\sin[(\omega-\omega_L)\,\tau]\,\mathrm{Im}[Y_2(\tau)]\,, \tag{8.47}$$

where $Y_1(\tau)$ and $Y_2(\tau)$ are the correlation functions for the fluctuation operators, defined in (3.27). The functions $S_\theta(\omega)$ and $S_{\theta+\pi/2}(\omega)$ are called squeezing spectrum.

Hence, the incoherent spectrum can always be regarded as being made up of the sum of contributions $S_\theta(\omega)$ and $S_{\theta+\pi/2}(\omega)$ associated with the two quadrature components of the field. However, unlike $S_{\rm in}(\omega)$, either $S_\theta(\omega)$ or $S_{\theta+\pi/2}(\omega)$ can be negative at some frequencies. If either $S_\theta(\omega) < 0$ or $S_{\theta+\pi/2}(\omega) < 0$, the fluctuations of the corresponding quadrature component are squeezed below the vacuum limit.

Let us now make use the relation (8.42) together with (8.46) and (8.47) to analyze the fluorescence spectrum of a weakly driven two-level atom, discussed in Sect. 3.4. The functions $Y_1(\tau)$ and $Y_2(\tau)$, which are needed to evaluate $S_\theta(\omega)$ and $S_{\theta+\pi/2}(\omega)$ from (8.46), and $S_{\rm asy}(\omega)$ from (8.47), are readily calculated from (3.26). The function $Y_2(\tau)$ was already calculated, and its explicit form is given in (3.30). Note from (3.30) that $Y_2(\tau)$ is real, so that $S_{\rm asy}(\omega) = 0$. For the remaining function $Y_1(\tau)$, we find from (3.26), when $\Delta = 0$, that

$$Y_1(z) = -\frac{\Omega^2}{(\gamma^2+2\Omega^2)^2}\,\frac{\gamma^2(z+\frac{1}{2}\gamma)(z+\gamma) - \gamma\,\Omega^2 z + \Omega^4}{(z+\frac{1}{2}\gamma)\left[(z+\frac{1}{2}\gamma)(z+\gamma)+\Omega^2\right]}\,. \tag{8.48}$$

In the limit of a weak driving field ($\Omega \ll \gamma$), the inverse Laplace transform of (8.48) gives

$$Y_1(\tau) = -\frac{1}{2}\left(\frac{\Omega}{\gamma}\right)^2 \left\{ \mathrm{e}^{-[\frac{1}{2}\gamma - \mathrm{i}(\omega-\omega_L)]\tau} + \mathrm{e}^{-\left[\left(\frac{1}{2}\gamma+\frac{2\Omega^2}{\gamma}\right)-\mathrm{i}(\omega-\omega_L)\right]\tau} \right\}\,. \tag{8.49}$$

Finally, we substitute (8.49), together with $Y_2(\tau)$ given in (3.30), into (8.46) and obtain

$$S_\theta(\omega) = -\frac{\Omega^2}{\gamma}\,\frac{\frac{1}{2}\gamma\left(1+\frac{4\Omega^2}{\gamma^2}\right)}{\frac{1}{4}\gamma^2\left(1+\frac{4\Omega^2}{\gamma^2}\right)^2 + (\omega-\omega_L)^2}\,, \tag{8.50}$$

and

$$S_{\theta+\pi/2}(\omega) = \frac{\Omega^2}{\gamma}\,\frac{\frac{1}{2}\gamma}{\frac{1}{4}\gamma^2 + (\omega-\omega_L)^2}\,. \tag{8.51}$$

It is clear that $S_\theta(\omega)$ is always negative, so the fluorescence field is squeezed for all frequencies. Comparing (8.50) and (8.51) with the fluorescence spectrum (3.72), we see that the negative weight of one of the Lorentzians is due to the squeezing of the fluorescence field. Hence, we may conclude that the narrowing of the spectral line clearly seen in Fig. 3.5 is due to squeezing, a quantum nature of the fluorescence field.

8.3 Engineered Incoherent Driving of a Cavity

In the previous section we have shown that the incoherent part of the fluorescence spectrum of a weakly driven two-level atom can be decomposed into two Lorentzians, one with a positive and the other with a negative weight. We have found by calculating the squeezing spectra that the negatively weighted Lorentzian is related to a squeezed quadrature component of the field. We have found this interesting relation between negative-weighted Lorentzians and squeezing on a simple example of the fluorescence of a two-level atom driven by a weak laser field.

In this section we extend this concept to a strongly driven atom located inside a single-mode cavity. This model lies at the heart of laser physics and belongs to the class of "one-atom" lasers [8–10]. In search for squeezing-induced spectral line narrowing, we shall calculate the spectrum of the output cavity field. As we shall see, the spectral line is composed of two Lorentzians with one of the Lorentzians having a negative weight, but surprisely, we will find that the negatively weighted Lorentzian is not associated with squeezing of the fluctuations of the cavity field. The mechanism for the line narrowing is different and is not related to squeezing aspects of the field.

Consider a single two-level atom represented by the atomic dipole operators, S^+, S^- and S_z, and the transition frequency ω_a. The atom is located inside a single mode cavity and is driven by a coherent external laser field through the open side of the cavity. In addition, the atom is damped at the rate γ by spontaneous emission to modes other than the cavity mode. The external driving field is treated classically in our calculations and is characterized by frequency ω_L. The cavity field of frequency ω_c is treated as quantized and characterized by the annihilation and creation operators $\hat{a}_c$ and $\hat{a}_c^\dagger$, respectively, satisfying the commutation relation $[\hat{a}_c, \hat{a}_c^\dagger] = 1$.

The master equation for the density operator of the system atom plus the cavity field, in the interaction picture, is of the form

$$\frac{\partial \varrho}{\partial t} = -\frac{\mathrm{i}}{\hbar}\left[\hat{H}, \varrho\right] - \frac{1}{2}\gamma\,\mathcal{L}_a\varrho - \frac{1}{2}\kappa\,\mathcal{L}_c\varrho\,, \tag{8.52}$$

where

$$\begin{aligned}\hat{H} &= \hbar\Delta_a S_z + \hbar\Delta_c \hat{a}_c^\dagger \hat{a}_c - \frac{1}{2}\mathrm{i}\hbar\Omega\left(S^+ - S^-\right)\\ &\quad - \frac{1}{2}\mathrm{i}\hbar g\left(\hat{a}_c S^+ - S^-\hat{a}_c^\dagger\right)\end{aligned} \tag{8.53}$$

is the Hamiltonian of the system, and

$$\begin{aligned}\mathcal{L}_a\varrho &= S^+S^-\varrho + \varrho S^+S^- - 2S^-\varrho S^+\,,\\ \mathcal{L}_c\varrho &= \hat{a}_c^\dagger\hat{a}_c\varrho + \varrho\hat{a}_c^\dagger\hat{a}_c - 2\hat{a}_c\varrho\hat{a}_c^\dagger\,,\end{aligned} \tag{8.54}$$

are operators representing the damping of the atoms by spontaneous emission and of the field by cavity decay, respectively, g is the coupling strength of the atom to the cavity mode, Ω is the Rabi frequency of the laser field, and κ is the cavity decay rate. The parameters $\Delta_a = \omega_a - \omega_L$ and $\Delta_c = \omega_c - \omega_L$ are the detuning of the atomic transition frequency and the cavity frequency from the laser frequency, respectively.

The strong driving field can be viewed as a dressing field for the atom. Therefore, we begin by diagonalizing the atomic part of the Hamiltonian together with the interaction of the atom with the laser field

$$H_a = \hbar\Delta_a S_z - \frac{1}{2}\mathrm{i}\hbar\Omega\left(S^+ - S^-\right) , \tag{8.55}$$

to find the dressed states of the combined atom plus laser field system. We restrict our calculations to the case where the laser field frequency is on resonance with the atomic transition frequency, i.e., $\Delta_a = 0$. Since the driving field is treated classically in our calculations, we use the semiclassical dressed states, which are

$$\left|\tilde{1}\right\rangle = \frac{1}{\sqrt{2}}\left(|g\rangle + \mathrm{i}\,|e\rangle\right) , \quad \left|\tilde{2}\right\rangle = \frac{1}{\sqrt{2}}\left(|g\rangle - \mathrm{i}\,|e\rangle\right) . \tag{8.56}$$

Next, we couple the "dressed atom" to the cavity field. First, we replace the atomic operators by the dressed-state operators

$$\begin{aligned} S^- &= -\frac{\mathrm{i}}{2}\left(R_3 - R_{21} + R_{12}\right) , \quad S^+ = \frac{\mathrm{i}}{2}\left(R_3 - R_{12} + R_{21}\right) , \\ S_z &= -\frac{1}{2}\left(R_{12} + R_{21}\right) , \end{aligned} \tag{8.57}$$

where $R_{ij} = |\tilde{i}\rangle\langle\tilde{j}|$ are the dressed-atom dipole operators and $R_3 = R_{22} - R_{11}$.

In terms of the dressed-atom operators, the Hamiltonian (8.53) and $\mathcal{L}_a\varrho$ take the form

$$\hat{H} = \frac{1}{2}\hbar\Omega R_3 + \hbar\Delta_c\hat{a}_c^\dagger\hat{a}_c + \frac{1}{4}\hbar g\left[\hat{a}_c^\dagger\left(R_3 - R_{21} + R_{12}\right) + \mathrm{H.c.}\right] , \tag{8.58}$$

In the next step, we perform the unitary "dressing" transformation of the Hamiltonian $\hat{H}$

$$\tilde{H} = \exp(\mathrm{i}\tilde{H}_0 t/\hbar)\hat{H}\exp(-\mathrm{i}\tilde{H}_0 t/\hbar) , \tag{8.59}$$

with

$$\tilde{H}_0 = \frac{1}{2}\hbar\Omega R_3 + \hbar\Delta_c\hat{a}_c^\dagger\hat{a}_c , \tag{8.60}$$

and obtain the interaction Hamiltonian between the dressed atom and the cavity mode

$$\tilde{H}_1 = -\frac{1}{4}\hbar g\left(\hat{a}_c^\dagger R_3 \mathrm{e}^{\mathrm{i}\Delta_c t} + \hat{a}_c^\dagger R_{12}\mathrm{e}^{\mathrm{i}(\Delta_c-\Omega)t} - \hat{a}_c^\dagger R_{21}\mathrm{e}^{\mathrm{i}(\Delta_c+\Omega)t} + \mathrm{H.c.}\right) . \tag{8.61}$$

The Hamiltonian (8.61) describes the interaction of the dressed atom with the cavity field. We see that in the dressed-atom picture, the cavity frequency and the vacuum modes are tuned to the dressed-state transitions that occur at three characteristic frequencies, Δ_c and $\Delta_c \pm \Omega$. By matching the cavity field frequency to one of the dressed states frequencies, we may manipulate the strength of the interaction between the driven system and the cavity mode.

On carrying out this procedure, it is found that in the dissipative part of the master equation certain terms are slowly varying in time while the others are oscillating with frequencies 2Ω and 4Ω. Since we are interested in the case where the Rabi frequency Ω is much larger than the atomic and cavity damping rates, $\Omega \gg \gamma, \kappa$, we can invoke the secular approximation that consist in dropping these rapidly oscillating terms. These terms, if kept in the master equation, would make corrections to the dynamics of the system of the order of γ/Ω, and thus completely negligible. We therefore find that after discarding the rapidly oscillating terms in the dissipative part $\mathcal{L}_a\varrho$, the time evolution of the density operator is of the form

$$\frac{\partial\varrho}{\partial t} = g_1[\hat{a}_c^\dagger R_3 \mathrm{e}^{\mathrm{i}\Delta_c t} - \hat{a}_c R_3 \mathrm{e}^{-\mathrm{i}\Delta_c t}, \varrho] + g_1[\hat{a}_c^\dagger R_{12}\mathrm{e}^{\mathrm{i}(\Delta_c-\Omega)t} - \hat{a}_c R_{21}\mathrm{e}^{-\mathrm{i}(\Delta_c-\Omega)t}, \varrho] - g_1[\hat{a}_c^\dagger R_{21}\mathrm{e}^{\mathrm{i}(\Delta_c+\Omega)t} - \hat{a}_c R_{12}\mathrm{e}^{-\mathrm{i}(\Delta_c+\Omega)t}, \varrho] - \frac{1}{2}\gamma\mathcal{L}_a\varrho - \frac{1}{2}\kappa\mathcal{L}_c\varrho , \tag{8.62}$$

where $g_1 = g/4$ is the effective coupling constant. It is seen that the commutator part of the master equation (8.62) contains oscillatory terms involving the dressed atom and the cavity field. As we have already mentioned, we work in the strong coupling regime of $\Omega \gg g \gg \gamma, \kappa$. We concentrate below on the case of $\Delta_c = 0$, i.e., the cavity mode frequency tuned to the central frequency of the dressed atom. In this limit, the master equation (8.62) contains terms that are time independent and thus corresponding to the resonant interaction of the cavity field with the dressed atom. It also contains terms that have an explicit time dependence of the form $\exp(\pm 2\mathrm{i}\Omega t)$. These terms rapidly oscillate in time, and after discarding them, we get

$$\frac{\partial\varrho}{\partial t} = g_1[\hat{a}_c^\dagger R_3 - \hat{a}_c R_3, \varrho] - \frac{1}{2}\gamma_1\mathcal{L}_a\varrho - \frac{1}{2}\kappa\mathcal{L}_c\varrho , \tag{8.63}$$

where $\gamma_1 = \gamma/2$, and

$$\begin{aligned}\mathcal{L}_a\varrho &= \Big\{(\varrho - R_3\varrho R_3) + \frac{1}{2}\left(R_{12}R_{21}\varrho + \varrho R_{12}R_{21} - 2R_{21}\varrho R_{12}\right) \\ &\quad + \frac{1}{2}\left(R_{21}R_{12}\varrho + \varrho R_{21}R_{12} - 2R_{12}\varrho R_{21}\right)\Big\} , \\ \mathcal{L}_c\varrho &= \hat{a}_c^\dagger\hat{a}_c\varrho + \varrho\hat{a}_c^\dagger\hat{a}_c - 2\hat{a}_c\varrho\hat{a}_c^\dagger ,\end{aligned} \tag{8.64}$$

describe spontaneous dynamics between the dressed states of the system and of the cavity mode, respectively.

The master equation (8.63) enables us to derive equations of motion for expectation values of an arbitrary combination of the atomic and cavity field operators. In particular, for the dressed-atom population inversion, the number of photons in the cavity field, and the cavity field amplitudes, we find the following closed set of equations of motions

$$\begin{aligned}
\frac{\mathrm{d}}{\mathrm{d}t}\langle R_3\rangle &= -\frac{1}{2}\gamma_1\langle R_3\rangle, \\
\frac{\mathrm{d}}{\mathrm{d}t}\langle \hat{a}_c^\dagger\rangle &= -\frac{1}{2}\kappa\langle \hat{a}_c^\dagger\rangle + g_1\langle R_3\rangle \ , \\
\frac{\mathrm{d}}{\mathrm{d}t}\langle R_3\hat{a}_c\rangle &= g_1 - \frac{1}{2}\left(\gamma_1+\kappa\right)\langle R_3\hat{a}_c\rangle \ , \\
\frac{\mathrm{d}}{\mathrm{d}t}\langle \hat{a}_c^\dagger\hat{a}_c\rangle &= -\kappa\langle \hat{a}_c^\dagger\hat{a}_c\rangle + g_1\left(\langle \hat{a}_c^\dagger R_3\rangle + \langle R_3\hat{a}_c\rangle\right) \ , \\
\frac{\mathrm{d}}{\mathrm{d}t}\langle \hat{a}_c^{\dagger 2}\rangle &= -\kappa\langle \hat{a}_c^{\dagger 2}\rangle + 2g_1\langle \hat{a}_c^\dagger R_3\rangle \ ,
\end{aligned} \tag{8.65}$$

and the equations of motion for the remaining correlations functions, $\langle \hat{a}_c\rangle$ and $\langle \hat{a}_c^\dagger R_3\rangle$ are obtained by the Hermitian conjugate of the equations of motion for $\langle \hat{a}_c^\dagger\rangle$ and $\langle R_3\hat{a}_c\rangle$, respectively.

Solving the equations of motion (8.65) for the steady state, we obtain

$$\begin{aligned}
&\langle R_3\rangle = 0 \ , \quad \langle \hat{a}_c^\dagger\rangle = \langle \hat{a}_c\rangle = 0 \ , \\
&\langle R_3\hat{a}_c\rangle = \langle \hat{a}_c^\dagger R_3\rangle = \frac{2g_1}{\gamma_1+\kappa} \ , \quad \langle a_c^{\dagger 2}\rangle = \langle \hat{a}_c^\dagger\hat{a}_c\rangle = \frac{4g_1^2}{\kappa\left(\gamma_1+\kappa\right)} \ .
\end{aligned} \tag{8.66}$$

Let us first examine the stationary state of the cavity field. Since $\langle \hat{a}_c^\dagger\rangle = \langle \hat{a}_c\rangle = 0$, it is a vacuum state. Then if we look at the normally ordered variances of the quadrature components of the cavity field, $X_\theta = \hat{a}_c\mathrm{e}^{\mathrm{i}\theta} + \hat{a}_c^\dagger\mathrm{e}^{-\mathrm{i}\theta}$ and $X_{\theta+\pi/2} = \mathrm{i}(\hat{a}_c\mathrm{e}^{\mathrm{i}\theta} - \hat{a}_c^\dagger\mathrm{e}^{-\mathrm{i}\theta})$, where θ is the quadrature phase, we find

$$\begin{aligned}
\langle : \left(\Delta X_\theta\right)^2 : \rangle &= \frac{8g_1^2}{\kappa(\kappa+\gamma_1)}(1+\cos 2\theta) \ , \\
\langle : \left(\Delta X_{\theta+\pi/2}\right)^2 : \rangle &= \frac{8g_1^2}{\kappa(\kappa+\gamma_1)}(1-\cos 2\theta) \ .
\end{aligned} \tag{8.67}$$

We see that both variances are positive and can be reduced, maximally to the vacuum limit. For example, a choice of the quadrature phase $\theta = 0$ gives

$$\langle : \left(\Delta X_\theta\right)^2 : \rangle = \frac{16g_1^2}{\kappa(\kappa+\gamma_1)} \ , \quad \langle : \left(\Delta X_{\theta+\pi/2}\right)^2 : \rangle = 0 \ . \tag{8.68}$$

Since, in general, $\langle : \left(\Delta X_\theta\right)^2 : \rangle \neq \langle : \left(\Delta X_{\theta+\pi/2}\right)^2 : \rangle$, we have that the cavity field is in a classically squeezed vacuum state.

8.3.1 Spectrum of the Cavity Field

We now turn to investigate the spectrum of the steady-state cavity field. We can adopt the definition (1.59), which with the help of (1.1) can be written as

$$S(\omega) = 2\mathrm{Re}\left\{2\varepsilon_0 c\lambda \int_0^\infty \mathrm{d}\tau \sum_{\boldsymbol{k}s} \frac{\hbar\omega_{\boldsymbol{k}}}{2\varepsilon_0 \mathcal{V}} \langle \hat{a}^\dagger_{\boldsymbol{k}s}(0)\hat{a}_{\boldsymbol{k}s}(\tau)\rangle \mathrm{e}^{\mathrm{i}(\omega-\omega_{\boldsymbol{k}})\tau}\right\} , \tag{8.69}$$

which determines the spectrum of a multimode three-dimensional field. Since the cavity field is highly directional, it is more appropriate to assume that the field is in the form of a quasi-monochromatic beam of cross-section A and bandwidth $\Delta\omega_k/2\pi = \kappa$ centered at the cavity frequency ω_c. In this case, we may replace the spherical volume $\mathcal{V}$ by a cylinder of area A and length L and treat the set of modes $\boldsymbol{k}s$ as having only one direction and a single polarization. Then, we can evaluate the sum in (8.69) in the limit $L \to \infty$ by replacing it with a one-dimensional integral. Thus, we can write

$$2\pi\varepsilon_0\lambda \sum_{\boldsymbol{k}s} \frac{\hbar\omega_{\boldsymbol{k}}}{2\varepsilon_0\mathcal{V}} \to \frac{1}{2\pi\omega_c} \int_{[\Delta\omega_k]} \mathrm{d}\omega_k \omega_k \approx \frac{\Delta\omega_k}{2\pi} = \kappa . \tag{8.70}$$

Hence, the spectrum (8.69) becomes

$$S(\omega) = 2\mathrm{Re}\left\{\kappa \int_0^\infty \mathrm{d}\tau \, \langle \hat{a}^\dagger_c(0)\hat{a}_c(\tau)\rangle \mathrm{e}^{\mathrm{i}(\omega-\omega_c)\tau}\right\} . \tag{8.71}$$

We may write the cavity field operators in the form $\hat{a}_c(t) = \langle \hat{a}_c(t)\rangle + \delta\hat{a}_c(t)$, where $\delta\hat{a}_c(t)$ is a part of the cavity operator that describes fluctuations of the cavity field about its average value. In this case, the spectrum can be decomposed into a sum of two terms

$$S(\omega) = [S_{\mathrm{coh}}(\omega) + S_{\mathrm{in}}(\omega)] , \tag{8.72}$$

where

$$S_{\mathrm{coh}}(\omega) = \kappa\langle \hat{a}^\dagger\rangle_s \langle \hat{a}\rangle_s \delta(\omega - \omega_L) \tag{8.73}$$

is the coherent part of the spectrum, and

$$S_{\mathrm{in}}(\omega) = 2\mathrm{Re}\left\{\kappa \int_0^\infty \mathrm{d}\tau \, \langle \delta\hat{a}^\dagger_c(0)\delta\hat{a}_c(\tau)\rangle_s \mathrm{e}^{\mathrm{i}(\omega-\omega_c)\tau}\right\} \tag{8.74}$$

is the incoherent part. The subscript "s" stands for steady-state value.

In analogy to (8.42), we can expressed the incoherent part of the spectrum in terms of the squeezing spectra

$$\begin{aligned} S_{\theta}(\omega) &= \kappa\,\mathrm{Re}\int_0^{\infty} \mathrm{d}\tau \cos[(\omega-\omega_c)\,\tau]\Big[\langle\delta\hat{a}_c^{\dagger}(0)\delta\hat{a}_c(\tau)\rangle_s + \mathrm{e}^{2\mathrm{i}\theta}\langle\delta\hat{a}_c^{\dagger}(0)\delta\hat{a}_c^{\dagger}(\tau)\rangle_s\Big]\,, \\ S_{\theta+\frac{\pi}{2}}(\omega) &= \kappa\,\mathrm{Re}\int_0^{\infty} \mathrm{d}\tau \cos[(\omega-\omega_c)\,\tau]\Big[\langle\delta\hat{a}_c^{\dagger}(0)\delta\hat{a}_c(\tau)\rangle_s - \mathrm{e}^{2\mathrm{i}\theta}\langle\delta\hat{a}_c^{\dagger}(0)\delta\hat{a}_c^{\dagger}(\tau)\rangle_s\Big]\,, \end{aligned} \tag{8.75}$$

and

$$S_{\mathrm{asy}}(\omega) = -2\kappa\int_0^{\infty} \mathrm{d}\tau\ \sin[(\omega-\omega_c)\,\tau]\,\mathrm{Im}[\langle\delta\hat{a}_c^{\dagger}(0)\delta\hat{a}_c(\tau)\rangle_s]\,, \tag{8.76}$$

By means of the quantum regression theorem [11] one can easy show, using (8.65), that the two-time correlations functions appearing in (8.74), (8.75) and (8.76) satisfy the following equations of motion

$$\begin{aligned} \frac{\mathrm{d}}{\mathrm{d}t}\langle\delta\hat{a}_c^{\dagger}\delta\hat{a}_c(t)\rangle_s &= -\frac{1}{2}\kappa\langle\delta\hat{a}_c^{\dagger}\delta\hat{a}_c(t)\rangle_s + g_1\langle\delta\hat{a}_c^{\dagger}\delta R_3(t)\rangle_s\,, \\ \frac{\mathrm{d}}{\mathrm{d}t}\langle\delta\hat{a}_c^{\dagger}\delta\hat{a}_c^{\dagger}(t)\rangle_s &= -\frac{1}{2}\kappa\langle\delta\hat{a}_c^{\dagger}\delta\hat{a}_c^{\dagger}(t)\rangle_s + g_1\langle\delta\hat{a}_c^{\dagger}\delta R_3(t)\rangle_s\,, \\ \frac{\mathrm{d}}{\mathrm{d}t}\langle\delta\hat{a}_c^{\dagger}\delta R_3(t)\rangle &= -\frac{1}{2}\gamma_1\langle\delta\hat{a}_c^{\dagger}\delta R_3(t)\rangle_s\,. \end{aligned} \tag{8.77}$$

The solution of (8.77), subject to the initial conditions (8.66), is

$$\begin{aligned} \langle\delta\hat{a}_c^{\dagger}\delta\hat{a}_c(t)\rangle_s &= \frac{4g_1^2}{\kappa\left(\kappa^2-\gamma_1^2\right)}\left[\kappa\mathrm{e}^{-\frac{1}{2}\gamma_1 t} - \gamma_1\mathrm{e}^{-\frac{1}{2}\kappa t}\right]\,, \\ \langle\delta\hat{a}_c^{\dagger}\delta\hat{a}_c^{\dagger}(t)\rangle_s &= \langle\delta\hat{a}_c^{\dagger}\delta\hat{a}_c(t)\rangle_s\,. \end{aligned} \tag{8.78}$$

When (8.78) is used in (8.74), we readily find the incoherent part of the spectrum

$$S_{\mathrm{in}}(\omega) = \frac{4g_1^2\kappa\gamma_1}{\kappa^2-\gamma_1^2}\left[\frac{1}{\frac{1}{4}\gamma_1^2+(\omega-\omega_c)^2} - \frac{1}{\frac{1}{4}\kappa^2+(\omega-\omega_c)^2}\right]\,. \tag{8.79}$$

The spectrum is composed of two Lorentzians, one contributing with a positive and the other with a negative weight. The resulting subtraction of the Lorentzians gives

$$S_{\mathrm{in}}(\omega) = \frac{g_1^2\kappa\gamma_1}{\left[\frac{1}{4}\gamma_1^2+(\omega-\omega_c)^2\right]\left[\frac{1}{4}\kappa^2+(\omega-\omega_c)^2\right]}\,. \tag{8.80}$$

If one notices that

$$S_{\rm cav}(\omega) = \frac{\frac{1}{2}\kappa}{\left[\frac{1}{4}\kappa^2 + (\omega - \omega_c)^2\right]} \tag{8.81}$$

is the spectrum of an empty cavity, and

$$S_{\rm da}(\omega) = \frac{\frac{1}{2}\gamma_1}{\left[\frac{1}{4}\gamma_1^2 + (\omega - \omega_c)^2\right]} \tag{8.82}$$

is the spectrum of radiation field spontaneously emitted by the dressed-atom at the central component of the Mollow triplet, we than can write the spectrum (8.80) as a convolution

$$S_{\rm in}(\omega) = \left(\frac{1}{2}g\right)^2 S_{\rm da}(\omega) S_{\rm cav}(\omega)\ . \tag{8.83}$$

This expression shows that the spectrum $S_{\rm in}(\omega)$ is the cavity response convolved with the spectral line shape of the dressed-atom spontaneous emission. This can be interpreted as driving the cavity mode by the incoherent process of spontaneous emission from the dressed-atom.

The convolution of two Lorentzians can result in narrowing of the spectral line below the linewidths of the two Lorentzians involved. This is illustrated in Fig. 8.3, where we plot the spectrum for $g_1/\gamma_1 = 0.1$ and several different values of κ/γ_1. In order to demonstrate narrowing of the spectral line below $\gamma_1/2$ and the cavity linewidth $\kappa/2$, we plot the spectrum together with two Lorentzians, one with the bandwidth $\kappa/2$ and the other with the natural linewidth $\gamma_1/2$. It is seen from the figure that the spectral line is narrower than both $\kappa/2$ and $\gamma_1/2$. For $\kappa \ll \gamma_1/2$ the bandwidth of the spectral line approaches $\kappa/2$.

Finally, we point out that the structure of the spectrum (8.79) is very similar in form to that found in Sect. 3.4 for the fluorescence spectrum of a weakly driven two-level atom in free space. We have demonstrated in Sect. 8.2 that the negative sign appeared in the spectrum (3.72) because the fluorescence field was squeezed. One could expect that a similar effect occurs here for the cavity field. However, this is not the case. When we make use of (8.78) in (8.75) and (8.76), we find the resulting squeezing spectra

$$S_\theta(\omega) = \frac{1}{2}S_{\rm in}(\omega)(1 + \cos 2\theta)\ ,\ \ S_{\theta+\frac{\pi}{2}}(\omega) = \frac{1}{2}S_{\rm in}(\omega)(1 - \cos 2\theta)\ , \tag{8.84}$$

and $S_{\rm asy}(\omega) = 0$. It is clear that both $S_\theta(\omega)$ and $S_{\theta+\frac{\pi}{2}}(\omega)$ are positive, therefore there is no squeezing. Thus, the negative weight of one of the Lorentzians in (8.79) is not caused by squeezing. However, the distribution of the fluctuations between the quadratures still depends on the phase θ and, in general, is anisotropic. One then could conclude that the negative weight occurs because of the asymmetry in the distribution of the fluctuations between the two quadratures of the cavity field that $S_\theta(\omega) \neq S_{\theta+\frac{\pi}{2}}(\omega)$. As we shall see below, this is not the case. We shall consider a

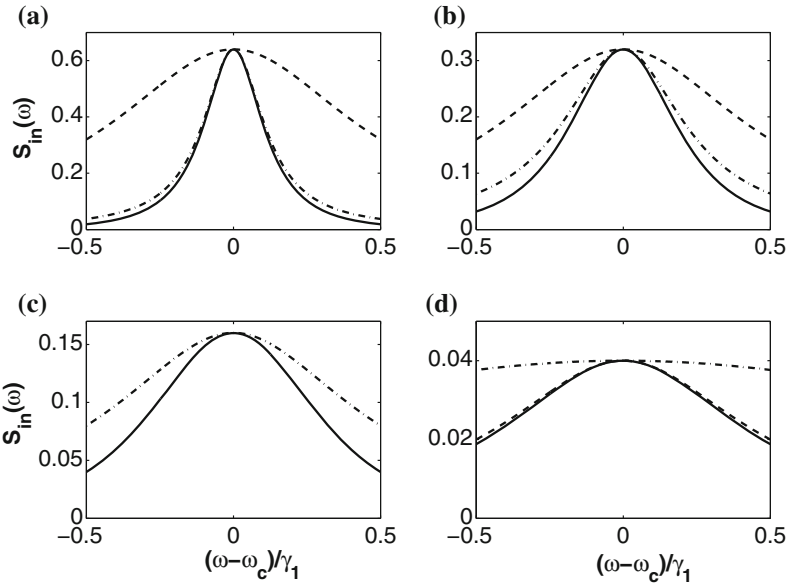

Fig. 8.3 The incoherent spectrum of the cavity field for $g_1 = 0.1\gamma_1$ and for several values of κ: **a** $\kappa = 0.25\gamma_1$, **b** $\kappa = 0.5\gamma_1$, **c** $\kappa = \gamma_1$, and **d** $\kappa = 4\gamma_1$. The *solid line* is the spectrum of the cavity field $S_{\rm in}(\omega)$, the *dashed line* is the Lorentzian $(4\gamma_1 g_1^2/\kappa)\left[\frac{1}{4}\gamma_1^2 + (\omega-\omega_c)^2\right]^{-1}$, the *dashed-dotted line* is the Lorentzian $(4g_1^2\kappa)\left[\frac{1}{4}\kappa^2 + (\omega-\omega_c)^2\right]^{-1}$

two-level atom driven in free space by a thermal field of a finite bandwidth and find the spectrum of the emitted field very similar in form to that of (8.79) but, unfortunately, we find that in this case a negative weight occurs with $S_\theta(\omega) = S_{\theta+\pi/2}(\omega)$.

8.4 Subnatural Linewidths in a Thermal Field

In this section, we specialize our search for subnatural linewidths to a simple model of a two-level atom driven in a free space by a thermal field of finite bandwidth [12, 13]. The starting point for our treatment of the driven two-level atom is the equation of motion for the slowly varying part $\tilde{S}^-(t)$ of the atomic lowering operator $S^-(t)$

$$\dot{\tilde{S}}^-(t) = -\left(\frac{1}{2}\gamma - \mathrm{i}\Delta\right)\tilde{S}^-(t) + 2\frac{\omega_a}{\hbar}\boldsymbol{\mu}_{eg}\cdot\hat{\boldsymbol{E}}_s^{(+)}(0,t)S_z(t)\,, \tag{8.85}$$

where

$$\tilde{S}^-(t) = S^-(t)\mathrm{e}^{\mathrm{i}\omega_L t}, \quad \hat{\boldsymbol{E}}_s^{(+)}(0,t) = \hat{\boldsymbol{E}}_F^{(+)}(0,t)\mathrm{e}^{\mathrm{i}\omega_L t}\,, \tag{8.86}$$

are the slowly varying parts of the atomic lowering operator and the positive frequency part of the external electric field, respectively. In (8.85), γ is the natural decay rate of the atom, ω_L is the central frequency of the driving field, $\Delta = \omega_a - \omega_L$ is the detuning of the field frequency from the atomic resonance, and $S_z(t)$ is the atomic inversion operator.

We are interested in the low-intensity limit of the driving field, in which the atom remains more or less in its ground state, $\langle S_z(t)\rangle \simeq -\frac{1}{2}$. Then a direct integration of (8.85) yields

$$\tilde{S}^-(t) = \tilde{S}^-(0)\mathrm{e}^{(-\frac{1}{2}\gamma+\mathrm{i}\Delta)t} - \frac{\omega_a}{\hbar}\mathrm{e}^{(-\frac{1}{2}\gamma+\mathrm{i}\Delta)t}\int_0^t \mathrm{d}t_1\, \boldsymbol{\mu}_{eg}\cdot\hat{\boldsymbol{E}}_s^{(+)}(0,t_1)\mathrm{e}^{(\frac{1}{2}\gamma-\mathrm{i}\Delta)t_1}\,. \quad (8.87)$$

In order to determine the fluorescence and squeezing spectra, we have to calculate the averages $\langle\tilde{S}^{\pm}(t)\rangle$ and the two-time correlation functions $\langle\tilde{S}^+(t)\tilde{S}^-(t+\tau)\rangle$ and $\langle\tilde{S}^{\pm}(t)\tilde{S}^{\pm}(t+\tau)\rangle$. These functions are obtained by multiplying $\tilde{S}^-(t+\tau)$ and $\tilde{S}^+(t+\tau)$ from the left by $\tilde{S}^+(t)$, respectively, and then taking expectation values. This together with the assumption that the atom was initially in its ground state yields

$$\begin{aligned}
\langle\tilde{S}^-(t)\rangle &= -\mu_{eg}\frac{\omega_a}{\hbar}\mathrm{e}^{(-\frac{1}{2}\gamma+\mathrm{i}\Delta)t}\int_0^t \mathrm{d}t_1\,\langle\hat{E}_s^{(+)}(t_1)\rangle\mathrm{e}^{(\frac{1}{2}\gamma-\mathrm{i}\Delta)t_1}\,,\\
\langle\tilde{S}^+(t)\tilde{S}^-(t+\tau)\rangle &= \mu_{eg}^2\left(\frac{\omega_a}{\hbar}\right)^2\mathrm{e}^{-\gamma t}\mathrm{e}^{-(\frac{1}{2}\gamma-\mathrm{i}\Delta)\tau}\int_0^t \mathrm{d}t_1\,\mathrm{e}^{(\frac{1}{2}\gamma+\mathrm{i}\Delta)t_1}\\
&\quad\times\int_0^{t+\tau}\mathrm{d}t_2\,\mathrm{e}^{(\frac{1}{2}\gamma-\mathrm{i}\Delta)t_2}\langle\hat{E}_s^{(-)}(t_1)\hat{E}_s^{(+)}(t_2)\rangle\,, \qquad (8.88)
\end{aligned}$$

and

$$\begin{aligned}
\langle\tilde{S}^+(t)\tilde{S}^+(t+\tau)\rangle &= \mu_{eg}^2\left(\frac{\omega_a}{\hbar}\right)^2\mathrm{e}^{-(\frac{1}{2}\gamma+\mathrm{i}\Delta)(2t+\tau)}\int_0^t \mathrm{d}t_1\,\mathrm{e}^{(\frac{1}{2}\gamma+\mathrm{i}\Delta)t_1}\\
&\quad\times\int_0^{\tau}\mathrm{d}t_2\,\mathrm{e}^{(\frac{1}{2}\gamma+\mathrm{i}\Delta)t_2}\langle\hat{E}_s^{(-)}(t_1)\hat{E}_s^{(-)}(t_2)\rangle\,, \qquad (8.89)
\end{aligned}$$

where $\mu_{eg} = |\boldsymbol{\mu}_{eg}|$ and we have assumed that $\boldsymbol{\mu}_{eg}\cdot\hat{\boldsymbol{E}}_s^{(+)}(0,t) = \mu_{eg}\hat{E}_s^{(+)}(t)$ and $\boldsymbol{\mu}_{eg}\cdot\hat{\boldsymbol{E}}_s^{(-)}(0,t) = \mu_{eg}\hat{E}_s^{(-)}(t)$.

The field correlation functions, which appear in (8.88) and (8.89), depend on the statistics of the driving field. We shall take a thermal field of finite bandwidth, characterized by the correlation functions

$$\begin{aligned}
\left(\frac{\mu_{eg}\omega_a}{\hbar}\right)^2\langle\hat{E}_s^{(-)}(t_1)\hat{E}_s^{(+)}(t_2)\rangle &= \gamma\,\lambda N\mathrm{e}^{-\lambda|t_1-t_2|}\,,\\
\left(\frac{\mu_{eg}\omega_a}{\hbar}\right)^2\langle\hat{E}_s^{(-)}(t_1)\hat{E}_s^{(-)}(t_2)\rangle &= 0\,,\\
\langle\hat{E}_s^{(+)}(t_1)\rangle = \langle\hat{E}_s^{(-)}(t_1)\rangle &= 0\,, \qquad (8.90)
\end{aligned}$$

where N is proportional to the number of photons in the driving mode and λ is its bandwidth.

When (8.90) are inserted into (8.88) and (8.89) and the result of the integration used in (8.40), we then find that in the steady state the fluorescence spectrum is of the form

$$S_{\rm in}(\omega) = U(\lambda, N)\left[\frac{B_\lambda}{\lambda^2 + (\omega - \omega_L)^2} - \frac{D_\lambda}{\frac{1}{4}\gamma^2 + (\omega - \omega_L + \Delta)^2}\right], \tag{8.91}$$

where

$$U(\lambda, N) = \frac{\frac{1}{4}\gamma^2\lambda^2 N}{\left[\left(\frac{1}{2}\gamma + \lambda\right)^2 + \Delta^2\right]\left[\left(\frac{1}{2}\gamma - \lambda\right)^2 + \Delta^2\right]}, \tag{8.92}$$

and

$$\begin{aligned} B_\lambda &= \left(\frac{1}{4}\gamma^2 - \lambda^2\right) + \Delta^2 - 2\Delta(\omega - \omega_L), \\ D_\lambda &= \left(\frac{1}{4}\gamma^2 - \lambda^2\right) - \Delta^2 - 2\Delta(\omega - \omega_L + \Delta). \end{aligned} \tag{8.93}$$

Clearly, the spectrum is composed of two Lorentzians centered at different frequencies, one of the bandwidth λ is centered at the frequency of the driving field ω_L and the other of the bandwidth $\gamma/2$ is centered at the atomic transition frequency ω_a. The Lorentzian centered at the atomic frequency ω_a has a negative weight. As we have already seen, this can lead to a narrowing of the spectral line below the bandwidths λ and $\gamma/2$ involved in the problem. Since, $\langle \tilde{S}^+(t)\tilde{S}^+(t+\tau)\rangle = 0$, we have from (8.46) that $S_\theta(\omega)$ and $S_{\theta+\pi/2}(\omega)$ are positive. Hence, no squeezing is produced in the fluorescence field. Therefore, in our simple model, there is no connection between the negative weight of the spectral component and squeezing in the fluorescence field. We may conclude that the feature of negative Lorentzians contributing to the spectrum is not unique to quantum squeezing in the radiation field.

Figure 8.4 shows the fluorescence spectrum for $\Delta = 0$, $N = 0.1$ and several different values of λ/γ. In order to demonstrate narrowing of the spectral line below λ and the natural linewidth $\gamma/2$, we plot the spectrum together with two Lorentzians, one with the bandwidth λ and the other with the natural linewidth $\gamma/2$. It is seen from the figure that the spectral line is narrower than both λ and $\gamma/2$. For $\lambda \gg \gamma/2$ the bandwidth of the spectral line approaches $\gamma/2$.

It is interesting to note that the spectrum can be written as the product of the atom response, Lorentzian of the bandwidth $\gamma/2$, with the spectrum of the incident field. We easily find that the spectrum (8.91), when $\Delta = 0$, can be written as

$$S_{\rm in}(\omega) = \frac{\frac{1}{4}\gamma^2\lambda^2 N}{\left[\lambda^2 + (\omega - \omega_a)^2\right]\left[\frac{1}{4}\gamma^2 + (\omega - \omega_a)^2\right]} = N(\lambda, \omega)S_a(\omega), \tag{8.94}$$

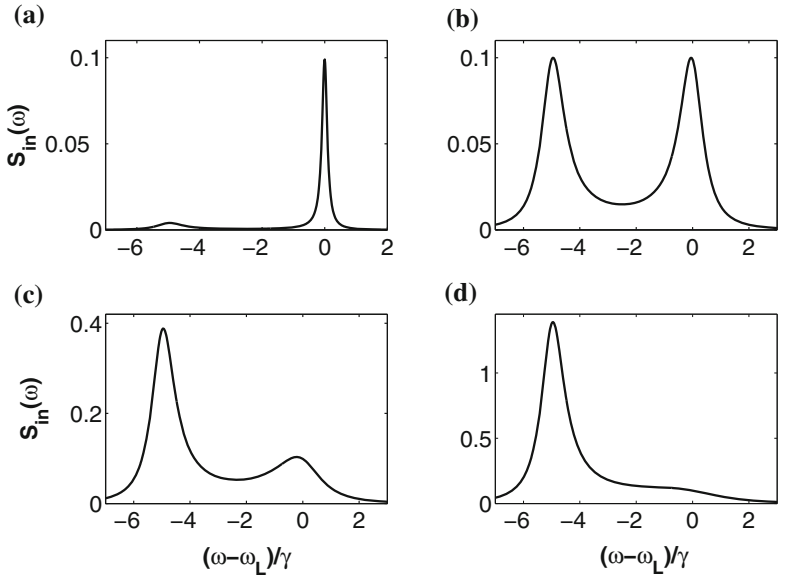

Fig. 8.4 The fluorescence spectrum of a two-level atom driven by a thermal field with $N = 0.1$, $\Delta = 5\gamma$ and for several values of λ: **a** $\lambda = 0.1\gamma$, **b** $\lambda = 0.5\gamma$, **c** $\lambda = \gamma$, and **d** $\lambda = 2\gamma$

where

$$N(\lambda, \omega) = \frac{\lambda^2 N}{\left[\lambda^2 + (\omega - \omega_a)^2\right]}, \tag{8.95}$$

is the spectrum of the incident thermal light, and

$$S_a(\omega) = \frac{\frac{1}{4}\gamma^2}{\left[\frac{1}{4}\gamma^2 + (\omega - \omega_a)^2\right]}. \tag{8.96}$$

is the atomic absorption spectrum of the linewidth $\gamma/2$. The convolution (3) is characteristics of the linear response model [14, 15], as the evolution of the atomic dipole moment depends linearly on the amplitude of the incident field. This feature can lead to narrowing of the spectral line independent of the shape and statistics of the driving field.

In concluding this section, we comment that the Lorentzian centered at ω_a exhibits a negative weight only for small detunings Δ, when the excitation spectrum of the bandwidth λ overlaps with the atomic absorption spectrum of the bandwidth $\gamma/2$. It has been shown in the context of the interaction between a partially coherent field and a two-level atom [14, 15], that such an overlapping repeatedly reinitiate the transient response of the atomic dipole, which then radiates at frequency ω_a. This reinitiate leads to a negative amplitude of the peak at ω_a. The structure of the fluorescence spectrum (8.91) shows many similarities to that considered in [14, 15].

8.5 Engineered Squeezed Vacuum Reservoir

Our special interest in previous two chapters were situations in which the radiative properties of atoms are significantly modified by the interaction of the atoms with a squeezed vacuum field. We have seen that such situations generally are realized in practice by the coupling of atoms in the output of a source of squeezed light. However, there are many practical difficulties in the confirmation of the modifications, especially those unique to the quantum nature of squeezed light.

In this section, we shall explore the idea of Lütkenhaus et al [16] of engineering a squeezed vacuum-type interaction in an atom rather than coupling the atom to an externally produced squeezed vacuum field. We shall examine dynamics of a four-level system driven by a set of lasers and investigate how this system could formally behave as a two-level system damped by a squeezed vacuum field. The analogy to a single two-level atom damped by a squeezed vacuum field is exploited and discussed in details.

To begin with let us first introduce the notation for the transition dipole operators between the levels of the system. As seen from Fig. 8.5, there are four possible transitions in the system which will be represented by transition raising and lowering operators

$$\begin{aligned} S_1^+ &= |3\rangle\langle 1| \ , \quad S_1^- = |1\rangle\langle 3| \ , \quad S_2^+ = |4\rangle\langle 2| \ , \quad S_2^- = |2\rangle\langle 4| \ , \\ S_3^+ &= |3\rangle\langle 2| \ , \quad S_3^- = |2\rangle\langle 3| \ , \quad S_4^+ = |4\rangle\langle 1| \ , \quad S_4^- = |1\rangle\langle 4| \ . \end{aligned} \tag{8.97}$$

The transition $|1\rangle \leftrightarrow |4\rangle$ is driven by a resonant laser field of the Rabi frequency Ω_1, while the transition $|2\rangle \leftrightarrow |3\rangle$ is driven by a resonant laser field of the Rabi frequency Ω_2. In practical terms the transitions between the energy levels, shown in Fig. 8.5, correspond to those of a $J = 1/2$ to $J = 1/2$ transition in a $^{198}Hg^+$ ion [16, 17]. The upper levels of the ion decay to the ground levels with different polarizations of the transition dipole moments. The transition dipole moments of the $|4\rangle \leftrightarrow |1\rangle$ and $|3\rangle \leftrightarrow |2\rangle$ transitions are circularly polarized, the σ^+ and σ^- transitions. On the other hand, the transition dipole moments of the $|3\rangle \leftrightarrow |1\rangle$ and $|4\rangle \leftrightarrow |2\rangle$ transitions are linearly polarized, the π^+ and π^- transitions. The transitions $|3\rangle \leftrightarrow |1\rangle$ and $|4\rangle \leftrightarrow |2\rangle$, which are not driven by the laser fields, spontaneously decay with a rate γ_e.

The dynamics of the system are determined by the density operator ϱ. In a rotating frame defined by the unitary operator

$$U = \mathrm{e}^{\mathrm{i}(A_{33}+A_{44})\omega_L t} \ , \tag{8.98}$$

where $A_{33} = |3\rangle\langle 3|$ and $A_{44} = |4\rangle\langle 4|$, the master equation for the density operator of the system $\tilde{\varrho} = U\varrho U^\dagger$, has the form

$$\frac{\partial \tilde{\varrho}}{\partial t} = -\frac{\mathrm{i}}{\hbar}\left[\hat{H}_L, \tilde{\varrho}\right] - \frac{1}{2}\gamma_e \mathcal{L}_a \tilde{\varrho} \ , \tag{8.99}$$

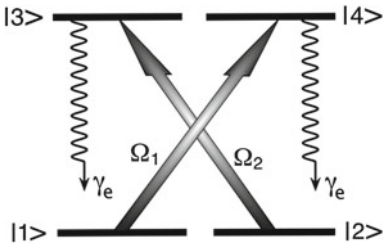

Fig. 8.5 Energy level diagram of a four-level system composed of two ground levels $|1\rangle$ and $|2\rangle$ and two *upper* levels $|3\rangle$ and $|4\rangle$. The transitions $|1\rangle \leftrightarrow |4\rangle$ and $|2\rangle \leftrightarrow |3\rangle$ are driven by lasers of the Rabi frequencies Ω_1 and Ω_2, respectively. The laser frequencies are on resonance with the atomic transition frequencies. The *upper* levels are damped to ground levels by spontaneous emission with a rate γ_e

where

$$\hat{H}_L = -\frac{1}{2}\mathrm{i}\hbar\Omega_1\left(S_4^+ - S_4^-\right) - \frac{1}{2}\mathrm{i}\hbar\Omega_2\left(S_3^+\mathrm{e}^{-\mathrm{i}\psi_L} - S_3^-\mathrm{e}^{\mathrm{i}\psi_L}\right) \tag{8.100}$$

is the interaction Hamiltonian of the laser fields with the atomic transitions, and

$$\begin{aligned}\mathcal{L}_a\tilde{\varrho} = &\left(S_1^+ + S_2^+\right)\left(S_1^- + S_2^-\right)\tilde{\varrho} + \tilde{\varrho}\left(S_1^+ + S_2^+\right)\left(S_1^- + S_2^-\right)\\ &-2\left(S_1^- + S_2^-\right)\tilde{\varrho}\left(S_1^+ + S_2^+\right)\ ,\end{aligned} \tag{8.101}$$

are operators representing the damping of the atom by spontaneous emission. The damping contains terms corresponding to the $|3\rangle \leftrightarrow |1\rangle$ and $|4\rangle \leftrightarrow |2\rangle$ transitions, as well as, cross terms which can lead to spontaneously generated coherences between the upper levels [17]. It should be noted here that there are also possible spontaneous transitions from $|3\rangle$ to $|2\rangle$ and from $|4\rangle$ to $|1\rangle$ in the $^{198}\mathrm{Hg}^+$ ion. However, these spontaneous transitions are not essential in our calculations. If included, these terms would lead to collision-type terms in the master equation of the effective system [16].

Let us write the Rabi frequencies in the form

$$\Omega_1 = \Omega u_1 \quad \text{and} \quad \Omega_2 = \Omega u_2\ , \tag{8.102}$$

and introduce the following operator

$$D = u_1 S_4^- + u_2\mathrm{e}^{\mathrm{i}\psi_L}S_3^-\ . \tag{8.103}$$

We then can write (8.100) as

$$\hat{H}_L = -\frac{1}{2}\mathrm{i}\hbar\Omega\left(D^\dagger - D\right)\ , \tag{8.104}$$

which is in the form of the interaction Hamiltonian of a laser field of the Rabi frequency Ω driving a single transition determined by the transition operators D and $D^\dagger$.

When we use the atomic states representation for the density operator

$$\tilde{\varrho} = \sum_{i,j=1}^{4} \varrho_{ij} \, |i\rangle \, \langle j| \ , \tag{8.105}$$

we find that the density operator can be written in the form

$$\tilde{\varrho} = P_e \tilde{\varrho} P_e + P_e \tilde{\varrho} P_g + P_g \tilde{\varrho} P_e + P_g \tilde{\varrho} P_g \ , \tag{8.106}$$

where P_e and P_g are projection operators defined as

$$P_e = |3\rangle \, \langle 3| + |4\rangle \, \langle 4| \quad \text{and} \quad P_g = |1\rangle \, \langle 1| + |2\rangle \, \langle 2| \ . \tag{8.107}$$

Clearly, the four-level system can be viewed as a two-level system with a single "global" upper $|e\rangle$ and ground $|g\rangle$ levels.

To proceed further, it is convenient to introduce the following operators

$$\varrho_{gg} = P_g \tilde{\varrho} P_g \ , \ \varrho_{ee} = P_e \tilde{\varrho} P_e \ , \ \varrho_{eg} = P_e \tilde{\varrho} P_g \ , \ \varrho_{ge} = P_g \tilde{\varrho} P_e \ , \tag{8.108}$$

which are density operators representing, respectively, the ground levels, the upper levels, and coherences between them.

From the master equation (8.99) we then obtain the following equations of motion

$$\begin{aligned}
\frac{\partial}{\partial t} \varrho_{ee} &= -\gamma_e \varrho_{ee} - \frac{1}{2} \Omega \left(D^\dagger \varrho_{ge} + \varrho_{eg} D \right) \ , \\
\frac{\partial}{\partial t} \varrho_{eg} &= -\frac{1}{2} \gamma_e \varrho_{eg} + \frac{1}{2} \Omega \left(D^\dagger \varrho_{gg} + \varrho_{ee} D^\dagger \right) \ , \\
\frac{\partial}{\partial t} \varrho_{ge} &= -\frac{1}{2} \gamma_e \varrho_{ge} + \frac{1}{2} \Omega \left(\varrho_{gg} D + D \varrho_{ee} \right) \ , \\
\frac{\partial}{\partial t} \varrho_{gg} &= -\frac{1}{2} \Omega \left(D \varrho_{eg} + \varrho_{ge} D^\dagger \right) + \gamma_e \left(S_1^- + S_2^- \right) \varrho_{ee} \left(S_1^+ + S_2^+ \right) \ ,
\end{aligned} \tag{8.109}$$

In the derivation of these equations we have made use of the following operator properties

$$\begin{aligned}
P_g D = D \ , \quad D P_e = D \ , \\
P_g \left(S_1^- + S_2^- \right) = S_1^- + S_2^- \ , \quad \left(S_1^- + S_2^- \right) P_e = S_1^- + S_2^- \ .
\end{aligned} \tag{8.110}$$

We would like to point out that the equations of motion (8.109) resemble very much the equations of motion (3.15) for the dipole operators of a two-level atom driven by coherent laser field of the Rabi frequency Ω.

If the upper levels are rapidly damped that $\Omega \ll \gamma_e$, we may assume that the population of the upper levels and the coherences does not change appreciably in time. Then, we can make the adiabatic approximation to eliminate the upper levels. Thus, we get

$$\begin{aligned} \varrho_{eg} &\approx \frac{\Omega}{\gamma_e}\left(D^\dagger \varrho_{gg} + \varrho_{ee} D^\dagger\right) , \\ \varrho_{ge} &\approx \frac{\Omega}{\gamma_e}\left(\varrho_{gg} D + D \varrho_{ee}\right) . \end{aligned} \tag{8.111}$$

When (8.111) are substituted into the equation of motion for ϱ_{ee}, we get

$$\varrho_{ee} \approx -\frac{\Omega^2}{2\gamma_e^2} D^\dagger \varrho_{gg} D . \tag{8.112}$$

When the results (8.111) and (8.112) are inserted in the equation of motion for ϱ_{gg}, and with the help of (8.110), we arrive at

$$\frac{\partial}{\partial t}\varrho_{gg} = -\frac{\Omega^2}{2\gamma_e}\left(F^\dagger F \varrho_{gg} + \varrho_{gg} F^\dagger F - 2F \varrho_{gg} F^\dagger\right) , \tag{8.113}$$

where

$$F = u_1 S^- + u_2 \mathrm{e}^{\mathrm{i}\psi_L} S^+ , \tag{8.114}$$

in which $S^+ = |2\rangle\langle 1|$ and $S^- = |1\rangle\langle 2|$ are the raising and lowering operators of the two-level system composed of the two ground levels of the four-level atom.

Expression (8.113) is in the form of a master equation for the reduced density operator ϱ_{gg} involving only the ground levels of the atom. When we write (8.113) explicitly in terms of the S^+ and S^- operators, we find ($\varrho \equiv \varrho_{gg}$):

$$\begin{aligned} \frac{\partial}{\partial t}\varrho = &-u_1^2 \frac{\Omega^2}{2\gamma_e}(S^+ S^- \varrho + \varrho S^+ S^- - 2S^- \varrho S^+) \\ &- u_2^2 \frac{\Omega^2}{2\gamma_e}(S^- S^+ \varrho + \varrho S^- S^+ - 2S^+ \varrho S^-) \\ &- u_1 u_2 \frac{\Omega^2}{2\gamma_e}\left(2S^+ \varrho S^+ \mathrm{e}^{2\mathrm{i}\psi_L} + 2S^- \varrho S^- \mathrm{e}^{-2\mathrm{i}\psi_L}\right) . \end{aligned} \tag{8.115}$$

Clearly, the ground levels show a dynamics which is analogous to that of a two-level atom damped by a squeezed vacuum field.

We now compare the master equation (8.115) with the master equation (6.65) for the density operator of a two-level atom illuminated by a squeezed vacuum field produced by a squeezing source

$$\frac{\partial}{\partial t}\varrho = -\frac{1}{2}\gamma\,(N+1)\,(S^+S^-\varrho + \varrho S^+S^- - 2S^-\varrho S^+)$$
$$-\frac{1}{2}\gamma N(S^-S^+\varrho + \varrho S^-S^+ - 2S^+\varrho S^-)$$
$$-\frac{1}{2}\gamma|M|\left(2S^+\varrho S^+\mathrm{e}^{2\mathrm{i}\Phi} + 2S^-\varrho S^-\mathrm{e}^{-2\mathrm{i}\Phi}\right), \tag{8.116}$$

where N is the number of photons in the squeezed field and the parameter $|M|$, which determines the degree of squeezing, may fall into one of the two separate regions

$$|M| < N \quad \text{or} \quad N < |M| \leq \sqrt{N(N+1)}. \tag{8.117}$$

As determined in Sect. 6.2.2, if $|M|$ falls into the region of $|M| < N$, the field corresponds to the so-called classically squeezed field in the sense that fluctuations in one of the quadratures of the field amplitudes are reduced but not below the shot-noise level. If $|M|$ falls into the region of $N < |M| \leq \sqrt{N(N+1)}$, the field is then a quantum squeezed field in the sense that the fluctuations of one of the quadratures are suppressed below the shot-noise level. The equality $|M| = \sqrt{N(N+1)}$ corresponds to a perfectly squeezed field.

Matching coefficients in (8.115) and (8.116), we find

$$\left(u_1^2 - u_2^2\right)\frac{\Omega^2}{\gamma_e} \to \gamma\,,$$
$$\frac{u_2^2}{u_1^2 - u_2^2} \to N\,,$$
$$\frac{u_1 u_2}{u_1^2 - u_2^2} \to |M|\,,$$
$$\psi_L \to \Phi\,. \tag{8.118}$$

The inequality (8.117) now reads

$$|M| = \frac{u_1 u_2}{u_1^2 - u_2^2} = \sqrt{N(N+1)}\,, \tag{8.119}$$

which shows that $|M|$ always falls into the quantum region of the correlations, and the correlations are maximal, $|M| = \sqrt{N(N+1)}$. Thus, we see clearly that the two ground states of a suitably driven four-level atom can effectively behave as a two-level system damped by a perfectly squeezed vacuum field.

In summary of this chapter, we have demonstrated that there are ways to engineer collective interactions between distant atoms and a squeezed reservoir for a two-level system. The effects analogous to the collective damping and the dipole–dipole interaction were predicted and observed experimentally.

References

1. Q.A. Turchette, C.S. Wood, B.E. King, C.J. Myatt, D. Leibfried, W.M. Itano, C. Monroe, D.J. Wineland: Phys. Rev. Lett. **81**, 3631 (1998)
2. S.-B. Zheng, G.-C. Guo: Phys. Rev. Lett. **85**, 2392 (2000)
3. S. Natali, Z. Ficek: Phys. Rev. A **75**, 042307 (2007)
4. R.H. Lehmberg: Phys. Rev. A **2**, 883, 889 (1970)
5. Z. Ficek, R. Tanaś: Phys. Rep. **372**, 369 (2002)
6. S. Osnaghi, P. Bertet, A. Auffeves, P. Maioli, M. Brune, J.M. Raimond, S. Haroche: Phys. Rev. Lett. **87**, 037902 (2001)
7. P.R. Rice, H.J. Carmichael: J. Opt. Soc. Am. B **5**, 1661 (1988)
8. L. Florescu, S. John, T. Quang, R.Z. Wang: Phys. Rev. A **69**, 013816 (2004)
9. L. Florescu: Phys. Rev. A **74**, 063828 (2006)
10. R. Tan, G.X. Li, Z. Ficek: Phys. Rev. A **78**, 023833 (2008).
11. M. Lax: Phys. Rev. **172**, 350 (1968)
12. R. Vyas, S. Singh: Phys: Rev. **A45**, 8095 (1992)
13. Z. Ficek, J. Seke: Physica A **258**, 477 (1998)
14. P.L. Knight, P.W. Milonni: Phys. Rep. **66**, 21 (1980)
15. M.G. Raymer, J. Cooper: Phys. Rev. **A20**, 2238 (1979)
16. N. Lütkenhaus, J.I. Cirac, P. Zoller: Phys. Rev. A **57**, 548 (1998)
17. M. Kiffrer, J. Evers, C.H. Keitel: Phys. Rev. A **73**, 063814 (2006)

Chapter 9
Beating Quantum Limits in Optical Spectroscopy

In Chaps. 6 and 7 we have discussed the effect of nonclassical squeezed light on optical spectra. A variety of classic and standard problems in optical spectroscopy have been re-examined with squeezed light included in the formulations. We have seen how the introduction of squeezed light led to many unusual effects in optical spectroscopy. Examples include a reduction in the linewidth of the fluorescence spectra, population inversion, and the decay to a pure state. We now turn on the subject of precision optical spectroscopy, which deals with the fundamental laws of physics imposing limits to the precision in measurements and interferometry. Consequently, this chapter begins with a discussion of the concepts of the fundamental limits in physics. The limits, called standard limits to the precision of measurements, determine how precisely a physical quantity can be measured. Three apparently distinct limits are known: The standard quantum limit and the Heisenberg limit, both imposed by quantum fluctuations of light, and the diffraction limit imposed by the wave nature of light. All detection systems are subject to these limits. After discussing the basic concepts of the standard limits, a study is made of some techniques, called quantum strategies, that have been developed to beat the diffraction and the standard quantum limits. We shall illustrate how one can beat the limits using nonclassical squeezed and entangled light. We shall see that the ability to produce squeezed light and entangled (correlated) light beams is leading us into a remarkably new domain of quantum physics in which detectors can resolve two closely spaced points or spectral lines with the minimal resolvable limit significantly reduced or even completely suppressed. This realm of physics is now known as quantum image spectroscopy or precision optical spectroscopy. Thereafter, we shall examine how one can improve the signal-to-noise ratio with a quantum squeezed field, and the spectral resolution with entangled light. Following this development, we describe several experiments that demonstrated the improvement of the spectral resolution with entangled light beams.

Z. Ficek and R. Tanaś, *Quantum-Limit Spectroscopy*, Springer Series in Optical Sciences 200, DOI 10.1007/978-1-4939-3740-0_9

9.1 Optical Interferometry: Classical Analysis

There are several types of systems and apparatus utilized in producing interference phenomena. There are those involving regular atomic structures or flat surfaces with very narrow parallel slits which divide the amplitude of an incident beam into two or more parts and then recombine these parts to produce interference. Another types of devices utilize beamsplitters rather than slits to divide the amplitude of the incident beam. In the former, the resolution of the interference fringes is limited to sizes and in particular to the separation between the slits that cannot be made infinitely small, as clearly shown by the familiar interference formula

$$d \sin\theta = n\lambda \,, \tag{9.1}$$

where d is the separation between the slits, θ is the angle under which the nth interference maximum is observed, and λ is the wavelength of the incident beam.

In the systems involving beamsplitters, the incident beam is split into two separate parts at the same point and lengths of the propagation paths from the beamsplitter to a recombination point, which usually is at another beamsplitter, can be infinitesimally changed by changing the propagation directions of these paths. In practice, it is often done by a displacing a perfectly reflecting mirror used to change the direction of the paths.

9.1.1 Mach–Zehnder Interferometer

The Mach–Zehnder interferometer is a fundamental instrument in optical interferometry which utilizes beamsplitters in producing interference effects. In the interferometer exceedingly small displacements or phase shifts of optical fields can be measured. The essential parts of the interferometer are shown in Fig. 9.1. It is composed of an input beamsplitter at which a field propagating in either mode a or b, or in both modes is divided by a partial reflection and transmission into two fields forming two arms of the interferometer. The fields are then directed by reflecting them from mirrors M to another (output) beamsplitter at which they are recombined into a single or two beams leaving the interferometer through the output modes e and f. The mirrors can be fixed or movable and by moving one of the mirrors, a phase shift ϕ can be created due to unequal lengths of the two arms of the interferometer.

The problem we intend to consider is to what precision one can measure the phase difference ϕ between the two arms of the interferometer. Let us start by considering the completely classical approach to the interferometer that a classical light field of an amplitude E_a is injected into the interferometer through the mode a and no field is present in the mode b ($E_b = 0$). If we assume that the light is injected through a lossless 50/50 beamsplitter, the amplitudes of the emerging fields E_c and E_d are $E_c = \mathrm{i}E_a/\sqrt{2}$ and $E_d = E_a/\sqrt{2}$, respectively. Here, we have included the fact that

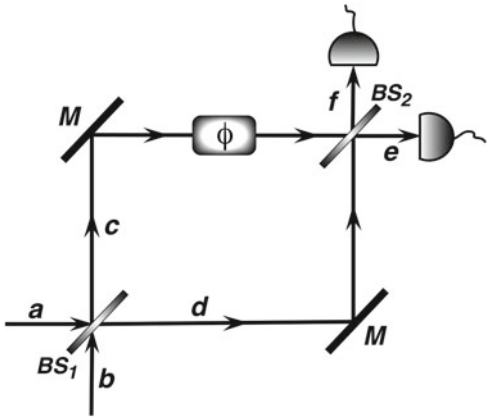

Fig. 9.1 Schematic diagram of a Mach–Zehnder interferometer. Two input modes a and b interact at a beamsplitter BS_1 and proceed as modes c and d through two arms. The arms might be unbalanced that the mode c could encounter a phase shift ϕ relative to the mode d. The modes are directed, by reflection from mirrors M, toward another beamsplitter (BS_2) from which they emerge as output modes e and f that are then monitored by two photodetectors

upon reflection from a beamsplitter the field changes phase by $\pi/2$ and there is no phase change of the transmitted field. The fields in the modes c and d are then subject of reflection from the mirrors M and, in addition, the mode c encounters a phase shift ϕ en route to another lossless 50/50 beamsplitter BS_2, that remains reasonably constant. Thus, at the second beamsplitter the amplitudes of the modes are

$$E_c = -E_a \mathrm{e}^{\mathrm{i}\phi}/\sqrt{2}\,, \quad E_d = \mathrm{i}E_a/\sqrt{2}\,. \tag{9.2}$$

Hence, the amplitudes of the output fields in the modes e and f are

$$\begin{aligned} E_e &= \frac{1}{\sqrt{2}}\,(E_c + \mathrm{i}E_d) = \frac{1}{2}E_a\left(-\mathrm{e}^{\mathrm{i}\phi} - 1\right)\,, \\ E_f &= \frac{1}{\sqrt{2}}\,(\mathrm{i}E_c + E_d) = \frac{1}{2}E_a\left(-\mathrm{i}\mathrm{e}^{\mathrm{i}\phi} + \mathrm{i}\right)\,, \end{aligned} \tag{9.3}$$

where a $\pi/2$ phase shift has been included between the reflected and transmitted fields. Therefore, the output field intensities are of the form

$$I_e = E_e^* E_e = I_a \cos^2(\phi/2)\,, \quad I_f = E_f^* E_f = I_a \sin^2(\phi/2)\,. \tag{9.4}$$

The intensities exhibit periodic variation with the phase ϕ and therefore may provide information about the phase difference between the two arms of the interferometer. In the case of the balanced condition of $\phi = 0$, all of the energy which enters the interferometer through the mode a emerges out from the interferometer in the mode e,

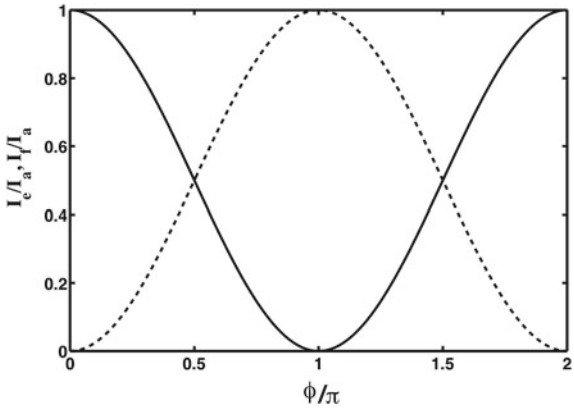

Fig. 9.2 Variation of the intensities I_e (*solid line*) and I_f (*dashed line*) of the output modes with the phase ϕ

as illustrated in Fig. 9.2. This makes the mode e as a bright mode and leaves the mode f as a dark mode, $I_f = 0$. A change of the phase ϕ by π will cause all the energy to appear in the formerly dark mode f.

Note that the output intensities (9.4) can be written as

$$I_e = \frac{1}{2} I_a \left(1 + \cos\phi\right) \ , \quad I_f = \frac{1}{2} I_a \left(1 - \cos\phi\right) \ , \tag{9.5}$$

from which we see that the intensities are composed of the phase dependent as well as the phase independent terms. For small variations of the phase, the phase independent terms dominate over the other terms. This would make difficult to detect small variations of the phase by analyzing either of the output intensities. For this reason, we should consider a different way of detecting small variations of the phase.

The usual way to circumvent this problem is to take the difference between the two output intensities. It is easy to see, the phase independent terms have the same sign, but the phase dependent (interference) terms appear with opposite signs. Therefore, the difference of the two intensities depends only on the phase dependent (interference) term

$$I_D \equiv I_e - I_f = I_a \cos\phi \, . \tag{9.6}$$

We now wish to establish how well the interferometer can be used to estimate the phase shift ϕ. A possible way is to determine a displacement of the intensity difference ΔI_D with a small change of the phase $\Delta\phi$. It is easy to see, if we take a derivative ΔI_D with respect to $\Delta\phi$, we find that for small changes it can be approximated by

$$\frac{\Delta I_D}{\Delta\phi} = \frac{\partial I_D}{\partial\phi} \ , \tag{9.7}$$

from which we find

$$\Delta\phi = \frac{\Delta I_D}{|\partial I_D/\partial\phi|} \,. \tag{9.8}$$

Differentiating the expression for I_D, we obtain

$$\Delta\phi = \frac{\Delta I_D}{|\partial I_D/\partial\phi|} = \frac{\Delta I_D}{|I_a \sin\phi|} \,. \tag{9.9}$$

In this way we find that the precision to which the phase can be determined varies with the phase itself. Specifically, the precision $\Delta\phi$ with which the phase can be determined in the interferometer depends on the displacement (fluctuations) ΔI_D of the intensity I_D and on its rate of change with respect to the phase ϕ. The precision is largest for phases at which $\partial I_D/\partial\phi$ is maximal. According to (9.8), it happens for phases at which $\sin\phi = 1$. Thus, for a given displacement ΔI_D, the smallest phase shifts can be detected at the phase differences $\phi = \pm\pi/2$. It should be noted here that a smaller value of $\Delta\phi$ indicates a reduction in the uncertainty of the phase and thus an increase in the sensitivity of the interferometer.

In closing this section, we would like to point out that although we have derived (9.8) for the phase precision through measurement of the difference current I_D, it is, in principle, possible to estimate the phase precision $\Delta\phi$ through measurement of an arbitrary variable of the system. The same procedure which led to (9.8) then leads to the following expression

$$\Delta\phi = \frac{\Delta A(\phi)}{|\partial\langle A(\phi)\rangle/\partial\phi|} \,, \tag{9.10}$$

where $A(\phi)$ and $\Delta A(\phi)$ are a variable and its associated uncertainty.

9.2 Standard Quantum Limit

The relation (9.8), that has been derived from completely classical arguments, indicates that if one could eliminate all the technical imperfections in the measurement of the intensity I_D, then it would be possible to detect any amount of the phase shift no matter how small it is. In classical terms, there are no restrictions on the fluctuations of the intensity I_D that can, in principle, be measured with perfect precision ($\Delta I_D = 0$), so that the phase shift too could be measured with perfect precision ($\Delta\phi = 0$).

Obviously, the classical arguments do not take into account the fact that in real experiments even if all the technical imperfections are removed, the intensity still suffers an imperfection resulting from the quantum fluctuations of the field amplitude. We now include quantum effects and show that the laws of quantum mechanics

impose limitations on the sensitivity of precision measurement of amplitude and phase changes that prevent them to be measured simultaneously with the same precision.

The fundamental limits encountered in optical physics are usually classified into three types; the standard quantum limit (SQL) or shot noise limit (SNL), the Heisenberg limit (HL), and the diffraction limit (DL). These limits set the upper bound on the sensitivity of traditional (classical) methods of the measurements. The upper bound results from the Heisenberg uncertainty principle for energy and time

$$\Delta E \Delta t \geq \hbar \,, \tag{9.11}$$

where ΔE is the uncertainty in energy and Δt is the uncertainty in time. For a monochromatic wave $E = n\hbar\omega$, where ω is the frequency of the wave and n is the number of photons.

Since $\Delta E = \hbar\omega\Delta n$ and $\omega\Delta t = \Delta\phi$, the energy–time uncertainty relation (9.11) can be transferred to the following photon number and phase uncertainty relation[1]

$$\Delta n \Delta\phi \geq 1 \,, \tag{9.12}$$

from which it follows immediately that the phase uncertainty scales as

$$\Delta\phi \geq \frac{1}{\Delta n} = \frac{1}{\sqrt{\langle(\Delta n)^2\rangle}} \,, \tag{9.13}$$

where $\langle(\Delta n)^2\rangle = \langle n^2\rangle - \langle n\rangle^2$ is the variance of the number of photons.

The inequality (9.13) shows that the precision in determining the phase is bounded by the inverse of the standard deviation of the number of photons. However, as long as the inequality holds in (9.13), which happens for a chaotic (thermal) field, it does not necessary mean that with an increasing Δn, the uncertainty of the phase is also decreasing. The situation differs when the field is in a coherent state. In this case, the equality holds in (9.13) and $\langle(\Delta n)^2\rangle = \langle n\rangle$, indicating that the lowest limit imposed by the Heisenberg uncertainty on the uncertainty of a phase measurement is given by

$$\Delta\phi_{\mathrm{SQL}} = \frac{1}{\sqrt{\langle n\rangle}} \,. \tag{9.14}$$

The limit is called the standard quantum limit (SQL). There are several possible ways to obtain the result (9.14), that the proportionality between the uncertainty in the phase and the inverse squared root of the average number of photons is a general characteristic of the standard quantum limit. Since the coherent state is the quantum state that comes closest to the traditional characterization of the electromagnetic field, the SQL limit is well suited for making comparison between classical and quantum theories of the field.

[1] This relation is true for small values of $\Delta\phi$ which are of interest here. We do not even touch problems related to a quantum phase operator.

9.2.1 Standard Quantum Limit in a Mach–Zehnder Interferometer

We now include the quantum nature of the field in a Mach–Zehnder interferometer to show how to distinguish different limits in the precision of measurement of the phase ϕ. It is done by representing the modes of the interferometer in terms of annihilation and creation operators that we replace the classical field amplitudes $E_a, E_a^*, E_b, \ldots, E_f^*$ by the corresponding annihilation and creation operators $\hat{a}, \hat{a}^\dagger, \hat{b}, \ldots, \hat{f}^\dagger$. The annihilation operators of the two modes of the interferometer, $\hat{c}$ and $\hat{d}$, are related to the annihilation operators of the input modes as

$$\hat{c} = \frac{1}{\sqrt{2}}\left(\mathrm{i}\hat{a} + \hat{b}\right) , \quad \hat{d} = \frac{1}{\sqrt{2}}\left(\hat{a} + \mathrm{i}\hat{b}\right) , \tag{9.15}$$

where the operators of the input modes obey the usual commutation relations

$$[\hat{a}, \hat{a}^\dagger] = [\hat{b}, \hat{b}^\dagger] = 1 , \quad [\hat{a}, \hat{b}] = [\hat{a}^\dagger, \hat{b}^\dagger] = [\hat{a}^\dagger, \hat{b}] = [\hat{a}, \hat{b}^\dagger] = 0 , \tag{9.16}$$

and the operators of the modes c and d satisfy an analogous set of commutation relations.

On the way to the second beamsplitter, the modes undergo perfect reflections from the mirrors and the mode c gains an additional phase shift ϕ, so that at the second beamsplitter the annihilation operators are of the form

$$\hat{c} = \frac{\mathrm{i}}{\sqrt{2}}\left(\mathrm{i}\hat{a} + \hat{b}\right)\mathrm{e}^{\mathrm{i}\phi} , \quad \hat{d} = \frac{\mathrm{i}}{\sqrt{2}}\left(\hat{a} + \mathrm{i}\hat{b}\right) . \tag{9.17}$$

Then, the annihilation operators of the two output modes of the interferometer are

$$\begin{aligned} \hat{e} &= -\frac{1}{2}\left[\left(\hat{a} + \mathrm{i}\hat{b}\right) + \left(\hat{a} - \mathrm{i}\hat{b}\right)\mathrm{e}^{\mathrm{i}\phi}\right] , \\ \hat{f} &= \frac{\mathrm{i}}{2}\left[\left(\hat{a} + \mathrm{i}\hat{b}\right) - \left(\hat{a} - \mathrm{i}\hat{b}\right)\mathrm{e}^{\mathrm{i}\phi}\right] . \end{aligned} \tag{9.18}$$

Note that in the absence of phase difference between the two arms of the interferometer ($\phi = 0$), the operators of the output modes are equal to the operators of the input modes, subject of a π phase shift between them, ($\hat{e} = -\hat{a}$, $\hat{f} = -\hat{b}$).

The relations (9.18) show that the various measurable quantities of the output fields, such as amplitudes, intensities, correlations, etc., can be expressed in terms of the properties of the input fields. For instance, without specifying the state of the input modes, the average number of photons in each of the two output modes are

$$\begin{aligned} \langle n_e \rangle &= \frac{1}{2}\left[\langle \hat{n}_a \rangle + \langle \hat{n}_b \rangle + (\langle \hat{n}_a \rangle - \langle \hat{n}_b \rangle)\cos\phi + 2\mathrm{Re}\{\langle \hat{a}^\dagger \hat{b} \rangle\}\sin\phi\right] , \\ \langle n_f \rangle &= \frac{1}{2}\left[\langle \hat{n}_a \rangle + \langle \hat{n}_b \rangle - (\langle \hat{n}_a \rangle - \langle \hat{n}_b \rangle)\cos\phi - 2\mathrm{Re}\{\langle \hat{a}^\dagger \hat{b} \rangle\}\sin\phi\right] , \end{aligned} \tag{9.19}$$

and the average value of the difference in the photon numbers of the two output modes is

$$\langle n_d \rangle \equiv \langle n_e \rangle - \langle n_f \rangle = (\langle \hat{n}_a \rangle - \langle \hat{n}_b \rangle) \cos\phi + 2\mathrm{Re}\{\langle \hat{a}^\dagger \hat{b} \rangle\} \sin\phi \,, \tag{9.20}$$

where $\hat{n}_a = \hat{a}^\dagger \hat{a}$ and $\hat{n}_b = \hat{b}^\dagger \hat{b}$ are the photon number operators of the input modes a and b, respectively.

Similarly, the uncertainty in the difference between the photon numbers of the two output modes is given by

$$\langle (\Delta n_d)^2 \rangle = \langle \left(\Delta \hat{u}\right)^2 \rangle \cos^2\phi + \langle \left(\Delta \hat{w}\right)^2 \rangle \sin^2\phi + \langle \Delta\hat{u}\Delta\hat{w} \rangle \sin(2\phi) \,, \tag{9.21}$$

where $\hat{u} = \hat{a}^\dagger \hat{a} - \hat{b}^\dagger \hat{b}$ and $\hat{w} = \hat{a}^\dagger \hat{b} + \hat{b}^\dagger \hat{a}$. The measurable quantities $\langle n_d \rangle$ and $\langle (\Delta n_d)^2 \rangle$ depend, of course, on the initial state of the input modes. Therefore, we will focus on the physical consequences of choosing different initial states of the input modes.

There are several possible ways to confirm the scaling (9.14) for the phase sensitivity using the results (9.20) and (9.21) for the output of a Mach–Zehnder interferometer. It can be obtained from a consideration of the phase uncertainty (9.8) or from a consideration of the signal-to-noise ratio (SNR). Since $I_D \sim \langle n_d \rangle$ and $\Delta I_D \sim \sqrt{\langle (\Delta n_d)^2 \rangle}$, we can write the relation (9.8) as

$$\Delta\phi = \frac{\Delta I_D}{\partial I_D / \partial\phi} = \frac{\sqrt{\langle (\Delta n_d)^2 \rangle}}{\partial \langle n_d \rangle / \partial\phi} \,. \tag{9.22}$$

When one of the input modes, say a, is prepared in a coherent state $|\alpha\rangle$ and the other input mode b is left in the vacuum state $|0\rangle$, then most of the terms in (9.20) and (9.21) are zero. For example, $\langle \hat{b}^\dagger \hat{b} \rangle = 0$, $\langle \hat{a}^\dagger \hat{b} \rangle = 0$. Hence, the average value of n_d and its variance are for this state

$$\langle n_d \rangle = \langle n \rangle \cos\phi \,, \quad \langle (\Delta n_d)^2 \rangle = \langle n \rangle \,, \tag{9.23}$$

where $\langle n \rangle \equiv \langle \hat{n}_a \rangle = |\alpha|^2$ is the average number of photons in the coherent field.

Next, since the slope $\partial \langle n_d \rangle / \partial\phi = -\langle n \rangle \sin\phi$ and using the result of (9.8) that the sensitivity in the phase maximizes at $\phi = \pm\pi/2$, the relation (9.22) simplifies to

$$\Delta\phi = \frac{1}{\sqrt{\langle n \rangle}} \,, \tag{9.24}$$

which is the result (9.14) for the SQL obtained from the Heisenberg uncertainty relation.

Consider now another quantity that can be directly measured in a Mach–Zehnder interferometer, the signal-to-noise ratio. The ratio also carries the information about small changes of the phase difference between the two arms of the interferometer. The

signal-to-noise ratio is defined as the ratio of the mean number of photons to their root-mean-square deviation (variance). In a Mach–Zehnder interferometer that interests us here, the standard quantum limit in the phase uncertainty can be understood and evaluated in terms of the signal-to-noise ratio by invoking the interference between the input modes when one of the modes is in the coherent state and the other is in the vacuum state. The signal measured is set by the average value of the difference in photon number, $\langle n_d \rangle$, and the noise level is set by the variance of the difference in photon numbers, $\langle (\Delta n_d)^2 \rangle$, so that

$$\mathrm{SNR} = \frac{\langle n_d \rangle}{\sqrt{\langle (\Delta n_d)^2 \rangle}} \,. \tag{9.25}$$

To estimate the sensitivity of the SNR to the phase ϕ, we introduce a small change in the phase $\Delta\phi$ from its original value ϕ, and obtain

$$\langle n_d \rangle = \langle n \rangle \cos(\phi + \Delta\phi) \,, \quad \langle (\Delta n_d)^2 \rangle = \langle n \rangle \,. \tag{9.26}$$

According to (9.8), the sensitivity in the phase maximizes at $\phi = \pm\pi/2$. Under this condition and assuming that the change in the phase is small ($\Delta\phi \ll 1$), we have $\cos(\phi + \Delta\phi) \approx \Delta\phi$, from which we readily find

$$\langle n_d \rangle = \langle n \rangle \Delta\phi \,, \quad \langle (\Delta n_d)^2 \rangle = \langle n \rangle \,. \tag{9.27}$$

The SNR is therefore just

$$\mathrm{SNR} = \frac{\langle n \rangle \Delta\phi}{\sqrt{\langle n \rangle}} \,. \tag{9.28}$$

Setting the SNR equal to unity (SNR $= 1$), that the minimum signal which could be measured equals to the noise level, we readily obtain for the uncertainty of the phase

$$\Delta\phi = \frac{1}{\sqrt{\langle n \rangle}} \,, \tag{9.29}$$

which is of the same form as the previously obtained from the Heisenberg uncertainty relation (9.14). This is also known as the shot noise limit and gives the smallest detectable phase change or phase difference that can be measured in the Mach–Zehnder interferometer when one of the input modes is in the vacuum state.

To complete our discussion on the method of achieving the phase sensitivity in a Mach–Zehnder interferometer at the SQL, we point out that the results (9.24) and (9.29) are not limited to the coherent state only. In fact, the results are valid for an arbitrary state injected into the mode a provided that the mode b is left in the ordinary vacuum state. It is easy to see. If the mode b is in the ordinary vacuum state $|0\rangle$, then most of the terms in (9.20) and (9.21), i.e., all terms involving the $\hat{b}$ and $\hat{b}^\dagger$

operators are zero. Hence, if we discard all the contributions from the mode b to the expressions $\langle n_d \rangle$ and $\langle (\Delta n_d)^2 \rangle$, we obtain

$$\langle n_d \rangle = \langle \hat{n}_a \rangle \cos\phi\,, \quad \langle (\Delta n_d)^2 \rangle = \langle \left(\Delta \hat{n}_a\right)^2 \rangle \cos^2\phi + \langle \hat{n}_a \rangle \sin^2\phi\,. \tag{9.30}$$

We see that without specifying the state of the mode a, the variance $\langle (\Delta n_d)^2 \rangle$ depends on the state of the mode a through the variance $\langle \left(\Delta \hat{n}_a\right)^2 \rangle$. However, the variance $\langle \left(\Delta \hat{n}_a\right)^2 \rangle$ is multiplied by $\cos^2\phi$ that at the optimized phase $\phi = \pm\pi/2$ vanishes. Therefore, at the optimized phase, the variance $\langle (\Delta n_d)^2 \rangle$ is independent of the fluctuations of the number of photons in the mode a. With these identifications, the expressions for $\langle n_d \rangle$ and $\langle (\Delta n_d)^2 \rangle$ as given in (9.30) reduce to (9.23) and (9.27), those leading to the standard quantum limit.

Summarizing, unlike the completely classical approach, where detectable phase changes can be zero, the smallest detectable phase changes as given by the standard quantum limit (9.29) can never vanish that one can determine an unknown phase only up to a specific uncertainty $\Delta\phi$. We should point out, the SQL as given by (9.29) is not "standard" for any phase ϕ. This phase sensitivity is achieved only for phase changes near $\phi = \pm\pi/2$. For phases different than $\pm\pi/2$, the changes $\Delta\phi$ could be much larger than that determined by the SQL. In addition, the SQL does not represent the ultimate limit in optical measurements and, as we shall see, the phase sensitivity can be improved by applying a nonclassical light such as squeezed or entangled light to one or both input modes of the interferometer.

9.3 Beyond the Standard Quantum Limit

We have learnt in Chap. 1 that fluctuations in one of the quadrature components of the amplitude of a squeezed field are reduced beyond the standard quantum limit. The notion of reduced fluctuations beyond the SQL is not restricted to the quadrature components of the field amplitudes but can be extended to any complimentary observables, in particular, to phase measurements in interferometry, and beating the SQL in sensitivity of phase changes is known as phase supersensitivity. To demonstrate that the SQL imposed on the sensitivity of precision measurement of phase changes can be beaten in an interferometer, we consider two examples of input states of a Mach–Zehnder interferometer that involve nonclassical states of light. In the first, we suppose that the input modes a and b are independent of each other, but is a in the coherent state $|\alpha\rangle$ and the mode b is in a single-mode squeezed vacuum state. Since nonclassical states are often generated by the creation of correlations between different modes rather than inside a single mode, in the second example we assume that the input modes of the interferometer are no longer independent of each other, but are prepared in a mutually correlated (entangled) state. As we shall see, the input entangled light can enhance the sensitivity of the interferometer to the Heisenberg limit, the ultimate limit to the precision of measurements. The possibility of

beating the SQL and reaching the Heisenberg limit is therefore of a great fundamental interest in understanding how quantum features can be advantageous and may lead to important applications in the precision measurements.

9.3.1 Beating the SQL with Squeezed Light

To demonstrate that the standard quantum limit imposed on sensitivity of phase measurements can be beaten by applying squeezed light, we look at the situation where the input mode a of a Mach–Zehnder interferometer is in the coherent state $|\alpha\rangle$ and the mode b is in a squeezed vacuum state

$$|0, \xi\rangle = \mathrm{e}^{\frac{1}{2}\left(\xi^* \hat{a}^2 - \xi \hat{a}^{\dagger 2}\right)} |0\rangle \ , \tag{9.31}$$

where $\xi = r \exp(\mathrm{i}\theta)$ is a complex squeezing parameter. This problem was originally treated by Caves [1], and the results of these treatments are quoted here.

In the squeezed vacuum state

$$\langle \xi, 0| \hat{b}^\dagger |0, \xi\rangle = \langle \xi, 0| \hat{b} |0, \xi\rangle = 0 \ , \quad \langle \xi, 0| \hat{b}^\dagger \hat{b} |0, \xi\rangle = \sinh^2 r \ , \tag{9.32}$$

and

$$\langle \xi, 0| \left(\hat{b}\mathrm{e}^{-\mathrm{i}\theta} + \hat{b}^\dagger \mathrm{e}^{\mathrm{i}\theta}\right)^2 |0, \xi\rangle = \mathrm{e}^{-2r} \ . \tag{9.33}$$

Notice that by putting the mode b in the squeezed vacuum state $|0, \xi\rangle$ we, in fact, no longer have a true vacuum, the average number of photons in the mode b is not equal to zero. However, it is still true that $\langle \hat{b}^\dagger \rangle = \langle \hat{b} \rangle = 0$, as seen from (9.32), so that the average amplitude of the field in the squeezed state (9.31) is zero. For this reason the squeezed field is called "vacuum" field. Note that in the squeezed vacuum state not only the averages $\langle \hat{b}^\dagger \rangle$ and $\langle \hat{b} \rangle$ are zero, but also higher order correlation functions involving an odd number of the b operators are all zero.

With the assumption that the mode a is in the coherent state α, the mode b is in the squeezed vacuum state $|0, \xi\rangle$, and the modes are independent of each other that the averages $\langle \hat{a}^\dagger \hat{b} \rangle$, etc., can be factorized, we then find

$$\langle n_d \rangle = \left(\langle n \rangle - \sinh^2 r\right) \cos\phi \ , \tag{9.34}$$

where the two contributions to $\langle n_d \rangle$ are from the coherent excitation and the squeezed vacuum, respectively. The variance of the difference of the number of photons for the squeezed vacuum state can be shown to be and

$$\langle (\Delta n_d)^2 \rangle = \sinh^2 r + \langle n \rangle \left[\cosh(2r) - \sinh(2r) \cos(\theta - \psi_L)\right] \ , \tag{9.35}$$

where ψ_L is the phase of the coherent field. It is apparent from (9.35) that by changing the phase ψ_L, the noise level in the difference in photon numbers of the output modes can be reduced below that of the ordinary vacuum.

If we introduce a small change of the phase $\Delta\phi$ and choose the phase angle ψ_L so that $\psi_L = \theta$, and optimizing the phase $\phi = \pi/2$, the SNR is of the form

$$\mathrm{SNR} = \frac{\left(\langle n\rangle - \sinh^2 r\right)\Delta\phi}{\sqrt{\langle n\rangle \mathrm{e}^{-2r} + \sinh^2 r}} \,. \tag{9.36}$$

We can simplify the expression (9.36) assuming that the number of photons in the coherent state input mode a significantly exceeds the number of photons in the squeezed vacuum mode b, i.e., $\langle n\rangle \gg \sinh^2 r$. Under this approximation, we readily find that the SNR is given by

$$\mathrm{SNR} = \frac{\langle n\rangle \Delta\phi}{\mathrm{e}^{-r}\sqrt{\langle n\rangle}} \,. \tag{9.37}$$

Comparing (9.37) with (9.26), we see that the effect of the squeezed field is merely to modify the variance (fluctuations) of the number of photons.

Setting $\mathrm{SNR} = 1$, it is straightforward to see that the smallest detectable phase shift in the presence of squeezed light is

$$\Delta\phi = \frac{1}{\mathrm{e}^{r}\sqrt{\langle n\rangle}} = \frac{\Delta\phi_{\mathrm{SQL}}}{\mathrm{e}^{r}} \,. \tag{9.38}$$

When $r = 0$ the squeezing is absent, mode b is in the vacuum state and then (9.38) reduces to the SQL.

Sometimes it is convenient to introduce the parameter $\mathcal{S}(\phi)$, defined by

$$\mathcal{S}(\phi) = \frac{\Delta\phi_{\mathrm{SQL}}}{\Delta\phi} = \frac{1}{\sqrt{\langle n\rangle}\Delta\phi} \,, \tag{9.39}$$

as a measure of the departure of the estimated phase sensitivity $\Delta\phi$ from the SQL. It is clear from (9.39) that $\mathcal{S}(\phi) > 1$ means beating the SQL, and the larger value of $\mathcal{S}(\phi)$ implies the greater phase supersensitivity. For the squeezing input we have $\mathcal{S} = \mathrm{e}^{r}$, from which we see that as long as $r > 1$ the phase sensitivity is significantly enhanced above the SQL. It is clear that the performance of the optimized squeezed state interferometer is much better than that of its vacuum state counterpart. For example, with 90% squeezing ($\mathrm{e}^{2r} = 10$) the sensitivity of the interferometer would be improved as much as if one had increased the input field intensity ($\sim \langle n\rangle$) by a factor of ten.

One could notice from (9.38) that the improvement in the phase sensitivity is proportional to the factor e^{r} that increases with the squeezing parameter r. However, an increase of r leads to the increase of the number of photons in the squeezed field that in the limit of $r \gg 1$ may be comparable to the number of photons in the

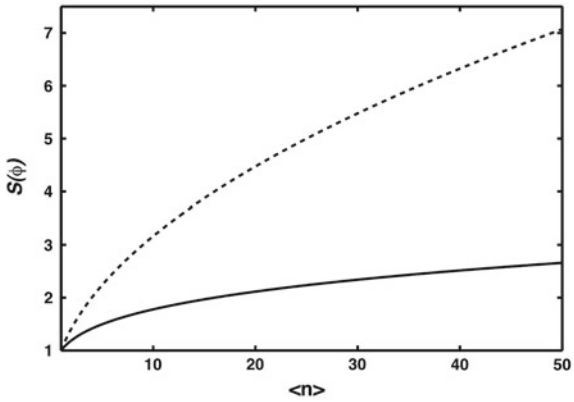

Fig. 9.3 Variation of the sensitivity $\mathcal{S}(\phi)$ with the average number of photons $\langle n \rangle$ in a Mach–Zehnder interferometer with the injected single-mode squeezed vacuum field (*solid line*). The *dashed line* represents the ultimate limit for the sensitivity, the $\sqrt{\langle n \rangle}$ scaling characteristic of the Heisenberg limit

coherent field. Strictly speaking, for $r \gg 1$ the approximation of $\langle n \rangle \gg \sinh^2 r$ may not be longer valid. In order to incorporate the effect of the number of photons in the squeezed field, we go back to the expression (9.36) and optimise the ratio of the mean photon numbers of the coherent and squeezed modes. Simple calculations show that the ratio maximizes at $\sinh^2 r \approx \sqrt{\langle n \rangle}/2$. At this optimum ratio, the sensitivity $\mathcal{S}(\phi)$ with the input squeezed state is

$$\mathcal{S}(\phi) = \langle n \rangle^{1/4} , \tag{9.40}$$

which shows that $\mathcal{S}(\phi) > 1$ for all values of $\langle n \rangle$. Figure 9.3 shows the behavior of $\mathcal{S}(\phi)$ as a function of $\langle n \rangle$. The behavior is compared to the $\sqrt{\langle n \rangle}$ scaling characteristic of the Heisenberg limit for the phase sensitivity. It is clearly seen that the sensitivity of a phase measurement is significantly enhanced by the squeezed light. However, the sensitivity is still much smaller than that corresponding to the Heisenberg limit.

9.3.2 *Experimental Evidence of Beating the SQL with Squeezed Light*

First experimental studies of phase sensitivity with squeezed light were performed by Xiao et al. [2] and Grangier et al. [3], who demonstrated an improvement of sensitivity in measurement of phase changes beyond the standard quantum limit. Here, we discuss in some details the experiment by Xiao et al. [2] that utilizes a Mach–Zehnder interferometer with the input squeezed light and at the output ports a scheme involving a balanced homodyne detection that demonstrated relative phase changes between two arms of the interferometer below the standard quantum limit. An outline of the experiment is shown in Fig. 9.4.

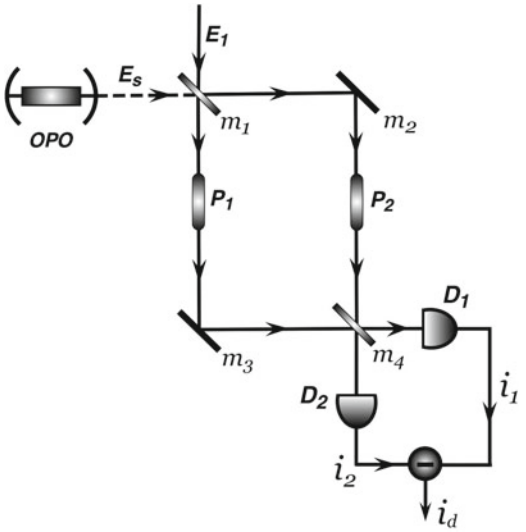

Fig. 9.4 Schematic diagram of the Xiao et al. [2] experiment for detecting phase changes beyond the standard quantum limit

The Mach–Zehnder interferometer is formed by two 50/50 beamsplitters (m_1, m_4) and two perfectly reflecting mirrors (m_2, m_3). The field injected into one of the input arms is a strong coherent field $E_1(t) = |E_1| \exp[-\mathrm{i}(\omega_c t - \theta)]$ of frequency ω_c and phase θ that can be varied in some way. The field E_s in the other input arm is a weak field in an arbitrary state. In the experiment two different states of the field E_s have been used. In the first, the input field was in the vacuum state to setup the standard quantum limit in the experiment. Then, the vacuum state was replaced by injecting squeezed light produced by an optical parametric oscillator (OPO). Phase modulators P_1 and P_2 are introduced into the arms of the interferometer to create a phase difference between the two arms of the interferometer. It was done by applying a time varying voltage $V(t) = V\cos(\omega t)$ to the modulator P_1 which introduced a modulation of the relative phase between the two arms $\phi(t) = \phi_0 + 2\delta\cos(\omega t)$. The outputs of the m_4 beamsplitter are detected by two photodetectors D_1 and D_2 of a balanced homodyne detection scheme that measures relative phase variation between the two arms of the interferometer. The measured output signal is the difference current $i_d = i_1 - i_2$.

A small modulation δ to the relative phase produced a difference photocurrent, an rms signal

$$i_d = \sqrt{2}e\eta|E_1|^2\delta\,, \tag{9.41}$$

where e is the charge of photoelectrons, η is an efficiency factor of the interferometer including the quantum efficiency of the detectors. This signal was first measured against the vacuum noise i_v in the difference photocurrent associated with the total power reaching the detectors

$$i_v^2 = 2e^2\eta|E_1|^2 B \,, \tag{9.42}$$

where B is the detection bandwidth (integration time B^{-1}). Thus, the SNR in the case of the vacuum state of the normally open input mode of m_1 is

$$\text{SNR} \equiv i_d^2/i_v^2 = \eta|E_1|^2\delta^2/B \,, \tag{9.43}$$

and SNR $= 1$ implies the SQL for the phase change

$$\delta = [B/(\eta|E_1|^2)]^{1/2} = 1/\sqrt{\langle n\rangle} \,, \tag{9.44}$$

where $\langle n\rangle$ is the average number of photoelectrons detected in the time interval B^{-1}.

When squeezed light is injected into the open input mode, the signal is exactly the same as in (9.41). However, the noise in the difference photocurrent changes to

$$i_n^2 = i_v^2\left[1 + \eta_{sq}S(\nu, \theta + \pi/2)\right] \,, \tag{9.45}$$

and then the SNR is

$$\text{SNR} = \frac{\eta|E_1|^2}{B\left[1 + \eta_{sq}S(\nu, \theta + \pi/2)\right]}\delta^2 \,, \tag{9.46}$$

where η_{sq} is the efficiency with which the squeezed light propagates through the interferometer, and $S(\nu, \theta + \pi/2)$ is the squeezing spectrum of the fluctuations in the phase quadrature $\theta + \pi/2$ of the difference photocurrent. This equation shows that the SNR can be enhanced by the factor $[1 + \eta_{sq}S(\nu, \theta + \pi/2)]^{-1}$, if the injected light is in a squeezed state for which $S(\nu, \theta + \pi/2) < 0$.

Experimental results for the measured fluctuations of the difference current, $\Phi = 10\log_{10}[1+\eta_{sq}S(\nu, \theta+\pi/2)]$, are shown in Fig. 9.5. The fluctuations were measured as a function of time and a time variation of the phase difference $\phi(t)$ between the two arms was realized by applying the time varying voltage to the modulator p_1. The dashed horizontal line in the figure marks the SNL of the interferometer that was determined by illuminating both detectors with uncorrelated light from the input laser beam with no modulation to the phase and with no squeezing input to the left port of the beamsplitter m_1. Figure 9.5a shows the time variation of the fluctuations Φ with a vacuum state in the input left port of the beamsplitter m_1. Clearly, with the vacuum state no reduction of the noise below the shot noise level ($\Phi = 0$) has been observed. Figure 9.5b gives experimental results when the vacuum field in the left port of m_1 is replaced by a squeezed field, and shows evidence for beating the SQL. The beating of the SQL or, equivalently, reduction of the noise beyond the SNL is indicated by negative values of Φ. In the experiment, more than 3 dB reduction of the noise below the SNL has been observed.

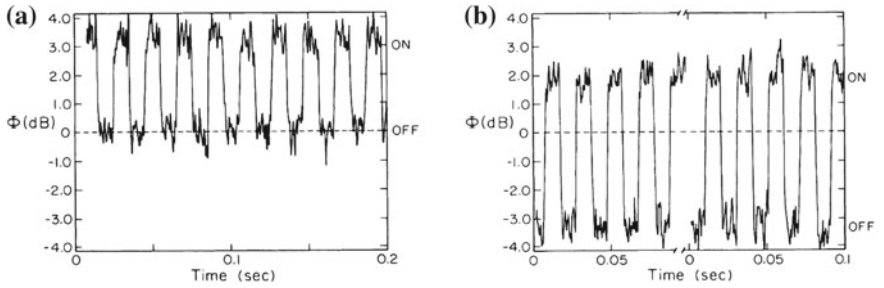

Fig. 9.5 Measured level of fluctuations $\Phi = 10\log_{10}[1+\eta_{sq}S(\nu, \theta+\pi/2)]$ of the difference current as a function of time for fixed frequency $\nu/2\pi = 1.6$ MHz, the detection bandwidth $B = 100$ kHz and the phase θ adjusted for a minimum noise level. Frame **a** shows the level of fluctuations with a vacuum state input to the left port of the beamsplitter m_1, and frame **b** shows the level of fluctuations when the vacuum state of the left port is replaced by a squeezed state of the injected squeezed light. In both frames, the *dashed horizontal line* at $\Phi = 0$ marks the SNL of the interferometer that was determined with no modulation to the phase and with no squeezing input to the *left* port of the beamsplitter. Reprinted with permission from M. Xiao, L.A. Wu, H.J. Kimble: Phys. Rev. Lett. **59**, 278 (1987). Copyright (1987) by the American Physical Society

9.3.3 Beating the SQL with Entangled Light: Heisenberg Limit

We should stress that the improvement of the phase sensitivity beyond the standard quantum limit with a squeezed state is not the ultimate limit that could be achieved in interferometry. The sensitivity can be further improved and ultimately limited to a phase uncertainty that scales as the inverse of $\langle n\rangle$, usually called the *Heisenberg limit* (HL).

Before proceeding with the discussion of the method of improving the phase sensitivity up to the Heisenberg limit, it is appropriate to explain the physical motivation of dealing with two scaling limits for the phase uncertainty, the SQL and HL, even so both refer to laws of quantum mechanics. The reason is in the fact that the SQL is set up by a coherent field that is a quantum field for which there exists a classical analogue, whereas a quantum field without a classical analogue is required to reach the Heisenberg limit. For this reason the SQL is sometimes called classical limit and therefore beating the SQL can be used as a test of quantum nature of the field. In this sense the SQL is always clearly distinguishable from the Heisenberg limit.

We now turn to the main problem of how to the increase sensitivity up to the Heisenberg limit in a Mach–Zehnder interferometer, and show that this may be done by applying an entangled state to the input modes of the interferometer. Suppose that the input modes are initially prepared in an entangled state

$$|\Psi\rangle = \frac{1}{\sqrt{2}}\left(|m\rangle_a\,|n\rangle_b + |n\rangle_a\,|m\rangle_b\right)\ , \tag{9.47}$$

where $|m\rangle_a$ and $|n\rangle_b$ are single mode states with m photons in the mode a and n photons in the mode b, respectively. As before, we may estimate the sensitivity $\Delta\phi$ of a small phase difference between the two arms of a Mach–Zehnder interferometer by measuring the photon number difference $\langle n_d\rangle$ and the photon number variance $\langle(\Delta n_d)^2\rangle$ of the output modes of the interferometer.

With the input entangled state (9.47), the term of importance in reaching the HL is the second term in (9.20), which is zero when the input modes are independent of each other and at least one of the modes is in a vacuum state. The term is clearly different from zero if the modes are correlated, which will certainly be the case for the input entangled state. It is straightforward to show that with the input entangled state (9.47), the quantities which are needed to determine the average $\langle n_d\rangle$, as defined in (9.20), are given by

$$\begin{aligned}\langle\hat{n}_a\rangle = \langle\hat{n}_b\rangle &= \frac{1}{2}N\,,\\ 2\mathrm{Re}\{\langle\hat{a}^\dagger\hat{b}\rangle\} &= \begin{cases} n & \text{if} \quad m = n+1\\ m & \text{if} \quad n = m+1\\ 0 & \text{otherwise}\,,\end{cases}\end{aligned} \tag{9.48}$$

where $N = m+n$ is the total number of photons in the input modes. Clearly, with the result (9.48), the first term in the output signal, $\langle n_d\rangle$, is zero independent of n and m. This means that a nonzero contribution to the output signal would come only from the second term in (9.20). Note that this term made no contribution to the output signal when the mode b was in the ordinary and squeezed vacuum state. A close look at (9.48) reveals that the second term would make a nonzero contribution only if either $m = n+1$ or $n = m+1$, that the numbers of photons in the modes differ by one. Thus, if we choose $m = n+1$ we then find that a nonzero signal in the difference between photon numbers of the output modes

$$\langle n_d\rangle = n\sin\phi\,, \tag{9.49}$$

can be produced only by an input entangled state of the form

$$|\Psi\rangle = \frac{1}{\sqrt{2}}\left(|n+1\rangle_a\,|n\rangle_b + |n\rangle_a\,|n+1\rangle_b\right)\,, \tag{9.50}$$

with $n = (N-1)/2$.

If we confine ourselves to the state (9.50) for which the averages $\langle\hat{a}^\dagger\hat{a}^\dagger\hat{b}\hat{b}\rangle = \langle\hat{b}^\dagger\hat{b}^\dagger\hat{a}\hat{a}\rangle = \langle\hat{a}^\dagger\hat{a}^\dagger\hat{a}\hat{b}\rangle = \langle\hat{a}^\dagger\hat{b}^\dagger\hat{b}\hat{b}\rangle = \ldots = 0$, we find that the variance $\langle(\Delta n_d)^2\rangle$ in the difference between photon numbers of the output modes is

$$\langle(\Delta n_d)^2\rangle = 1 + n\,(n+4)\sin^2\phi\,. \tag{9.51}$$

With these results for $\langle n_d\rangle$ and $\langle(\Delta n_d)^2\rangle$, we can now calculate the uncertainty of the phase estimation $\Delta\phi$ with the input entangled state. When we substitute (9.49)

and (9.51) into (9.22), we find that

$$\Delta\phi = \frac{\sqrt{1 + n\,(n+4)\sin^2\phi}}{n\cos\phi}\,. \tag{9.52}$$

It is clear from this result that $\Delta\phi$ is minimized when $\sin\phi = 0$ ($\phi = 0$). Hence, the minimum uncertainty in ϕ for the entangled state (9.50) is

$$\Delta\phi = \frac{1}{n}\,, \tag{9.53}$$

and then the sensitivity corresponding to this scaling is

$$\mathcal{S}(\phi) = \sqrt{n}\,. \tag{9.54}$$

This is the ultimate limit for scaling of the phase sensitivity, called the Heisenberg limit. This shows that entangled states can be constructed between the input modes that allow the interferometer to achieve a phase sensitivity which for a given number of photons n scales as $1/n$.

Note that the phase at which the phase sensitivity maximizes with the input entangled state is not the same as those at which the phase sensitivity maximizes with independent input modes. With the input entangled state, the phase sensitivity optimizes at $\phi = 0$, whereas for independent input modes the phase sensitivity optimizes at $\phi = \pm\pi/2$. Thus, the phase sensitivity is, in general, phase dependent which shows that a precise control of ϕ is required in order to reach the HL. This is illustrated in Fig. 9.6 which shows the variation of the phase sensitivity $\Delta\phi$ with the number of photons n for different phases ϕ. As can be seen from the figure, the sensitivity decreases rapidly with increasing ϕ. It is interesting to note that for $\phi \neq 0$ and a large number of photons ($n \gg 1$), the sensitivity becomes independent of n.

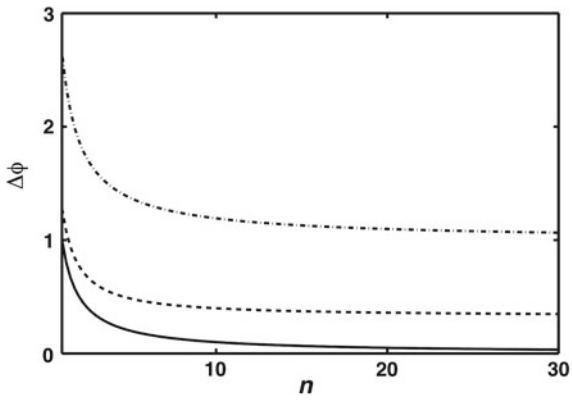

Fig. 9.6 Variation of the phase sensitivity $\Delta\phi$ with the number of photons n in a Mach–Zehnder interferometer for different phases: $\phi = 0$ (*solid line*), $\phi = \pi/10$ (*dashed line*), $\phi = \pi/4$ (*dashed-dotted line*). The input modes are prepared in the entangled state (9.50)

Finally, we would like to point out that the same result as given in (9.53) can also be obtained by analyzing the SNR. Namely, if the phase is shifted by $\Delta\phi$ from its original value ϕ, we have for the output signal

$$\langle n_d \rangle = n \sin(\phi + \Delta\phi) \ . \tag{9.55}$$

As before, we may expand the sine function into a series and find that for $\Delta\phi \ll 1$ the signal maximizes at $\phi = 0$ to give

$$\langle n_d \rangle = n\Delta\phi \ . \tag{9.56}$$

If we now make use of (9.55) and (9.51) for SNR, we readily find from (9.25) that at the optimized phase $\phi = 0$, the signal-to-noise ratio is

$$\text{SNR} = n\Delta\phi \ . \tag{9.57}$$

Setting SNR $= 1$ gives the smallest phase variation $\Delta\phi = 1/n$, which is the same result as that given by (9.53). Hence, an application of the entangled state to the input modes allows to reach the Heisenberg limit for the phase sensitivity in a Mach–Zehnder interferometer. In other words, nonclassical features of entanglement are reflected in enhanced sensitivity of phase measurements.

9.3.4 Approaching the Heisenberg Limit Without Entanglement

The experimental realization of squeezed light of a high degree of squeezing and the creation of entangled states between light beams have opened a possibility to enhance the sensitivity of optical interferometers beyond the SQL. Different measurement strategies have been proposed which led to the observation of a substantial enhancement of the sensitivity. However, achieving a phase sensitivity close to the Heisenberg limit is still a challenging problem in the laboratory. Although the simple model involving an input entangled state to the Mach–Zehnder interferometer is able to reach the HL for the phase sensitivity, it is difficult to realize in practice. There are several practical limitations imposed by internal losses of the interferometer and external losses due to imperfections of the detection process. It has been shown that the effect of losses can be detrimental in beating the SQL by changing the scaling characteristics of the HL toward the $1/\sqrt{\langle n \rangle}$ scaling.

The main difficulty in practical experiments is in the preparation of the input modes in suitable entangled states. Entanglement is a relatively young field in which much of the effort is still aimed at creating entangled systems of photons or particles. This led researchers to consider other strategies that would not require entangled states on input to the interferometer. It has been demonstrated that the HL in a

Mach–Zehnder interferometer can be achieved if, instead of injecting an entangled state to the interferometer, one could create a maximally entangled state $(|n,0\rangle + |0,n\rangle)/\sqrt{2}$ after the first beamsplitter, i.e., a NOON state between the internal modes c and d of the interferometer. This can be achieved, for example, by preparing each of the input modes in a photon number state with a precisely equal number of photons, $|n/2, n/2\rangle \equiv |n/2\rangle_a\,|n/2\rangle_b$. However, with the input state $|n/2, n/2\rangle$, the difference in the number of photons of the two output modes is zero. In other words, there is no output difference signal, and thus no information about ϕ can be obtained. It is easy to see. If the input modes are prepared in photon number states with a precisely equal number of photons, we then have

$$\langle \hat{n}_a \rangle = \langle \hat{n}_b \rangle = n/2\,, \quad 2\mathrm{Re}\{\langle \hat{a}^\dagger \hat{b} \rangle\} = 0\,, \tag{9.58}$$

and consequently zero the difference signal, $\langle n_d \rangle = 0$. Evidently, we have to modify the experimental arrangement.

We may consider the same interferometer configuration as described before, the standard Mach–Zehnder interferometer shown in Fig. 9.1, but with a slightly modified detection system. Instead of measuring a difference current, one may choose to measure a probability of detecting n photons in one of the outputs of the interferometer, either mode e or f, that is the nth order correlation function

$$P_{(ne)} = \frac{1}{n!}\left\langle \left(\hat{e}^\dagger\right)^n \left(\hat{e}\right)^n \right\rangle\,, \quad \text{or} \quad P_{(nf)} = \frac{1}{n!}\left\langle \left(\hat{f}^\dagger\right)^n \left(\hat{f}\right)^n \right\rangle\,, \tag{9.59}$$

and a joint (coincidence) probability $P_{((n-m)e,mf)}$ of a simultaneous detection of $(n-m)$ photons in the mode e and m photons in the mode f, that is given by

$$P_{((n-m)e,mf)} = \left\langle \left(\hat{e}^\dagger\right)^{n-m} \left(\hat{f}^\dagger\right)^m \left(\hat{e}\right)^{n-m} \left(\hat{f}\right)^m \right\rangle\,, \tag{9.60}$$

where m and $(n-m)$ are arbitrary nonnegative integers, and the factor $n!$ results from all possible permutations of the field operators.

Similar to the difference in the number of photons and its fluctuations, the probabilities are expected to be dependent on the phase ϕ that for $n \geq 2$ can be regarded as the higher order interference. The phase sensitivity of the interferometer can then be inferred from the resolution of the interference fringes.

Let us now illustrate in some detail how this could work. For simplicity, we focus on situations when only a few photons are present in the input modes. First consider the simplest possible case of a single photon state $|1,0\rangle$, a single photon in mode a and no photons in mode b. In this case, the probabilities of detecting the single photon in one of the output modes e or f are

$$P_{(1e)} = \frac{1}{2}\left(1 + \cos\phi\right)\,, \quad P_{(1f)} = \frac{1}{2}\left(1 - \cos\phi\right)\,. \tag{9.61}$$

The probabilities exhibit a cosine modulation with the phase ϕ, the first-order interference effect. Since the coefficient of the cosine is equal to unity, the interference occurs with perfect visibility. Note that the probabilities (9.61) have the same dependence on the phase ϕ as the output field intensities (9.5), which were derived classically. Therefore, we shall use these probabilities as a classical limit for the variation of the probabilities with the phase ϕ.

If we prepare the input modes in a two-photon state $|1, 1\rangle$, with one photon appearing simultaneously in each of the two input modes, the probability of detecting two photons in either mode e or f is

$$P_{(2e,0f)} = P_{(0e,2f)} = \frac{1}{4}(1 - \cos 2\phi) \ , \tag{9.62}$$

and the probability of detecting one photon in each of the two output modes is

$$P_{(1e,1f)} = \frac{1}{2}(1 + \cos 2\phi) \ . \tag{9.63}$$

The probabilities are given by particularly simple expressions showing that interference effects are present in the two-photon detection probability. Once again the interference occurs with perfect visibility, but the oscillations of the two-photon probabilities with the phase ϕ are two times faster than that of the one-photon probabilities. This leads to the fringe spacing $\pi/2$, twice smaller than that of single photons.

It should be noted here, that the increase of the phase oscillations or equivalently the decrease of the fringe spacing indicates an increase of the resolution of the interferometer. For example, if the phase difference $\phi = k\Delta x$, that it is due to a difference Δx in the lengths of the two arms of the interferometer, then with a single photon state, one can resolve differences to no smaller than $\Delta x = \lambda/2$, where λ is the wavelength of the employed light. This lower limit of $\Delta x = \lambda/2$ imposed on Δx is called the *diffraction limit*. It follows, that with the two-photon state $|1, 1\rangle$, the diffraction limit can be beaten and the resolution improved to $\Delta x = \lambda/4$. The improved resolution is often called the phase super-resolution. We defer the detailed discussion of the variation of the resolution with the number of photons to Sect. 9.4.

Returning to our original problem of the two-photon probabilities, it is interesting to point out that with the input state $|1, 1\rangle$ to the interferometer, the probabilities for the internal modes c and d of the interferometer are

$$P_{(2c,0d)} = P_{(0c,2d)} = \frac{1}{2} \ , \quad P_{(1c,1d)} = 0 \ . \tag{9.64}$$

Note an interesting fact that one never finds one photon in each internal mode of the interferometer. More generally, the state of the internal modes is a maximally entangled NOON state $(|2, 0\rangle + |0, 2\rangle)\sqrt{2}$.

The expressions (9.61) and (9.62) suggest that if we would continue these considerations to n photons, we could obtain the n-order probabilities of the same simple form as (9.61) and (9.62) but with the cosine term oscillating n times faster than that

of single photons. This is not the case, because these simple functions become very different when $n > 2$ photons are present, except for very special cases. For example, if we prepare the input modes in a four-photon state $|2, 2\rangle$, with two photons appearing simultaneously in each of the input modes, the fourth-order probabilities are

$$P_{(4e,0f)} = P_{(0e,4f)} = \frac{9}{64}\left(1 - \frac{4}{3}\cos 2\phi + \frac{1}{3}\cos 4\phi\right) ,$$
$$P_{(2e,2f)} = \frac{11}{32}\left(1 + \frac{12}{11}\cos 2\phi + \frac{9}{12}\cos 4\phi\right) . \tag{9.65}$$

It is seen that the forms of the fourth-order probabilities differ from the desired cosine form (9.61) in two ways. Firstly, the coefficient of the cosine terms are not equal to unity, indicating that the visibility of the fringe pattern is reduced. Secondly, apart from the oscillatory term $\cos 4\phi$, there is an additional oscillatory term $\cos 2\phi$, so that the variation of the interference pattern may not be strictly harmonic.

The reason for these appreciable differences is in the fact that with the input state $|2, 2\rangle$ the internal modes of the interferometer, c and d, are not in a NOON state $(|4, 0\rangle + |0, 4\rangle)/\sqrt{2}$ as one could expect, but rather in a superposition of the NOON state and the state $|2, 2\rangle$. It is easily verified using (9.17) that the fourth-order probabilities for the modes c and d are

$$P_{(4c,0d)} = P_{(0c,4d)} = \frac{3}{8} , \quad P_{(2c,2d)} = \frac{1}{4} . \tag{9.66}$$

Consequently, the state of the internal modes of the interferometer is

$$|\Psi\rangle_{cd} = \sqrt{\frac{3}{8}}\,(|4, 0\rangle + |0, 4\rangle) + \sqrt{\frac{1}{4}}\,|2, 2\rangle . \tag{9.67}$$

Fortunately, the probabilities (9.65) are not the only possible probabilities that could be measured at the output of the interferometer. We can demonstrate that there are fourth-order probabilities which can depend on the oscillatory factor $\cos 4\phi$ alone [4]. In other words, there are fourth-order probabilities or equivalently fourth-order correlation functions that do not include the oscillatory factor $\cos 2\phi$ associated with the $|2, 2\rangle$ component of the state vector $|\Phi\rangle_{cd}$.

To obtain the desired cosine form (9.61), we try to unbalance the symmetry by introducing an asymmetrical fourth-order joint probability function of three photons detected in the mode e (f) and a single photon in mode f (e). In this case, we find

$$P_{(3e,1f)} = P_{(1e,3f)} = \frac{3}{16}\,(1 + \cos 4\phi) . \tag{9.68}$$

Clearly, the variation of the probabilities with ϕ is of the desired cosine form (9.61). The visibility of the interference pattern is unity and the fringe spacing is $\pi/4$. That is, the asymmetrical fourth-order probabilities $P_{(3e,1f)}$ and $P_{(1e,3f)}$ are valuable

functions which permit to observe interference effects with a super-resolution of the interference fringes that continues as π/n.

We might mention that beating the diffraction limit for the fringe resolution does not imply beating the SQL for the phase sensitivity. However, we can determine phase sensitivity $\Delta\phi$ from a knowledge of the phase dependent coincidence probability P_n. For this purpose, it is found convenient to use probabilities of the form (9.61) that produce a sinusoidal interference pattern with the fringes oscillating periodically with $n\phi$. We can associate the phase sensitivity $\Delta\phi$ with the probability P_n by using the general formula (9.10), from which we have

$$\Delta\phi = \frac{\Delta P_n}{|\partial P_n/\partial\phi|} , \tag{9.69}$$

where

$$P_n = \frac{\eta}{2}(1 + V\cos n\phi) , \tag{9.70}$$

is the joint probability of detecting n photons, and $\Delta P_n = \sqrt{P_n(1-P_n)}$ is its associated uncertainty. In writing P_n, we have included the detection efficiency η and the visibility V of the interference fringes that might not be perfect in an experiment.

Since the slope, $\partial P_n/\partial\phi = -(\eta/2)nV\sin n\phi$ maximizes at $n\phi = \pm\pi/2$, we readily find the minimum uncertainty in the phase

$$\Delta\phi = \frac{\sqrt{\eta(2-\eta)}}{\eta V}\frac{1}{n} , \tag{9.71}$$

and then the sensitivity

$$\mathcal{S}(\phi) = \frac{\eta V}{\sqrt{\eta(2-\eta)}}\sqrt{n} . \tag{9.72}$$

We see that the phase uncertainty approaches the scaling $1/n$, the form characteristic for the Heisenberg limit. Thus, an entangled state of the input modes of the interferometer is not essential for a phase sensitivity to maintain the scaling $1/n$. Of course, how close the uncertainty $\Delta\phi$ can approach the scaling $1/n$ depends on the efficiency η and the visibility V. It is easily verified from (9.71) and (9.72) that the principal effect of η and V is to degrade the phase sensitivity. It follows therefore that the sensitivity has its largest value, $\mathcal{S}(\phi) = \sqrt{n}$, corresponding to the HL when $\eta = 1$ and $V = 1$. This also shows that for a given n and η, there is a threshold value for the visibility to beat the SQL, that $\mathcal{S}(\phi) > 1$ when

$$V > \sqrt{\frac{(2-\eta)}{\eta n}} = V_{th} . \tag{9.73}$$

Thus, it is still possible to beat the SQL and maintain the $1/n$ scaling for the sensitivity characteristic of the HL even with an imperfect efficiency and reduced visibility.

Let us now apply these considerations to the higher order probabilities to examine a possibility of beating the SQL and reaching the HL with a two ($n = 2$) and four ($n = 4$) photon interferometer. We look at the expressions (9.63) and (9.68) for the coincidence probabilities P_2 and P_4 that produce a regular interference pattern with the fringes oscillating periodically with $n\phi$. For $n = 2$, we have $\eta = 1$, which yields the threshold value for the visibility $V_{th} = 1/\sqrt{2} = 0.707$. This shows that beating of the SQL with the input state $|1, 1\rangle$ is possible for the visibility of the second-order interference fringes $V > 0.707$. For the input state $|2, 2\rangle$, with $n = 4$ photons, we have from (9.68) for the efficiency $\eta = 3/8$. Substituting this value into expression (9.73), we find $V_{th} = 1.04$, which is of course impossible to achieve. Clearly, the SQL cannot be beaten, although the coincidence probability $P_{3e,1f}$ exhibits the super-resolution of the interference fringes.

9.3.5 *Beating the Heisenberg Limit*

It is generally believed that the Heisenberg limit is the ultimate limit to the phase sensitivity, which cannot be beaten [5–8]. Actually, some work on nonlinear detection schemes has uncovered ways in which the phase sensitivity may be reduced *below* the Heisenberg limit [9–13]. Therefore, one may wonder whether the Heisenberg limit really is a true quantum limit to the precision of measuring phase in interferometry. Specifically, nonlinear transformations, which occur in the propagation of light in nonlinear media, can produce sensitivity $\Delta\phi = 1/n^k$, where k is the order of the nonlinearity. Clearly, nonlinear transformations can break the Heisenberg limit leading to a better precision in measuring phase. A somewhat different point of view of this improved sensitivity has been presented by Zwierz et al. [14, 15]. According to their explanation, the nonlinearity in the transformation process introduces a subtle complication that the limit $\Delta\phi = 1/n$ determined from a linear transformation process cannot be treated as the Heisenberg limit.

In order to demonstrate this point of view in more details, let us consider a system prepared initially in a quantum state determined by the density operator $\varrho(0)$. Suppose that the state undergoes an evolution to a state $\varrho(\phi)$ by an unitary operator $U(\phi) = \exp(-\mathrm{i}\phi\mathcal{H})$, where $\mathcal{H}$ is the generator of translations in ϕ. We use the quantum Cramér-Rao bound [16], which gives the ultimate limit for the precision of ϕ that can be achieved. According to the general theory of quantum parameter estimation, $\Delta\phi$ is bounded by the quantum Cramér-Rao bound [17, 18], which is related to the Fisher information as

$$\Delta\phi \geq \frac{1}{\sqrt{T\,F(\phi)}}\,, \tag{9.74}$$

where T is the number of measurements made in estimating the precision and $F(\phi)$ is the quantum Fisher information.

Comparing (9.74) with (9.29) and (9.53), we see that the SQL is obtained when the Fisher information scales linearly with respect to T, and the Heisenberg limit is obtained in a single-shot experiment ($T = 1$) when the Fisher information scales quadratically with the number of measurements.

The Fisher information can be related to a statistical distance between quantum states

$$F(\phi) = \left(\frac{ds}{d\phi}\right)^2 , \tag{9.75}$$

where $s(\psi, \phi)$ is a statistical distance between quantum states

$$s(\psi, \phi) = \arccos(|\langle\psi\,|\phi\rangle\,|) , \tag{9.76}$$

in which $|\psi\rangle$ and $|\phi\rangle$ are two pure states. The distance between $\varrho(0)$ and $\varrho(\phi)$ can then be represented by the pure states $|\psi(0)\rangle$ and $|\psi(\phi)\rangle$:

$$|\psi(\phi)\rangle = \mathrm{e}^{-\mathrm{i}\phi\mathcal{H}}\,|\psi(0)\rangle \ . \tag{9.77}$$

If we place an upper bound on the derivative of s, $ds/d\phi \leq |\langle\mathcal{H}\rangle|$, and take a single-shot ($T = 1$) measurement, we then get for $\Delta\phi$:

$$\Delta\phi \geq \left(\frac{ds}{d\phi}\right)^{-1} = \frac{1}{|\langle\mathcal{H}\rangle|} , \tag{9.78}$$

which shows that the Heisenberg limit can be determined by $|\langle\mathcal{H}\rangle|$. Thus, if the transformation process is linear with $\mathcal{H} = \hat{n}$, the Heisenberg limit is given by $1/n$, and the limit varies to $1/n^k$ when the transformation process is nonlinear with $\mathcal{H} = \hat{n}^k$. It might therefore be thought that the Heisenberg limit can be beaten. However, according to (9.78), this widely held belief is a misconception surrounding the subject. In fact, rather than talking about beating the Heisenberg limit with a nonlinear transformation process of order k, one should simply talk about the variation of the Heisenberg limit from $1/n$ to $1/n^k$. Alternatively, the limit of $\Delta\phi = 1/n^k$ with $k > 1$ could be called *super-Heisenberg* limit [19].

A possibility of achieving the super-Heisenberg limit with nonlinear processes has been discussed for several nonlinear systems, in particular, for a Kerr-like medium [20], the Bose–Einstein condensates [21], optomechanical systems [22] and atomic ensembles [23, 24].

The super-Heisenberg limit has been demonstrated experimentally by Napolitano et al. [25], who made use of the atomic ensemble. We shall not go into details of the experiment, but just briefly mention that the experiment involved an ensemble of $N \approx 10^6$ cold ^{87}Rb atoms held in an optical dipole trap and prepared in a state determined by the nonlinear Hamiltonian describing a paramagnetic Faraday rotation

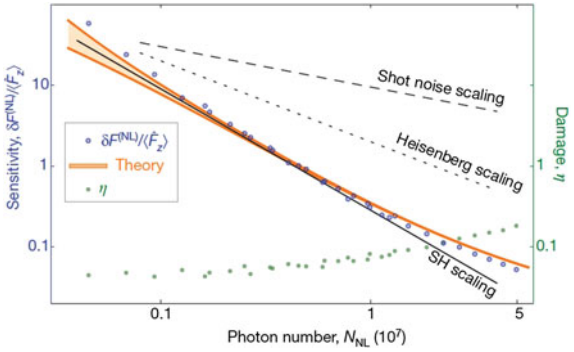

Fig. 9.7 Fractional sensitivity $\Delta F_z/\langle \hat{F}_z \rangle$ plotted as a function of a large number of photons N_{NL} corresponding to the nonlinear regime of the interaction. The *black long dashed line* indicates the SQL, the black short *dashed line indicates* the linear Heisenberg limit $1/N$, and the *black solid line* indicates the super-Heisenberg limit, $1/N^{3/2}$. The *blue circles* indicate the measured sensitivity and the *orange solid line* is the theoretical result. Also shown, as green circles, is the level of the damage of the atomic magnetization. Reprinted by permission from Macmillan Publishers Ltd: [Nature] (M. Napolitano, M. Koschorreck, B. Dubost, N. Behbood, R.J. Sewell, M.W. Mitchell: Nature **471**, 486 (2011)), copyright (2011)

$$H = \alpha^{(1)} \hat{F}_z S_z + \beta^{(1)} \hat{F}_z S_z S_0 \,, \tag{9.79}$$

where S_z is the z component of the collective Stokes operators, $S_0 = N/2$, and $\langle \hat{F}_z \rangle$ is on-axis atomic magnetization, which plays the role of the susceptibility χ. The parameters $\alpha^{(1)}$ and $\beta^{(1)}$ depend on the detuning δ_p of the pumping field. The Hamiltonian is composed of linear, $\alpha^{(1)} \hat{F}_z S_z$, and nonlinear, $\beta^{(1)} \hat{F}_z S_z S_0$ terms. Both terms cause rotation of the polarization of a probe pulse monitoring the atomic ensemble. The experiment determined the sensitivity of measuring the magnetization as

$$\Delta F_z = \langle \hat{F}_z \rangle \frac{\Delta\phi}{\phi} = \frac{1}{A(\delta)N^{1/2} + B(\delta)N^{3/2}} \,, \tag{9.80}$$

where ϕ is the rotation angle (the Faraday rotation angle), $A(\delta) \sim \alpha^{(1)}$, $B(\delta) \sim \beta^{(1)}$, and N is the number of photons with circular plus- and minus-polarization eigenstates $|+\rangle$ and $|-\rangle$ described by the Stokes parameters. We see that the sensitivity scales as $1/\sqrt{N}$ for a small number of atoms and shifts to a $1/N^{3/2}$ scaling for a large N. It is evident that at large N, the sensitivity ΔF_z may reach the super-Heisenberg limit of $1/N^{3/2}$, which is better than the Heisenberg limit $1/N$.

Figure 9.7 shows the experimental results for the fractional sensitivity $\Delta F_z/\langle \hat{F}_z \rangle$ at large numbers of photons. The orange solid line indicates the prediction of the theory. The results clearly demonstrate the sensitivity at the super-Heisenberg limit. The damage to the atomic magnetization is small showing the nondestructive nature of the measurement.

9.3.6 *Experimental Evidence of Beating the SQL in a Four-Photon Interferometry*

A four-photon interferometry demonstrating beating of the SQL has been performed by the O'Brien's group in Bristol [26, 27]. The main element of the experimental apparatus, shown schematically in Fig. 9.8, was the so called displaced Sagnac interferometer, in which the clockwise and anticlockwise modes are displaced from each other, i.e., the modes do not overlap. The optical path lengths of the internal modes of the displaced interferometer are more stable than in a Mach–Zehnder interferometer. The Sagnac interferometer works in the same way as the Mach–Zehnder interferometer, with the output mode amplitudes related to the input mode amplitudes through the same relations as given in (9.18). A variable phase shift between the modes c and d was realized by changing the angle of the phase plate (PP) located in the mode d of the interferometer. The output photons were detected using a set of single photon counting modules (SPCM). In these experiments, the fourth-order probability $P_{3e,1f}$ was effectively measured and a phase sensitivity better than the SQL was demonstrated. The experimental method is interesting in that it furnishes one of the very few successful applications of the four-photon entangled field interferometry.

Before proceeding with a detailed discussion of the experimental results, we should first clarify how it was experimentally possible to demonstrate beating of the SQL with the coincidence probability $P_{3e,1f}$, if the above theoretical analysis predicts no beating of the SQL is possible in $P_{3e,1f}$. To claim that a sensitivity better than the SQL can be achieved in the interferometer, the authors considered a more general measure than that leading to the criterion (9.73). The measure of the phase sensitivity, more appropriate for this experimental situation, has been suggested by

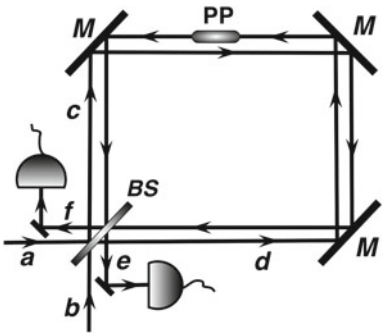

Fig. 9.8 Schematic diagram of the experiments of Nagata et al. [26] and Okamoto et al. [27] to demonstrate phase sensitivity beyond the SQL with $N = 4$ photons. The experiment involved a displaced Sagnac interferometer with the input modes a and b prepared in the state $|2, 2\rangle$ by excitation with a two-mode entangled field generated via spontaneous parametric downconversion from a pumped type I phase matched BBO crystal. A phase plate (PP) was inserted into the mode d to create a variable phase shift ϕ between the internal modes of the interferometer

Resch et al. [28], from considerations of the efficiency at which the initial photons in the state $|2, 2\rangle$ are used to generate the output state of the form (9.61).

Let us briefly outline the approach of Resch et al. [28] of determining the phase uncertainty with the state $|2, 2\rangle$ on input to the interferometer. The principle of the approach relays on the efficiency at which the n initial resources (photons) were used to generate the output state of the form (9.61). The SQL is set by

$$\Delta\phi_{\mathrm{SQL}} = \frac{1}{\sqrt{n/\eta}}\,, \tag{9.81}$$

which shows that the SQL decreases when the efficiency η decreases. To beat the SQL, we need to obtain a precision better than that determined by

$$\Delta\phi = \frac{2\Delta P_{(3f,1f)}}{\eta V}\frac{1}{n} = \frac{\sqrt{\eta(2-\eta)}}{\eta V}\frac{1}{n}\,, \tag{9.82}$$

where η is the efficiency at which the initial photons are used to generate the output state of the form (9.61). Thus, beating the SQL requires a visibility

$$V > \sqrt{\frac{2-\eta}{n}} = V_{th}\,. \tag{9.83}$$

In the case of the input state $|2, 2\rangle$, we have $n = 4$, and according to (9.68), $\eta = 3/8$, so that this time the threshold visibility required to beat the SQL is $V_{th} = 0.637$. Even at the worst case for the fluctuations, $\Delta P_{(3e,1f)} = 1/2$, beating the SQL requires a visibility $V_{th} = 1/\sqrt{\eta n} = 0.816$. Clearly, according to the criterion (9.83), the SQL can be beaten in the interferometer.

Figure 9.9 shows the experimental results of the measurements of the coincidence probabilities $P_{(1e)}$ (frame A), $P_{(1e,1f)}$ (frame B), and $P_{(3e,1f)}$ (frame C) versus the phase difference ϕ between two paths of the interferometer. The frame A serves as a reference for the demonstration that the period of the oscillations of the nth coincidence counts is n times faster than the period of the oscillations of the single photon counts. We see that the period of the oscillations increases as π/n, which confirms that the measured probabilities are those of the form (9.61). A high visibility level was observed with $V = 96 \pm 1\%$ for $n = 2$ and $V = 91 \pm 6\%$ for $n = 4$ interference fringes. These visibilities are clearly greater than the threshold values of $V_{th} = 70.7\%$ for $n = 2$ and $V_{th} = 81.6\%$ for $n = 4$, required to beat the SQL.

It is interesting, however, that the SQL can be beaten according to the criterion (9.73) if one considers a sum of the probabilities $P_{(3e,1f)}$ and $P_{(1e,3f)}$ rather than only one of them. When both probabilities are simultaneously measured, the total probability reads

$$P_{(3e,1f)} + P_{(1e,3f)} = \frac{3}{8}\left(1 + \cos 4\phi\right)\,. \tag{9.84}$$

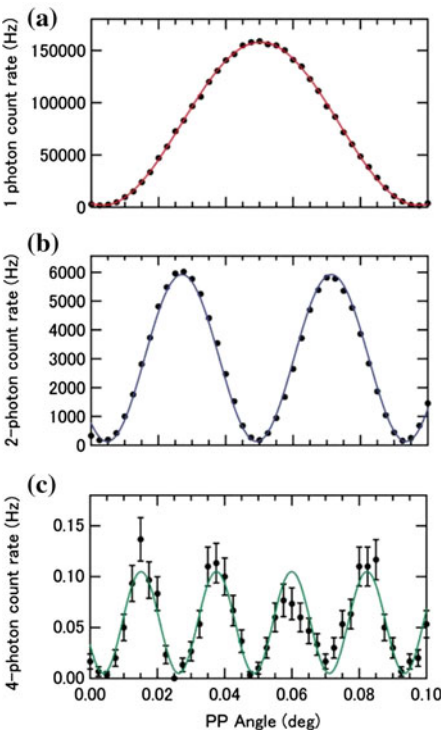

Fig. 9.9 Experimental results obtained by Nagata et al. [26] for the photon counts as a function of the PP angle, i.e., the phase difference ϕ between the two paths of the interferometer. Part **a** shows results for single photon counts, part **b** shows results for the two-photon coincidence counts, and **c** shows results for the fourfold coincidence counts of three photons in mode e (or f) and one photon in mode f (or e). From T. Nagata, R. Okamoto, J.L. OŐBrien, K. Sasaki, S. Takeuchi: Science **316**, 726 (2007). Reprinted with permission from AAAS

This shows an improvement of the efficiency η to $\eta = 3/4$, at which the threshold visibility is smaller than one, $V_{th} = 0.645$. According to the criterion (9.73), beating of the SQL is now possible with a visibility $V > 0.645$.

An experimental demonstration of beating the SQL in the sum of the probabilities, $P_{(3e,1f)} + P_{(1e,3f)}$, was reported by Okamoto et al. [27] who generalized the experiment of Nagata et al. [26] to include measurements of the probability $P_{(1e,3f)}$ of detecting one photon in mode e and three photons in mode f. When both detection events are taken, the SQL can be beaten with a visibility $V > 0.645$.

Figure 9.10 shows plots of measured single photon counts, part (a), and fourfold coincidence counts, part (b), together with their standard deviations, as a function of the phase plate (PP) angle. The part (a) serves as a reference for the demonstration that the period of the oscillations of the fourfold coincidence counts is $1/4$ of the period of the oscillations of the single photon counts. The visibility of the interference fringes seen in part (b) is $V = 82 \pm 6\%$, which is greater than the threshold value of $V_{th} = 0.645$ required to beat the SQL. With the efficiency $\eta = 3/4$, it gives the phase sensitivity $\mathcal{S}(\phi) = 1.30$. Thus, the phase sensitivity achieved in the interferometer was 1.3 times greater than the SQL. It is interesting to note that the value $\mathcal{S}(\phi) = 1.30$ corresponds to beating the SQL by 65% toward the Heisenberg limit of $\mathcal{S}(\phi) = 2$.

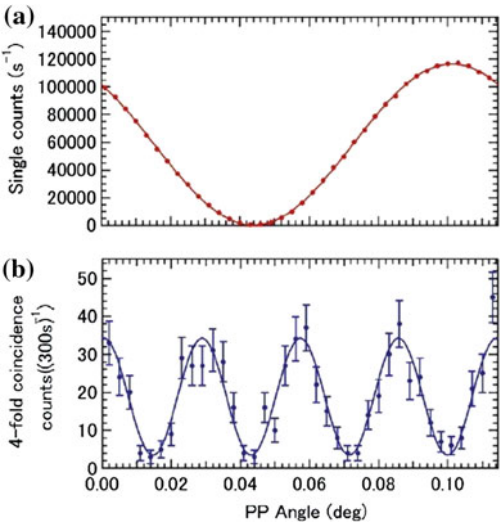

Fig. 9.10 Experimental results obtained by Okamoto et al. [27] for the photon counts as a function of the phase plate angle. Part **a** shows results for single photon counts and part **b** shows results for the fourfold coincidence counts of three photons in mode e (or f) and one photon in mode f (or e). Reprinted with permission from R. Okamoto, H.F. Hofmann, T. Nagata, J.L. OŐBrien, K. Sasaki, S. Takeuchi: New J. Phys. **10**, 073033 (2008)

9.3.7 Effect of Losses and Imperfections

We have seen in Sect. 9.3.4 that in a practical situation (in the real world) there are significant coherence losses between the internal modes of the interferometer. Apart from the coherence losses there are losses at the input state generation and also due to the imperfection of detectors [29–31]. In particular, the generation of the perfect NOON state is very complicated. The creation of a NOON states relies on quantum (nonclassical) interference between multi-photon amplitudes, which should be unaffected by the degree of distinguishability between the photons or photon statistics at the detector [32]. Therefore, it is important to find solutions to minimize these experimental losses.

A possible solution has been proposed by Datta et al. [33] who suggested to use the Holland–Burnett state (HB) instead of the NOON state as the resource state for the supersensitivity. They have demonstrated that the HB states are experimentally more immune to losses than the NOON states. The HB state is generated in a Mach–Zehnder interferometer with the input 50:50 beamsplitter by driving the interferometer with two Fock states $|n\rangle$ containing equal number of photons [34].

Let us discuss in some details the issues of imperfections and the advantage of using the HB state raised by Datta et al. [33]. Consider first losses in the interferometer, which mostly occur at the process of the phase accumulation (phase shift) in the arm c of the interferometer, shown in Fig. 9.1. The system start with a state $|\Phi\rangle = |n\rangle\,|n\rangle$, containing n photons in each of the two input arms to the interferometer. The losses in the arm c of the interferometer, in which the phase is accumulated can be modeled as

$$\hat{c} \to \sqrt{\eta}\,\hat{c}\,\mathrm{e}^{\mathrm{i}\phi} + \sqrt{1-\eta}\,\hat{e}\,, \tag{9.85}$$

where η is the transmissivity coefficient of the mode $\hat{c}$ and $\hat{e}$ is the annihilation operator of an unaccessible environment mode. The subsequent state of the input modes is

$$|\Phi\rangle = \frac{1}{2^n} \sum_{m=0}^{n} \sum_{p=0}^{2m} C_m B_{m,p} \, |2m-p\rangle_c \, |2n-2m\rangle_d \, |p\rangle_e \ , \tag{9.86}$$

where $C_m = 2m!\sqrt{(2n-2m)!}\exp(2im\phi)/m!(n-m)!$, $B_{m,p} = \eta^{m-p/2}(1-\eta)^{m/2}/\sqrt{(2m-p)!p!}$, $|2m-p\rangle_c$ is the state of the arm c, $|2n-2m\rangle_d$ is the state of the arm d, $|p\rangle_e$ is the state of the environment, and p is the number of photons lost to the environment.

The changes in the initial state as a result of the phase shift in the arm c can be quantified by the quantum Fisher information. It describes changes of the state $|\Phi\rangle$, which are determined by the statistical distance between $|\Phi\rangle$ and $|\Phi\rangle_\phi = d\,|\Phi\rangle\,/d\phi$. Note that (9.86) involves the state of the environment. Since we are interested in determining changes in the state of the interferometer alone, we may write (9.86) as

$$|\Psi\rangle = \sum_{p=0}^{2m} |\psi_p\rangle \, |p\rangle_e \ , \tag{9.87}$$

with

$$|\psi_p\rangle = \frac{1}{2^n} \sum_{m=0}^{n} C_m B_{m,p} \, |2m-p\rangle_c \, |2n-2m\rangle_d \ , \tag{9.88}$$

and trace over the states of the environment. We then arrive to the following expression for the quantum Fisher information

$$F(\phi) = 4\left({}_\phi\langle\psi_p \, |\psi_p\rangle_\phi - |\langle\psi_p \, |\psi_p\rangle_\phi|^2 \right) \ . \tag{9.89}$$

Figure 9.11 shows the quantum Fisher information of the NOON, HB and optimal loss-tolerant states plotted as a function of η for the total $2n = 20$ input photons. The optimal loss-tolerant states is one giving the best possible precision in optical two-mode interferometry.

Note a significant difference in the sensitivity to the losses of the NOON and HB states. With the HB states one can beat the SQL with the efficiency $\eta = 0.5$ while the efficiency $\eta > 0.8$ is required to beat the SQL with the NOON state. The results clearly show that the HB states are more immune to the losses in the interferometer than the NOON states.

Further Research on Quantum Metrology

The experiments described in Sects. 9.3.4 and 9.3.6 were first successful demonstrations of the beating of the standard quantum limit and achieving the supersensitivity close to the Heisenberg limit. Since then the fields of quantum metrology and the precise spectroscopy have been investigated by many authors. Several different schemes

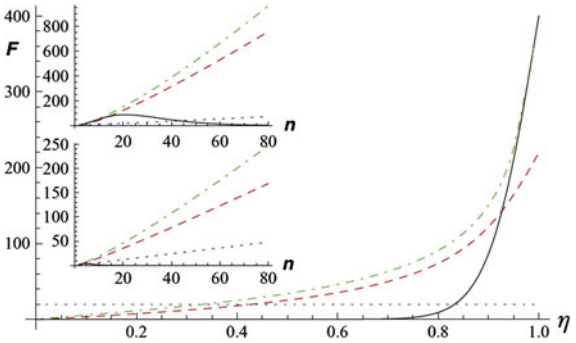

Fig. 9.11 Quantum Fisher information $F(\phi)$ versus η for $2n = 20$ input photons. The *blue dotted line* is the SQL of the quantum Fisher information, the *red dashed line* is the result for the HB state and the *green dashed-dotted line* is the result for the optimal loss-tolerant state. The *two insets* show the quantum Fisher information as a function of the number of photons n for $\eta = 0.9$ (*top*) and $\eta = 0.6$ (*bottom*). Reprinted with permission from A. Datta, L. Zhang, N. Thomas-Peter, U. Dorner, B.J. Smith, I.A. Walmsley: Phys. Rev. A **83**, 063836 (2011). Copyright (2011) by the American Physical Society

for achieving supersensitivity have been proposed such as optomechanical systems, parity detection scheme, [35–44]. Alternative schemes for reaching the Heisenberg limit involving different type of nonclassical states such entangled coherent states and twin Fock states have also been demonstrated [45–49]. Interesting schemes have been proposed to improve quantum metrology using quantum error correction [50–52], and to restore the Heisenberg limit in noisy environment [53–55]. These schemes are important in connection with precision measurement of gravitational waves, where optimal sensitivity is ultimately limited by their detection noise.

Following these developments, several workers have studied the application of quantum metrology in the high precision spectroscopy to improve the frequency standard and atomic clocks [56] Moreover, it was shown that precision near the Heisenberg limit can be attained without requiring single particle resolved state detection [57].

9.4 Quantum Optical Lithography

In the preceding sections we have seen how the laws of quantum mechanics led to the fundamental limits encountered in optical interferometry and demonstrated how one could achieve supersensitivity, the phase sensitivity better than that determined by the standard quantum limit. In this section, we continue our study of the fundamental limits and turn our attention to the diffraction limit. One of the fundamental facts leading to the occurrence of the diffraction limit is that the resolution of an optical detector is limited by diffraction on its optical elements due to the wave nature of the incident light. The light tends to scatter around the optical elements and

measured objects, limiting the achievable resolution. The resolution criterion, called the classical resolution limit, was established by Abbe and Rayleigh at the end of the nineteenth century [58, 59]. It states that two closely spaced points cannot be resolved if the distance between them is smaller than $\lambda/\mathcal{A}$, where λ is the wavelength of the employed light and $\mathcal{A}$ is called the numerical aperture of the detector. Although the Abbe and Rayleigh's analysis were done for diffraction, they are equally valid for interferometry. In the simple interference experiment involving two slits or two point sources of light, distance Δx, the adjusted interference minima or maxima correspond to a phase difference $k\Delta x = \pi$, where $k = 2\pi/\lambda$. Thus, two sources can be resolved if the distance between them is no smaller than $\Delta x = \lambda/2$. This limit is called the diffraction limit or Rayleigh criterion for resolution.

The diffraction limit, of course, is not a fixed bound for resolution. It can be changed and there are several methods to improve the spatial resolution. In any case it is clear from the formula $\lambda/\mathcal{A}$ that in diffraction one may always increase the resolution by increasing the size of the numerical aperture $\mathcal{A}$. In both diffraction and interference, the resolution can be increased by reducing the wavelength λ of the employed light. For example, some technological approaches consider light in the vacuum ultraviolet or soft x-ray regime in order to resolve objects at 100 nm or below. However, from a laboratory point of view, it is not always practical to reduce the wavelength. The reason is that energy of light increases with shortening the wavelength, being ultraviolet or soft x-rays light might easily destroy the system investigated. Therefore, it is practically important to find other ways to improve the spatial resolution of lithographic systems.

Rather than making the diffraction limit $\lambda/2$ as small as possible, one can consider methods that use only a fraction of the energy, or equivalently, a fraction of the wavelength of the employed light. That is, use methods to write lithographic features with resolution that is a fraction of that achievable according to the diffraction limit. Such a resolution could be achieved by making use of quantum effects such as entangled photons in the incident fields. By utilizing the quantum nature of entangled n-photon states, one can achieve the spatial resolution of a lithographic feature n times higher than that determined by the diffraction limit, spatial *super-resolution* [60, 61]. In other words, the resolution obtained with n-photon entangled light of wavelength λ is equivalent to that obtained with a classical light of wavelength λ/n.

Let us turn into a detailed study of methods that can lead to a super-resolution, the spatial resolution better than that determined by the diffraction limit. Before going into details, we would like to point out that the advantage of the super-resolution over the supersensitivity is that the former can be determined solely from the fringe pattern. Therefore, a typical device for optical lithography is configured like a Mach–Zehnder interferometer except that the output beamsplitter is replaced by a sensitive screen that could be a photographic plate or lithographic resist, as illustrated in Fig. 9.12. The input modes a and b are mixed at the beamsplitter (BS) and the resulting modes c and d are then brought to interference on the screen S after a phase shift ϕ is introduced between them.

The physical quantity that is typically measured in optical lithography is the n-photon absorption rate, or equivalently a joint (coincidence) rate P_n of a simultaneous

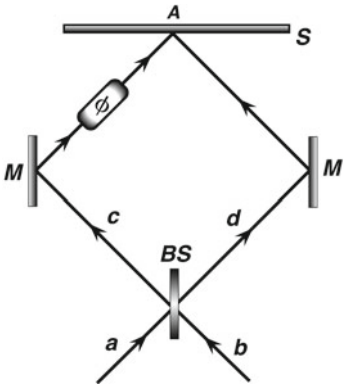

Fig. 9.12 Schematic diagram of an interferometer relating to optical lithography, controlled writing of lithographic features on a screen S. The interferometer is similar to a Mach–Zehnder interferometer, shown in Fig. 9.1, except that the output beamsplitter is replaced by a sensitive screen S that responds by means of multi-photon absorption of the superposition field of the phase ϕ shifted internal modes of the interferometer

deposition of n photons on the screen at the coincidence point A. The rate P_n is given by the nth order correlation function of the superposition field $u = c + d$ as

$$P_n = \frac{1}{n!} \left\langle (\hat{u}^\dagger)^n (\hat{u})^n \right\rangle , \tag{9.90}$$

where $\hat{u}$ is the annihilation operator representing the total field detected at the coincidence point

$$\hat{u} = \hat{c} + \hat{d} = \frac{1}{\sqrt{2}} \left(1 + \mathrm{i}\mathrm{e}^{\mathrm{i}\phi}\right) \hat{a} + \frac{1}{\sqrt{2}} \left(\mathrm{i} + \mathrm{e}^{\mathrm{i}\phi}\right) \hat{b} . \tag{9.91}$$

With the relations (9.90) and (9.91), we can determine the dependence of the rate on the state of the input modes of the interferometer and on the number of photons used in the process of depositing a lithographic feature on the screen S.

One can notice that the theory of the optical lithography proceeds along the lines of that for the phase sensitivity presented above in Sect. 9.3.4, except that the correlations between the internal modes are considered instead of the output modes of the interferometer. We shall not carry it again but should point out that the coincidence probabilities of the output modes, as calculated in Sect. 9.3.4 also provide the information about the spatial resolution.

We now proceed to examine the rate (9.90) for different input states of the interferometer. We start with a simple input state, a single photon state $|1_a, 0_b\rangle$, that at given time there is only one photon in mode a and no photons in mode b. In this case, the rate is of the form

$$P_1 = \langle \hat{u}^\dagger \hat{u} \rangle = 1 - \sin\phi , \tag{9.92}$$

The rate exhibits a periodic variation with the phase ϕ, an interference effect. The phase difference between a maximum and an adjacent minimum of the interference pattern is $\phi = \pi$, from which we readily find the minimum resolution $\Delta x = \lambda/2$, that is equal to the diffraction limit. Thus, with single photons used, a lithographic feature can be deposited on the screen with the same resolution as those given by the diffraction limit.

It is interesting to find the state of the internal modes of the interferometer. Since the probability of finding the photon in either mode c or d is equal to $1/2$, one finds readily that the internal modes are in the state

$$|\Phi\rangle_{cd} = \frac{1}{\sqrt{2}} \left(|1_c, 0_d\rangle + |0_c, 1_d\rangle\right) , \tag{9.93}$$

which is a $n = 1$ NOON state. We see that although a nonclassical state is created between the internal modes of the interferometer, the result for the resolution is the same as that of the classical theory.

Consider now the case when two photons are used to deposit a lithographic feature on the screen. Here, we have two possibilities for the input states. In the first, both photons are in either mode a or mode b, i.e., the photon number state of the input modes is either $|2_a, 0_b\rangle$ or $|0_a, 2_b\rangle$. In the other, one photon appears simultaneously in each mode, i.e., the photon number state of the input modes is $|1_a, 1_b\rangle$.

In the first case, when the input photon number state $|2_a, 0_b\rangle$ is used, the following solution for the coincidence rate P_2 is obtained

$$P_2 = \frac{1}{2}\langle \hat{u}^\dagger \hat{u}^\dagger \hat{u}\hat{u}\rangle = \frac{3}{2} - 2\sin\phi - \frac{1}{2}\cos 2\phi , \tag{9.94}$$

which can be written in a compact form as

$$P_2 = (1 - \sin\phi)^2 \equiv P_1^2 . \tag{9.95}$$

When the input photon number state $|1_a, 1_b\rangle$ is used, the probability takes the form

$$P_2 = 1 + \cos 2\phi . \tag{9.96}$$

The behavior of the probability P_2, or equivalently the two-photon absorption rate is very different for these two input states. For the input state $|2_a, 0_b\rangle$, the two-photon coincidence rate is equal to the square of the single photon rate, $P_2 = P_1^2$, which implies that the two incident photons are independently absorbed by the detector (screen). This property is not limited to two photons only. It can be easily generalized to an arbitrary n-photon number state $|n_a, 0_b\rangle$ to yield

$$P_n = (1 - \sin\phi)^n = P_1^n . \tag{9.97}$$

Clearly, the rate of the n-photon absorption is n times that of the single photon rate, corresponding to n independent absorption processes of the incident photons. In other words, the result (9.97) implies that the process of absorption of n photons incident on the screen is completely coherent.

More interesting is the result (9.96) for the coincidence rate with the input state $|1_a, 1_b\rangle$ which, evidently, does not factorize into single photon rates, $P_2 \neq P_1^2$. It follows therefore that in this case, the photons are not absorbed independently, but have certain characteristic correlation properties.

This conclusion is especially evident if one examines the state of the internal modes of the interferometer. When two photons are involved, the space of the internal states of the interferometer is spanned by a three-state vector, $|1_c, 1_d\rangle$, $|2_c, 0_d\rangle$, $|0_c, 2_d\rangle$. For the input state $|2_a, 0_b\rangle$, it is easily verified that the probabilities for the internal states are

$$P_{(2c,0d)} = P_{(0c,2d)} = \frac{1}{4}\,, \quad P_{(1c,1d)} = \frac{1}{2}\,, \tag{9.98}$$

and then the corresponding state of the internal modes is of the form

$$|\Phi\rangle_{cd} = \sqrt{\frac{1}{4}}\,(|2_c, 0_d\rangle + |0_c, 2_d\rangle) + \sqrt{\frac{1}{2}}\,|1_c, 1_d\rangle\ . \tag{9.99}$$

A different situation arises if the state of the input modes is $|1_a, 1_b\rangle$. In this case, the probabilities are

$$P_{(2c,0d)} = P_{(0c,2d)} = \frac{1}{2}\,, \quad P_{(1c,1d)} = 0\,, \tag{9.100}$$

and consequently the state of the internal modes is a maximally entangled NOON state

$$|\Phi\rangle_{cd} = \sqrt{\frac{1}{2}}\,(|2_c, 0_d\rangle + |0_c, 2_d\rangle)\ . \tag{9.101}$$

There is an important difference between the states (9.99) and (9.101). The state (9.99) resulting from the input state $|2_a, 0_b\rangle$ contains a contribution of the state $|1_c, 1_d\rangle$ that is absent in the probability when the input state is replaced by $|1_a, 1_b\rangle$. The reason is in the distinguishability of the detected photons. The input state $|2_a, 0_b\rangle$ possesses both photons in the mode a, so that when a photon is detected in either mode c or d, one can say from which mode it originated. In other words, the detected photons are distinguishable. The situation is completely different when the input state is $|1_a, 1_b\rangle$. In this case, when a photon is detected in either c or d, one cannot say from which mode it originated. Thus, the photons are indistinguishable, or equivalently, the photons are entangled. It is clear that the correlations between the photons deposited on the screen could be described as having their origin in the correlations of the entangled NOON state created between the internal modes of the interferometer.

Notice a common feature of the two-photon coincidence rates (9.94) and (9.96) which is basic to the concept of super-resolution. The rates contain a term $\cos 2\phi$ whose the presence may lead to a sinusoidal oscillation of the interference pattern twice faster than that of the one-photon excitation pattern. This oscillation could then result in a resolution of the interference fringes at the limit $\Delta x = \lambda/4$, one-half of the diffraction limit.

It is easily verified from (9.96) that the term $\cos 2\phi$ produces an interference pattern with a resolution $\Delta x = \lambda/4$. This conclusion is not so obvious for the probability (9.94) which involves two oscillatory terms, $\sin\phi$ and $\cos 2\phi$. In fact, the presence of the two terms is disadvantageous for achieving a resolution better than the diffraction limit. The disadvantageous is that the two terms produce an interference pattern whose the variation with ϕ is not sinusoidal. This is illustrated in Fig. 9.13, which shows the coincidence rate (9.94) as a function of ϕ for different number of photons. For $n = 1$ the interference pattern is seen to oscillate sinusoidally with the phase ϕ but with an increasing n, the pattern becomes progressively less sinusoidal. Thus, the advantage gained from the presence of the $\cos 2\phi$ term lies not in the frequency of the oscillations but in the sharpness of the interference maxima. The effect of the $\cos 2\phi$ term is to narrow the maxima of the interference pattern.

It is interesting to compare the results for the resolution arising from the use of independent photons with the corresponding results arising from the use of entangled photons. Figure 9.14 shows the behavior of the coincidence rates (9.92), (9.96) and (9.97) as a function of the phase ϕ. The dashed-dotted line shows the one-photon rate P_1 that sets up the diffraction limit for the resolution. Beating of a diffraction limit with multi-photon states shows up clearly as a sharpening of the interference maxima. For the input quantum state $|1_a, 1_b\rangle$, the resolution is evidently $\Delta x = \lambda/4$, twice larger than that at the diffraction limit. When $n = 2$ independent photons are used, the resolution is far from approaching $\lambda/4$. Also shown is the interference pattern when the input state is an $n = 5$ photon number state $|5_a, 0_b\rangle$. We see that the same super-resolution $\Delta x = \lambda/4$, that is achieved with $n = 5$ independent photons,

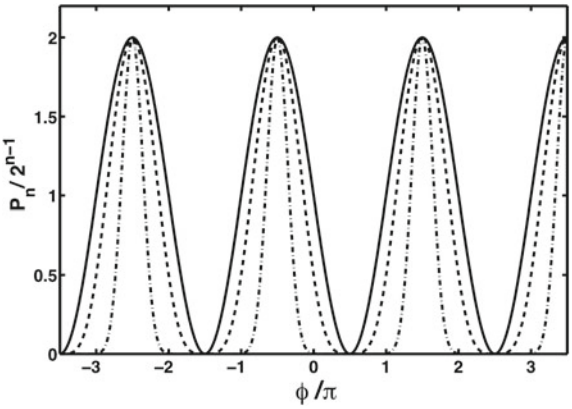

Fig. 9.13 The normalized coincidence rate $P_n/2^{n-1}$ of the absorption of n independent photons plotted as a function of the phase shift ϕ for different number of photons: $n = 1$ (*solid line*), $n = 2$ (*dashed line*), and $n = 10$ (*dashed-dotted line*)

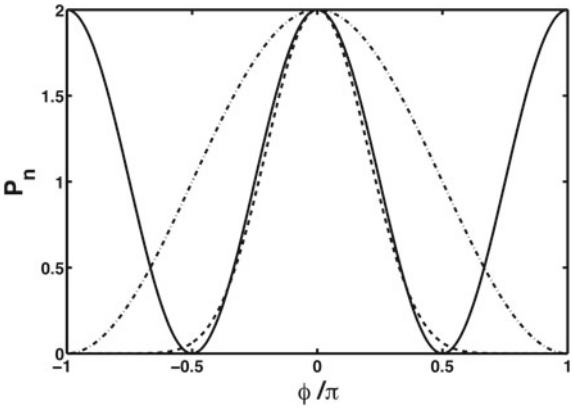

Fig. 9.14 The coincidence rate P_n as a function of the phase shift ϕ for different photon number states of the input modes of the interferometer. The *solid line* is the rate (9.96) corresponding to the input state $|1_a, 1_b\rangle$. The *dashed line* is the normalized rate $P_5/16$ corresponding to the input state $|5_a, 0_b\rangle$, and *dashed-dotted line* is the rate P_1 for the input state $|1_a, 0_b\rangle$. Since the locations of the interference maxima depend on the state of the input modes, the plots for $P_5/16$ and P_1 were uniformly phase shifted, $\phi \to \phi - \pi/2$, to superpose the interference maxima of all the plots at the same $\phi = 0$

can be achieved with $n = 2$ entangled photons. This clearly illustrates the power of entangled states that devices utilizing entanglement can perform with less required resources.

9.4.1 Experimental Evidence of Multi-Photon Super-Resolution Without Entanglement

There have been several experimental demonstrations of a super-resolution of $\Delta x = \lambda/4$ achievable with $n = 2$ photons. The experiments can be divided into two groups, those configured like a Mach–Zehnder interferometer illustrated in Fig. 9.12, and those using other setups such as slits and gratings. The later group employed entangled light to achieve the super-resolution, whereas the former demonstrated the super-resolution without entanglement.

The first successful demonstration of beating the diffraction limit with two-photon ($n = 2$) entangled light was reported by D'Angelo et al. [62], who used slits to create two separate beams for a phase shifted interference and an OPO as a source of entangled pairs of photons. More similar experiments using slits and a grating have since been successfully performed by others. These experiments have been extensively discussed in the literature and, therefore, we will not go into more details with them. In this section, we rather focus on the problem of beating the diffraction limit in systems employing a Mach–Zehnder interferometer and a classical input light. In particular, we shall discuss in details an experiment by Chang et al. [63].

The aim of the experiment was to measure the super-resolution of $\Delta x = \lambda/4$ with a classical light source depositing $n > 2$ independent photons on the lithographic screen of a Mach–Zehnder interferometer.

We have already discussed and illustrated in Fig. 9.13 that the super-resolution of $\Delta x = \lambda/4$ can be achieved in a Mach–Zehnder interferometer type system with $n = 5$ independent photons. Chang et al. [63] argued that the super-resolution of $\lambda/4$ can be achieved in this system with less photons, $n = 3$, if one considers a simultaneous measurement of a sum of three-photon coincidence probabilities, $P_3(\phi)$ and $P_3(\phi + \pi)$. It is easy to see, with the sum of the coincidence three-photon probabilities, one has

$$\begin{aligned} P_3(\phi) + P_3(\phi + \pi) &= (1 - \sin\phi)^3 + [1 - \sin(\phi + \pi)]^3 \\ &= 5 - 3\cos(2\phi) = 5\,[1 - V\cos(2\phi)]\ , \end{aligned} \tag{9.102}$$

where $V = 3/5$ is the visibility of the interference fringes. Evidently, the total probability (9.102) produces an interference pattern with the fringe resolution $\Delta x = \lambda/4$, the resolution enhanced by a factor of two compared to the diffraction limit of $\lambda/2$. However, the visibility of these interference fringes is not perfect, $V = 3/5$, but it might be large enough to observe the rapidly oscillating interference fringes.

The concept of the super-resolution with $n = 3$ unentangled photons proposed by Chang et al. [63] was then tested by them experimentally. The experiment employed a Mach–Zehnder interferometer as discussed earlier and illustrated in Fig. 9.12. For the detecting screen, a UV lithographic material was used sensitive to multi-photon excitations. A femtosecond pulse laser was used as a source of light. The laser pulses of a wavelength 800 nm were injected to the interferometer through one of the input modes. Another mode was left unexcited. The laser pulses were divided into two beams at the input beamsplitter and then directed by perfectly reflecting mirrors to a coincidence point on the screen. A glass plate was placed in one of the two arms of the interferometer to introduce a phase shift between the arms. The phase difference was changed by rotating the glass plate.

Using this scheme, Chang et al. [63] observed an interference pattern with a resolution twice better than that given by the diffraction limit. The experimental results are shown in Fig. 9.15. When a single pulse of a wavelength $\lambda = 800$ nm was sent to the interferometer, an interference pattern was observed with sharp and non-sinusoidal fringes separated by 425 nm, a half of the wavelength of the used light. As it has been discussed above and illustrated in Fig. 9.13, a non-sinusoidal shape of the interference pattern ensures the multi-photon nature of absorption in the lithographic screen. The observed fringe separation of 425 nm corresponded to a resolution nearly $\Delta x = \lambda/2$, the diffraction limit. This interference pattern is shown in the part (a) of the figure. However, when a sequence of two pulses was sent to the interferometer such that for the second pulse the field in one arm of the interferometer was phase shifted by π in relative to another arm, an interference pattern was observed with the fringe separation suppressed to roughly 213 nm. The result for the interference pattern is shown in Fig. 9.15b. This figure shows that a resolution twice better than that given by the diffraction limit was achieved.

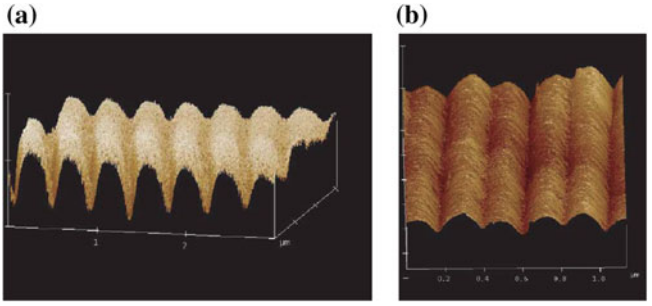

Fig. 9.15 Images of the interference fringes recorded on the lithographic screen in the experiment by Chang et al. [63]. Part **a** shows the interference pattern for a single pulse exposure, and part **b** shows the interference pattern for a sequence of two exposures. From H.J. Chang, H. Shin, M.N. O'Sullivan-Hale, R.W. Boyd: J. Mod. Opt. **53**, 2271 (2006), reprinted by permission of the publisher (Taylor and Francis Ltd, http://www.tandfonline.com)

9.4.2 Multi-Photon Super-Resolution with Entanglement

The preceding discussion focused on the possibility of achieving a super-resolution with classical light. Of greatest interest, however, is the case when a quantum field containing a large number of photons ($n > 2$) is applied to the input modes of the interferometer. As we have already seen, devices utilizing entangled fields can perform with less required resources. However, there is a subtle problem with achieving a super-resolution with a multi-photon quantum field. Following the result (9.96) for the probability P_2 one could expect that by preparing the input modes of the interferometer in an n-photon state $|(n/2)_a, (n/2)_b\rangle$, the joint probability P_n should have the form

$$P_n = 1 + \cos(n\phi) \,, \tag{9.103}$$

and then the resolution of the interference pattern would be improved to the limit of $\Delta x = \lambda/(2n)$. It is not difficult to show that for P_n to be of the simple form (9.103), it is necessary that the state of the internal modes of the interferometer is an n-photon NOON state

$$|\Phi\rangle_{cd} = \frac{1}{\sqrt{2}} \left(|n, 0\rangle + |0, n\rangle\right) \,. \tag{9.104}$$

One might hope that the NOON state could be easily created with the input n-photon state $|(n/2)_a, (n/2)_b\rangle$. Unfortunately, this hope is unfounded because in a Mach–Zehnder interferometer an increase of the number of photons is equally effective in loosing the ability for creating the NOON state between the internal modes of the interferometer. In particular, restricting ourselves to $n = 4$, we get for the coincidence probability

$$P_4 = \frac{11}{32}\left(1 + \frac{12}{11}\cos 2\phi + \frac{9}{12}\cos 4\phi\right) . \tag{9.105}$$

Evidently, the probability P_4 is not of the form (9.103) that makes it impossible to maintain the $\lambda/8$ scaling for the resolution. The probability contains an additional oscillatory factor $\cos 2\phi$ which may obscure the pure harmonic oscillations with periodicity $\pi/4$ induced by the factor $\cos 4\phi$. Thus, not only the classical but also quantum methods can suffer from super-resolution with $n > 2$.

The presence of the additional oscillatory factor can be traced to the state of the internal modes of the interferometer. We have already encountered this problem in Sect. 9.3.4, where we calculated the state of the internal modes of the standard Mach–Zehnder interferometer for $n = 4$ photons and the input photon number state $|2_a, 2_b\rangle$. The four-photon state of the internal modes is therefore of the form

$$|\Phi\rangle_{cd} = \sqrt{\frac{3}{8}}\left(|4, 0\rangle + |0, 4\rangle\right) + \sqrt{\frac{1}{4}}\,|2, 2\rangle \ . \tag{9.106}$$

Clearly, not only the NOON state is populated but also the state $|2, 2\rangle$ that is responsible for the oscillatory factor $\cos 2\phi$ in the coincidence probability (9.105). We may state that the creation of the NOON state in a Mach–Zehnder interferometer is highly effective for small number of photons. The efficiency degrades rapidly with an increasing number of photons.

In concluding this section, we briefly comment on practical difficulties one could face when implementing the quantum lithography. Apart from the difficulty of creating an entangled NOON state with a large number of photons, there are practical problems of producing the required input number state for large n with identical numbers of photons and simultaneously inject them into the interferometer. A further practical difficulty is with photographic or lithographic materials used for the depositing screen. The material should change its behavior only when absorbing n photons simultaneously, not changing the behavior after absorbing only a fraction k ($k < n$) of the total number of photons.

9.4.3 *Experimental Evidence of Super-Resolution with Four-Photon Entangled Light*

As pointed out above, with the use of a field containing $n > 2$ photons, the super-resolution scaled as $1/n$ cannot be achieved in the simple configuration involving a single Mach–Zehnder interferometer. Therefore, a different interferometer configuration has been proposed and experimentally realized by the Zeilinger's group in Vienna [64], where the super-resolution scaled as $1/n$ with a four-photon ($n = 4$) correlated field was demonstrated. In their experiment two Mach–Zehnder interferometers were used, with the input beamsplitters replaced by a parametric down-conversion process simultaneously exciting internal modes of both interferometers, as illustrated in Fig. 9.16. The parametric process might reasonably be called a

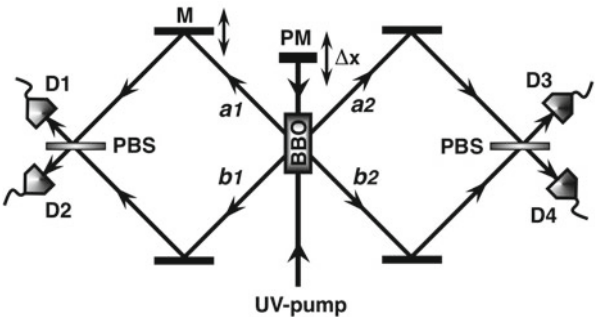

Fig. 9.16 Outline of the experimental setup used by Walther et al. [64] to demonstrate a super-resolution of $\Delta x = \lambda/8$ in a four-photon interferometry. The setup was composed of two Mach–Zehnder interferometers with the input beamsplitters replaced by a parametric downconversion process. The parametric process generated entangled pairs of photons with one photon from each pair sent to the arms of different interferometers. A phase difference ϕ between photons sent to arms $(a1, a2)$ and those sent to arms $(b1, b2)$ was created by displacing the pump mirror PM

"quantum beamsplitter" since it generates correlated (entangled) pairs of photons. In this configuration, photons from each pair generated in the parametric process go into the arms of different interferometers.

Pulsed femtosecond Ti:S laser light was used to pump a type II BBO crystal which, by the process of spontaneous downconversion generated entangled pairs of photons, with one photon from each pair sent to the arm $a1$ of the interferometer on the left and the other photon sent into the arm $a2$ of the interferometer on the right. The pump beam was then reflected by a mirror PM back onto the crystal to generate more entangled pairs of photons with photons from each pair now sent to the arms $b1$ and $b2$ in the respective interferometers. The phase shift ϕ of the photons sent through the upper paths $(a1, a2)$ with respect to the photons sent through the bottom paths $(b1, b2)$ of the interferometers was varied by varying the position of the reflection mirror PM. The overlap of the paths of the interferometers was done by a fine adjustment of the position of the mirror M. The photons were mixed at the beamsplitters (PBS) and the combined beams were passed through linear polarisers before being detected by photodetectors D. The beamsplitters transmit horizontally polarized light $|H\rangle$ and reflect vertically polarized light $|V\rangle$, where H (V) stands for horizontal (vertical) polarization of the photon. In their experiment, Walther et al. [64] achieved on average approximately 0.05 photons per second in coincidence and a visibility of the four-photon interference fringes approximately 61%.

The experiment involved measurements of the polarization correlations of two and four photons emitted into different interferometers. In the two-photon coincidence measurements, only a single pair of photons was generated during the double pass of the pump beam through the BBO crystal. In the four-photon coincidence measurements, two pairs of photons were generated during the double pass of the pump beam through the crystal. In this case, there are two possibilities for the generation of the two pairs of photons. Two pairs of photons can be emitted on either

pass of the pump beam or one pair can be emitted on each pass of the pump beam. In the first case both pairs of photons can be emitted to the modes $(a1, a2)$ or $(b1, b2)$. In the second case, one pair is emitted to modes $(a1, a2)$ and the other is emitted to modes $(b1, b2)$.

The experimental setup was aligned to create the following maximally entangled states between the internal modes of the interferometer for each pair of photons emitted into the modes $(a1, a2)$ or $(b1, b2)$:

$$\begin{aligned} \left|\Phi^{+}\right\rangle_{a} &= \frac{1}{\sqrt{2}}\left(|H_{a1}H_{a2}\rangle + |V_{a1}V_{a2}\rangle\right) , \\ \left|\Phi^{+}\right\rangle_{b} &= \frac{1}{\sqrt{2}}\left(|H_{b1}H_{b2}\rangle + |V_{b1}V_{b2}\rangle\right) . \end{aligned} \tag{9.107}$$

Since the beamsplitters transmit the horizontally polarized light and reflect vertically polarized light, one can predict the state which contributed to the detection probability of a photon at each of the output modes. For example, if only one pair of photons is generated on a double pass of the laser beam through the crystal, a single photon detected at D_2 and D_3 will either result from the state $|H_{D2}H_{D3}\rangle$ or $|V_{D2}V_{D3}\rangle$ of the output modes, which leads in a maximally entangled state

$$|\Phi\rangle_{D2D3} = \frac{1}{\sqrt{2}}\left(|H_{D2}H_{D3}\rangle + \mathrm{e}^{2\mathrm{i}\phi}\,|V_{D2}V_{D3}\rangle\right) . \tag{9.108}$$

If two pairs of photons are generated on the double pass of the laser beam through the crystal such that both pairs are sent to the same pair of modes, either $(a1, a2)$ or $(b1, b2)$, a detection of a single photon at each of the output modes results from either $|H_{D2}H_{D3}V_{D1}V_{D4}\rangle$ or $|V_{D2}V_{D3}H_{D1}H_{D4}\rangle$, which leads in a maximally entangled state

$$|\Phi\rangle_{D} = \frac{1}{\sqrt{2}}\left(|H_{D2}H_{D3}V_{D1}V_{D4}\rangle + \mathrm{e}^{4\mathrm{i}\phi}\,|V_{D2}V_{D3}H_{D1}H_{D4}\rangle\right) . \tag{9.109}$$

Knowing the output state, we may find the two-photon coincidence probability of detecting photons in given modes by performing a projection measurement into the linear polarization basis

$$|\pm\rangle_{Di} = \frac{1}{\sqrt{2}}\left(|H_{Di}\rangle \pm |V_{Di}\rangle\right) , \quad i = 1, 2, 3, 4 . \tag{9.110}$$

For example, using (9.108) and (9.110), we readily find the coincidence probability of detecting a single photon in each of the output modes $D2$ and $D3$:

$$P_{D2,D3} = |\langle +|_{D2}\,\langle -|_{D3}\,|\Phi\rangle_{D2D3}|^2 = \frac{1}{4}\left(1 - \cos 2\phi\right) . \tag{9.111}$$

Similarly, using (9.109) and (9.110) one can find the four-photon coincidence probability of detecting a single photon in each of the output modes as

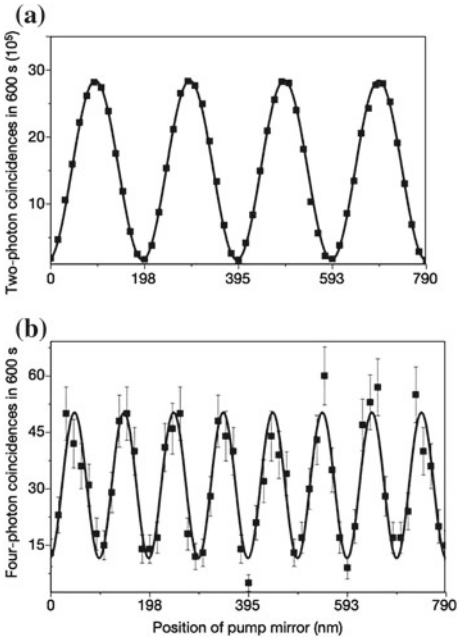

Fig. 9.17 Experimental results for **a** the two-photon coincidence probability $P_{D2,D3}$ and **b** the four-photon coincidence probability $P_{D1,D2,D3,D4}$, demonstrating the pure multi-photon interference patterns. The *squares* are the experimental data and the *solid line* represents theoretical results respectively (9.111) for the two-photon coincidence probability and (9.112) for the four-photon probability. Reprinted by permission from Macmillan Publishers Ltd: [Nature] (P. Walther, J.-W. Pan, M. Aspelmeyer, R. Ursin, S. Gasparoni, A. Zeilinger: Nature (London) **429**, 158 (2004)), copyright (2004)

$$P_{D1,D2,D3,D4} = |\langle +|_{D1} \langle +|_{D2} \langle -|_{D3} \langle +|_{D4} |\Phi\rangle_D|^2$$
$$= \frac{1}{16} (1 - \cos 4\phi) \ . \tag{9.112}$$

Figure 9.17 gives experimental results for two- and four-photon coincidence probabilities plotted as a function of the displacement of the pump mirror PM. A pumped BBO crystal emitted pairs of entangled photons at a wavelength 790 nm into the modes of the interferometer. The observed oscillations at a wavelength 395 nm for the two-photon case and at a wavelength 194 nm for the four-photon case clearly demonstrated the super-resolutions of $\Delta x = \lambda/4$ for the two-photon case and $\Delta x = \lambda/8$ for the four-photon case.

A slightly different procedure was used to demonstrate the pure four-photon interference pattern without any contribution from the two-photon interference. The experimental setup was aligned such that on the first pass of the pump through the crystal, a pair of photons emitted into the modes $(a1, a2)$ was in the state

$$\left|\Phi^+\right\rangle = \frac{1}{\sqrt{2}} (|H_{a1} H_{a2}\rangle + |V_{a1} V_{a2}\rangle) \ , \tag{9.113}$$

and on the second pass of the pump through the crystal, a pair of photons emitted into the modes $(b1, b2)$ was in a state

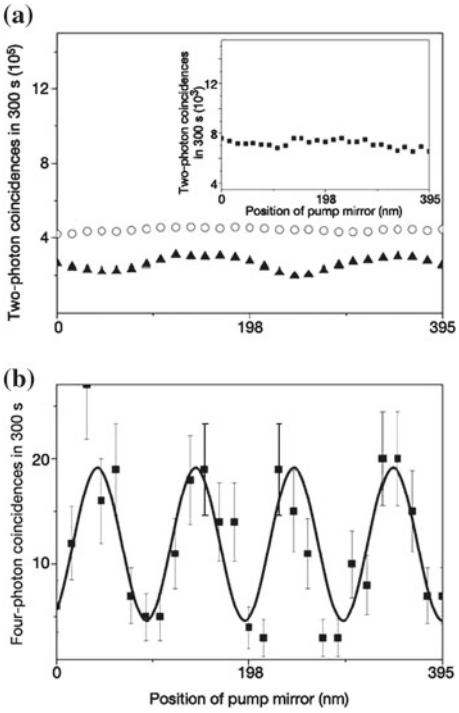

Fig. 9.18 Experimental demonstration of four-photon interference without any contribution from the two-photon interference. Part **a** shows the two-photon coincidence probability for three different pairs of the output modes, whereas part **b** shows the four-photon coincidence probability. Reprinted by permission from Macmillan Publishers Ltd: [Nature] (P. Walther, J.-W. Pan, M. Aspelmeyer, R. Ursin, S. Gasparoni, A. Zeilinger: Nature (London) **429**, 158 (2004)), copyright (2004)

$$\left|\Psi^{-}\right\rangle = \frac{1}{\sqrt{2}}\left(|H_{b1}V_{b2}\rangle - |V_{b1}H_{b2}\rangle\right) \ . \tag{9.114}$$

Since the beamsplitters transmit the horizontally polarized light and reflect vertically polarized light, a superposition of these states at the beamsplitter does not result in any interference terms. In the case of a double emission of both entangled pairs of photons sent to the same modes of the interferometer, the four-photon coincidence probability exhibits a four-photon interference.

The experimental results are shown in Fig. 9.18. The two-photon coincidence probabilities for various pairs of photodetectors are shown in frame (*a*) of the figure. Clearly, no oscillations of the probabilities were observed. The absence of the oscillations in the two-photon coincidence probability indicates that there are no two-photon correlations under these conditions. In contrast, the four-photon probability shows the characteristic $\cos 4\phi$ dependence predicted by (9.103). Thus, the resolution of the interference fringes at $\Delta x = \lambda/8$ was observed in the entangled four-photon interferometry.

In conclusion of this section, we point out that in principle, the scheme of Walther et al. [64] could be extended to a larger number of photons if many modes or many interferometers are used. What appears necessary to support such a possibility are an appropriately designed set of the interferometers and some arrangement for a source of a large and controlled number of correlated pairs of photons.

9.4.4 Super-Resolution with Classical Light

According to the above discussions, super-resolution can be achieved with a quantum field. However, there is a possibility to achieve a super-resolution by employing only *classical* light. The starting point of these investigations was a result found by Hemmer et al. [65–67], according to which a super resolution can be achieved by illuminating the lithographic screen with two counterpropagating frequency modulated (signal) fields and two control fields that assist a directional resonance for photons of the signal fields. This configuration of the fields leads to a multi-photon absorption process of the signal photons in the lithographic material [68].

A different example of a system in which one could achieve a super-resolution with classical light is the work of Kiffner et al. [69], in which a method based on the creation of a position dependent dark state in a multilevel Λ-type system driven on resonance by counterpropagating phase shifted laser fields. The physical process responsible for the creation of the dark state is the phenomenon of coherent population trapping. By a suitable choice of the Rabi frequencies of the driving fields it is possible to achieve a sinusoidal oscillation in space of the ground states populations with the wave number n times longer or accordingly, the wavelength n times shorter than that of the driving fields. A practical difficulty is the requirement of n fields and multi-lambda systems.

Perhaps, the most interesting is the proposal of Liao et al. [70–72] demonstrating how to achieve a super-resolution by preparing two-level molecules composing the lithographic screen in a position dependent state via coherent Rabi oscillations. The screen is exposed by two counterpropagating beams of Gaussian pulses that form a position dependent standing wave. The resolution depends on the number of Rabi cycles during the pulse duration. For very short pulses, the resolution at the diffraction limit can be achieved and a resolution beyond the diffraction limit is obtained by extending the duration of the pulses.

Super-resolution with classical light has been observed in some remarkable experiments by the Pan's group in Hefei, China [73]. In these experiments two-photon Raman transition of ^{87}Rb atoms was driven by a pulse standing-wave laser field of wavelength λ and the position dependent Rabi frequency $\Omega(x) = \Omega_0 \cos(2\pi x/\lambda_{\mathrm{SW}})$, where $\lambda_{\mathrm{SW}} = \lambda/\sin(\theta/2)$, with θ being the relative angle between the two fields forming the standing wave. The atom patterns for up to 9π Raman pulses creating the spatial resolution up to $\lambda/18$ were achieved via coherent Rabi oscillations.

Figure 9.19 shows recordings of the phase resolutions for durations of the laser pulses varying from 1π to 9π. As seen from the figure, periodic atomic patterns with spatial localization of atoms inside areas $\lambda_{\mathrm{SW}}/2$ have been created.

In closing this section, we would like to point out that one of trends of current research in the area of quantum lithography is the study of super-resolution in terms of quantum Fisher information [74, 75], which provides the inverse of the Crámer-Rao bound, the lowest variance achievable for an unbiased estimator [76].

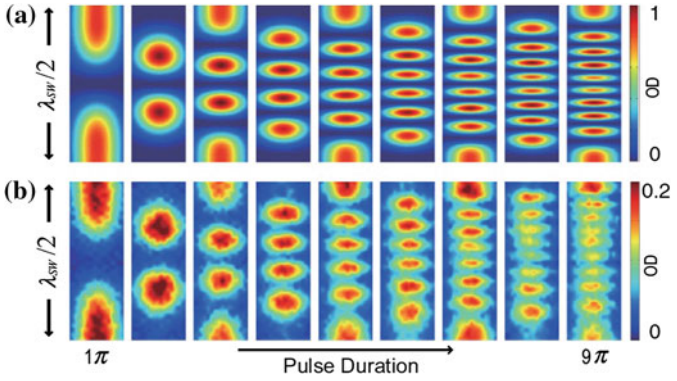

Fig. 9.19 The theoretical, frame **a** and experimental, frame **b**, results for the localization of atoms driven by standing-wave laser pulses of the duration varying from 1π to 9π. Reprinted with permission from J. Rui, Y. Jiang, G.-P. Lu, M.-J. Zhu, B. Zhao, X.-H. Bao, J.-W. Pan: Phys. Rev. A **93**, 033837 (2016). Copyright (2016) by the American Physical Society

Among other examples of super-resolution is quantum optical coherence tomography [77–79], a technique widely used for medical diagnostics, where it is employed to generate high-resolution 3D images [80].

References

1. C.M. Caves: Phys. Rev. D **23**, 1693 (1981)
2. M. Xiao, L.A. Wu, H.J. Kimble: Phys. Rev. Lett. **59**, 278 (1987)
3. P. Grangier, R.E. Slusher, B. Yurke, A. LaPorta: Phys. Rev. Lett. **59**, 2153 (1987)
4. O. Steuernagel: Phys. Rev. A **65**, 033820 (2002)
5. V. Giovannetti, S. Lloyd, L. Maccone: Phys. Rev. Lett. **108**, 260405 (2012)
6. M.J.W. Hall, D.W. Berry, M. Zwierz, H.M. Wiseman: Phys. Rev. A **85**, 041802 (2012)
7. D.W. Berry, M.J.W. Hall, M. Zwierz, H.M. Wiseman: Phys. Rev. A **86**, 053813 (2012)
8. D.W. Berry, M.J.W. Hall, H.M. Wiseman: Phys. Rev. Lett. **111**, 113601 (2013)
9. A. Luis: Phys. Lett. A **329**, 8 (2004)
10. J. Beltrán, A. Luis: Phys. Rev. A **72**, 045801 (2005)
11. S. Boixo, S.T. Flammia, C.M. Caves, J. Geremia: Phys. Rev. Lett. **98**, 090401 (2007)
12. S.M. Roy, S.L. Braunstein: Phys. Rev. Lett. **100**, 220501 (2008)
13. P.M. Anisimov, G.M. Raterman, A. Chiruvelli, W.N. Plick, S.D. Huver, H. Lee, J.P. Dowling: Phys. Rev. Lett. **104**, 103602 (2010)
14. M. Zwierz, C.A. Pérez-Delgado, P. Kok: Phys. Rev. Lett. **105**, 180402 (2010)
15. M. Zwierz, C.A. Pérez-Delgado, P. Kok: Phys. Rev. A **85**, 042112 (2012)
16. C.W. Helstrom: Phys. Lett. **25A**, 101 (1967)
17. S.L. Braunstein, C.M. Caves: Phys. Rev. Lett. **72**, 3439 (1994)
18. S.L. Braunstein, C.M. Caves, G.J. Milburn, Ann. Phys. (N.Y.) **24**, 135 (1996)
19. S. Boixo, A. Datta, M.J. Davis, S.T. Flammia, A. Shaji, C.M. Caves: Phys. Rev. Lett. **101**, 040403 (2008)
20. A. Rivas, A. Luis: New J. Phys. **14**, 093052 (2012)
21. S. Choi, B. Sundaram: Phys. Rev. A **77**, 053613 (2008)

22. M.J. Woolley, G.J. Milburn, C.M. Caves: New J. Phys. **10**, 125018 (2008)
23. A.M. Rey, L. Jiang, M.D. Lukin: Phys. Rev. A **76**, 053617 (2007)
24. B.A. Chase, B.Q. Baragiola, H.L. Partner, B.D. Black, J.M. Geremia: Phys. Rev. A **79**, 062107 (2009)
25. M. Napolitano, M. Koschorreck, B. Dubost, N. Behbood, R.J. Sewell, M.W. Mitchell: Nature **471**, 486 (2011)
26. T. Nagata, R. Okamoto, J.L. O'Brien, K. Sasaki, S. Takeuchi: Science **316**, 726 (2007)
27. R. Okamoto, H.F. Hofmann, T. Nagata, J.L. O'Brien, K. Sasaki, S. Takeuchi: New J. Phys. **10**, 073033 (2008)
28. K.J. Resch, K.L. Pregnell, R. Prevedal, A. Gilchrist, G.J. Pryde, J.L. O'Brien, A.G. White: Phys. Rev. Lett. **98**, 223601 (2007)
29. P.J. Mosley, J.S. Lundeen, B.J. Smith, P. Wasylczyk, A.B. UÕRen, C. Silberhorn, I. A. Walmsley: Rev. Lett. **100**, 133601 (2008)
30. C. Söller, O. Cohen, B.J. Smith, I.A. Walmsley, C. Silberhorn: Phys. Rev. A **83**, 031806(R) (2011)
31. Z. Li-Jian, X. Min: Chin. Phys. B **22**, 110310 (2013)
32. C.K. Hong, Z.Y. Ou, L. Mandel: Phys. Rev. Lett. **59**, 2044 (1987)
33. A. Datta, L. Zhang, N. Thomas-Peter, U. Dorner, B.J. Smith, I.A. Walmsley: Phys. Rev. A **83**, 063836 (2011)
34. M.J. Holland, K. Burnett: Phys. Rev. Lett. **71**, 1355 (1993)
35. X. Guo-Yong, G. Guang-Can: Chin. Phys. B **22**, 110601 (2013)
36. A. Luis, A. Rodil: Phys. Rev. A **87**, 034101 (2013)
37. Y. Israel, S. Rosen, Y. Silberberg: Phys. Rev. Lett. **112**, 103604 (2014)
38. D.-W. Wang, M.O. Scully: Phys. Rev. Lett. **113**, 083601 (2014)
39. X. Xu, J.M. Taylor: Phys. Rev. A **90**, 043848 (2014)
40. D. Li, B. T. Gard, Y. Gao, C.-H. Yuan, W. Zhang, H. Lee, J.P. Dowling: arXiv:1603.09019 [quant-ph], (2016)
41. S. Ragole, J. M. Taylor: arXiv:1601.02549 [cond-mat.quant-gas], (2016)
42. O. Hosten, N.J. Engelsen, R. Krishnakumar, M.A. Kasevich: Nature **529**, 505 (2016)
43. S. R. Shepard, F. I. Moxley, III, J. P. Dowling: Phys. Rev. A **93**, 033805 (2016)
44. H.F.H. Cheung, Y.S. Patil, L. Chang, S. Chakram, M. Vengalattore: arXiv:1601.02324 [quant-ph], (2016)
45. L. Czekaj, A. Przysiezna, M. Horodecki, P. Horodecki: Phys. Rev. A **92**, 062303 (2015)
46. R. Demkowicz-Dobrzański, M. Jarzyna, J. Kolodynski: Progress in Optics **60**, 345 (2015)
47. J. Huang, X. Qin, H. Zhong, Y. Ke, C. Lee: Scientific Reports **5**, 178894 (2015)
48. T. Tanaka, P. Knott, Y. Matsuzaki, S. Dooley, H. Yamaguchi, W.J. Munro, S. Saito: Phys. Rev. Lett. **115**, 170801 (2015)
49. C.-P. Wei, X.-Y. Hu, Ya-Fei, Z.-M. Zhang: Chin. Phys. B **25**, 040601 (2016)
50. W. Dür, M. Skotiniotis, F. Fröwis, B. Kraus: Phys. Rev. Lett. **112**, 080801 (2014)
51. G. Arrad, Y. Vinkler, D. Aharonov, A. Retzker: Phys. Rev. Lett. **112**, 150801 (2014)
52. E.M. Kessler, I. Lovchinsky, A.O. Sushkov, M.D. Lukin: Phys. Rev. Lett. **112**, 150802 (2014)
53. A.W. Chin, S.F. Huelga, M.B. Plenio: Phys. Rev. Lett. **109**, 233601 (2012)
54. J. Jeske, J.H. Cole, S.F. Huelga: New J. Phys. **16**, 073039 (2014)
55. E. Rocco, R.N. Palmer, T. Valenzuela, V. Boyer, A. Freise, K. Bongs: New J. Phys **16**, 093046 (2014)
56. J. Borregaard, A.S. Sorensen: Phys. Rev. Lett. **111**, 090801 (2013)
57. E. Davis, G. Bentsen, M. Schleier-Smith: Phys. Rev. Lett. **116**, 053601 (2016)
58. E. Abbe: Archiv für Mikroskopische Anatomie **9**, 413 (1873)
59. L. Rayleigh: Phil. Mag. **8**, 261 (1879)
60. V. Giovannetti, S. Lloyd, L. Maccone, J.H. Shapiro: Physical Review A **79**, 013827 (2009)
61. L.A. Rozema: Phys. Rev. Lett. **112**, 223602 (2014)
62. M. De Angelo, Y.-H. Kim, S.P. Kulik, Y. Shih: Phys. Rev. Lett. **92**, 233601 (2004)
63. H.J. Chang, H. Shin, M.N. O'Sullivan-Hale, R.W. Boyd: J. Mod. Opt. **53**, 2271 (2006)

64. P. Walther, J.-W. Pan, M. Aspelmeyer, R. Ursin, S. Gasparoni, A. Zeilinger: Nature (London) **429**, 158 (2004)
65. P.R. Hemmer, A. Muthukrishnan, M.O. Scully, M.S. Zubairy: Phys. Rev. Lett. **96**, 163603 (2006)
66. Q. Sun, P.R. Hemmer, M.S. Zubairy: Phys. Rev. A **75**, 065803 (2007)
67. W. Ge, P.R. Hemmer, M.S. Zubairy: Phys. Rev. A **87**, 023818 (2013)
68. M. Al-Amri, Z. Liao, M.S. Zubairy: Adv. At. Mol. Opt. Phys. **66**, 1 (2012)
69. M. Kiffner, J. Evers, M.S. Zubairy: Phys. Rev. Lett. **100**, 073602 (2008)
70. Z. Liao, M. Al-Amri, M.S. Zubairy: Phys. Rev. Lett. **105**, 183601 (2010)
71. Z. Liao, M. Al-Amri, T. Becker, W.P. Schleich, M.O. Scully, M.S. Zubairy: Phys. Rev. A **87**, 023405 (2013)
72. Z. Liao, M. Al-Amri, M.S. Zubairy: Phys. Rev. A **88**, 053809 (2013)
73. J. Rui, Y. Jiang, G.-P. Lu, M.-J. Zhu, B. Zhao, X.-H. Bao, J.-W. Pan: Phys. Rev. A **93**, 033837 (2016)
74. M. Tsang, R. Nair, X. Lu: arXiv:1511.00552 (2015)
75. W.-K. Tham, H. Ferretti, A. M. Steinberg: arXiv:1606.02666 (2016)
76. G. Tóth, L. Apellaniz: J. Phys. A: Math Theor. **47**, 424006 (2014)
77. M.B. Nasr, D.P. Goode, N. Nguyen, G. Rong, L. Yang, B.M. Reinhard, B.E.A. Saleh, M.C. Teich: Optics Commun **282**, 1154 (2008)
78. G. Tóth, W. Wieczorek, D. Gross, R. Krischek, C. Schwemmer, H. Weinfurter: Phys. Rev. Lett. **105**, 250403 (2010)
79. M.D. Mazurek, K.M. Schreiter, R. Prevedel, R. Kaltenbaek, K.J. Resch: Scientific Rep. **3**, 1582 (2013)
80. S.R. Arridge: Inverse Problems **15**, R41 (1999)

Chapter 10
Dipole Squeezing and Spin Squeezed States

In the preceding chapters, we have demonstrated how squeezed light applied to optical systems may lead to the prediction of subnatural linewidths in the radiation spectra and the possibility to improve the precision of measurements beyond the standard quantum limit. The reason for this was that squeezed light is an example of a nonclassical state of the electromagnetic field with quantum fluctuations in one of the two field quadrature components reduced below the limit set by the vacuum or shot-noise fluctuations. The concept of squeezed states of light was introduced in the context of the field observables, the quadrature components of the electromagnetic field, which can be measured and which are represented by Hermitian operators given in terms of the boson creation and annihilation operators. As we have seen, two-photon correlations in the field modes or between modes are required in order to reduce quantum fluctuations in one of the quadrature components below the vacuum level.

The notion of squeezed states is not restricted to the boson variables, but can be extended to any set of Hermitian quantum mechanical variables. The best known example of such variables is the angular momentum, in particular, spin variables. In fact the concept of squeezed states can be applied to any set of observables represented by operators obeying a Lie algebra, for example, the $SU(2)$ and $SU(1, 1)$ Lie algebras and their generalizations. We have seen that in terms of the boson variables the generation of squeezed states requires a nonlinear two-photon process or nonlinear systems involving two-photon transitions. This may not be required in atomic systems where interactions involve atomic dipole moments that are determined in terms of angular momentum (spin) variables.

In this chapter, we extend the concept of squeezed states to other observables such as the spin operators and introduce the fundamental noise limits imposed by quantum mechanics on the fluctuations of the spin. The concepts of dipole, planar, and spin squeezing are introduced, and we demonstrate how to distinguish between these three forms of squeezing. In a series of examples, carried out in the context of spin operators describing dipole moments of two-level atoms, we illustrate how these different forms of squeezing in the spin variables can be produced and what their properties are, and to what degree the fluctuations of the spin variables can

Z. Ficek and R. Tanaś, *Quantum-Limit Spectroscopy*, Springer Series in Optical Sciences 200, DOI 10.1007/978-1-4939-3740-0_10

be squeezed. The planar squeezing has an interesting property that it can exhibit squeezing simultaneously in two components of the spin. This is possible owing to the fact that the $SU(2)$ algebra of the spin involves three quadrature components in contrast to the field variables that involve only two quadrature components. In addition, we use the relation between the field and atomic dipole variables, derived in Chap. 2, and discuss the relation between the quantum fluctuations of the field radiated by oscillating atomic dipoles, such as coherently driven two-level atoms. We show that the quantum fluctuations of the field variables are not always directly related in a simple fashion to the quantum fluctuations of the spin variables. Consequently, it is possible to find situations in which the quantum fluctuations of the field radiated by an atomic system are not squeezed even when the quantum fluctuations of the atomic spin variables are squeezed. The later part of the chapter is devoted to the relation between spin squeezing and entanglement. We compare spin squeezing with two measures of entanglement, concurrence, and negativity.

10.1 Dipole Squeezing in a Spin-$\frac{1}{2}$ System

In Chap. 2 the concept of squeezed states was introduced for the field variables. Squeezed states of the electromagnetic field were distinguished by the property that the quantum fluctuations in one of the two noncommuting quadrature components of the electromagnetic field are reduced below the vacuum limit. In principle, the concept of squeezed states can be introduced to any pair noncommuting Hermitian operators. The best known example of such operators that are directly connected to radiative properties of atoms are angular momentum or spin operators.

Consider the spin operator $\boldsymbol{S}$ of a spin-$\frac{1}{2}$ system. Physically, it usually consists of a two-level atom. We may express $\boldsymbol{S}$ in terms of its Cartesian components, S_x, S_y, S_z, which obey the familiar cyclic commutation relations

$$[S_i, S_j] = \mathrm{i}\epsilon_{ijk} S_k \,, \tag{10.1}$$

where suffixes i, j, k denote the components of the spin operator and ϵ_{ijk} is the Levi-Civita symbol. Hence, the quantum fluctuations associated with a pair of spin components S_i and S_j are limited by the Heisenberg uncertainty principle

$$\sqrt{\langle(\Delta S_i)^2\rangle\langle(\Delta S_j)^2\rangle} \geq \frac{1}{2}|\langle S_k\rangle| \,, \tag{10.2}$$

where $\Delta S_i = S_i - \langle S_i\rangle$. In the coherent state $\langle(\Delta S_i)^2\rangle = \langle(\Delta S_j)^2\rangle = \frac{1}{2}|\langle S_k\rangle|$. In analogy to the definition of squeezed states for the bosonic variables (2.47), we can define a squeezed state of the spin variables as one for which either of the following inequalities holds

$$\langle(\Delta S_i)^2\rangle < \frac{1}{2}|\langle S_k\rangle| \quad \text{or} \quad \langle(\Delta S_j)^2\rangle < \frac{1}{2}|\langle S_k\rangle|\,. \tag{10.3}$$

Spin states leading to reduced quantum fluctuations characterized by the inequalities (10.3) are called squeezed states of the i or j component of the spin. We shall later refer to the condition (10.3) as the "natural" definition of squeezing of the spin for the simple reason that (10.3) is a natural generalization of the definition (2.47) to the case of spin variables.

The definition (10.3) of squeezing in spin variables, although a natural generalization of the definition for boson variables, it is fundamentally different from (2.47). This is because the right-hand side of (10.3), the vacuum or shot-noise level of the spin fluctuations, $\frac{1}{2}|\langle S_k\rangle|$, depends explicitly on the state of the system. Consequently, the shot-noise or vacuum fluctuations of the spin components can vary with the varying state of the system. It is in contrast to the vacuum level of the fluctuations of the bosonic variables where the right-hand side of (2.47) is a constant independent of the state of the field.[1]

As an example illustrating the idea of squeezing in spin variables, we consider a practical model of a single two-level atom represented by a spin$\frac{1}{2}$ system with two energy states $|g\rangle$ and $|e\rangle$ separated by an energy $\hbar\omega_a$. The atom is characterized by the transition dipole moment $\boldsymbol{\mu}$ between the energy states which can be represented by spin raising and lowering operators $S^+ = |e\rangle\langle g|$ and $S^- = |g\rangle\langle e|$ as

$$\boldsymbol{\mu} = \boldsymbol{\mu}_{eg}S^+ + \boldsymbol{\mu}_{ge}S^-\,, \tag{10.4}$$

where $\boldsymbol{\mu}_{ij}$ is the dipole matrix element $\boldsymbol{\mu}_{ij} = \langle i|\,\boldsymbol{\mu}\,|j\rangle$ connecting atomic energy states i and j, $(i, j = g, e)$. For simplicity, we assume that the atom has no permanent dipole moments in its energy states, $\boldsymbol{\mu}_{gg} = \boldsymbol{\mu}_{ee} = 0$. Thus, quantum fluctuations of the atomic dipole moment can be studied in terms of the fluctuations of the components of the spin-$\frac{1}{2}$ system.

In order to examine squeezing in the spin variables, we evaluate the variances of the components S_x and S_y and readily find that

$$\begin{aligned}\left\langle(\Delta S_x)^2\right\rangle &= \frac{1}{4}\langle\left(S^+ + S^-\right)^2\rangle - \langle S_x\rangle^2 = \frac{1}{4} - \langle S_x\rangle^2\,,\\ \left\langle(\Delta S_y)^2\right\rangle &= -\frac{1}{4}\langle\left(S^+ - S^-\right)^2\rangle - \langle S_y\rangle^2 = \frac{1}{4} - \langle S_y\rangle^2\,,\end{aligned} \tag{10.5}$$

where we have used the fact that for the spin-$\frac{1}{2}$ system $(S^{\pm})^2 \equiv 0$. This simplifies the variances to depend solely on the average values of the x and y components of the spin. Equivalently, we may conclude that the fluctuations depend on the average

[1] The dependence of the right-hand side of (10.3) on the state involved means that an equality in (10.3) can be achieved for two distinct states. The equality can be achieved with or without of both sides reaching a local or absolute minimum value. States for which an equality is achieved with both sides reaching a local or absolute minimum are called the minimum uncertainty states. States for which only an equality is achieved are called the intelligent states [1–3].

atomic dipole moment. For this reason squeezing of a spin component is often called in the literature as dipole squeezing. This also shows that the condition for dipole squeezing is fundamentally different than that for squeezing in boson variables which required a two-photon nonlinear process. Dipole squeezing would be observed if a dipole moment were created in the atom [4]. As we shall see below, no two-photon process is required to create a nonzero dipole moment in the atom.

We introduce quantities F_x and F_y as direct indicators of the extent of squeezing in the x and y components of the spin

$$F_x \equiv \left\langle (\Delta S_x)^2 \right\rangle - \frac{1}{2}|\langle S_z \rangle| = \frac{1}{4} - \langle S_x \rangle^2 - \frac{1}{2}|\langle S_z \rangle|\,,$$
$$F_y \equiv \left\langle (\Delta S_y)^2 \right\rangle - \frac{1}{2}|\langle S_z \rangle| = \frac{1}{4} - \langle S_y \rangle^2 - \frac{1}{2}|\langle S_z \rangle|\,. \tag{10.6}$$

A negative value of either F_x or F_y will indicate squeezing of the x or y component of the spin, and the largest the negative value the greater the squeezing. Expressions (10.6) show, what seems to contradict with our intuition, that a larger vacuum level of the fluctuations means a smaller dipole moment required or, equivalently, easier to achieve squeezing.

To determine the smallest value of $\langle S_x \rangle$ or $\langle S_y \rangle$ required for squeezing to occur in the spin components, we must determine what are possible values the term $\frac{1}{2}|\langle S_z \rangle|$ could take in a spin-$\frac{1}{2}$ system. If we take the energies of the atomic states $|e\rangle$ and $|g\rangle$ to be $E_e = \frac{1}{2}\hbar\omega_a$ and $E_g = -\frac{1}{2}\hbar\omega_a$, respectively, the atomic energy is then given by $\hbar\omega_a S_z$, so that S_z is the atomic inversion operator. Maxima of the average inversion are $\langle S_z \rangle = \frac{1}{2}$ when the atom is in the state $|e\rangle$ and $\langle S_z \rangle = -\frac{1}{2}$ when it is in state $|g\rangle$. Hence, for any state of the atom $|\langle S_z \rangle| \leq \frac{1}{2}$, and therefore always $\frac{1}{2}|\langle S_z \rangle| \leq \frac{1}{4}$. It follows from (10.6) that in the limit of $\frac{1}{2}|\langle S_z \rangle| \approx \frac{1}{4}$, the squeezing quantities are

$$F_x \approx -\langle S_x \rangle^2\,, \quad F_y \approx -\langle S_y \rangle^2\,, \tag{10.7}$$

which indicate that, in general, there is no lower limit on the magnitude of the dipole moment; even a small $\langle S_x \rangle$ or $\langle S_y \rangle$ would lead to squeezing in the spin components. In addition, it suggests that large squeezing would be predicted if the vacuum level were maximized, $\frac{1}{2}|\langle S_z \rangle| \approx \frac{1}{4}$, and simultaneously a large dipole moment was created. However, this hope is unfounded because the preparation of the atom in a state at which $\frac{1}{2}|\langle S_z \rangle| \approx \frac{1}{4}$ is equally effective in destroying the atomic dipole moment. For atomic states at which $\frac{1}{2}|\langle S_z \rangle| = \frac{1}{4}$, the atomic dipole moment vanishes, $\langle S_x \rangle = \langle S_y \rangle = 0$. On the other hand, for atomic states at which $\frac{1}{2}|\langle S_z \rangle| < \frac{1}{4}$, the atomic dipole moment is different from zero and squeezing may occur. However, the average $\langle S_x \rangle$ or $\langle S_y \rangle$ must exceed a threshold value of $\frac{1}{4} - \frac{1}{2}|\langle S_z \rangle|$ for F_x or F_y to be negative.

To show this more explicitly, let us express the spin vector $\boldsymbol{S}$, which represents the state of the system, in terms of its spherical polar components S, θ, and ϕ, that are related to its Cartesian components by

$$S_x = S\sin\theta\cos\phi\,,\quad S_y = S\sin\theta\sin\phi\,,\quad S_z = S\cos\theta\,, \tag{10.8}$$

where S is the magnitude of the total spin of the system, $0 \le \theta \le \pi$ and $0 \le \phi \le 2\pi$. For a pure state $S = \frac{1}{2}$, and $S < \frac{1}{2}$ for a mixed state. A pure state is represented geometrically by points on a sphere of radius $S = \frac{1}{2}$. The north pole ($\theta = 0$) of this sphere corresponds to the upper (excited) state $|e\rangle$ of the atom and the south pole ($\theta = \pi$) to the lower (ground) state $|g\rangle$. Any other point corresponds to a superposition of these states that can be written as

$$|\psi_A\rangle = \cos\frac{\theta}{2}\,|e\rangle + \mathrm{e}^{\mathrm{i}\phi}\sin\frac{\theta}{2}\,|g\rangle\ . \tag{10.9}$$

The average values of the spin components specified by the polar variables are

$$\langle S_x\rangle = \frac{1}{2}\sin\theta\cos\phi\,,\quad \langle S_y\rangle = \frac{1}{2}\sin\theta\sin\phi\,,\quad \langle S_z\rangle = \frac{1}{2}\cos\theta\,, \tag{10.10}$$

from which it is easy to see that $\langle S_x\rangle$ and $\langle S_y\rangle$ are different from zero only if $\theta \neq 0$ or π. In this case, $|\langle S_z\rangle| < \frac{1}{2}$. When $\theta = 0$ or π, the atom is in its upper ($\theta = 0$) or in lower ($\theta = \pi$) energy state at which $\langle S_z\rangle = \pm\frac{1}{2}$, and there is no dipole moment, $\langle S_x\rangle = \langle S_y\rangle = 0$. This means that states with $\theta = 0, \pi$ cannot lead to squeezing of the spin components. The x and y components can be different from zero only if the system is in a superposition of the atomic energy states. This means that states with $\theta \neq 0, \pi$ can lead to squeezing.

We now make use of (10.10) to express (10.6) in terms of the polar variables and arrive to

$$\begin{aligned} F_x &= \frac{1}{4}\left(1 - \sin^2\theta\cos^2\phi - |\cos\theta|\right)\,,\\ F_y &= \frac{1}{4}\left(1 - \sin^2\theta\sin^2\phi - |\cos\theta|\right)\,. \end{aligned} \tag{10.11}$$

First, note that

$$F_x + F_y = \frac{1}{4}\left(1 - |\cos\theta|\right)^2\,, \tag{10.12}$$

which is always positive indicating that the x and y components of the spin cannot be simultaneously squeezed. For states with $\cos^2\phi = 1$, i.e., $\phi = n\pi$, we have

$$F_x = \frac{1}{4}|\cos\theta|\left(|\cos\theta| - 1\right)\,,\quad F_y = \frac{1}{4}\left(1 - |\cos\theta|\right)\,, \tag{10.13}$$

from which we see that squeezing is possible only in the x component and may occur for all values of θ except $\theta = 0$ and π, at which $F_x = F_y = 0$. The case of $\sin^2\phi = 1$ is obtained from (10.13) by exchanging $F_x \leftrightarrow F_y$. Note that for $\theta = \pi/2$ at which

the right-hand side of the Heisenberg uncertainty principle (10.2) is equal to zero, both F_x and F_y are nonnegative for all values of ϕ. It follows that squeezing of the spin components results from the noncommutivity of the operators S_x and S_y.

It is straightforward to show that the most negative value of F_x (or F_y), corresponding to optimum dipole squeezing is achieved for $\theta = \pi/3$ and $2\pi/3$, in which cases $F_x = -\frac{1}{16}$. It follows that the optimum squeezing is observable in principle only if the spin vector lies on a two-dimensional plane oriented in a direction set by the azimuthal angle $\phi = n\pi$, for the x component, or $\phi = (n + \frac{1}{2})\pi$ for the y component to be maximally squeezed.

The above considerations are illustrated in Fig. 10.1, which shows the variation of F_x with θ and ϕ. It is seen that $F_x > 0$ everywhere except for values of the azimuthal phase $\phi = 0$, π and 2π. For those phases squeezing is possible for all values of θ and the maximum squeezing of $(F_x)_{\min} = -\frac{1}{16}$ is achieved for $\theta = \pi/3$ and $2\pi/3$. However, for $\theta = \pi/2$ at which S_z vanishes, the variance $F_x \geq 0$ for all values of ϕ. At this value of θ the right-hand side of the Heisenberg uncertainty principle (10.2) is also equal to zero.

10.1.1 Application to Resonance Fluorescence

We now apply these considerations explicitly to the fluorescence field produced by a two-level atom. We consider a two-level atom of level spacing $\hbar\omega_a$, damping rate γ, and transition dipole moment $\boldsymbol{\mu}_{12}$, continuously driven by a coherent laser field whose the strength is characterized by the Rabi frequency Ω_0. Under the influence of the driving field, the atom is continuously re-excited by the field after emitting a fluorescent photon. This excitation reestablish the atomic dipole moment and makes it to oscillate continuously in time which produces more fluorescent photons.

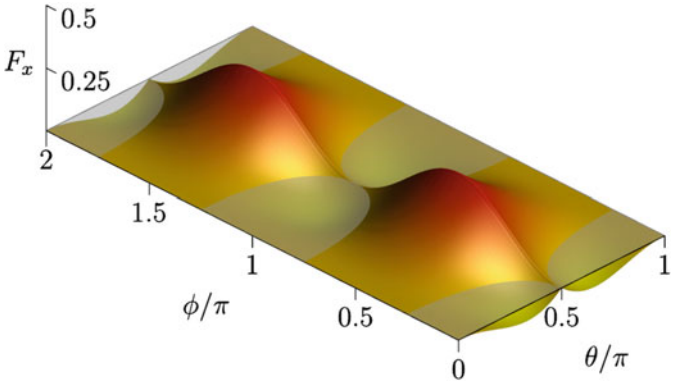

Fig. 10.1 The variation of the squeezing factor F_x with the spherical polar components θ and ϕ. Negative values of F_x indicate the presence of squeezing

As demonstrated in Chap. 1.6, expression (1.90), the fluorescence intensity is directly proportional to the expectation value of the atomic dipole operators. Therefore, we shall focus on squeezing properties of the atomic dipole moment that can be determined by evaluating the quantities F_x and F_y. We postpone the explicit evaluation of squeezing properties of the emitted fluorescence field to Sect. 10.3.

As we have seen, the evaluation of the squeezing factors requires the knowledge of the average values of the spin components, $S_x(t)$, $S_y(t)$ and $S_z(t)$. In order to find the average values we shall make use of the optical Bloch equations (3.17) that were derived in Sect. 3.1. If we restrict our analysis to the case in which the laser frequency is tuned exactly to the atomic transition frequency and the atom is in the ground state at time $t = 0$, the solutions of the Bloch equations are of the following form

$$\begin{aligned}
\langle S_x(t)\rangle &= \frac{-\gamma\,\Omega_0}{2\Omega_0^2+\gamma^2}\left[1-\mathrm{e}^{-\frac{3}{4}\gamma t}\left(\cos\Omega t-\frac{4\Omega_0^2-\gamma^2}{4\gamma\,\Omega}\sin\Omega t\right)\right],\\
\langle S_y(t)\rangle &= 0\,,\\
\langle S_z(t)\rangle &= \frac{-\frac{1}{2}\gamma^2}{2\Omega_0^2+\gamma^2}\left[1+\frac{2\Omega_0^2}{\gamma^2}\mathrm{e}^{-\frac{3}{4}\gamma t}\left(\cos\Omega t+\frac{3\gamma}{4\Omega}\sin\Omega t\right)\right], \qquad (10.14)
\end{aligned}$$

with $\Omega = (\Omega_0^2 - \frac{1}{16}\gamma^2)^{\frac{1}{2}}$.

Because $\langle S_y(t)\rangle = 0$, it makes that only the x component of the atomic dipole moment can be squeezed. When the results (10.14) are used in (10.6) for F_x, we readily find

$$\begin{aligned}
F_x(t) = \frac{1}{4} &- \frac{\gamma^2\Omega_0^2}{\left(2\Omega_0^2+\gamma^2\right)^2}\left[1-\mathrm{e}^{-\frac{3}{4}\gamma t}\left(\cos\Omega t-\frac{4\Omega_0^2-\gamma^2}{4\gamma\,\Omega}\sin\Omega t\right)\right]^2\\
&- \frac{1}{4}\frac{\gamma^2}{2\Omega_0^2+\gamma^2}\left|1+\frac{2\Omega_0^2}{\gamma^2}\mathrm{e}^{-\frac{3}{4}\gamma t}\left(\cos\Omega t+\frac{3\gamma}{4\Omega}\sin\Omega t\right)\right|, \qquad (10.15)
\end{aligned}$$

which shows that the squeezing factor will oscillate in time at the Rabi frequency Ω, but with the amplitude decreasing in time with the rate γ.

Before examining the transient behavior of the factor $F_x(t)$, let us first consider its steady-state properties. By taking the limit $t \to \infty$, the expression (10.15) simplifies to

$$F_x(\infty) = \frac{1}{2}\Omega_0^2\frac{\left(2\Omega_0^2-\gamma^2\right)}{\left(2\Omega_0^2+\gamma^2\right)^2}\,, \qquad (10.16)$$

from which it is seen that $\Omega_0 < \gamma/\sqrt{2}$ is the condition for squeezing in the steady state and the most negative value of $F_x(\infty)$ is achieved when $\Omega_0 = \gamma/\sqrt{6}$, in which case $F_x(\infty) = -\frac{1}{32}$. Thus, the steady-state squeezing occurs only in the restricted range of the Rabi frequency and the maximum value of the steady-state squeezing is twice as smaller as the optimum value possible in the spin-$\frac{1}{2}$ system.

As we have already mentioned, in the steady state the atomic dipole does not show as much squeezing as it was predicted by the expression (10.13), and the squeezing also occurs in a restricted range of the Rabi frequency Ω_0. In searching for a better squeezing in the system, we extend our analysis to the transient regime and study the time evolution of the squeezing factor $F_x(t)$ from its initial value at $t = 0$.

An example of the time evolution of F_x and its variation with the Rabi frequency is shown in Fig. 10.2. For small Rabi frequencies squeezing is seen to occur at longer times and shifts toward shorter times as Ω_0 increases. The effect of increasing Rabi frequency is also to increase the amount of squeezing and to shift the maximum squeezing, the minimum value of F_x, toward a shorter time. It is apparent that optimum squeezing of $F_x = -\frac{1}{16}$ is reached at the time $t \approx 0.2/\gamma$ when $\Omega_0 \geq 5\gamma$. Thus, optimum dipole squeezing in a two-level atom may be produced via strong-field excitation of the atom.

We conclude this section with a brief comment about some complications that may arise in an attempt to extend the definition of squeezing (10.3) to the normally ordered average values of the atomic dipole operators. We ascribe the term "normally ordered" to average values in which operator products are ordered such that all the spin raising operators S^+ appear to the left of the lowering operators S^-. The normally ordered variances $\langle :(\Delta S_x)^2: \rangle$ and $\langle :(\Delta S_y)^2: \rangle$ are simply related to the conventional variances as

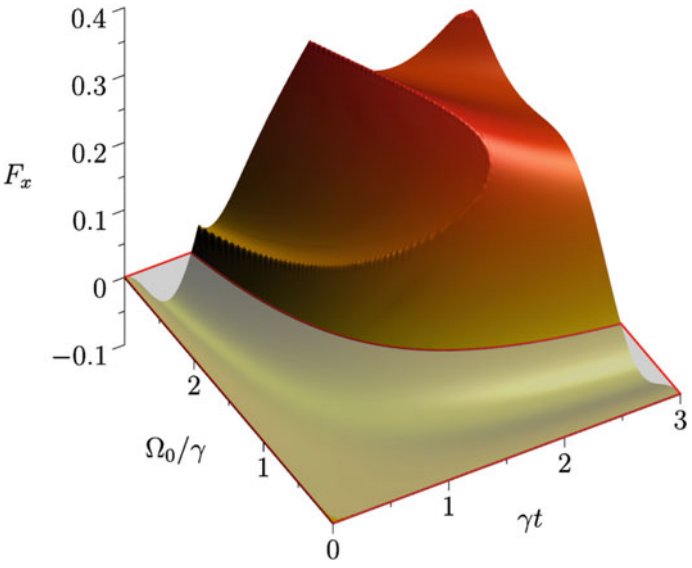

Fig. 10.2 Variation of the quantity F_x with time γt and the Rabi frequency Ω_0/γ

$$\langle :(\Delta S_x)^2: \rangle = \langle (\Delta S_x)^2 \rangle + \frac{1}{2}\langle S_z \rangle ,$$
$$\langle :(\Delta S_y)^2: \rangle = \langle (\Delta S_y)^2 \rangle + \frac{1}{2}\langle S_z \rangle . \tag{10.17}$$

It is easily verified that the criterion for squeezing (10.3) is equivalent to the condition that either

$$\langle :(\Delta S_x)^2: \rangle - \frac{1}{2}\langle S_z \rangle - \frac{1}{2}\,|\langle S_z \rangle| < 0 ,$$
or
$$\langle :(\Delta S_y)^2: \rangle - \frac{1}{2}\langle S_z \rangle - \frac{1}{2}\,|\langle S_z \rangle| < 0 . \tag{10.18}$$

It follows that, in general, the squeezing condition (10.3) does not imply negative values of the normally ordered variances. Evidently, an additional condition is required that the average inversion $\langle S_z \rangle$ should be negative for $\langle :(\Delta S_x)^2: \rangle < 0$ or $\langle :(\Delta S_y)^2: \rangle < 0$ to imply squeezing. For a positive $\langle S_z \rangle$, the dipole is squeezed if either

$$\langle :(\Delta S_x)^2: \rangle < \langle S_z \rangle , \quad \text{or} \quad \langle :(\Delta S_y)^2: \rangle < \langle S_z \rangle . \tag{10.19}$$

Thus, it is possible that the spin components may exhibit squeezing even though their normally ordered variances are positive.

Barnett [5], see also [6–8], proposed to use the antinormally ordered variances of the atomic dipole moment to quantify dipole squeezing when $\langle S_z \rangle$ is positive. Antinormally ordered average values have operator product ordered such that all the raising operators S^+ appear to the right of the lowering S^- operators. The antinormally ordered variances $\langle \dot{:}(\Delta S_x)^2 \dot{:} \rangle$ and $\langle \dot{:}(\Delta S_y)^2 \dot{:} \rangle$ are related to the conventional variances as

$$\langle \dot{:}(\Delta S_x)^2 \dot{:} \rangle = \langle (\Delta S_x)^2 \rangle - \frac{1}{2}\langle S_z \rangle ,$$
$$\langle \dot{:}(\Delta S_y)^2 \dot{:} \rangle = \langle (\Delta S_y)^2 \rangle - \frac{1}{2}\langle S_z \rangle , \tag{10.20}$$

and then the criterion for squeezing (10.3) is equivalent to the condition that either

$$\langle \dot{:}(\Delta S_x)^2 \dot{:} \rangle + \frac{1}{2}\langle S_z \rangle - \frac{1}{2}\,|\langle S_z \rangle| < 0 ,$$
or
$$\langle \dot{:}(\Delta S_y)^2 \dot{:} \rangle + \frac{1}{2}\langle S_z \rangle - \frac{1}{2}\,|\langle S_z \rangle| < 0 . \tag{10.21}$$

Clearly, if $\langle S_z \rangle$ is positive the condition (10.21) reduces to

$$\langle :(\Delta S_x)^2: \rangle < 0 \quad \text{or} \quad \langle :(\Delta S_y)^2: \rangle < 0\,, \tag{10.22}$$

for the dipole moment to be squeezed. We may summarize that the squeezing criterion (10.3) is equivalent to the condition that the normally or antinormally ordered variance of either S_x or S_y component of the spin is negative.

In the practical situation of a driven two-level atom, the atomic inversion (10.14) oscillates in time between positive and negative values. This is illustrated in Fig. 10.3 where we plot the time evolution of $\langle S_z(t) \rangle$ for several different values of the Rabi frequency Ω_0. It is apparent that $\langle S_z(t) \rangle$ oscillates in time and at some periods of time $\langle S_z(t) \rangle$ takes positive values. However, in the steady state $\langle S_z(\infty) \rangle$ is negative for all Ω_0. Thus, we may conclude that as long as $\langle S_z(t) \rangle$ is negative, $\langle :(\Delta S_x)^2: \rangle < 0$ or $\langle :(\Delta S_y)^2: \rangle < 0$ implies dipole squeezing. As we have seen this condition can be realized in the steady state but in the transient regime it can be satisfied only in some period of time. When $\langle S_z(t) \rangle$ is positive, $\langle :(\Delta S_x)^2: \rangle < 0$ or $\langle :(\Delta S_y)^2: \rangle < 0$ implies dipole squeezing.

We will return to this problem in Sect. 10.3, where we discuss a general relationship between the fluctuations of the radiation field emitted by two-level atoms and squeezing of the atomic dipole moments.

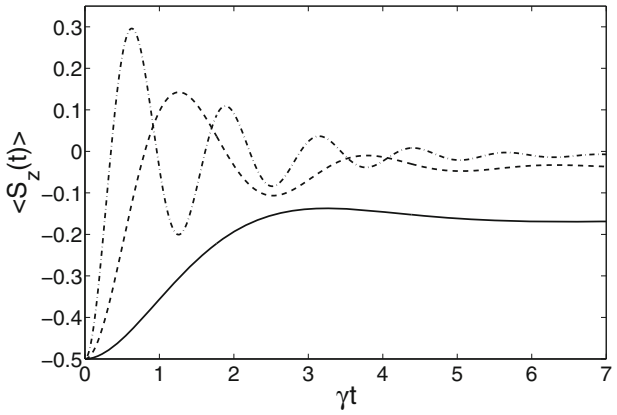

Fig. 10.3 Time evolution of the atomic inversion $\langle S_z(t) \rangle$, as given by the expression (10.14), plotted for several values of the Rabi frequency Ω_0: $\Omega_0 = \gamma$ (*solid line*), $\Omega_0 = 2.5\gamma$ (*dashed line*), and $\Omega_0 = 5\gamma$ (*dashed-dotted line*)

10.2 Dipole Squeezing in a Spin-$\frac{N}{2}$ System

The concept of dipole squeezing can be extended to a collection of $N > 1$ spin-$\frac{1}{2}$ systems. For example, N two-level atoms. The systems can be composed of few atoms or an ensemble of large number of atoms confined to a finite volume, or arranged in a linear chain or a plane. The linear dimensions of the area occupied by the atoms can be large or small compared with the radiation wavelength.

We define the total (collective) dipole raising and lowering operators

$$S^+ = \sum_{i=1}^{N} S_i^+ \mathrm{e}^{\mathrm{i}\boldsymbol{k}\cdot\boldsymbol{R}_i}\,, \quad S^- = \sum_{i=1}^{N} S_i^- \mathrm{e}^{-\mathrm{i}\boldsymbol{k}\cdot\boldsymbol{R}_i}\,, \tag{10.23}$$

where the phase factors $\exp(\pm\mathrm{i}\boldsymbol{k}\cdot\boldsymbol{R}_i)$ model the spatial redistribution of the atoms. Then, we define collective operators, S_x, S_y, and S_z, the Cartesian components of the collective spin

$$S_x = \frac{1}{2}(S^+ + S^-)\,, \quad S_y = \frac{\mathrm{i}}{2}(S^+ - S^-)\,, \quad S_z = \sum_{i=1}^{N} S_z^i\,. \tag{10.24}$$

It is straightforward to verify that these operators satisfy the usual angular momentum commutation relations

$$[S_i, S_j] = \mathrm{i}\epsilon_{ijk} S_k\,, \quad i, j, k = x, y, z\,. \tag{10.25}$$

The commutation relation (10.25) prompts us to write the uncertainty relation

$$\sqrt{\langle(\Delta S_i)^2\rangle\langle(\Delta S_j)^2\rangle} \geq \frac{1}{2}|\langle S_k\rangle|\,, \tag{10.26}$$

from which we obtain the condition for squeezing that either

$$\langle(\Delta S_i)^2\rangle < \frac{1}{2}|\langle S_k\rangle| \quad \text{or} \quad \langle(\Delta S_j)^2\rangle < \frac{1}{2}|\langle S_k\rangle|\,. \tag{10.27}$$

When comparing (10.27) with (10.3), one could argue that there are no differences between the conditions for squeezing of the collective and those of a single spin-$\frac{1}{2}$ dipole operators. The conditions (10.27) are formally the same as (10.3), the corresponding ones for a dipole squeezing in a single spin-$\frac{1}{2}$ system.

Although it is not explicitly seen, the variance (10.27) is different from the variance (10.3). For example, if we expand the variance of the x component of the collective spin, we arrive to the following expression:

$$\langle(\Delta S_x)^2\rangle = \frac{1}{2}\left(\langle S^+S^-\rangle - \langle S_z\rangle\right) + \frac{1}{4}\left(\langle S^+S^+\rangle + \langle S^-S^-\rangle\right) - \langle S_x\rangle^2 . \tag{10.28}$$

The important difference is that in the present case there are terms involving squares of the dipole operators, $(S^+)^2$ and $(S^-)^2$. Such terms vanish of course when the system consists of a single spin. In mathematical terms, the presence of these terms is a consequence of the fact that the square of the collective spin-up or spin-down operator is not in general equal to zero:

$$\left(S^{\pm}\right)^2 = \sum_{i=1}^{N}\sum_{j\neq i=1}^{N} S_i^{\pm}S_j^{\pm}\mathrm{e}^{\pm\mathrm{i}\boldsymbol{k}\cdot(\boldsymbol{R}_i+\boldsymbol{R}_j)} , \tag{10.29}$$

since products of spin-raising or spin-lowering operators belonging to different atoms ($i \neq j$) are nonzero.

Thus, the variance of the collective spin may be said to be characterized by dipole operators and squares of the dipole operators. The averages $\langle S^+S^+\rangle$ and $\langle S^-S^-\rangle$ in (10.28) reflect the addition of multiatom effects to those of single atom effects already discussed in the preceding section. In physical terms, the presence of those terms is a manifestation of two-photon absorption and emission processes that may occur in multiatom systems. This can easily be understood by considering the energy-level structure of a multiatom system. For a better clarity, let us illustrate this on a simple example of a system composed of $N = 2$ atoms only. In the case of two identical and noninteracting atoms of lower and upper energy states $|g_i\rangle$, $|e_i\rangle$ $(i = 1, 2)$, the Hilbert space of the system is spanned by a complete orthonormal set of four state vectors

$$\begin{aligned} |1\rangle &= |g_1\rangle \otimes |g_2\rangle , \quad |2\rangle = |e_1\rangle \otimes |g_2\rangle , \\ |3\rangle &= |g_1\rangle \otimes |e_2\rangle , \quad |4\rangle = |e_1\rangle \otimes |e_2\rangle , \end{aligned} \tag{10.30}$$

with the corresponding energies

$$E_1 = -\hbar\omega_a , \quad E_2 = E_3 = 0 , \quad E_4 = \hbar\omega_a . \tag{10.31}$$

The state $|1\rangle$ is the ground state corresponding to no excitation present in the system, the states $|2\rangle$ and $|3\rangle$ are single-quantum states corresponding to a single excitation present in either atom 1 or 2, and the state $|4\rangle$ is a double-quantum state corresponding to single excitations present in each atom.

Figure 10.4 shows the energy-level structure of the system with possible transitions. We see that apart from single-photon transitions from the double-quantum state $|4\rangle$ to the single-quantum states $|2\rangle$ and $|3\rangle$, and from the single-quantum states to the ground state $|1\rangle$, there are possible two-photon transitions from $|4\rangle$ to the state $|1\rangle$. These transitions involve a simultaneous absorption or emission of two photons,

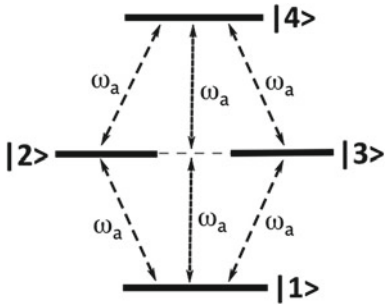

Fig. 10.4 An energy-level scheme of a system composed of two independent two-level atoms each of the transition frequency ω_a

as indicated in Fig. 10.4. We may note an important point, the two-photon transition $|4\rangle \leftrightarrow |1\rangle$ has no dipole moment. It is easy to show. The matrix element of the transition dipole moment between the energy states $|4\rangle$ and $|1\rangle$ is

$$\begin{aligned}\langle 4|\,\boldsymbol{\mu}\,|1\rangle &= \langle 4|\,(\boldsymbol{\mu}_1+\boldsymbol{\mu}_2)\,|1\rangle = \langle e_1|\,\langle e_2|\,\boldsymbol{\mu}_1\,|g_1\rangle\,|g_2\rangle + \langle e_1|\,\langle e_2|\,\boldsymbol{\mu}_2\,|g_1\rangle\,|g_2\rangle \\ &= \boldsymbol{\mu}_{ge}^{(1)}\,\langle e_2|\,g_2\rangle + \boldsymbol{\mu}_{ge}^{(2)}\,\langle e_1|\,g_1\rangle = 0\,,\end{aligned} \tag{10.32}$$

since $\langle e_1|\,g_1\rangle = 0$ and $\langle e_2|\,g_2\rangle = 0$.

Returning to (10.28), we find convenient to write the variance in terms of the normally ordered operators

$$\langle(\Delta S_x)^2\rangle = \langle :(\Delta S_x)^2: \rangle - \frac{1}{2}\langle S_z\rangle\,, \tag{10.33}$$

where $\langle :(\Delta S_x)^2: \rangle$ can be written as

$$\langle :(\Delta S_x)^2: \rangle = \frac{1}{2}\langle S^+S^-\rangle - \langle S_x\rangle^2 + \frac{1}{2}\langle A_x\rangle\,, \tag{10.34}$$

with

$$\langle A_x\rangle \equiv \frac{1}{2}(\langle S^+S^+\rangle + \langle S^-S^-\rangle)\,. \tag{10.35}$$

It is seen that there are three terms contributing to $\langle :(\Delta S_x)^2: \rangle$. The physical consequences of the three terms are as follows: The first term $\langle S^+S^-\rangle$, familiar from the definition of the radiation intensity, is always positive. It satisfies the nonnegative definiteness condition that for an arbitrary operator $\hat{O}$, $\langle \hat{O}^\dagger \hat{O}\rangle \geq 0$. It sets the level of fluctuations that have to be beaten for the variance to be negative. The second term $\langle S_x\rangle^2$ represents the contribution of a component of the average dipole moment. Finally, the third term $\langle A_x\rangle$ represents a multispin or collective contribution that involves two-photon correlation functions. Note that, in general, the correlation functions $\langle S^\pm S^\pm\rangle$ are complex. For this reason, the functions are often referred to as anomalous correlation functions. However, $\langle A_x\rangle$ is always real and may be either

positive or negative. This makes the term very interesting that if $\langle A_x \rangle$ is sufficiently large and negative, it may reduce the variance below the threshold for squeezing even if $\langle S_x \rangle$ is zero.

The contributions from the average dipole moment and from the two-photon correlations represent two fundamental processes by which the fluctuations of the total spin of a collective system may be reduced below the threshold for squeezing. These constitute two "sources" of squeezing in a multiatom system.

One can notice from (10.34) that $\langle : (\Delta S_x)^2 : \rangle$ can be reduced below the threshold for squeezing in several different situations, for example, when either $\langle S_x \rangle \neq 0$, $\langle A_x \rangle = 0$ or $\langle S_x \rangle = 0$, $\langle A_x \rangle \neq 0$. Another interesting situation, which according to (10.33) could be the most effective in the generation of squeezing, is that of $\langle S_x \rangle \neq 0$ and $\langle A_x \rangle < 0$. Let us discuss in more detail the situation in which one could encounter either $\langle S_x \rangle \neq 0$, $\langle A_x \rangle = 0$ or $\langle S_x \rangle = 0$, $\langle A_x \rangle \neq 0$. The situation of $\langle S_x \rangle \neq 0$ and $\langle A_x \rangle < 0$ requires a special attention and will be discussed separately in the following section.

To illustrate the generation of squeezing in the cases $\langle S_x \rangle \neq 0$, $\langle A_x \rangle = 0$ and $\langle S_x \rangle = 0$, $\langle A_x \rangle \neq 0$, we require an atomic system in which either the average values of the dipole raising and lowering operators or the average value of the square of the operators are nonzero. Such a situation may be realized by employing a three-level atom in a ladder configuration or in a system composed of two two-level atoms. We concentrate here on the system of two identical two-level atoms.

In order to distinguish between the contributions of $\langle S_x \rangle$ and $\langle A_x \rangle$ to $\langle : (\Delta S_x)^2 : \rangle$, we have to include the dipole–dipole interaction Ω_{12} to the dynamics of the atoms that shifts of the single-quantum states from their resonant values. As a result of the shift, the single-photon transitions, at which $\langle S_x \rangle$ dominates over $\langle A_x \rangle$, occur at frequencies $\omega_a \pm \Omega_{12}$, whereas the two-photon transitions, at which $\langle A_x \rangle$ dominates over $\langle S_x \rangle$, occur at frequency ω_a. For a large Ω_{12}, the one- and two-photon transitions should be well separated and then one could easily distinguish between squeezing produced by $\langle S_x \rangle$ and that produced by $\langle A_x \rangle$.

As it was shown in Chap. 4, the dipole–dipole interaction not only shifts the energies of the single-quantum states but also leads to collective states of the system by creating the symmetric $|s\rangle$ and antisymmetric $|a\rangle$ superpositions of the single-quantum states. We may associate the expectation values $\langle S_x \rangle$ and $\langle A_x \rangle$ with the coherences between the collective states

$$\langle S_x \rangle = \frac{1}{\sqrt{2}} \left(\varrho_{es} + \varrho_{sg} + \varrho_{se} + \varrho_{gs} \right) , \quad \langle A_x \rangle = \frac{1}{2} \left(\varrho_{eg} + \varrho_{ge} \right) . \tag{10.36}$$

We see that there is a clear physical distinction between $\langle S_x \rangle$ and $\langle A_x \rangle$. The quantity $\langle S_x \rangle$ is a real part of the sum of one-photon coherences between the collective states, $\varrho_{es} + \varrho_{sg}$, whereas $\langle A_x \rangle$ is a real part of two-photon coherence ϱ_{eg}. It is interesting to note that $\langle S_x \rangle$ contains coherences that involve the ground $|g\rangle$, upper $|e\rangle$, and the symmetric $|s\rangle$ states only. There are no contributions from coherences involving the antisymmetric state $|a\rangle$. The reason is that $\langle S_x \rangle$ is the symmetrical combination of

the atomic raising and lowering operators and as such it then involves coherences only between the symmetric states of the system.

We now demonstrate that squeezing can be generated in the two-atom system by both one- and two-photon coherences. We consider two identical two-level atoms, each of transition frequency ω_a, damping rate γ, separated by a distance $\boldsymbol{R}_{12}$ and driven by a coherent laser field of the Rabi frequency Ω. We assume that the atoms are separated by a small distance at which the dipole–dipole interaction is important and we use the results derived in Chap. 3 for the steady-state values of the atomic correlation functions to derive an analytical expression for $\langle : (\Delta S_x)^2 : \rangle$. We then obtain

$$\begin{aligned}\langle : (\Delta S_x)^2 : \rangle = \frac{\Omega^2}{2D^2} \Big\{ & D\left(\gamma^2 + 4\Delta_L^2 + \Omega^2\right) \\ & - \frac{1}{2}\left[2\gamma\Omega^2 + (\gamma + \gamma_{12})\left(\gamma^2 + 4\Delta_L^2\right)\right]^2 \\ & + D\left[\frac{1}{4}\gamma(\gamma + \gamma_{12}) - \Delta_L(\Delta_L - \Omega_{12})\right]\Big\}, \end{aligned} \tag{10.37}$$

with $D = \Omega^4 + (\gamma^2 + 4\Delta_L^2)\Omega^2 + (\gamma^2 + 4\Delta_L^2)[\frac{1}{4}(\gamma + \gamma_{12})^2 + (\Delta_L - \Omega_{12})^2]$. It is not difficult to verify from the steady-state solutions that the average inversion $\langle S_z \rangle$ is negative for all values of the parameters involved. Thus, according to (10.18), the condition for dipole squeezing is $\langle : (\Delta S_x)^2 : \rangle < 0$.

The normally ordered variance (10.37) has been plotted in Fig. 10.5 as a function of the laser detuning Δ_L and the Rabi frequency Ω of the driving field for a small separation between the atoms ($R_{12} = 0.05\lambda$). At that separation $\gamma_{12} \approx 0.97\gamma$ and $\Omega_{12} \approx 23\gamma$. It is seen from Fig. 10.5 that for a weak driving field there is a large squeezing generated at a detuning equal to the dipole–dipole frequency shift Ω_{12} and outside that frequency $\langle : (\Delta S_x)^2 : \rangle = 0$. The detuning $\Delta_L = \Omega_{12}$ corresponds to the laser frequency on resonance with the frequency of the $|s\rangle \rightarrow |g\rangle$ transition. In this situation the two-atom system behaves not as a true four-level system but as an effective two-level system. For this reason, squeezing generated by an effective two-level system might reasonably be called "two-level squeezing".

The magnitude of the two-level squeezing depends strongly on the Rabi frequency. As the Rabi frequency Ω is increased from small to large values, the two-level squeezing decreases and simultaneously a squeezing develops at $\Delta_L = 0$. Clearly, with an increasing Ω there is a switching of the squeezing generation from the detuning $\Delta_L = \Omega_{12}$ to $\Delta_L = 0$.

In order to understand the origin of squeezing at the detunings $\Delta_L = 0$ and $\Delta_L = \Omega_{12}$, we plot in Fig. 10.6 the quantities $\langle S_x \rangle^2$ and $\langle A_x \rangle$ as a function of Δ_L for two different values of the Rabi frequency. When the atoms are driven by a weak laser field, the quantity $\langle S_x \rangle^2$, which involves one-photon coherences exhibits a pronounced peak at $\Delta_L = \Omega_{12}$ while the quantity $\langle A_x \rangle$, which involves two-photon

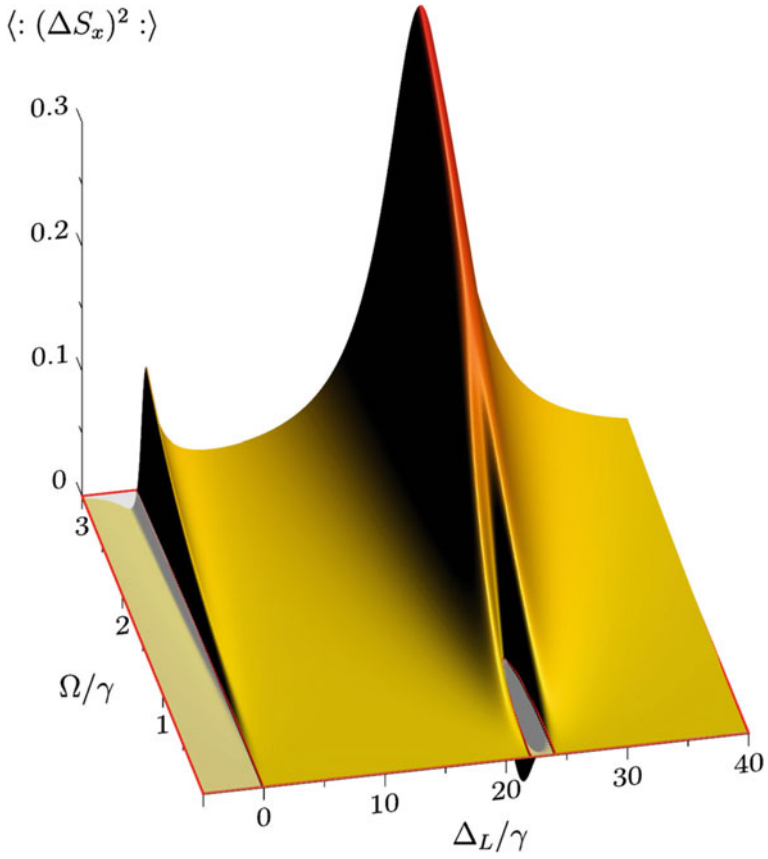

Fig. 10.5 Variation of the normally ordered variance $\langle : (\Delta S_x)^2 : \rangle$ with the laser detuning Δ_L and the Rabi frequency Ω for $\bar{\boldsymbol{\mu}} \perp \bar{\boldsymbol{R}}_{12}$ and $R_{12} = 0.05\lambda$

coherences, is practically zero for all Δ_L with a very small dispersive structure at $\Delta_L = 0$. Clearly, the origin of the squeezing at $\Delta_L = \Omega_{12}$ is in the one-photon coherence ϱ_{sg}. For a strong driving field, an enhancement of $\langle A_x \rangle$ is seen at $\Delta_L = 0$, thus provides the dominant contribution to the normally ordered variance. This clearly indicates that the origin of the squeezing at $\Delta_L = 0$ is in the two-photon coherence ϱ_{eg}. Since the two-photon coherence can be created in a system composed of a least two atoms, this type of squeezing might reasonably be called "multiatom squeezing". In fact, it corresponds to spin squeezing, the concept of multiatom squeezing solely generated by the two-photon coherence. We shall discuss the concept and properties of spin squeezing in detail in Sect. 10.5.

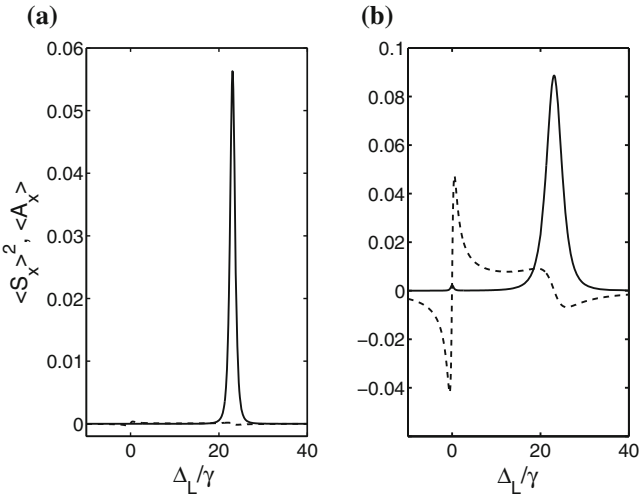

Fig. 10.6 The quantities $\langle S_x \rangle^2$ (*solid line*) and $\langle A_x \rangle$ (*dashed line*) plotted as a function of the laser detuning Δ_L for $\bar{\boldsymbol{\mu}} \perp \bar{\boldsymbol{R}}_{12}$, $R_{12} = 0.05\lambda$ and different Ω: **a** $\Omega = .25\gamma$, **b** $\Omega = 3\gamma$

10.3 Atomic Dipole Squeezing and Field Squeezing

We have demonstrated in Sect. 10.1.1 that a two-level atom driven by a coherent laser field can produce dipole squeezing. The squeezing is intrinsically connected to a nonzero dipole moment of the atom. According to (1.90), the emitted field operators are linearly proportional to the atomic dipole operators. Therefore, one could expect that squeezing in the dipole fluctuations should lead to squeezing in the fluorescence field fluctuations. Unfortunately, this is not always true that squeezing in the fluctuations of the atomic dipoles is linearly proportional to squeezing in the fluctuations of the radiation field emitted by the dipoles.

In this section, we examine a relationship between the fluctuations of the atomic dipole moments and the fluctuations of the field emitted. In order to establish this relationship, we consider the positive frequency part of the field detected at a point $\boldsymbol{r}$ far from the atom is given by the formula (1.31), which for the case of a single two-level atom located at the origin is given by

$$\hat{\boldsymbol{E}}^{(+)}(\boldsymbol{r}, t) = \hat{\boldsymbol{E}}_F^{(+)}(\boldsymbol{r}, t) + \boldsymbol{\Psi}_{eg}(\boldsymbol{r}) S^+(t) \,, \tag{10.38}$$

where $\boldsymbol{\Psi}_{eg}(\boldsymbol{r})$ is the geometrical factor, $S^+(t) \equiv \hat{\Lambda}_{eg}^n(t)$ is the atomic spin raising operator, and $\hat{\boldsymbol{E}}_F^{(+)}(\boldsymbol{r}, t)$ is the free field amplitude. The analysis we present here, although formulated for a single atom, is quite general and may be applied to an arbitrary number of atoms.

If the free field at the position of the detector is in the vacuum state, that $\hat{\boldsymbol{E}}_F^{(+)}(\boldsymbol{r},t)\,|0\rangle \equiv 0$, then the fluctuations of the quadrature components of the fluorescence field are given by

$$\begin{aligned}\langle(\Delta\hat{\boldsymbol{E}}_x(\boldsymbol{r},t))^2\rangle &= \boldsymbol{\Psi}_{eg}^2(\boldsymbol{r})\left\langle(\Delta S_x)^2\right\rangle ,\\ \langle(\Delta\hat{\boldsymbol{E}}_y(\boldsymbol{r},t))^2\rangle &= \boldsymbol{\Psi}_{eg}^2(\boldsymbol{r})\left\langle(\Delta S_y)^2\right\rangle .\end{aligned} \tag{10.39}$$

The fluctuations of the fluorescence field components are thus completely determined by fluctuations of the atomic dipole moment, $\langle(\Delta S_x)^2\rangle$ and $\langle(\Delta S_y)^2\rangle$, respectively. The field fluctuations are directly measurable in schemes involving homodyne or heterodyne detection, as demonstrated in Chap. 1, and give information about squeezing of the field.

Let us return to the definition of squeezing in the field components. As we have seen, the usual way to identify squeezing in the field components is to test for the condition that either

$$\langle(\Delta\hat{\boldsymbol{E}}_x(\boldsymbol{r},t))^2\rangle < C \quad \text{or} \quad \langle(\Delta\hat{\boldsymbol{E}}_y(\boldsymbol{r},t))^2\rangle < C\ , \tag{10.40}$$

where C is a positive constant. An equivalent condition, which is more convenient in the study of the relation between squeezing in the field and dipole components, is that written in terms of the normally ordered expectation values

$$\langle{:}\,(\Delta\hat{\boldsymbol{E}}_x(\boldsymbol{r},t))^2\,{:}\rangle < 0 \quad \text{or} \quad \langle{:}\,(\Delta\hat{\boldsymbol{E}}_y(\boldsymbol{r},t))^2\,{:}\rangle < 0\ , \tag{10.41}$$

where

$$\begin{aligned}\langle{:}\,(\Delta\hat{\boldsymbol{E}}_x(\boldsymbol{r},t))^2\,{:}\rangle &= \boldsymbol{\Psi}_{eg}^2(\boldsymbol{r})\left\langle{:}\,(\Delta S_x)^2\,{:}\right\rangle ,\\ \langle{:}\,(\Delta\hat{\boldsymbol{E}}_y(\boldsymbol{r},t))^2\,{:}\rangle &= \boldsymbol{\Psi}_{eg}^2(\boldsymbol{r})\left\langle{:}\,(\Delta S_y)^2\,{:}\right\rangle .\end{aligned} \tag{10.42}$$

These expressions reveal the linear relation between the normally ordered variances of the field and the dipole operators. This implies that, for example, the x component of the fluorescence field is negative if $\langle{:}\,(\Delta S_x)^2\,{:}\rangle$ is negative. A negative value of $\langle{:}\,(\Delta\hat{\boldsymbol{E}}_x(\boldsymbol{r},t))^2\,{:}\rangle$ means squeezing in the x component of the fluorescence field. However, $\langle{:}\,(\Delta S_x)^2\,{:}\rangle < 0$ does not necessary mean squeezing in the x component of the atomic dipole moment. According to (10.18), the x component of the atomic dipole moment is squeezed if

$$\langle{:}(\Delta S_x)^2{:}\rangle < \frac{1}{2}\langle S_z\rangle + \frac{1}{2}\,|\langle S_z\rangle|\ . \tag{10.43}$$

This shows that the x component of the dipole moment can be squeezed even though $\langle{:}\,(\Delta S_x)^2\,{:}\rangle$ is positive. Since $\langle S_z\rangle$ can be positive as well as negative, it is then

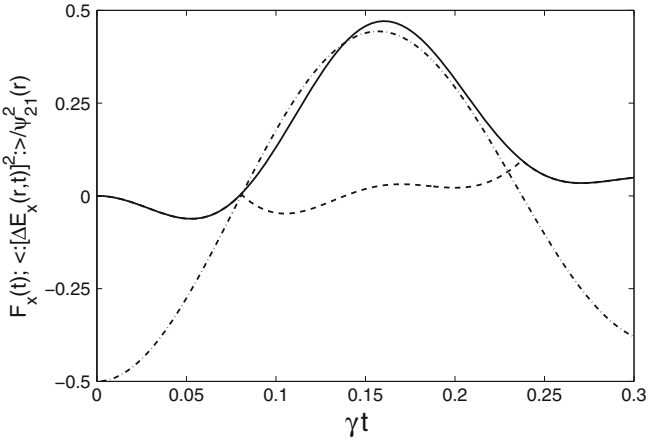

Fig. 10.7 Time evolution of the normally ordered variance of the fluorescence field $\langle :(\Delta \hat{\boldsymbol{E}}_x(\boldsymbol{r}, t))^2 : \rangle$ (*solid line*) and the dipole squeezing factor $F_x(t)$ (*dashed line*), as given in (10.15), for a two-level atom driven by a coherent laser field of the Rabi frequency $\Omega_0 = 20\gamma$. The atom was initially in the ground state. The dashed-dotted line shows the time evolution of the atomic inversion $\langle S_z \rangle$

clear from (10.43) that *only* for a negative $\langle S_z \rangle$, the condition for squeezing in the x component of the dipole moment is equivalent to the requirement that $\langle :(\Delta S_x)^2 : \rangle < 0$.

Thus, we conclude that squeezing will be produced in the fluorescence field if both the normally ordered variance of the atomic dipole operators and the average atomic inversion are negative. An example of this situation is shown in Fig. 10.7, where we contrast the normally ordered variance of the fluorescence field with the dipole squeezing factor F_x. We see that squeezing occurs at short times and is initially large but disappears quickly as time progresses. The dependence of the field squeezing on the sign of $\langle S_z \rangle$ is clearly evident. At times when $\langle S_z \rangle$ is negative, a squeezed atomic dipole moment generates squeezed light, whereas at times where $\langle S_z \rangle$ is positive, the squeezed dipole moment does not produce squeezing in the radiated field. Clearly, the generation of squeezing in the radiation field is strongly dependent on the expectation value of the atomic inversion [5–7, 9, 10].

10.4 Planar Squeezing

In this section, we shall illustrate the concept of planar squeezing, introduced by He et al. [11, 12], which is an interesting modification of the concept of dipole squeezing discussed in the above section. The idea of planar squeezing is to look for reduced (squeezed) fluctuations of the total spin vector $\boldsymbol{S}$ in a plane the vector $\boldsymbol{S}$ lies. In this case, the expectation value of the spin vector has only two components with the other component equal to zero. For example, if the expectation value of the spin vector $\langle \boldsymbol{S} \rangle$ lies in the $X - Y$ plane such that it forms an angle ϕ with the x-axis

$$\langle S_x\rangle = S\cos\phi\,, \quad \langle S_y\rangle = S\sin\phi\,, \quad \langle S_z\rangle = 0\,, \tag{10.44}$$

where $S = \sqrt{\langle S_x\rangle^2 + \langle S_y\rangle^2}$ and $\tan\phi = \langle S_y\rangle/\langle S_x\rangle$.

In this case, the following Heisenberg uncertainty principles are obeyed

$$\begin{aligned}
&\sqrt{\langle(\Delta S_x)^2\rangle\langle(\Delta S_y)^2\rangle} \geq 0\,, \quad X-Y \text{ plane}\,,\\
&\sqrt{\langle(\Delta S_y)^2\rangle\langle(\Delta S_z)^2\rangle} \geq \frac{1}{2}|\langle S_x\rangle|\,, \quad Y-Z \text{ plane}\,,\\
&\sqrt{\langle(\Delta S_z)^2\rangle\langle(\Delta S_x)^2\rangle} \geq \frac{1}{2}|\langle S_y\rangle|\,, \quad Z-X \text{ plane}\,.
\end{aligned} \tag{10.45}$$

From the uncertainty relation in the $X-Y$ plane, we see that there is no lower limit to the fluctuations of the quadrature variances $\langle(\Delta S_x)^2\rangle$ and $\langle(\Delta S_y)^2\rangle$. In other words, both quadratures $\langle(\Delta S_x)^2\rangle$ and $\langle(\Delta S_y)^2\rangle$ can simultaneously be reduced below the quantum limit, with the uncertainty being absorbed by the z component. This is in contrast to the dipole squeezing where only the fluctuations in one of the quadratures can be reduced below the quantum limit with the fluctuations in both the other components greatly increased above the quantum limit. Example of the error ellipsoide for planar squeezing is illustrated in Fig. 10.8.

Although the right-hand side of the uncertainty relation in the $X-Y$ plane is equal to zero, the variances of S_x and S_y cannot be simultaneously zero, that it is not possible to choose a state of the total spin such that both variances $\langle(\Delta S_x)^2\rangle$ and $\langle(\Delta S_y)^2\rangle$ are zero. This is because the variance of the z component, perpendicular to the direction of the average spin vector, is limited, according to (10.45) by the Heisenberg uncertainty relations.

Let us consider an example that illustrates a possible application of the concept of planar squeezing just considered. In the example, we shall demonstrate that the concept of planar squeezing can be used to improve the precision in determining of an unknown rotation (phase shift) of a spin state.

Suppose that the total spin vector $\boldsymbol{S}$ lies in the $X-Y$ plane and, with no loss of generality, we choose axis such that $\boldsymbol{S}$ is oriented in the x direction, so that

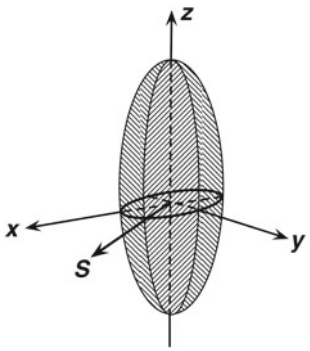

Fig. 10.8 Illustration of the concept of planar squeezing. The spin vector $\boldsymbol{S}$ lies in the $X-Y$ plane. Since $\langle S_z\rangle = 0$, the fluctuations of the x and y components can simultaneously be reduced (squeezed) below the quantum limit

$\langle S_y\rangle = \langle S_z\rangle = 0$. Let us now rotate the spin around the z-axis with an angle ϕ. After the rotation, the magnitude of the spin vector, $\tilde{S}(\phi) = |\tilde{\boldsymbol{S}}(\phi)|$, is

$$\tilde{S}(\phi) = S_x \cos\phi + S_y \sin\phi \,, \tag{10.46}$$

where $\tilde{S}(\phi)$ is the spin after the rotation. We then have for the variance and the average value of the rotated spin

$$\begin{aligned} \langle[\Delta\tilde{S}(\phi)]^2\rangle &= \langle(\Delta S_x)^2\rangle\cos^2\phi + \langle(\Delta S_y)^2\rangle\sin^2\phi + \mathrm{cov}(S_x, S_y)\sin 2\phi \,, \\ \langle\tilde{S}(\phi)\rangle &= \langle S_x\rangle\cos\phi \,, \end{aligned} \tag{10.47}$$

where $\mathrm{cov}(S_x, S_y) \equiv \frac{1}{2}\langle S_x S_y + S_y S_x\rangle - \langle S_x\rangle\langle S_y\rangle$ is the covariance.

To evaluate the precision to which the angle ϕ can be determined, we use the definition (9.10) of the uncertainty $\Delta\phi$, and find that in a state where $\mathrm{cov}(S_x, S_y) = 0$, the precision is

$$\Delta\phi = \frac{\Delta\tilde{S}(\phi)}{\left|\partial\langle\tilde{S}(\phi)\rangle/\partial\phi\right|} = \frac{\sqrt{\langle(\Delta S_x)^2\rangle\cos^2\phi + \langle(\Delta S_y)^2\rangle\sin^2\phi}}{|\langle S_x\rangle\sin\phi|} \,. \tag{10.48}$$

We see that the total noise of the rotated spin is determined by the planar variance. Therefore, the precision in determining ϕ can be improved by planar squeezing, in which $\langle(\Delta S_x)^2\rangle$ and $\langle(\Delta S_y)^2\rangle$ can be simultaneously reduced below the quantum limit.

10.5 Spin Squeezing

In this section, we explain the concept of spin squeezing, in particular, what makes spin squeezing different from the dipole and planar squeezing considered in the preceding sections. Unfortunately, the notion of spin squeezing is not unique in the literature. There are several different definitions of the spin squeezing parameter which is used to determine the degree of spin squeezing [13, 14]. The definition depends on the context where squeezing is considered and were introduced for certain considerations. We shall discuss the concept of introducing the spin squeezing parameter following the definition introduced by Kitagawa and Ueda [15]. It has been widely used to identify nonclassical states in atomic and molecular systems and, the most importantly, it is has been recognized as a good measure of multiparticle entanglement. As we shall see, the spin squeezing parameter introduced by Kitagawa and Ueda is qualitatively equivalent to the negativity and concurrence, the criteria for pairwise entanglement.

There are at least three reasons for studying spin squeezing. The first of these is simply to study further the idea of reducing quantum noise below the quantum limit.

The second reason is to gain a deeper understanding of the role of the multiatom correlations in the reduction of the noise below the quantum limit. Spin squeezing parameters only involve the second-order correlation functions (moments) of the collective angular momentum operators. The involvement of the collective operators makes spin squeezing very useful in the many-body physics, in particular, in the Bose–Einstein condensates, where particles cannot be addressed individually, only the collective operators can be measured. The third reason is that spin squeezing is significant for both entanglement detection and high-precision measurements.

The basic idea of spin squeezing is simple and is illustrated in Fig. 10.9. Suppose that in a Cartesian coordinate system (x, y, z), the total spin has the components $\boldsymbol{S} = (S_x, S_y, S_z)$. We would like to make a rotation of the coordinates such that in a new coordinate system (n_1, n_2, n_3) the average spin vector $\langle \boldsymbol{S} \rangle$ would have only one nonzero component. To illustrate this, we make a double rotation of the Cartesian coordinates with a polar angle θ and an azimuthal angle ϕ and arrive at

$$\boldsymbol{S} = S_{n_1}\hat{n}_1 + S_{n_2}\hat{n}_2 + S_{n_3}\hat{n}_3 \,, \tag{10.49}$$

where $\hat{n}_i$ $(i = 1, 2, 3)$ is the unit vector in the n_i direction, and the components S_{n_i} are related to the Cartesian components by the equations

$$\begin{aligned} S_{n_1} &= S_x \cos\theta\cos\phi + S_y \cos\theta \sin\phi - S_z \sin\theta \,, \\ S_{n_2} &= -S_x \sin\phi + S_y \cos\phi \,, \\ S_{n_3} &= S_x \sin\theta\cos\phi + S_y \sin\theta \sin\phi + S_z \cos\theta \,. \end{aligned} \tag{10.50}$$

As it is illustrated in Fig. 10.9, the axis $\boldsymbol{n_1}$ and $\boldsymbol{n_2}$ lie in the N_s plane and $\boldsymbol{n_3}$ is normal to the plane.

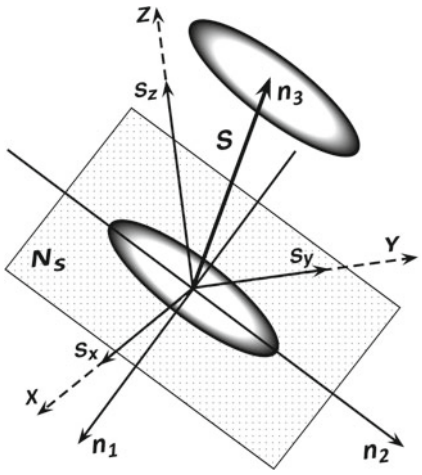

Fig. 10.9 Space relation between the components of the total spin vector $\boldsymbol{S}$. In the Cartesian coordinate system, the spin vector has components (S_x, S_y, S_z). In a doubly rotated coordinate system (n_1, n_2, n_3) the spin vector is aligned along the $\boldsymbol{n}_3$ axis, so that $\boldsymbol{n}_1$ and $\boldsymbol{n}_2$ lie in the plane N_s normal to $\boldsymbol{S}$

Since we would like the average spin $\langle \boldsymbol{S} \rangle$ to be oriented in the direction normal to the plane N_s, we find from (10.50) that the average values of the components S_{n_1} and S_{n_2} vanish when

$$\tan\phi = \frac{\langle S_y \rangle}{\langle S_x \rangle} \quad \text{and} \quad \tan\theta = \frac{\sqrt{\langle S_x \rangle^2 + \langle S_y \rangle^2}}{\langle S_z \rangle} \,. \tag{10.51}$$

We now see that by a suitable rotation of the coordinates, we are able to find directions at which the average values of the spin components S_{n_1} and S_{n_2} are zero, $\langle S_{n_1} \rangle = \langle S_{n_2} \rangle = 0$. Physically, it corresponds to the lack of the average dipole moment in the $\boldsymbol{n}_1$ and $\boldsymbol{n}_2$ directions.

In the directions $\boldsymbol{n}_1$ and $\boldsymbol{n}_2$, the average dipole moment is zero, but the variances of the operators S_{n_1} and S_{n_2} are, in general, nonzero. It is easily verified from (10.50) that the components S_{n_i} satisfy the the usual angular momentum commutation relations

$$[S_{n_i}, S_{n_j}] = \mathrm{i}\epsilon_{ijk} S_{n_k} \,, \quad i, j, k = 1, 2, 3 \,, \tag{10.52}$$

from which the fluctuations in S_{n_1} and S_{n_2} are constrained by the uncertainty relation

$$\sqrt{\langle (\Delta S_{n_1})^2 \rangle \langle (\Delta S_{n_2})^2 \rangle} \geq \frac{1}{2} |\langle S_{n_3} \rangle| \,. \tag{10.53}$$

Then the fluctuations of the spin are squeezed if the variance of one of the spin components satisfies the condition

$$\langle (\Delta S_{n_i})^2 \rangle \leq \frac{1}{2} |\langle S_{n_3} \rangle| \,, \quad i = 1, 2 \,. \tag{10.54}$$

Thus, instead of measuring fluctuations of the spin components S_x, S_y or S_z, we may chose to measure fluctuations of the spin components S_{n_1} or S_{n_2} that lie in the plane N_s normal to the direction of the total spin and have average values equal to zero, $\langle S_{n_1} \rangle = \langle S_{n_2} \rangle = 0$. We then have

$$\begin{aligned}
\langle (\Delta S_{n_1})^2 \rangle &= \frac{1}{4} \left(\langle S^+ S^- \rangle + \langle S^- S^+ \rangle \right) \cos^2\theta + \langle S_z^2 \rangle \sin^2\theta \\
&\quad + \frac{1}{2} \left(\langle A_x \rangle \cos 2\phi + \langle A_y \rangle \sin 2\phi \right) \cos^2\theta \\
&\quad - \frac{1}{4} \left[\left(\langle S^+ S_z \rangle + \langle S_z S^+ \rangle \right) \mathrm{e}^{-\mathrm{i}\phi} + \text{c.c.} \right] \sin 2\theta \,, \\
\langle (\Delta S_{n_2})^2 \rangle &= \frac{1}{4} \left(\langle S^+ S^- \rangle + \langle S^- S^+ \rangle \right) \\
&\quad - \frac{1}{2} \langle A_x \rangle \cos 2\phi - \frac{1}{2} \langle A_y \rangle \sin 2\phi \,,
\end{aligned} \tag{10.55}$$

where

$$\langle A_y \rangle = \frac{1}{2\mathrm{i}} \left(\langle S^+ S^+ \rangle - \langle S^- S^- \rangle \right) . \tag{10.56}$$

When $\langle S_{n_1} \rangle = \langle S_{n_2} \rangle = 0$, the absolute value of $\langle S_{n_3} \rangle$ is equal to the magnitude of the total spin, $|\langle S_{n_3} \rangle| = \langle S \rangle$. This suggests to introduce a parameter

$$\xi^H_{n_i} \equiv \frac{\langle (\Delta S_{n_i})^2 \rangle}{\frac{1}{2} |\langle S_{n_3} \rangle|} , \quad i = 1, 2 , \tag{10.57}$$

as a measure of the degree of spin squeezing. The superscript H refers to the Heisenberg uncertainty principle. Whenever $\xi^H_{n_i} < 1$, there is spin squeezing in the system. Evidently, the rotation to the coordinate system (n_1, n_2, n_3) makes an important difference in the nature of the fluctuations and then squeezing of the S_{n_i} components of the spin. The variance in (10.57) depends only on the multiatom correlations with no contribution from the average value of the atomic dipole moment. Referring to (10.33), the rotation of the coordinates such that $\langle S_{n_1} \rangle$ and $\langle S_{n_2} \rangle$ are both zero is equivalent of extracting squeezing generated by $\langle A_x \rangle$ from those generated by $\langle S_x \rangle$ when simultaneously $\langle S_x \rangle \neq 0$ and $\langle A_x \rangle \neq 0$. In other words, the variances $\langle (\Delta S_{n_1})^2 \rangle$ and $\langle (\Delta S_{n_2})^2 \rangle$ involve only the two-photon coherences with no any contribution from the first-order coherences. This makes squeezing generated solely by the multiatom correlations different from the dipole squeezing and is referred to as spin squeezing.

However, the definition of the spin squeezing parameter (10.57) is not unique. As we have already mentioned, there are several different definitions of the spin squeezing parameter present in the literature [13, 14]. For example, Kitagawa and Ueda proposed a slightly different definition [15], that instead of taking the ratio between the variance $\langle (\Delta S_{n_i})^2 \rangle$ and the one half of the absolute value of the average value of the total spin, $|\langle S_{n_3} \rangle|/2$, they proposed to take a ratio between the variance and the one half of the total spin of a given system, $S/2$:

$$\xi^S_{n_i} \equiv \frac{\langle (\Delta S_{n_i})^2 \rangle}{\frac{1}{2} S} , \quad i = 1, 2 , \tag{10.58}$$

where the superscript S refers to the total spin S.

Comparing (10.58) with (10.57), we find that the definitions are related to each other through

$$\xi^S_{n_i} = \left(\frac{|\langle S_{n_3} \rangle|}{S} \right) \xi^H_{n_i} . \tag{10.59}$$

Since $S \geq |\langle S_{n_3} \rangle|$, it is apparent from (10.59) that $\xi^S_{n_i} \leq \xi^H_{n_i}$. Evidently, $\xi^H_{n_i}$ is a stronger condition for spin squeezing than $\xi^S_{n_i} < 1$.

Note that these two definitions coincide, $\xi^S_{n_i} = \xi^H_{n_i}$ when $|\langle S_{n_3} \rangle| = S$. Such a situation one can encounter in a system composed of a large number of spins,

where we can introduce a bosonic representation of the atomic operators. In this approach, we make use of the Holstein–Primakoff representation [16] that transforms the collective atomic operators into harmonic oscillator annihilation and creation operators $\hat{c}$ and $\hat{c}^\dagger$ of a single bosonic mode

$$S^+ = \hat{c}^\dagger \sqrt{N - \hat{c}^\dagger \hat{c}}, \quad S_z = \hat{c}^\dagger \hat{c} - N/2 \,. \tag{10.60}$$

If the number of atoms in the excited state is much smaller than the total number of atoms, i.e., $\langle \hat{c}^\dagger \hat{c} \rangle \ll N$, we can expand the square root in (10.60) and neglect terms of the order of $O(1/N)$. Then the collective atomic operators can be approximated as

$$S^+ \approx \sqrt{N} \hat{c}^\dagger \,, \quad S_z \approx -N/2 \,. \tag{10.61}$$

Evidently, $|\langle S_z \rangle| = S = N/2$, that $|\langle S_{n_3} \rangle|$ is equal to the magnitude of the total spin. For this reason, the parameter $\xi^S_{n_i}$ is often called as the analogue of bosonic squeezing.

We now illustrate the above analysis by examining three examples where spin squeezing could be generated. In all of the examples, we consider two identical two-level atoms located at a small distance that the atomic dipole moments could behave collectively. In the first, we demonstrate the occurrence of spin squeezing if the atoms are prepared in a suitable superposition state. In the second example, we show that atoms can decay to a pure spin squeezed state if located in a broadband squeezed vacuum field. Finally, we show that the system of two atoms interacting with a coherent laser field can be dynamically driven to a spin squeezed state.

Example 1: Atoms Initially Prepared in a Two-Photon State

The simplest technique for generating spin squeezing would be by preparing a system composed of two two-level atoms in a superposition state

$$|\eta\rangle = \cos\eta \, |g_1, g_2\rangle + \sin\eta e^{i\psi} \, |e_1, e_2\rangle \,, \tag{10.62}$$

which is a superposition of only the ground and the upper states of the two-atom system. The parameter η is defined in the range $(0, \pi/2)$, and ψ is defined in the range $(0, 2\pi)$. We note that the system prepared in the state (10.62) exhibits strong two-photon correlations, that

$$\langle \eta | \, A_x \, | \eta \rangle = \sin(2\eta) \cos\psi \,, \quad \langle \eta | \, A_y \, | \eta \rangle = -\sin(2\eta) \sin\psi \,. \tag{10.63}$$

The correlations are maximal when $\eta = \pi/4$ and $\psi = 0$ or $\pi/2$, in which case $\langle \eta | \, A_{x(y)} \, | \eta \rangle = \pm 1$ and the superposition state (10.62) becomes a maximally entangled state. On the other hand, the correlations vanish when $\eta = 0$ and $\eta = \pi/2$, at which the state (10.63) reduces, respectively, to the ground and upper states of the system.

It should be noted here, that if the system is prepared in a superposition state involving a single excitation state and the ground state

$$|\zeta\rangle = \cos\zeta\,|g_1 g_2\rangle + \sin\zeta e^{i\psi}\,|e_1 g_2\rangle\ , \tag{10.64}$$

then no spin squeezing will be generated. It is easily verified that in the state (10.64), the two-photon correlations are zero, $\langle A_x\rangle = 0$ and $\langle A_y\rangle = 0$. Nevertheless, the system prepared in the state (10.64) may exhibit dipole squeezing since the average values of the dipole operators can be nonzero

$$\langle\zeta|\,S_x\,|\zeta\rangle = \frac{1}{2}\sin(2\zeta)\cos\psi\,, \quad \langle\zeta|\,S_y\,|\zeta\rangle = -\frac{1}{2}\sin(2\zeta)\sin\psi\,. \tag{10.65}$$

Clearly, dipole squeezing can be created for all values of ζ except those discrete values of ζ, $(\zeta = 0, \pi/2, \pi)$, for which the superposition state reduces to either $|g_1 g_2\rangle$ or $|e_1 g_2\rangle$.

To examine the occurrence of spin squeezing in the system prepared in the state (10.62) we must look first at the average values of the Cartesian components of the collective spin, S_x, S_y, S_z, to see how to make a rotation to new coordinates (n_1, n_2, n_3) in which the total spin would have only one component. A simple calculation using (10.62) shows that

$$\langle\eta|\,S_x\,|\eta\rangle = 0\,, \quad \langle\eta|\,S_y\,|\eta\rangle = 0\,, \quad \langle\eta|\,S_z\,|\eta\rangle = \cos(2\eta)\,. \tag{10.66}$$

We see that the average values of the x and y components of the spin are zero. This means no rotation to a new reference frame is required that the Cartesian system is a suitable coordinate system in which we can search for spin squeezing. In other words, $(n_1, n_2, n_3) = (x, y, z)$ and squeezing of the fluctuations of either S_x or S_y component will correspond to spin squeezing.

We next use (10.63) and (10.66) to evaluate the spin squeezing parameters, as defined in (10.57). For $\theta = \phi = 0$ the parameters take the following forms:

$$\begin{aligned} \xi_{n_1} &\equiv \xi_x = [1 + \sin(2\eta)\cos\psi]\ , \\ \xi_{n_2} &\equiv \xi_y = [1 - \sin(2\eta)\cos\psi]\ . \end{aligned} \tag{10.67}$$

Since $\sin(2\eta)$ is positive for all values of η, $\eta \in (0, \pi/2)$, the expressions (10.67) show that the phase ψ determines which component of the collective spin may be squeezed. When the phase ψ is chosen so that $\cos\psi > 0$, spin squeezing may occur in the y component, $\xi_y < 1$, whereas with $\cos\psi < 0$ spin squeezing may occur in the x component of the spin. Note that the case of $\cos\psi > 0$ corresponds to symmetric superposition states $|\eta\rangle$, while $\cos\psi < 0$ corresponds to antisymmetric superposition states. In both cases, perfect spin squeezing of $\xi_x = 0$ or $\xi_y = 0$ is obtained for $\eta = \pi/4$, at which the state $|\eta\rangle$ is a maximally entangled state. The state $|\eta\rangle$ that exhibits spin squeezing is referred to as a spin squeezed state.

To complete the discussion of this example, we would like to point out that with a specific choice of the phase ψ, the spin squeezed state (10.62) becomes a minimum uncertainty state for all η. If the phase ψ is chosen such that $\cos\psi = 1$, it is then straightforward to show that

$$\sqrt{\langle(\Delta S_{n_1})^2\rangle\langle(\Delta S_{n_2})^2\rangle} = \frac{S}{2}\sqrt{\xi_{n_1}\xi_{n_2}} = \frac{1}{2}|\cos(2\eta)| = \frac{1}{2}|\langle S_{n_3}\rangle| \,. \tag{10.68}$$

Thus, with the choice of the phase such that $\cos\psi = 1$, the spin squeezed state (10.62) becomes a minimum uncertainty state with reduced fluctuations in S_y. A change of the phase to $\cos\psi = -1$ results in a minimum uncertainty state with reduced fluctuations in S_x. Hence, the change of the phase ψ is accomplished by the transfer of the fluctuations from the y to the x component of the collective spin.

Example 2: Atoms Damped by a Squeezed Vacuum Field

As a second example, we consider a system of two two-level atoms interacting with a broadband squeezed vacuum field which is characterized by strong two-photon correlations. The correlations create two-photon transitions in the atomic system transferring population from the ground state $|g\rangle$ to the upper state $|e\rangle$ without population of the intermediate states $|s\rangle$ and $|a\rangle$. To make the situation as simple as possible, we assume that the atoms are separated by a distance much smaller than the atomic transition wavelength and interact only with squeezed vacuum modes. We also take the phase of the squeezed vacuum $\psi_s = 0$ for maximum squeezing in one of the quadratures of the vacuum field.

Under the influence of the squeezed vacuum field, the expectation values of the spin components in the steady state are

$$\langle S_x\rangle = \langle S_y\rangle = 0 \,, \quad \langle S_z\rangle = -\frac{(2N+1)^2 - 4M^2}{(2N+1)(3N^2+3N+1-3M^2)} \,, \tag{10.69}$$

and

$$\langle S^+S^-\rangle + \langle S^-S^+\rangle = 2\left[1 + \frac{N(N+1) - M^2}{3N^2+3N+1-3M^2}\right] \,,$$
$$\langle S^+S^+\rangle = \langle S^-S^-\rangle = \frac{M}{(2N+1)(3N^2+3N+1-3M^2)} \,, \tag{10.70}$$

where N is the number of photons in the modes of the squeezed field and $M \leq \sqrt{N(N+1)}$ determined the degree of correlations between the modes.

Since $\langle S_x\rangle$ and $\langle S_y\rangle$ are zero, we can determine spin squeezing in the xy plane without any rotation. Thus, substituting (10.70) in (10.57) and taking into account that $\theta = \phi = 0$, we obtain

$$\xi_{n_1} = \frac{(2N+1)(4N^2+4N+1-4M^2)+2M}{(2N+1)(3N^2+3N+1-3M^2)} ,$$
$$\xi_{n_2} = \frac{(2N+1)(4N^2+4N+1-4M^2)-2M}{(2N+1)(3N^2+3N+1-3M^2)} . \tag{10.71}$$

It follows from (10.71) that depending on whether M is positive or negative, either ξ_{n_1} or ξ_{n2} can be reduced below one. Let us examine the spin squeezing parameters for $M > 0$ more closely. It is apparent from (10.71) that in this case only ξ_{n_2} can be reduced below one. For a thermal field, one sets $M = 0$, and the parameters can be shown to greater than one irrespective of the value of N. For a classically squeezed field, for which $M = N$, the parameter ξ_{n_2} reduces to

$$\xi_{n_2} = 1 + \frac{N(2N-1)}{(2N+1)(3N+1)} , \tag{10.72}$$

which is smaller than one whenever $N < \frac{1}{2}$. Hence, spin squeezing may occur but is restricted to small N. For a quantum squeezed field, for which $M = \sqrt{N(N+1)}$, the parameter ξ_{n_2} becomes

$$\xi_{n_2} = 1 - \frac{2\sqrt{N(N+1)}}{(2N+1)} . \tag{10.73}$$

It is clear that ξ_{n_2} is always smaller than one, so spin squeezing occurs for all N, and ξ_{n_2} achieves its minimum value of $\xi_{n_2} = 0$ at $N \to \infty$. In this case, we may speak of perfect spin squeezing.

It is easily verified from (10.69) and the uncertainty relation (10.53) that for the quantum squeezed vacuum with $M = \sqrt{N(N+1)}$, the spin squeezing (10.73) corresponds to a minimum uncertainty state. If one concerns about the explicit form of the state, the procedure is to write the density operator ϱ of the two-atom system in the basis of the collective (Dicke) states $\{|g\rangle , |a\rangle , |s\rangle , |e\rangle\}$, in which ϱ takes the form

$$\varrho = \begin{pmatrix} \varrho_{gg} & 0 & 0 & \varrho_{ge} \\ 0 & 0 & 0 & 0 \\ 0 & 0 & \varrho_{ss} & 0 \\ \varrho_{eg} & 0 & 0 & \varrho_{ee} \end{pmatrix} . \tag{10.74}$$

The diagonalization of (10.74) results in superposition states

$$|\eta_1\rangle = \left[(P_1 - \varrho_{ee})\,|g\rangle + \varrho_{eg}\,|e\rangle\right] / \sqrt{(P_1 - \varrho_{ee})^2 + \left|\varrho_{eg}\right|^2} ,$$
$$|\eta_2\rangle = \left[\varrho_{ge}\,|g\rangle + \left(P_2 - \varrho_{gg}\right)|e\rangle\right] / \sqrt{\left(P_2 - \varrho_{gg}\right)^2 + \left|\varrho_{eg}\right|^2} ,$$
$$|\eta_3\rangle = |s\rangle ,$$
$$|\eta_4\rangle = |a\rangle , \tag{10.75}$$

with the corresponding eigenvalues

$$
\begin{aligned}
P_1 &= \frac{1}{2}\left(\varrho_{gg}+\varrho_{ee}\right)+\frac{1}{2}\sqrt{\left(\varrho_{gg}-\varrho_{ee}\right)^2+4\left|\varrho_{eg}\right|^2}\,,\\
P_2 &= \frac{1}{2}\left(\varrho_{gg}+\varrho_{ee}\right)-\frac{1}{2}\sqrt{\left(\varrho_{gg}-\varrho_{ee}\right)^2+4\left|\varrho_{eg}\right|^2}\,,\\
P_3 &= \varrho_{ss}\,,\\
P_4 &= 0\,.
\end{aligned}
\tag{10.76}
$$

In general, the states (10.75) are mixed states. However, for perfect correlations $|\tilde{M}|^2=\tilde{N}(\tilde{N}+1)$ the populations P_2 and P_3 are zero leaving the population only in the state $|\eta_1\rangle$. Hence, the state $|\eta_1\rangle$ is a pure state of the system of two atoms driven by a squeezed vacuum field.

From (10.75), we find that the pure entangled state $|\eta_1\rangle$ is given by

$$
|\eta\rangle=\sqrt{\frac{N+1}{2N+1}}\,|g_1,g_2\rangle+\sqrt{\frac{N}{2N+1}}\,|e_1,e_2\rangle\ , \tag{10.77}
$$

The pure state (10.77) is nonmaximally entangled state, it reduces to a maximally entangled state for $N\gg 1$. The entangled state is analogous to the pairwise atomic state or the multiatom squeezed state, predicted in the small sample model of two coupled atoms.

The pure entangled state $|\eta_1\rangle$ is characteristic not only of the two-atom Dicke model, but in general of the Dicke model of an even number of atoms. The N-atom Dicke system interacting with a squeezed vacuum can decay to a state in which the density operator is given by

$$
\varrho=C_n\left(\mu S^-+\nu S^+\right)^{-1}\left(\mu S^++\nu S^-\right)^{-1}\ , \tag{10.78}
$$

if N is odd, or

$$
\varrho=|\Upsilon\rangle\langle\Upsilon|\ , \tag{10.79}
$$

if N is even, where C_n is the normalization constant, $S^{\pm}$ are the collective atomic operators, $\mu^2=\nu^2+1=\tilde{N}+1$, and $|\Upsilon\rangle$ is defined by

$$
\left(\mu S^-+\nu S^+\right)|\Upsilon\rangle=0\,. \tag{10.80}
$$

Thus, for an even number of atoms the stationary state of the system is the pure pairwise atomic state.

Example 3: Two Atoms Driven by a Coherent Field

Consider now a system of two dipole–dipole interacting atoms, damped by the ordinary vacuum field and driven by a coherent laser field. As demonstrated earlier in Sect. 10.2 of this chapter, two dipole–dipole interacting and coherently driven atoms

can produce squeezing in the steady-state fluorescence at two different detunings of the laser field from the atomic resonance. The variance $\langle : (\Delta S_x)^2 : \rangle \equiv F_{\theta=0}$, shown in Fig. 10.5, exhibits not only the large squeezing at finite detuning Δ_L, but also a small squeezing near $\Delta_L = 0$. In contrast to the squeezing at finite Δ_L, which is an example of dipole squeezing, the source of squeezing at $\Delta_L = 0$ is not easy to understand. In this example, we shall demonstrate that the squeezing effect at $\Delta_L = 0$ is intrinsically connected to the two-photon coherence and, in fact, is an example of spin squeezing.

For clarity, we simplify the calculations assuming that the angular frequency of the quadrature components $\omega = \omega_L$ and the fluorescence field is observed in the direction perpendicular to the interatomic axis, $\bar{r} \perp \boldsymbol{R}_{12}$. This choice, of course, involves no loss of generality. In this case, the normally ordered variance $\langle : \Delta \boldsymbol{E}_\theta^2 : \rangle$, written in terms of the density matrix elements of the collective system reads

$$F_\theta \equiv \frac{\langle : \Delta \boldsymbol{E}_\theta^2 : \rangle}{\Psi_{eg}(\boldsymbol{r})} = \frac{1}{4} \left\{ 2\varrho_{ee} + 2\varrho_{ss} + \varrho_{eg} \mathrm{e}^{2\mathrm{i}\theta} + \varrho_{ge} \mathrm{e}^{-2\mathrm{i}\theta} - \left[\left(\varrho_{es} + \varrho_{sg} \right) \mathrm{e}^{\mathrm{i}\theta} + \left(\varrho_{se} + \varrho_{gs} \right) \mathrm{e}^{-\mathrm{i}\theta} \right]^2 \right\} . \tag{10.81}$$

This equation shows that the variance depends on phase θ not only through the one-photon coherences ϱ_{es} and ϱ_{sg}, but also through the two-photon coherences ϱ_{eg} and ϱ_{ge}. This dependence suggests that there are two different processes that can lead to squeezing in the two-atom system. The one-photon coherences cause squeezing near one-photon resonances $|e\rangle \to |s\rangle$ and $|s\rangle \to |g\rangle$, whereas the two-photon coherences cause squeezing near the two-photon resonance $|g\rangle \to |e\rangle$.

In order to evaluate the variance (10.81), we make use the analytical solutions (4.33) for the steady-state populations and coherences, which were derived in Sect. 4.2.2. It is not difficult to find from (4.33) that at $\Delta_L = 0$ and in the limit of $\Omega_{12} \gg \tilde{\Omega}, \gamma$ the coherences between the collective states reduce to

$$\varrho_{es} \approx \frac{\mathrm{i}\tilde{\Omega}^3}{\gamma \Omega_{12}^2} , \qquad \varrho_{sg} \approx -\frac{\tilde{\Omega}}{\Omega_{12}} , \qquad \varrho_{eg} \approx -\frac{\mathrm{i}\tilde{\Omega}^2}{\gamma \Omega_{12}} . \tag{10.82}$$

In this regime, the coherences ϱ_{sg} and ϱ_{eg} are of order of magnitude Ω_{12}^{-1}, but ϱ_{eg} dominates over the one-photon coherence ϱ_{sg} when the driving field is strong. Thus, the squeezing generated at $\Delta_L = 0$ is due to the two-photon coherences between the collective states. We have already learnt that the two-photon coherence creates the superposition state $|\eta\rangle$ which, as described above in Example 1, exhibits spin squeezing.

Figure 10.10 shows the steady-state variance F_θ, evaluated according to (10.81) and (4.33) and plotted as a function of Δ_L for $R_{12} = 0.05\lambda$, $\Omega = 3\gamma$, $\bar{r} \perp \boldsymbol{R}_{12}$ and different phases θ. We see that a large squeezing is generated near the one- and two-photon resonances. It is also seen that near the two-photon resonance a change by $\pi/4$ of the phase θ changes a dispersion-like structure of F_θ into an absorption-like type.

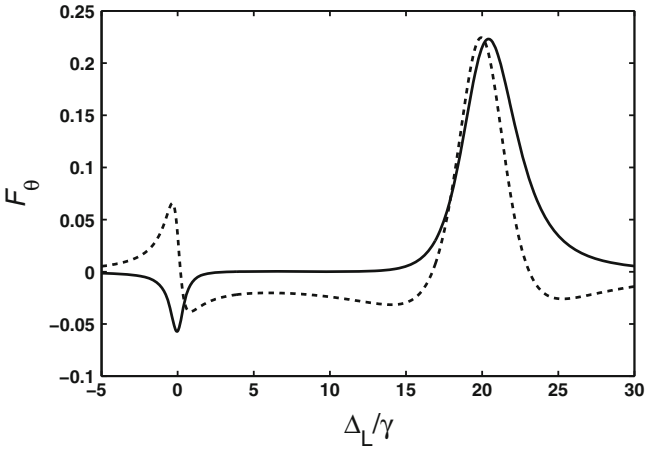

Fig. 10.10 The steady-state variance F_θ plotted as a function of Δ_L for $\Omega = 3\gamma$, $\Omega_{12} = 20\gamma$ and different values of the quadrature phase θ: $\theta = 0$ (*dashed line*), $\theta = 3\pi/4$ (*solid line*)

The analytical form of the variance F_θ can be written down directly with the help of the steady-state solutions (4.33). In the case illustrated in Fig. 10.10, in which the dipole–dipole interaction is much stronger than the Rabi frequency that, on the other hand, is much stronger than the damping rate γ, $\Omega_{12} \gg \Omega \gg \gamma$, the variance takes the form

$$F_\theta = \frac{\Omega^2}{\Omega_{12}} \left[\frac{\Delta_L}{\left(\gamma^2 + 4\Delta_L^2\right)} \cos 2\theta + \frac{\gamma}{\left(\gamma^2 + 4\Delta_L^2\right)} \sin 2\theta \right] . \tag{10.83}$$

In writing (10.83) we have retained only those terms which contribute near $\Delta_L = 0$. Expression (10.83) predicts a dispersion-like structure for $\theta = 0$ or $\pi/2$, and an absorption-like structure for $\theta = \pi/4$. Moreover, we see that the presence of the dipole–dipole interaction is essential to obtain squeezing near the two-photon resonance. This means that the generation of the spin squeezing is a clear indication of a totally different process which can appear in a two-atom system. The dipole–dipole interaction shifts the collective states that induces two-photon transitions responsible for the origin of the two-photon coherence.

10.6 Spin Squeezing and Entanglement

Interest in spin squeezed states or shortly in spin squeezing has been greatly stimulated by the need to determine a direct measure of an entanglement between atoms or ions. Similar to the dipole squeezing, the spin squeezing is itself a nonclassical phenomenon, and therefore it is essential to use the quantum picture in the description of

the behavior of the atomic spins. As we have already demonstrated, spin squeezing is manifested by a reduction of the noise level caused by multiatom or collective spin fluctuations that falls below the standard quantum limit even if the fluctuations of each spin separately are well above the vacuum noise level. Since the correlated quantum correlations result from the collective behavior of the spins, the single spin contribution to the noise level is not taken into account.

10.6.1 Relation Between Entanglement and the Kitagawa and Ueda Spin Squeezing Parameter

We illustrate our considerations of the relation between entanglement and the Kitagawa and Ueda spin squeezing parameter on the simplest collective system, the two-atom Dicke model. Among several measures of entanglement proposed in the literature [17, 18], we shall use the negativity criterion for entanglement, which requires to evaluate eigenvalues of the partial transposition of ϱ written on the basis of the product states (10.30). In general, the density matrix has the form

$$\varrho = \begin{pmatrix} \varrho_{11} & \varrho_{12} & \varrho_{13} & \varrho_{14} \\ \varrho_{21} & \varrho_{22} & \varrho_{23} & \varrho_{24} \\ \varrho_{31} & \varrho_{32} & \varrho_{33} & \varrho_{34} \\ \varrho_{41} & \varrho_{42} & \varrho_{43} & \varrho_{44} \end{pmatrix} . \tag{10.84}$$

The matrix partially transposed to ϱ with respect to the first atom has the form

$$(\varrho)^{T_1} = \begin{pmatrix} \varrho_{11} & \varrho_{21} & \varrho_{13} & \varrho_{23} \\ \varrho_{12} & \varrho_{22} & \varrho_{14} & \varrho_{24} \\ \varrho_{31} & \varrho_{41} & \varrho_{33} & \varrho_{43} \\ \varrho_{32} & \varrho_{42} & \varrho_{34} & \varrho_{44} \end{pmatrix} \tag{10.85}$$

Matrix partially transposed with respect to the second atom is the matrix transposed to (10.85). Both of them are Hermitian and have the same eigenvalues.

In a collective system, such as the Dicke model, the product states (10.30) do not correspond in general to the eigenstates of the system. Therefore, it is more proper to work in terms of the collective states (4.5), introduced in Sect. 4.1, which are the eigenstates of the collective system. When we express the elements of the density matrix (9.2) in terms of elements between the collective states, the density matrix takes the form

$$(\varrho)^{T_1} = \begin{pmatrix} \varrho_{gg} & \frac{1}{\sqrt{2}}\varrho_{sg} & \frac{1}{\sqrt{2}}\varrho_{gs} & \frac{1}{2}\varrho_{ss} \\ \frac{1}{\sqrt{2}}\varrho_{gs} & \frac{1}{2}\varrho_{ss} & \varrho_{ge} & \frac{1}{\sqrt{2}}\varrho_{se} \\ \frac{1}{\sqrt{2}}\varrho_{sg} & \varrho_{eg} & \frac{1}{2}\varrho_{ss} & \frac{1}{\sqrt{2}}\varrho_{es} \\ \frac{1}{2}\varrho_{ss} & \frac{1}{\sqrt{2}}\varrho_{es} & \frac{1}{\sqrt{2}}\varrho_{se} & \varrho_{ee} \end{pmatrix} \tag{10.86}$$

where we have taken into account the fact that in the Dicke model the antisymmetric state $|a\rangle$ does not participate in the dynamics of the system.

There are obviously four eigenvalues of the matrix (10.86). In general, it is not easy to the properties of the eigenvalues. However, for a simple problem in which the one-photon coherences are zero, $\varrho_{sg} = \varrho_{es} = 0$, the matrix (10.86) reduces to the so-called X-state form

$$(\varrho)^{T_1} = \begin{pmatrix} \varrho_{gg} & 0 & 0 & \frac{1}{2}\varrho_{ss} \\ 0 & \frac{1}{2}\varrho_{ss} & \varrho_{ge} & 0 \\ 0 & \varrho_{eg} & \frac{1}{2}\varrho_{ss} & 0 \\ \frac{1}{2}\varrho_{ss} & 0 & 0 & \varrho_{ee} \end{pmatrix} \tag{10.87}$$

In this case, one can readily find that the eigenvalues are of the form

$$\begin{aligned} p_{1,2} &= \frac{1}{2}\varrho_{ss} \pm |\varrho_{eg}| \,, \\ p_{3,4} &= \frac{1}{2}\left\{ \left(\varrho_{ee} + \varrho_{gg}\right) \pm \left[\left(\varrho_{ee} - \varrho_{gg}\right)^2 + \varrho_{ss}^2 \right]^{\frac{1}{2}} \right\} . \end{aligned} \tag{10.88}$$

We see from (10.88) that p_2 can be negative. Hence, the degree of entanglement is simply

$$E = \max\left(0, -2p_2\right) = 2|\varrho_{eg}| - \varrho_{ss} \,. \tag{10.89}$$

The negativity criterion depends only on the matrix elements $|\varrho_{eg}|$ and ϱ_{ss}, and tells us that the two-photon coherence $|\varrho_{eg}|$ must be grater than $\varrho_{ss}/2$ to obtain entanglement between the atoms. Thus, the two-photon coherence is necessary to produce entanglement. Recalling that two-photon coherence creates the superposition state $|\eta\rangle$, which exhibits spin squeezing, we should expect that there is a connection between entanglement and spin squeezing.

In order to determine the relation between entanglement and spin squeezing, we express the spin components $\langle S_x\rangle$, $\langle S_y\rangle$, $\langle S_z\rangle$ in terms of the density matrix elements of the system. A simple calculation using the relations (4.14) shows that

$$\begin{aligned} \langle S_x\rangle &= \left[\left(\varrho_{es} + \varrho_{sg}\right) + \left(\varrho_{se} + \varrho_{gs}\right)\right] \,, \\ \langle S_y\rangle &= \mathrm{i}\left[\left(\varrho_{es} + \varrho_{sg}\right) - \left(\varrho_{se} + \varrho_{gs}\right)\right] \,, \\ \langle S_z\rangle &= \varrho_{ss} + 2\varrho_{ee} - 1 \,. \end{aligned} \tag{10.90}$$

Since the one-photon coherences are real, $\langle S_y\rangle = 0$, and then the Bloch vector has the components $\boldsymbol{B} = (\langle S_x\rangle, 0, \langle S_z\rangle)$. Thus, we can study spin squeezing by a single rotation of the nonzero spin components around the y-axis. Let $\boldsymbol{n}_3$ be the direction of the total spin in the new (rotated) reference frame. Then the variances calculated in the directions $\boldsymbol{n}_1$ and $\boldsymbol{n}_2$ perpendicular to the direction of the total spin can be written as

$$\langle\left(\Delta S_{\boldsymbol{n}_1}\right)^2\rangle_\perp = \langle S_z^2\rangle \sin^2\alpha + \langle S_x^2\rangle \cos^2\alpha - \langle S_x S_z\rangle \sin 2\alpha \,,$$
$$\langle\left(\Delta S_{\boldsymbol{n}_2}\right)^2\rangle_\perp = \langle S_y^2\rangle \,, \tag{10.91}$$

where $\tan\alpha = \langle S_x\rangle/\langle S_z\rangle$.

When (10.88) are used in (10.91), we readily find that the Kitagawa and Ueda's parameters become

$$\xi^S_{\boldsymbol{n}_1} = 2\,(1-\varrho_{ss})\sin^2\alpha + \left(1+\varrho_{ss}+2\varrho_{eg}\right)\cos^2\alpha \,,$$
$$\xi^S_{\boldsymbol{n}_2} = 1+\varrho_{ss}-2\varrho_{eg} \,. \tag{10.92}$$

From the structure of (10.92) it is clear that the necessary condition to obtain spin squeezing is to create two-photon coherences ϱ_{ge}. For $\varrho_{eg} < 0$, the right-hand side of $\xi^S_{\boldsymbol{n}_1}$ can be less than 1, whereas the right-hand side of $\xi^S_{\boldsymbol{n}_2}$ are always greater than 1. Thus, spin squeezing can be observed only in the $\xi^S_{\boldsymbol{n}_1}$ component. On the other hand, for $\varrho_{eg} > 0$, the right-hand side of only $\xi^S_{\boldsymbol{n}_2}$ can be less than 1 indicating that in this case spin squeezing can be observed only in the $\xi^S_{\boldsymbol{n}_2}$ component.

When we compare (10.92) with (10.89) we readily see that the condition for entanglement ($E > 0$) is completely equivalent to the condition for spin squeezing predicted by the Kitagawa and Ueda's parameter $\xi^S_{\boldsymbol{n}_2}$, and there is a simple relation

$$E = \max\left\{0,\, 1-\xi^S_{\boldsymbol{n}_2}\right\} \,. \tag{10.93}$$

A value of $\xi^S_{\boldsymbol{n}_2} < 1$ indicates spin squeezing and at the same moment there is entanglement ($E > 0$) between the atoms. In addition, the degree of entanglement is equal to the degree of spin squeezing [19]. Thus, we conclude that the Kitagawa and Ueda parameter is the sufficient and necessary condition for entanglement in a two-atom system determined by the density operator (10.87). Note that this is not true if the parameter $\xi^H_{\boldsymbol{n}_2}$ is used in a search for entanglement. Since, $\xi^H_{\boldsymbol{n}_2} \geq \xi^S_{\boldsymbol{n}_2}$ there might be entangled states which are not spin squeezed according to $\xi^H_{\boldsymbol{n}_2}$. It is clearly seen if we make use of the relation (10.59) in (10.93), which gives

$$E = \max\left\{0,\, 1-\left(\frac{|\langle S_{n_3}\rangle|}{S}\right)\xi^H_{n_2}\right\} \,. \tag{10.94}$$

Then since $|\langle S_{n_3}\rangle| \leq S$, we see that the measure E could be positive ($E > 0$) even if $\xi^H_{n_2} > 1$. Hence, $\xi^H_{n_2}$ may not detect entangled states which, on the other hand, could be detected by $\xi^S_{n_2}$.

10.6.2 Relation Between Entanglement and the Spectroscopic Spin Squeezing Parameter

Apart from the spin squeezing parameters $\xi^H_{\boldsymbol{n}_i}$ and $\xi^S_{\boldsymbol{n}_i}$ there is yet another spin squeezing parameter often used in the literature, the spectroscopic spin squeezing parameter

introduced in the context of Ramsey spectroscopy as a ratio of the variance of the phase measurement $(\Delta\phi)^2$ to the variance $(\Delta\phi_{\rm SQL})^2$ at the standard quantum limit [20]

$$\xi^R_{n_i} = \frac{(\Delta\phi)^2}{(\Delta\phi_{\rm SQL})^2} = \frac{2S\langle\left(\Delta S_{\boldsymbol{n}_i}\right)^2\rangle_\perp}{\langle S_{\boldsymbol{n}_3}\rangle^2} \,. \tag{10.95}$$

Comparing (10.95) with (10.57) and (10.58), we find

$$\xi^S_{n_i} = \frac{|\langle S_{n_3}\rangle|}{S}\xi^H_{n_i} = \left(\frac{\langle S_{\boldsymbol{n}_3}\rangle}{S}\right)^2 \xi^R_{n_i} \,. \tag{10.96}$$

Since, $|\langle S_{n_3}\rangle| \leq S$, we see that the spin squeezing parameters satisfy the following inequality:

$$\xi^S_{n_i} \leq \xi^H_{n_i} \leq \xi^R_{n_i} \,. \tag{10.97}$$

Evidently, among these three parameters, $\xi^R_{n_i}$ is the most stringent parameter to detect spin squeezing. On the other hand, $\xi^R_{n_i}$ is the most weaken parameter to detect entangled states in the two-atom Dicke model. Since the spin squeezing parameters are in general state dependent we stress that these conclusions, which apply to the two-atom Dicke model, may not apply to other systems.

We now illustrate the application of these relations to the two-atom Dicke model and consider two cases. In the first, we assume that the Dicke model is damped by a broadband squeezed vacuum field. In the second, we assume that the Dicke model is driven by a coherent laser field is damped to the ordinary vacuum reservoir.

The spin squeezing parameters $\xi^H_{n_2}$ and $\xi^R_{n_2}$ are readily calculated from the previously derived expression (10.92) for $\xi^S_{n_2}$. Using (10.92) in (10.96), we arrive at the following relation:

$$\xi^S_{n_2} = \frac{\xi^H_{n_2}}{U} = \frac{\xi^R_{n_2}}{U^2} \,, \tag{10.98}$$

where

$$U = (\varrho_{ee} - \varrho_{gg})\cos\alpha + \sqrt{2}(\varrho_{es} + \varrho_{sg})\sin\alpha \,. \tag{10.99}$$

Thus, we expect that these three parameters will give different predictions about spin squeezing.

Consider first the two-atom Dicke system damped by a broadband squeezed vacuum field. We make use of the steady-state solutions (6.116) for the density matrix elements, derived previously in Sect. 6.3.5. When (6.116) are used in (10.90), we find for the average values of the spin components

$$\langle S_x\rangle = \langle S_y\rangle = 0\,,$$
$$\langle S_z\rangle = \frac{-(2N+1)^2+4|M|^2}{(2N+1)(3N^2+3N+1-3|M|^2)}\,. \tag{10.100}$$

Since $\langle S_x\rangle = \langle S_y\rangle = 0$, we can determine spin squeezing in the xy-plane without any rotation ($\alpha = 0$). In this case, $(n_1, n_2, n_3) = (x, y, z)$.

Figure 10.11 shows the entanglement measure E and the spin squeezing parameters plotted as a function of N for classical ($|M| = N$) and quantum ($|M| = \sqrt{N(N+1)}$) squeezed vacuum fields. For a classical squeezed field entanglement is seen to occur only in a restricted range of N. Correspondingly, spin squeezing also occurs in a restricted range of N. We see significant differences in the prediction of spin squeezing by the parameters $\xi^H_{n_2}$, $\xi^H_{n_2}$, and $\xi^R_{n_2}$. When the atoms are damped by the quantum squeezed field, entanglement occurs over entire range of N. It is apparent that whenever there is entanglement between the atoms, all the parameters ξ_{n_2} exhibit spin squeezing. Therefore, presence of spin squeezing is a conclusive test for entanglement. However, the reverse is not true. There are ranges of N at which $\xi^H_{n_2} > 1$ and $\xi^R_{n_2} > 1$ even though the atoms are entangled. However, in all cases it turns out that $\xi^S_{n_2} < 1$ whenever the atoms are entangled and the degree of spin squeezing is equal to the degree of entanglement. Thus, we must conclude that not all the spin squeezing parameters correctly detect entanglement between the atoms.

As our second example, we consider the two-atom Dicke model driven by a coherent laser field ($\Omega \neq 0$) and damped by the ordinary vacuum field, ($M = N = 0$). The steady-state values of the density matrix elements needed to evaluate the negativity and the spin squeezing parameters can be obtained from the equations of motion (4.25). Putting $\gamma_s = 2\gamma$, $\Delta_L = \Omega_{12} = 0$, $\Omega_\alpha = -i\Omega_0$ and $\Omega_\beta = 0$ in (4.25), we can solve the set of the coupled equations analytically for the steady state, and get

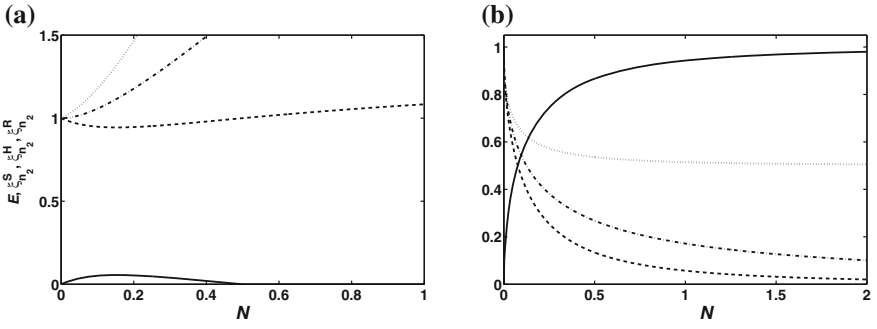

Fig. 10.11 Negativity E (*solid line*) and the spin squeezing parameters $\xi^S_{n_2}$ (*dashed line*), $\xi^H_{n_2}$ (*dashed-dotted line*), and $\xi^R_{n_2}$ (*dotted line*) plotted as a function of N for **a** the classical squeezed vacuum field with $M = N$, **b** the quantum squeezed vacuum field with $M = \sqrt{N(N+1)}$

$$\varrho_{ee} = \frac{\Omega_0^4}{D}\,, \quad \varrho_{ss} = \frac{\left(\Omega_0^2 + 2\gamma^2\right)\Omega_0^2}{D}\,,$$
$$\varrho_{es} = \varrho_{se} = \frac{\sqrt{2}\gamma\,\Omega_0^3}{D}\,, \quad \varrho_{eg} = \varrho_{ge} = \frac{2\gamma^2\Omega_0^2}{D}\,,$$
$$\varrho_{sg} = \varrho_{gs} = \frac{\sqrt{2}\gamma\,\Omega_0\left(\Omega_0^2 + 2\gamma^2\right)}{D}\,, \tag{10.101}$$

where $D = 3\Omega_0^4 + 4\gamma^2\Omega_0^2 + 4\gamma^4$.

When (10.101) is used in (10.90), we readily find that $\langle S_x\rangle \neq 0$, $\langle S_y\rangle = 0$ and $\langle S_z\rangle \neq 0$. Thus, we can determine spin squeezing by a single rotation of the nonzero spin components around the y-axis with an angle α given by $\tan\alpha = \langle S_x\rangle/\langle S_z\rangle$.

Figure 10.12 illustrates the variation of E and the spin squeezing parameters with Ω_0. It is apparent that entanglement appears for $\Omega < \sqrt{2}\gamma$ and mirrors the spin squeezing determined by the parameter $\xi^S_{n_2}$. As one would expect from the above discussion, there are significant differences in the prediction of spin squeezing by the parameters $\xi^H_{n_2}$, $\xi^H_{n_2}$ and $\xi^R_{n_2}$. The range of Ω_0 over which $\xi^H_{n_2} < 1$ and $\xi^R_{n_2} < 1$ is smaller than that over which the atoms are entangled.

In summary of this section, we stress that different spin squeezing parameters give somewhat different predictions of entanglement in the two-atom Dicke model. It is interesting and perhaps surprising that the Kitagawa and Ueda spin squeezing parameter, which is recognized as the appropriate measure of spin squeezing of massive systems, is found as the sufficient and necessary condition for entanglement in a system containing only two atoms. We would like to emphasize that not all entangled states of the Dicke model are spin squeezed. In other words, entanglement and spin squeezing are two distinct features of quantum states of a two-atom system that do not always occur together.

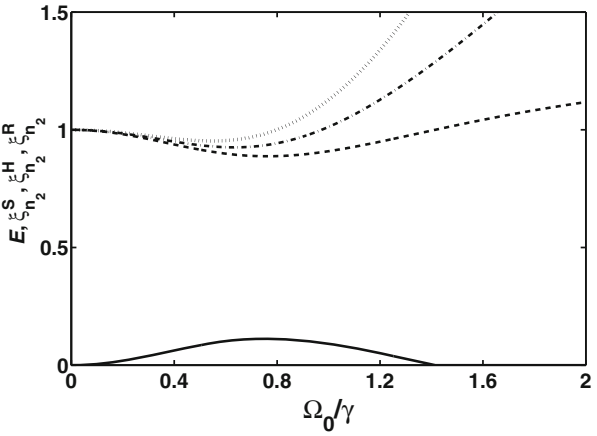

Fig. 10.12 Negativity E (*solid line*) and the spin squeezing parameters $\xi^S_{n_2}$ (*dashed line*), $\xi^H_{n_2}$ (*dashed-dotted line*), and $\xi^R_{n_2}$ (*dotted line*) plotted as a function of the Rabi frequency Ω_0

Further Applications of Spin Squeezing

Spin squeezing has demonstrated to be a fruitful concept both for the measure of entanglement and for precision spectroscopy [13]. Experimental realizations with cold atomic ensembles [21, 22] and with Bose−Einstein condensates [23–25] have made spin squeezing suitable for quantum metrology. Especially, the application of spin squeezing to the problem of beating the quantum limit in the precision measurement and atomic clocks has been the subject of a great deal of research activity [13, 26]. One of the limitations to the precision of measurements and of atomic clocks is the quantum noise caused by the measurement of the atomic state. We have seen in Chap. 9 that the SQL can be overcome by entangling the field modes. Similarly, one can overcome the SQL by entangling atoms. Hence, performing spin squeezing, it is possible to robustly generate such entanglement and therefore surpass the SQL of precision in atomic clocks. An experimental protocol to generate spin squeezed states close to the Heisenberg limit was proposed [27].

References

1. C. Aragone, G. Guerri, S. Salamo, J.L. Tani: J. Phys. A **15**, L149 (1974)
2. K. Wódkiewicz, J.H. Eberly: J. Opt. Soc. Am. B **2**, 458 (1985)
3. M.A. Dupertuis, A.N. Kireev: Quantum Opt. **2**, 119 (1990)
4. C.H.H. Schulte, J. Hansom, A.E. Jones, C. Matthiesen, C. Le Gall, M. Atatüre: Nature **525**, 222 (2015)
5. S.M. Barnett: Optics Commun. **61**, 432 (1987)
6. K. Wódkiewicz, P.L. Knight, S.J. Buckle, S.M. Barnett: Phys. Rev. A **35**, 2567 (1987)
7. S.M. Barnett, P.L. Knight: Phys. Scr. **21**, 5 (1988)
8. B.J. Dalton, Z. Ficek, P.L. Knight: Phys. Rev. A **50**, 2646 (1994)
9. Z. Ficek, R. Tanaś, S. Kielich: Phys. Rev. A **29**, 2004 (1984)
10. Z. Ficek, R. Tanaś, S. Kielich: Acta Phys. Pol. A**67**, 583 (1985)
11. Q.Y. He, S.G. Peng, P.D. Drummond, M.D. Reid: Phys. Rev. A **84**, 022107 (2011)
12. Q.Y. He, T.G. Vaughan, P.D. Drummond, M.D. Reid: New J. Phys. **14**, 093012 (2012)
13. J. Ma, X.-G. Wang, C.P. Sun, F. Nori: Physics Rep. **509**, 89 (2011)
14. B. Dalton, J. Goold, B. Garraway, M. Reid: arXiv:1506.06892 (2015)
15. M. Kitagawa, M. Ueda: Phys. Rev. A **47**, 5138 (1993)
16. T. Holstein, H. Primakoff: Phys. Rev. **58**, 1098 (1940)
17. A. Peres: Phys. Rev. Lett. **77**, 1413 (1996)
18. P. Horodecki: Phys. Lett. A **232**, 333 (1997)
19. A. Messikh, Z. Ficek, M.R.B. Wahiddin: Phys. Rev. A **68**, 064301 (2003)
20. D.J. Wineland, J.J. Bollinger, W.M. Itano, D.J. Heinzen: Phys. Rev. A **46**, R6797 (1992); **50**, 67 (1994)
21. K. Hammerer, A.S. Sorensen, E.S. Polzik: Rev. Mod. Phys. **82** 1041 (2010)
22. C.F. Ockeloen, R. Schmied, M.F. Riedel, P. Treutlein: Phys. Rev. Lett. **111**, 143001 (2013)
23. C. Gross, T. Zibold, E. Nicklas, J. Estéve, M.K. Oberthaler: Nature **464**, 1165 (2010)
24. M.F. Riedel, P. Boehi, Y. Li, T.W. Haensch, A. Sinatra, P. Treutlein: Nature **464**, 1170 (2010)
25. W. Muessel, H. Strobel, D. Linnemann, D. B. Hume, M. K. Oberthaler: Phys. Rev. Lett. **113**, 103004 (2014)
26. D. Leibfried, M. Barrett, T. Schaetz, J. Britton, J. Chiaverini, W. Itano, J. Jost, C. Langer, D. Wineland: Science **304**,1476 (2004)
27. L. Pezze, L.A. Collins, A. Smerzi, G.P. Berman, A.R. Bishop: Phys Rev A **72**, 043612 (2005)

Index

Z. Ficek and R. Tanaś, *Quantum-Limit Spectroscopy*, Springer Series in Optical Sciences 200, DOI 10.1007/978-1-4939-3740-0